

1069

heat water
and
transfer

the

NN08201.1069

bare soil surface

h.f.m. ten berge

HEAT AND WATER TRANSFER AT THE BARE SOIL SURFACE

Aspects affecting thermal imagery

STELLINGEN

1. Bij de beschrijving van de verdamping van onbegroeide bodem dient men ervan uit te gaan dat de fysische toestand van bodem en van aangrenzende atmosfeer van elkaar afhankelijk zijn.

dit proefschrift.

2. De door Philip en De Vries gegeven beschrijving van gekoppeld vocht- en warmtetransport geeft een overschatting van de door temperatuurgradiënten geïnduceerde vloeistofflux.

Philip, J.R. and D.A. de Vries, 1957. Moisture movement in porous materials under temperature gradients. Trans. Amer. Geophys. Union 38: 222-231.

3. De vergelijkingen tussen thermodynamische en mechanistische beschrijvingen van gekoppeld vocht- en warmtetransport, zoals te vinden in de bodemfysische literatuur, negeren het verband tussen enerzijds de bevochtigingswarmte van de vaste fase en anderzijds de temperatuurafhankelijkheid van de oppervlaktespanning van het water. Dientengevolge zijn deze vergelijkingen steeds onvolledig en inconsequenter uitgewerkt.

Nielsen, D.R., R.D. Jackson, J.W. Cary, and D.D. Evans, 1972. Soil Water. Am. Soc. of Agron. Special Issue.

Jury, W.A., 1973. Simultaneous transport of heat and moisture through a medium sand. Dissertatie Univ. of Wisconsin.

Chu, S.Y., G. Sposito, and W.A. Jury, 1983. The cross-coupling transport coefficient for the steady flow of heat in soil under a gradient of water content. Soil Sci. Soc. Am. J. 47: 21-25.

4. Het concept 'matrix flux potentiaal' verdient ook voor praktische toepassingen meer aandacht dan er tot op heden aan geschonken werd.

Shaykewitch, C.F., and L. Stroosnijder, 1977. The concept of matric flux potential applied to simulation of evaporation from soil. Neth. J. agric. Sci. 25: 63-82.

5. Het stemt tot verbazing dat de toenemende interesse in ruimtelijke variabiliteit van bodemeigenschappen niet gepaard gaat met een vergrote belangstelling voor de temporele variabiliteit van deze eigenschappen.

Soil Spatial Variability. Proceedings of a workshop of the ISSS and the SSSA, Las Vegas, USA, November 30 - December 1, 1984. Eds. D.R. Nielsen and J. Bouma. Pudoc, Wageningen, 1985.

6. Bij de selectie van proefvelden voor bodemfysisch onderzoek wordt in het algemeen te weinig rekening gehouden met het relaxatie gedrag van de atmosferische grenslaag na terreinovergangen.

Kroon, L.J.M., 1985. Profile derived fluxes above inhomogeneous terrain: a numerical approach. Dissertatie Landbouwhogeschool, Wageningen.

7. De drie voudige betekenis van het woord 'valideren' lijkt sommige modelbouwers ertoe te verleiden de grondleggende fase te vergeten ten behoeve van de latere fasen.
8. De behoudendheid van mensen ten aanzien van waardevolle nieuwe technieken, zoals bijvoorbeeld teledetectie of numerieke simulatie, wordt helaas in de hand gewerkt doordat enthousiaste gebruikers zelf vaak nalaten een foutenanalyse te verstrekken bij operationeel gebruik.
9. Het beoordelen van teledetectieprodukten op basis van slechts kwantitatieve aspecten doet sommigen te gemakkelijk eraan voorbijgaan dat dergelijke produkten in kwalitatieve zin van grote praktische zowel als wetenschappelijke waarde kunnen zijn.
10. Een optimale beschikbaarheid van computerfaciliteiten aan de Landbouwhogeschool zou een verhoging van de arbeidscapaciteit opleveren ter waarde van 3 à 4 miljoen gulden per jaar.
11. Het moderne massa-toerisme leidt veleer tot onderlinge vervreemding van culturen dan tot serieuze wederzijdse verkenningen.
12. Juist in een klimaat van snelle verbreiding van informatie-technologie verdient het subsidiëren van muziekscholen hoge prioriteit, als middel ter ontwikkeling van het vermogen tot communicatie tussen mensen.
13. De door het Centraal Bureau Motorrijtuigenbelastingen voorgestelde opheffing van wegenbelasting op 'klassieke mobielen' dient te worden toegejuicht omdat dit zou leiden tot een meer gevarieerd straatbeeld.
14. Ook in de wetenschap wordt kleur vaak ontleend aan stellingnamen die als 'al te grijs' kunnen worden aangemerkt.

Stellingen behorend bij het proefschrift:

Heat and water transfer at the bare soil surface: aspects affecting thermal imagery.

H.F.M. ten Berge, 14 februari 1986

Promotoren: **dr. G.H. Bolt,**
hoogleraar in de bodemscheikunde en de bodemnatuurkunde,
dr. L. Wartena,
hoogleraar in de landbouwweerkunde en de omgevingsnatuurkunde
Co-promotor: **dr. L. Stroosnijder**

NN08201, 1069

H.F.M. ten Berge

**HEAT AND WATER TRANSFER
AT THE BARE SOIL SURFACE:
Aspects affecting thermal imagery**

Proefschrift
ter verkrijging van de graad van
doctor in de landbouwwetenschappen,
op gezag van de rector magnificus,
dr. C.C. Oosterlee,
in het openbaar te verdedigen
op vrijdag 14 februari 1986
des namiddags te vier uur in de aula
van de Landbouwhogeschool te Wageningen

ISN = 240242

This study was carried out at the
Department of Soil Science and Plant Nutrition
Wageningen Agricultural University,
De Dreijen 3,
NL 6703 BC Wageningen
The Netherlands

LANDBOUWHOOGESCHOOL
WAGENINGEN

Aan mijn beide ouders.

VOORWOORD

Het tot stand komen van dit proefschrift is voor mij een hoogtepunt en daarom een goede gelegenheid om allen, die mij bij het ten grondslag liggen-de werk direct of indirect geholpen hebben, te bedanken.

Mijn vader en moeder wil ik graag eerst noemen. Zij hebben mij een grote vrijheid gegeven en mijn studie in alle stadia mogelijk gemaakt en aangemoedigd. Het plotseling afscheid van mijn eerste leermeester, twee jaar geleden, doet mij daarom ook nu intens verdriet.

Dr. Leo Stroosnijder heeft dit onderzoek voorbereid en een grote invloed gehad op het eindresultaat. Ik wil je bedanken, Leo, voor de toewijding en het enthousiasme waarmee je mij hebt begeleid, en voor de gesprekken van velerlei aard die hiermee gepaard gingen. Het doet mij veel plezier dat je de reis uit Indonesië onderneemt om als co-promotor hierbij aanwezig te kunnen zijn.

Mijn eerste promotor, Prof. G.H. Bolt, heeft mij veel aandacht geschenken, aanvankelijk vooral waar het theoretische problemen betrof, maar later ook bij de redactionele aspecten van het schrijven. Hooggeleerde Bolt, met genoegen denk ik aan de lange discussies, waarbij u de voedzame huiselijke lunch vrijwillig inruilde voor taaiere kost. Mijn hartelijke dank voor alle hulp en adviezen.

Veel dank gaat ook uit naar mijn tweede promotor, Prof. L. Wartena. Beste Bert, verschillende malen heb je mij moed ingeblazen door te laten zien welke in de praktijk belangrijke en interessante vragen zijn. De erg plezierige samenwerking met jou heeft ervoor gezorgd dat deze studie zich inderdaad op het grensvlak bodem-atmosfeer afspeelde.

Verder gaat mijn dank uit naar Dr. Ad Driedonks (KNMI) voor zijn waardevolle adviezen.

Karin Sijlmans en Inge Stakman hebben zeer veel energie besteed aan het typen van dit proefschrift, maar vooral ook aan de coördinatie van de ermee gepaard gaande bezigheden in de eindfase. Karin en Inge, ik ben jullie veel dank verschuldigd. Ook Herma Roseboom wil ik hartelijk danken voor de geboden hulp.

Voor het beschikbaar maken van een aantal gegevens ben ik Dr. R.D. Jackson (USDA Water Conservation Lab), Prof. C.H.M. van Bavel en Dr. Robert Lascano (Texas A & M University) zeer erkentelijk, evenals Dr. T.J. Schmugge (NASA Goddard Space Flight Centre).

Het vele tekenwerk is uitgevoerd door de heer Rijpma. Voor de snelle en zorgvuldige behandeling van de bij voortduring aangevoerde tekeningen ben ik hem zeer erkentelijk.

De heer Van Baren en zijn medewerkers, wil ik danken voor het fotografische werk.

Op het Rekencentrum heb ik veel hulp ontvangen van de heren Koster en Van Hoof, en van de groep voorlichting.

Verder wil ik graag mijn dank uitspreken aan Gerard Nieuwenhuis (ICW) voor de zeer waardevolle hulp bij mijn FLEVO veldexperimenten, en aan Wil Ackerman, Simon Maasland, Marion de Heus, Arnold Bregt, Hans Bronswijk, Annemiek van der Meijden en Coen Ritsema, die mij allen enthousiast geholpen hebben bij het verzamelen van gegevens.

Tot slot mijn dank aan al die medewerkers van de vakgroep die het werk op het lab tot aangenaam verpozen maken en daarmee een belangrijke motor zijn voor hun omgeving.

CONTENTS

Abstract		
List of symbols		
1 INTRODUCTION		
1.1	Bare soils and remote sensing	1
1.2	Structure of the thesis	4
2 SOIL TEMPERATURE MODELS		9
2.1	Correlative models	9
2.2	Physical models	10
2.2.1	Analytical models	11
2.2.2	Numerical models	16
3 TRANSPORT PROCESSES. THEORY AND MODELLING		20
3.1	General overview	20
3.2	The surface energy balance	24
3.3	Radiation	26
3.3.1	Shortwave radiation terms	26
3.3.2	Longwave radiation terms	30
3.4	Transport in the atmospheric boundary layer	34
3.4.1	Exchange at the surface	34
3.4.2	Boundary layer development	39
3.5	Transport of heat in the soil	47
3.5.1	Conduction	48
3.5.2	Coupling: heat associated with changes in soil water entropy	54
3.5.3	Convective heat transport in the gas phase	58
3.6	Transport of water in the soil	59
3.6.1	Coupling: non-isothermal transport in the liquid phase; the formulation of $p(r,T)$	60
3.6.2	The moisture characteristic, hydraulic conductivity and matric flux potential	66
3.6.3	Coupling: non-isothermal transport in the vapour phase; the formulation of $p(r,T)$	74
3.6.4	The transport coefficient of water vapour in soil; enhancement effects	81

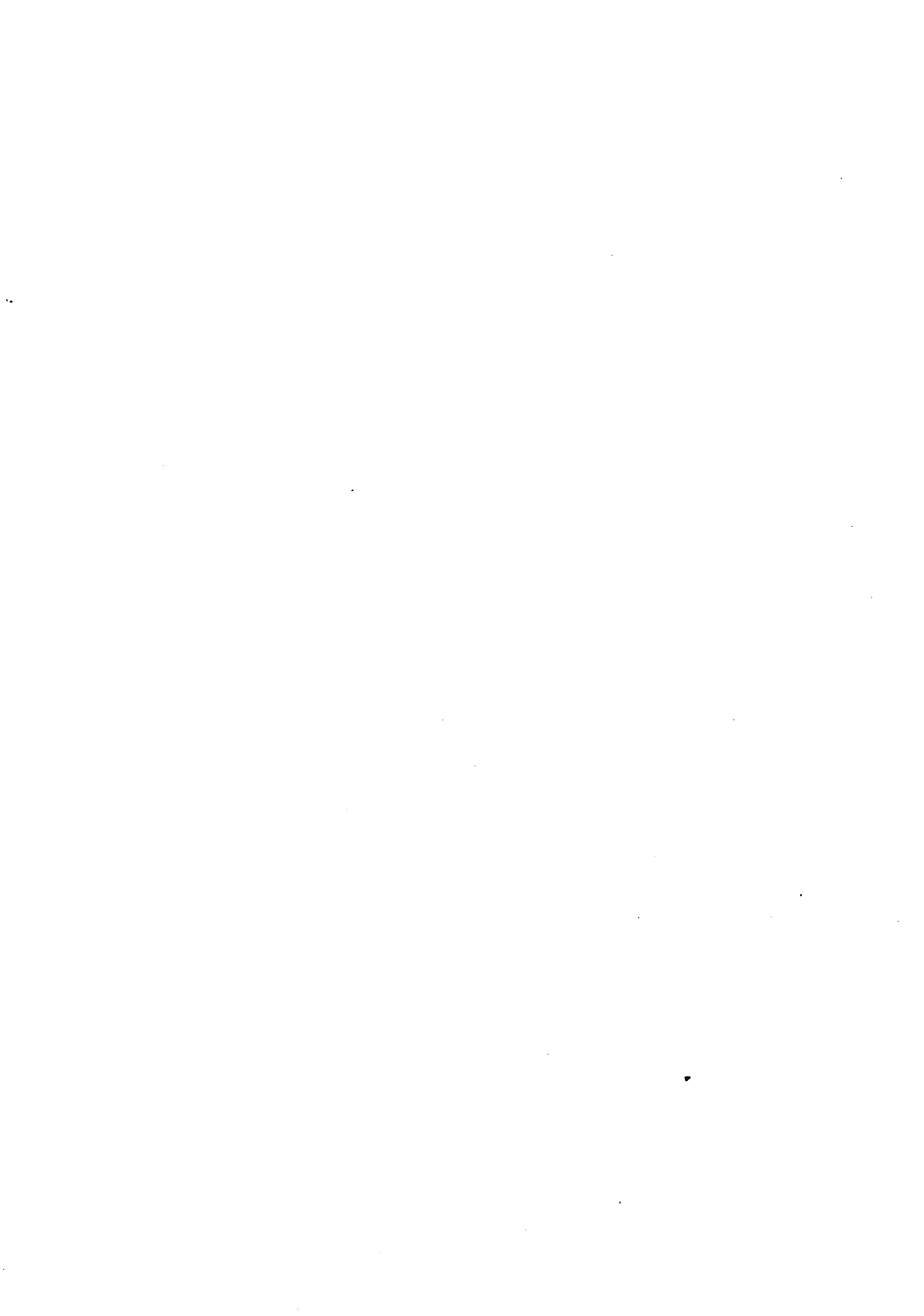
4 EXPERIMENTS	88
4.1 Introduction	88
4.2 Variability and errors	89
4.3 Location and general conditions	93
4.4 Boundary conditions: the fluxes	97
4.5 Boundary conditions: the state variables	101
4.6 System parameters and functions	104
4.7 Output and initial conditions: soil state variables and fluxes	122
5 VALIDATION	127
5.1 Experimental validation	127
5.1.1 Error variance analysis	128
5.1.2 FLEVO-1	132
5.1.3 FLEVO-2	144
5.1.4 TEXAS	152
5.1.5 ARIZONA	156
5.2 Comparison of the simulation model with an analytical solution under limiting conditions	162
5.3 Brief evaluation of simulated boundary layer development	167
6 SENSITIVITY ANALYSIS	174
6.1 Approaches to sensitivity analysis	174
6.2 Relevance of boundary layer development to soil processes	177
6.3 Sensitivity of some variables to major soil parameters; the drying stages I and III	181
6.4 Stage II: development of the dry surface layer; a case study	189
6.5 Comments on the relation T_s -LE	202
7 THERMAL REMOTE SENSING: STATE OF THE ART AND PERSPECTIVES FOR BARE SOILS	204
7.1 Determination of soil state variables	206
7.2 Determination of the latent heat flux	212

Literature

APPENDIX 1	Listing of the SALSA model	A1
APPENDIX 2	Algorithm for the calculation of soil thermal conductivity according to the De Vries (1963) model	A16
APPENDIX 3	On the derivation of equation 3.59	A18
APPENDIX 4	Some additional considerations based on TIP	A21
APPENDIX 5	Heat transfer by convection in the soil under a gradient in virtual temperature	A24
APPENDIX 6	Determination of the matric flux potential curve for core samples; a new method	A26
APPENDIX 7	Description of the surface step method to determine soil thermal conductivity on core samples (Stroosnijder, 1984)	A29
APPENDIX 8	Details on FLEVO, TEXAS, ARIZONA experiments	A31
APPENDIX 9	The Nicholaichuck model	A36
APPENDIX 10	Listings of the programs NICAN and LINTRA	A39

Samenvatting

Curriculum Vitae



ABSTRACT

Surface temperature as assessed by means of thermal infra red remote sensing is affected by a number of soil properties. The sensitivity of surface temperature and surface energy fluxes to variations in physical soil properties is studied by means of a numerical simulation model.

The model developed here takes into account the mutual interdependence between soil and atmosphere. The transport processes in the soil are discussed in detail, and are partially revised. Developments in the atmospheric boundary layer are based on the production rates of turbulent kinetic energy.

Many physical data on soil hydraulic, thermal and radiative properties are summarized. The ranges over which these properties appear to vary are used to set extreme parameter values for studying model sensitivity.

Several field experiments were conducted to study in detail the behaviour of topsoil moisture and temperature; a total of four different experimental datasets is used for model validation.

Sensitivity to basic soil physical properties is determined for the three classical stages of drying. The 'falling rate' stage is discussed in more detail in terms of two new soil parameters, characterizing the matric flux potential curve. These appear to have a strong influence on dry layer development, and hence on the sensitivity of surface temperature to soil physical properties.

The possibilities to assess bare soil conditions and surface fluxes by means of thermal infra red imagery appear, from the presented results, to be very limited, even when detailed wind and global radiation data for the site under study are known.

A review of methods, used in thermal imagery interpretation, is included; also, most of the existing simulation models on this topic are summarized.

LIST OF SYMBOLS

symbol	description	Unit
a	parameter in soil water pressure - temperature relation	Pa K ⁻¹
a	parameter in dimensionless gradient atmosphere	-
a	albedo	-
a	sky emissivity parameter	-
a_{dry}	dry soil albedo	-
a_{wet}	wet soil albedo	-
A	gravimetric soil moisture content at h=0.8	kg kg ⁻¹
A	interfacial area	m ²
A	parameter in $\Phi(\theta)$ relation with saturation as reference	kg m ⁻¹ s ⁻¹
A'	parameter in $\Phi(\theta)$ with field capacity as reference	kg m ⁻¹ s ⁻¹
b	sky emissivity parameter	-
b	parameter in soil water pressure-temperature relationship	m ³ m ⁻³
B	parameter in $\Phi(\theta)$ function with saturation as reference	-
B'	parameter in $\Phi(\theta)$ function with field capacity as reference	-
c	cloud cover	-
c	parameter in soil water pressure-temperature relationship	Pa K ⁻¹
c	constant relating transport coefficient to turbulent kinetic energy	-
C_a	volumetric heat capacity air	J m ⁻³ K ⁻¹
C_c	volumetric heat capacity clay	J m ⁻³ K ⁻¹
C_o	volumetric heat capacity volumetric matter	J m ⁻³ K ⁻¹
C_p	heat capacity of air at constant pressure	J kg ⁻¹ K ⁻¹
C_q	volumetric heat capacity quartz	J m ⁻³ K ⁻¹
C_s	volumetric heat capacity bulk soil	J m ⁻³ K ⁻¹
C_w	volumetric heat capacity water	J m ⁻³ K ⁻¹
D_a	water vapour diffusivity in free air	m ² s ⁻¹
D_e	effective water vapour diffusivity	m ² s ⁻¹
$D_{T,liq}$	thermal liquid diffusivity	m ² s ⁻¹ K ⁻¹
D_θ	isothermal soil water diffusivity	m ² s ⁻¹
e	turbulent kinetic energy	J kg ⁻¹
e	vapour pressure	Pa

E	surface water vapour flux	$\text{kg m}^{-2} \text{s}^{-1}$
f	Coriolis parameter	s^{-1}
f_a	volume fraction air	$\text{m}^3 \text{m}^{-3}$
f_c	volume fraction clay	$\text{m}^3 \text{m}^{-3}$
f_o	volume fraction organic matter	$\text{m}^3 \text{m}^{-3}$
f_q	volume fraction quartz	$\text{m}^3 \text{m}^{-3}$
F	free Helmholtz energy	J
g	gravity constant	m s^{-2}
G_s	soil heat flux density of the surface	W m^{-2}
h	relative humidity soil air	-
h	lag (in semivariance)	-
H	sensible heat flux (atmosphere)	W m^{-2}
H	partial specific enthalpy	J kg^{-1}
ΔH_a	heat of adsorption (heat of wetting)	J kg^{-1}
ΔH_v	heat of vaporisation	J kg^{-1}
\bar{H}_v	partial specific enthalpy of soil water in a reference state	J kg^{-1}
ΔH_v^*	heat of vaporisation	J mol^{-1}
j_l	flux density of liquid water	$\text{kg m}^{-2} \text{s}^{-1}$
$j_{q,w}$	heat flux density associated with water transport	W m^{-2}
j_s	total entropy flux density	$\text{W m}^{-2} \text{K}^{-1}$
j_v	water vapour flux density	$\text{kg m}^{-2} \text{s}^{-1}$
j_w	water flux density	$\text{kg m}^{-2} \text{s}^{-1}$
j_q	total heat flux density	W m^{-2}
k	Von Kármán constant	
K	hydraulic conductivity	$\text{kg m}^{-1} \text{Pa}^{-1} \text{s}^{-1}$
K_H	transport coefficient (atmosphere) for heat	$\text{m}^2 \text{s}^{-1}$
K_M	transport coefficient (atmosphere) for momentum	$\text{m}^2 \text{s}^{-1}$
K_s	hydraulic conductivity at saturation	$\text{kg m}^{-1} \text{Pa}^{-1} \text{s}^{-1}$
K_v	transport coefficient (atmosphere) for vapour	$\text{m}^2 \text{s}^{-1}$
λ	length scale (atmosphere)	m
L	latent heat of vaporisation (= ΔH_v)	J kg^{-1}

L	Monin-Obukhov length	m
LE	latent heat flux density (atmosphere)	W m^{-2}
LE_{pot}	potential latent heat flux density (atmosphere)	W m^{-2}
m	Van Genuchten parameter	-
M	molecular weight	kg mol^{-1}
n	cloud parameter	-
n	Van Genuchten parameter	-
p	soil water pressure (extramatic phase)	Pa
p'	soil water pressure (matric phase)	Pa
\bar{p}	pressure (atmosphere)	Pa
\tilde{p}	soil vapour pressure	Pa
p_r	soil water pressure at specific location r	Pa
p_{sc}	field scaled soil water pressure	Pa
q	specific humidity	kg kg^{-1}
q	scaled deviation	-
r_a	atmospheric resistance	s m^{-1}
r_{aH}	atmospheric resistance to heat transfer	s m^{-1}
r_{aM}	atmospheric resistance to momentum transfer	s m^{-1}
r_{av}	atmospheric resistance to vapour transfer	s m^{-1}
R	gas constant	$\text{J mol}^{-1}\text{K}^{-1}$
R	radiance	$\text{W Sr}^{-1} \text{m}^{-2}$
R'	reflectance	W m^{-2}
R_e	emitted radiation	W m^{-2}
R_{glob}	global radiation (radiant flux density)	W m^{-2}
R_{ld}	longwave downward radiation	W m^{-2}
R_n	net radiation	W m^{-2}
R_{nl}	net longwave radiation	W m^{-2}
Ri	Richardson number	-
S	total system entropy (in Appendix 3 only)	J
S	partial specific entropy of soil water in 'extramatic' state	$\text{J kg}^{-1} \text{K}^{-1}$
S'	partial specific entropy of soil water in 'matric' state	$\text{J kg}^{-1} \text{K}^{-1}$

\bar{s}_w	partial specific entropy of soil water in a reference state	$J \text{ kg}^{-1} \text{ K}^{-1}$
\tilde{s}_w	partial specific entropy of soil water in vapour state	$J \text{ kg}^{-1} \text{ K}^{-1}$
t	time	s
T	temperature	$^{\circ}\text{C}$ or K
T_a	air temperature	$^{\circ}\text{C}$
T_c	cloud temperature	K
T_s	surface temperature	$^{\circ}\text{C}$
T_{sky}	sky radiation temperature (8-14 μm)	$^{\circ}\text{C}$ or K
T_{sr}	surface radiation temperature (8-14 μm)	$^{\circ}\text{C}$ or K
u	wind speed (in x direction)	m s^{-1}
u'	temporal deviation from \bar{u}	m s^{-1}
u^*	friction velocity	m s^{-1}
\bar{u}	time-averaged wind speed	m s^{-1}
u_g	geostrophic wind speed (in x direction)	m s^{-1}
U	internal energy	J
v	wind speed (in y direction)	m s^{-1}
v'	temporal deviation from \bar{v}	m s^{-1}
\bar{v}	time averaged wind speed	m s^{-1}
\bar{v}	specific volume of 'extramatic' water	$\text{m}^3 \text{ kg}^{-1}$
v'	specific volume of 'matric' water	$\text{m}^3 \text{ kg}^{-1}$
\tilde{v}	specific volume of water vapour	$\text{m}^3 \text{ kg}^{-1}$
v_g	geostrophic wind speed (in y direction)	m s^{-1}
w	blackbody emittance	W m^{-2}
x	horizontal space coordinate	m
y	horizontal space coordinate	m
z	vertical space coordinate	m
z_m	measurement height	m
z_o	roughness length	m

α	constant in formulation length scale atmosphere	-
α	absorptivity	-
α	Van Genuchten parameter in moisture characteristic expression	Pa^{-1}
α	tortuosity correction factor	-
α_r	scale factor of location r	-
β	parameter in dimensionless gradient atmosphere	-
β	regression coefficient	$\text{K W}^{-1} \text{m}^2$
β	Bowen ratio	-
β	phenomenological diffusion enhancement coefficient	-
γ	semivariance	-
γ_{lg}	interfacial tension liquid-gas	N m^{-1}
γ_{ls}	interfacial tension liquid-solid	N m^{-1}
γ_{gs}	interfacial tension gas-solid	N m^{-1}
ϵ_{dry}	dry soil emissivity	-
ϵ_{sky}	apparent sky emissivity	-
ϵ_{wet}	wet soil emissivity	-
ζ	stability parameter	-
η	dynamic viscosity	Pa s
η_3	component in the z-direction of unit vector along rotation axis	-
θ	volumetric moisture content	$\text{m}^3 \text{m}^{-3}$
θ	potential temperature	K
θ_{crit}	volumetric moisture content at which albedo reaches minimum value	$\text{m}^3 \text{m}^{-3}$
θ_r	residual moisture content	$\text{m}^3 \text{m}^{-3}$
θ_s	volumetric moisture content at saturation	$\text{m}^3 \text{m}^{-3}$
$\theta_{1.5}$	soil moisture content at $p = -1.5 \text{ MPa}$	$\text{m}^3 \text{m}^{-3}$
θ_{30}	soil moisture content at $p = -30 \text{ MPa}$	$\text{m}^3 \text{m}^{-3}$
θ_*	scaled temperature	K
λ	thermal conductivity soil	$\text{W m}^{-1} \text{K}^{-1}$
λ	wavelength	μm
λ_a	thermal conductivity air	$\text{W m}^{-1} \text{K}^{-1}$
λ_c	thermal conductivity clay	$\text{W m}^{-1} \text{K}^{-1}$
λ_o	thermal conductivity organic matter	$\text{W m}^{-1} \text{K}^{-1}$
λ_q	thermal conductivity quartz	$\text{W m}^{-1} \text{K}^{-1}$
λ_w	thermal conductivity water	$\text{W m}^{-1} \text{K}^{-1}$
μ	chemical potential	J kg^{-1}

μ_{w_i}	chemical potential of water in phase i	$J \ kg^{-1}$
v	mass flow correction factor	-
ν	kinematic viscosity air	$m^2 \ s^{-1}$
ξ	correction factor for local temperature gradient	-
Ξ	relative moisture content	-
ρ	density of surface air	$kg \ m^{-3}$
ρ	reflectivity	-
ρ_c	density of clay	$kg \ m^{-3}$
ρ_l	longwave reflectivity	-
ρ_l	density of soil liquid	$kg \ m^{-3}$
ρ_v	water vapour density	$kg \ m^{-3}$
σ	Stefan-Bolzman constant	$W \ m^{-2} \ K^{-4}$
τ	transmissivity	-
τ_x	flux of x-momentum	$kg \ m^{-1} \ s^{-2}$
τ_y	flux of y-momentum	$kg \ m^{-1} \ s^{-2}$
ϕ	geographical latitude	rad
ϕ	wetting angle	rad
ϕ	azimuth	rad
ϕ_M	dimensionless gradient of momentum	-
ϕ_H	dimensionless gradient of temperature	-
Φ	matric flux potential	$kg \ m^{-1} \ s^{-1}$
ψ	soil water potential	$J \ kg^{-1}$
ψ	elevation	rad
Ψ_H	stability correction factor (heat)	-
Ψ_M	stability correction factor (momentum)	-
Ω	angular frequency of earth's rotation	rad s^{-1}

CHAPTER 1. INTRODUCTION

1.1 Bare soils and remote sensing

Although the hydraulic and thermal behaviour of bare topsoils may seem somewhat irrelevant in the context of agricultural production, in reality it deserves due attention. Bare soil surfaces occur, during short or more extended periods of the year, in all climatological zones that have significance to agriculture. Often, the lack of a crop cover is due to adverse physical conditions, imposed by temporal, large scale meteorological situations. In the humid temperate and cold regions, large tracts of arable land remain bare in wintertime due to low temperatures. Under mediterranean conditions, both winter cold and (late) summer drought may put a limit to crop growth, and in the semi-arid and subhumid tropics, arable land is often cultivated during a short growing season; there, drought and sometimes also high temperatures inhibit plant establishment and growth during the dry season. In semi-arid zones, also rangeland may be very sparsely vegetated during a considerable part of the year.

Aside from this seasonal absence of vegetation, certain crops are cultivated in a manner that keeps most of the soil surface bare continuously, and in some dry farming systems one may find rotation schemes that include a year fallow, in order to store soil moisture for the next growing season.

After the oceans, the soil surface is the major distributor of solar energy on the earth's surface, and accordingly surface conditions have a strong influence on our every-day environment. Heat and mass, momentum and kinetic energy are carried away from or towards the surface by a variety of transport processes in the soil and the atmospheric boundary layer, thus providing a buffering mechanism that maintains the earth habitable. The transitions from liquid water flow to vapour transfer, from molecular diffusion to bulk mass transport, and from conductive to radiative heat transfer all occur at or near the soil-atmosphere interface. The interaction between surface and atmosphere is also essential in the production of turbulence; in addition, the surface can be viewed as a sink for the horizontal components of momentum.

For bare surfaces, soil physical properties determine to a large extent the hydraulic and thermal response of the topsoil to variations in atmo-

spheric conditions. With respect to seasonal variations, examples of agro-nomical interest are the Spring warming of seedbed and rootzone in cold and temperate climates, the process of slaking and crust formation, and in dryland agriculture the storage and conservation of soil water. The physical response of the topsoil to daily variations plays a role in e.g. the germination physiology of weed and crop seeds, in the occurrence of groundfrost, the movement of solutes (herbicides), the formation of dew (and associated pests in developing canopies) etc., but is also linked with seasonal developments in soil temperature and moisture profiles.

Soil management practices often aim at influencing these physical processes in the topsoil. A variety of tillage and crop residue treatment systems has been developed ever since the commencement of human activities in agriculture, and new (and old) concepts are still being evaluated, mostly by empirical analysis. The recent development of the so called 'alley cropping systems' may serve in this context to illustrate the continuing interest in the management of surface processes, both in soil and in atmosphere.

During the last two decades, remote sensing techniques have become increasingly attractive as a means of obtaining information about the conditions and processes occurring at the earth's surface. In relation to bare soils, mainly radar, passive microwave and thermal infrared (TIR) systems, either airborne or operating from satellites, have been used. These techniques provide information about a thin surface layer of the soil, i.e. a layer of a few tens of micrometers (TIR) up to a few centimeters (microwave) thickness. Although the absolute value of the measured variable in these cases often is of little interest, the relative ease at which data can be collected by remote sensing - with desired frequency and from large areas - is a promising aspect in itself. If surface signals could be interpreted quantitatively in terms of physical processes, the inventory of relevant time-dependent phenomena would be greatly helped. Such 'monitoring' not only would yield a (continuous) record of conditions that determine (potential) plant environment, it also would be helpful in the evaluation of soil treatments and might permit the survey of more permanent material properties, associated with surface processes.

Consequently, along with the development of remote sensing capabilities, the need has evolved to relate 'superficial' signals, as registered by

sensors, to processes and conditions that have a practical significance. Two approaches to this problem have been followed in soils and remote sensing literature: the empirical (statistical) approach, and the analyses based upon physical models of reality.

In the empirical/statistical approach, the signal is directly correlated to the variable of practical interest. Examples of such analyses are given by Bouter and Janse (1979) (topsoil moisture, roughness and radar backscatter), Stolp and Janse (1985) (surface slaking and radar backscatter), Lynn (1984a) (soil texture, organic matter and multispectral reflectance), Heilman and Moore (1980) and Idso et al (1975a) (topsoil moisture and radiation temperature), Idso et al (1975b) (topsoil moisture and albedo), Reginato et al (1976) (evaporation and radiation temperature), ten Berge et al (1983) (texture, moisture and radiation temperature), Lynn (1985) (soil taxonomy and radiation temperature), Lamers (1985) (surface slaking and radiation temperature) and many other authors.

The methods alternative to the above approach employ physical relations between fluxes and state variables (e.g. moisture content, temperature) in combination with relations between measured variables or derived parameters and the actual conditions of interest. Examples of the latter type are models expressing thermal inertia in terms of soil moisture content and bulk density (e.g. Pratt and Elyett, 1979), or microwave emittance in terms of moisture content and temperature (e.g. Tsang et al, 1975; Choudhury et al, 1982; Dobson et al, 1985). The former type of relations constitute procedures that use the remotely measured course of a surface state variable as a starting point to finally calculate the desired surface flux or state variable. The balance concept (for mass or energy) is usually involved here. If the goal is to obtain fluxes and soil state variables (profiles), straightforward physical models are often used, with the remotely sensed boundary conditions and known system parameters as input (as applied by e.g. Stroosnijder et al. (1985) and Prevot et al (1984) in soil water regime calculations and by Hares et al (1985) in monitoring the soil thermal regime). If on the other hand system parameters, (e.g. thermal inertia) and surface fluxes are sought, one encounters the so-called inversion problem: now the measured course of a state variable must be used to infer system parameters and fluxes, instead of being imposed to calculate the development of state variables. Then, analytical balance approximations can be used, for

example to estimate evaporation and thermal inertia (Price, 1980). To this purpose also semi-analytical approaches are followed, as exemplified by Menenti (1984) in an extensive treatment of the calculation of evaporation from thermal imagery.

As an alternative to cope with the inversion problem, 'lookup' tables have been constructed, using numerical simulation models (Rosema, 1975; Schieldge et al., 1980).

Of the remotely sensible variables, attention is focussed in the present work upon soil surface temperature. Temperature plays a central role in both the mass and the energy balance of the bare soil surface, and it can be obtained with fair accuracy. For these reasons, surface temperature would seem to be an attractive variable to be measured by remote sensing, thus enabling one to keep track of topsoil behaviour. Naturally then questions arise as to which phenomena could actually be followed using thermal infrared technology, which accuracy can be hoped for, and how much noise can be expected from effects one is not interested in.

In an attempt to answer the above questions, the present study was developed along the lines of the school of C.T. de Wit, and the approach could be referred to as 'systems analysis' in the terminology of some authors. The aims are the following:

- to compile the available theory, relevant to exchange processes at bare soil surfaces, in the form of a simulation model
- to present an overview of measured data with reference to bare soils, comprising both system parameters and time sequences of state variables
- to show by sensitivity analysis how the developed simulation model can be used as a tool to study the transport processes, and the surface temperature in relation to soil physical properties, and, consequently, how such a model can aid in the interpretation of thermal imagery.
- to draw conclusions, though not exhaustive, on the promises of thermal infrared remote sensing for bare soil monitoring.

1.2 Structure of the thesis

Figure 1.1 shows the 'flowpaths' of the approach followed, along with references to the various chapters of the present thesis.

In Chapter 2, the existing models concerning topsoil dynamics in a

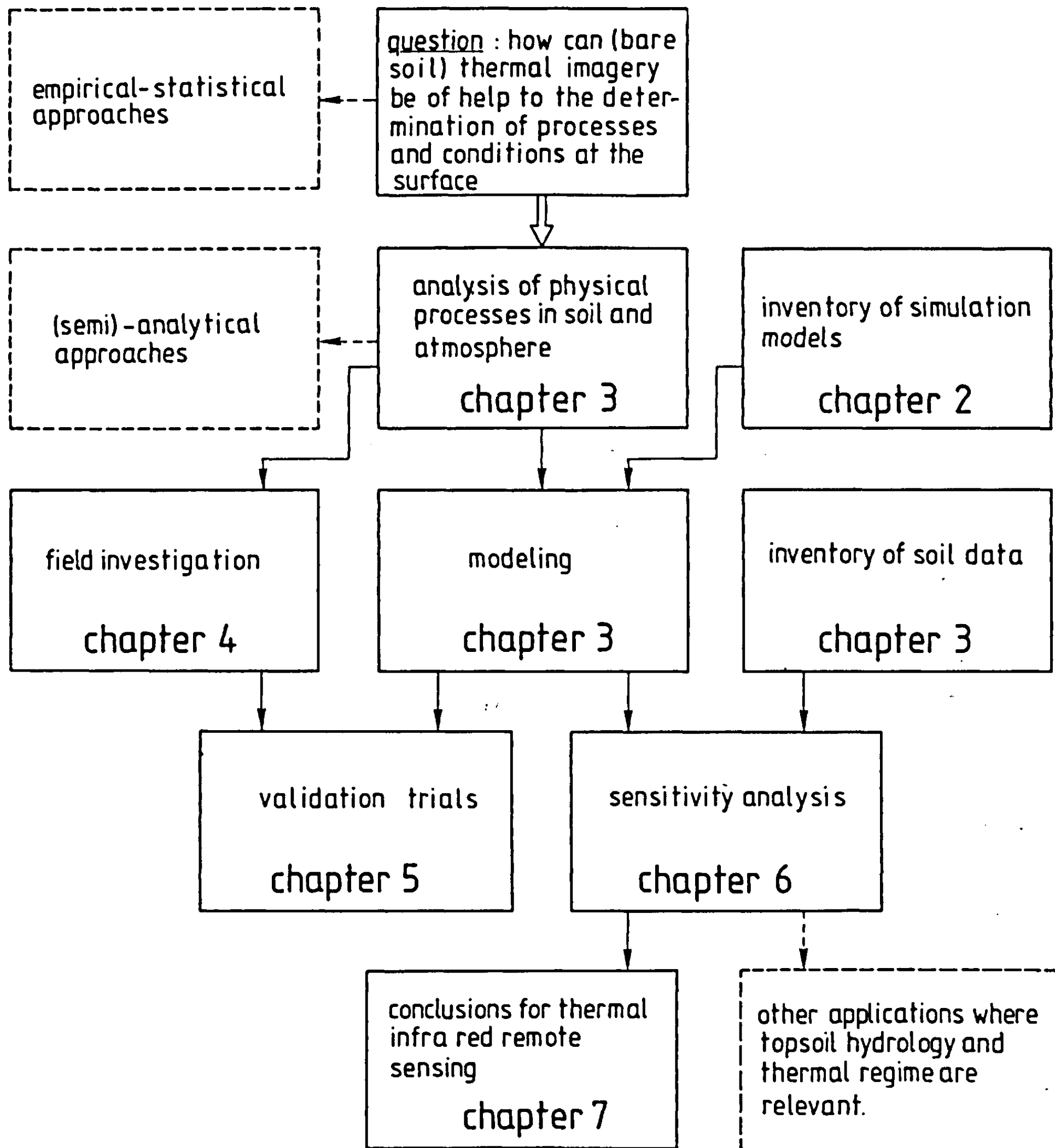


Figure 1.1 Outline of the thesis. Alternative lines of interest, not followed in the present study, are marked by broken lines.

natural environment, known to the author, are briefly reviewed and classified. It appears that a large number of models have been constructed during the past fifteen years, each with its specific application aims. Whereas for the various models the required boundary conditions and the assumptions in describing the transport processes may vary strongly, they have in common that they all predict soil temperatures under field conditions.

The theory underlying the presented model SALSA is treated in Chapter 3, along with the simplifications introduced to arrive at the model formulation as listed at the end of each (sub)section. Fragments of the model are based on models already existing, such as those by Van Keulen (1975), Van Bavel and Lascano (1979), and Nieuwstadt and Driedonks (1979).

Bearing in mind the number of described models as listed in the second chapter, one might question the need for 'yet another' numerical simulation model. Nevertheless, it was felt that several - in modelling generally accepted - formulations call for a revision. These relate to the phenomenon of coupling between mass and heat transfer in the soil, and to the dependence of atmospheric conditions on surface processes. With respect to the former, some theoretical developments, leading to a simplification of the description of non-isothermal soil water transport, are presented. Regarding the atmospheric processes, existing concepts from the field of boundary layer meteorology have been adopted in the formulation of the simulation model. For a realistic description of the present system, soil and atmospheric boundary layer are to be viewed as mutually dependent. Profiles of soil temperature and soil moisture are influenced by atmospheric conditions, and these in turn are dependent on the state of the soil. This implies that boundary conditions must be chosen with care, which often has not been done in modelling efforts. The choice of boundary conditions, of course, depends on the purpose of the modelling activity. The SALSA model offers, besides some minor variations, two options: either the upper boundary of the system is taken close to the surface (e.g. at screen height) and measured conditions at this level are imposed as boundary conditions, or the system is extended to include the complete boundary layer. In the latter case, boundary conditions are taken at some height above the mixed layer, and the diurnal development of this layer is simulated on the basis of surface fluxes, along with soil profile developments.

An additional requirement entertained was to compose a clearly struc-

tured model that could be used also for other applications than the present, e.g. as a reference model in parametrization, or as an instruction tool for educational purposes. Chapter 3 also provides an extensive collection of data pertaining to soil radiative, thermal and hydraulic functions and parameters, relevant to surface phenomena.

Two field experiments (FLEVO and TEXAS) have been conducted to obtain data for model validation. An additional set of observations (Jackson, 1973) is used to represent semi-arid conditions. Thus, datasets pertaining to different climatic conditions were compiled for this study. The measurement procedures and some results are discussed in Chapter 4. In the same chapter, attention is paid to the involved errors, both due to the problem of spatial variability, which is discussed in some detail, and to measurement errors.

The courses of soil state variables and surface fluxes as actually measured, hereafter called 'dynamic variables' in order to express their time-dependence, are compared in Chapter 5 to the simulation results as an attempt to model validation. With this particular intention, the uncertainty in measured dynamic variables and in model output (due to input errors) are taken into account. The latter involves a brief sensitivity analysis over those domain intervals, identified as input error intervals.

The measured field data are only suitable for a validation of the 'cut-off' version of the model, that is, the algorithm that does not include boundary layer development but uses imposed atmospheric conditions close to the surface instead. Predicted diurnal boundary layer behaviour could not be verified due to a lack of data, but is evaluated briefly on the basis of common knowledge. In addition, performance of the soil compartment is tested against an analytical solution of the simplified surface energy balance.

In Chapter 6, model sensitivity analysis and its results are discussed. The major point of interest is the sensitivity of surface temperature to variations in soil parameters. Dividing the drying process into three stages, the parameter perturbation method is used, combined with statistical evaluation. Besides surface temperature, the total daily evaporation, air temperature and saturation deficit are interesting variables of which sensitivity is studied.

Included is also a case study on the development of dry surface layers in relation to soil hydraulic properties, and finally the relation between surface temperature and evaporation rate is analyzed briefly.

Chapter 7 discusses some assumptions generally made in the interpretation of thermal infrared imagery, in the light of the results of the experiments and sensitivity study. This is not meant to be a complete overview of TIR possibilities and shortcomings, but rather an illustration of the type of use of models such as the one presented here.

CHAPTER 2. SOIL TEMPERATURE MODELS

Different types of models to predict soil temperature under field conditions have been described in soil literature in the last ten to fifteen years. They can be grouped according to various criteria. Examples of such possible criteria are the time scale of prediction (annual, seasonal, monthly, daily or hourly), the required input (air temperature, radiation, wind speed etc.), the inherent structure (correlative vs physical), the supposed application (agronomical prediction, imagery interpretation, technological or military purposes), the solution schemes used (analytical vs numerical), the underlying assumptions with respect to the involved physical processes, etcetera.

In this chapter, a distinction is made between regression-type models, and the models based on equations that express physical relationships. The latter group is subsequently divided into analytical and numerical models.

2.1 Correlative models

The models of this type use empirical relations, mostly between soil temperature and standard meteorological variables, and usually predict soil temperatures for one or more fixed depths.

Most of these regression models are 'coarse' in the sense that they do not specify soil conditions or surface cover. They may be designed to predict for a given depth the mean annual soil temperature as a function of altitude and latitude (Vann and Cline, 1975; Aldridge and Cook, 1983; Schmidlin et al, 1983) or mean monthly soil temperature as a function of mean air temperature (Chang and Boyer, 1977; Ouellet, 1973; Reimer and Shaykewich, 1980; Toy et al, 1978). Also, daily maximum and minimum soil temperature values have been modelled, e.g. as a function of date (Meikle and Treadway, 1979; Meikle and Gilchrist, 1983). Hasfurther and Burman (1974) modelled daily mean soil temperatures, using again air temperature as the input variable. Expressions for the diurnal course of soil temperature, based on observed maximum and minimum values of soil temperature were presented by Parton and Logan (1981).

Examples of rather detailed models, specifically for bare and residue covered soils, are those by Ghuman and Lal (1982) for a tropical soil, and by Cruse et al. (1980) for a temperate soil; these were used, respectively,

to predict daily variations and averages of soil temperature. They do take into account surface conditions, a characteristic rarely encountered in empirical soil temperature models. The model by Gupta et al. (1981) shows the same feature; it might be considered as a 'hybrid' model, as it combines an empirical formulation of surface temperature (as a function of air temperature) with a numerical solution of the soil heat flow equation.

Whereas these models may be very useful in crop growth or pest modelling because of their relative simplicity (computing costs), they do not serve the present purpose of modelling in detail the diurnal course of surface processes. Physical soil properties are usually not taken into account in the applied statistical analyses underlying these models, and often the basic bulk data refer to a variety of vegetative covers. Moreover, temperatures are generally predicted for some depth, and not for the actual soil surface, which is the location of interest in the present context. In view of these drawbacks, such models as mentioned above will not be taken into account any further.

2.2 Physical models

The models listed in the Tables 2.1 and 2.2 are based upon physical relations between fluxes, state variables, and soil properties. They all predict the development of surface temperature and soil temperature profiles, mostly on a diurnal basis. An exception is the model by Pratt et al (1980), which does not predict surface temperature, but instead uses this variable to infer thermal soil properties and evaporation rate. It is included because of its operational value to image interpretation.

Mainly bare soil models are considered here. The available models dealing with vegetation-covered surfaces have been evaluated as well if the 'canopy compartment' is not modelled separately but is viewed as an integral, inert part of the soil system. Another condition for models to be treated here is that at least the surface energy balance equation and the Fourier or heat conduction equation are involved.

The energy balance equation deals with the partitioning of energy over the various terms:

$$(2.1) \quad R_n + G_s + H + LE = 0 \quad (\text{W m}^{-2})$$

where R_n is the net radiation, G_s the soil heat flux at the surface, and H and LE the sensible and latent heat fluxes above the surface, respectively. The Fourier equation expresses the local rate of change in heat content as the divergence of the heat flux G , for the one-dimensional case as:

$$(2.2) \quad \frac{\partial(CT)}{\partial t} = - \frac{dG}{dz} = \lambda \frac{d^2 T}{dz^2} \quad (\text{W m}^{-3})$$

In this equation, T is the soil temperature (K), C the bulk volumetric heat capacity ($\text{J m}^{-3}\text{K}^{-1}$), and λ the thermal conductivity of the soil ($\text{W m}^{-1}\text{K}^{-1}$); t and z are the time and space coordinates respectively. In many of the listed models, eq. (2.2) is the only differential equation to be solved. The latter is always subject to a zero flux or constant temperature condition at some depth (e.g. 0.5 m). In contrast, the surface boundary has been treated in different ways. The soil thermal regime was extensively studied by van Duin (1956) and de Vries (1963) for the case where the surface temperature or heat flux follows a prescribed course. Alternatively, the surface conditions are based upon the energy balance equation, the formulation of which ranges from rough approximations, omitting one or more terms, to very detailed expressions, in the various reviewed models. Other differential equations than eq. (2.2) are sometimes involved, to describe mass transport processes that are linked to the energy balance, as the water supply to the surface is a key factor determining the partitioning of energy at the surface over the different terms.

2.2.1 Analytical models

Analytical solutions of eq. (2.2) subject to conditions that satisfy eq. (2.1) can only be achieved by the introduction of strongly simplifying assumptions. This renders analytical models only rough descriptions of reality, not suitable for detailed sensitivity analysis with respect to soil properties. Hence, the analytical solutions will be treated only briefly here. They offer, on the other hand, the advantage of low computer cost; and sometimes show more clearly the relations that constitute the system.

The methods used for the solution of eqs. (2.1) and (2.2) involve the use of either linear Fourier series or Laplace transforms (Jaeger, 1953; Carslaw and Jaeger, 1959). In general, analytical solutions can be obtained if the surface soil heat flux is written as a function that consists of only

first order terms in T_s , the surface temperature (Jaeger, 1953). Heschinger (1979), in an extensive treatise on the Fourier approach, showed how the surface soil heat flux can be expressed in the form

$$(2.3) \quad G_s(t, T_s) = a(t, \bar{T}_s) + b(t, \bar{T}_s)$$

and decomposed all other involved surface fluxes (H , LE , and R_n) in Fourier terms, to derive the functions $a(t, \bar{T}_s)$ and $b(t, \bar{T}_s)$. Essentially the same approach, with some variations, was followed by Watson (1975), Price (1977), Pratt et al. (1980), Moustafa et al. (1981) and Buchan (1982).

Laplace transforms were applied by Watson (1973), Nicholaichuck (1974), and Milly (1984). In the former two cases, the surface energy balance was simplified to an extreme extent. Watson completely omitted the sensible and latent heat fluxes above the surface, and Nicholaichuck imposed a constant evaporation rate at the surface. The analysis by Milly (1984) has a more general validity, allowing all surface fluxes to be variable; it imposes a periodic net radiation term as a forcing function. It also includes an advanced description of soil liquid and vapour fluxes. A major drawback of all these analytical models is the linearisation of the relevant differential equations, resulting in the constancy of transport coefficients and capacities. In particular this is not realistic for the soil water diffusivity, which is taken independent of moisture content in the Nicholaichuck and Milly models; the remaining models on the other hand are based on even stronger simplifications, omitting soil water transport completely.

Table 2.1 lists the major features of some analytical models in terms of assumptions made with respect to the energy balance, and to transport processes in soil and atmosphere. Some representatives of both the Fourier and the Laplace type models are given.

Table 2.1 Analytical models

Source	Energy balance	Radiation
Price (1977)/ Pratt et al. (1980)	$G = c_1 + c_2 T_s$ $H = c_3(T_a - T_s)$ $LE = c_4(\bar{e}_a - \bar{e}_{sur} - f(T_s))$	R_{glob} periodic $R_{ld} = f(T_a)$
Hechinger (1979)	R_N, H, LE, G all periodic $G = f_1(t, T_s)$ $+ f_2(t, T_s)T_s$	$T_s^4 = \bar{T}_s^4 + 4\bar{T}_s^3$. periodic $f(T_s)$ $R_{ld} = f(T_a, e_a, c, T_c)$
Moustafa et al (1981)	$LE = 0$ $T_a + ((1-a)R_{glob} - R_{nl})/r_a$ periodic	net longwave radiation $R_{nl} \equiv \epsilon(\sigma T_a^4 - R_{ld})$ constant
Buchan (1982)	$LE = 0$ or $LE = LE_{pot}$	R_{glob} periodic $R_{ld} = f(T_a, c, T_c)$
Watson (1973)	$H = LE = 0$	$R_n = (1-a)R_{glob} +$ $f(T_{sky}) - \epsilon\sigma T_s^4$; R_{glob} periodic; T_{sky} constant (day/night values)
Nicholaichuck (1974) Gibbs and Baca (1981)	$(R_n + \rho C_p T_a / r_a)$ and LE constant	no subdivision of R_n
Milly (1984)	R_n, G, H, LE all variable	R_n periodic

Table 2.1 - continued -

atmosphere	soil	driving variables/ boundary conditions
r_a constant; boundary conditions e_a, u constant. $T_a = c_5(T_s - \bar{T}_s) + \bar{T}_a$ no stability correction	only heat conduction	$\bar{u}, \bar{e}_a, \bar{T}_a, \bar{e}_{sur}$ (24 h averages)
r_a , and boundary conditions T_a, e_a, u all periodic; at night: T_a and e_a linear in $f(t)$; stability correction by iteration optional	only heat conduction; surface humidity $f(T_s, \theta)$; groundwater table specific groundwater temperature specified	c, T_c ; * T_a, e_a, u
r_a constant T_a see energy balance	only heat conduction	T_a, R_{glob}, R_{nl}
r_a by logarithmic wind profile; no stability correction; T_a, e_a, u, c all periodic	only heat conduction	$T_a, e_a, u, R_{glob}, c, T_c$
no fluxes	only heat conduction	T_{sky}, c
no separate formulation of fluxes; see energy balance	heat and water flow; zero vapor flow	T_a, LE, R_n
$H = c_1 (T_s - T_a)$ $LE = c_2 (q_s - q_a)$ (no stability correction)	heat: conduction; water: thermal and isothermal vapor flow; isothermal liquid flow	T_a, q_a, R_n, u

* c in this column
represents cloud cover

Table 2.1 - continued -

developed for	tests/applications	remarks
remote sensing: thermal inertia	HCMM data	use of reference thermal inertia point
remote sensing: thermal inertia	against numerical model by Soer (1977)	extensive treatment Fourier analysis
ground shelter-heat storage technology	field data Kuwait	arid climate only
agronomic forecasting	field data Aberdeen	attention to time- averaging
remote sensing thermal inertia (geology)		Laplace transform
transport contaminants	against numerical model by Gibbs and Baca, 1981	Laplace transform
theoretical analysis soil water transport		Laplace transform

2.2.2 Numerical models

Of the numerical models published, a selection is listed in Table 2.2. The format of this table differs somewhat from that of Table 2.1 since the numerical models can be characterized easiest by naming the standard formulations adopted to take into account the various processes.

Again only models are listed that solve the soil heat flow equation in conjunction with the surface energy balance. Some of the models mentioned are not limited to bare soil conditions only, but are nevertheless considered because of their general character, which renders them applicable to bare surfaces as well. Examples of these are the models by Zdunkovski and Trask (1971), Palagin (1976) and Smith (1977), the latter two of which deal with tundra surfaces. The well-known TERGRA model by Soer (1977) is not listed here since it was developed specifically for vegetated surfaces.

The studies by Sasamori (1970), Delsol et al (1971), Zdunkovski and Trask (1971), and Carlson and Boland (1978) are basically focussed upon developments in the atmospheric boundary layer. In the corresponding models, soil transport processes are included only to formulate the lower boundary conditions, set to the atmospheric boundary layer. Of these, the model by Sasamori (1970) provides the most complete description of the soil compartment. The Carlson and Boland (1978) study uses the course of boundary layer state variables over heterogeneous urban-rural terrain as the integrated result of surface fluxes, in order to infer 'effective' surface conditions. Such an approach has hardly been used in agronomical research, but it might prove useful in that context as well.

The budget of turbulent kinetic energy (see section 3.4) is not incorporated in any of the listed models, although the one by Carlson and Boland makes use of some assumptions that are based upon consideration of the kinetic energy budget of the mixed layer as a whole. Instead, the turbulent exchange coefficients in these models are derived from wind shear and local stability parameters.

For the other cases listed in Table 2.2, the emphasis is shifted towards soil and surface processes. These models have often been developed to study specific surface phenomena, e.g. snowmelt (Palagin, 1976; Smith, 1977), the effect of tillage operations (Hammel et al, 1981; Mahrer, 1982), or for the interpretation of remote sensing imagery (Rosema, 1975; Camillo et al, 1983).

Some models take into account the water flow equation, mostly along with a formulation for vapour flow as well. In those cases, the expressions proposed by Philip and de Vries (1957) are adopted to calculate transport coefficients for the coupled water and heat transfer processes. For a critique on this point see sections 3.5 and 3.6.

The models by Schroeder et al (1978) and Mahrer (1982) have the specific feature of taking surface geometry into account, involving a two dimensional description. Although not designed for this purpose, such models may prove useful to image interpretation studies, because of their capability to cope with the aspect problem on rough surfaces.

With respect to the boundary conditions, required to run the models, the same distinction as made above between 'soil' and 'atmospheric' models applies. The models with emphasis on soil processes usually require wind speed, air temperature, and vapour pressure or specific humidity at a height close to the surface, e.g. at 1.5 or 2.0 m. Global radiation is either required as a measured input variable, or it is calculated as a function of latitude, season, and time of the day. In the latter case, a transmissivity parameter is usually employed to characterize the atmosphere. More elaborate radiation models are adopted in the studies by Njoku et al (1980), Camillo et al (1983), Zdunkovski and Trask (1971) and Carlson and Boland (1978). The longwave downward radiation term is in most models derived from air temperature at screen height and cloud cover, which are to be entered as input variables.

The models designed for boundary layer studies use values for potential temperature (sometimes also specific humidity) and geostrophic wind at some height above the mixed layer as boundary conditions (Sasamori, 1970; Zdunkovski and Trask, 1971); alternatively, the ambient lapse rates of potential temperature and specific humidity are used instead of fixed values of these variables (Carlson and Boland, 1978; Delsol et al, 1971).

Detailed comparisons between predictions and observations have been performed in few cases only. Examples of field experiments designed for model validation are those by Smith (1977), Njoku et al (1980), and Lascano and Van Bavel (1983).

Table 2.2 Numerical models

	energy balance					atmosphere			soil		
	R_n , H, G, LE, incl. R_n subdivided	BL development*	kin. energy budget	stability correction	Paulson integration	water flow eq. soil	non-isothermal lbg.	isothermal vapour	non-isothermal vapour	soil latent heat	albedo $f(\theta)$
1. Sasamori (1970)	+	+	+	-	+	-	+	+	+	+	-
2. Delsol et al (1971)	+	+	+	-	+	-	-	-	-	-	-
3. Zdunkovski and Trask (1971)	-	+	+	-	+	-	-	-	-	-	-
4. Van Keulen (1975)	+	+	-	-	-	-	+	-	+	-	+
5. Rosema (1975)	+	+	-	-	+	-	+	+	+	+	+
6. Palagin (1976)	-	+	-	-	-	-	-	-	-	+	-
7. Smith (1977)	+	+	-	-	+	+	-	-	-	-	+
8. Kahle (1977)	+	+	-	-	-	-	-	-	-	-	-
9. Vauclin et al (1983)	+	+	-	-	+	-	+	-	-	+	+
10. Carlson and Boland (1978)	+	+	+	-	+	+	-	-	-	-	-
11. Schroeder et al (1978)	+	-	-	-	-	-	+	+	+	+	+
12. Van Bavel and Lascano (1979)	+	+	-	-	-	-	+	-	-	+	+
13. Njoku et al (1980)	+	+	-	-	+	-	+	+	+	-	+
14. Hammel et al (1981)	+	+	-	-	+	+	+	-	+	-	+
15. Mahrer (1982)	+	+	-	-	+	+	-	-	-	-	-
16. Camillo et al (1983)	+	+	-	-	-	-	+	+	+	-	+
17. Milly (1984)	+	+	-	-	+	-	+	-	+	-	+

* BL: atmospheric boundary layer

Table 2.2 - continued -

driving variables/ boundary cond.	developed for	test/application	remarks
1. T_{pot} , q , u_G , all above BL; R_{glob}	BL study	-	constant flux layers, time coeff. analysis.
2. T_{pot} , q , u_G , all above BL; R_{glob} , R_{ld}	circulation scale atmosphere study	-	atmosphere 3-dim. soil 1-dim.
3. R top atmosphere T_{pot} top BL	nocturnal BL study	-	no evaporation; radiat. divergence incl.
4. T_a , e_a , u , cloud cover, R_{glob}	soil water balance arid regions	lab columns and field exp. Israel	T_s calculation explicit
5. T_a , e_a , u , cloud cover; R calculated	TIR imagery interpretation	data Jackson (1973)	-
6. T_a , $(R_{glob}+R_{ld})$	snowmelt study	Mozhaisk, USSR	no evaporation; heat of freezing incl.
7. T_a , e_a , u , P_{atm} , cloudcover, R_{glob}	snowmelt study	Eureka, Canada	LE-H relation predetermined
8. T_a , q_a , u ; R top atmosphere	TIR imagery interpretation	Mojave desert, California	-
9. T_a , e_a , u , R_{glob}	agronomical study	-	-
10. u_a ; R calculated	urban-rural complex study	Nebraska; Hay, Australia; Los Angeles	2-layer atmosphere; surface moisture availability parameter
11. T_a , e_a , u , R_n	engineering, agronomical study	-	2-dim.; surface geometry incl.
12. T_a , T_d , u , precipitation, R_{glob}	agronomical study	College Station, Texas	see also Lascano and Van Bavel (1983)
13. T_a , q_a , u , or dT_a/dz , dq_a/dz , du/dz	TIR and microwave imagery interpretation	Bakersfield, California	see also Schieldge et al (1982); radiation transfer model included
14. T_a , q_a , u , R_{glob}	tillage effect study	Lacrosse, Washington	
15. T_a , q_a , u ; R calculated	tillage effect study	Rehovot, Israël	2-dim.; shading included
16. T_a , e_a , u ; R_{glob}	TIR and Microwave imagery interpretation	Ruthe, West Germany	see also Camillo and Schmugge (1981) several radiation options
17. T_a , q_a , u , R_{glob} R_{ld}	moisture regime study	- study	quantitative analysis thermal effects

CHAPTER 3. TRANSPORT PROCESSES. THEORY AND MODELLING

3.1 General overview

This chapter deals with the theory of transport processes in soil and atmosphere, and formulates the simulation model SALSA (Soil-Atmosphere Linking Simulation Algorithm), which serves as a basis for the present study.

Figure 3.1a shows the relational diagram of the soil-atmosphere system. Although basically the interest is in the surface energy balance, it is convenient to take into account a total of four types of budgets: those of mass, heat, momentum, and turbulent kinetic energy. To distinguish between soil and atmosphere state variables, different names for the same quantities in the respective sections of the biosphere are used. Moreover, the equations for momentum transfer are treated for two horizontal components separately, so that a total of seven main variables results to characterize the state of the simulated system. These state variables are temperature and moisture content in the soil, potential temperature and specific humidity in the atmosphere, two orthogonal components of wind speed, and the turbulent kinetic energy. Alternatively, the dependence of atmospheric conditions on surface fluxes is not taken into account, and prescribed courses of temperature and humidity are used as boundary conditions at screen height. The relational diagram corresponding to this shorted version of the model is shown in Figure 3.1b.

In CSMP numerical simulation, each of the main state variables is calculated for each compartment of the discretized system by integration of its rate of change over time. The other state variables are then assumed to be in equilibrium with these, and are calculated subsequently. Calculated values of state variables apply to the centres of compartments; the fluxes operate at compartment interfaces. In the atmosphere, 11 layers are distinguished, increasing in thickness from 3 m at the surface to hundreds of meters at the top of the boundary layer. In the soil, compartment size increases downward from a few millimeters to several centimeters, and a total of 25 layers is used. A global flow diagram of the SALSA model is presented in Figure 3.2. The algorithm is written in computational order in the simulation language CSMP (IBM, 1975).

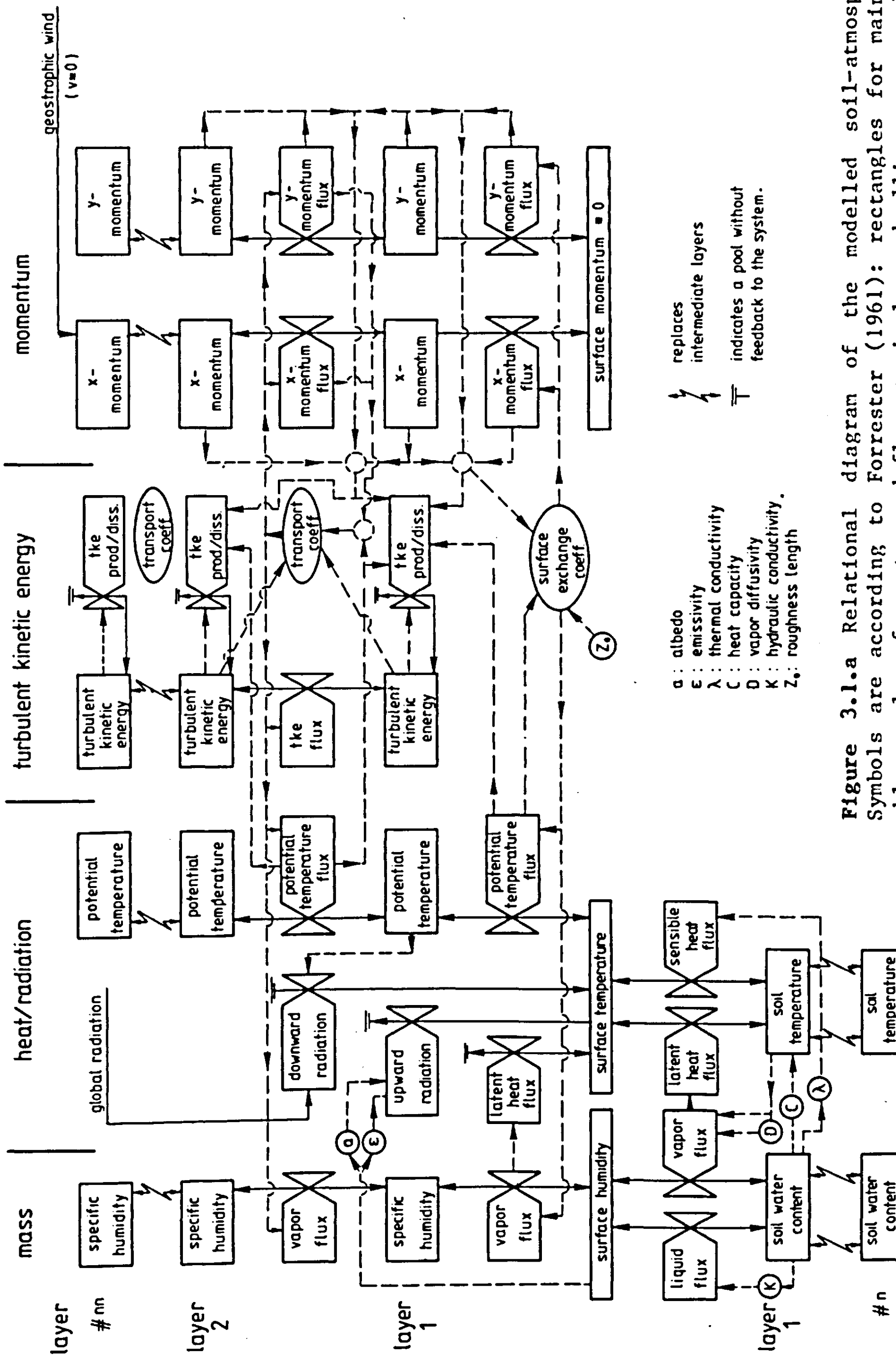


Figure 3.1.a Relational diagram of the modelled soil-atmosphere system.
 Symbols are according to Forrester (1961): rectangles for main state variables, valves for rates and fluxes; circles and ellipses are used here to indicate auxiliary soil and atmospheric boundary layer variables. Solid lines represent flows of quantities, broken lines flows of information. Boundary conditions are underlined. Within each column, the indication of feedback mechanisms between flux and state variable (gradient) – usually indicated by broken lines – has been omitted.

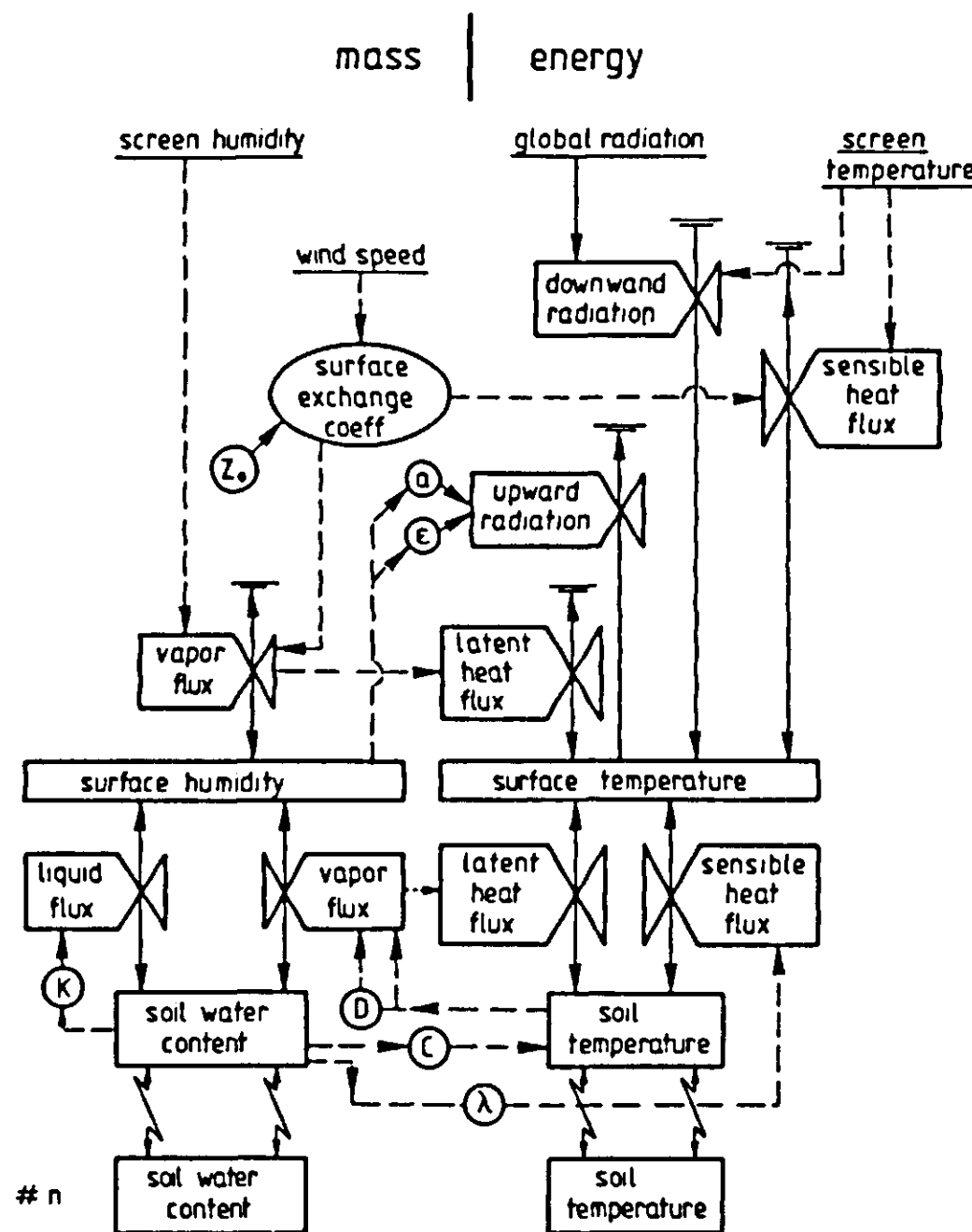


Figure 3.1.b Relational diagram of the simplified system, employing prescribed atmospheric boundary conditions at screen height. For the interpretation of symbols see figure 3.1.a.

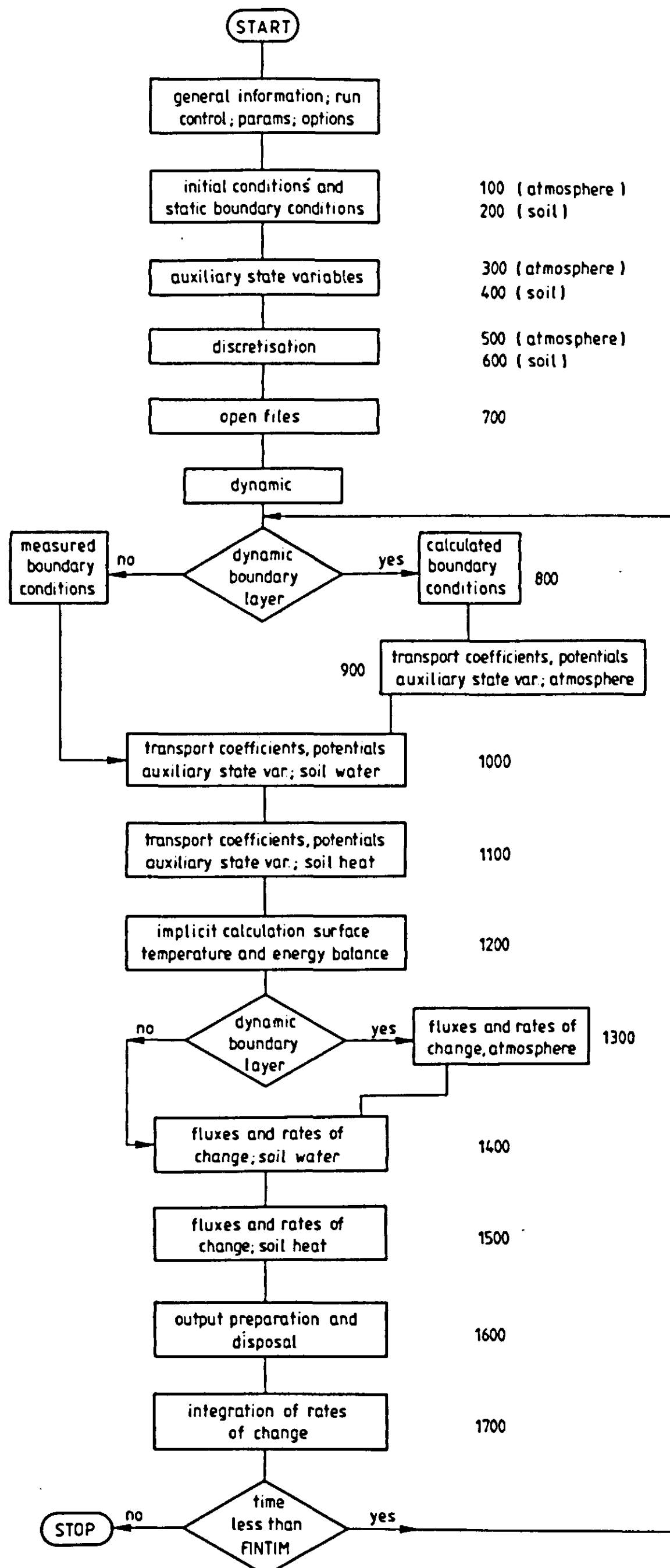


Figure 3.2 Global flow diagram of the model SALSA. Numbers refer to line numbers employed in the CSMP algorithm (Appendix 1).

As will be done at the end of each paragraph, the CSMP expressions involved for the main equations discussed are finally listed:

* integration of rates of change

$$W = \text{INTGRL(WI,WRCH,25)}$$

$$T = \text{INTGRL(TI,TRCH,25)}$$

$$Q = \text{INTGRL(QI,QRCH,11)}$$

$$TP = \text{INTGRL(TPI,TPRCH,11)}$$

$$U = \text{INTGRL(UI,URCH,11)}$$

$$V = \text{INTGRL(VI, VRCH, 11)}$$

$$TKE = \text{INTGRL(TKEI,TKERCH,11)}$$

In the following paragraphs, the energy balance will be discussed first (subsection 3.2) as it provides the key equation for the present system. Subsequently, the respective terms appearing in this equation, and the related mechanisms, will be treated: radiative transfer (3.3), bulk turbulent transport in the atmosphere (3.4), and soil thermal and hydraulic processes (3.5 and 3.6, respectively).

3.2 The surface energy balance

The central equation that sets boundary conditions to both the soil and the atmosphere subsystems is the energy balance equation of the surface (Lettau, 1957; Geiger, 1961):

$$(3.1) \quad R_n + H + LE + G = 0 \quad (\text{W m}^{-2})$$

where R_n is net radiation, H and LE are the sensible and latent heat fluxes respectively, and G is the soil heat flux. The equation implies that the surface itself has no capacity, i.e. no energy can be stored in it. The same will be assumed for matter. Also, eq. (3.1) states that fluxes towards the surface have a sign opposite to those directed away from it. Throughout the programmed model, all fluxes are designated positive if directed towards the surface, and negative if directed away from it. In the text, this rule is not strictly applied, for the sake of convention.

A strong feedback exists between the fluxes in eq. (3.1) and surface properties. Net radiation, the sum of incoming and outgoing radiation terms, is affected by soil moisture content and temperature, as these variables influence soil albedo, emissivity and emittance, respectively. The atmospheric

sensible and latent heat fluxes are governed by surface temperature and humidity, and by air temperature, air humidity and some exchange coefficient. This latter coefficient depends on the magnitude of the sensible heat flux itself (stability), on wind speed, and on surface roughness. The soil heat flux is determined by thermal conductivity and heat capacity of the soil, both of which are functions of soil moisture content.

A complication that should be touched upon explicitly in this context is the relation between G and LE in eq. (3.1). Often the soil heat flux is expressed as $G = -\lambda(\partial T/\partial z)_s$, where the index refers to the soil surface. In the case of a dry soil surface, however, a large fraction of the required latent heat of evaporation is supplied by downward conduction through the solid soil mass. Therefore, the use of G as calculated by the above expression (or as measured by heat flux plates) in eq. (3.1) is theoretically erroneous. Instead, the soil heat flux for field application of eq. (3.1) could be calculated by a variety of calorimetric methods (e.g. Horton, 1982; Kimball and Jackson, 1975). This subject has been elaborated upon by Menenti (1984), who presented several evaporation formulas that incorporate the above; this complication has also been recognized and accounted for by several modellers (e.g. Van Keulen, 1975), but is often not given due account.

The examples mentioned show the mutual dependence among surface properties and the various fluxes composing the energy balance. With respect to the surface temperature, Van Keulen (1975) presented an elegant solution of the energy balance equation in the form of an explicit expression for this surface variable. Nevertheless, for the sake of clarity it is preferred to use an implicit solution for surface temperature in the present simulation study, since errors are introduced easily when amending a program including such involved explicit expressions. An implicit solution as applied here was also used by Van Bavel and Lascano (1979).

The relevant CSMP lines then read:

```
*      surface energy balance, implicit loop
TS0 = T(1)
TS  = IMPL(TS0,0.05,FOTS)
..... (surface fluxes) .....
FOTS = (NETRAD+H)/(CHSOIL(1)/DZ(1))+T(1)
```

The various fluxes appearing in these lines will be discussed in the following.

3.3. Radiation

3.3.1 Shortwave radiation terms

Global radiation

Global radiation, the major fraction of daytime incoming radiation, sets one of the main boundary conditions to the system. It is the shortwave radiant flux density (W m^{-2}) received at the surface, resulting from the integration of radiance ($\text{W m}^{-2}\text{Sr}^{-1}$) over a solid angle $2\pi \text{ Sr}$. The term 'shortwave' is only roughly delineated by the spectral transparency of the glass domes employed on solarimeters. Global radiation then is defined as

$$(3.2) R_{\text{glob}} = \int_{\phi=0}^{2\pi} \int_{\psi=0}^{\pi/2} \int_{\lambda=0,3}^{\lambda \approx 3\mu\text{m}} R(\lambda, \phi, \psi) d\lambda d\psi d\phi \quad (\text{W m}^{-2})$$

where ϕ is the azimuth angle (rad), ψ the elevation (rad), λ the wavelength, and R the spectral radiance. Global radiation in modelling is frequently calculated from latitude, date and time (e.g. Goudriaan, 1977) and such relations could be used as an alternative to a measured course of global radiation, as employed in the present model.

Albedo

For a given surface and wavelength, the sum of reflectivity ρ , absorptivity α and transmissivity τ equals unity. As the soil is considered to be an opaque body, it is assumed that $\alpha+\rho=1$. Reflectivity depends on the wavelength of incoming radiation, and in general increases with wavelength up to $\lambda=1.2 \mu\text{m}$ (Gerberman, 1979; Van der Heide and Koolen, 1980; Coulson and Reynolds, 1971). As surface reflectivity also is dependent on azimuth and elevation, it will be clear that the overall fraction of shortwave radiation, reflected by the surface, in reality is not a constant, but is dependent on atmospheric conditions and the position of the sun. Therefore albedo, the overall fraction of global radiation that is reflected, is defined as

$$(3.3) \quad a \equiv \frac{\int_{\phi=0}^{2\pi} \int_{\psi=0}^{\pi/2} \int_{\lambda=0,3}^{3\mu\text{m}} \rho(\lambda, \phi, \psi) R(\lambda, \phi, \psi) d\lambda d\phi d\psi}{\int_{\phi=0}^{2\pi} \int_{\psi=0}^{\pi/2} \int_{\lambda=0,3}^{3\mu\text{m}} R(\lambda, \phi, \psi) d\lambda d\phi d\psi}$$

which roughly corresponds to the reflected fraction of shortwave radiation as measured with a double dome solarimeter.

For bare soils, several authors reported a dependence of albedo on solar elevation (Feddes, 1971; Aase and Idso, 1975; Idso, 1975). It is generally found that albedo for bare soils reaches a maximum at incidence angles ranging from 70 to 80 degrees. At a solar elevation of less than 10 degrees, Coulson and Reynolds (1971) measured a decrease of reflectivity over a wide range of wavelengths, which was attributed to the high ratio of diffuse to direct radiation that naturally occurs at sunrise and sunset. Kalma and Badham (1972) also pointed at cloud cover as a factor affecting soil albedo. Recently, Menenti (1984) mentioned several expressions to account for solar zenith and for the distribution of radiation over direct and diffuse components. The latter author also reported strong dependence of albedo on local time (for rough-surface playa soils). Most other authors reporting on bare field soils gave only a moderate dependence, noticeable in early morning and late afternoon. This was also the case in the field experiments conducted for the present study (Chapter 5). As this dependence is evident only at hours when total global radiation is low, relations between albedo and solar elevation were not adopted in the present model. Also, albedo was assumed to be independent of cloud cover and fraction of diffuse radiation, since the experiments discussed here yielded only minor variations in albedo under strongly changing sky conditions.

Of course soil conditions affect albedo. The influence of surface roughness on albedo as reported by Van der Heide and Koolen (1980) from slaking experiments, and by Bowers and Hanks (1965) may very well be related to differences in distribution of incidence angles for different surface geometries. Mineral composition and organic matter content are known to have strong effects on albedo. Hanks and Bowers increased albedos of different soils by up to a factor two, oxidizing the small amounts (<1.5%) of organic matter and carbonates present in the samples. Gerberman (1979) mentioned a general increase of dry soil albedo with quartz content in a soil mixing

Table 3.1 Albedo values for wet and dry soils

soil type	wet	dry	source
Dune sand	0.24	0.37	Buttner and Sutter, 1935
Arenosa sand	0.22	0.38	Graser and Van Bavel, 1982
Lufkin sandy loam	0.19	0.33	Graser and Van Bavel, 1982
Yuma sand	0.18	0.42	Gold and Ben Asher, 1976
Buffalo silty clay	0.17	0.32	this report
Blue loam	0.16	0.23	Kondrat'ev, 1954
Grey soil	0.15	0.27	Budyko, 1958
Norwood silty clay	0.15	0.23	Graser and Van Bavel, 1982
Williams loam	0.14	0.26	Aase and Idso, 1975
Avondale loam	0.14	0.30	Idso et.al. 1975
Tippera clay loam	0.14	0.23	Kalma and Badham, 1971
Swifterbant silt loam	0.13	0.31	this report
Grey brown loam	0.12	0.21	Graham and King, 1961
Grey soil	0.11	0.27	Kondrat'ev, 1954
Clay loam with flints	0.11	0.18	Monteith, 1959
Red-brown clay loam	0.10	0.20	Piggin and Schwertfeger, 1973
Sandy loam	0.10	0.17	Feddes, 1971
Oudelande sandy loam (slaked)	0.10	0.30	Van der Heide and Koolen, 1980
Oudelande sandy loam (unslaked)	0.08	0.20	Van der Heide and Koolen, 1980
Grey sand	0.09	0.18	Angström, 1925
Black mould	0.08	0.14	Angström, 1925
Latosol	0.08	0.14	Ekern, 1965
Clay	0.08	0.14	Feddes, 1971
Black soil	0.08	0.14	Kondrat'ev, 1954
Black soil	0.07	0.14	Chia, 1967

(part of this table is taken from Idso and Reginato, 1974)

experiment, a result comparable to that by Karamanov (1970) who studied the effect of ferric coatings on quartz grains. Table 3.1 lists albedo values for a wide range of soils under both wet and dry conditions.

The effect of moisture on albedo is marked. Angström (1925) proposed to express the relation between dry soil albedo and albedo at saturation as

$$(3.4) \quad a_{wet} = \frac{a_{dry}}{n^2(1-a_{dry}) + a_{dry}}$$

where n is the index of refraction of the liquid. This expression was supported by Planet (1970) after experiments employing fluids with different refraction indices. However, the simple relation $a_{dry} = 2 a_{wet}$, suggested by Idso and Reginato (1974), holds better in reality, as demonstrated in Figure 3.3. This relation might be safely employed in modelling when more accurate data are not available.

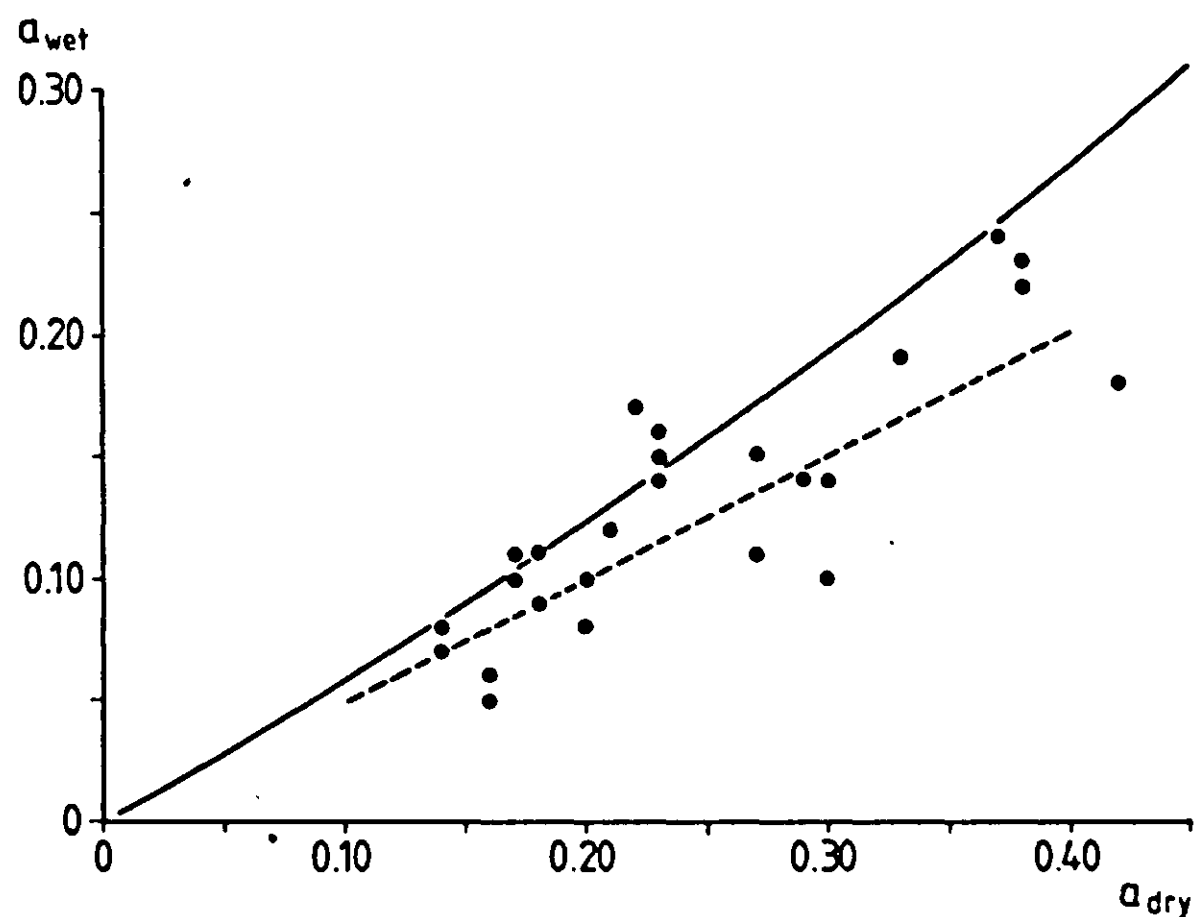


Figure 3.3 Wet soil albedo versus dry soil albedo for the soils listed in Table 3.1. Solid line: Angström's formula; broken line: $a_{dry} = 2 a_{wet}$.

For intermediate moisture contents, only few data are available. Under laboratory conditions, Graser and Van Bavel (1982) measured an exponential decrease of albedo with increasing moisture content on core samples. From field experiments, Idso et al. (1975) reported a linear dependence of albedo on volumetric water content for Avondale loam. Also the Flevoland and Texas measurements, both discussed in this report, result in a linear relationship, although the Texas data show much scatter. For these three cases, the data are shown in Chapter 4 (Figures 4.15-4.17). The linear relationship between albedo and soil moisture content as determined for the three different field situations mentioned above will be used in the present study:

$$(3.5) \quad a(\theta) = a_{wet} + \frac{\theta_{crit} - \theta}{\theta_{crit}} (a_{dry} - a_{wet})$$

where θ_{crit} is the moisture content below which albedo starts increasing during drying.

The program statements involved for shortwave radiation are

```
GLORAD = AFGEN(GLORTB,TIME)
ALB     = AWET+(ADRY-AWET)*(WCRITA-W(1))/WCRITA
```

Alternatively, global radiation data are read from an input file, e.g.:

```
READ(50,860) GLORAD, .....
860 FORMAT(2IX,5F)
```

3.3.2 Longwave radiation terms

Sky radiation

Thermal sky radiation, more precisely incoming longwave radiant flux density or longwave irradiance (W m^{-2}), also constitutes an important term in the surface energy balance, its value ranging from 200 to 500 W m^{-2} . It is defined in analogy to global radiation as an integral over azimuth, elevation and wavelength (see eq. 3.2). In practice, the longwave radiation often is taken to be a function of air temperature at screen height (1.5 m) of the form

$$(3.6) \quad R_{ld} = \epsilon_{sky} \sigma T_a^4$$

which defines the apparent sky emissivity ϵ_{sky} as an empirical constant; σ is the Stefan-Bolzmann constant. It must be noted that the value of ϵ_{sky} also is the result of an integration over the sky hemisphere (Jacobs, 1982). Effective sky temperature, another variable sometimes used in this context, is defined by

$$(3.7) \quad T_{sky} = \left(\frac{1}{\sigma} R_{ld} \right)^{\frac{1}{4}} \quad (\text{K})$$

i.e. the air temperature following from eq. (3.6) under the assumption $\epsilon=1$. The apparent (clear) sky emissivity has been related to water content in the atmosphere, i.e. vapour pressure or specific humidity, by empirical formulas employing powers or exponential functions of these properties. Gupta (1983) recently reviewed this type of expressions. In the present study, the rela-

tion proposed by Brunt (1939) is used:

$$(3.8) \quad \epsilon_{\text{sky}} = a + b/e$$

where e is the vapour pressure at screen height. Table 3.2 lists some measured values for the constants a and b . It must be realized that measuring techniques and circumstances (characteristics of the governing air mass) definitely affect the values found for these parameters (Wartena et al, 1973). For cloudy skies, Sellers (1965) formulated the apparent emissivity as

$$(3.9) \quad \epsilon_{\text{sky}} = \epsilon_{\text{sky}}(0)(1+nc^2)$$

where c is the fraction of cloud cover, and n is a parameter ranging from 0.04 for high (Cirrus) cloud, to 0.2 for low cloud (Monteith, 1973). In the simulation model described in this report, eqs. (3.6-3.9) are used to calculate longwave radiant flux density from the sky hemisphere.

Surface emittance

The longwave radiation leaving the surface (apparent emittance) consists of the terms emittance and reflection. As a reminder, the assumptions underlying the formulation of emittance will be set forth.

Planck's law for black body radiation expresses the spectral radiant flux density per unit of solid angle in a direction normal to the surface, $R_{n\lambda}$, as a function of wavelength and absolute temperature. Applying Lambert's cosine law, the spectral radiant emittance R_λ is found by integration of $R_{n\lambda}$ over a hemisphere (2π Sr). Finally, integration of R_λ over the whole wavelength interval yields the well known Stefan-Boltzmann law:

$$(3.10) \quad R_{le} = \epsilon \sigma T_s^4 \quad (\text{W m}^{-2})$$

where R_{le} is the (longwave) emittance, σ the Stefan-Boltzmann constant ($5.67 \cdot 10^{-8} \text{ W m}^{-2}\text{K}^{-4}$) and T_s is the temperature of the emitting body (K); the emissivity ϵ is introduced as a reduction factor for non-black body behaviour, and is equal to the absorption factor for the corresponding wavelengths (Kirchoff's law). For the present case, the soil is assumed to be a gray (ϵ independent of λ) body with a flat, homogeneous surface, obeying Lambert's law. Analogous to the case for the visible spectrum, opaqueness is assumed for thermal radiation as well.

Table 3.2 Constants for longwave sky radiation

a	b (mbar ⁻¹)	source
0.51-0.60	0.059-0.065	Unsworth and Monteith, 1975
0.60-0.75	0.017-0.057	Wartena et al, 1973
0.605-0.75	0.048	Sellers, 1965
0.61	0.050	Budyko, 1958
0.62	0.035	Stroosnijder and Van Heemst, 1982

Table 3.3 Soil emissivity values

soil type	wet/dry	ϵ	$\lambda(\mu\text{m})$	source
Silica sand	.	0.893	8-13	Idso and Jackson, 1969
Superstition	.	0.948	8-13	Idso and Jackson, 1969
Silica sand coarse	dry	0.914	8-12	Buettner and Kern, 1965
Silica sand coarse	wet	0.936	8-12	Buettner and Kern, 1965
Silica sand fine	.	0.928	8-12	Buettner and Kern, 1965
Silica sand	dry	0.898	8-12	Buettner and Dana, 1968
White sand	dry	0.890	10.4-11	Schurer, 1976
White sand	wet	0.925	10.4-11	Schurer, 1976
Plainfield sand	dry	0.90	8-12	Fuchs and Tanner, 1968
Plainfield sand	wet	0.94	8-12	Fuchs and Tanner, 1968
Avondale loam	dry	0.967	8-13	Idso and Jackson, 1969
Avondale loam	wet	0.980	7.5-16	Conaway and Van Bavel, 1967
Swifterbant silt loam	dry	0.91	8-14	this report
Swifterbant silt loam	wet	0.94	8-14	this report
Pine silty clay	.	0.965	8-13	Idso and Jackson, 1969
Arid soil eastern Washington	.	0.93-0.97	8-12	Buettner and Dana, 1968
14 diff. soils SE USA	.	0.94-0.99	10.4-12.6	Taylor, 1979

Emissivity is a soil specific property that ranges from 0.9 (dry quartz sand) to approximately 1.0, depending on organic matter, mineral composition and moisture content. As can be seen from the data listed in Table 3.3, the difference in ϵ , found between wet and dry soil, usually amounts 0.02-0.04. Relatively few data are available on the relation between emissivity and other soil properties. Some interesting results have been achieved in this respect by using quotients of measured emittances in small wavelength bands within the thermal range, thus eliminating temperature. This yields quotients of spectral emissivities, sensitive to surface properties (Palluconi, 1983).

Although differences in soil emissivity are hardly significant in the energy balance of bare soils (negligible effect on actual surface temperature), they are important in the interpretation of thermal infra red imagery. Differences in ϵ have been reported to make cool, wet sand appear warmer on surface imagery than warm, dry sand (Buettner and Kern, 1963). In this report, the dependence of ϵ on soil moisture is expressed by the empirical relationship

$$(3.11) \quad \epsilon(\theta) = \epsilon_{\text{dry}} + \frac{\theta}{\theta_s} (\epsilon_{\text{wet}} - \epsilon_{\text{dry}})$$

where θ_s is the moisture content at saturation (cf. Chapter 4).

The reflection compound of longwave radiation leaving the soil surface is calculated as a fraction $(1-\alpha)$ of incoming thermal radiation, where α is the absorptivity, assumed equal to the emissivity. Naturally, the same type of assumptions as discussed for reflection in the visible spectrum apply for this integral quantity. Emissivity values are usually measured in the 'atmospheric window' (roughly 8-14 μm) for the obvious reason that this is the most attractive wavelength interval for remote sensing. At the same time however, a large fraction of the sky radiation - aside from cloud radiation - naturally is of other wavelengths, which makes the use of ϵ in the 8-14 μm interval open to question in this context; accurate data of reflectivity in the desired intervals are not known to the present author, but an estimate of 0.05-0.15 can be derived from the ARIZONA data, discussed later in this report. From those data, a significant dependence of longwave reflectivity on soil moisture content cannot be recognized.

The CSMP lines involved for longwave radiation read:

```
EMISKY = (SKYA+SKYB*(SQRT(0.01*VPA)))*(1.+CLON*CLOC*CLOC)
EMISOI = EDRY+(EWET-EDRY)*W(1)/WSAT(1)
LONGIN = EMISKY*BOLZ*((T1+TZERO)**4)
TS      = IMPL(TS0,0.1,FOTS)
RADEMI = -EMISOI*BOLZ*(TS+TZERO)**4
..... (surface fluxes) .....
FOTS   = (NETRAD+H)/(CHSOIL(1)/DZ(1))+T(1)
```

The radiation terms discussed in the subsections 3.3.1 and 3.3.2 are now merged into the net radiation term, which is included in the energy balance implicit loop because of the temperature dependence of the emittance term:

```
TS      = IMPL(TS0,0.1,FOTS)
..... (surface fluxes) .....
NETRAD = (1.-ALB)*GLORAD+RADEMI+(1.-LONREF)*LONGIN
IF      (IFNET.EQ.1) NETRAD = AFGEN(NETRTB,TIME)
FOTS   = (NETRAD+H)/(CHSOIL(1)/DZ(1))+T(1)
```

As indicated, net radiation can be used optionally as a driving variable of the system, thus excluding uncertainties in the radiative properties of soil and sky, as may be useful in testing the remainder of the model with experimental data.

3.4. Transport in the atmospheric boundary layer

3.4.1. Exchange at the surface

As was set forth in section 3.1, boundary conditions to the system can be chosen such that either the model simulates atmospheric boundary layer development, or that this simulation is not included. The equations for surface exchange are almost identical for the two cases, and will be discussed first. Air temperature, humidity and wind speed at given height above the surface, e.g. screen height, are either given, or are calculated as a result of surface fluxes (subsection 3.4.2). Given these conditions, the surface fluxes of momentum, heat and mass are expressed as functions of the vertical gradients of the relevant properties, under the assumption of no advection.

Although the flux of momentum itself is of no direct interest to the surface energy balance, it is important because the atmospheric 'resistance' to heat and mass transport is closely related to this flux. The objective now is to write the vertical turbulent fluxes of respectively momentum, heat and vapour as

$$(3.12a) \quad \tau_x = \rho \frac{u(z_m) - u(z_o)}{r_{aM}} \quad (\text{kg m}^{-1}\text{s}^{-2})$$

$$(3.12b) \quad \tau_y = \rho \frac{v(z_m) - v(z_o)}{r_{aM}} \quad (\text{kg m}^{-1}\text{s}^{-2})$$

$$(3.13) \quad H = \rho C_p \frac{T(z_m) - T(z_o)}{r_{aH}} \quad (\text{W m}^{-2})$$

$$(3.14) \quad E = \rho \frac{q(z_m) - q(z_o)}{r_{aV}} \quad (\text{kg m}^{-2}\text{s}^{-1})$$

where the x , y indicate momentum in the x - and y -directions; z_o is the roughness length (m), and z_m is the height (m) at which the state variables are measured or calculated; u, v are the horizontal wind velocity components (m s^{-1}), T the air temperature ($^{\circ}\text{C}$) and q the specific humidity of the air ($\text{kg water/kg dry air}$); for the 'resistances' r_a , the indices M, H, and V refer to momentum, heat and vapour respectively. In the calculation of these fluxes it is assumed that T and q at height z_o are equal to their values at the soil surface, and that $u(z_o)=0$. Now the remainder of this paragraph will focus on the formulation of r_a .

An important characteristic in that formulation is atmospheric stability, a function of the ratio between fluxes of momentum and sensible heat. In an unstable situation, temperature decreases with height, which implies a decrease of atmospheric resistance by the effect of buoyancy. Following Obukhov (1946), stability is expressed by the dimensionless parameter $\zeta \equiv z/L$, where z is the height (m) and L is the well known Monin-Obukhov length (m), defined as

$$(3.15) \quad L \equiv \frac{\theta u_*^3}{k g(H/\rho C_p)} = \frac{\theta}{k} \frac{|\tau/\rho|^{3/2}}{g(H/\rho C_p)} \quad (\text{m})$$

(k is the von Kármán constant (0.41), and g the acceleration by gravity). The friction velocity u_* is defined by the relation $\tau \equiv \rho u_*^2$ and the potential temperature θ by the equation $\theta = T(1000/p)^{0.288}$, where T and p are the actual temperature (K) and pressure (mbar) of the air, respectively. Potential temperature is the temperature an air parcel would obtain if brought dry adiabatically to a pressure of 1000 mbar. For the first meters of the surface layer, θ is usually set equal to T . The stability parameter ζ has been related to the non-dimensional gradients of potential temperature and wind velocity by the semi-empirical so-called flux-profile relationships. Reviews on this topic were given by Dyer (1974), Businger (1975), Viswanadham (1982) and others. These dimensionless gradients are defined as (Businger, 1975):

$$(3.16) \quad \phi_M(z) \equiv \frac{k z}{u_*} \frac{\partial u(z)}{\partial z}$$

$$(3.17) \quad \phi_H(z) \equiv \frac{k z}{\theta_*} \frac{\partial \theta(z)}{\partial z}$$

where $\theta_* \equiv (H/\rho C_p)/u_*$. The flux-profile relationships for the unstable situation are of the form

$$(3.18) \quad \phi_{M,H} = (1-a \zeta)^b$$

where a and b are empirical constants, approximately 16 and -0.25 for momentum, and 16 and -0.50 for heat transfer respectively; for stable stratification, the relation $\phi_M = \phi_H = 1 + \beta \zeta$ is used, with $\beta = 4.7$ (Businger, 1963; Businger et al. 1971).

The eqs. (3.16) and (3.17) employ local derivatives at height z . In numerical simulation, as distance is discretized into steps or compartments, the transcription of these equations into the finite difference form may be hazardous for cases where the gradient changes rapidly with height, i.e. close to the surface. Therefore, the integral form of eqs. (3.16) and (3.17), derived by Paulson (1970), was used for the expression of surface fluxes in the present model. Paulson's integration, employing eq. (3.18), results in the wind and temperature profile equations respectively:

$$(3.19) \quad u = \frac{u_*}{k} \left(\ln \left(\frac{z}{z_{o,M}} \right) - \Psi_M \right) \quad (\text{m s}^{-1})$$

$$(3.20) \quad \theta = \theta_o + \frac{\theta^*}{k} \left(\ln\left(\frac{z}{z_{o,H}}\right) - \Psi_H \right) \quad (K)$$

The roughness lengths $z_{o,M}$ and $z_{o,H}$ are assumed to be equal. It is directly verified that for neutral stratification ($\Psi_M=0$) eq. (3.19) reduces to the well known logarithmic wind profile equation (e.g. Monteith 1963; 1973). Now the combination of eqs. (3.12) and (3.19) yields (with $\tau=\rho u_*^2$) for the resistance to momentum transfer

$$(3.21) \quad r_{aM} = \frac{1}{k^2 u} \left(\ln\left(\frac{z}{z_o}\right) - \Psi_M \right)^2 \quad (s m^{-1})$$

Similarly, (with $\theta=T$), eqs. (3.13) and (3.20) combine to

$$(3.22) \quad r_{aH} = \frac{1}{k^2 u} \left(\ln\left(\frac{z}{z_o}\right) - \Psi_M \right) \left(\ln\left(\frac{z}{z_o}\right) - \Psi_H \right) \quad (s m^{-1})$$

The stability correction functions Ψ_M and Ψ_H in eqs. (3.19-3.22) are defined (Paulson, 1970) for unstable stratification as

$$(3.23) \quad \Psi_M = 2 \ln((1+\phi_M^{-1})/2) + \ln((1+\phi_M^{-2})/2) - 2 \arctan(\phi_M^{-1}) + \pi/2$$

$$(3.24) \quad \Psi_H = 2 \ln((1+\phi_H^{-1})/2)$$

and for stable conditions as

$$(3.25) \quad \Psi_M = \Psi_H = -\beta \zeta$$

On the basis of similarity theory it is assumed that the aerodynamic resistance of the atmospheric boundary layer is identical for all transported constituents, expressed as conservative properties, this resistance being related only to the eddy structure of the flow. As specific humidity q is such a property, r_{av} in eq. (3.14) is taken equal to r_{aH} .

The set of eqs. (3.12-3.14) and (3.21-3.25), in combination with the energy balance equation, enables one to calculate stability and aerodynamic resistance with a single-level air temperature only; to this purpose, the Paulson integration allows the use of soil surface temperature - calculated from the surface energy balance - in conjunction with air temperature. This procedure was also applied by Hammel (1981) and Mahrer (1982). In program-

ming, the variables $\Psi_{M,H}$ are tabulated as functions of the stability parameter ζ . (An actually remotely sensed surface temperature of course is far too inaccurate to be used for application in such expressions).

The above theory programmed reads:

```
PSIM      = AFGEN(PSIMTB,STAPAR(1))
PSIH      = AFGEN(PSIHTB,STAPAR(1))
SURWIN    = SQRT(U(1)*U(1)+V(1)*V(1))
RAM       = ((ALOG(ZZ(1)/ZNOT)-PSIM)**2)/(SURWIN*KAR**2)
RAH       = ((ALOG(ZZ(1)/ZNOT)-PSIH)*(ALOG(ZZ(1)/ZNOT)-PSIM)/...
            (SURWIN*KAR**2))
RAV       = RAH
TS        = IMPL(TS0,0.01,FOTS)
..... (radiation terms) .....
H         = RHOAIR*CP*(T1-TS)/RAH
FOTS     = (NETRAD+H)/(CHSOIL(1)/DZ(1))+T(1)
E         = RHOAIR*(Q1-QS)/RAV
LE        = LVAP*E
QFLX(1)  = E/RHOAIR
TPFLX(1) = H/(RHOAIR*CP)
UVOFNX(1) = U(1)/RAM
VVOFLX(1) = V(1)/RAM
```

(wind velocity and momentum are split into the two orthogonal horizontal components). Note that eqs. (3.12-3.14) and (3.21-3.25) are only used for the calculation of surface fluxes, i.e. the fluxes between the soil surface and the lowermost compartment of the boundary layer. For the remainder of the atmospheric boundary layer, the expressions expounded in the next paragraph, including the calculation of stability, are used when the option switch IFBLD is set to 1 (boundary layer development included). For the alternative case, IFBLD=0, the following CSMP lines must be included here to account for the stability parameter:

*option: IFBLD = 0

```
950      TPAV(1)      = 0.5+(TS+T1)
          TPFLX(1)     = H/(RHOAIR*CP)
          OBU(1)       = (TPAV(1)+TZERO)*(ABS(RMOFLX(1))**1.5)/...
                        (KAR*G*TPFLX(1))
```

```
STAPAR(1)      = 0.5*ZZ(1)/OBU(1)
IF (STAPAR(1).LT.-3.) STAPAR(1) = -3.
IF (STAPAR(1).GT.1.) STAPAR(1) =1.
```

3.4.2 Boundary layer development

The atmospheric boundary layer is the lower part of the atmosphere, that by turbulent mixing responds to the diurnal course of fluxes at the earth's surface. During daytime, its height usually ranges between a few hundred meters and a few kilometres, occasionally up to the tropopause (approximately 10 km) for very unstable situations. The daytime boundary layer develops rapidly as a result of intensive mixing due to surface heating. At night, turbulence fades out as one of its major sources, buoyancy, reverses its effect, and a stable stratification is built up by radiative cooling of the surface. The nocturnal boundary layer may typically extend to heights in the order of a few hundred meters.

The diurnal development of this boundary layer is the subject of discussion in this paragraph. It involves the equations of motion, of enthalpy and mass conservation, the gradient expressions of the fluxes, and the kinetic energy budget equation. The theory set forth here is used only in the extended soil-atmosphere model (Figure 3.1.a) and may be of minor importance to those interested in soil behaviour under given boundary conditions close to the surface. The work by Nieuwstadt and Driedonks (1979) on the nocturnal boundary layer was used as a guideline in the formulation of the one-dimensional model.

The equations of motion

Following the Reynolds theory, the three orthogonal components of velocity along the axes x, y and z respectively are usually written as

$$(3.26) \quad \begin{aligned} u &= \bar{u} + u' \\ v &= \bar{v} + v' \\ w &= \bar{w} + w' \quad \text{with } \bar{u}' = \bar{v}' = \bar{w}' = 0 \end{aligned}$$

where the bars indicate time averages, and u' , v' , w' are the turbulent fluctuations about the mean; w is taken along the vertical axis. The fluidum is considered incompressible, except where the buoyancy term is concerned

and density depends on temperature (a Boussinesque approximation; for a summary of Boussinesque assumptions see Busch (1973) and Nieuwstadt and Van Dop (1981)). The equations of motion for the mean horizontal flow are then written as

$$(3.27a) \frac{\partial \bar{u}}{\partial t} + \bar{u} \frac{\partial \bar{u}}{\partial x} + \bar{v} \frac{\partial \bar{u}}{\partial y} + \bar{w} \frac{\partial \bar{u}}{\partial z} = - \frac{1}{\rho} \frac{\partial \bar{p}}{\partial x} + v \left[\frac{\partial^2 \bar{u}}{\partial x^2} + \frac{\partial^2 \bar{u}}{\partial y^2} + \frac{\partial^2 \bar{u}}{\partial z^2} \right] - \\ \text{I} \quad \text{II} \quad \text{III} \quad \text{IV} \\ - \frac{\partial u'v'}{\partial y} - \frac{\partial u'w'}{\partial z} + 2\Omega \eta_3 \bar{v} \quad (\text{m s}^{-2}) \\ \text{V} \quad \text{VI}$$

$$(3.27b) \frac{\partial \bar{v}}{\partial t} + \bar{u} \frac{\partial \bar{v}}{\partial x} + \bar{v} \frac{\partial \bar{v}}{\partial y} + \bar{w} \frac{\partial \bar{v}}{\partial z} = - \frac{1}{\rho} \frac{\partial \bar{p}}{\partial y} + v \left[\frac{\partial^2 \bar{v}}{\partial x^2} + \frac{\partial^2 \bar{v}}{\partial y^2} + \frac{\partial^2 \bar{v}}{\partial z^2} \right] - \\ - \frac{\partial u'v'}{\partial x} - \frac{\partial v'w'}{\partial z} - 2\Omega \eta_3 \bar{u} \quad (\text{m s}^{-2})$$

where v is the kinematic viscosity and Ω is the angular frequency of rotation of the earth; η is the unit vector, parallel to the axis of rotation, and η_3 , its component along the z -axis, equals $\sin \phi$ at latitude ϕ . The equation for the mean flow in the vertical (analogous to eqs. (3.27), but including a buoyancy term) is omitted as it is supposed that the mean flow \bar{w} can be neglected in comparison to its fluctuations w' .

In the Eulerian expressions 3.27, term I is the rate of change of the local mean flow velocity at a point with fixed coordinates in space. The terms II represent acceleration due to advection of momentum; III denotes acceleration down the pressure gradient; IV and V are the viscous stress terms and Reynolds terms respectively (when multiplied by ρ , these are the divergencies of the fluxes of momentum by viscous forces and turbulence respectively). Finally, the last term, VI, in eqs. (3.27) is due to the rotation of the earth.

As molecular interaction plays a very minor role in momentum transfer in the atmosphere as compared to turbulence, the term IV can virtually be neglected. Further simplification is achieved when the advection terms II are omitted. This is a more serious limitation, since advection may play a significant role, e.g. in the nocturnal boundary layer when vertical mixing is low (Nieuwstadt and Driedonks, 1979). Nevertheless, advection is neglected for practical reasons at the moment. Moreover, horizontal divergences of

the turbulent fluxes $\partial(\overline{u'v'})/\partial x$ and $\partial(\overline{u'v'})/\partial y$ are considered small as compared to $\partial(\overline{u'w'})/\partial z$ and $\partial(\overline{v'w'})/\partial z$, and are neglected. If then the vertical fluxes of momentum are written as:

$$(3.28) \quad \tau_x = \rho \overline{u'w'} \quad \text{and} \quad \tau_y = \rho \overline{v'w'} \quad (\text{kg m}^{-1} \text{s}^{-2})$$

the equations of motion reduce to

$$(3.29a) \quad \frac{\partial \bar{u}}{\partial t} = - \frac{1}{\rho} \frac{\partial \bar{p}}{\partial x} - \frac{\partial}{\partial z} \frac{\tau_x}{\rho} + f \eta \bar{v} \quad (\text{m s}^{-2})$$

$$(3.29b) \quad \frac{\partial \bar{v}}{\partial t} = - \frac{1}{\rho} \frac{\partial \bar{p}}{\partial y} - \frac{\partial}{\partial z} \frac{\tau_y}{\rho} - f \eta \bar{u} \quad (\text{m s}^{-2})$$

where the Coriolis parameter f is defined by $f\eta=2\Omega\eta_3$ (s^{-1}); for simplicity, the bars to indicate mean values will be left out in the following. Geostrophic wind is used to substitute for the pressure gradient term in eqs. 3.29. For a given height z , the relations between pressure gradient and geostrophic wind are given by (e.g. Busch, 1973) $u_g = (-1/f\rho)(\partial p/\partial y)$ and $v_g = (1/f\rho)(\partial p/\partial x)$.

The difference between geostrophic winds at different levels, called thermal wind, is a function of the horizontal temperature gradient. The neglect of thermal wind in replacing the pressure gradient term by geostrophic wind at a prescribed level may introduce a significant error in the case of strong horizontal temperature gradients; since the required input conditions will seldom be available, however, thermal wind is neglected, following Nieuwstadt and Driedonks. Then finally the equations of motion as used in the present model become

$$(3.30a) \quad \frac{\partial u}{\partial t} = f(v - v_g) - \frac{\partial}{\partial z} \frac{\tau_x}{\rho} \quad (\text{m s}^{-2})$$

$$(3.30b) \quad \frac{\partial v}{\partial t} = - f(u - u_g) - \frac{\partial}{\partial z} \frac{\tau_y}{\rho} \quad (\text{m s}^{-2})$$

Conservation of mass and enthalpy

Omitting the advection terms and horizontal turbulent flux divergence as indicated above, the conservation equation for enthalpy in the vertical is written as (Businger, 1981).

$$(3.31) \quad \frac{\partial \theta}{\partial t} = - \frac{d}{dz} (\bar{w} \bar{\theta} + \overline{w' \theta'}) + \sum S_i \quad (K s^{-1})$$

where again θ is the potential temperature and the terms S_i represent sources and sinks of enthalpy. These include changes in local enthalpy due to thermal conduction, divergence of net radiation, dissipation of kinetic energy, and changes in mass content, composition or state of a given parcel of air. All these terms will be neglected here. For most terms this means no severe violation of reality as they are very small. Only the change of state of available water may constitute an important term. If cloud formation occurs, also divergence of net radiation becomes important. Therefore the omission of these terms in eq. (3.31) limits the validity of the model to cases where no condensation in the atmosphere occurs. The equation now reduces to

$$(3.32) \quad \frac{\partial \theta}{\partial t} = - \frac{d}{dz} \left(\frac{H}{\rho C_p} \right) \quad (K s^{-1})$$

Similarly, the equation of mass conservation is expressed for water vapour as

$$(3.33) \quad \frac{\partial q}{\partial t} = - \frac{d}{dz} (\bar{w} \bar{q} + \overline{w' q'}) = - \frac{d}{dz} \left(\frac{E}{\rho} \right) \quad (kg_{water} kg_{air}^{-1} s^{-1})$$

Fluxes in terms of gradients

The fluxes in the boundary layer are expressed somewhat different from the surface fluxes, described in the previous paragraph. For momentum, sensible heat and moisture, the equations are

$$(3.34) \quad \frac{\tau_x}{\rho} = - K_M \frac{du}{dz} ; \quad \frac{\tau_y}{\rho} = - K_M \frac{dv}{dz} \quad (m^2 s^{-2})$$

$$(3.35) \quad \frac{H}{\rho C_p} = - K_H \frac{d\theta}{dz} \quad (K m s^{-1})$$

$$(3.36) \quad \frac{E}{\rho} = - K_V \frac{dq}{dz} \quad (kg_{water} kg_{air}^{-1} m s^{-1})$$

(clearly, combination with eqs. (3.30, 3.31, 3.32) resp. yields the well known second order flow equations). Although this gradient formulation is a coarse approximation, based on similarity with molecular transfer processes, it is still the most widely used approach, because of its simplicity and relatively low computer cost (Businger, 1981). The transport coefficients K

are expressed as functions of e , the available local turbulent kinetic energy:

$$(3.37) \quad K_{M,H,V} = \lambda_{M,H,V} (c e)^{\frac{1}{2}} \quad (\text{m}^2 \text{s}^{-1})$$

where the kinetic energy is in J/kg. The length scales $\lambda_{M,H,V}$ are functions of the dimensionless gradients ϕ (section 3.4.1) and are given by

$$(3.38) \quad \lambda_{M,H,V}^{-1} = \frac{\phi_{M,H,V}(\zeta)}{k z} + \alpha \frac{f}{|u_g|} \quad (\text{m}^{-1})$$

where $\phi_M^2 = \phi_H^2 = \phi_V^2$ (Businger, 1975); for the empirical constants a and c , the values $4 \cdot 10^{-4}$ and 0.2 respectively are used (Nieuwstadt and Driedonks, 1979).

The kinetic energy budget

The system is closed by the turbulent kinetic energy (TKE) equation (Tennekes and Lumley, 1972; Driedonks, 1981):

$$(3.39) \quad \frac{\partial e}{\partial t} = \frac{\tau_x}{\rho} \frac{du}{dz} + \frac{\tau_y}{\rho} \frac{dv}{dz} + \frac{g}{T} \frac{H}{\rho C_p} + \frac{d}{dz} K_M \frac{de}{dz} - \frac{(c e)^{3/2}}{\lambda_M} \quad (\text{J kg}^{-1} \text{s}^{-1})$$

I II III IV V

The term I is the local rate of change of TKE per unit of mass; II are the mechanical production terms of TKE due to vertical wind shear; III is the TKE production by buoyancy, IV represents the divergence of the vertical TKE flux, and the last term is the loss of TKE due to dissipation, where the constant c is identical to that in eq. (3.37). Driedonks (1981) extensively discussed the relative importance of each term at different locations in the developing boundary layer.

Boundary conditions

The lower boundary conditions to the atmosphere, dictated by the surface energy balance, have been treated in paragraph 3.4.1, except for the TKE flux; this term is taken zero at the surface. The conditions at the upper boundary of the system are in the present study defined as:

$$\begin{aligned} u &= u_g \\ v &= v_g \equiv 0 \\ \tau_x &= \tau_y \equiv 0 \\ H &\equiv 0 \\ E &\equiv 0 \\ \frac{\partial e}{\partial z} &\equiv 0 \end{aligned}$$

It will be clear that the use of these boundary conditions requires that the height of the upper boundary be chosen above the actual top of the developing boundary layer. Casting the resulting equations of motion, conservation of mass and enthalpy, and the TKE budget with their respective boundary conditions into CSMP expressions gives:

* option: IFBLD=1

* initial condtions (to be specified)

TABLE UI(1-11) =
TABLE VI(1-11) =
TABLE TPI(1-11) =
TABLE QI(1-11) =
TABLE TKEI(1-11) =
TABLE UVOFNX(1-11) =
TABLE VVOFLX(1-11) =
TABLE TPFLX(1-11) =
H =
RAM =

* (the latter five lines required for initial STAPAR calculation)

* boundary conditions (see also 3.4.1)

TABLE TKEFLX(1) = 0
TABLE UVOFNX(12) = 0
TABLE VVOFLX(12) = 0
TABLE MOFLX(12) = 0
TABLE TPFLX(12) = 0
TABLE QFLX(12) = 0
TABLE TKEFLX(12) = 0

* dynamic

* transport coefficients

* stability at interfaces

900 TPAV(1) = 0.5*(TS+TP(1))
 DO 905 I = 2,NN
 TPAV(I) = (TP(I)*TCMM(I)+TP(I-1)*...
 TCMM(I-1))/(TCMM(I)+TCMM(I-1))

905 CONTINUE
 DO 930 I = 1,NN
 RMOFLX(I) = SQRT(UVOFLX(I)**2+VVOFLX(I)**2)
 OBU(I) = (TPAV(I)+TZERO)*((ABS(RMOFLX(I)))**1.5)/...
 (KAR*G*TPFLX(I))
 STAPAR(I) = ZZ(I)/OBU(I)
 IF(STAPAR(I).LT.-3.) STAPAR(I)=-3.
 IF(STAPAR(I).GT.1.) STAPAR(I)=1.
 IF(STAPAR(I).GE.0.) GOTO 910
 PHIM(I) = (1.-16.*STAPAR(I))**(-0.25)
 PHIH(I) = PHIM(I)*PHIM(I)
 GOTO 920

910 PHIM(I) = 1.+4.7*STAPAR(I)
 PHIH(I) = PHIM(I)

920 INVLM(I) = PHIM(I)/(KAR*ZZ(I))+INVCOR
 INVLH(I) = PHIH(I)/(KAR*ZZ(I))+INVCOR

930 CONTINUE

* local turbulent transport coefficients at interfaces
 DO 940 I = 2,NN
 TKEAV(I) = (TCMM(I)*TKE(I)+TCMM(I-1)*TKE(I-1))/...
 (TCMM(I)+TCMM(I-1))
 KM(I) = (1./INVLM(I))*((YUC*TKEAV(I))**0.5)
 IF(TKEAV(I).LE.0) KM(I)=0
 KH(I) = KM(I)*INVLM(I)/INVLH(I)
 KV(I) = KH(I)

940 CONTINUE

* fluxes and rates of change, atmosphere

UVOLX(1)	= U(1)/RAM
VVOLX(1)	= V(1)/RAM
TPFLX(1)	= H/(RHOAIR*CP)
QFLX(1)	= E/RHOAIR
TKEFLX(1)	= 0.0
DO 1310	I = 2,NN
UVOLX(I)	= KM(I)*(U(I)-U(I-1))/DZZ(I)
VVOLX(I)	= KM(I)*(V(I)-V(I-1))/DZZ(I)
TPFLX(I)	= KH(I)*(TP(I)-TP(I-1))/DZZ(I)
QFLX(I)	= KH(I)*(Q(I)-Q(I-1))/DZZ(I)
TKEFLX(I)	= KM(I)*(TKE(I)-TKE(I-1))/DZZ(I)

1310 CONTINUE

* flux divergencies atmosphere

DO 1320	I = 1,NN
DIVUVOLX(I)	= (UVOLX(I+1)-UVOLX(I))/TCMM(I)
DIVVVOLX(I)	= (VVOLX(I+1)-VVOLX(I))/TCMM(I)
DIVTP(I)	= (TPFLX(I+1)-TPFLX(I))/TCMM(I)
DIVTKE(I)	= (TKEFLX(I+1)-TKEFLX(I))/TCMM(I)
DIVQ(I)	= (QFLX(I+1)-QFLX(I))/TCMM(I)

1320 CONTINUE

* acceleration by pressure gradient

DO 1330	I = 1,NN
ACCPRY(I)	= -CORIOL*(U(I)-UG)
ACCPRX(I)	= +CORIOL*(V(I)-VG)

1330 CONTINUE

* TKE production, $J \text{ kg}^{-1} \text{s}^{-1}$

* EPRSXR, EPRSRY, EPRBUO at interfaces weighed, EPRDIS at centres

DUDZZ(1)	= U(1)/DZZ(1)
DVDZZ(1)	= V(1)/DZZ(1)
DO 1340	I = 2,NN
DUDZZ(I)	= (U(I)-U(I-1))/DZZ(I)
DVDZZ(I)	= (V(I)-V(I-1))/DZZ(I)

1340 CONTINUE

```
DO 1350      I = 1,NN
              = (UVOLX(I)*DUDZZ(I)*DZZ(I)+UVOLX(I+1)*...
                DUDZZ(I+1)*DZZ(I+1))/(DZZ(I)+DZZ(I+1))
              = (VVOLX(I)*DVDZZ(I)*DZZ(I)+VVOLX(I+1)*...
                DVDZZ(I+1)*DZZ(I+1))/(DZZ(I)+DZZ(I+1))
              = -(TPFLX(I)*DZZ(I)+TPFLX(I+1)*DZZ(I+1))*G/...
                ((TP(I)+TZERO)*(DZZ(I)+DZZ(I+1)))
              = -((YUC*TKE(I))**1.5)*(INVLM(I)+INVLM(I+1))/2.
1350      CONTINUE
              EPRDIS(1)      = -((YUC*TKE(1))**1.5)*INVLM(1)
* rates of change of main state variables
DO 1360      I = 1,NN
              = (EPRSXRX(I)+EPRSRY(I)+EPRBUO(I)+...
                +EPRDIS(I)+DIVTKE(I))
              URCH(I)        = ACCPRX(I)+DIVUV0(I)
              VRCH(I)        = ACCPRY(I)+DIVVVO(I)
              TPRCH(I)       = DIVTP(I)
              QRCH(I)        = DIVQ(I)
1360      CONTINUE
(see also section 3.1)
```

3.5 Transport of heat in the soil

The one-dimensional flow equation for heat in the soil can be written as

$$(3.41) \quad \frac{\partial(CT)}{\partial t} = \lambda \frac{d^2 T}{dz^2} + \sum_i P_i \quad (\text{K s}^{-1})$$

where λ is the thermal conductivity ($\text{W m}^{-1}\text{K}^{-1}$), C the volumetric heat capacity ($\text{J m}^{-3}\text{K}^{-1}$) and the P_i terms represent the temperature changes by other than conduction mechanisms. These are associated with liquid or gas movement, and some are still poorly understood. In the case of actual measurements, the terms P_i are often omitted and all heat transport is ascribed to conduction. Thermal conductivity in the above equation is then replaced by λ^* , the apparent thermal conductivity. The use of λ^* in modelling of coupled flow is not attractive at this stage, for reasons explained in the

next subsection, and hence the two main heat transfer terms are calculated separately in the present model.

In this section, heat transport by conduction is discussed first (3.5.1). Subsequently, the heat associated with a change of state of the soil water will be treated (3.5.2), and finally some remarks concerning heat transfer by convective mass flow of air are made (3.5.3).

The above in CSMP statements:

* divergence of soil heat flux and rate of change of soil temperature

```
DO 1530      I = 1,N  
        DIVHFL(I) = (HFLX(I+1) - HFLX(I))/TCM(I)  
        TRCH(I) = DIVHFL(I)/HCSOIL(I)  
1530      CONTINUE
```

3.5.1 Conduction

Naturally, soil thermal conductivity and heat capacity have a strong influence on soil thermal behaviour. Both can be formulated on the basis of soil composition.

Heat capacity

The heat capacity is defined on the basis of the capacities of the different soil components (De Vries, 1963):

$$(3.42) \quad C_s = f_q C_q + f_c C_c + f_o C_o + \theta C_w + f_a C_a \quad (\text{Jm}^{-3} \text{K}^{-1})$$

where f is the volume fraction and C the volumetric heat capacity of the components clay, quartz, organic matter, water and air respectively; θ is the volume fraction of soil water. Water content determines heat capacity to a large extent, since water has a much higher specific heat capacity than the other soil constituents as shown in Tabel 3.4.

Table 3.4 Thermal properties of soil components (after Van Wijk and De Vries, 1963)

Component	density Mg m^{-3}	specific heat $\text{J g}^{-1} \text{K}^{-1}$	thermal conductivity $\text{W m}^{-1} \text{K}^{-1}$	thermal diffusivity $10^{-6} \text{m}^2 \text{s}^{-1}$
Quartz	2.66	0.80	8.80	4.18
Clay minerals	2.65	0.90	2.92	1.22
Organic matter	1.30	1.92	0.25	0.10
Water	1.00	4.18	0.57	0.14
Air (20 °C)	1.20×10^{-3}	1.01	0.025	20.50

Thermal conductivity

Thermal conductivity is less obviously related to soil composition than heat capacity. Aside from the conductivities of the individual soil particles, also the arrangement and shape factors of the particles affect bulk thermal conductivity. Extremes in soil conductivity may differ by a factor 100 (Hillel, 1980), although for arable soils variability is somewhat less and a factor 10 seems more appropriate to characterize the range of occurring λ -values. Several empirical expressions for $\lambda(\theta)$ have been proposed, e.g. Woodside and Messmer (1961) and Nerpin and Chudnovski (1970). Table 3.5 lists measured thermal conductivities at different water contents as collected from literature; most data refer to apparent thermal conductivity.

In the SALSA model, either tabulated (measured) functions of λ vs θ are used, or λ is calculated on the basis of the electrical conductivity analogy by De Vries (1963, 1975). De Vries's model considers soil as a continuous medium (gas or liquid), in which soil particles and water or air respectively are dispersed. Conductivity is then calculated as a weighted average of the conductivities of the individual components. For $\theta > 0.05$, the liquid is used as the continuous phase, and the expression becomes

$$(3.43) \quad \lambda = \frac{k_{\text{q}} f_q \lambda_q + k_{\text{cw}} f_c \lambda_c + k_{\text{ow}} f_o \lambda_o + k_{\text{ww}} \theta \lambda_w + k_{\text{aw}} f_a \lambda_a}{k_{\text{q}} f_q + k_{\text{cw}} f_c + k_{\text{ow}} f_o + k_{\text{ww}} \theta + k_{\text{aw}} f_a} \quad (\text{W m}^{-1} \text{K}^{-1})$$

Table 3.5 Thermal conductivity of soil materials

	θ	λ_{dry} $\text{W m}^{-1}\text{K}^{-1}$	θ	λ_{wet} $\text{W m}^{-1}\text{K}^{-1}$	ρ Mg m^{-3}	source
Fairbanks sand	.00	0.33	.21	2.30	1.70	de Vries, 1963
sand	.00	0.30	.40	1.68	1.46	van Duin, 1956
sand	.00	0.20	.27	1.70	1.50	Hartmann et al. 1972
sand	.01	0.25	.23	1.13	1.30	Hartmann et al. 1972
sand	.00	0.15	.38	2.3	1.60	Riha et al. 1980
pumice (Ac)	.00	0.16	.70	0.71	0.76	Cochran et al. 1967
pumice (Cl)	.00	0.10	.80	0.63	0.44	Cochran et al. 1967
loamy sand	.00	0.20	.21	1.80	1.50	Hartmann et al. 1972
loamy sand	.01	0.20	.18	1.22	1.30	Hartmann et al. 1972
loamy sand	.01	0.30	.35	1.50	1.69	Sepaskhah and Boersma, 1979
Avondale loam	.09	0.42	.30	1.18	1.40	Kimball et al. 1976
loam	.01	0.20	.50	1.00	1.18	Sepaskhah and Boersma, 1979
silt loam	.08	0.30	.50	0.90	1.25	Riha et al, 1980
Yolo silt loam	.16	0.75	.40	1.18	1.35	Wierenga et al, 1969
Muir silty clay loam	.04	0.30	.31	0.90	1.25	Asrar and Kanemasu, 1983
silty clay loam	.01	0.20	.55	1.0	1.16	Sepaskhah and Boersma, 1979
Healy clay	.03	0.16	.36	1.55	.36-.61*	de Vries, 1963
clay	.00	0.40	.40	1.26	1.33	Van Duin, 1956
Fairbanks peat	.02	0.05	.80	0.45	.84-.79*	de Vries, 1963
peat	.00	0.04	.60	0.34		Van Duin, 1963
forest litter	.02	0.10	.55	0.30	0.21	Riha et al, 1980

* porosity

The weight factors k_{q_w} , k_{c_w} , k_{o_w} , and k_{a_w} depend on the ratio of specific thermal conductivity of resp. quartz, clay, organic matter, water and air to that of water ($k_{ww} \equiv 1$). At very low water contents, ($\theta < 0.02$), air is viewed as the continuous phase, and an equivalent expression is used, including an empirical correction factor:

$$(3.44) \quad \lambda = 1.25 * \frac{k_{qa} f_q \lambda_q + k_{ca} f_c \lambda_c + k_{oa} f_o \lambda_o + k_{wa} \theta \lambda_w + k_{aa} f_a \lambda_a}{k_{qa} f_q + k_{ca} f_c + k_{oa} f_o + k_{wa} \theta + k_{aa} f_a} \quad (\text{W m}^{-1}\text{K}^{-1})$$

with $k_{aa} \equiv 1$.

For component x in medium y , k_{xy} is defined for a temperature gradient in the direction i as

$$(3.45) \quad k_{xy_i} = 1/(1 + (\lambda_x/\lambda_y - 1) \cdot g_{x_i})$$

where g_{x_i} is the shape factor for direction i , determined by the ratio of the main axes of the particle. The particles are assumed to be spheroid-shaped. If it is assumed that the particle axes have random directions in the bulk soil, the weight factors are calculated by

$$(3.46) \quad k_{xy} = \frac{1}{3} (k_{xy_{i=1}} + k_{xy_{i=2}} + k_{xy_{i=3}})$$

which results for spheroids in

$$(3.47) \quad k_{xy} = \frac{2}{3} \frac{1}{(1 + (\lambda_x/\lambda_y - 1)g_{x_i})} + \frac{1}{3} \frac{1}{(1 + (\lambda_x/\lambda_y - 1)(1 - 2g_{x_i}))}$$

with $i=1$.

De Vries (1975) mentioned an inaccuracy of 5% in the λ -predictions for soil by the above equations, increasing to a 10% inaccuracy for the range where neither water nor air are considered as the continuous medium ($0.02 < \theta < 0.05$). A program to perform the entire procedure of the λ -calculation is included (Appendix 2), and an example of the result is given for Swifterbant silt loam (Chapter 4). The sensitivity of the calculated λ to several parameters will be illustrated in the next chapter.

Several authors compared predictions by the analog model to measured data of thermal conductivity from both laboratory and field experiments. Although some reported disagreement (Nagpal and Boersma, 1973; Hadas, 1977b), others found good agreement between measured and calculated values (De Vries, 1963; Cochran et al., 1967; Wieringa et al., 1969; Sepaskhah and Boersma, 1979; Horton, 1982). The air shape factor g_a in the above model is sometimes used to match calculations with data. Kimball et al. (1976) extensively discussed this air shape factor, indicating its dependence on temperature and moisture content. Horton (1982) found best agreement when using the values of the air shape factor given by Kimball et al. In this report, an error interval is introduced to account for uncertainty in g_a where the λ -model is applied in simulation of field soil temperatures, rather than optimizing the fit between predicted and observed courses by adaptation of g_a .

The continuing discussions on thermal conductivity in soils literature indicates the difficulties involved in both the actual measurement of λ and the determination of the parameters required for the De Vries model. How relevant λ really is with respect to soil surface temperature behaviour, will be studied in Chapter 6.

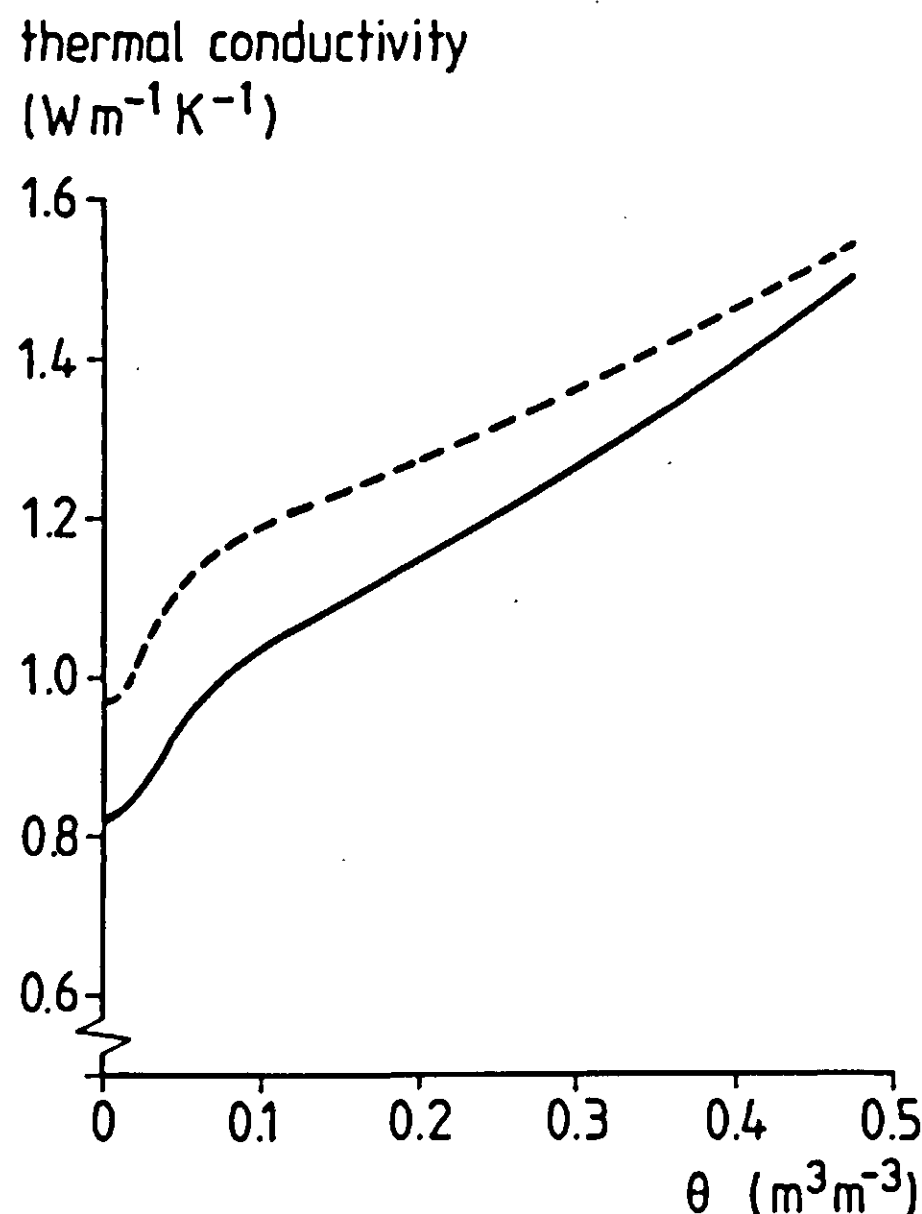


Figure 3.4 Thermal conductivity and apparent thermal conductivity as calculated by the De Vries model (saturated soil air).

Summarized in program statements, the previous theory states:

* non dynamic soil thermal properties, De Vries, 1975
430 IF (IFCHTB.EQ.1) GOTO 500
KAW = 0.66/(1.+((CHA/CHW)-1.)*GA)+0.33/...
 (1.+((CHA/CHW)-1.)*(1.-2.*GA))
KQW = 0.66/(1.+((CHQ/CHW)-1.)*GQ)+0.33/...
 (1.+((CHQ/CHW)-1.)*(1.-2.*GQ))
KOW = 0.66/(1.+((CHO/CHW)-1.)*GO)+0.33/...
 (1.+((CHO/CHW)-1.)*(1.-2.*GO))
KCW = 0.66/(1.+((CHC/CHW)-1.)*GC)+0.33/...
 (1.+((CHC/CHW)-1.)*(1.-2.*GC))

KWA = $0.66/(1.+((CHW/CHA)-1.)*GW)+0.33/...$
 $(1.+((CHW/CHA)-1.)*(1.-2.*GW))$
KQA = $0.66/(1.+((CHQ/CHA)-1.)*GQ)+0.33/...$
 $(1.+((CHQ/CHA)-1.)*(1.-2.*GQ))$
KOA = $0.66/(1.+((CHO/CHA)-1.)*GO)+0.33/...$
 $(1.+((CHO/CHA)-1.)*(1.-2.*GO))$
KCA = $0.66/(1.+((CHC/CHA)-1.)*GC)+0.33/...$
 $(1.+((CHC/CHA)-1.)*(1.-2.*GC))$
DO 440 I = 1,N
CHSL02(I) = $1.25*(KWA*0.02*CHW+KOA*FO(I)*CHO+KQA*FQ(I)*...$
 $CHQ+KCA*FC(I)*CHC+(POR(I)-.02)*CHA)/(KWA*...$
 $.02+KOA*FO(I)+KQA*FQ(I)+KCA*FC(I)+(POR(I)-.02))$
CHSL05(I) = $(.05*CHW+KOW*FO(I)*CHO+KQW*FQ(I)*CHQ+KCW*...$
 $FC(I)*CHC+KAW*(POR(I)-.05)*CHA)/(.05+KOW*...$
 $FO(I)+KQW*FQ(I)+KCW*FC(I)+KAW*(POR(I)-.05))$
KFCSA(I) = KOA*FO(I)*CHO+KQA*FQ(I)*CHQ+KCA*FC(I)*CHC
KFSA(I) = KOA*FO(I)+KQA*FQ(I)+KCA*FC(I)
KFCSW(I) = KOW*FO(I)*CHO+KQW*FQ(I)*CHQ+KCW*FC(I)*CHC
KFSW(I) = KOW*FO(I)+KQW*FQ(I)+KCW*FC(I)
440 CONTINUE

DYNAMIC

* Transport coefficients, potentials, auxiliary state soil (thermal)
* heat capacity profile
1100 DO 1105 I = 1,N
HCSOIL(I) = FC(I)*HCC+FQ(I)*HCQ+FO(I)*HCO+W(I)*HCW
1105 CONTINUE
* soil thermal conductivity, De Vries
1110 IF (IFCHTB.EQ.1) GOTO 1150
DO 1140 I = 1,N
FA(I) = POR(I)-W(I)
IF (W(I).GT.0.02) GOTO 1120
CHSOIL(I) = $1.25*(CHW*W(I)*KWA+FA(I)*CHA+KFC SA(I))/...$
 $(KFSA(I)+KWA*W(I)+FA(I))$
GOTO 1140
1120 IF (W(I).GT.0.5) GOTO 1130
CHSOIL(I) = CHSL02(I)+(W(I)-0.02)*(CHSL05(I)-CHSL02(I))...

```
/0.03  
GOTO 1140  
1130 CHSOIL(I) = W(I)*CHW+FA(I)*KAW*CHA+KFCSW(I)/...  
                  (W(I)+KAW*FA(I)+KFSW(I))  
1140 CONTINUE  
      GOTO 1170  
* thermal conductivity from table  
1150 DO 1160 I=1,N  
      CHSOIL(I) = BDRAT(I)*AFGEN(CHTB,W(I))  
1160 CONTINUE  
* local average thermal conductivity  
1170 CHAV(1) = CHSOIL(1)  
      DO 1180 I = 2,N  
      CHAV(I) = (CHSOIL(I-1)*TCM(I-1)+CHSOIL(I)*TCM(I))/...  
                  (TCM(I-1)+TCM(I))  
1180 CONTINUE  
* soil heat flux by conduction  
      HFLCON(1) = -(TS-T(1))*CHSOIL(1)/DZ(1)  
      DO 1500 I = 2,N  
      HFLCON(I) = CHAV(I)*(T(I)-T(I-1))/DZ(I)  
1500 CONTINUE
```

3.5.2 Coupling: heat associated with changes in soil water entropy

Soil water may be present in various states, each of which is characterized by a corresponding entropy. The condition of local thermodynamic equilibrium signifies that at any point, the local chemical potentials μ_i and the temperatures T_i are the same for all phases. Then, when water passes from one state into another, the change in entropy is accompanied by the release or absorption of a certain amount of heat ΔH , equal to $T(S_1 - S_2)$, where S_1 and S_2 are the partial specific entropies ($J \text{ kg}^{-1}\text{K}^{-1}$) of the respective phases. This follows from the equilibrium condition and the relation

$$(3.48) \quad \mu = H - TS \quad (\text{J } \text{kg}^{-1})$$

where H is the partial specific enthalpy ($\text{J } \text{kg}^{-1}$). Although in reality soil

water state changes gradually in space, it is considered satisfactory to distinguish three phases, each with its characteristic transport coefficient, pressure (p), partial specific entropy (S) and specific volume (V). These three phases are the 'free' or 'extrameric' liquid phase, the adsorbed or 'meric' phase, and the vapour phase (Kay and Groenevelt, 1974). (See also 3.6.1).

Heat of wetting

When liquid water is added to dry soil, a change in temperature is noticed due to the heat of wetting, ΔH_a , that is liberated when water molecules are adsorbed by the soil particles and their state changes from 'free' (liquid) to 'meric'. The heat of wetting has also been called 'heat of transport' (Nielsen et al., 1972). This is somewhat confusing, since ΔH_a is not directly related to the transport itself but to a local change of state, and the latter term should be avoided, because it does not reflect the phenomenon involved specifically. Table 3.6 lists for a number of soil materials the ΔH_a values, as measured directly in adsorption or immersion experiments. It is shown that ΔH_a differs over a wide range of values, depending on the type of clay mineral and the adsorbed cation species. It is generally acknowledged that upon wetting up to a relative humidity of 20%, the heat of wetting has evolved almost completely. This state is identified with the presence of a monolayer of water molecules adsorbed on the active surfaces. The actual concern being the relevance of the reported data to the soil energy balance, it may be stated that the heat of evaporation of adsorbed water, down to a relative humidity of 20%, is equal to that of free water, i.e. $2.4-2.5 \cdot 10^6 \text{ J kg}^{-1}$. Only for the last molecular layer, this value is increased by 5-25%, as can be seen from Table 3.6. In the context of the surface energy balance, this amount can be neglected and hence the heat of adsorption is not accounted for by the present model. (Note that to derive ΔH_a from vapour adsorption experiments, the latent heat of vaporisation, ΔH_v , should be subtracted from the total value of ΔH).

Heat of vaporisation

In analogy to the above, the well known heat of vaporisation ΔH_v accompanies the increase in entropy when water evaporates. This particular change in free enthalpy, in contrast to ΔH_a , has been observed to contribute considerably to soil heat transport (e.g. Hadas (1977b) and Westcot and Wierenga

Table 3.6 Integral heat of adsorption ΔH_a (free liquid \rightarrow adsorbed liquid) for different soil materials

	$\text{kJ kg}_{\text{dry soil}}^{-1}$	$\text{kJ kg}_{\text{water}}^{-1}$	
	(complete wetting) (from dry to $h=0.2$)		
Millville silt loam	.	80	Cary et al, 1964
Millville silt loam	.	510	Kijne et al, 1964
Red.brown loam	.	380	Orchiston, 1953
Yellow-grey loam	.	360	Orchiston, 1953
Illite	8.2	350	Orchiston, 1954
Kaolinite	0.9	500	Orchiston, 1954
Kaolinite	12.3*	.	Greene.Kelly, 1962
Na-kaolinite	6.8*	.	East, 1950
Na-Wakefield clay	.	360	Goates and Bennet, 1957
Montmorillonite	52.9	420	Orchiston, 1954
Montmorillonite	70*	.	Green-Kelly, 1962
Na-montmorillonite	75*	.	Van der Marel, 1966
Ca-montmorillonite	95	791	Kijne, 1969
Li-montmorillonite	70	538	Kijne, 1969
NH ₄ -montmorillonite	39	709	Kijne, 1969
Na-montmorillonite	28	700	Kijne, 1969

* Calculated from original data assuming specific surface areas of 500 and 25 $\text{m}^2 \text{g}^{-1}$ for montmorillonite and kaolinite, respectively.

(1974) for field and laboratory experiments respectively). Surface condensation, in addition to conductive heat transport, may play an important role in the surface energy balance at night, compensating for radiative cooling and thus maintaining net radiation at a steady minimum level. A brief model study on this topic will be discussed in Chapter 6.

As mentioned before, the latent heat carried by the vapour is usually taken into account by the use of a so-called 'apparent thermal conductivity', λ^* . As an example, Figure 3.4 shows its contribution as calculated by the De Vries model (eqs 3.43, 3.44), in which λ_a can either signify the true conductivity of air (for a prediction of λ), or the apparent conductivity of air, i.e. including vapour diffusion (to yield λ^*). Since both vapour diffusivity and vapour density are temperature dependent, this also applies

to λ^* . It must be realized however, that these curves represent only the case of saturated soil air. In other cases, the effect of vapour movement on heat transfer may even be in the reverse direction, such as happens when vapor diffuses down the gradient of relative humidity towards the warm soil surface, which probably occurs commonly at very shallow depth during daytime. Then, vapour flow decreases apparent thermal conductivity. For these reasons the use of λ^* is avoided in the SALSA model, where an accurate description of surface energy fluxes is essential to the prediction of temperature and moisture content near the surface.

Heat flux associated with water transport

The heat flux through soil with simultaneous water transport is easily misinterpreted, and different definitions are possible (De Groot and Mazur, 1962; Chu et al., 1983). Using eq. (3.48), the flux of free enthalpy can be seen as the total heat flux (Katchalsky and Curran, 1965):

$$(3.49) \quad j_q = T j_s + \sum_i \mu_{w_i} j_{w_i} \quad (\text{W m}^{-2})$$

where j_s is the total entropy flux (by conduction and mass transport) and j_{w_i} are the different fluxes of water in state i , with chemical potential μ_{w_i} . This equation, combined with eq. (3.48), is identical with

$$(3.50) \quad j_q = T j_s - T \bar{S}_w \sum_i j_{w_i} + \bar{H}_w \sum_i j_{w_i} \quad (\text{W m}^{-2})$$

where the first two terms on the RHS constitute the so-called 'reduced heat flux' (Bolt and Groenevelt, 1972; Kay and Groenevelt, 1974) and the entropy \bar{S}_w refers to a particular chosen state of the water (the enthalpy \bar{H}_w then corresponds to that same state). If the condition is imposed that the water after transportation has attained this reference entropy, then this reduced heat flux represents the total sensible heat flux due to both conduction and change of state. However, if the water is not brought to the \bar{S}_w -state, the choice of this state loses significance, as does the term 'reduced heat flux'.

The last term in eq. (3.50) is the total 'flux of reference enthalpy', carried by the water. For a more extensive discussion of these coupling phenomena in the context of thermodynamics of irreversible processes see subsection 3.6.1 and Appendix 4.

Neglecting the heat of wetting, and forgetting for a moment the conduction term, substitution of ΔH_v for $(Tj_s - TS_w j_w)$ in eq. (3.50) yields for the local change of soil heat content due to water transport:

$$(3.51) \quad \left[\frac{\partial}{\partial t} (CT) \right]_w = - \frac{d}{dz} j_{q,w} = - \Delta H_v \frac{d}{dz} j_v - \frac{d}{dz} (\bar{H}_w j_w) \quad (J m^{-3} s^{-1})$$

where j_v is the vapour flux, j_w is the total water flux, and $j_{q,w}$ is the total heat flux associated with water transport.

In the discussed model, the LHS derivative of this equation is calculated as $C(\partial T / \partial t)$ and the last term on the RHS is omitted, thus cancelling $T(\partial C / \partial t)$ against the divergence of $\bar{H}_w j_w$. It can be shown that this is not a severe simplification; it implies the neglect of the part $j_w (\partial \bar{H}_w / \partial z)$ of the divergence of $j_w \bar{H}_w$. This term is small indeed: even under a temperature gradient of 100 K m^{-1} , a flux of 1 mm h^{-1} would give rise to a temperature change of only approximately 0.1 K h^{-1} .

Consequently, the latent heat flux in the soil is programmed as:

* soil heat flux by vapour transport

```
DO 1510           I = 1,N  
                  HFLVAP(I) = LVAP*WFLVAP(I)  
1510    CONTINUE
```

Using eq. (3.51) - with the simplification mentioned - as the only term P_i in eq. (3.41), combination of these equations gives in CSMP statements:

* total soil heat flux

```
DO 1520           I = 1,N  
                  HFLX(I) = HFLCON(I)+HFLVAP(I)  
1520    CONTINUE
```

3.5.3 Convective heat transport in the gas phase

Recently, Menenti (1984) suggested that free convection of soil air in cracked desert soils might contribute to the transport of heat from the soil surface downward. The stratification of hot and dry air overlying cool and moist air in a soil profile would cause instability, since air density de-

creases with increasing humidity. The gradient of virtual temperature, i.e. the temperature that dry air would have at the actual density and pressure of the (moist) air under consideration, thus indicates whether or not instability might occur.

In appendix 5 it is shown that the suggested mechanism, heat being supplied to the evaporation front below the surface by descending dry hot air which is subsequently transformed into moist cool air-, cannot act if the heat required for evaporation is supplied solely by convection. If indeed another source of heat would enable evaporation to take place, the contribution of the convective heat flux should be less than 10%.

Although thermal convection in the soil gas phase apparently is not important as a mechanism to transport energy downward during daytime, it surely needs further study as a process that enhances heat and vapour movement at night and in early morning, when temperature gradients are reversed.

3.6 Transport of water in the soil

The general flow equation for one-dimensional, liquid water transport in the soil is written as

$$(3.52) \quad \rho_1 \frac{\partial \theta}{\partial t} = \frac{d}{dz} \left(K(\theta, T) \frac{dp(\theta, T)}{dz} \right) - \rho_1 g \frac{d}{dz} K(\theta, T) \quad (\text{kg m}^{-3}\text{s}^{-1})$$

where p is the pressure potential (Pa), K is the hydraulic conductivity ($\text{kg m}^{-1}\text{Pa}^{-1}\text{s}^{-1}$), ρ_1 is the density of the liquid, g the acceleration by gravity, and θ the volumetric water content. The moisture characteristic $p(\theta)$ and the hydraulic conductivity function $K(\theta)$ will be treated in subsection 3.6.2, along with the so-called 'matric flux potential' concept. The latter is a combination of the $p(\theta)$ and $K(\theta)$ functions, that may be used as a substitute for these; this substitution offers several advantages.

Since moisture transport near the soil surface is rarely isothermal, attention must be paid to the phenomenon of coupling between heat and moisture fluxes in analogy to the discussion concerning the soil heat flux (3.5.2). As demonstrated in Chapter 2, various models that include coupling phenomena have been published, and some aspects have been evaluated quantitatively recently by simulation studies (e.g. Milly, 1984; Hopmans and Dane, 1985). Nevertheless, it is felt that a thorough analysis is required here.

This analysis (subsection 3.6.1) yields a new connection between the classical approaches, underscoring the final conclusion that in the liquid phase, transport due to a temperature gradient can be neglected. For its counterpart, the transport of heat associated with water transport, see 3.5.2. In appendix 4, the involved Onsager reciprocal relations are discussed in the context of thermodynamics of irreversible processes (TIP).

The equivalent of eq. (3.52) for vapour transfer is expressed as

$$(3.53) \quad \rho_1 \frac{\partial \theta}{\partial t} = \frac{d}{dz} \left(D_e(\theta, T) \frac{dp_v(\theta, T)}{dz} \right) \quad (\text{kg m}^{-3}\text{s}^{-1})$$

where ρ_v is the vapour density (kg m^{-3}) and D_e the effective vapour diffusivity (m^2s^{-1}). In analogy to the case for liquid transfer, some comments will be given on the theory of coupling and on the relation $\rho_v(\theta)$ (3.6.3); also the effective diffusivity D_e , including the various enhancement mechanisms that have been discussed in literature (3.6.4), will be touched upon.

The combination of eqs (3.52) and (3.53) cast into CSMP statements gives

```
*      soil water flux divergence; rate of change of moisture content  
      DO 1480      I = 1, N  
      DIVWFL(I)    = (WFLX(I+1)-WFLX(I))/TCM(I)  
      WRCH(I)      = DIVWFL(I)/RHOL  
1480    CONTINUE
```

3.6.1 Coupling: non-isothermal transport in the liquid phase; the formulation of $p(\theta, T)$

In soils literature, two different approaches have been followed to analyse coupling between mass and heat transport: the 'mechanistic' approach by Krischer and Rohnalter (1940) and Philip and De Vries (1957) on the one hand, and the 'thermodynamic' approach on the other hand (Taylor and Cary, 1964; Cary, 1965; Weeks, 1968).

Mechanistic approach

The mechanistic analysis employs the concepts of fluid mechanics and heat conduction. Using the gradient of the hydrostatic pressure (here tensiometer

pressure p) as the only driving force for liquid flow, Philip and De Vries indicated that at constant value of the volumetric water content θ , a T-gradient should induce a liquid flow in the direction of the cold side, following the effect of temperature on the surface tension γ . They divided the flux due to a tensiometer pressure gradient into two components, one due to a gradient of the water content, and another due to a temperature gradient:

$$(3.54) \quad j_1 = -K \left(\frac{\partial p}{\partial \theta} \right)_T \frac{d\theta}{dz} - K \left(\frac{\partial p}{\partial T} \right)_\theta \frac{dT}{dz} \quad (\text{kg m}^{-2}\text{s}^{-1})$$

where p , the pressure component of the total water potential, actually is the Laplace pressure jump Δp across a curved liquid-gas interface; Δp is dictated by the relation between equivalent pore radius R , wetting angle ϕ and the interfacial tension of the liquid-gas interface, γ_{lg} , according to

$$(3.55) \quad \Delta p = - \frac{2}{R} \cos \phi \cdot \gamma_{lg} \quad (\text{Pa})$$

The derivative $(\partial p / \partial T)$ as used in eq. (3.54) now follows directly from differentiation of eq. (3.55) with respect to temperature:

$$(3.56) \quad \left(\frac{\partial p}{\partial T} \right)_\theta = \frac{p}{\gamma_{lg}} \frac{\partial \gamma_{lg}}{\partial T} \quad (\text{Pa K}^{-1})$$

where the wetting angle is kept constant. Since γ_{lg} decreases with increasing temperature, it follows (with p negative) that the 'thermal liquid diffusivity' $D_{T,liq} \equiv K(\partial p / \partial T)_\theta$, causes water to flow in the direction of decreasing temperature.

Experimental evidence of the temperature dependence of $p(\theta)$ has been reported by several authors. In general, a hyperbolic relationship of the form $(\partial p / \partial T) = a(\theta - b)^{-1} + c$ can be fitted to the data (Ritsema, 1985). The empirical constants a , b and c , as calculated from the original data, are listed in Table 3.7 to give an impression of the magnitude of the temperature effect on extramatrix liquid pressure. It will be clear that this relation is only meant to summarize the data and has no direct physical significance, as appears for θ approaching the b -value.

Table 3.7 Constants in empirical $(\partial p/\partial T)_\theta = \theta$ relationship, eq. 4.13

	a (Pa K ⁻¹)	b	c (Pa K ⁻¹)	
Sand	6.90	.069	-32	Constantz, 1982
Fine sand	0.40	.035	+17	Wilkinson and Klute, 1962
Silt	8.40	.085	+240	Wilkinson and Klute, 1962
Fine silt	37.50	.000	-97	Chahal, 1965
Sandy loam	13.60	.150	-46	Constantz, 1982
Silt loam	277.20	.000	-1249	Taylor and Stewart, 1960
Silt loam	44.40	.210	-167	Maridasan and Jensen, 1972
Silt loam	104.20	.180	-512	this report

Thermodynamic approach

The thermodynamic analysis involves the use of the general framework of thermodynamics of irreversible processes, TIP, together with the Clapeyron equations to formulate the coupling coefficients. Selecting again the gradient of the tensiometer pressure p as the superficial driving force, Bolt and Groenevelt (1972) and particularly Kay and Groenevelt (1974) indicated that at a constant value of this tensiometer pressure, a T-gradient would induce liquid flow from the cold to the warm side, i.e. in the opposite direction from the situation sketched above. The reasoning of these authors is elaborated upon below.

On the basis of the local entropy of soil water, many different phases could be distinguished, amongst others comprising ice, bulk liquid and vapour. For the present purpose, only the liquid phase is considered in more detail. On the scale of a pore then, a gradual change in local entropy can be found within the liquid phase: it decreases as the solid-liquid interface is approached as a result of the force field extending from the solid surface. Thus an infinity of subphases could be defined. For each subphase i , the macroscopic gradient in chemical potential μ_w , is expressed as a linear combination of pressure and temperature gradients by the Gibbs-Duhem equation:

$$(3.57) \quad \frac{d\mu_w}{dz} = -S_i \frac{dT}{dz} + V_i \frac{dp_i}{dz} \quad (\text{J kg}^{-1}\text{m}^{-1})$$

where S_i , V_i , and p_i are the partial specific entropy, volume and pressure respectively. This implies that the pressure gradients are different for the distinguished subphases when a temperature gradient exists. Kay and Groenevelt (1974) simplified this picture by distinguishing two phases of the liquid water: the 'extrameric' water, i.e. water outside the force field emanating from the solid phase, and water under direct influence of these surface forces. For brevity, the latter will be called 'matric' water, although it is stressed that both phases may be present at the same time within the soil matrix. 'Extrameric' water is the water as present in a measuring device, such as a psychrometer or a tensiometer. The measured tensiometer pressure gradient is a gradient in the pressure p of the 'extrameric' liquid, in equilibrium with the soil water (i.e. also at the same local temperature!).

If now, following Kay and Groenevelt (1974), ∇p_i is used as the driving force to be balanced by the friction forces arising during movement of the liquid phase(s) i , thermal osmosis may be ascribed to the difference between ∇p and ∇p_i . Such a difference must come about for non-zero values of ∇T , as will become clear in the following. The condition of local thermodynamic equilibrium implies that the chemical potentials μ_{w_i} are the same for all subphases. If then the water, present in the soil system, is satisfactorily typified by some average value of the 'matric' phase pressure $p'(\neq p)$ and specific volume $V' \approx \bar{V}$, combination of this equilibrium condition with eq (3.57) yields the well-known Clapeyron equation:

$$(3.58) \quad \bar{V}(dp - dp') = (S - S')dT \equiv \Delta \bar{H}_a \frac{dT}{T} \quad (\text{J kg}^{-1})$$

where S' is the partial specific entropy of liquid in the 'matric' phase, and S represents the same quantity for the 'extrameric' phase; the positive value of the heat of wetting $\Delta \bar{H}_a \equiv T(S - S')$, signifies that $dp' < dp$ for $dT > 0$. Thus thermoosmosis ($dp \equiv 0!$) is directed towards the warm side. It follows then directly that the last RHS term of eq (3.54) overestimates the thermally induced liquid flow, since $\nabla p'$ should be used as the driving force instead of ∇p . Some measured values of $\Delta \bar{H}_a$ were listed in Table 3.6.

Connecting mechanistic and thermodynamic approaches

Clearly, the appearance of a ∇T driven flux in eq (3.54) is, within the context of the mechanistic approach, incurred by the substitution of $\nabla \theta$ for the

assumed primary driving force for the liquid phase, ∇p . As such it has no direct relation with the coupling phenomenon inferred within the context of TIP, when constructing the matrix of fluxes and conjugated forces. As was shown by Kay and Groenevelt and summarized in the previous section, such a coupling should indeed be expected when ∇p is used as the overall driving force conjugated to the liquid flux; its form is then found with the help of eq (3.58).

As a result, the actual VT driven flux at constant θ must be found by summing up of both effects discussed above. By making use of the extensive analysis by Kay and Groenevelt (1974) and Groenevelt and Kay (1974) on the one hand, and of the thermodynamics of the solid-liquid interfacial region on the other hand, it may be shown that in addition to having opposite directions, the magnitude of the two VT driven fluxes is likely to be of the same order. The required analysis, described in more detail in Appendix 3, involves the relation between the interfacial tensions of the gas-liquid and liquid-solid interfaces, and their respective temperature dependences. As a result, finally the connection between the two approaches sketched above appears as:

$$(3.59) \quad (dp)_\theta = \left(\frac{\partial p}{\partial T}\right)_\theta dT = \frac{\Delta \bar{H}}{\bar{V} T} dT \quad (\text{Pa})$$

Combination of eqs (3.58) and (3.59) shows that the assumed average driving force for flow of 'matric' water, $\nabla p'$, must be zero. As indicated in Appendix 3, this result is based upon the assumption that all soil water be in the matric state, and that $\nabla p'$ therefore is the overall driving force. It may now be objected that this assumption is not realistic; it can be shown, however, that for any schematized division of soil water into two subphases, the driving forces on the respective subphases due to a temperature gradient cancel each other (Appendix 3). It must be added that in reality of course not only the driving forces, but also the mobilities of water in the different phases determine the fluxes, and that as a result the flow towards the cold side will win out in the situation with $\nabla \theta = 0$. Presently, this difference is neglected, assuming that the qualitative analysis of compensation gives enough justification for doing so. It is stressed that the previous analysis directly leads to the conclusion that the widely accepted Philip and De Vries formulation of thermally induced liquid flow does not take into account true coupling in the thermodynamic sense; such coupling

arises from the relation between pressure and entropy differences between the distinguished phases (eq. 3.58).

The remaining driving forces for liquid water movement now are $(\partial p / \partial \theta)_T \nabla \theta$ and $(\partial p' / \partial \theta)_T \nabla \theta$ for the two-phase situation, and only the latter term if all water is assumed to be in the 'matric' state. According to the Clapeyron equation (3.58), the derivatives $(\partial p / \partial \theta)_T$ and $(\partial p' / \partial \theta)_T$ must be equal, and they simply represent the slope of the well known moisture characteristic curve (next subsection). This slope is used in the discussed model to calculate water flow in the liquid phase.

Having eliminated the gradient of temperature as a substantial driving force for movement in the liquid phase, the dependence of $(\partial p / \partial \theta)_T$ on temperature still remains. This relation can hardly be analysed on a theoretical basis, the moisture characteristic itself being an empirical datum. Empirical results are therefore invoked here to study this derivative. Data from different authors, applying to a wide range of soils, θ -values and temperatures were analysed, and the results are shown in Figure 3.5.

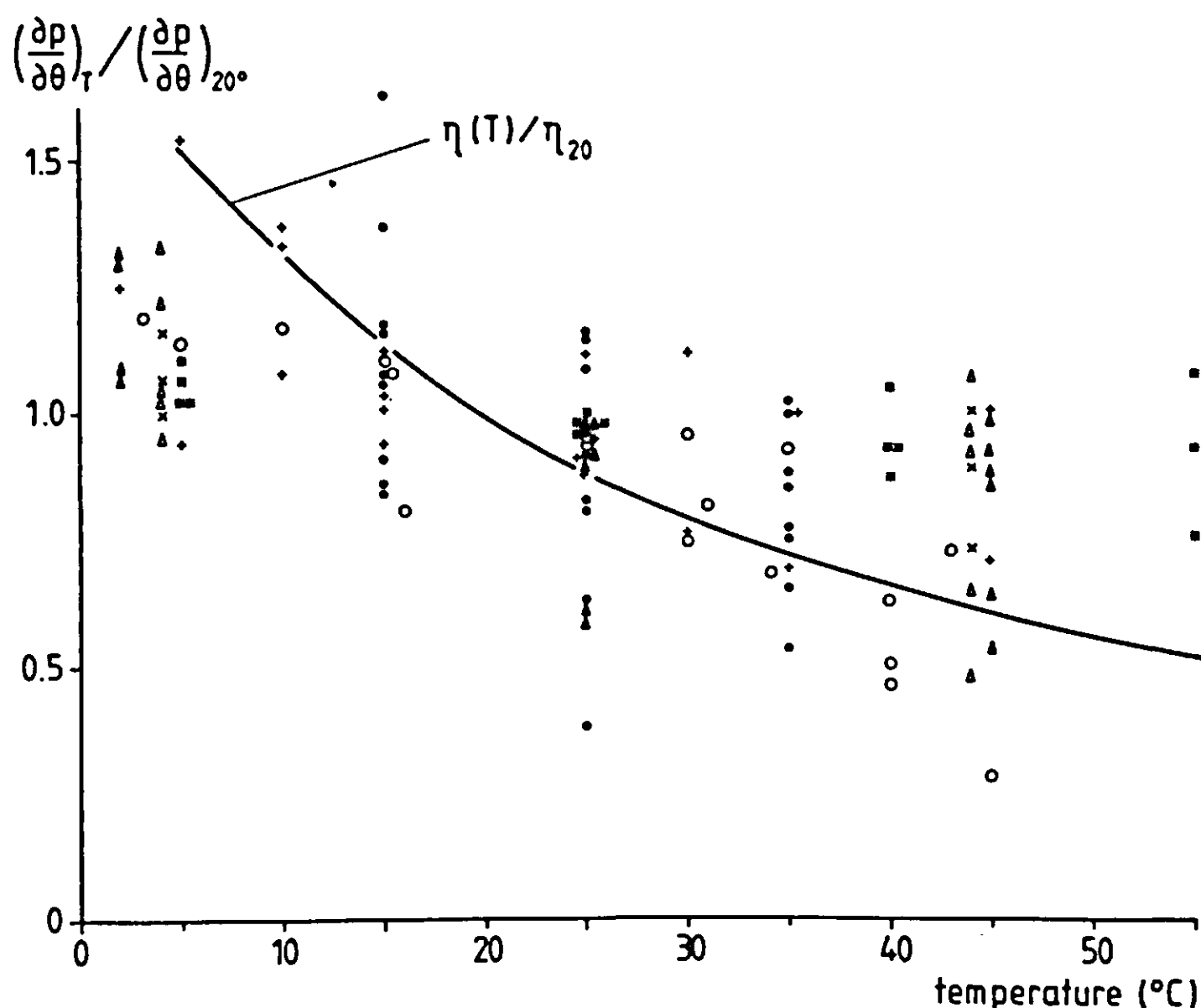


Figure 3.5 The ratio $(\frac{\partial p}{\partial \theta})_T / (\frac{\partial p}{\partial \theta})_{20^\circ}$ versus temperature as calculated from literature data, applying to a variety of soil water contents. o silt loam, Haridasan and Jensen (1972); o silt loam, Taylor and Stewart (1960); x fine sand, Wilkinson and Klute (1962); Δ silt, Wilkinson and Klute (1962); Δ sandy loam, Constantz (1982); + silt loam, this report; * fine silt, Chahal (1965).

This figure shows as a function of T the ratio of $(\frac{\partial p}{\partial \theta})_T$ to its value at a reference temperature (20°C). In view of these results, it seems important to take temperature into account when calculating $p(\theta)$. However, since ∇p is multiplied by K in calculating the flux, the $K(T)$ relation also must be studied in this context. As K_θ is inversely proportional to the temperature-dependent viscosity of liquid, the ratio of viscosity $\eta(T)$ (see also 3.6.2) to its value at reference temperature T_o is plotted in Figure 3.5 as well, showing that both effects mentioned tend to compensate one another:

$$(3.60) \quad \frac{\eta(T)}{\eta(T_o)} \approx \frac{(\frac{\partial p}{\partial \theta})_T}{(\frac{\partial p}{\partial \theta})_{T_o}}$$

Hence the temperature dependence of the moisture characteristic slope is not taken into account in the SALSA model.

3.6.2 The moisture characteristic, hydraulic conductivity and matric flux potential

The moisture characteristic

The relation between moisture content and pressure potential is determined by soil texture and structure. Empirical and semi-empirical models have been proposed to express the moisture characteristic on the basis of these properties (e.g. Arya and Paris, 1981; Gupta and Larson, 1979) but a main problem remains the distribution of total pore space over the fractions related to particle size classes and those related to structure. In the present model it is therefore preferred to use measured relationships, which may be specified in the form of an analytical expression. The function proposed by Van Genuchten (1980) is employed here, as it can be fitted to curves from a wide range of soils:

$$(3.61) \quad p = -\frac{1}{\alpha} (\Xi^{-1/m} - 1)^{1/n} \quad (\text{Pa})$$

where Ξ is the relative saturation according to

$$(3.62) \quad \Xi \equiv \frac{\theta - \theta_r}{\theta_s - \theta_r}$$

with θ_r and θ_s as the residual moisture content and the moisture content at saturation, respectively. The parameters α , n , and θ_r can be determined for a given set of $p(\theta)$ measurements by the optimisation procedure SOHYP (Van Genuchten, 1979). The parameter α appears to be related to soil structure, and n and θ_r to texture; m is defined by $m \equiv 1-1/n$. For the present purpose, data from a number of soils, covering a wide range of textures, have been analysed using SOHYP, resulting in the sets of parameter values listed in Tabel 3.8. A distinct advantage of Van Genuchten's function is that it allows one to use the theoretically based $K(\theta)$ model given by Mualem (1976), as elaborated upon by Van Genuchten (1980).

At very low water contents, the above concept presents some difficulties, as it is based on transport in the liquid phase only. By eqs. (3.61) and (3.62), the residual water content θ_r is defined as the moisture content where an infinitely high pressure must be exerted to liberate more water from the matrix. At infinitely low pressure potential however, no vapour transport could occur either, since the vapour concentration would approach zero. Of course this paradox is due to the fact that liquid continuity and mobility ceases at very low θ -values. Therefore θ_r has no physical meaning in terms of pressure and should not be used as such.

In the model SALSA, the above set of equations is used down to the (quite arbitrary) pressure potential of -1.5 MPa, where the relative humidity h is still approximately 100%. For moisture contents lower than the corresponding $\theta_{-1.5}$, liquid pressure is calculated from relative humidity, making use of the Kelvin equation (eq. 3.73) and adsorption isotherms for water to soil particles. (The liquid pressure is then only of interest for $\theta > \theta_r$; at lower θ , hydraulic conductivity is set to zero and pressure is not a relevant variable). The adsorption isotherms will be discussed in subsection 3.6.3.

Hysteresis

A theoretical concept of hysteresis to be used in the study of diurnal top-soil behaviour should take into account the hysteresis in both the $p(\theta)_T$ and the $p(T)_\theta$ relations. The former represents the classical hysteretic behaviour, for which some theoretical models have been formulated (Poulovassilis, 1962; Mualem, 1973; Mualem and Morel-Seytoux, 1978). Evidence of the latter case, for brevity called 'thermal' hysteresis, was reported already by Moore (1940), Gardner (1955), Taylor and Stewart (1960), and Richter (1972), and

Table 3.8 Hydraulic properties of various soils. The original $p(\theta)$ and $K(\theta)$ data for most soils were taken from references listed by Mualem and Dagan (1976)

Soil	α 10^{-4} Pa ⁻¹	n	θ_r	θ_s^{**}	K_s 10^{-8} kg m ⁻¹ s ⁻¹ Pa ⁻¹	A 10^{-6} kg m ⁻¹ s ⁻¹	B	Source
Beit Netofa clay	1.1390	1.1693	0.000	0.446	0.81	.	.	Rawitz, 1965
Rideau clay	8.2510	1.1740	0.000	0.478	34.20	639.0	0.0899	Staple, 1969
Yolo light clay	2.9200	1.2725	0.006	0.495	0.9950	36.9	0.125	Moore, 1939
Buffalo silty clay	7.1028	1.1275	0.000	0.416	7.90	51.9	0.0088	this report
Glendale clay loam	22.4680	1.5856	0.232	0.525	109.00	510.2	0.0965	Sisson et al., 1980
Avondale loam	2.2670	1.1929	0.000	0.400	27.80	642.0	0.0402	Jackson, 1973
Guelph loam	1.3470	1.7036	0.176	0.520	30.49	1816.5	0.0595	Elrick, 1964
Gilat loam	1.8000	3.2259	0.133	0.440	21.62	759.0	0.0208	Bresler et al., 1971
Swifterbant loam	46.7063	1.0927	0.033	0.430	5.20*	.	.	this report
Swifterbant silt loam	4.0397	1.1610	0.000	0.420	5.20*	.	.	this report
Grenville silt loam	0.6700	1.4346	0.149	0.475	6.40	496.4	0.0242	Staple, 1965
Columbia silt loam	1.4990	1.6260	0.095	0.400	5.85	315.9	0.0736	Davidson et al., 1963
Ida silt loam	0.8470	1.3895	0.049	0.550	9.22	355.2	0.0248	Green et al., 1964
Mont Cenis silt loam	1.8070	1.2814	0.000	0.442	1.41	150.4	0.1670	Vachaud, 1966
Yolo fine sandy loam	0.9440	3.1091	0.171	0.375	1.48	200.2	0.0726	Moore, 1939
Vernal sandy loam	5.6060	1.2562	0.000	0.475	22.10	485.9	0.1100	Nimah and Hanks, 1973
Bet Dagan 1 loamy sand	2.7610	3.0224	0.044	0.375	638.32	16313	0.0404	Russo and Bresler, 1980
Panoche soil	1.6560	1.8033	0.249	0.450	44.28	13119	0.0230	Nielsen et al., 1973
Gravelly sand G.E.-9	1.4960	2.8043	0.080	0.326	27.40	1365	0.0450	Reisenauer, 1963
Hygiene sandstone	0.8010	7.3563	0.150	0.250	124.96	12380	0.00897	Brooks and Corey, 1964
River sand	3.6260	5.2091	0.000	0.350	222.84	3841	0.0135	Jensen et al., 1967
Sable S2	10.0220	1.3741	0.000	0.410	409.58	470.9	0.00456	Stroosnijder, 1982
Lakefield fine sand 3	2.7140	3.5955	0.077	0.360	529.10	14463	0.0328	Elseftawy and Mansell, 1975
Lakefield fine sand 1	2.4070	3.6334	0.103	0.365	463.73	12149	0.0254	Elseftawy and Mansell, 1975
Uplands sand	7.0870	1.8103	0.049	0.304	182.92	2164	0.0605	Staple, 1969
Nahal Sanai sand	2.4700	5.7633	0.036	0.270	344.79	11038	0.0182	Bresler et al., 1971

* at -1 kPa

** or highest θ reported

was also found for Swifterbant silt loam in the study discussed in this report. However, observations are inconsistent. In addition to the well-known 'pore neck' explanation, both classical and 'thermal' hysteresis are possibly related to wetting angle hysteresis and changes in soil structure. Rose (1971) reported on hysteresis down to very low moisture contents, in the range of physical adsorption ($p \approx -1$ GPa) where significant liquid movement is unlikely; from this observation it can be expected that other than 'pore-neck' mechanisms are involved.

Although it is recognized (Chapter 5) that hysteresis may play a significant role in soil water evaporation cycles (see also Hillel (1976) for a simulation exercise), the phenomenon is not included in the model discussed in this report; hysteresis is viewed as a refinement at a stage where 'coarser' effects of soil properties on the surface energy balance still have to be generalized. In case the user wishes to incorporate $p(\theta)_T$ hysteresis into the model, the formulation by Dane and Wierenga (1975) seems to be attractive, although computation costs will rise dramatically.

Hydraulic conductivity

For the description of moisture flow in simulation models, the $K(\theta)$ relation can be introduced in different ways. One possibility is the use of a tabulated $K(\theta)$ function, obtained by direct measurement. Various techniques are available for the measurement of hydraulic conductivity, most of which are fairly time-consuming. Rather fast is the 'hot air method', which however may easily yield erroneous results, if the proper precautions are not taken (Van Grinsven et al., 1985). Aside from its rapidity - the large field variability in K requires numerous measurements - a major advantage of this method is that the $K(\theta)$ relation is also obtained for relatively low θ -values. This is especially of interest in the present context, where evaporation rather than infiltration cases are studied.

As an alternative to the specification of tabulated $K(\theta)$ data, one might use parameters, obtained by fitting an expression to such data. A third possibility would be to make use of one of the (semi-) empirical models that relate hydraulic conductivity to the moisture characteristic curve, and usually involve as a 'matching point' a K -value near saturation (Brooks and Corey, 1964; Jackson, 1972; Campbell, 1974; Mualem, 1976).

In the SALSA model, the $K(\theta)$ function can either be specified as a table of measured data, or be calculated on the basis of the model by Mualem

(1976), using eqs. (3.61) and (3.62) to express the moisture characteristic. The resulting equation for the hydraulic conductivity reads:

$$(3.63) \quad K = K_s \varepsilon^{\frac{1}{m}} (1 - (1 - \varepsilon^{1/m})^m)^2 \quad (\text{kg m}^{-1}\text{Pa}^{-1}\text{s}^{-1})$$

where K_s is the conductivity at saturation and ε and m are defined as for eqs. (3.61) and (3.62). This implies that K is zero for $\theta \leq \theta_r$. Averaging of K -values at the interfaces of two neighbouring compartments in the model is done by using the square root from the product of the two K -values (Vauclin et al., 1979).

Aside from moisture content, also temperature affects the hydraulic conductivity, since the viscosity η (Pa s) is temperature dependent (see Figure 3.6). The $K(T)\theta$ function is usually expressed satisfactorily by the relation

$$(3.64) \quad K_\theta(T) = K_\theta(T_o) \frac{\eta(T_o)}{\eta(T)} \quad (\text{kg m}^{-1}\text{Pa}^{-1}\text{s}^{-1})$$

where T_o is a reference temperature (Philips and De Vries, 1957; Haridasan and Jensen, 1972; Rahi and Jensen, 1974; Saha and Triphathi, 1979). Constanz (1982) reported a stronger temperature influence than predicted by this relation, and other effects than the above mentioned may be present, but are not adopted in the model.

As shown in Figure 3.5 and discussed in 3.6.1, the $\eta(T)$ relation appears to counteract the effect of temperature on the slope $(\partial p/\partial \theta)_T$. Although this compensation is only a rough approximation and considerable scatter and inconsistency occur in the reported data of both $K(T)$ and $f(T) \equiv (\partial p/\partial \theta)_T$, it seems warranted to exclude both functions from the simulation model. In view of this, it was tested to what extent a difference in slope between the two functions affects hydraulic behaviour of the top-soil. The effect appeared negligible, and hence the temperature correction was omitted from the model.

Matric flux potential

According to Darcy's law, the flux density equation for flow in the vertical contains the sum of a 'matric' component and a gravity component:

$$(3.65) \quad j_w = -K \frac{dp}{dz} + \rho_1 g K \quad (\text{kg m}^{-2}\text{s}^{-1})$$

For the case where gravity is neglected, the flux by the matric term can be written as the gradient of a 'potential' Φ , called 'matric flux potential' (Raats, 1970). This matric flux potential is defined as

$$(3.66) \quad \Phi \equiv \int_{p=-\infty}^0 K(p) dp \quad (\text{kg m}^{-1} \text{ s}^{-1})$$

As the transport coefficient K is incorporated into Φ , the latter is not a true potential in the sense that its gradient should represent a force per unit mass or per unit volume; the name is therefore somewhat misleading. The transformation involved is also called the Kirchoff transform. Klute (1952) introduced the concept into soil physics, and it has been used since in mainly analytical solutions of the flow equation for infiltration from point, line or volume sources (e.g. Philip, 1971; Warrick, 1974; Raats, 1977). As the integral in the above equation converges for realistic $K(p)$ functions (Raats and Gardner, 1971), the $\Phi(p)$ and also $\Phi(\theta)$ curves all show the same characteristic shape (See Chapter 4).

In numerical simulation, the use of the matric flux potential has some advantages over the $K-p$ formulation (Shaykewich and Stroosnijder, 1977). The major gain is due to the fact that averaging of transport coefficients, a problem encountered in numerical solutions of the flow equation (e.g. Vauclin et al., 1979), is avoided. This is especially advantageous to the simulation of the evaporation process and of infiltration into dry soil, where very large potential gradients occur; in such cases it is difficult to choose a representative $K(\theta)$ value, which may result in significant errors in the calculated flux (numerical overshoot). The use of Φ also saves some computation time, since only the $\Phi(\theta)$ function is used instead of both $K(\theta)$ and $p(\theta)$, and the averaging procedures are left out. Moreover, the $\Phi(\theta)$ curve is more easily interpreted in terms of fluxes than a combination of $K(\theta)$ and $p(\theta)$, and an additional advantage is that the $\Phi(\theta)$ function can be measured directly over a wide range of θ by a relatively easy procedure, proposed in this report (Appendix 6).

A drawback is that the matric flux potential concept is only valid for homogeneous soils; it also loses its physical significance if hysteresis in the $p(\theta)$ function occurs, and if the driving force for liquid movement would be affected by temperature or by the temperature gradient, which however is supposed not to be the case (see 3.6.1).

In the present model, either the $\Phi(\theta)$ or the $K(\theta)-p(\theta)$ option can be chosen. In the former case, $\Phi(\theta)$ can be given in tabulated form, or can be specified by an analytical function, involving two empirical constants:

$$(3.67) \quad \Phi(\theta) = \frac{-A}{x + B} \quad (\text{kg m}^{-1} \text{ s}^{-1})$$

where x is defined as $x \equiv 1 - \theta/\theta_s$. The scale parameter A indicates the maximum stationary flux that can be attained through a soil slab of thickness unity, and the 'saturation constant' B is related to the shape of the curve. Table 3.8 lists these coefficients for a number of soils; it may be mentioned that eq. (3.67) very well approximates the $\Phi(\theta)$ curve for almost every soil given in the table included here (within 3% inaccuracy). So under the assumptions mentioned above, an extremely simple relationship suffices to describe the transport of liquid in the soil.

This subsection's contents as expressed in CSMP statements is listed below. Additionally, a parameter SCALE is introduced to allow for easy changes in hydraulic scale, affecting moisture characteristic, conductivity and matric flux potential. The subject of scaling will be discussed in Chapter 4.

* soil water pressure

```
IF           (IFMFLP.EQ.1.AND.IFGRAV.EQ.0) GOTO 1080
DO 1035    I = 1,N
            WREL(I) = (W(I)-WRES(I))/(WSAT(I)-WRES(I))
1035    CONTINUE
            IF           (IFMFLP.EQ.1) GOTO 1050
            DO 1045    I = 1,N
            IF           (W(I).LT.W15(I)) GOTO 1040
            P(I)        = -(1./VGA(I))*(WREL(I)**(-1./VGM(I))-1.)**
                           (1./VGN(I))
            GOTO 1045
1040    P(I)        = RHOL*RGAS*(T(I)+TZERO)*(ALOG(RH(I)))/MH20
1045    CONTINUE
            DO 1047    I = 1,N
            P(I)        = P(I)/SCALE
1047    CONTINUE
```

```
* hydraulic conductivity; Van Genuchten-Mualem
1050 IF (IFKTB.EQ.1) GOTO 1060
      DO 1055 I = 1,N
            IF (W(I).LE.WRES(I)) K(I)=0.0
            IF (W(I).GT.WRES(I)) K(I)=KSAT(I)* ...
                  SQRT(WREL(I))*(1.-(1.-WREL(I)**(1./VGM(I)))) ...
                  **VGM(I)**2.
1055 CONTINUE
      GOTO 1070

* hydraulic conductivity from table
1060 DO 1065 I = 1,N
      K(I) = AFGEN(KTB,W(I))
1065 CONTINUE

* average conductivity
1070 KAV(1) = 0.0
      DO 1075 I = 2,N
            KAV(I) = SCALE*SCALE*SQRT(K(I-1)*K(I))
1075 CONTINUE
      IF (IFMFLP.EQ.0) GOTO 1100

* MFLP profile; rational expression
1080 IF (IFMTB.EQ.1) GOTO 1090
      DO 1085 I = 1,N
            MFLP(I) = -SCALE*MFA*(1.-W(I)/WMFO)/(MFB+1.-W(I)/WMFO)
1085 CONTINUE
      GOTO 1100

* MFLP from table
1090 DO 1095 I = 1,N
            MFLP(I) = SCALE*AFGEN(MTB,W(I))
1095 CONTINUE
```

```
*      liquid flux; K-p option
WFLLIQ(1) = 0.
IF          (IFMFLP.EQ.1) GOTO 1420
DO 1410    I = 2,N
WFLLIQ(I)  = -KAV(I)*((P(I-1)-P(I))/DZ(I)+RHOL*G)
1410    CONTINUE
GOTO 1460

*      liquid flux; MFLP option, gravity included.
1420    IF          (IFGRAV.EQ.0) GOTO 1440
DO 1430    I = 2,N
WFLLIQ(I)  = (MFLP(I)-MFLP(I-1))/DZ(I)-KAV(I)*RHOL*G
1430    CONTINUE
GOTO 1460

*      liquid flux; MFLP option, no gravity
1440    DO 1450    I = 2,N
WFLLIQ(I)  = (MFLP(I)-MFLP(I-1))/DZ(I)
1450    CONTINUE
```

3.6.3 Coupling: non-isothermal transport in the vapour phase; the formulation of $\rho_v(\theta, T)$

Vapour transport in the soil plays an important role in the surface energy balance in cases where evaporation takes place below the surface, but probably also for moist surface conditions at night, when condensation in the topsoil may occur.

This subsection expounds, in a comparison between 'thermodynamic' and 'mechanistic' formulations, how the driving force for vapour transfer in eq. (3.53)- i.e. the gradient of vapour density $\rho(\theta, T)$ - is formulated. In this treatment, again local thermodynamic equilibrium is assumed between water phases in the soil. Probably this is realistic with an exception for extremely high infiltration rates into coarse soils (Milly, 1982). Furthermore the total gas pressure of soil air is assumed to be atmospheric, although some caution must be taken on this point (subsection 3.6.4).

The density gradient of water vapour can be written as (Philip and De Vries, 1957):

$$(3.68) \quad \frac{d\rho_v}{dz} = \left(\frac{\partial \rho_v}{\partial T}\right)_\theta \frac{dT}{dz} + \left(\frac{\partial \rho_v}{\partial \theta}\right)_T \frac{d\theta}{dz} \quad (\text{kg m}^{-4})$$

with on the RHS respectively the so-called 'thermal' and 'isothermal' terms, which will be discussed below in this order.

Vapour density versus temperature

The Clapeyron equation for the liquid-vapour system (Kay and Groeneveld, 1974) states

$$(3.69) \quad \tilde{V} dp - \tilde{V} \tilde{dp} = (S - \tilde{S}) dT \equiv \Delta H_v \frac{dT}{T} \quad (\text{J kg}^{-1})$$

where \tilde{p} and p are the pressure in the vapour and in the 'extramatic' liquid phases, respectively, and \tilde{V} , \tilde{V} and S , \tilde{S} are the specific volume ($\text{m}^3 \text{ kg}^{-1}$) and partial specific entropy ($\text{J kg}^{-1} \text{ K}^{-1}$) for both phases respectively; ΔH_v is the latent heat of vaporisation (J kg^{-1}). For a more precise description of the phases of soil liquid see subsection 3.6.1.

For thermoosmosis, in this context the transport of vapour due to a temperature gradient under the condition $dp=0$, combination of the universal gas law with eq. (3.69) yields

$$(3.70) \quad \tilde{dp} = \frac{\Delta H_v \tilde{p} M}{2 RT} dT \quad (\text{Pa})$$

But since it is preferred to use the moisture content θ as the independent variable instead of p , one is interested in the situation where $\nabla\theta=0$ and $\nabla T \neq 0$. In analogy to the case treated in paragraph 3.6.1, the driving force $\nabla\tilde{p}$ then is not obtained exactly by eq. (3.70), since the gradient of the extramatic pressure, ∇p , is not defined to be zero for this situation. The term $\tilde{V}(\partial p/\partial T)$ as encountered when defining $\nabla\tilde{p}$ from eq. (3.69), however, is two orders of magnitude smaller than $\tilde{V}(\tilde{\partial p}/\partial T)$, so the former can virtually be neglected, and eq. (3.70) remains a valid approximation, also for $d\theta=0$. Thus in contrast to the discussion of the connection between mechanistic and thermodynamic formulations for the liquid phases, where ∇p and $\nabla p'$ had the same order of magnitude but opposite directions, one finds here that the two gradients ∇p and $\nabla\tilde{p}$ are of the same direction but of different order of magnitude, at constant θ .

Furthermore, differentiation of the gas law with respect to temperature results in the relation

$$(3.71) \quad \frac{\partial \rho_v}{\partial T} = \frac{M}{RT} \frac{\partial \tilde{p}}{\partial T} - \frac{\tilde{p} M}{RT} \quad (\text{kg m}^{-3} \text{ K}^{-1})$$

where ρ_v is the vapour density (kg m^{-3}), R is the gas constant ($\text{J mol}^{-1} \text{ K}^{-1}$) and M the specific molar mass of water (kg mol^{-1}). So the transformation of $\partial \tilde{p}/\partial T$ into $\partial \rho_v/\partial T$ involves a second term on the RHS of eq. 3.71, which is negligible under natural field conditions; it represents only approximately 5% of the first term. This explains the absence of the latter term in the analysis by Jury and Letey (1979). Now the combination of eqs. (3.70) and (3.71) gives, with the simplifications mentioned, the expression used by Jury and Letey (1979):

$$(3.72) \quad \frac{\partial \rho_v}{\partial T} \approx \frac{\Delta H_v \tilde{p} M^2}{R T^2} = \frac{\Delta H_v^* \tilde{p} M}{R T^2} \quad (\text{kg m}^{-3} \text{ K}^{-1})$$

(where ΔH_v is expressed in J kg^{-1} and ΔH_v^* in J mol^{-1}). The terms on the LHS and RHS of eq. (3.72), multiplied by ∇T , represent the driving forces in respectively the 'mechanistic' formulation (Philip and De Vries, 1957) and the 'thermodynamic' terminology (e.g. Cary, 1963) of the so-called thermal vapour flux.

Usually, as also in the present case, the derivative $(\partial \rho_v/\partial T)_\theta$ is calculated as $h(\partial \rho_{vs}/\partial T)$, where h is the relative humidity and ρ_{vs} is the saturated vapour density. This implies the assumption that the term $\rho_s(\partial h/\partial T)$ is negligible, as was also mentioned by Philip and De Vries. This is in accordance with results found by Cary et al. (1964) and Kijne and Taylor (1964), who showed that at constant gravimetric water content the relative humidity h changed by only 1-5% of its average value, for temperatures ranging from 15 to 35 °C (Figure 3.6). However, few experimental data are available to verify the general validity of this behaviour for soil materials.

In Appendix 3, Figure A3.1 visualizes the theory of coupling as treated above and in subsection 3.6.1.

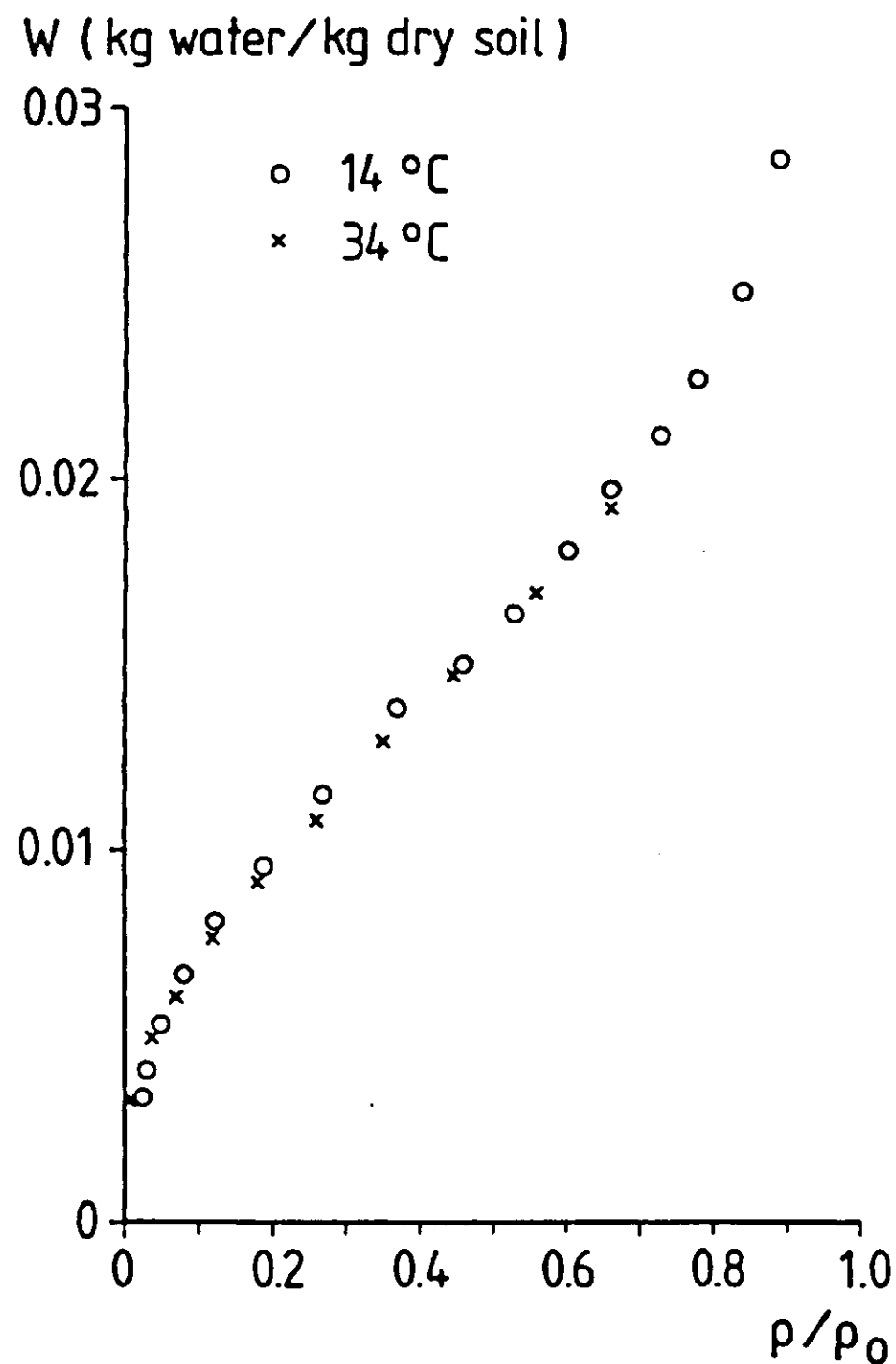


Figure 3.6 Adsorption isotherms for water on Millville silt loam at two temperatures, after Cary et al (1964).

Vapour density versus water content

At soil water pressures below -1.5 MPa, common at the soil surface, the decrease of relative humidity has a marked effect on vapour density in the soil atmosphere. Vapour fluxes then may be governed by the gradient in relative humidity and the second term in eq. (3.68) becomes important. Without this term, soils with a dry surface would not lose water during daytime, at least not by diffusion.

The derivative $\partial p_v / \partial \theta$ can be replaced by $\rho_s (\partial h / \partial \theta)$. In modelling, the relative humidity $h(\theta)$ is usually calculated by combination of the Kelvin equation:

$$(3.73) \quad h = \exp \left(\frac{\psi M}{RT} \right)$$

with a given moisture characteristic (ψ is the moisture potential in $J \text{ kg}^{-1}$). Here it is preferred not to do so, since the $p(\theta)$ curve often is based exclusively on measurements at higher θ -values and hence must be

extrapolated to the range of interest, where the curves are extremely steep. Instead, it seems more appropriate to employ adsorption isotherms of water to clay minerals, combined with an estimate of the clay content of the soil. Some of these adsorption isotherms are depicted in Figure 3.7, showing the characteristic sigmoidal shape found for soil materials (Thomas, 1928; Orchiston, 1954; Rose, 1971; Scotter, 1976).

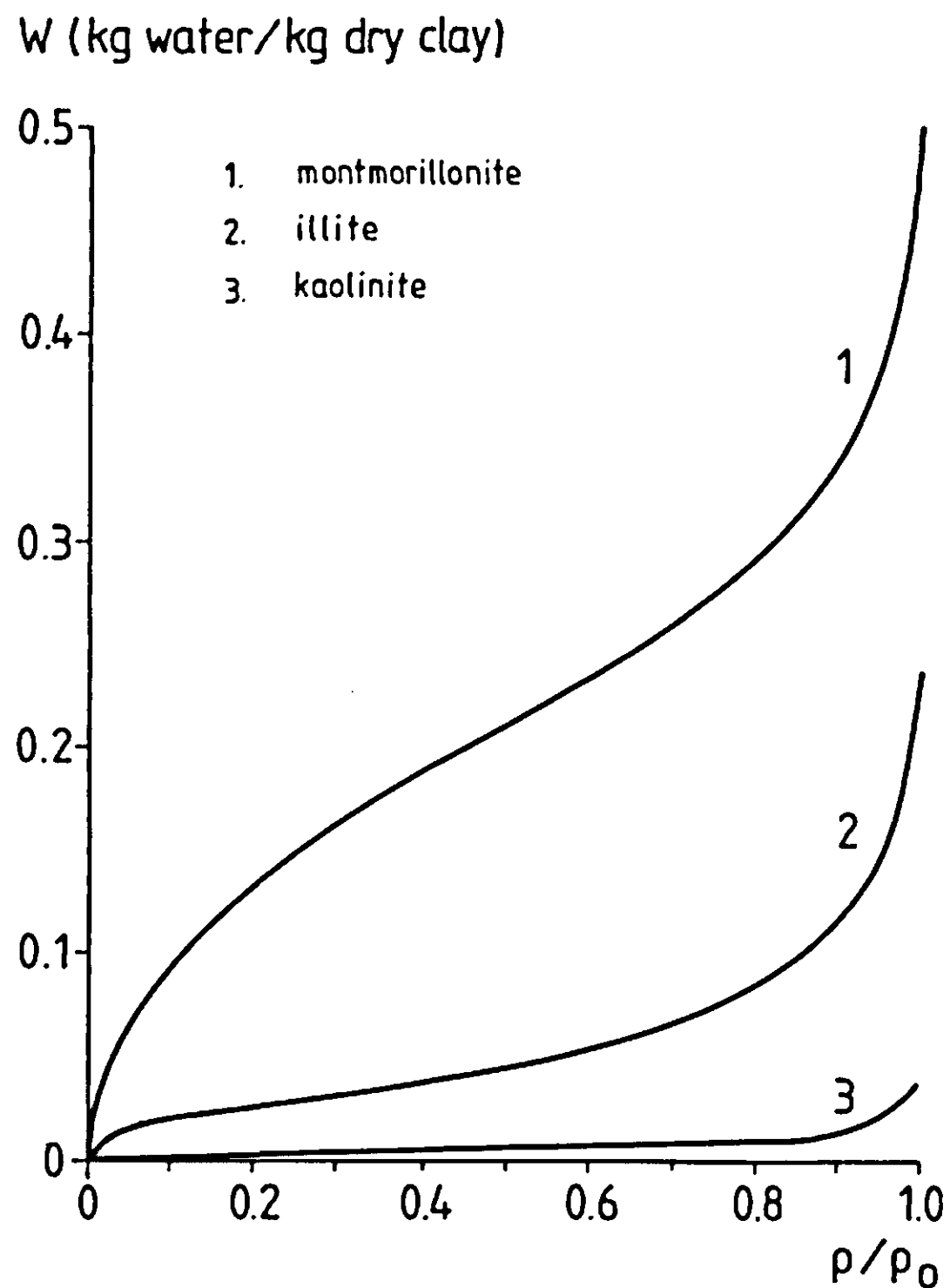


Figure 3.7 Adsorption isotherms for water on different clay minerals, after Orchiston (1954).

The clay content of soil materials largely determines the gravimetric water content at given relative humidity, as is well known from moisture characteristics. At low relative humidity ($h < 0.8$), the thickness of the water layer on the surface of clay platelets does not differ much from one clay mineral to another, although the species of adsorbed cations present may have a considerable influence (Table 3.9). In general, a monolayer of water molecules is thought to be adsorbed at $h = 0.2$, and twice the amount of water at $h = 0.6$ (Quirk, 1955; Orchiston, 1954; Vershinin et al., 1969).

The large differences in specific surface area of the various clay minerals, however, are reflected in the different isotherms. As is well known, the specific surface area of the different clays varies over about two orders of magnitude, in the following order: 5-50, 50-200 and 200-800 m^2g^{-1} for respectively kaolinite, illite and montmorillonite.

For application in the SALSA model, the exact shape of the isotherm is not relevant, and the curves are simplified to a set of linear segments, characterized by a single parameter A. This parameter represents the gravimetric moisture content (mass of liquid per mass of clay) at $h=0.8$. The corresponding volumetric water content is then calculated on the basis of the mass of clay per unit volume of bulk soil, and is here indicated by θ_{30} (-30 MPa being the pressure equivalent of a relative humidity $h=0.8$). A-values for different soil materials are listed in Table 3.9, along with the moisture content at $h=0.2$. It will be clear that also the influence of other adsorbing agents, e.g. hygroscopic salts, on the moisture regime can easily be taken into account in this manner.

Table 3.9 Characteristics of adsorption isotherms: gravimetric water content at relative humidities of 0.2 and 0.8.

	$h=0.2$	$h=0.8$	
	kg $\text{H}_2\text{O}/\text{kg dry soil}$		
loamy sand	0.01	0.025	Scotter, 1976
glauconite sand	0.015	0.06	Orchiston, 1954
Millville silt loam	0.010	0.024	Cary et al. 1964
Ca ⁺⁺ sat. chernozem	0.049	0.092	Vershinin et al, 1966
Hilo soil	0.05	0.12	Wadsworth, 1944
illite	0.05	0.08	Orchiston, 1954
clay	0.03	0.08	Scotter, 1976
Li-kaolinite	0.003	0.008	Jurinak, 1963
kaolinite	<0.005	0.005	Orchiston, 1954
montmorillonite	0.13	0.30	Orchiston, 1954
Ca-montmorillonite	0.12	.	Kijne, 1969
Na-montmorillonite	0.04	.	Kijne, 1969
Li-montmorillonite	0.13	.	Kijne, 1969
NH ₄ -montmorillonite	0.06	.	Kijne, 1969

As liquid pressure drops below -1.5 MPa ('wilting point', $h \approx 0.99$) relative humidity starts departing from unity and hence this point, indicated by $\theta_{1.5}$, is another mark to characterize the adsorption isotherm. So finally the model calculates $h(\theta)$ by the equations

$$(3.74) \quad h = \frac{\theta \rho_1}{f_c \rho_c} \frac{0.8}{A} \quad \text{for } 0 < \theta < \theta_{30}$$

$$(3.75) \quad h = 0.8 + 0.2 \left(\frac{\theta - \theta_{30}}{\theta_{1.5} - \theta_{30}} \right) \quad \text{for } \theta_{30} \leq \theta < \theta_{1.5}$$

$$(3.76) \quad h = 1.0 \quad \text{for } \theta_{1.5} \leq \theta$$

where ρ_1 is the specific density of the liquid and $f_c \rho_c$ the mass of clay per unit of bulk soil volume.

Isotherms by definition are valid for a specified temperature. The use of a given isotherm over a range of temperatures to calculate $h(\theta)$ therefore may raise some doubt. Nevertheless, as mentioned before in this subsection, experimental evidence suggests that $(\partial h / \partial T)_\theta$ is negligible and that the use of a single isotherm can be justified here.

In CSMP statements:

```
*      soil vapour state profile
1000   DO 1020      I = 1, N
          VPDS(I)      = AFGEN(VPDSTB,T(I))
          IF            (W(I).LT.W15(I)) GOTO 1005
          RH(I)        = 1.0
          GOTO 1015
1005   IF            (W(I).LT.W30(I)) GOTO 1010
          RH(I)        = 0.8 + 0.2*(W(I)-W30(I))/(W15(I)-W30(I))
          GOTO 1015
1010   RH(I)        = HRH(I)*W(I)*0.8
1015   VPD(I)        = RH(I)*VPDS(I)
1020   CONTINUE
          RHS          = RH(1)
```

3.6.4 The transport coefficient of water vapour in soil; enhancement effects

Diffusion enhancement

The transport of water vapour in soil is still subject to extensive discussion and the mechanisms involved are not fully understood yet. First, a short review on vapour diffusion is given, and subsequently some comments are made on convective mass transfer in the gas phase.

Originally, water vapour was viewed as an inert gas, the diffusion of which is determined by the concentration gradient and D_a , the diffusivity of vapour in free air (Krischer and Rohmalter, 1940):

$$(3.77) \quad j_v = - D_a v \alpha f_a \frac{dp}{dz} \quad (\text{kg m}^{-2}\text{s}^{-1})$$

where α , f_a , and v are correction factors for tortuosity, airfilled pore space and mass flow, respectively. Many experiments however have shown that the actual water vapour flux exceeds considerably the estimates made on the basis of molecular diffusion and the density gradient, determined by the bulk temperature gradient. This phenomenon is referred to as 'enhancement' of vapour transfer. Several explanations have been proposed. Philip and De Vries (1957), after distinguishing between a 'thermal' and an 'isothermal' component of the density gradient (eq. 3.68), suggested that enhancement is caused in the thermal term by two effects. One is the interaction between vapour and liquid; transport is increased by condensation on the 'warm' end of so-called 'liquid islands', accompanied by evaporation at the 'cool' end. The other effect would be the difference between local temperature gradient in the gas phase and the bulk soil temperature gradient. These authors formulated the thermal vapour flux by

$$(3.78) \quad j_v = - \left\{ (f_a + f(a)\theta) v \xi D_a \frac{\partial p}{\partial T} v \right\} \frac{dT}{dz} \quad (\text{kg m}^{-2}\text{s}^{-1})$$

and designated the term in major brackets as the 'thermal vapour diffusivity'. In the above equation, $f(a)$ is a function to account for liquid continuity, and ξ is a correction function for the local temperature gradient. Both $f(a)$ and ξ are defined more precisely but it is thought not relevant to cite the equations here.

Cary (1963), on the other hand, used a phenomenological coefficient β to account for all local interactions, without attempting to explain the enhancement phenomenon in further detail, and wrote the vapour flux as

$$(3.79) \quad j_v = -\beta D_a \frac{M_p}{R T} \frac{\Delta H_v^*}{2^3} \frac{dT}{dz} \quad (\text{kg m}^{-2}\text{s}^{-1})$$

(for the derivation and the use of symbols see subsection 3.6.3).

So β is simply the ratio of the measured vapour flux to the flux, calculated for molecular diffusion through free, saturated air under the same temperature gradient. Hence it not only accounts for the enhancement effects mentioned, but it also includes the corrections for pore space and path length.

The combination of eqs. (3.72), (3.78) and (3.79) shows that Cary's β should correspond to the term $(f_a + f(a)\theta)$ in eq. (3.78), and hence it can be combined directly with $D_a(\partial p_v / \partial T)VT$ to express the vapour flux density. Jury and Letey (1979) analysed, on the basis of this conclusion, experimental data from a number of sources. They showed that the Philip and De Vries formulation usually underestimates enhancement in the vapour phase, and elaborated further on the path length corrections. The coefficient nearly always appears to be greater than unity, whereas the corresponding term in the mechanistic formulation is reduced to values below one by the factor $f(a)\theta$. Measured β values seem to be fairly independent of moisture content as appears from the review by Jury and Letey (1979) (Table 3.10). Several models for the $\beta(\theta)$ relationship have been developed (Jury and Letey, 1979; Cary, 1979; Cass et al, 1984) but there is little agreement between them. In the present study, β is taken to be a constant, independent of θ .

The previous discussion regards 'thermal' vapour transfer only. Rose (1962a, b), however, suggested on the basis of experiments that the 'liquid island' enhancement mechanism is valid for isothermal diffusion as well. So based on the above, it seems warranted to combine Cary's β with the full density gradient in formulating the vapour flux by diffusion, as done in the SALSA model:

$$(3.80) \quad j_v = -\beta D_a(T) \frac{dp_v(\theta, T)}{dz} \quad (\text{kg m}^{-2}\text{s}^{-1})$$

Table 3.10 Reported values for the vapour diffusion enhancement factor β

Soil type	θ	ψ (mbar)	T($^{\circ}$ C)	β	source
Valentine sand	0.021	$2 \cdot 10^4$	41	1.53	Hanks et al, 1967
	0.045	$1 \cdot 10^3$	35	1.29	
	0.118	<100	30	1.06	
	0.328	<100	26	1.06	
	0.054	800	36	1.21	
	0.114	<100	35	1.15	
	0.154	<100	32	1.07	
	0.233	<100	29	1.11	
Jerome sandy loam	.	82	.	0.9	Nielsen et al, 1972
	.	310	.	1.4	
Portneuf silt loam	.	34	.	0.9	Nielsen et al, 1972
	.	270	.	3.8	
	.	550	.	3.1	
Rago silt loam	0.36	<10	41	0.75	Hanks et al, 1967
	0.071	$5 \cdot 10^4$	3	1.06	
	0.178	$2.7 \cdot 10^3$	33	0.95	
	0.236	950	30	1.08	
Columbia loam	.	66	7	1.80	Cary, 1965
	.	66	19	1.72	
	.	66	32	0.72	
	.	132	6	2.22	
	.	132	18	2.28	
	.	132	35	2.21	
	0.192	237	9	1.95	
	0.192	237	20	2.21	
	0.192	237	33	2.37	

Millville loam	0.159	540	15	2.87	Cary and Taylor, 1962a, b
	0.159	540	25	2.84	
	0.159	540	35	2.52	
	0.167	370	15	3.39	
	0.167	370	25	3.00	
	0.167	370	35	2.34	
<hr/>					
Pachappa loam	0.181	239	20	1.87	Weeks et al, 1968
	0.174	268	21	1.89	
	0.167	304	22	2.05	
	0.150	378	23	1.99	
	0.133	596	24	1.79	
<hr/>					
Silver Creek Silty clay	.	420	.	2.0	Nielsen et al, 1972
<hr/>					
Portneuf silt loam	0.00-0.35	.	32.5	0.4-2.1	Cass et al, 1984
Sand	0.01-0.19	.	32.5	0.4-2.0	
Sand	0.01-0.19	.	3.5	0.4-3.5	

(Most data in this table were collected and transformed by Jury and Letey, 1979, and by Nielsen et. al. 1972.)

Vapour flux enhancement by mass transfer

Thus far, the discussed theory has been restricted to diffusion. In addition the above, possibly two other enhancement mechanisms are acting in field situations. Hadas (1977) used the term 'mass transfer enhancement' to indicate their combined effect. The supposed mechanisms are forced convection of soil air by pressure fluctuations at the surface, and free or thermal convection under reversed temperature gradients.

Forced convective transfer was studied by Fukuda (1955), Scotter and Raats (1969), Kimball and Lemon (1971), and Farrell et al. (1966). The latter expressed the increase of effective vapour diffusivity as a function of soil air velocity and frequency of pressure fluctuations. The reported enhancement factors range from 1 for soil materials with particles smaller than 1 mm, to 2-4 for 5 mm aggregates, and up to a factor 100 for coarse

mulches (10 mm aggregates). These numbers may very well be of relevance to tilled soil.

Free convective transport was discussed by e.g. Hadas (1977a) and Menenti (1984). The former ascribed enhancement factors of about 3.5, derived by comparing day- and nighttime values of λ^* , to this process. For laboratory experiments, Hadas (1969) reported factors up to 5 for the combined effect of pressure and temperature fluctuations. Menenti extensively elaborated upon stability of soil air, making use of the critical Rayleigh number Ra_{cr} for different idealized cases. As shown by that author, free convection may start at different values of the Rayleigh number, depending on the chosen model. A difficulty encountered in the usual formulation of stability is the choice of a fixed gradient and corresponding characteristic length. By the nature of soil cooling, it seems promising to use instead the recently developed expressions for local stability in semi-infinite media, subject to surface cooling (Rudraiah et al. 1980; 1982). This has not yet been done in the present study.

Detailed verifications of enhancement effects for field situations are not available due to the complexity of the required measurements, but the subject certainly asks for more attention. Effective vapour diffusivity is one of the major factors affecting evaporation and surface temperature, as will be shown in Chapter 6, and at the same time one of the parameters that may be strongly influenced by soil management. The extensive and controversial discussion in literature regarding the effect of tillage and mulches on the surface energy balance, and particularly on evaporation, is partly due to the poor understanding of the processes mentioned above.

In the present model, mass enhancement is not formulated separately and must be effectuated by adaptation of the factor β , which then becomes a 'mixed' coefficient accounting for both diffusion enhancement and convective mass transfer.

These aspects of vapour transport are programmed as:

* effective soil vapour diffusivity profile
DO 1025 I = 1, N
 DATM(I) = DNOT*((T(I)+TZERO)/TZERO)**1.75
1025 CONTINUE

```
DO 1030      I = 2, N
              DAV(I)      = BCARY*(DATM(I)+DATM(I-1))/2
1030      CONTINUE
*
*      soil vapour flux
WFLVAP(1)    = -E
DO 1405      I = 2,N
              WFLVAP(I)    = DAV(I)*(VPD(I)-VPD(I-1))/DZ(I)
1405      CONTINUE
```

The total water flux is then given by

```
1460      DO 1470      I = 1,N
              WFLX(I)      = WFLLIQ(I)+WFLVAP(I)
1470      CONTINUE
```

3.7 Summary of option switches

The different option switches available in the SALSA model are summarized below; the names of the switches represent integer parameters, which can have a value of either 0 or 1:

IFBLD	: simulation of boundary layer development included (1), or not (0)
IFMFLP	: soil liquid transport expressed in terms of matric flux potential (1), or in terms of K-p (0)
IFMTB	: matric flux potential versus volumetric moisture content specified as a tabulated FUNCTION MTB = (1), or calculated by a rational function (0)
IFGRAV	: gravity term in soil water flow equation included (1), or not (0)
IFKTB	: soil hydraulic conductivity versus volumetric mois- ture content specified as a tabulated FUNCTION KTB = (1), or expressed in terms of Van Genuchten- Mualem parameters (0)
IFCHTB	: soil thermal conductivity versus volumetric moisture content specified as a tabulated FUNCTION CHTB = ... (1), or calculated by the De Vries model (0)

IFNET : course of net radiation imposed as measured boundary condition (1) or calculated as the sum of distinguished radiation terms (0).

CHAPTER 4. EXPERIMENTS

4.1 Introduction

Detailed field experiments to study the diurnal and spatial course of moisture content and temperature in bare topsoils have been performed in few cases only. The most extensive set of data available is that by Jackson and co-workers of the USDA Water Conservation Laboratory at Phoenix, Arizona. This group collected soil moisture and temperature data at small time- and depth intervals, along with meteorological data during several weeks in Spring 1971 (Jackson, 1973).

For the present study, two similar field experiments were conducted under different climatological and soil conditions, in order to obtain different independent data sets to be used for model validation trials. In 1982 an experiment was conducted in Oostelijk Flevoland, The Netherlands; a second experiment took place one year later in the USA (Texas). The 1982 experiment yielded two datasets, as the meteorological circumstances shifted markedly during the measurement period, dividing the results into two distinct series. Including the data by Jackson, a total of four different datasets from detailed bare soil energy balance experiments is therefore available to be discussed in this report: the Dutch sets FLEVO-1 and FLEVO-2 from a temperate region, and the sets TEXAS and ARIZONA from subhumid and semi-arid subtropical zones, respectively.

This chapter discusses the experimental setup, the type of measurements, the calculation procedures and the results for each of the field experiments. Summarized information on the ARIZONA data, as obtained from literature and personal communications, is also included. As the measurements will be used to compare model predictions with actual behaviour, the experiments are described here in terms of initial conditions, system parameters and functions, boundary conditions and 'output variables'.

The latter are the soil state variables, and the surface fluxes of heat and moisture; they are thus named since, in this context, they are to be predicted by simulation. Their measured values are not discussed here - they will be presented in Chapter 5, along with simulation results - but the measurement and calculation procedures and errors involved are treated in this chapter. The initial conditions are the profiles of soil state variables. At

the upper boundary of the system, incoming or net radiation, and rainfall (irrigation) determine the flux boundary conditions. Air temperature, humidity and windspeed at a given height above the soil surface are the state boundary conditions. The lower boundary conditions to the system are set by the fluxes of heat and moisture at a given depth. System parameters and functions express the soil radiative, thermal and hydraulic properties, and a soil-atmosphere exchange coefficient. Detailed specifications of equipment, measuring depths and heights, frequencies etc. for the subsequent datasets are listed in Appendix 8.

In all these experiments, soil behaviour was the principal subject of study. The atmospheric variables at screen height or lower were measured as boundary conditions. The data are not suited for checking models that include mixed layer development in the lower atmosphere, - such as the extended version of the SALSA model outlined in the previous chapter - because of the limited sizes of the experimental fields, and the lack of measurements at higher elevation above the surface.

4.2 Variability and errors

As model predictions are to be compared with observations, the uncertainties, both in measurements and in predictions, must be known. Comparisons between model performance and reality without specified errors, as often presented, have a rather limited significance at best. Before discussing the results of the measurements, some attention is paid therefore to error analysis. The term 'uncertainty' as used here refers to the expected deviation of a measured value at some point in the field from the actual value at the particular location for which a prediction is to be made. Clearly then, spatial variability may play an important role and must be studied when model predictions are to be compared with field observations.

In the present treatise, error variance is used as a measure of uncertainty. The next chapter shows how the total system error variance is composed of input measurement error variances on the one hand, resulting in prediction error variances, and 'output' measurement error variances on the other, and how these components are used in model validation. To the latter purpose, this chapter includes a brief discussion on errors in measured in- and output, i.e. errors in system parameters, boundary conditions and driving variables, and errors in fluxes and soil state variables, respectively.

Errors in measurement are due to calibration errors, to violation of certain assumptions underlying the experimental method, and to inertia of apparatus. Especially instantaneous values of boundary layer variables are sensitive to inertia problems. In the present experiments, all meteorological variables were integrated over half hour or one hour intervals, and it was assumed that the time-averaged values are representative for these intervals. Calibration errors were either known or estimated. Uncertainties due to erroneous model assumptions are often more difficult to deal with. An example is the measurement of thermal conductivity by means of the probe method in a field situation. In that case the contact resistance at the probe surface and inhomogeneity of the surrounding soil are discordant with the assumptions underlying the method. Also the measurements of hydraulic conductivity and matric flux potential curves are susceptible to this type of error. In such cases, error variance was estimated from a comparison between results obtained by different methods, or it was assumed that measurement errors are small in relation to field variability.

A special type of error variance is due to spatial variability. Since soil and atmosphere are laterally inhomogeneous, uncertainty is not only due to measurement errors, but also to the spatial dependence of the variable under consideration. For the boundary layer variables and radiation terms, this dependence was not measured and the simplifying assumption of lateral homogeneity is made. In soil physics and related fields, on the other hand, this problem of spatial variability has rapidly gained more attention during the last decade, and several techniques are now available to account for field variability of soil properties. For extensive reviews see Nielsen (1983) and Philip (1980). Two of these techniques, applied in this report, will be discussed briefly in the following: semivariance analysis and the scaling approach.

Semivariance analysis

Spatial variability analysis prior to detailed study of dynamic (i.e. time-dependent) soil behaviour can be useful to select sampling plots and to assess variability within these plots. Semivariance data were used to these purposes in the FLEVO and TEXAS experiments. Semivariance is defined as

$$(4.1) \quad \gamma(h) \equiv \frac{1}{2} \operatorname{var}(z(x) - z(x + h\Delta x))$$

where z is the value of the (soil) variable, x is the location, and h is the number of steps Δx between samples (Journel and Huijbregts, 1978). The estimator for semivariance used here is written as

$$(4.2) \quad \hat{\gamma}(h) = \frac{1}{2(N-h)} \sum_{i=1}^{N-h} (z(x_i) - z(x_i + h\Delta x))^2$$

where N is the number of observations. So the semivariance at level h is half the variance of the population of differences $(z(x) - z(x+h\Delta x))$ along a transect. It is an indicator of the spatial structure of the variable $z(x)$. It can be shown that $\gamma(h)$ is equal to the variance of variable z at level h in the case of second order stationarity, that is, when both the expectation and variance of z do not depend on the location. In that case one may write

$$(4.3) \quad \frac{1}{2} \text{var } (z(x) - z(x+h\Delta x)) = \frac{1}{2} (\text{var } z(x) + \text{var } z(x+h\Delta x)) - \\ - 2 \text{cov } (z(x), z(x+h\Delta x))$$

or

$$(4.4) \quad \gamma(h) = C(0) - C(h)$$

where $C(0) \equiv \text{var } z(x)$ and $C(h) \equiv \text{cov } (z(x), z(x+h\Delta x))$. Consequently, for $h\Delta x$ equal to the minimum sampling distance ($h=1$), $\gamma(h)$ appears to be the 'restvariance' of variable z : it represents the variance due to measurement errors and to spatial structure within the minimum sampling distance. As a by-product of semivariance analysis, this restvariance comes in very opportunely for the intended error variance analysis; the major aim of the semivariance study, however, is to reveal information about the spatial structure of soil properties over the field as a whole, which can be used as a basis for the selection of plots to study the (dynamic) behaviour of the soil in more detail. Both these aspects have been employed in the design of the discussed field experiments.

Scaling of hydraulic properties

The concept of scaling was developed in microhydrology to relate transport phenomena in media that have identical pore geometries, except for a multiplication factor called 'scale length'. Supposing this similitude of media

is valid, the water pressure potential for a particular medium is then derived from that of a reference medium at the same water content, and the involved scale length. For some well defined problems, solutions of the water flow equation can then be scaled by dimension analysis. For a detailed discussion see Miller (1980). Later, scaling on the basis of the similitude hypothesis was also applied to express field heterogeneity of soil hydraulic properties and soil water profiles during infiltration. Philip (1967) introduced the term scale heterogeneity to confine field heterogeneity to that specific class of variability that can be handled by scaling.

A clear picture of the scaling technique applied to the field heterogeneity problem was given by Warrick and Nielsen (1980). In general, scaling is effectuated by assigning a factor α_r to a particular point r such that the local hydraulic properties may be translated into a scaled value by multiplication with α_r^n . So one finds that $p_{sc} = \alpha_r^n p_r$, where p_r is the observed pressure for a given water content, and p_{sc} is a field averaged pressure at that particular water content. It can be shown that for similar media the scaled hydraulic conductivity must be expressed as $K_{sc} = \alpha_r^{-2} K_r$ (e.g. Warrick and Amoozegar-Fard, 1979). It follows then directly that the Kirchoff transform - which will be used later in this report - defined as:

$$(4.5) \quad \Phi \equiv \int_{p=-\infty}^0 K(p) dp$$

in a scaled form should be written as $\Phi_{sc} = \alpha_r^{-1} \Phi_r$. See also subsection 3.6.2. In describing lateral field heterogeneity, it is supposed that α_r is a site specific constant, valid for all values of water content and for all depths.

Rao et al. (1983) recently discussed the validity of the assumptions underlying the scaling technique in an extensive evaluation of the approach to field variability. They concluded that in their datasets three basic requirements were not met: (1) saturated water contents were not the same for all sites, (2) the values of the scaling factor, derived from different measured hydraulic properties, were not the same, and (3) the values of the scaling factor were not depth-independent. On the other hand, as they stated, Warrick et al. (1977) and Simmons et al. (1979) did not find this disagreement.

In this study the scaling factors for hydraulic conductivity and for moisture retention curves are supposed to be equal. In addition, a type of

'geometry scaling' has been introduced by using θ/θ_s , the moisture content relative to saturation, in the scaling procedure, instead of θ itself.

Scaled solutions would be attractive since they offer the possibility to translate the result of a single simulation run directly into solutions for similar media. It is noted here that even if soil materials at different locations differed only by a scale length parameter, probably no advantage could be taken in the present case from fully scaled solutions of the transport processes. The naturally imposed boundary conditions are variable in time. This is due to the diurnal course of evaporation and to coupling between heat and vapour transport. Then, as time is also scaled in the process, each value of the scale length would be connected to its own defined frequency of the imposed boundary conditions. Moreover, scaling of the flow equation might not be possible in the presence of coupling.

Irrespective of the above, scaling remains an effective tool for data compression; the frequency distribution of the scaling factor as derived from moisture retention curves is used both for field data representation - in the cases of the FLEVO and TEXAS experiments - and for the calculation of prediction error variances in modelling; (the latter by incorporating the scale factor in the numerically solved water flow equation).

4.3 Location and general conditions

The site of the FLEVO measurements was located in the polder Oostelijk Flevoland at the Ir. A.P. Minderhoudhoeve, an experimental farm of the Wageningen Agricultural University. Figure 4.1 shows the layout of the experimental field. Slight changes in soil texture were observed within the field, dividing it in areas of somewhat different hydraulic and thermal behaviour. The soils were named Swifterbant silt loam and Swifterbant loam respectively, although texture differences barely met the requirements for this distinction. The courses of two texture fractions along one of the indicated transects over the field are shown in Figure 4.2. Figure 4.3 gives the corresponding semivariograms. The soil surface was levelled by rolling the moist soil in Spring directly after superficial tillage.

Measurements of soil state variables were collected from plots, of which plots 3 and 4 (figure 4.1) were situated on loam soil, and 1 and 2 on silt loam, each plot measuring 4x4 m. These sites were located on the basis of a spatial variability study of moisture retention and texture data along

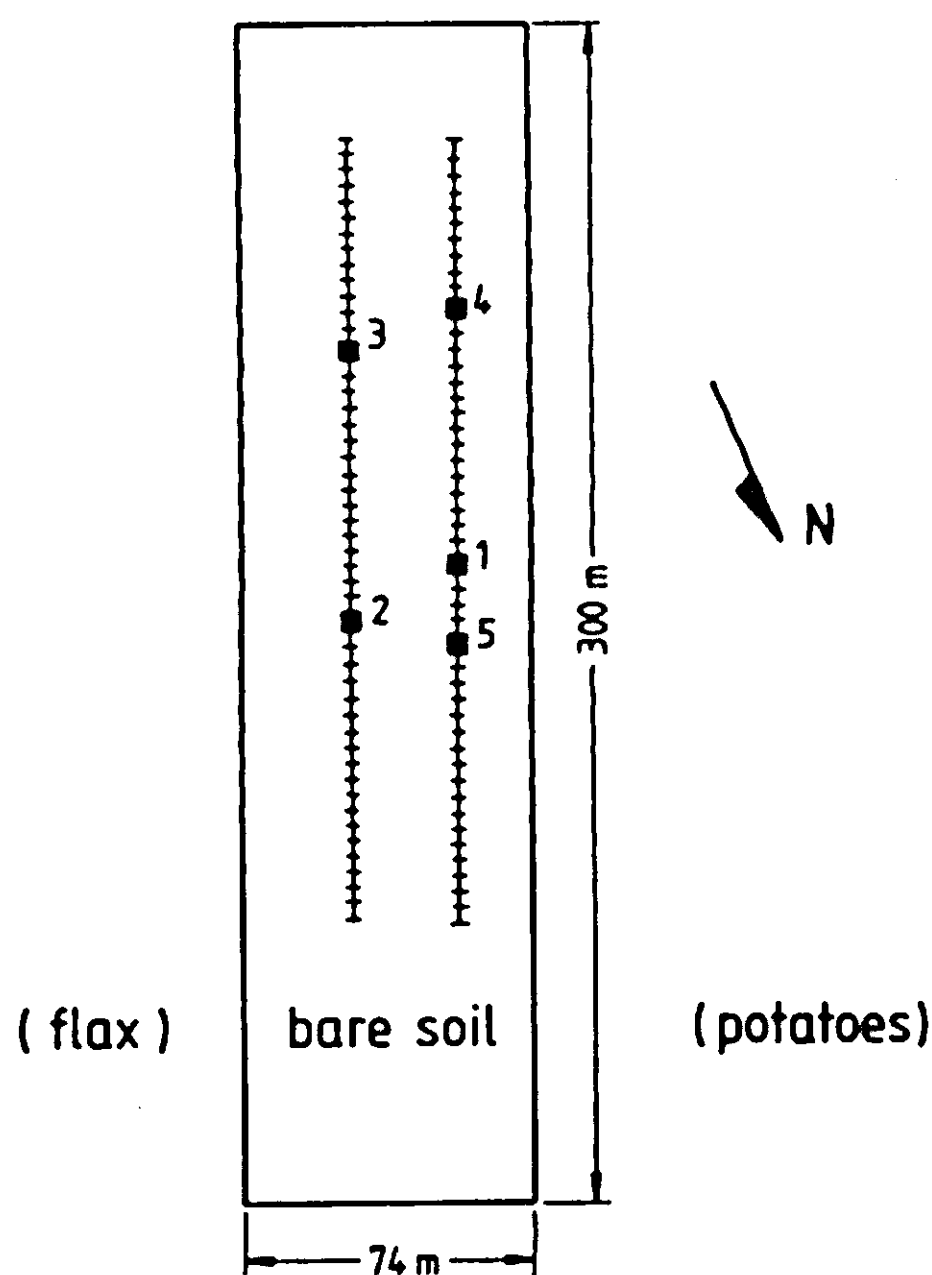


Figure 4.1 Design of the experimental field at the Ir. A.P. Minderhoudhoeve, Swifterbant, O.Flevoland. Numbers refer to plots for detailed measurements. Also indicated are the two transects with 50 observation spots each.

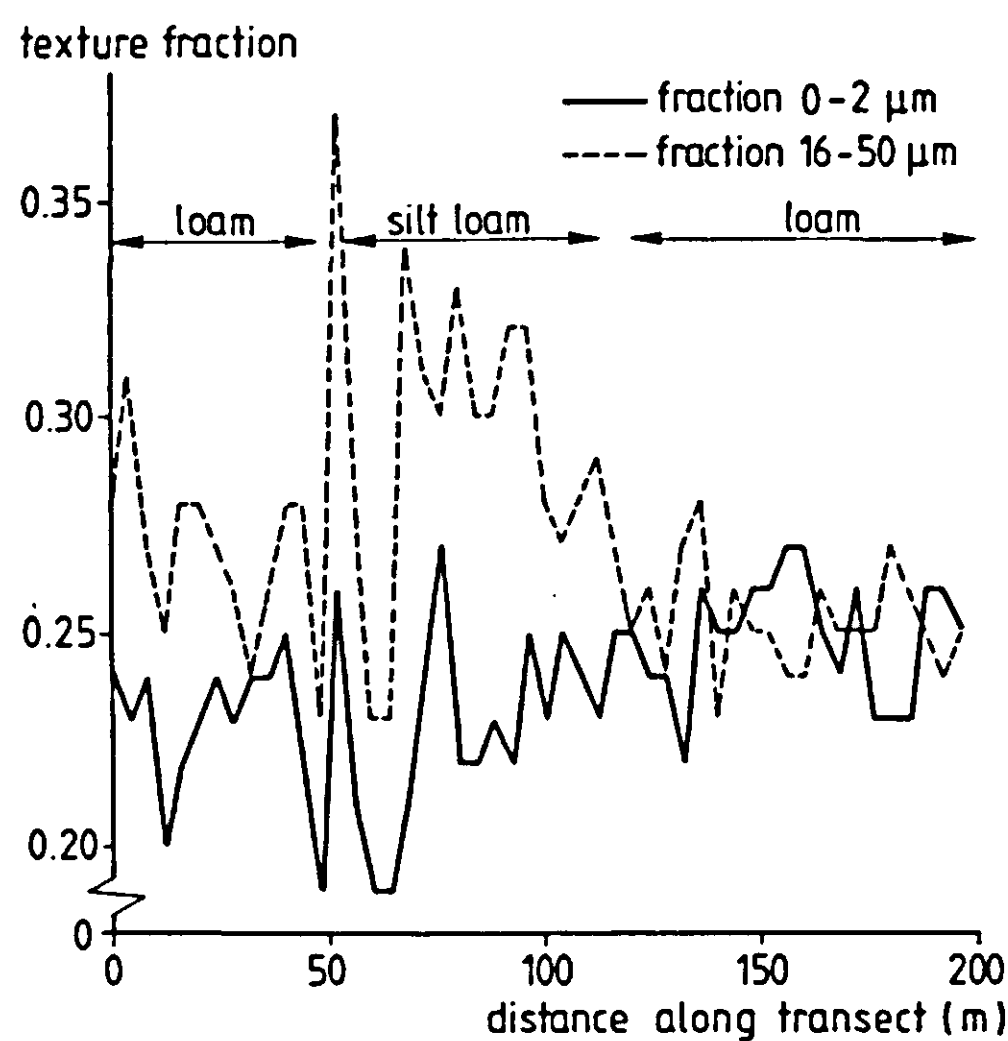


Figure 4.2 The course of two texture fractions along a transect running lengthwise over the field at Swifterbant.

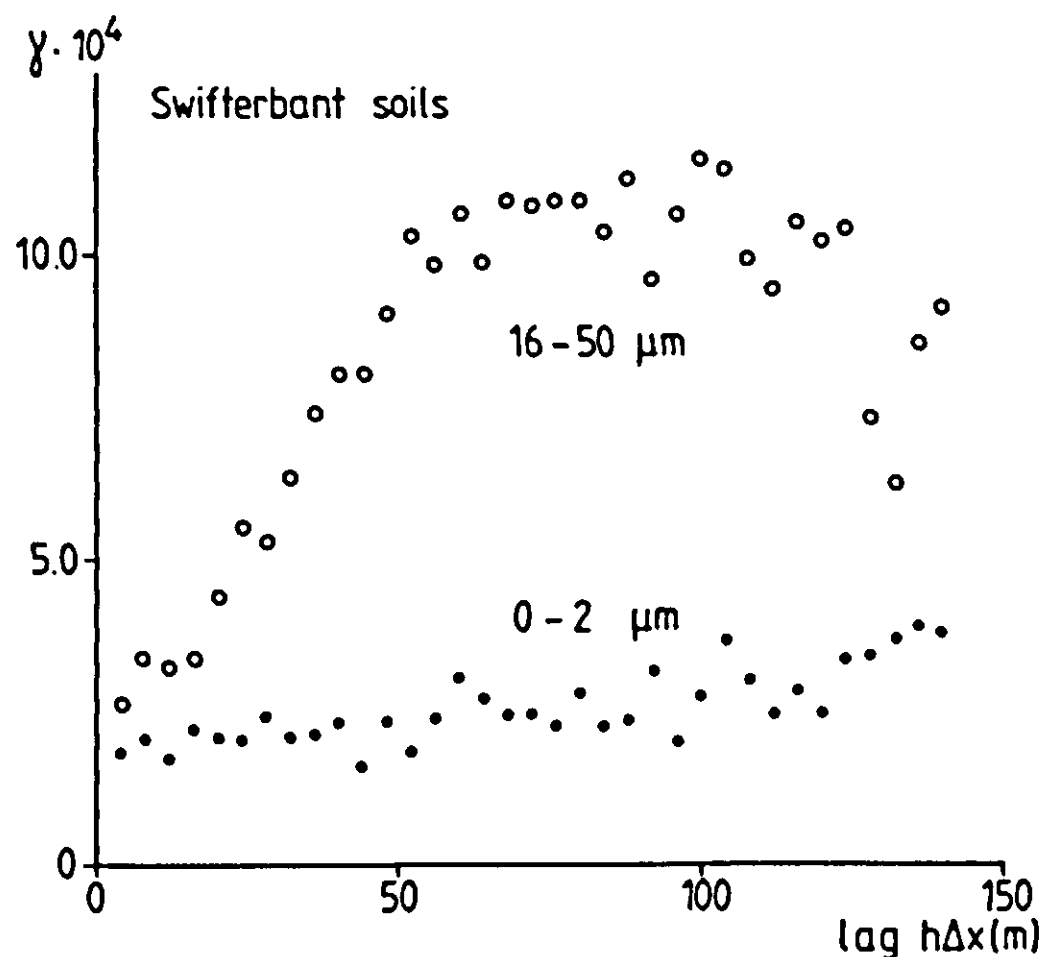


Figure 4.3 Semivariograms for two texture fractions.

the transects shown in Figure 4.1 (Ten Berge et al., 1983). As the minimum sampling distance along these transects also was 4 m, the semivariograms could be used to determine the momentary variance of the observations within the four plots, which is identified as the error variance (see previous section). Although strictly speaking this is correct only in the idealized case of isotropy and second order stationarity, an estimate of the variance is obtained in this way. In this report, time series of soil variables only from plots 1 (silt loam) and 4 (loam) are treated, as these plots represent the extremes occurring in the experimental field.

The 1982 campaign covered the period from May 28 to June 28. This period was characterized in the first two weeks by highly evaporative conditions, following an initially wet situation. During the second half of the experiment, low radiation, high humidity and scattered rain were predominant. For this reason, the two different sequences FLEVO-1 and FLEVO-2 are distinguished as separate sets.

The Texas field experiment was a joint effort with Texas A&M University. The campaign extended over five days, from June 21 to June 25, 1983. Figure 4.4 shows the experimental plot at Buffalo Ranch, situated near Snook, Texas. The soil is referred to as Buffalo silty clay. Analysis of the spatial structure of soil texture, measured at 100 sites, yielded the semivariograms shown in Figure 4.5. After Spring tillage, the soil was left

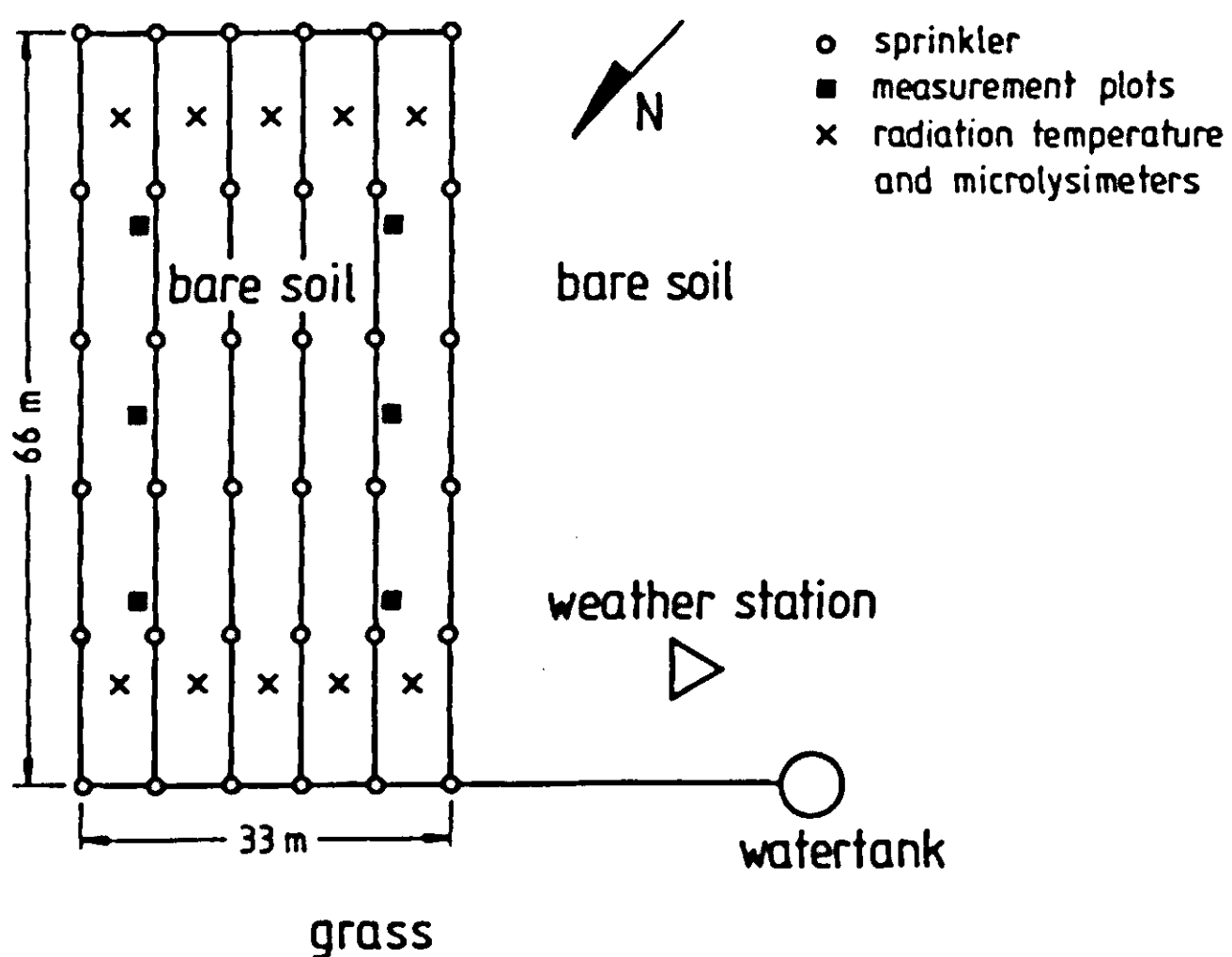


Figure 4.4 Design of the experimental plot at Buffalo Ranch, Snook, TEXAS.

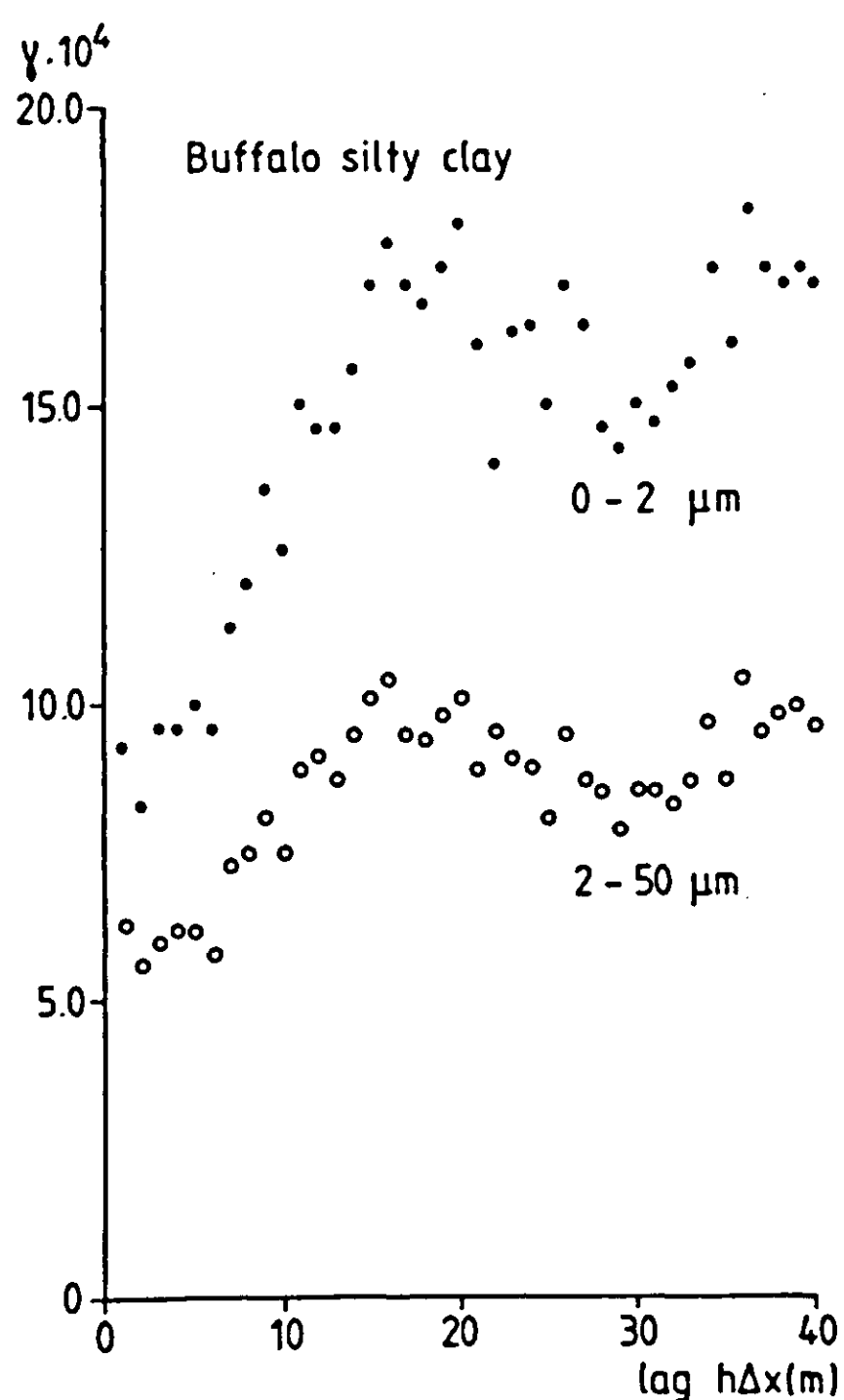


Figure 4.5 Semivariograms for two texture fractions in the TEXAS experiment.

fallow for two months. By the time of the experiment, the surface had smoothed by slaking from showers. The measurements commenced on a fairly dry soil; after two days, the field was flooded at midnight, and measurements were continued next morning to follow the drainage and drying phase. Figure 4.5 shows a range of 20 m for both texture fractions, implying that at distances of about 20 m, observations on these properties can be considered independent of one another, on the scale of the field observation. Based on this, the six plots for detailed study of dynamic soil properties were spaced approximately 20 m apart. In contrast to the FLEVO case, differences in soil behaviour between plots were small. Therefore the data from the six plots were pooled, and only averages and variances are reported to represent the field as a whole. So an estimate of the total variance $C(0)$ is used for the TEXAS field, whereas the 'reduced' variance $C(0)-C(h)$ is used for the FLEVO site because of the strong spatial structure in the latter case.

Only a summarized description of the ARIZONA experiment is given, merely to illustrate the assumptions on the dataset used in the next chapter. For more extensive treatments see Jackson (1973), Nakayama et al. (1973), Jackson et al. (1974), Idso et al. (1974), Idso et al. (1975) and Kimball et al. (1976), and Appendix 8. Several drying runs were executed in the 1970 and 1971 campaigns. In this report, only the data from March 8-11, 1971 are used. The experimental plots were located on a 72 x 90 m field of Avondale loam. The soil profile was supposed to be uniform down to a depth of 1 m. Three weighing lysimeters were available in the field, two of which were irrigated along with the rest of the field with 100 mm of water at the start of the experiment. Assumptions with respect to error variance are based on the FLEVO and TEXAS experiments.

4.4. Boundary conditions: the fluxes

Radiation

A choice may be made as to which radiation flux is used as the driving variable in the modelling effort. If global and sky radiation are used to determine the energy flux boundary condition, net radiation is viewed as an 'output' variable. If on the other hand net radiation is used, it must be realized that this term is influenced by the system one wishes to model. The radiation terms measured are treated briefly in the following.

During the FLEVO experiment, global radiation, reflected shortwave ra-

diation and net radiation were measured as integrated values over half hour periods. Daily totals of global radiation ranged between 21.5 and 23.5 MJ m⁻² day⁻¹ for set FLEVO-1, and between 14.5 and 16.5 MJ m⁻² day⁻¹ for the second period (the FLEVO-2 set).

Also at the TEXAS site, global and net radiation and reflected shortwave radiation were measured, in this case integrated over one hour time periods. Global radiation daily totals ranged from 20.7 to 25.3 MJ m⁻² day⁻¹. Daily totals of net radiation were between 8.1 and 13.1 MJ m⁻² day⁻¹.

In the ARIZONA dataset, four radiation terms are available: global radiation, reflected shortwave radiation, 'all wave' incoming radiation, and net radiation. The following daily totals characterize the prevailing conditions: global radiation 18.6-25.8, 'all wave' radiation 44.6-51.0, and net radiation 5.5-10.8 MJ m⁻² day⁻¹.

For all datasets, net longwave sky radiation $(1-\rho_1)R_{ld}$ can be estimated by using the relation

$$(4.6) \quad R_n = (1-a)R_{glob} + (1-\rho_1)R_{ld} + R_e$$

where ρ_1 is the surface reflectivity for longwave radiation and the subscripts n, glob, ld and e refer to net, global, longwave downward and emitted radiation terms respectively. The latter term is estimated as $R_e = -\epsilon\sigma T_s^4$, where the surface temperature T_s is in Kelvin, σ is the Stefan-Boltzmann constant, and ϵ the surface emissivity. Only for the ARIZONA dataset it is possible to separate incident and reflected longwave sky radiation from the measured data, making use of the additional relation

$$(4.7) \quad R_{ld} = R_{ad} - R_{glob}$$

where the first term on the RHS is the measured 'all wave' radiation; so the surface reflectivity for longwave radiation can also be derived.

For all radiation terms measured in the FLEVO, TEXAS and ARIZONA experiments, error variance is calculated from an estimated 5% coefficient of variation in the recorded signals. Figures 4.6-4.9 depict the courses of global radiation for the various experiments. As net radiation will be used in the TEXAS case as a driving variable, its path is shown as well in Fig. 4.8. The same applies to the longwave radiation term in the ARIZONA experiment. Net radiation for the FLEVO and ARIZONA sets will be shown in Chapter 5 as an output variable.

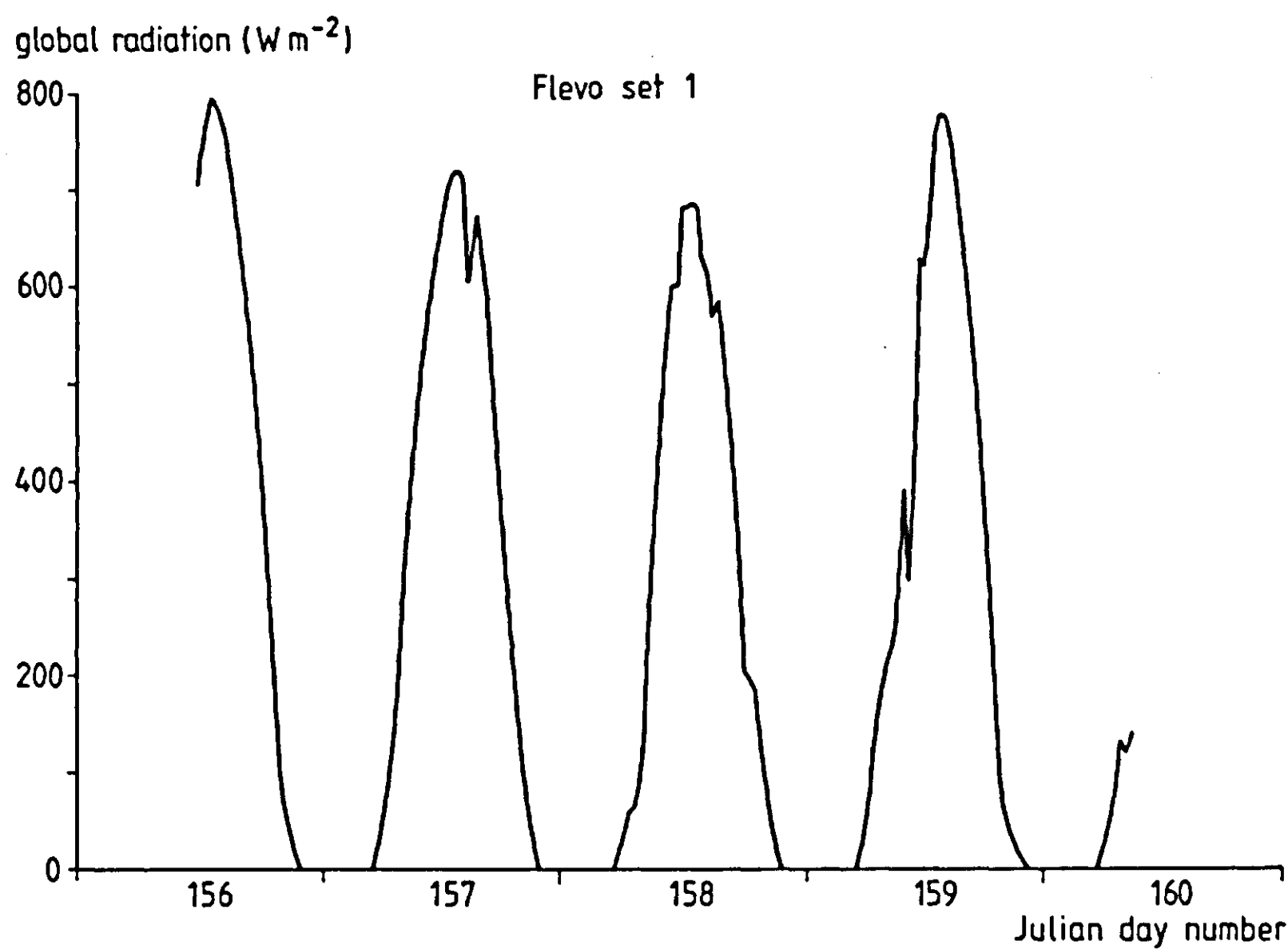


Figure 4.6 Measured global radiation, FLEVO set 1.

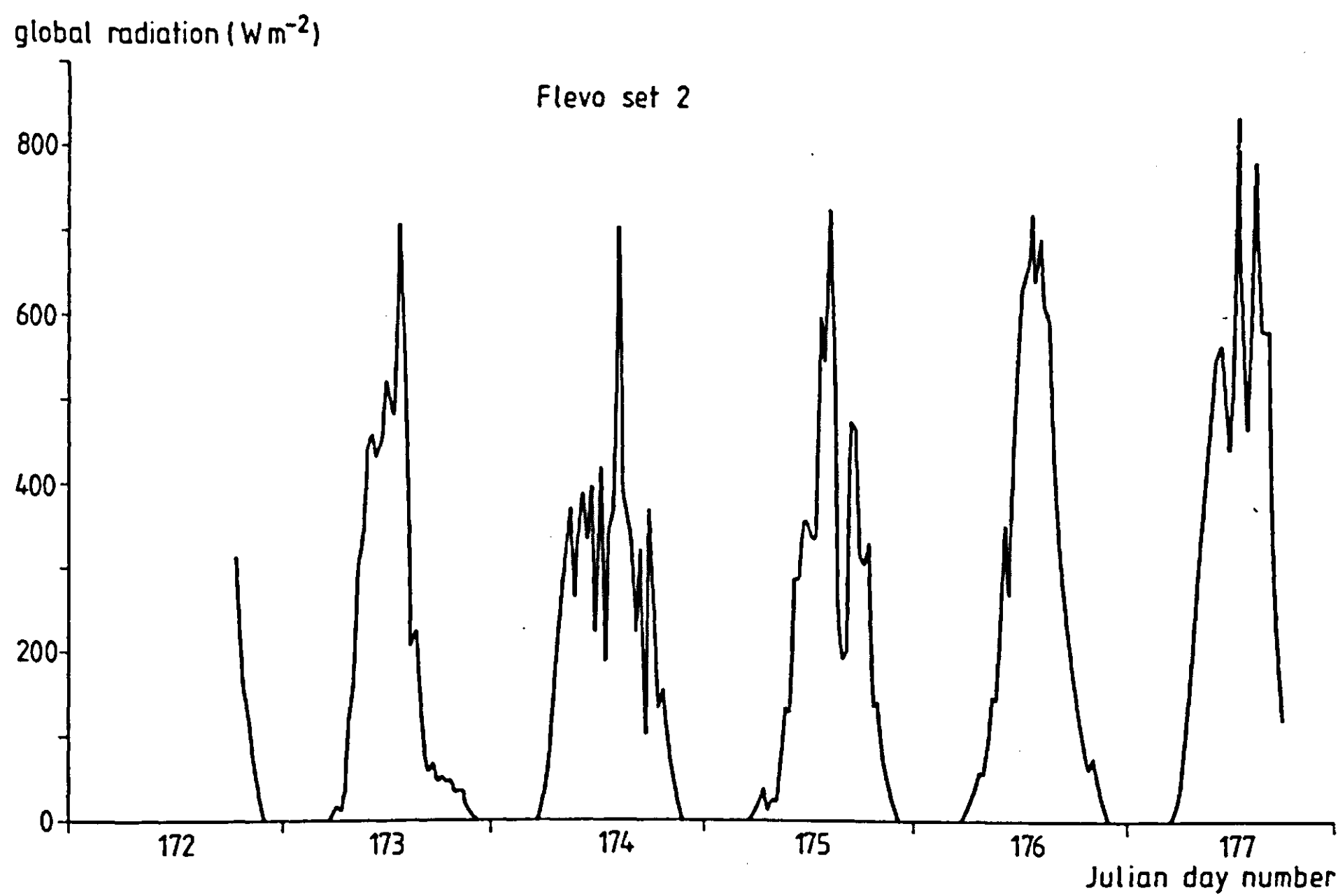


Figure 4.7 Measured global radiation, FLEVO sets 2.

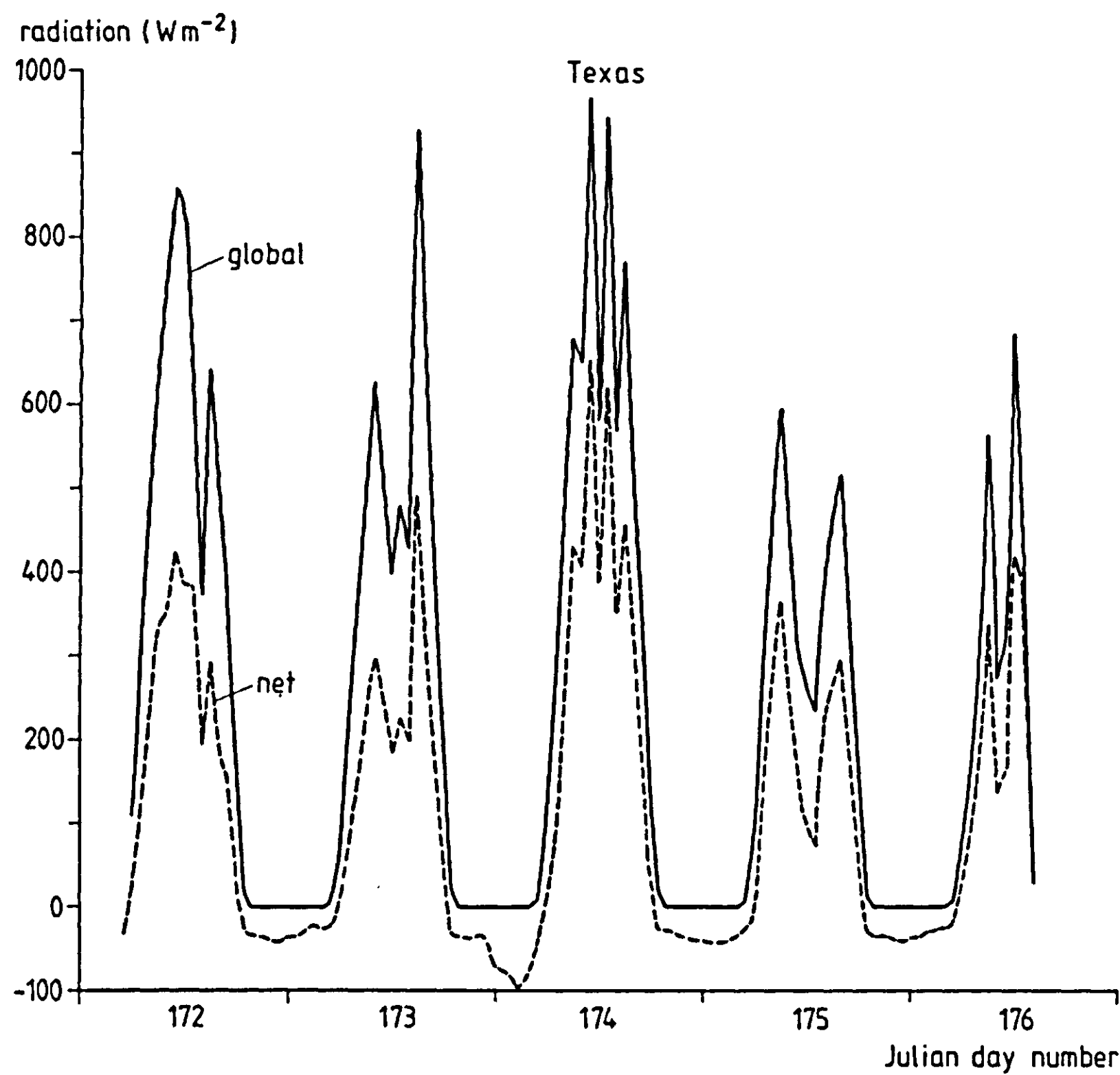


Figure 4.8 Measured radiation terms, TEXAS. (Net radiation is given as well since it will be used as a boundary condition in Chapter 5).

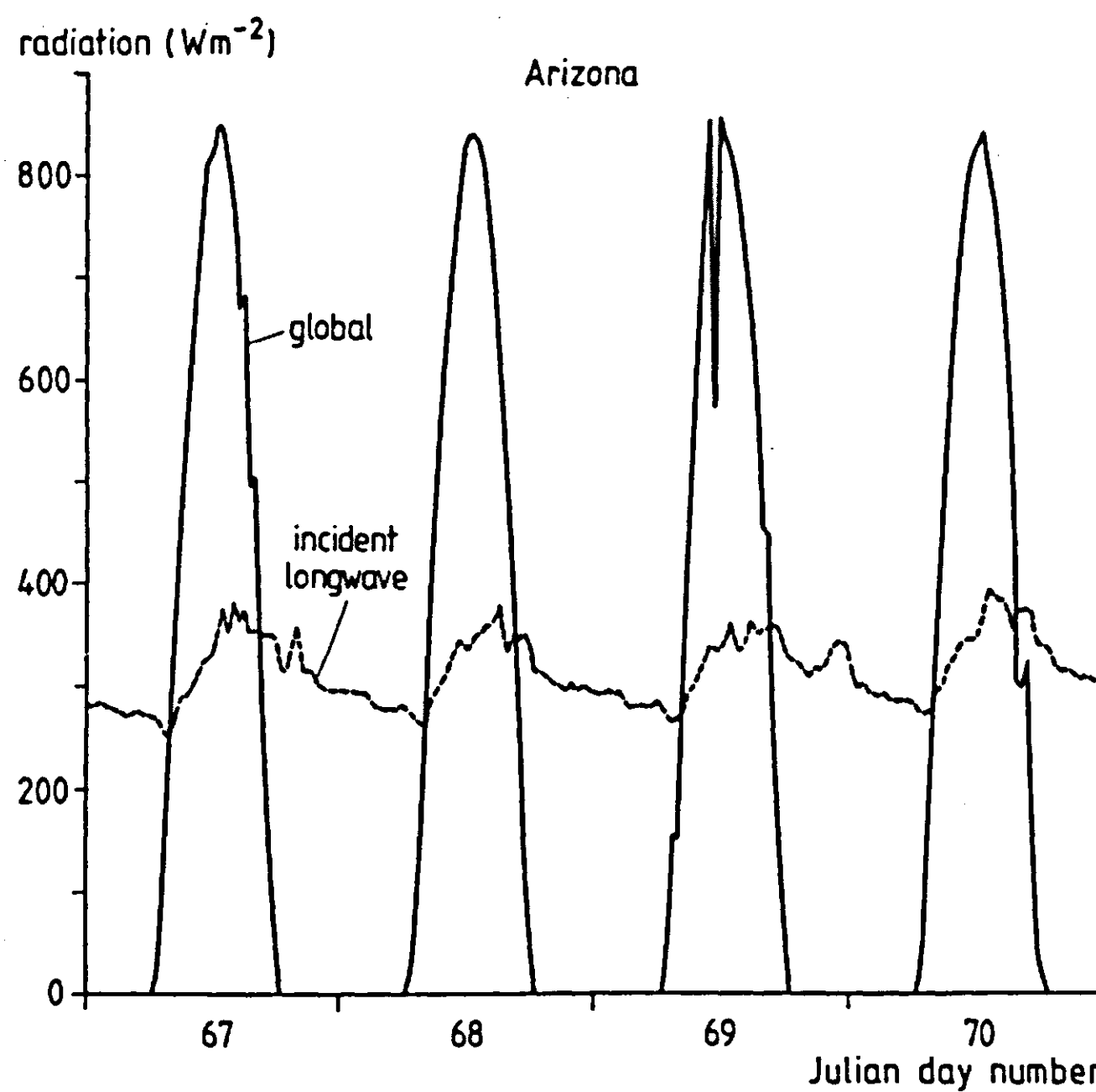


Figure 4.9 Measured radiation terms, ARIZONA.

Water

Rainfall occurred during the FLEVO experiments only in the second period, when a total of 33.4 mm was measured.

At the TEXAS site, water was distributed by sprinklers (Figure 4.4). On June 24, a shower added another 7.2 mm.

In the ARIZONA case, no water was supplied after initial wetting, so an influx of water as a driving variable was absent.

4.5 Boundary conditions: the state variables

Air temperature, vapour pressure and wind speed at 0.5 m height were measured as boundary conditions in the FLEVO experiment (Figure 4.10 and 4.11). Depending on the prevailing wind direction, the masts for profile measurements were moved so that a maximum fetch (ranging from 74 to 300 m length) over the bare soil surface was provided. It was assumed that these measurements represented the whole field, in spite of soil heterogeneity. Error standard deviations in dry and wet bulb temperatures were 0.1 K. This corresponds to an error of 15 Pa for the vapour pressure. The coefficient of variation in the wind speed data amounted to 4%. At the lower end of the soil profile (0.5 m), temperature and water potential were nearly constant. Temperature showed a slight trend of 1 K/week for both sets FLEVO-1 and FLEVO-2, due to seasonal warming.

Upper boundary conditions in the TEXAS set are vapour pressure, air temperature, and wind speed at 2 m height (Figure 4.12). Since the measurement of wind speed presented some problems during several time intervals, an average daily course has been calculated, which is supposed to apply to all measurement days. Soil moisture content was measured down to 0.5 m and temperature down to 1.0 m depth. The values of both these state variables were constant during the experiment.

For the ARIZONA experiment, daily averages for the different boundary conditions shifted considerably during the experimental period. Generally, vapour pressure was lower than for the other experiments. Vapour pressure, air temperature and windspeed were measured at various heights; the 0.5 m values, used as boundary conditions in this study, are shown in Figure 4.13. Soil temperature and moisture content were measured down to depths of 1.28 and 1.0 m respectively, and were constant at these depths. Errors in the measured values of atmospheric variables in the TEXAS and ARIZONA cases were taken identical to those specified for the FLEVO sets.

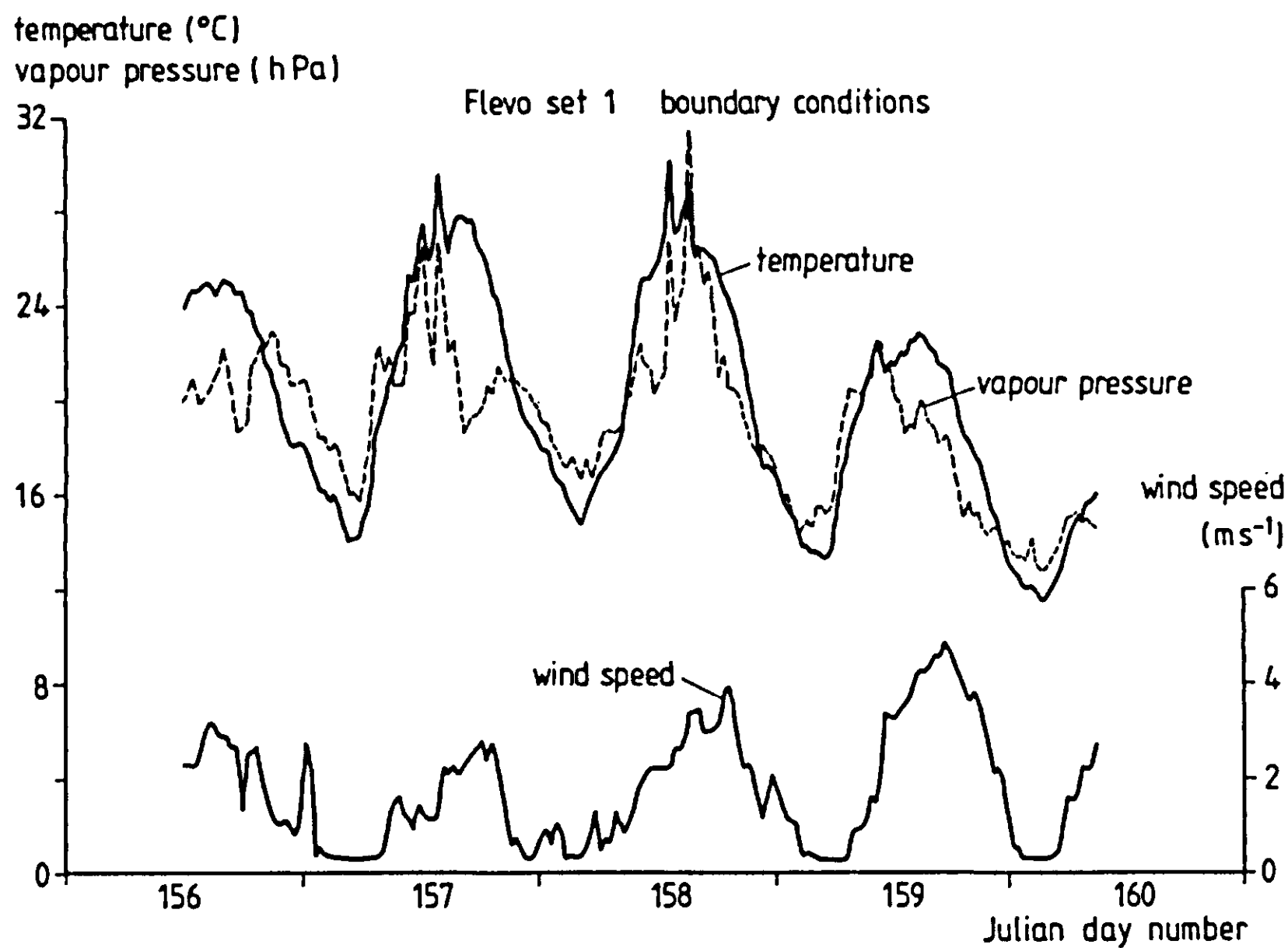


Figure 4.10 Atmospheric boundary conditions, measured at 0.5 m, FLEVO-set 1.

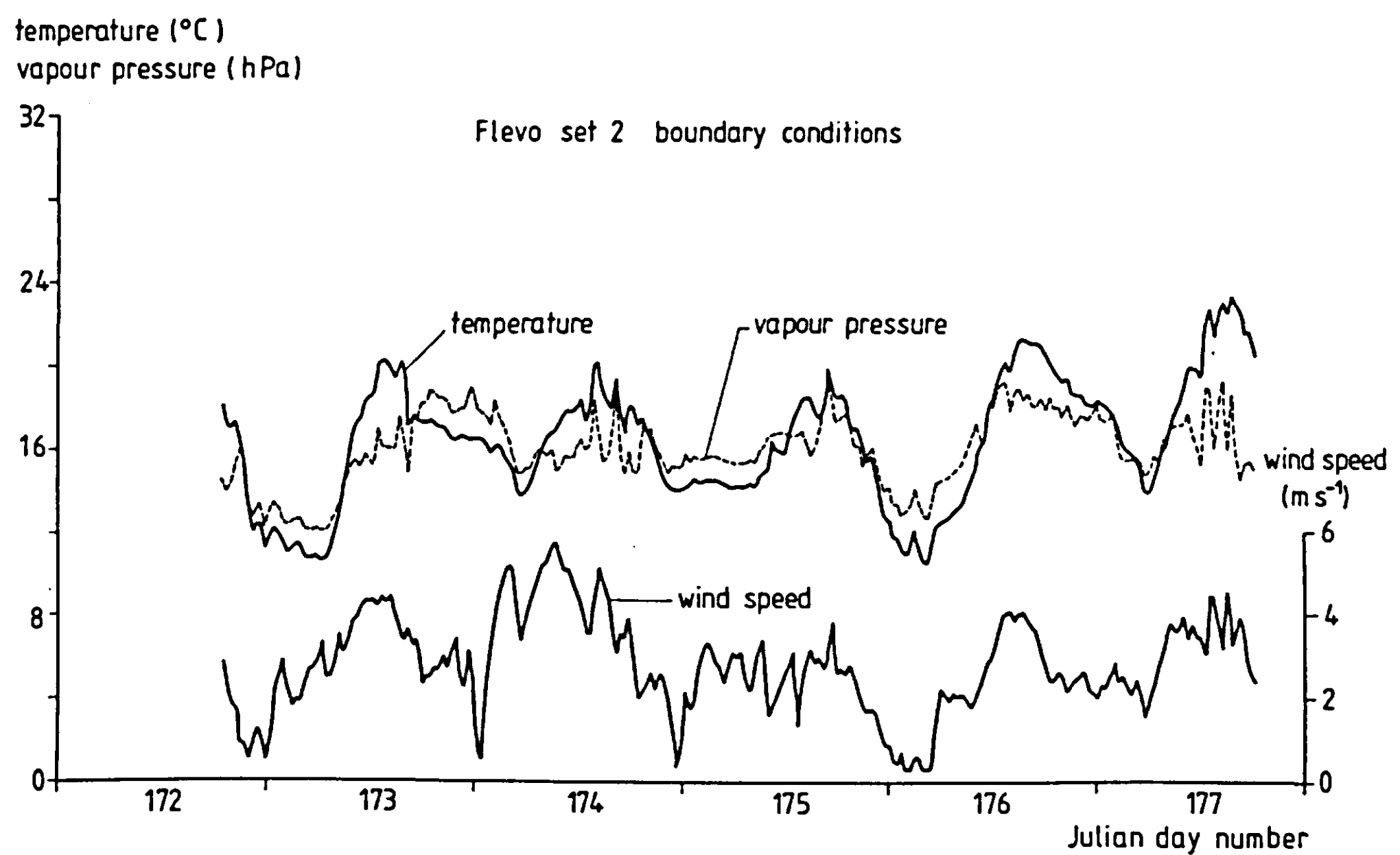


Figure 4.11 Atmospheric boundary conditions, measured at 0.5 m, FLEVO set 2.

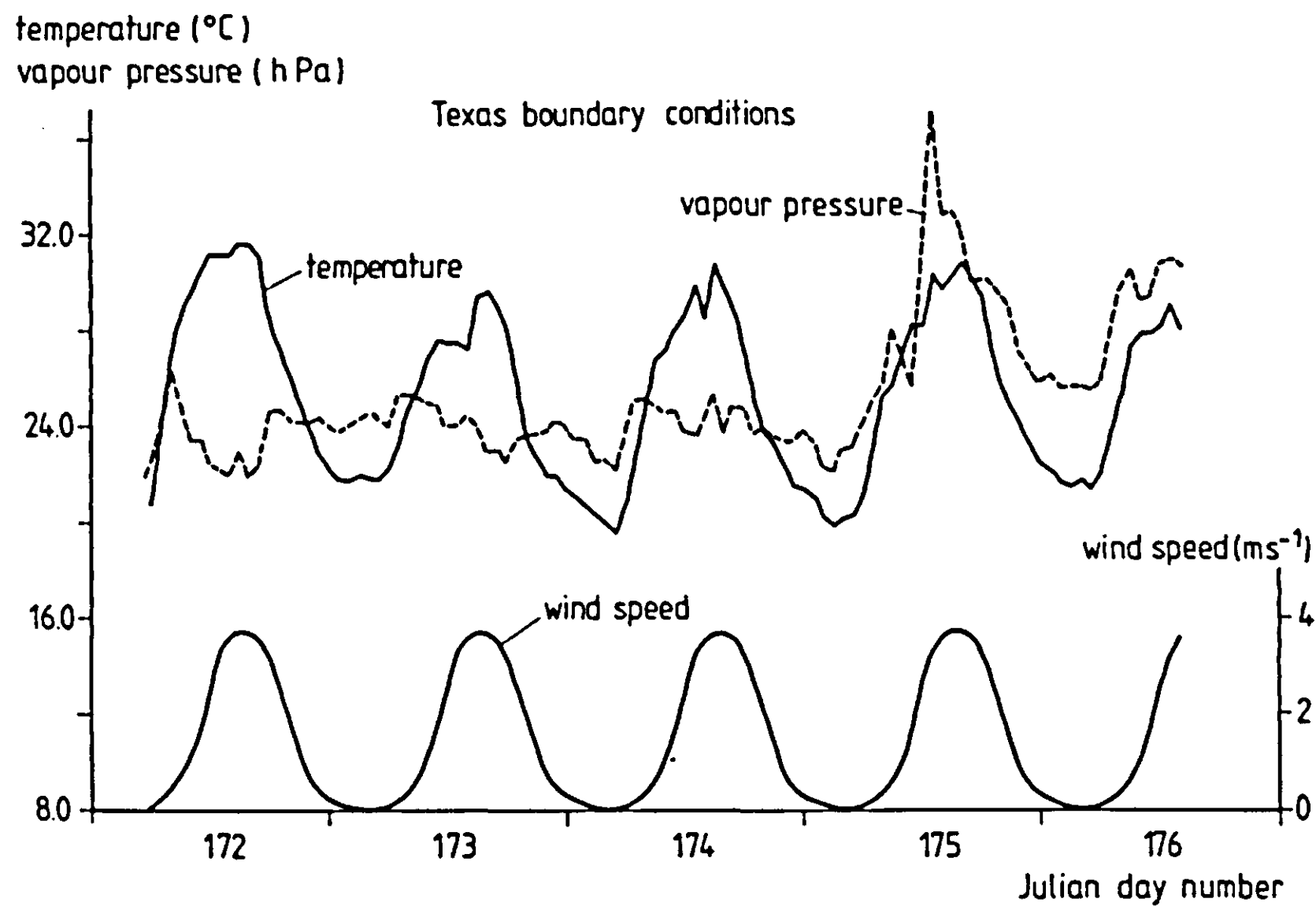


Figure 4.12 Atmospheric boundary conditions, measured at 2 m, TEXAS.

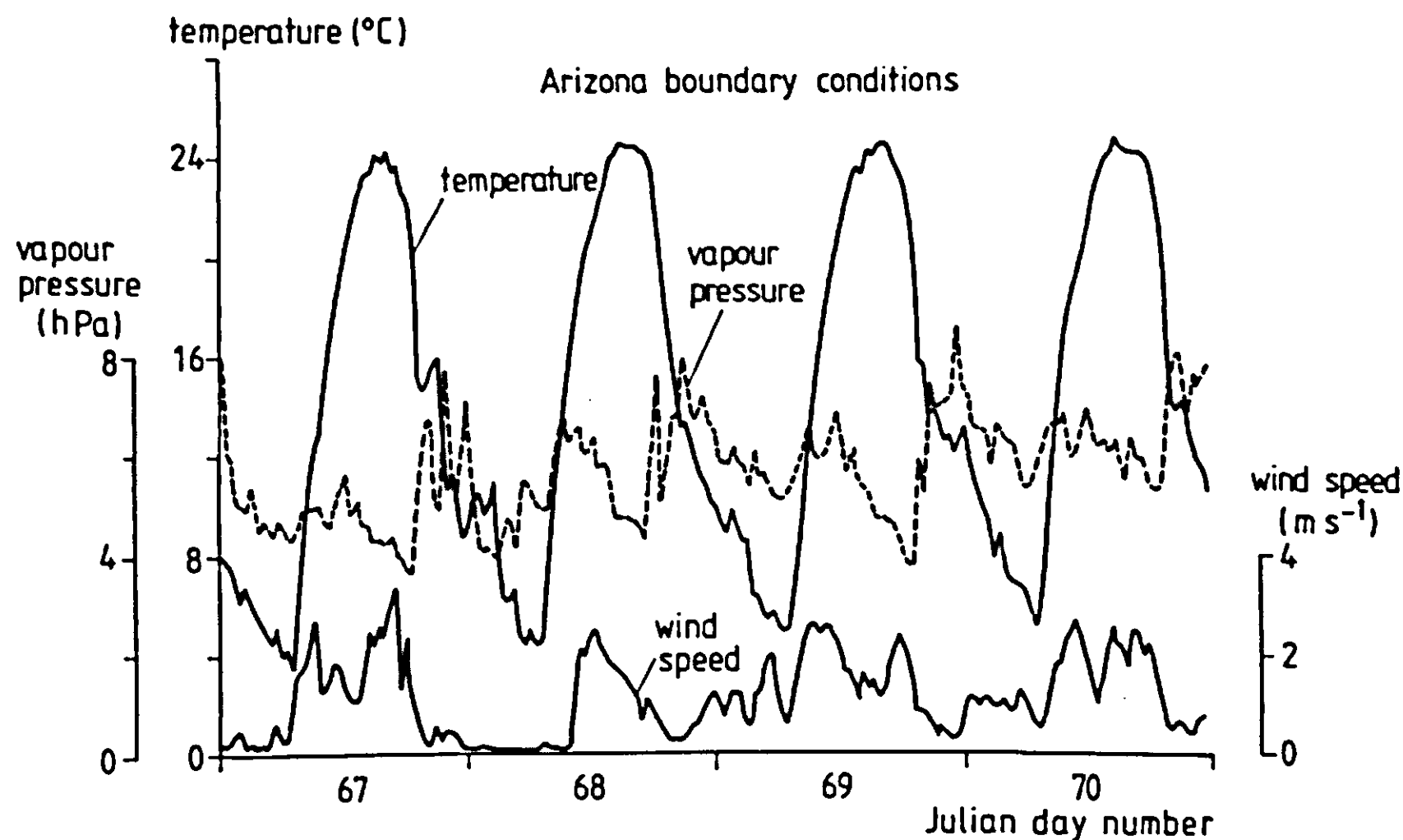


Figure 4.13 Atmospheric boundary conditions, measured at 0.5 m, ARIZONA.

4.6 System parameters and functions

The measured system parameters mostly express soil properties as functions of volumetric water content. These properties are the surface characteristics albedo and emissivity, the transport coefficients hydraulic and thermal conductivity, and the capacities for water (moisture characteristic) and heat. The only parameter not directly related to soil physical properties is the roughness length, a boundary layer property. Not all these functions were measured in each experiment, and in some instances estimates will have to be used for simulation purposes.

Roughness length

Roughness length (z_0), derived directly from wind profile measurements, could be assessed only for the FLEVO site. Although wind- and temperature profiles were measured continuously during a one month period, only few times were suitable for the determination of z_0 . Requirements for reliable determinations are near-neutral stability, a wind speed high enough for accurate anemometer performance, and the absence of rain in the preceding days, as moisture affects anemometer calibration; moreover, wind direction should allow for long enough fetch. Only observations corresponding to an absolute value for the Richardson number Ri less than 0.02 were used to derive z_0 ; (Ri is defined as $(g/T)(\partial T/\partial z)/(\partial u/\partial z)^2$). Combination of the log-linear wind profile equation with the assumption $\phi_H = \phi_M$ for the dimensionless gradients of temperature and windspeed (eqs. 3.16,17) gives the expression (Thom, 1975).

$$(4.8) \quad u(z) = \frac{u_*}{k} \ln \left(\frac{z-d}{z_0} \right) + 5(z-d-z_0) \frac{g}{T} \frac{dT}{du}$$

where d is the displacement height, generally taken zero for unvegetated surfaces. Equation 4.8 is supposed to be valid for stable and moderately unstable situations ($|Ri| < 0.1$). The values of u_* and z_0 were determined from the wind profiles (3 heights) by a non-linear optimisation procedure. This yielded z_0 values ranging between 0.02 and 0.15 mm for most days, although occasionally values up to 0.9 mm were determined.

As boundary layer variables were determined at a single level only in the TEXAS experiment, roughness length could not be derived from wind measurements.

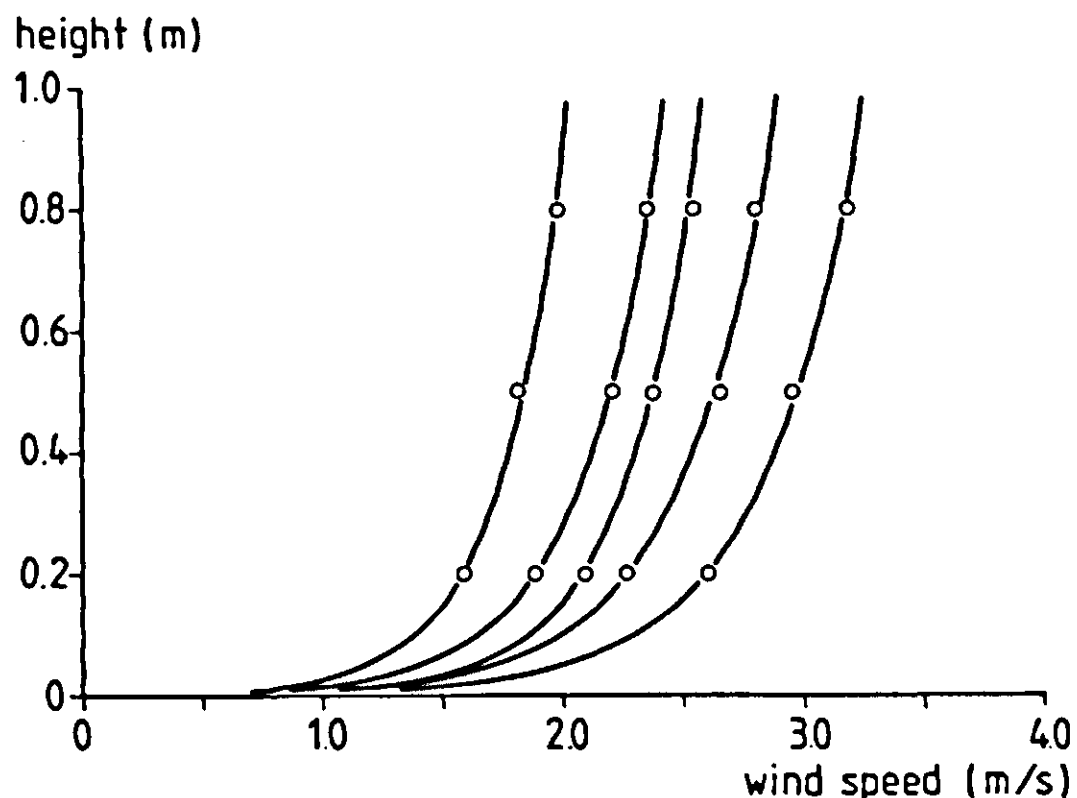


Figure 4.14 Some examples of wind-profiles, FLEVO set 2.

Although boundary layer variables were determined at several heights at the ARIZONA site, roughness length could not be determined from measured profiles of wind and temperature, probably due to fetch problems. Roughness length for the ARIZONA and TEXAS sets had to be assessed by matching simulated to measured soil heat fluxes respectively soil temperatures.

Albedo

Bare soil albedo was measured *in situ* as a function of moisture content in all three experiments. Double solarimeters were used, and topsoil moisture content was determined by gravimetric sampling of the top 5 mm layer; in the ARIZONA case, a 2 mm layer was sampled instead. The data were converted to volumetric water contents by using measured bulk density values.

To avoid effects of high incidence angles, data pertaining to early morning and late evening hours (global radiation < 100 W/m²) were omitted. For all three soils, albedo appears to be fairly well described by the relation

$$(4.9) \quad a(\theta) = a_{\text{wet}} \quad \theta > \theta_{\text{crit}}$$
$$a(\theta) = a_{\text{wet}} + \frac{\theta_{\text{crit}} - \theta}{\theta_{\text{crit}}} (a_{\text{dry}} - a_{\text{wet}}) \quad \theta < \theta_{\text{crit}}$$

For Swifterbant silt loam, a_{wet} and a_{dry} are, respectively, 0.13 and 0.31; for Buffalo silty clay, these numbers are 0.17 and 0.32, and the corresponding values for Avondale loam are 0.14 and 0.31. The critical volumetric

moisture contents for these three soils are, respectively, 0.26, 0.32 and 0.22.

At given soil moisture content, the error standard deviations in albedo, expressed by the above regression data are 0.020 for Swifterbant silt loam and Avondale loam, and 0.033 for Buffalo silty clay. Spatial dependence of $a(\theta)$ was not measured in either one of the experiments. Figures 4.15-4.17 show the $a(\theta)$ functions for the three different soils. The albedo-moisture content relation for Avondale loam was discussed in more detail by Idso et al., (1975).

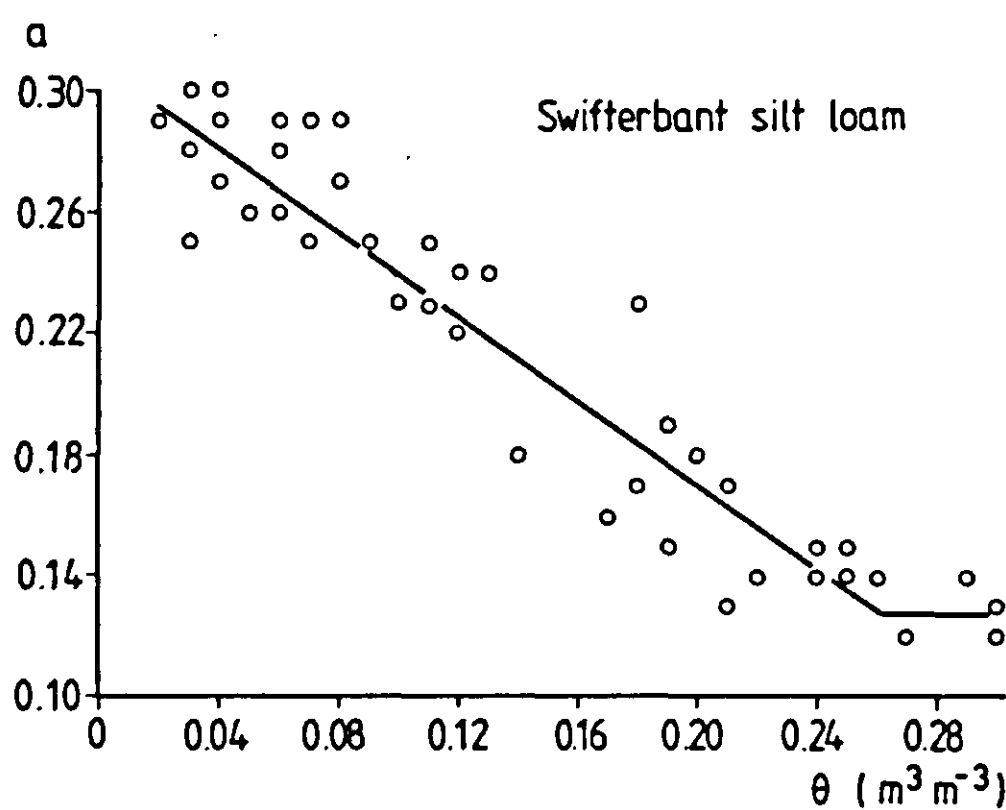


Figure 4.15 In-situ measured albedo versus volumetric moisture content (0-5 mm) for Swifterbant silt loam.

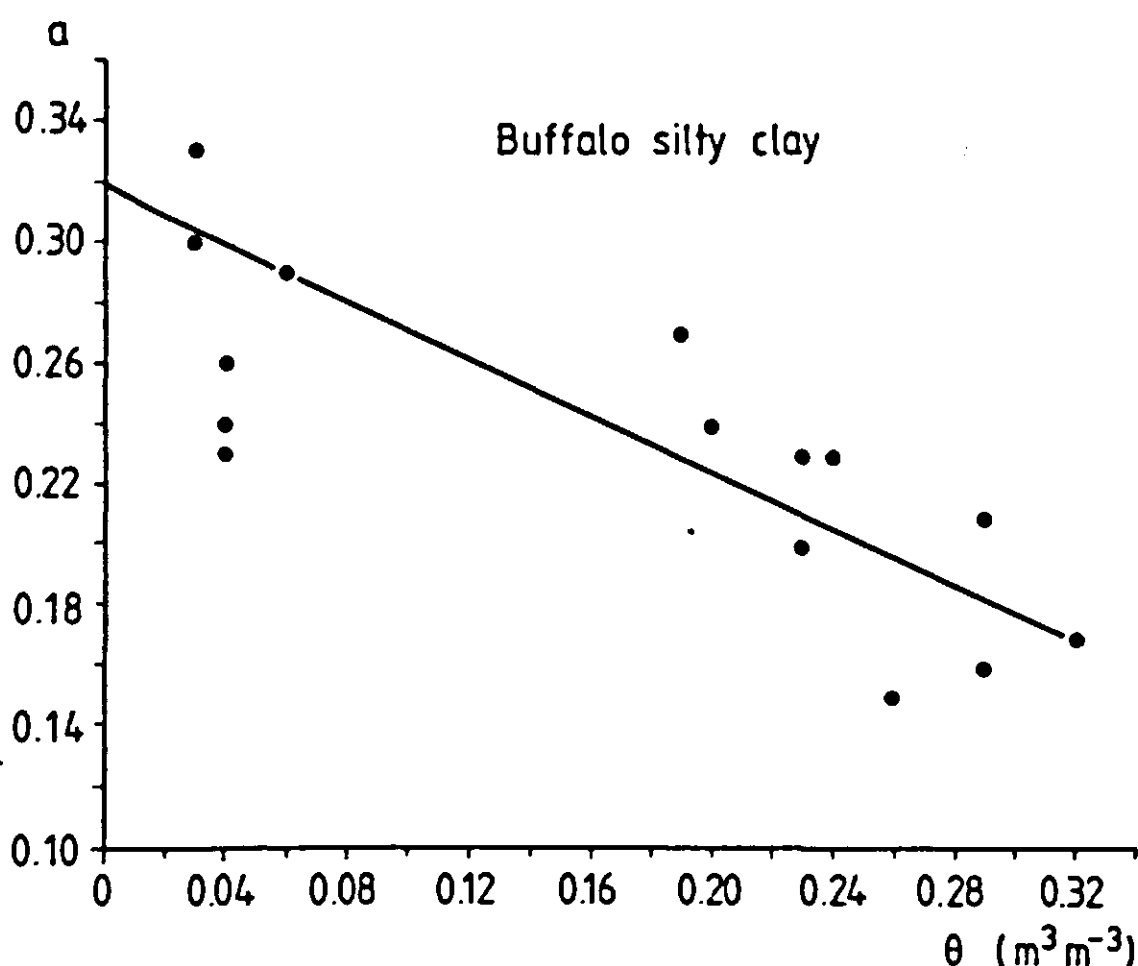


Figure 4.16 In-situ measured albedo versus volumetric moisture content (0-5 mm) for Buffalo silty clay.

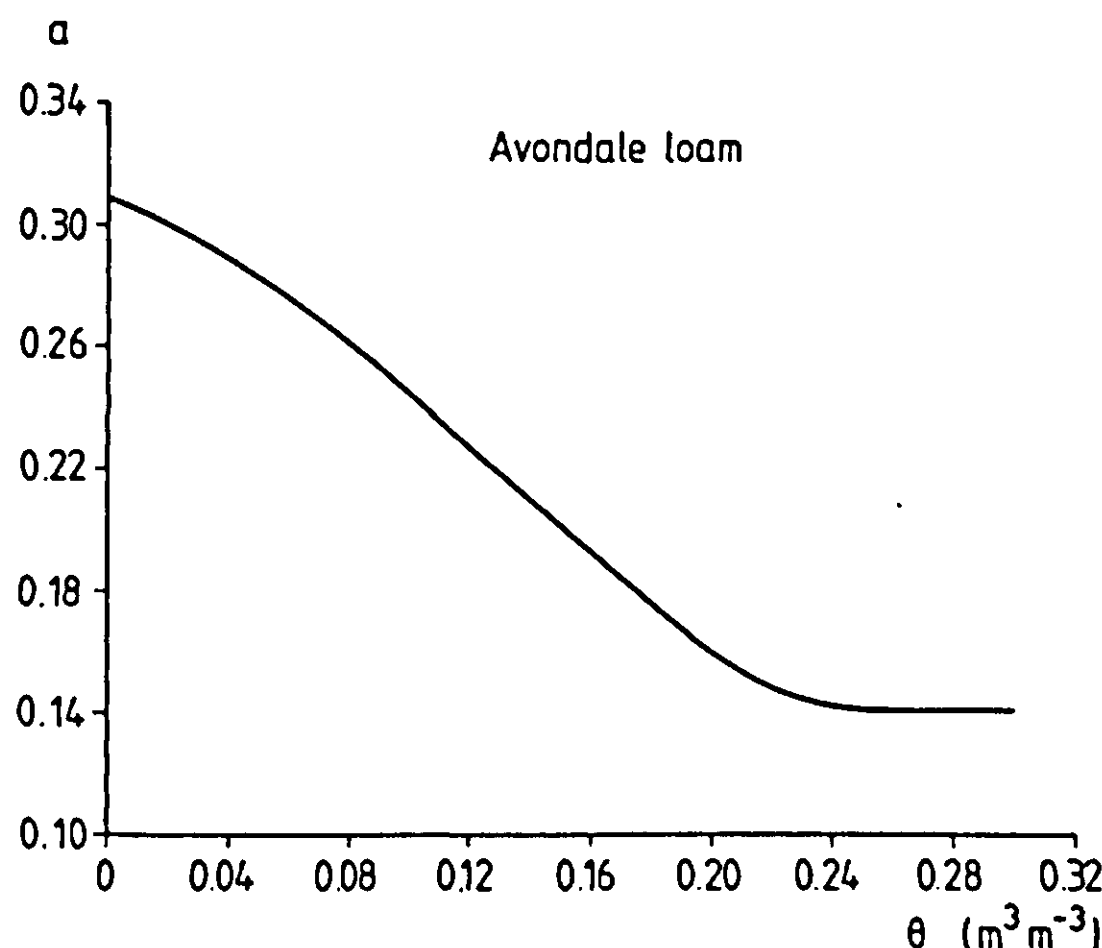


Figure 4.17 In-situ measured albedo vs. volumetric moisture content (0-2 mm) for Avondale loam.

Longwave reflectivity

Longwave reflectivity could be calculated from the measured data only in the ARIZONA case. Its value ranged between 0.05 and 0.15. In contrast to albedo, a relation with surface moisture content was not evident. An average value of 0.10 with an error standard deviation of 0.05 will be used for all data-sets.

Emissivity

Emissivity of Swifterbant silt loam, as a function of moisture content, is shown in Figure 4.18. Measurements were taken on core samples by the Fuchs and Tanner (1966) reflection method under stratus cloud cover, on the roof of the 'Dreijenborch' building at Wageningen, exhibiting an unobstructed horizon. Only under these conditions, distribution of radiance in the 8-14 μm wavelength interval over the sky hemisphere was fairly even and within the range of the measurement instrument. Although the data suggest a step increase of the emissivity as the moisture content increases (which physically could be explained on the basis of soil water energy state), a simple linear $\varepsilon(\theta)$ relationship is adopted because of the large scatter observed:

$$(4.10) \quad \varepsilon(\theta) = \varepsilon_{\text{dry}} + \frac{\theta}{\theta_s} (\varepsilon_{\text{wet}} - \varepsilon_{\text{dry}})$$

with $\varepsilon_{\text{dry}} = 0.90$ and $\varepsilon_{\text{wet}} = 0.94$. The scatter is partly due to inaccuracies in the non-destructive θ -determination, which involved averaging of weight changes over 100 cm^{-3} core samples. The results obtained by an alternative method, employing gravimetric moisture content of the top 5 mm layer instead, were not better, however. The error standard deviation in emissivity

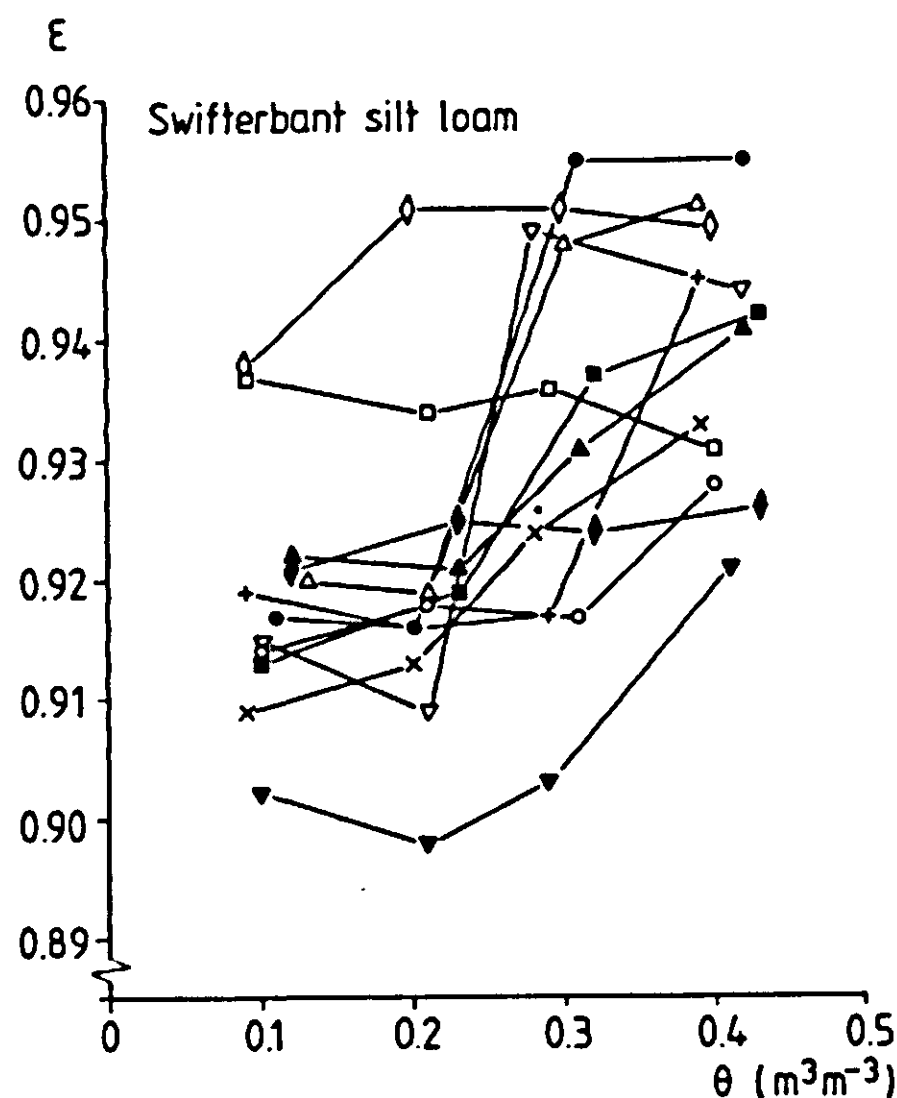


Figure 4.18 Emissivity ($8-14 \mu\text{m}$) measured on core samples of Swifterbant silt loam by the Fuchs-Tanner method.

For dry Avondale loam, Idso and Jackson (1969) reported an emissivity of 0.97. Conaway and Van Bavel (1967) measured for wet Avondale loam a value of 0.98. These values will be used with an assumed error standard deviation of 0.01.

For Buffalo silty clay, no emissivity values were measured. A value of 0.96 ± 0.03 will be used, based on literature data (Table 3.3).

Thermal soil properties

The damping depth of the diurnal temperature wave in homogeneous soil profiles can be inferred from the attenuation of the temperature amplitude and from the phase shift, both with respect to depth (De Vries, 1963). (Horton (1982) gave an excellent review of these and related methods). Fourier analysis yields these two characteristics for the different wave numbers, and from the resulting damping depths, thermal conductivity can be calculated, using an estimated soil heat capacity. However, at all three test sites, soil moisture distribution was such that thermal properties were definitely not constant with depth. Moreover, bulk density increased with depth at the FLEVO and TEXAS sites, and for these cases indeed a layer of increased thermal diffusivity was found at 0.2-0.3 m depth using amplitude attenuation of the first harmonics of the temperature wave.

Two other field methods were employed in the FLEVO experiment: direct measurement by heat probes, and the so-called 'null-alignment' method. Results of both methods are compared to predictions, made by the De Vries thermal conductivity model. However, since significant changes in moisture content occurred only in the top few centimetres, field measurements only yielded the $\lambda(z)$ function, rather than the $\lambda(\theta, z)$ or $\lambda(\theta, p)$ relation, needed in the intended dynamic simulation; additional laboratory measurements were therefore conducted to obtain $\lambda(\theta)$ for topsoil core samples, and to this purpose a new method was introduced.

Measurement of λ by heat probes inserted in the soil was extensively discussed by De Vries (1952), and later by several other authors, so the theoretical aspects are not repeated here. The probes were installed at various depths to measure in-situ thermal conductivity. Figure 4.19 shows the results for different depths. Some scatter is observed, which is possibly due to the problem of contact resistance, also discussed by Nagpal and Boersma (1973) and recently by Van Haneghem (1981).

Results obtained by the 'null-alignment' method proposed by Kimball and Jackson (1975) are also depicted in Figure 4.19. This calorimetric method employs $T(z)$ profiles at different times, and infers heat fluxes by numerical integration, making use of points with a zero temperature gradient. The procedure is analogous to what is known as the 'instantaneous profile' method for the determination of the unsaturated hydraulic conductivity curve, $K(\theta)$.

Figure 4.19 also shows thermal conductivity as predicted by the De Vries model on the basis of bulk density, texture and moisture content. Since both measurement procedures mentioned above yield apparent instead of true thermal conductivity, the vapour term was included in the De Vries model in order to obtain estimates that can be compared to the measured results (see also section 3.5). This vapour contribution to thermal conductivity was calculated for a temperature of 20° C, approximately the average profile temperature. As indicated in the previous chapter, the choice of the air shape factor g_a (eq. 3.45) reduces the predictive value of this conductivity model. For the curve as given in Figure 4.19, an air shape factor of 0.05 was used; higher values of g_a gave even higher estimates of λ (see also Figure 4.20).

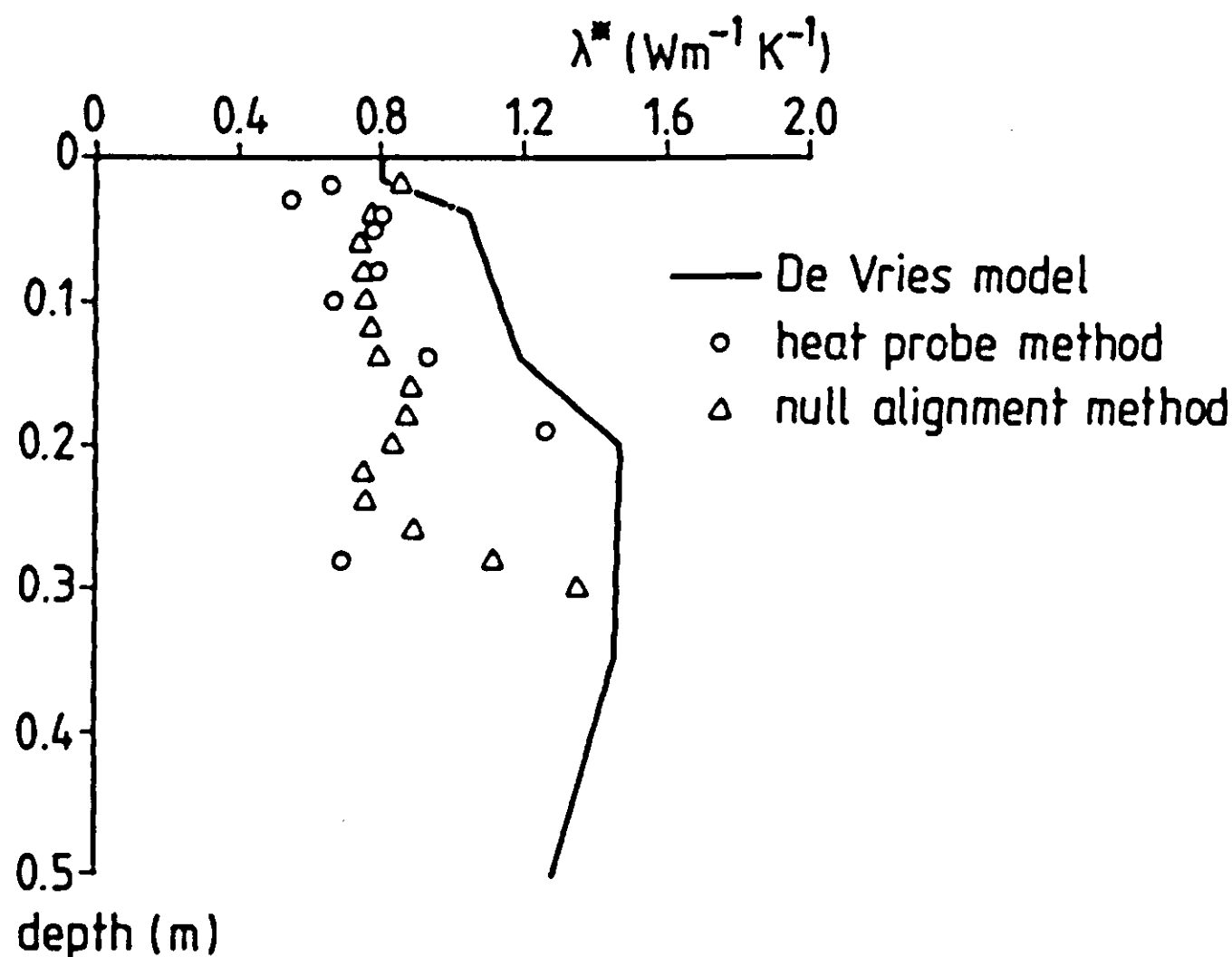


Figure 4.19 Profiles of apparent thermal conductivity, obtained by different methods, for Swifterbant silt loam.

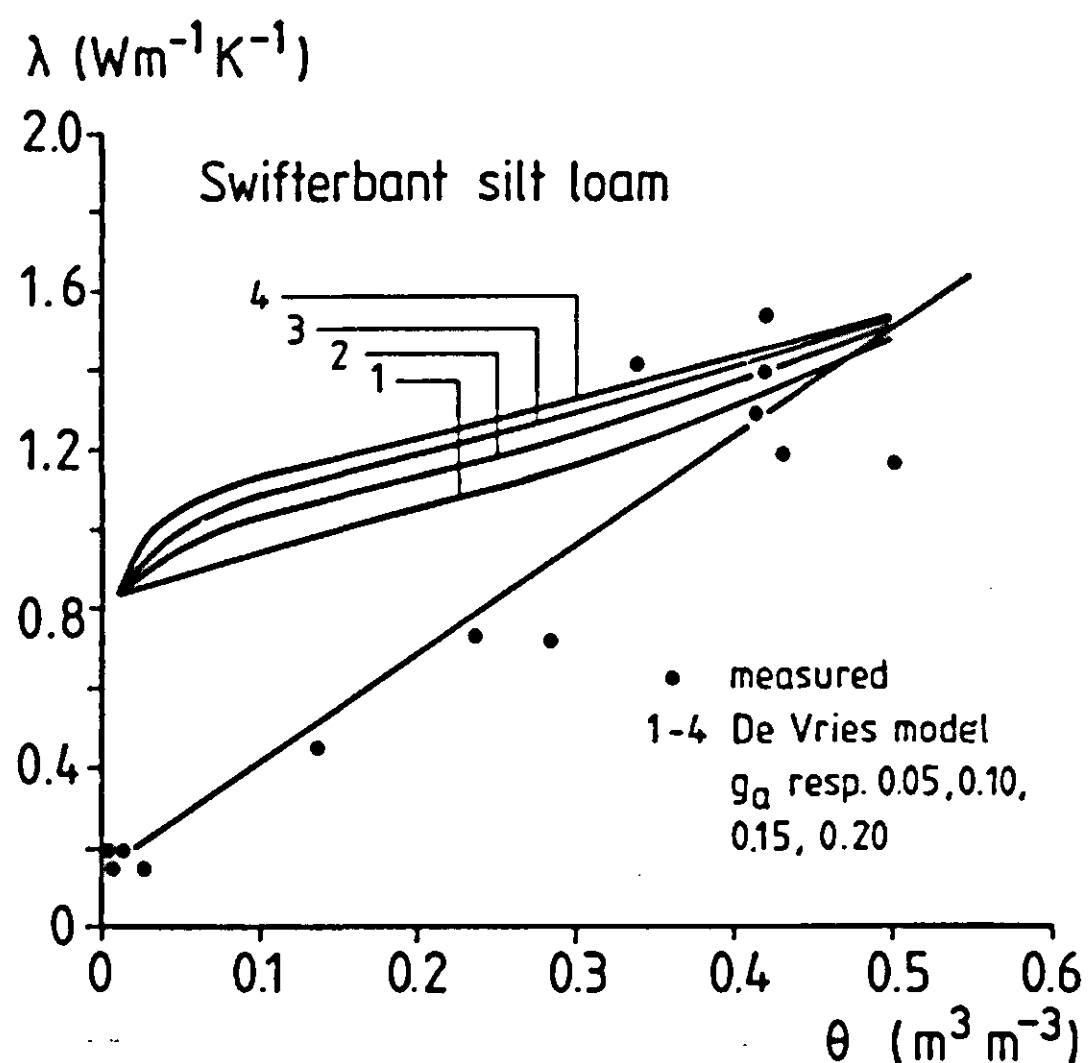


Figure 4.20 Apparent thermal conductivity of Swifterbant silt loam (0-5 cm), determined on core samples by the 'surface step' method.

It can be concluded from Figure 4.19 that for Swifterbant silt loam the conductivity model does not well predict λ as measured by the probe method nor by the null-alignment method, whereas the results of these latter methods are in fairly close agreement with one another.

Laboratory measurements of thermal conductivity were taken on a number of undisturbed core samples from the top 5 cm soil layer. A new method for the determination of λ in the surface region, described in Appendix 7, was

used. The method is based on the existence of a constant interface temperature when contact is made between two semi-infinite, homogeneous bodies, each with a given initial temperature. The method is referred to as the 'surface step' method, and it yields, like the discussed field methods, apparent thermal conductivity, provided that the heat capacity of the soil is known. The results are shown in Figure 4.20. These measured data are in agreement with the De Vries predictions only for the higher water contents. The data can be approximated by a straight line, as encountered frequently for aggregated field soils, in contrast to the typical curves for packed granular materials (e.g. Figure 3.4).

Two problems arise when a function, to be used in the context of a simulation model, must be defined from measured data as available here: (1) moisture content hardly varied at depths where field measurements of λ^* were made, and (2) true conductivity is used in simulation (section 3.5), whereas apparent thermal conductivity was measured. To overcome these, two simplifications present themselves: (1) $\lambda(\theta)$ curves for the different bulk densities (depths) are calculated from the laboratory-measured curve by simple multiplication with a factor ρ/ρ^* (where ρ^* is the reference bulk density), and (2) the vapour diffusion term (estimated at $0.05\text{--}0.10 \text{ W m}^{-1}\text{K}^{-1}$) is subtracted from the measured apparent thermal conductivity. The latter involves an increase in uncertainty, due to the choice of an average temperature and the unknown role of the enhancement factor (subsection 3.6.4). The function $\lambda(\theta, \rho)$ resulting from application of the above procedure to the Swifterbant data is given in Figure 4.21. Error coefficients of variation in this λ -function are estimated to amount to 20%, based on the scatter in field and laboratory measurements. In the next chapters, it will be assessed to what extent such an inaccuracy in λ affects predicted soil behaviour with respect to the surface energy balance and to soil temperatures.

Thermal conductivity was not measured for Buffalo silty clay. Instead, the De Vries model has been used to estimate λ , the results of which are depicted in Figure 4.22.

The $\lambda(\theta)$ function for Adelanto loam (Figure 4.23) was determined by Kimball and Jackson (1975) by the null-alignment method, which was introduced by these authors for that occasion. Their data are used in the present report.

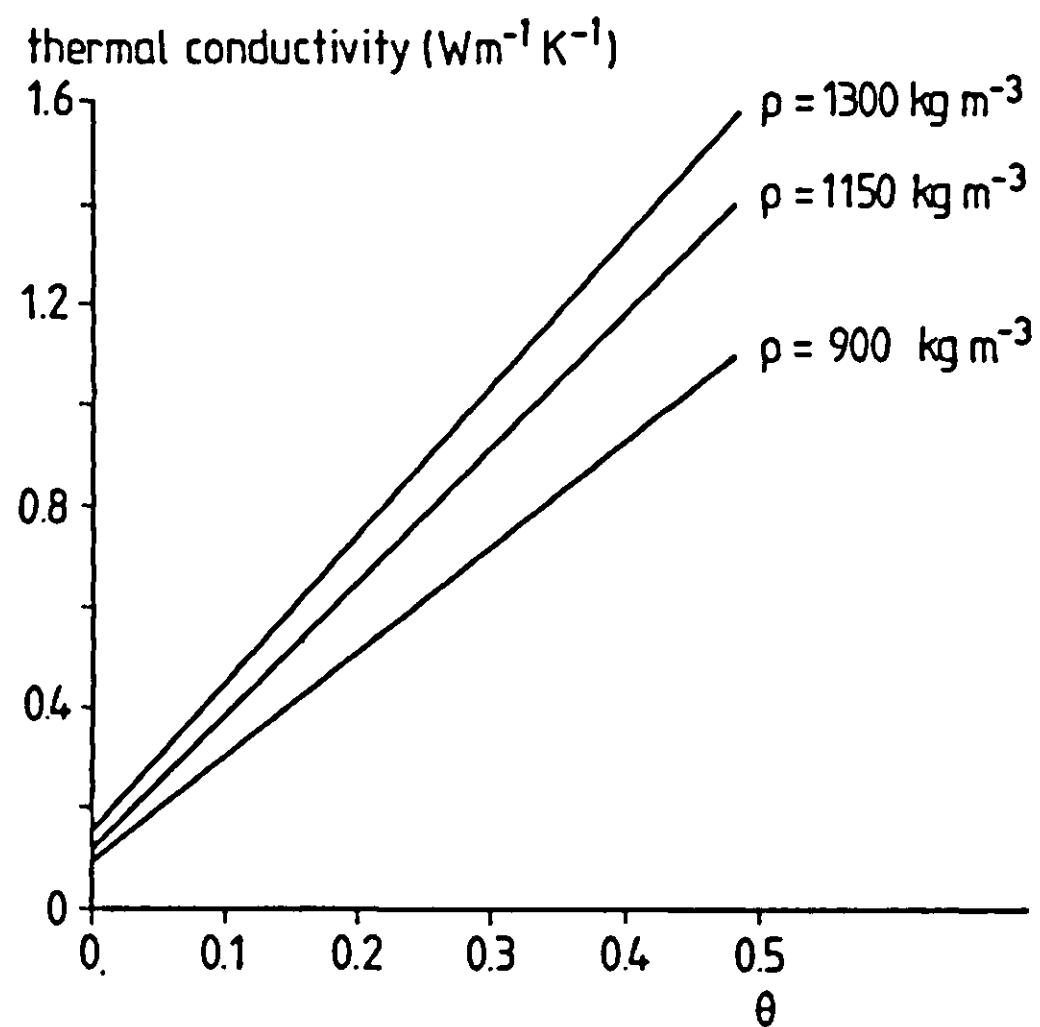


Figure 4.21 $\lambda(\theta, \rho)$ for Swifterbant silt loam as used in simulation (Chapter 5).

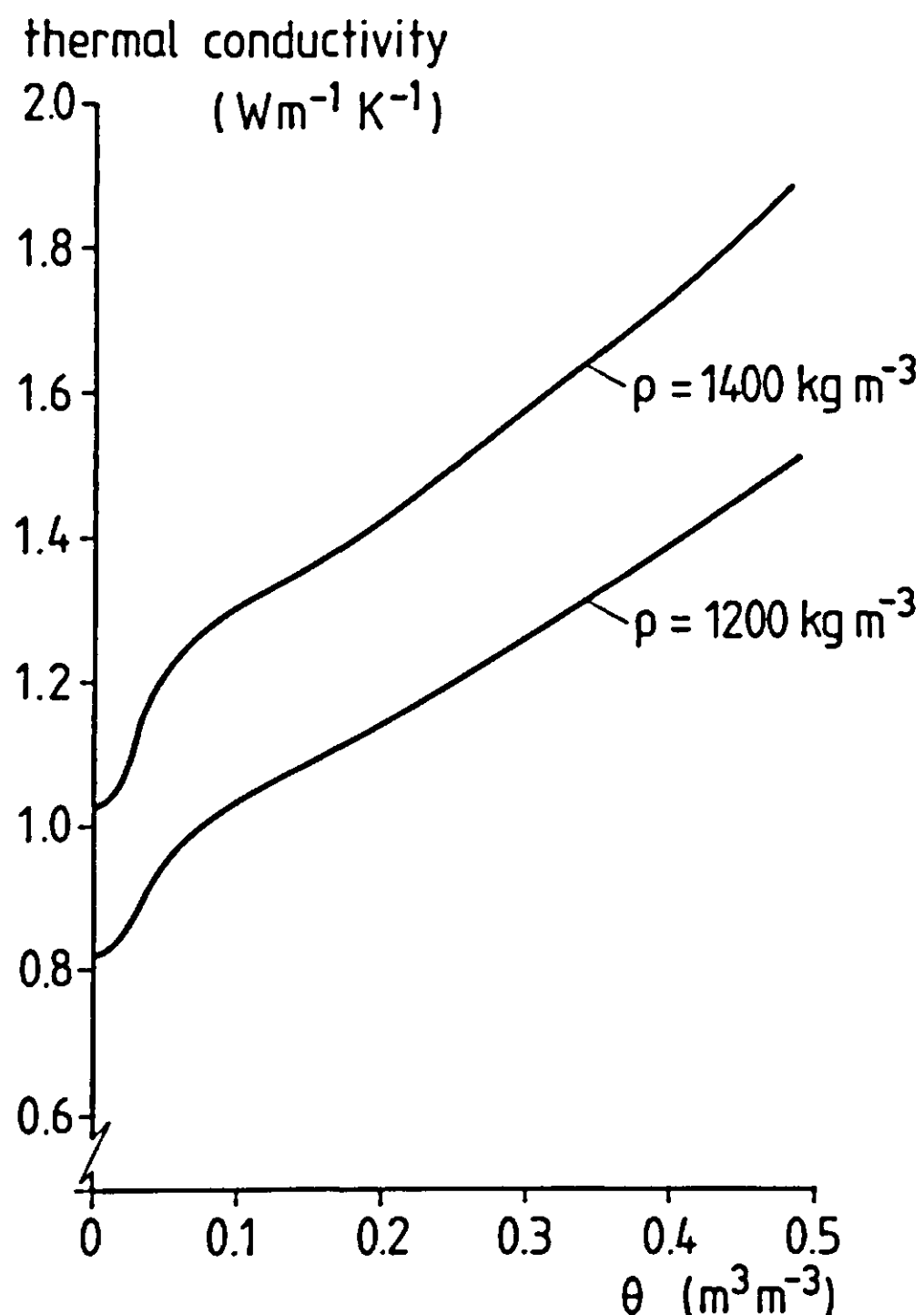


Figure 4.22 Thermal conductivity for Buffalo silty clay as calculated by the De Vries model ($g_a = 0.20$).

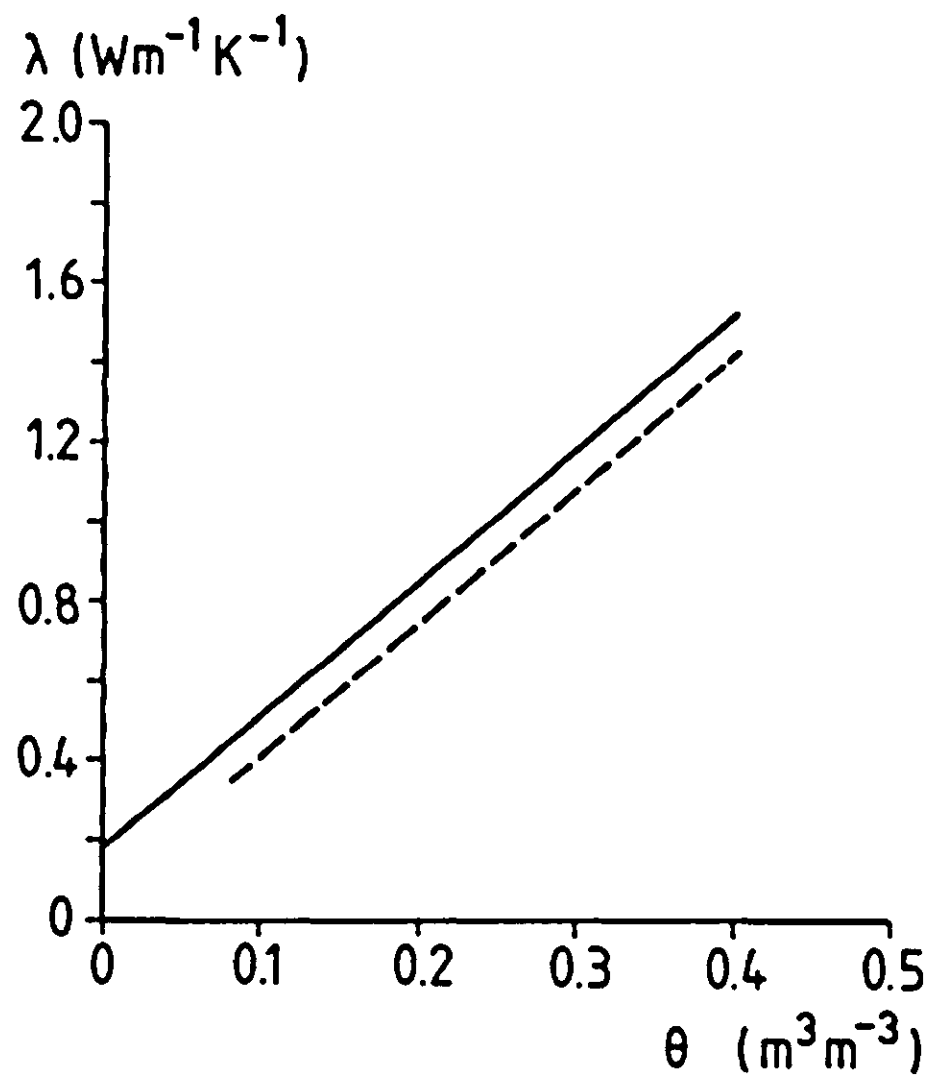


Figure 4.23 Apparent thermal conductivity for Adelanto loam, based on field observations by Kimball and Jackson (1975). The dotted line indicates the calculated true conductivity function.

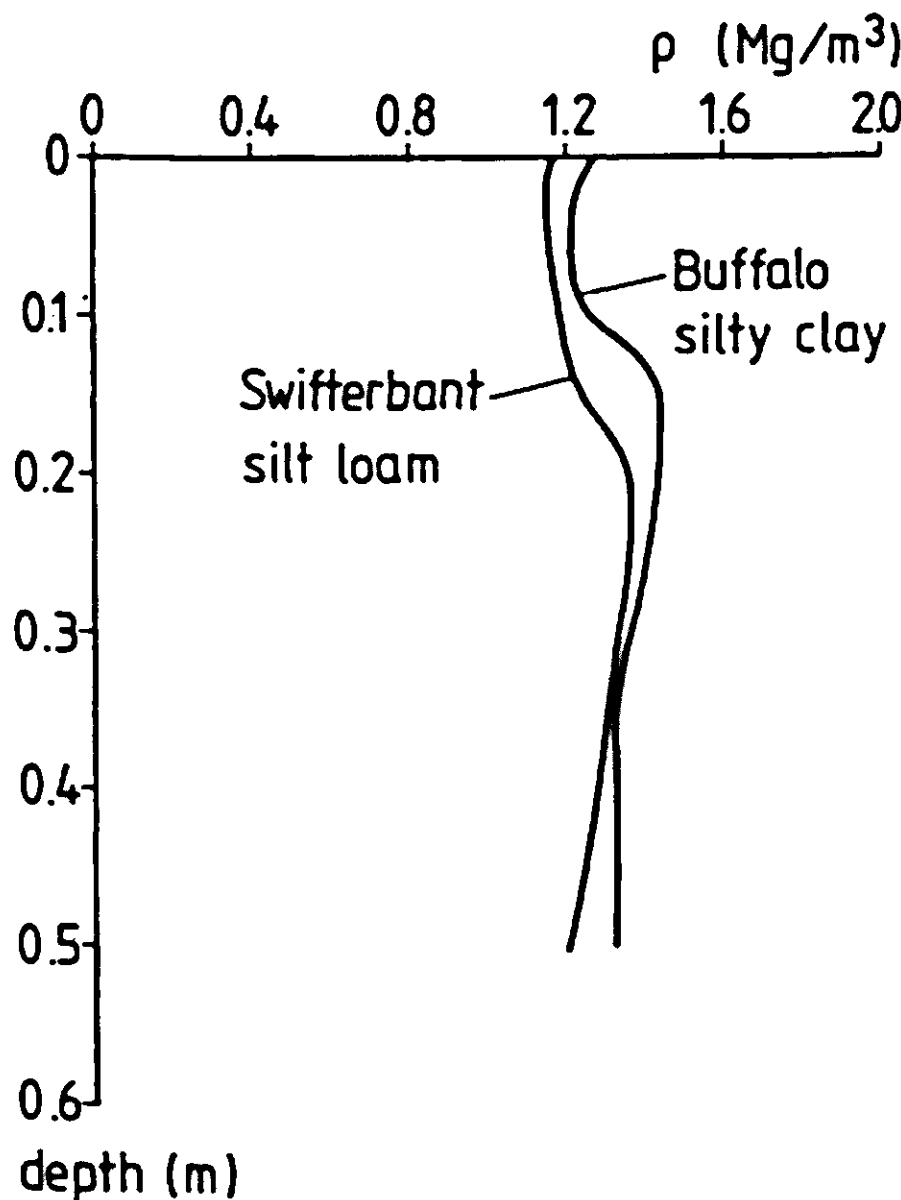


Figure 4.24 Bulk density (dry soil) profiles for the FLEVO and TEXAS sites.

Heat capacity profiles were calculated by eq. (3.42) from bulk density, moisture content and texture. Profiles of bulk density for the FLEVO and TEXAS experimental fields are given in Figure 4.24. Error standard deviations for bulk density are based on semivariance analysis for the FLEVO set,

and on total field variance in the TEXAS case; their values depend on depth and range up to 60 and 90 kg m³, respectively. Based on these numbers, errors in heat capacity were estimated at 0.06 and 0.10 (coefficient of variation), respectively.

The moisture characteristic

Moisture characteristics of the Swifterbant soils were determined as part of a spatial variability study. At 100 locations, core samples were taken from two depth intervals: the 0-5 cm and 5-10 cm layers. The samples were grouped into a loam and a silt loam class, and intermediate samples were left out. For each of the two groups, average curves were determined by first averaging - at given fixed pressure potentials - the corresponding measured moisture contents. Subsequently, Van Genuchten's expression for the moisture characteristic (eq. 3.61) was fitted to these averaged data. Figure 4.25 shows the results for the two soils. The fitting parameters α and n are $4.04 \cdot 10^{-4} \text{ Pa}^{-1}$ and 1.161 for the silt loam, and $4.67 \cdot 10^{-3}$ and 1.093 for the loam, respectively. (The fitting parameter α is, unlike the scaling factor α_r , not dimensionless).

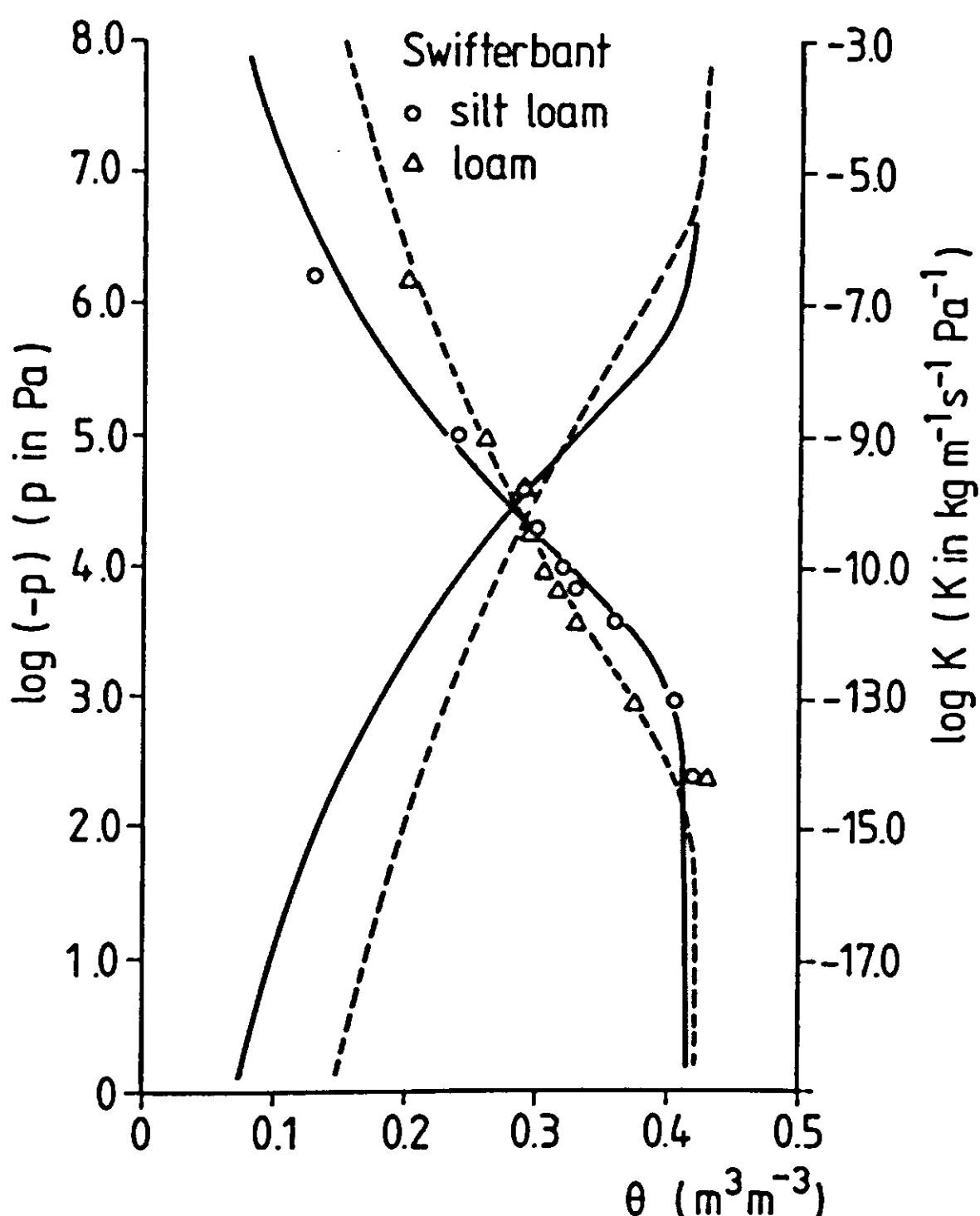
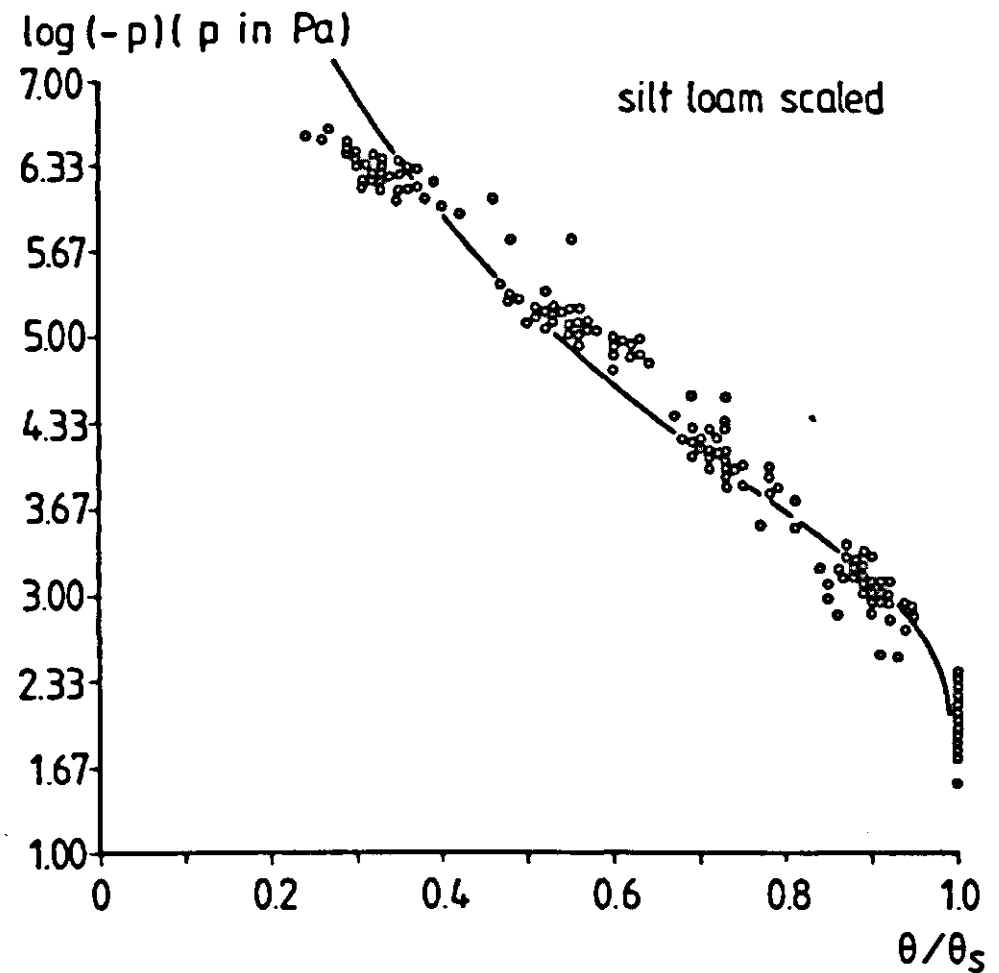
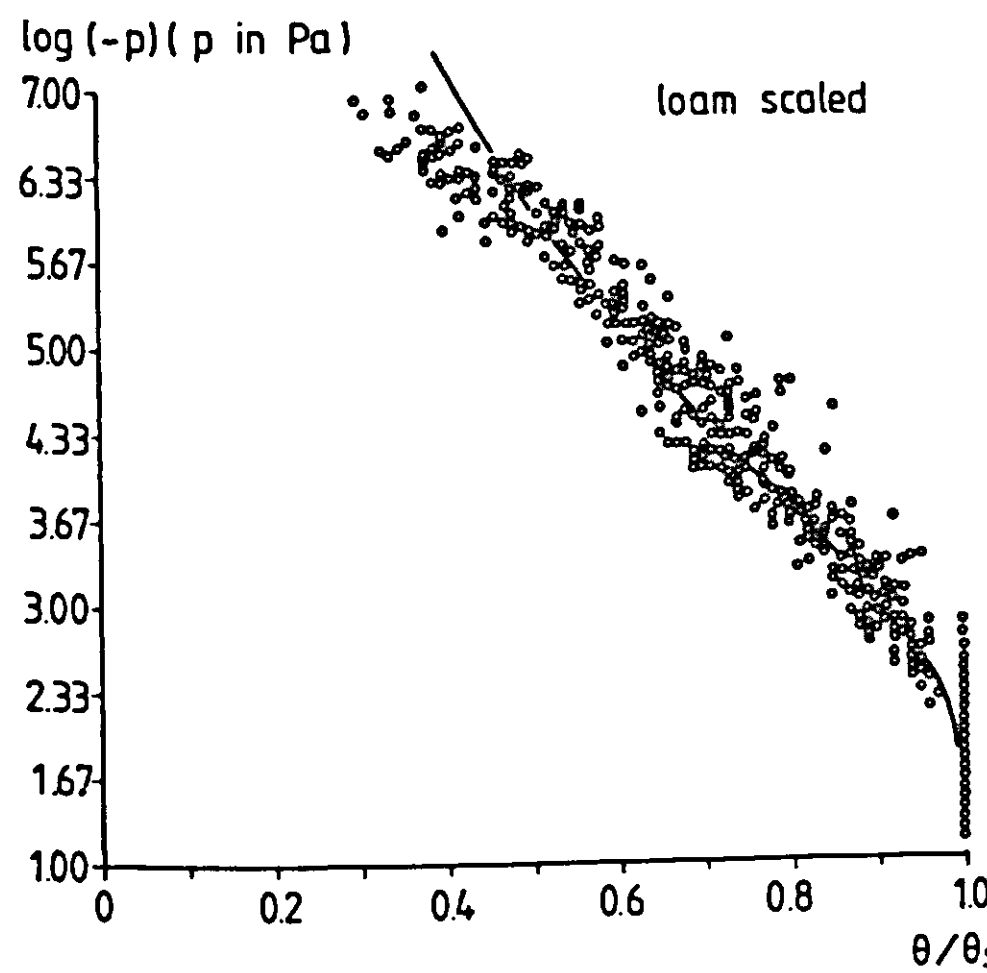
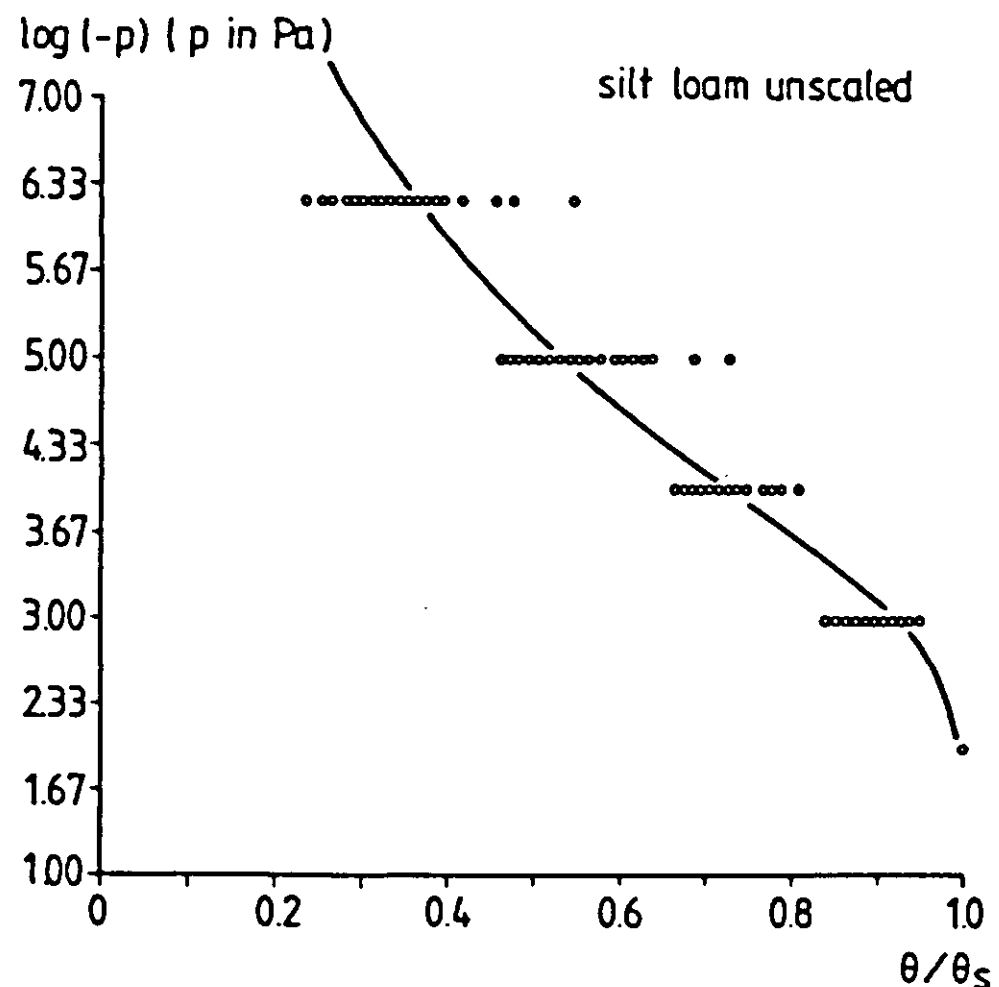
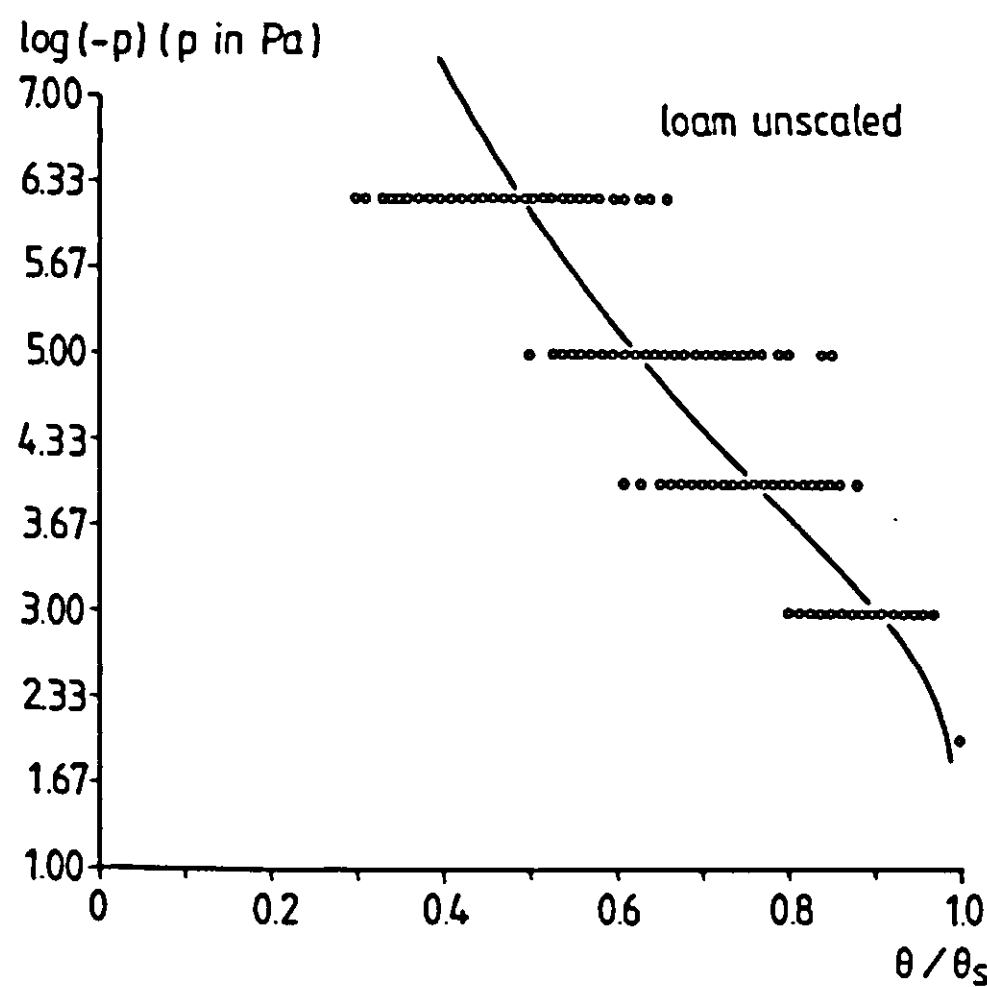
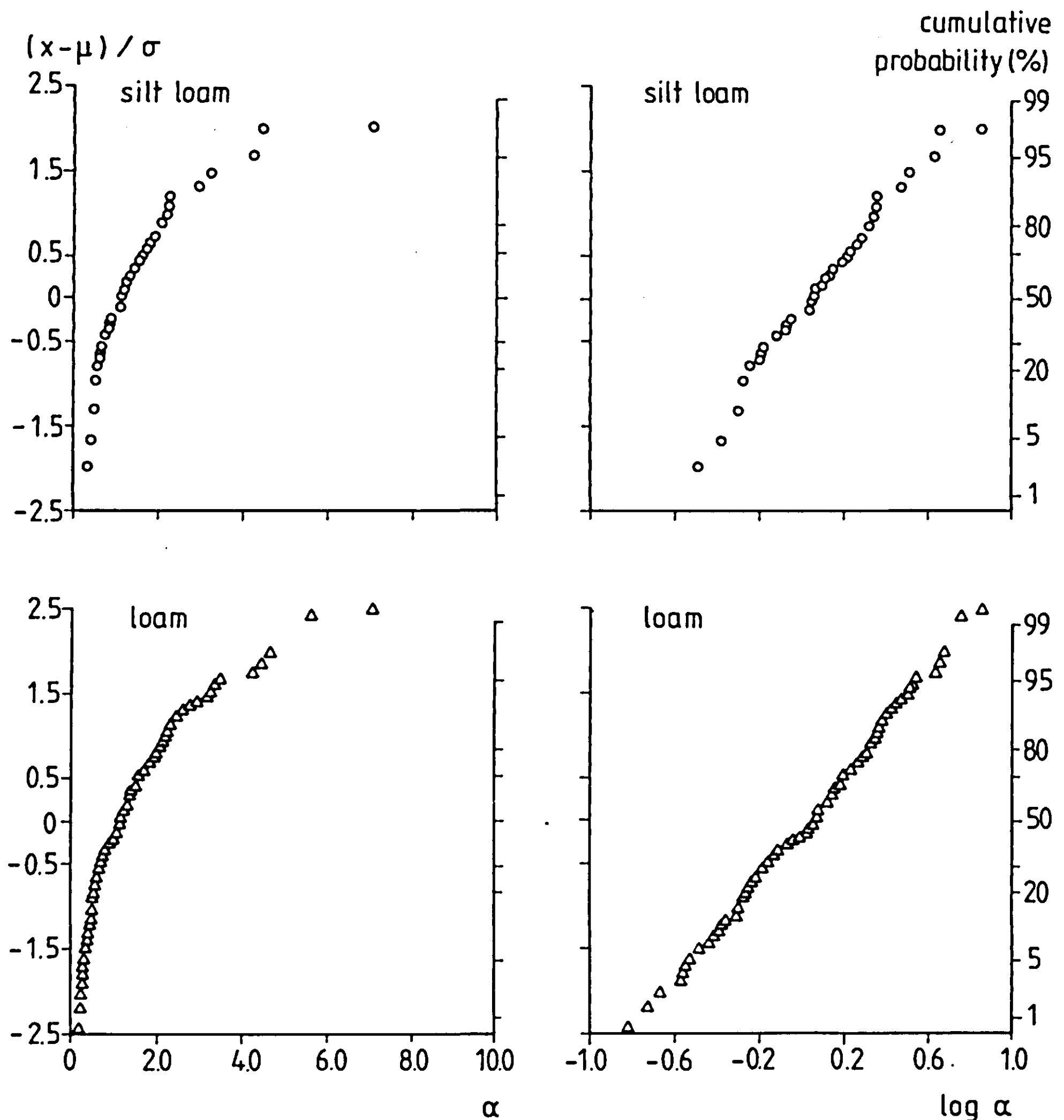


Figure 4.25 Moisture characteristics for Swifterbant silt loam and Swifterbant loam; the lines represent best fits to the Van Genuchten (1980) model. Indicated are also the hydraulic conductivity curves, calculated by the Van Genuchten-Mualem model.

Variability of the moisture characteristic, as explained in section 4.2, was taken into account by scaling. A prerequisite for scaling is that curves have similar shapes, that is, the $\log p$ - θ curves should run parallel. Since this is clearly not the case for the two Swifterbant soils, distinguished on the basis of texture, the loam and silt loam data were scaled separately. The scaled pressure p_{sc} was taken to be a function of $s \equiv \theta/\theta_s$, and was determined by fitting the curve given by eq. 3.61, with E replaced



Figures 4.26 – 4.29 Actual and scaled moisture characteristics for Swifterbant silt loam and Swifterbant loam.



Figures 4.30 – 4.33 Probability distribution of the scale factor α for both Swifterbant soils.

by s , to the whole set of datapoints pertaining to each texture class. This again was done by the optimization procedure 'SOHYP' (Van Genuchten, 1978). Subsequently, the scaling factor α_r was determined for each sample by minimizing the sum of squares

$$(4.11) \quad SSQ = \sum_{i=1}^N (\log p_{sc}(s) - \log \alpha_r p_r(s))^2$$

This optimization criterion is preferred to the alternative where pressures instead of their logarithms are used, since it reduces the weight of the points at low θ values; these points would determine the scaling factor almost entirely in the alternative case. Scaling by means of expression 4.11 reduced the variance $(1/(N-1)) \sum (p_{sc}(s) - p_r(s))^2$ by two orders of magnitude for both soils. Unscaled and scaled water pressures as a function of relative saturation are depicted in Figures 4.26-4.29 for both soils. The scale factors show log-normal distributions (Figures 4.30-4.33). Log α_r variances amount to 0.095 (silt loam) and 0.140 (loam) for the two Swifterbant soils. (Strictly speaking, the use of these numbers overestimates to some extent the variability at the 4 m level, in which one is interested for validation purposes, as explained before. It was, however, not well possible to do a semivariance analysis on the α -data in order to obtain the restvariance at this level, since for scaling the observations were grouped into the two texture classes silt loam and loam; as a result of this, the transects were divided into smaller sections representing loam and silt loam patches).

Also for Buffalo silty clay the hydraulic properties were determined on core samples. The moisture characteristic is given in Figure 4.34. Scaling

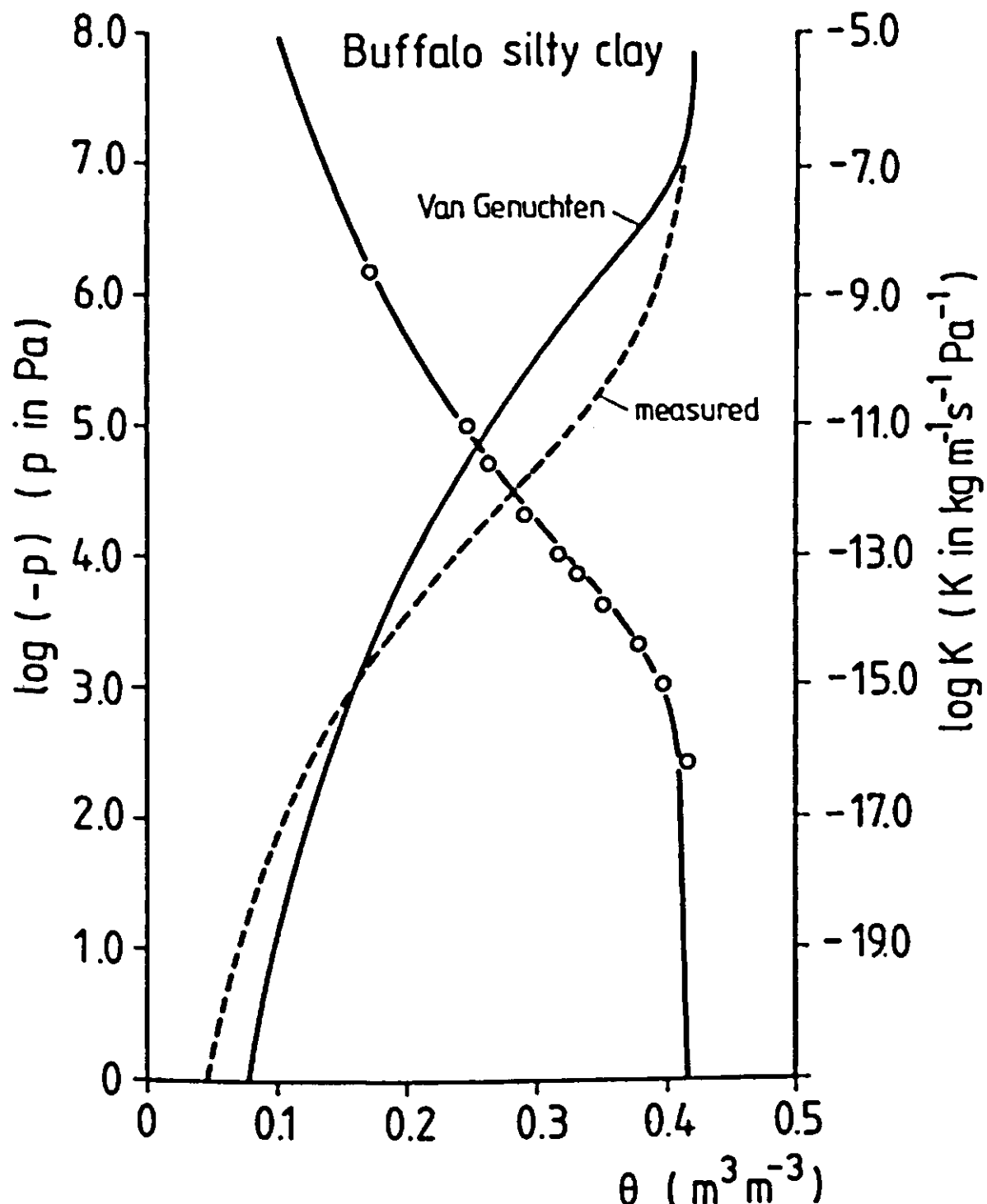


Figure 4.34 Hydraulic properties of Buffalo silty clay.

data were taken from Lascano and Stroosnijder (1984). These authors calculated the retention curves from texture data (100 sites) by the Arya and Paris (1981) model. To scale the pressure, they used the expression

$$(4.12) \quad s(p_{sc}) = \frac{1 - c}{(\alpha_r p_r(s)/A)^b + 1} + c$$

where A, b and c are parameters applying to a mean curve. As an optimization criterion to determine α_r they used the sum of squares

$\sum (s(\alpha_r p_r) - s(p_{sc}))^2$. Figure 4.35 shows the cumulative probability diagram for α_r . Its distribution is neither normal nor log-normal. At cumulative probabilities of 17 and 83%, α_r -values are 0.7 and 1.4 respectively. These levels represent the equivalents for the levels of $\mu \pm \sigma$, as used in the cases of normal distributions.

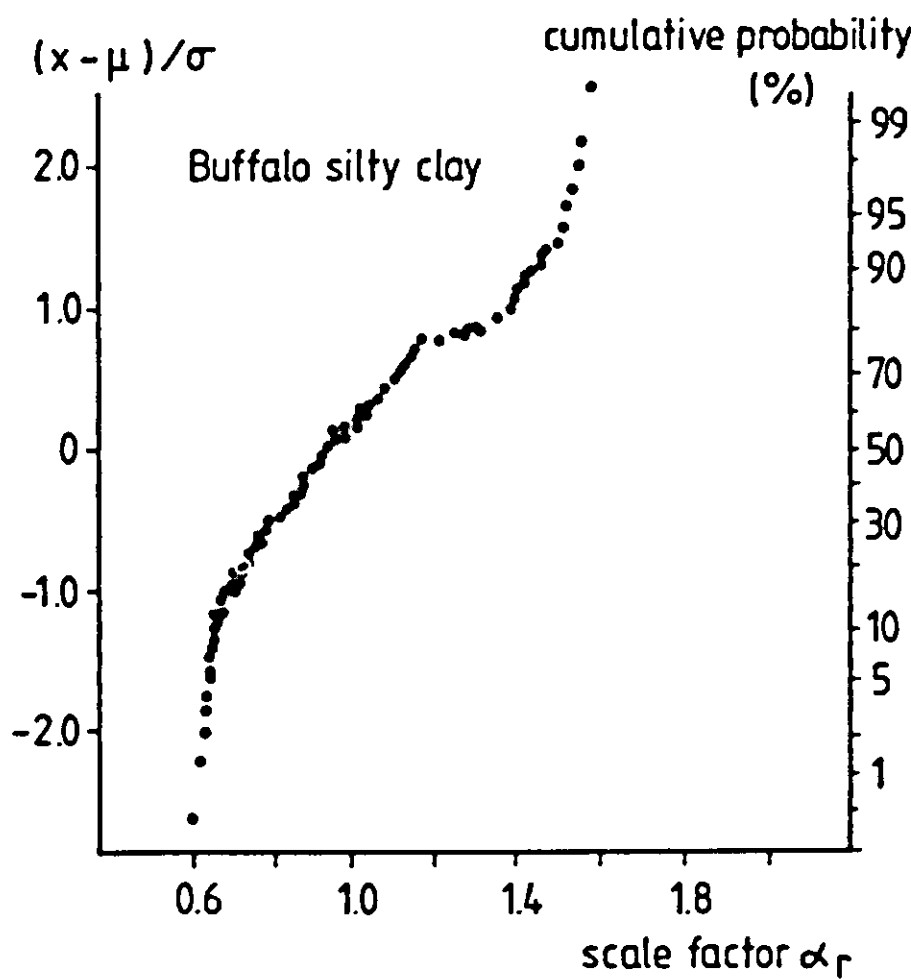


Figure 4.35 Probability distribution of the scale factor α for Buffalo silty clay.

The Adelanto loam moisture characteristic as taken from Jackson (1973) is depicted in Fig. 4.36. As no spatial variability data are available for the ARIZONA site, error variance is expressed by an assumed variance of 0.10 for $\log \alpha$.

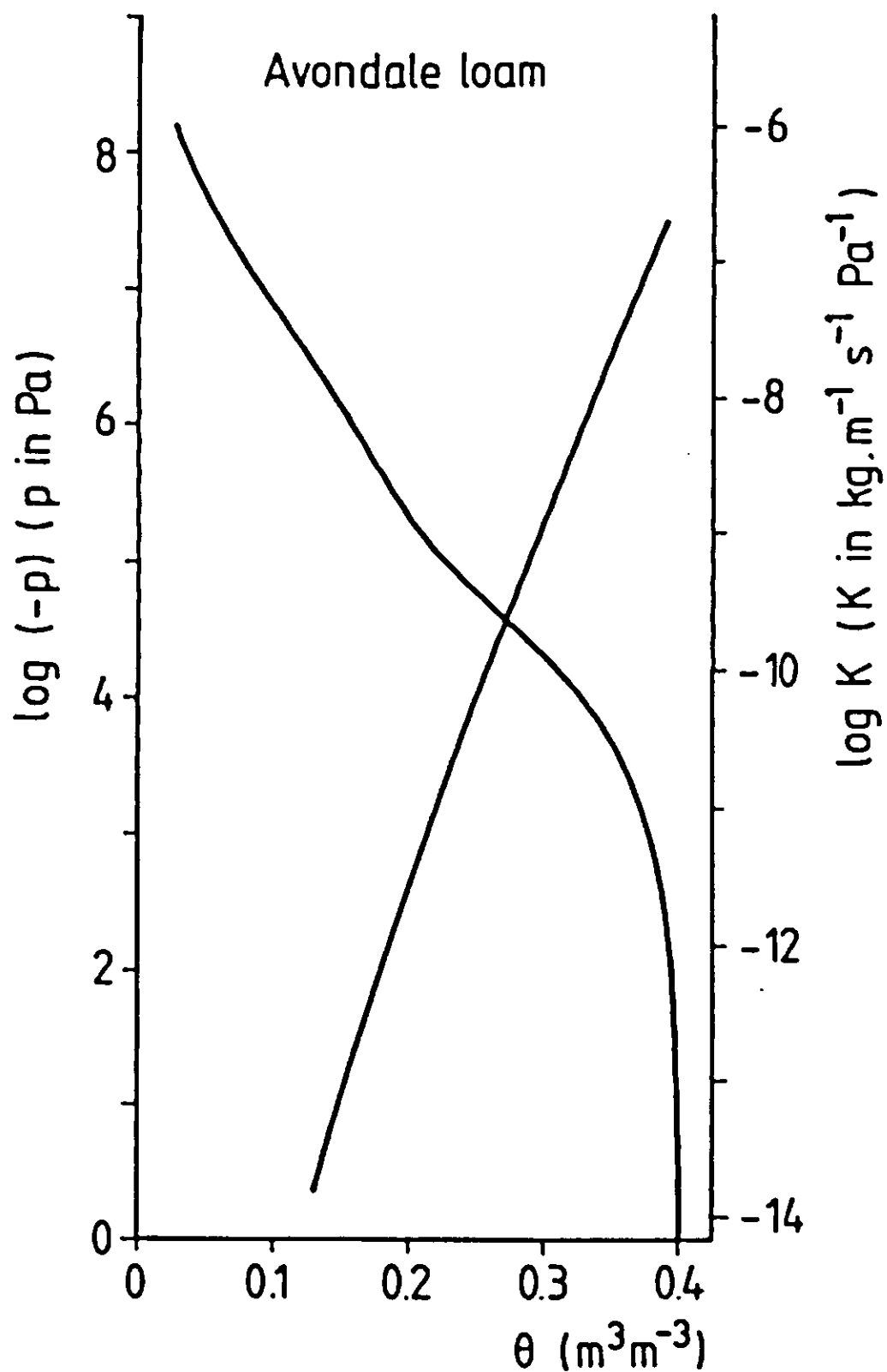


Figure 4.36 Hydraulic properties of Avondale loam (from: Jackson (1973)).

A remark must be made here on a special feature of the moisture characteristic, being its temperature dependence. During the FLEVO experiment, soil water pressures measured at various depths exhibited a marked diurnal course. Pressure potential increased (less negative) during daytime, and recovered during the night. To investigate whether this course could be explained fully by taking into account solely the temperature fluctuations, the effect of temperature on $p(\theta)$ was examined in the laboratory. Measurements were done on confined samples at constant θ , using pencil-type tensiometers and pressure transducers. The results are shown in Figure 4.37 for various water contents. These data can be summarised by the expression

$$(4.13) \quad \left(\frac{\partial p}{\partial T}\right)_\theta = a (\theta - b)^{-1} + c \quad (\text{Pa K}^{-1})$$

where the constants a , b and c have the values 104.2 Pa K^{-1} , 0.18 and 5.1 Pa K^{-1} (Ritsema, 1985). In section 3.6 it is demonstrated that a temperature

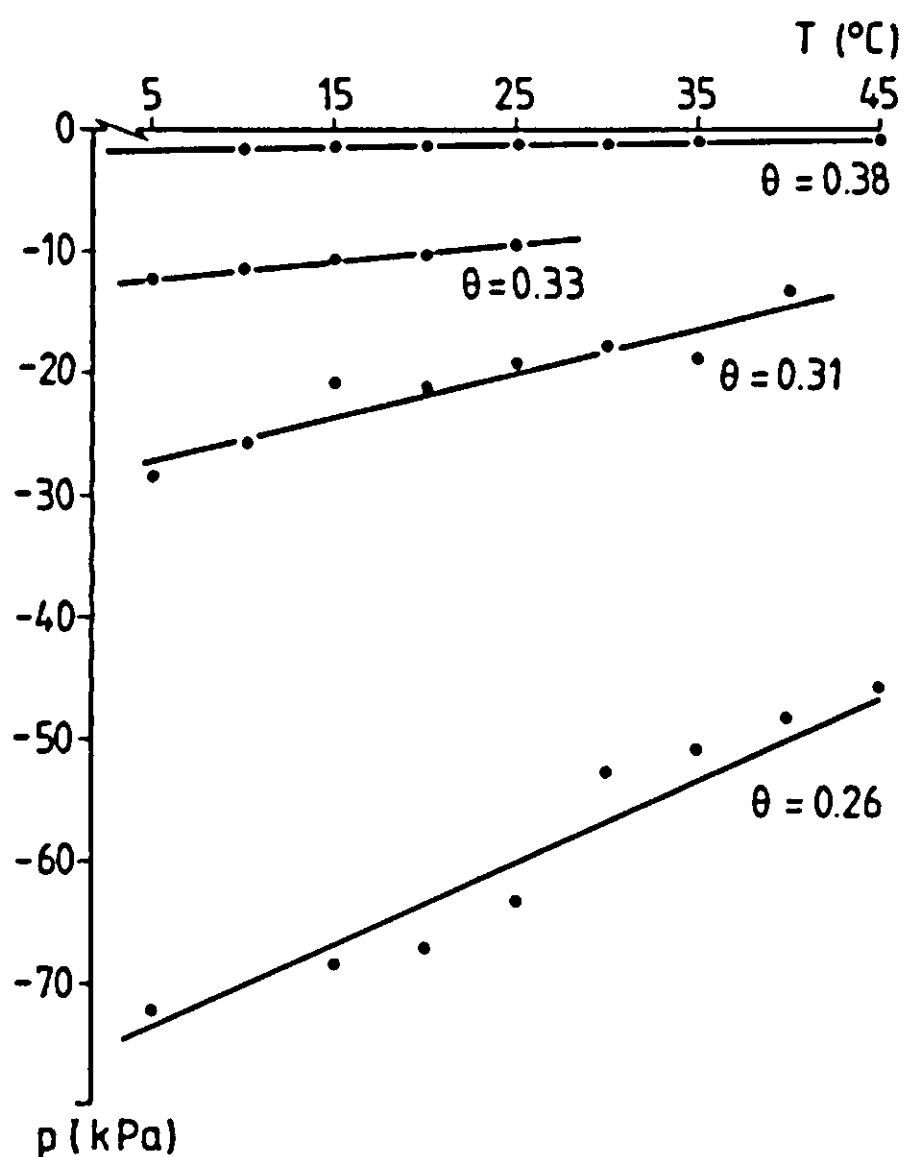


Figure 4.37 Temperature dependence of soil liquid pressure at various values of θ , obtained from laboratory measurements on core samples of Swifterbant silt loam. (See also Table 3.7).

induced pressure gradient should not be used as the driving force for flow, and so the above expression is not meant to be used in flux calculations. Nevertheless, the relation can be used to verify whether the observed pressure fluctuations observed in the field may have been due to temperature variations only. This will be done in Chapter 5 (Figure 5.13).

Hydraulic conductivity and matric flux potential

For the Swifterbant soils, $K(\theta)$ curves (Figure 4.25) were calculated according to the Van Genuchten-Mualem model (eq. 3.63). The parameter n , used in this equation, was derived from the average moisture characteristics of silt loam respectively loam, obtained as described before. As a matching point, measured K -values at $p=-1.0$ kPa were used.

According to the scaling concept for similar media, hydraulic conductivity at a given location r is related to the average value K_{sc} by the equation $K_r = \alpha_r^2 K_{sc}$, where α_r may be derived from the scaling of moisture characteristics. This relation was used here, and since the scaling factor shows a log-normal distribution, the estimated variability of K is based upon the variance of $\log \alpha_r$.

In addition, matric flux potential curves (section 3.6.2) were measured to characterize the hydraulic properties of the Swifterbant soils. The

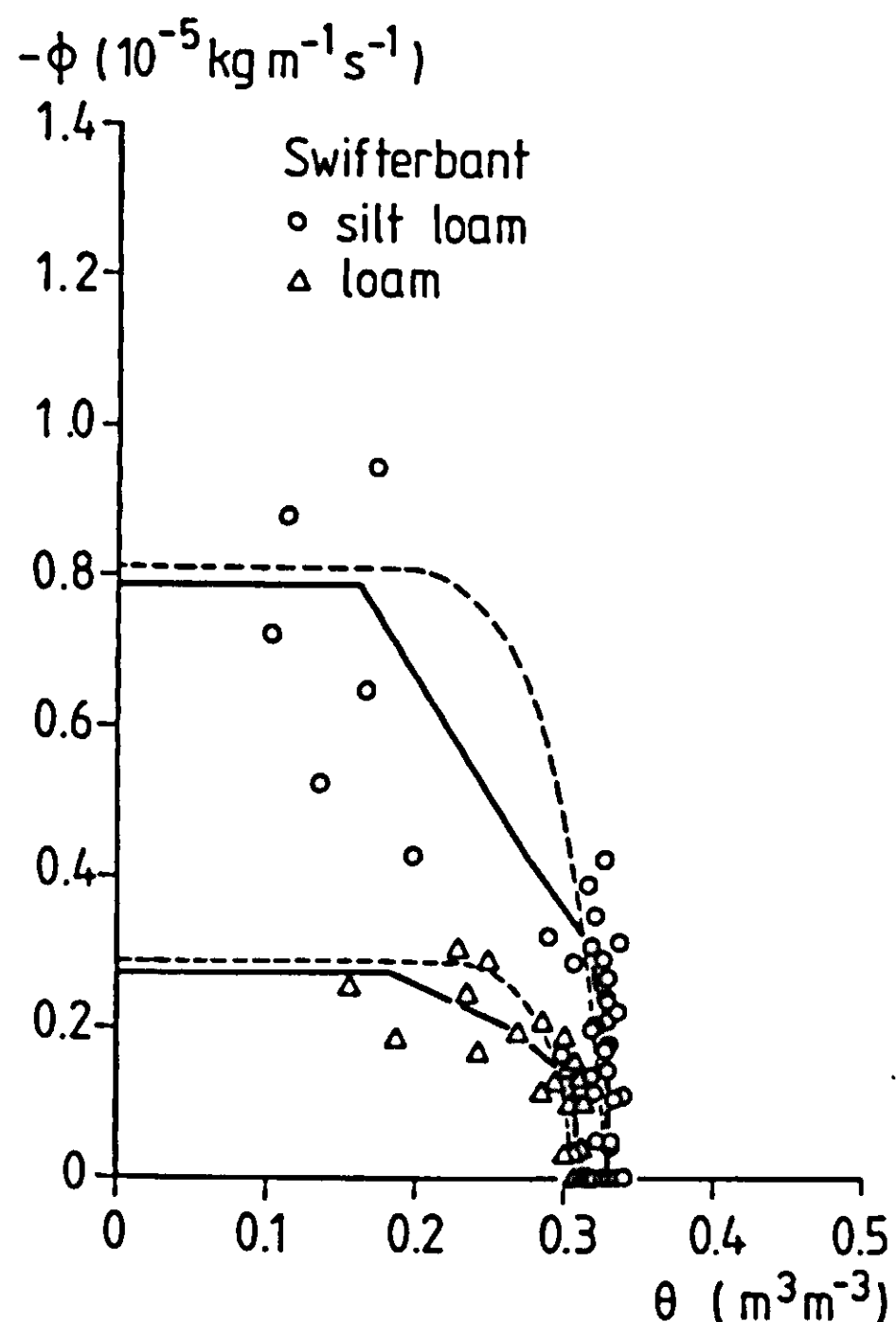


Figure 4.38 Measured matric flux potential curves of both Swifterbant soils. Solid lines were obtained by considering the total of eight core samples as a single soil volume, in applying the calculation procedures (Appendix 6). Broken lines are the result of numerical integration (see text).

curves by numerical integration (eq. 4.5). As an alternative, in this study a new steady state method was developed that enables one to measure directly the $\Phi(\theta)$ function (Appendix 6); this function then can be used as a substitute for the separate $K(\theta)$ and $p(\theta)$ curves. The measured results are shown in Figure 4.38, along with calculated curves obtained by numerical integration of the Van Genuchten-Mualem $K(\theta)$ curve, used in combination with the measured $p(\theta)$ curve, both of which are shown in Figure 4.25. The difference between the two Swifterbant soils, as demonstrated in Figure 4.38, is the main explanation of the difference in surface temperature as observed yearly from thermal imagery during Spring drying of the soils at the Ir. A.P. Minderhoudhoeve experimental farm. Variability in the $\Phi(\theta)$ function is again defined on the basis of the scaling factor, using the relation $\Phi_r = \alpha \Phi_{r sc}$.

Figure 4.34 shows the hydraulic conductivity of Buffalo silty clay as determined by the 'hot air method' (Arya et al., 1975) and as derived from the moisture characteristic (eg. 3.63). The $K(\theta)$ curve of Avondale loam as

presented by Jackson (1973) is shown in Figure 4.36. For both these soils, as for the FLEVO data, the scaling factors expressing the variability in moisture characteristics were used to define the variability in $K(\theta)$ as well.

4.7 Output and initial conditions: soil state variables and fluxes

The measured soil state variables are moisture content and temperature, and in the FLEVO experiment also the soil water tension in addition. These 'output' variables will serve at the start of the simulation runs as initial conditions.

The other 'output' variables are the fluxes of heat and moisture at the soil surface. The latter could only be assessed with sufficient accuracy for the FLEVO and ARIZONA experiments. Time sequences of 'output' variables will be presented in the next chapter for all datasets. Here only a brief description of the field situation is given. Appendix 8 summarizes more details on these measurements.

Soil moisture

At the FLEVO site, soil state variables were determined within small sampling plots at various locations in the field (Figure 4.1). As mentioned before, only the data from two plots (plots 1 and 4) are used in this report. The other plots gave comparable results.

Soil moisture content was determined by gravimetric sampling of four depth intervals of increasing thickness down to 55 mm. All samples were composites of five subsamples. A razor blade device was used for sectioning these top centimetres into thin layers by a single manipulation. To convert gravimetric to volumetric moisture contents, dry bulk densities of 1150 kg/m³ and 1050 kg/m³ were used for the silt loam and loam, respectively. These averages are based on a total of 100 transect samples. Throughout the experiment, significant changes in moisture content occurred only in the top 35 mm. Below this depth, changes were less than 2% by volume, and θ averaged 0.33 and 0.31 for silt loam and loam respectively, as determined by occasional gravimetric sampling.

Error variance in volumetric moisture content is due to within-plot variability of gravimetric moisture content and bulk density. For these properties, error standard deviations of 0.5-2.0 % by mass and 50 kg/m³

respectively were obtained from semivariograms. Based on these data, an average standard deviation of $0.025 \text{ m}^3/\text{m}^3$ may be estimated for volumetric water contents at all depths. It is well known that variability itself is dependent on the average level of moisture content, but extensive sampling for the study of spatial variability could only be done at a few occasions; hence the behaviour in time of spatial variability is hardly known.

Soil water tension was measured at various depths (Appendix 8). As mentioned in the previous section, a marked diurnal course was observed. The next chapter shows the relation of these fluctuations with those of soil temperature.

At the TEXAS site, moisture content of the top 30 mm was determined by gravimetric sampling. Samples were composed of ten subsamples to reduce scatter. For conversion to volumetric moisture content, a bulk density of 1220 kg/m^3 was used and an error standard deviation of 0.02 in θ was estimated. In addition, volumetric soil moisture content was measured by gamma attenuation and neutron moderation techniques for the complete profile (0-50 cm). Standard deviations of volumetric moisture content determined by gamma attenuation usually ranged from 0.01 to 0.04 below a depth of 10 mm. Only shortly after irrigation, standard deviations at these depths were larger, up to $0.10 \text{ m}^3/\text{m}^3$. Above a depth of 10 mm, variability was larger, the standard deviation rising to $0.09 \text{ m}^3/\text{m}^3$.

In the ARIZONA experiment, the complete profile was sampled gravimetrically in layers of increasing thickness, and samples were composed of several subsamples per layer. On the basis of the other two experiments, standard deviations of $0.02 \text{ m}^3/\text{m}^3$ are assumed.

Soil temperature

Soil temperature profiles were measured down to 0.5 m depth at the Swifterbant site. Measurement errors were 0.1 K, but again the corresponding variance is larger due to spatial variability. Like for soil water content, spatial variability of soil temperature depends on drying stage, depth and time of the day. Semivariance analyses of noon soil temperatures at 10 mm depth under fair weather conditions yield standard deviations of 0.2-0.4 K at the 4 m distance level. A value of 0.4 K is used for all depths and drying stages for the FLEVO experiment.

At the TEXAS site, where soil temperatures were determined at four depths in six plots, standard deviations ranged from 0.2 to 1.5 K for all depths. Contrary to the other experiments, the actual standard deviations

are available for all observations.

Profiles of soil temperature in the ARIZONA experiment were measured at small depth increments down to 1.28 m. An error standard deviation of 1 K due to spatial variability and measurement error is assumed for all depths.

Surface radiation temperature

The measured surface radiation temperature T_{sr} used in this report is defined by

$$(4.14) \quad \sigma T_{sr}^4 = \int_{\lambda=8}^{14 \text{ } \mu\text{m}} \{ \varepsilon(\lambda) W(\lambda, T_s) + R'(\lambda) \} d\lambda \quad (\text{W m}^{-2})$$

where $W(\lambda, T_s)$ is the blackbody emittance at temperature T_s , and $R'(\lambda)$ the reflectance by sky radiation. For the FLEVO and TEXAS experiments, this radiation temperature was actually measured by ground based and handheld IR thermometers, respectively. For the FLEVO measurements, the error standard deviation of the detector was 0.25 K in the relevant temperature range. The within-plot error standard deviation for radiation temperature as derived from semivariance analysis ranged from 0.5 to 1.0 K. Combined with the measurement error, this results in an error standard deviation of 1.03 K.

True surface temperature may deviate from radiation temperature by several K due to ambient radiation and to the fact the emissivity does not equal unity. The accurate measurement of sky radiation temperature requires various precautions (e.g. Jacobs, 1982); this variable was not measured regularly in the discussed experiments. As the surface radiation temperature is to be predicted by the SALSA model for a comparison with measured data, sky radiation temperature should be taken into account in the simulation to convert the actual surface temperature - as results from the energy balance equation - into radiation temperature by adding reflected ambient radiation to calculated emittance. To this purpose, sky radiation temperatures are assumed to vary over a 40 K range, which will increase the expected error variance in predicted surface radiation temperature by 2.25 K^2 (subsection 5.1.1).

In the TEXAS case, IR-temperature data were collected at ten sites. During daytime, standard deviations were between 1.0 and 1.5 K. At night these values decreased to 0.2-0.3 K. Sky radiation temperatures, measured over the hemisphere each time when surface temperature measurements were taken, were averaged arithmetically. Averages ran between 279 and 298 K.

Surface temperature for the ARIZONA experiment was determined by ther-

mocouples. A standard deviation of 1.0 K is assumed for these temperature data.

The surface fluxes can be calculated from the measured data only for the FLEVO and ARIZONA experiments. For the TEXAS case, evaporation was to be assessed by the use of microlysimeters. These however gave so much scatter in the results that a reliable record of the evaporative flux could not be obtained.

The fluxes of interest are the net radiation, the sensible and latent heat fluxes above the surface, and the soil heat flux. Net radiation was already discussed in section 4.4, along with the other radiation terms. The remaining fluxes will be discussed below.

Soil heat flux

The surface soil heat flux for both the FLEVO and ARIZONA datasets was determined from the development of soil temperature profiles in the top 0.30 and 0.16 m respectively, by numerical integration of the heat content profile. The required heat flux at a depth of 0.30 m was calculated from the temperature gradient and an estimated value of the apparent thermal conductivity in the FLEVO-case (section 4.6). For the ARIZONA experiment, the flux at 0.16 m was calculated from the first harmonic of the temperature wave at that depth.

It must be noted that, other than by the use of flux plates, this calorimetric method does not take into account that particular fraction of the surface heat flux that is spent on evaporation within the topsoil. This is convenient and correct in the present cases, where the procedures used to assess the evaporation term (Bowen ratio method and weighing lysimeters) do already take into account this subsurface evaporative heat loss (or gain). The errors involved, both in the estimated heat flux at 0.30 and 0.16 m depths and the calculated flux divergence above these depths, amount to approximately 10%. As the two terms are summed up to yield the surface heat flux, the coefficient of variation in the latter term is to be taken at 10% as well.

Latent heat flux

The latent heat flux was determined at the FLEVO site by the Bowen ratio method, using the combined equations:

$$(4.15) \quad H + LE = -R_n - G$$

and

$$(4.16) \quad \beta \equiv \frac{H}{LE} = \gamma \frac{dT}{de}$$

where β is the Bowen ratio and γ the psychrometer constant. The gradients of wet and dry bulb temperature were measured separately from the absolute values of these variables, to obtain relatively accurate figures for β . Measurements were made at 0.2 and 0.5 m. Error standard deviations in differences (between heights) for wet and dry bulb temperature (amplified signals) amount to 0.0025 K. For most daytime conditions ($dT/dz > 0.04 \text{ K m}^{-1}$; $de/dz > 10 \text{ Pa m}^{-1}$) this corresponds to a maximum error of 10% in the Bowen ratio. Combined with errors in net radiation and soil heat flux, this results in a relative error in the evaporation term that ranges usually between 10 and 20% during daytime.

In addition to the above method, total daily evaporation was determined on several days by the use of microlysimeters (Boast and Robertson, 1982). This was done in order to compare evaporative losses from the two different soils (loam and silt loam). The silt loam consistently showed a higher daily total evaporation than the loam, the difference ranging from 15 to 40%. For predicted differences in evaporation rate, see Chapter 5.

Evaporation for the ARIZONA dataset was determined by weighing lysimeters, with an accuracy of 0.05 mm/d. Vapour fluxes could not be assessed by the Bowen ratio method using de and dT derived from the 0.20 and 0.50 m measurements, possibly due to advection problems.

Sensible heat flux

The sensible heat flux was found along with the latent heat flux by application of equations 4.15 and 4.16 for the FLEVO data. The error variance was calculated as a function of time, and corresponds to a relative error of 10 to 20% during daytime. This figure increases at low net radiation, but in those cases the absolute error is usually below 5 W m^{-2} , as is also the case for the latent heat flux.

For the Arizona experiment the sensible heat flux was determined as a rest term, using measured net radiation and evaporative heat flux, and the soil heat flux calculated as described above.

CHAPTER 5. VALIDATION

In the present chapter, several attempts to validation of the SALSA model will be made. The results of the experiments discussed in the previous chapter are the basis of the experimental validation, presented in section 5.1. In the comparison of the theory with these experimental datasets only the shortened version of the model (Figure 3.1.b) will be used, since the available data are too limited in nature to be used for the prediction of boundary layer development. Hence the upper boundary conditions to the system are the measured values of air temperature, humidity and wind speed over the respective experimental fields, and the measured course of global or net radiation.

In section 5.2 an analytical solution of the surface energy balance equation is used in a test to merely check the correctness of the numerical formulations. A qualitative validation of the 'complete' model, i.e. including boundary layer development, is discussed in section 5.3, where a number of general boundary layer characteristics is inspected on the basis of common knowledge.

5.1 Experimental validation

The experimental results of the FLEVO, TEXAS and ARIZONA field studies will be used in a comparison with model predictions. Attention will be focussed in this section on the measured and simulated courses of surface fluxes (R_n , G, H, LE) and on the developments in surface radiation temperature, topsoil moisture content, and soil temperature (the latter two at various depths). These variables were named 'output variables' to indicate that they are to be predicted by simulation; since the measured values of these variables are used for validation, they have not yet been presented in the previous chapter.

In the validation of models by field observations, it is useful to take into account the errors involved in variables cq. system parameters. These are due to measurement inaccuracy and to spatial variability. This applies both to the fluxes and state variables actually measured, and to their predicted values; errors in the latter are due to errors in the system parameters and boundary conditions, used as input to the model.

5.1.1 Error variance analysis

The expected value of the error variance of some predicted variable $z_j \equiv f(x_i, i=1, n)$ can be expressed as a function of (1) the error variances in input variables x_i , and (2) the sensitivity of the prediction to changes in input. Thus for the case of non-correlated input-variables x_i , the expected variance in the output variable z_j is written as (e.g. Hahn and Shapiro, 1967)

$$(5.1) \quad E[\text{var}(z_j)] = \sum_{i=1}^n \left(\frac{\partial z_j}{\partial x_i} \right)^2 \text{var}(x_i) + \sum_{i=1}^n \left(\frac{\partial z_j}{\partial x_i} \right) \left(\frac{\partial^2 z_j}{\partial x_i^2} \right) \mu_3(x_i)$$

where n is the number of independent variables x_i and the derivative $\partial z_j / \partial x_i$ is the sensitivity of the function z_j to changes in x_i . μ_3 is the third moment about the mean. The second term in eq. 5.1 is assumed to be negligible, and if the derivatives are replaced by finite differences, the expected error variance is expressed in the linearized form

$$(5.2) \quad E[\text{var}(z_j)] = \sum_{i=1}^n \left(\frac{\Delta z_j}{\Delta x_i} \right)^2 \text{var}(x_i)$$

The variables z_j in the present case are the various model output variables, i.e. the surface energy fluxes and the soil state variables.

The sensitivity $(\Delta z_j / \Delta x_i)$ was assessed by running the simulation model for two values of x_i , differing by the error standard deviation $\sigma(x_i)$. (This implies $n+1$ runs in order to determine $E[\text{var}(z_j)]$!). As explained before, the error variance of x_i comes about by measurement errors and spatial dependence of x_i . It is assumed that the sensitivity as defined here is constant over small Δx_i intervals, and that the error in x_i is normally distributed; furthermore, interactions between the effects $(\Delta z_j / \Delta x_i)$ for the various x_i are neglected. The above procedure was applied in a hydrological context by e.g. Coleman and DeCoursey (1976) in a comparison between different evapotranspiration formulas. As can be expected, the variance as calculated by eq. (5.2) depends on the state of the system, and hence in the following its course in time is to be employed.

Now if for each output variable a measured course $z_j(t)$ and a predicted course $\hat{z}_j(t)$ are available, along with the associated variances for both time series, the evaluation of the prediction may take into account these variances by the use of the quotient q , defined as

$$(5.3) \quad q(t) \equiv \frac{\hat{z}_j(t) - z_j(t)}{\sqrt{[var(z_j(t)) + var(\hat{z}_j(t))]}}$$

The course of this quotient, which is similar to the Student t parameter, will be inspected as an indicator of model validity in the subsections 5.1.2-5.1.5 for the respective data sets. Predictions will be considered reasonable in this context if the value of q ranges between -2 and +2.

For the FLEVO and ARIZONA experiments, the observed behavior may now be compared to the predicted course over a time span of about four days for the following variables:

- net radiation
- soil heat flux ($z=0$)
- latent heat flux
- sensible heat flux
- surface radiation temperature
- soil temperature (3 depths)
- volumetric soil moisture (four depth intervals)

For the TEXAS case, only the state variables will be inspected, as the fluxes could not be established in the field with sufficient accuracy.

Table 5.1 summarizes the error standard deviations or coefficients of variation of the measured input variables as used in the simulation runs, and also includes for the system parameters - which do not vary in time - the values used as a reference. For more details the reader is referred to Chapter 4. The uncertainty in the predictions, caused by input errors, is expressed by the expected variance according to eq. 5.2. The corresponding standard deviations or coefficients of variation are listed in Table 5.2. Where ranges are indicated instead of single values, the relevant properties depend strongly on the state of the system. Table 5.2 also shows the error standard deviations in the measured series of 'output' variables. Employing these numbers and following the procedure described in this subsection, the course of q (as defined by eq. 5.3) was calculated for each output variable. To prevent problems in the use of this procedure caused by division through very small numbers, - as might occur for the variances of the nighttime fluxes - a q -value of zero was assigned in cases where the difference $|\hat{z}_j(t) - z_j(t)|$ is less than a critical value c . The resulting q -t series are shown for each dataset; where a c -value has been used, this is indicated in the corresponding figures.

Table 5.1 Inputs for validation runs: reference value and standard deviation or coefficient of variation.

variable	FLEVO 1 and 2		TEXAS		ARIZONA	
	ref.	σ or cv(%)	ref.	σ or cv(%)	ref.	σ or cv(%)
global radiation	1)	5%	1)	5%	1)	5%
air temperature	1)	0.1 K	1)	0.1 K	1)	0.1 K
vapour pressure	1)	15 Pa	1)	15 Pa	1)	15 Pa
wind speed	1)	4%	1)	10%	1)	4%
initial soil T	f(z)	0.4 K	f(z)	1.0 K	f(z)	1.0 K
initial soil θ	f(z)	0.025	f(z)	0.04	f(z)	0.02
cloud cover	f(t)	20%
a (eq. 3.8)	0.70	0.05
b (eq. 3.8)	0.04	0.02 mb ⁻¹
n (eq. 3.8)	0.10	0.05
sky rad. temperature	273 K	20 K	278 K	15 K	.	.
roughness length	0.08 mm	0.06 mm	0.8	.	0.015 mm	.
albedo	f(θ) 1)	0.02	.	.	f(θ)	0.02
soil emissivity	f(θ) 1)	0.01	0.96	0.03	0.97	0.01
longwave reflectivity	0.10	0.05	.	.	0.10	0.05
thermal conductivity	f(θ,ρ) 1)	20%	f(θ,ρ) 4)	20%	f(θ)	20%
heat capacity	f(θ,ρ) 1)	6%	f(θ,ρ) 1)	10%	f(θ)	10%
hydraulic scale α	1.0 2)	-0.51/+1.04	1.0	-0.3/+0.4	1.0	-0.5/+1.0
	1.0 3)	-0.58/+1.37				
β (eq. 3.81)	2.0	1.0	2.0	1.0	2.0	1.0

1) see chapter 4, 2) siltloam, 3) loam, 4) De Vries model.

.: irrelevant to the chosen modeloption

Table 5.2. Error standard deviations in measured and predicted output variables.

	FLEVO-1	FLEVO-2	TEXAS	ARIZONA
net radiation	0-20 a)	20-80	0-20	20-40
soil heat flux	0-20 a)	10-40	0-15	5-25
sensible heat flux	0-25 a)	5-80	0-15	5-15
latent heat flux	0-35 a)	10-100	0-35	5-35
surface rad. temp.	1.0	2-6	1.0	2.0-3.0
soil temp. T1 b)	0.4	1.5-2.5	0.4	1.0-2.0
soil temp. T2 b)	0.4	0.5-1.8	0.4	0.5-1.5
soil temp. T3 b)	0.4	0.5-1.5	0.4	0.5-1.5
vol. moisture θ_1 c)	0.025	0.05-0.15	0.025	0.01-0.05
vol. moisture θ_2 c)	0.025	0.05-0.15	0.025	0.01-0.04
vol. moisture θ_3 c)	0.025	0.02-0.03	0.025	0.02
vol. moisture θ_4 c)	0.025	0.02-0.03	0.025	0.02

a) calculated as 5, 10, 20 20% (FLEVO) and 5, 10, 20, 15% (ARIZONA) of actually measured values for R_n , G, H, LE, respectively.

b) FLEVO: 3, 11, 20 cm; TEXAS: 5, 10, 25 cm; ARIZONA: 1, 5, 16 cm.

c) FLEVO: 0-5, 5-15, 15-35, 35-55 mm; TEXAS: 0-5, 5-15, 15-30 mm; ARIZONA: 0-5, 5-10, 10-30, 30-50 mm.

5.1.2 FLEVO-1

The FLEVO-1 set typically represents some days of fine late Spring weather in the Netherlands (see also Chapter 4). The initial condition of the soil was homogeneously wet after heavy showers, and the strong drying conditions brought about high initial evaporation rates. Subsequent drying of the topsoil dramatically affected the Bowen ratio, rendering this series of data an interesting case for model validation. Moreover, the occurrence of two soil types within a single trial field offers an extra opportunity to test model performance. The data used for the silt loam case were taken from plot 1; the loam data used here refer to plot 4 (Figure 4.1). The model options chosen for the FLEVO-1 analysis are:

IFBLD = 0 (no boundary layer simulation)
IFMFLP = 1 (use of matric flux potential)
IFMTB = 1 (matric flux potential specified in a table)
IFGRAV = 0 (gravity not taken into account in water flow equation)
IFCHTB = 1 (soil thermal conductivity specified in a table)
IFNET = 0 (net radiation not used as boundary condition)

The results of one particular simulation run are depicted in the Figures 5.1-5.4 (surface energy fluxes) and 5.7-5.14 (state variables), along with the time series of actual observations. The inputs for this run were taken as listed in Table 5.1, and 'matching' was limited to varying the inputs within the range of the error standard deviations indicated in that table. The corresponding q-t series are shown in Figures 5.6 (fluxes) and 5.15 (state variables).

Some remarks must be made first regarding the two soil types distinguished in the experimental field. In terms of system parameters, the two soils are assumed to differ only in hydraulic properties and - slightly - in topsoil bulkdensity (Chapter 4). Of the surface fluxes, net radiation and the soil heat flux were observed for the silt loam plot specifically. In the measurement of sensible and latent heat fluxes, however, the use of the Bowen ratio method introduces the complication that the obtained fluxes represent some 'field averaged' values, which cannot be ascribed to a single specified soil type. Therefore, in the simulation effort, the model was run for the two soil types respectively (using identical boundary conditions), and for both situations the simulated sensible and latent heat fluxes are

depicted in Figures 5.3 and 5.4, along with the observations. According to the above one would then expect that, in the case of correct simulation, the observed courses of these two fluxes lie somewhere between the extremes, as simulated for the two soil types.

In contrast, the developments in topsoil moisture content and radiation temperature are of course site specific; these were observed separately for the loam and silt loam plots. The results, therefore, are also presented separately (Figures 5.7-5.12). A continuous record of soil temperatures of the loam site is not available, but incidental measurements revealed negligible differences with the silt loam plot at depths below 0.03 m.

Soil water pressure, as measured by a total of 28 tensiometers (equipped with mercury manometers), clearly showed a diurnal periodicity, the suction decreasing during the day and rising at night. Since one would rather expect the suction to increase during daytime, this behaviour called for a series of more detailed measurements under laboratory conditions, regarding the effect of temperature on the $p(\theta)$ relationship. The results of these measurements were shown in Figure 4.37 and condensed in eq. (4.13). Figure 5.13 is added here to merely illustrate the behaviour of topsoil water suction under field conditions, rather than to verify model predictions (SALSA neglects the effect of temperature on $p(\theta)$ as explained before). The broken line in Figure 5.13 represents the development of soil water suction as calculated from eq. (4.13), using the field-measured T- and θ -values (for the latter, a linear decrease in time was assumed, see Figure 5.12) at the depth of the corresponding tensiometer cup. It can be concluded that the observed diurnal pattern may be ascribed fully to temperature fluctuations, without taking into account moisture migration.

Evaluation of flux predictions

To prevent confusion, it is recalled here that fluxes are assigned a positive value if directed towards the surface, and a negative value when directed away from it. Of the surface fluxes, net radiation (Figure 5.1) is described fairly well. For daytime conditions, this needs not surprise, since global radiation as a measured driving variable constitutes a major fraction of net radiation. At night, when this flux is determined solely by surface emittance and sky radiation, predictions are also good. It is mentioned that for the sky emissivity parameters a and b (eq. 3.8) constant values were used, whereas in reality these values may vary over a

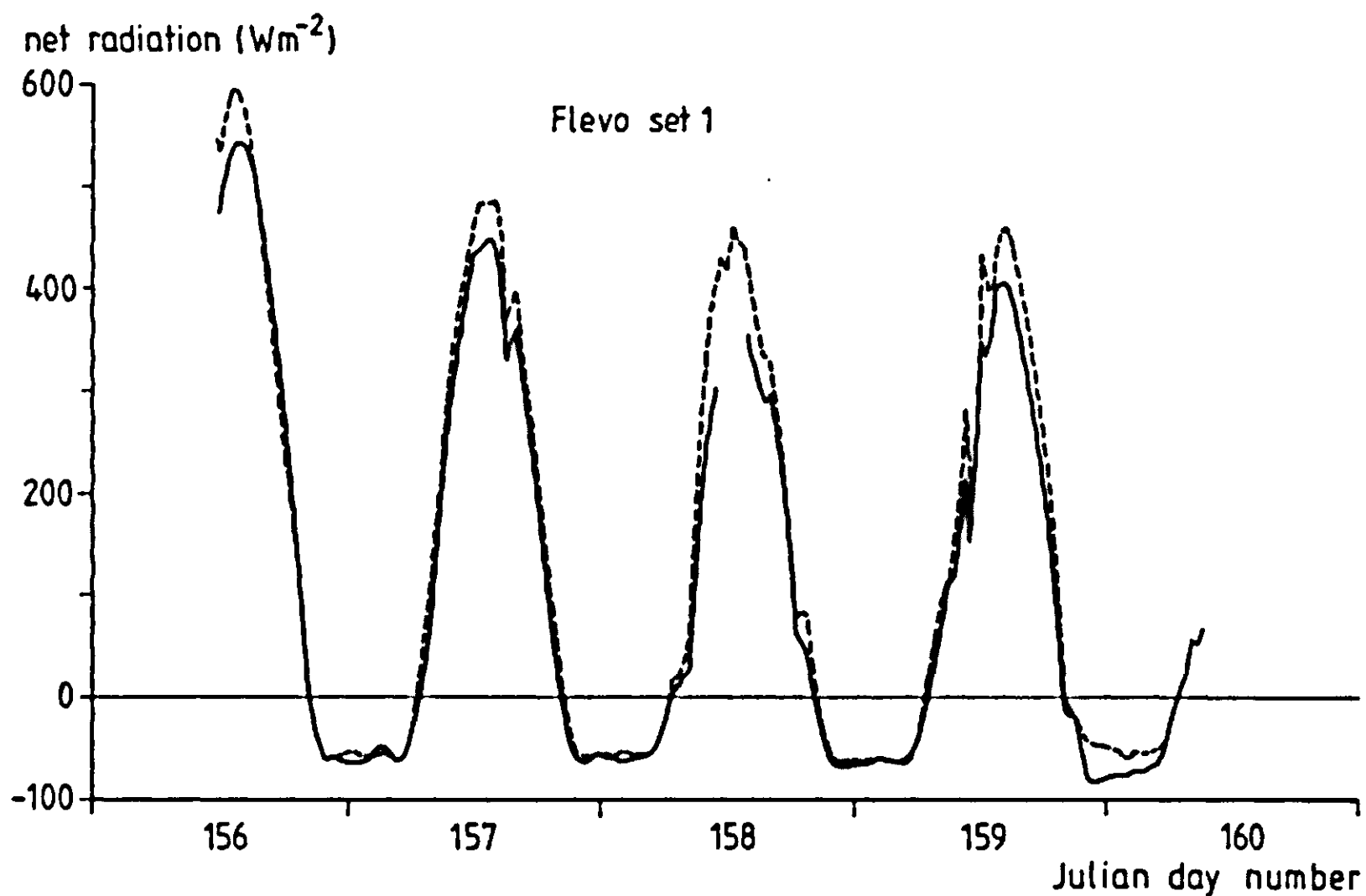


Figure 5.1 Measured (—) and simulated (----) net radiation.

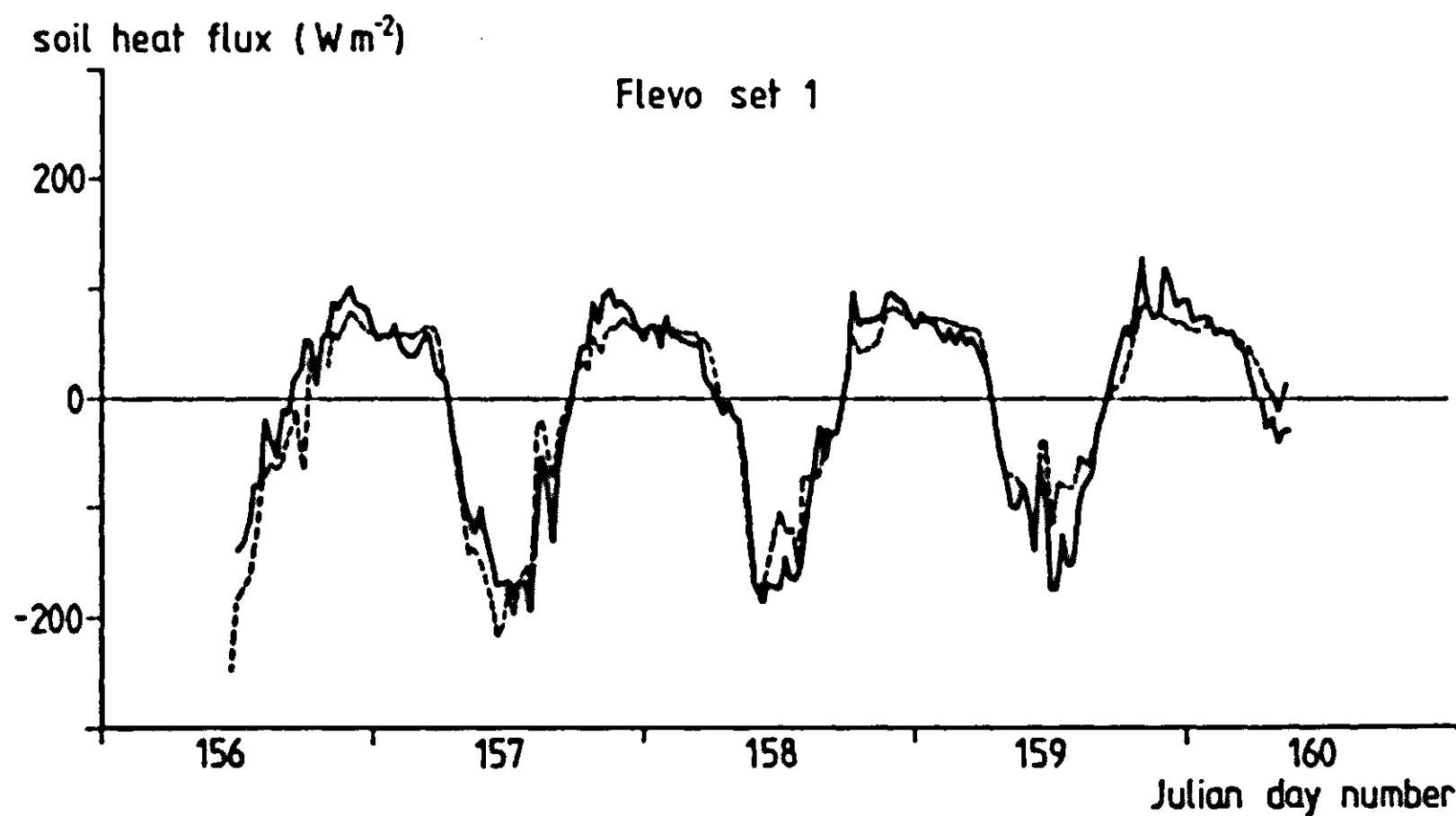


Figure 5.2 Measured (—) and simulated (----) soil heat flux.

considerable range (Table 5.1). In the specific case discussed here, these possible variations account for up to 75% of the expected error variance in the nighttime predictions of net radiation. A deviation in net radiation as observed for the night 159/160 may be explained by variations in a and b . The q -values for net radiation (Fig. 5.6) range between -1 and +1 throughout the experiment period, which is considered satisfactory.

The soil heat flux at the surface is also described reasonably well, although the peaks in both curves (Figure 5.2) do not always match. This causes q to fluctuate stronger than in the case of other surface energy fluxes. The accuracy attained in the registration of peaks and dips in the surface soil heat flux (by integration of temperature profiles) is limited by the spacing of temperature sensors just below the surface. Also, in contrast to most other variables, soil temperatures were registered in terms of momentary half hour values, i.e. without integration. These are probable causes of the observed discrepancy between measurement and simulation results. To illustrate that this validation is fairly sound, one may be reminded that all predicted surface fluxes are calculated by the model directly from the linearized gradients between the surface and the centres of the first soil and atmosphere compartments, respectively. The surface heat flux associated with soil heating or cooling is then obtained after subtraction of the predicted surface latent heat flux from the conduction flux between the surface and the centre of the first compartment; it has, therefore, no direct relation with the flux derived from measured temperature profiles.

The latent and sensible heat fluxes, as determined in the field by the Bowen ratio method, fit rather well between the simulated courses depicted in Figures 5.3 and 5.4 for the two respective soils. Only during the first day, the model underestimates the latent heat flux considerably. It may be noted also that the decrease in daily maximum latent heat flux, observed during the four subsequent days after the 'wet' start, is steeper than the corresponding decrease in the predicted values for both soils. (The inverse applies, somewhat mitigated, to the sensible heat flux). This may be due to the neglect of hysteresis in the soil hydraulic properties: the use of desorption curves implies an overestimation of the nighttime moisture redistribution (surface wetting). Overestimation of vapour transfer within the topsoil may also be a plausible explanation. A value of 2 was used here for the phenomenological coefficient β (eq. 3.81). In the field, no measures were taken to separate vapour and liquid transport in the soil.

The q - t series shown in Figure 5.6 for latent and sensible heat fluxes refer to the 'silt loam' simulation. (The predictions for the 'loam' case, when compared to field observations, will give better q -figures on days 159-160, and poorer results on the first two days). With q ranging mostly between -1.5 and +1.5, the discrepancy between prediction and observation is considered acceptable.

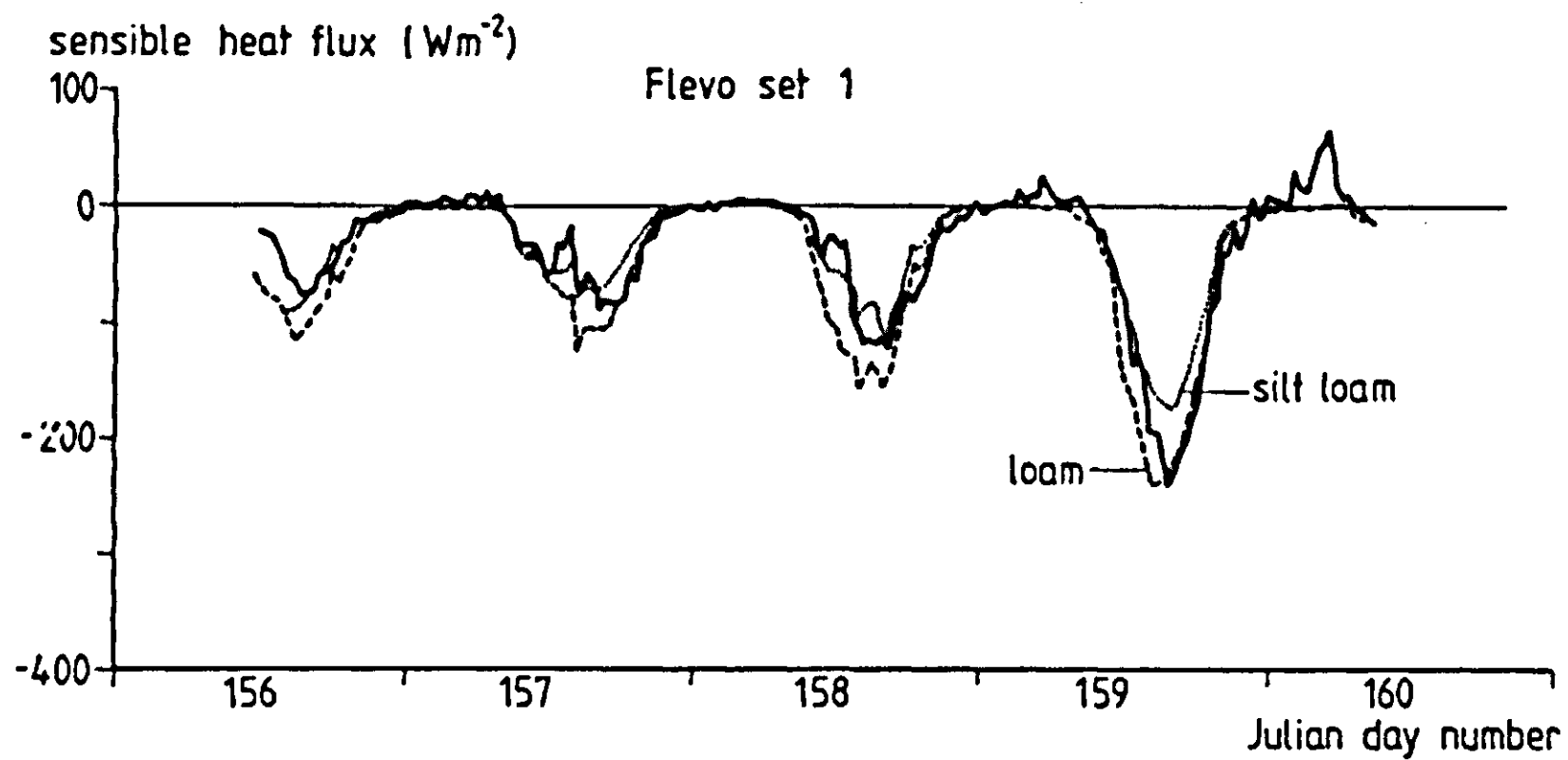


Figure 5.3 Measured (—) and simulated (---- and) sensible heat flux.

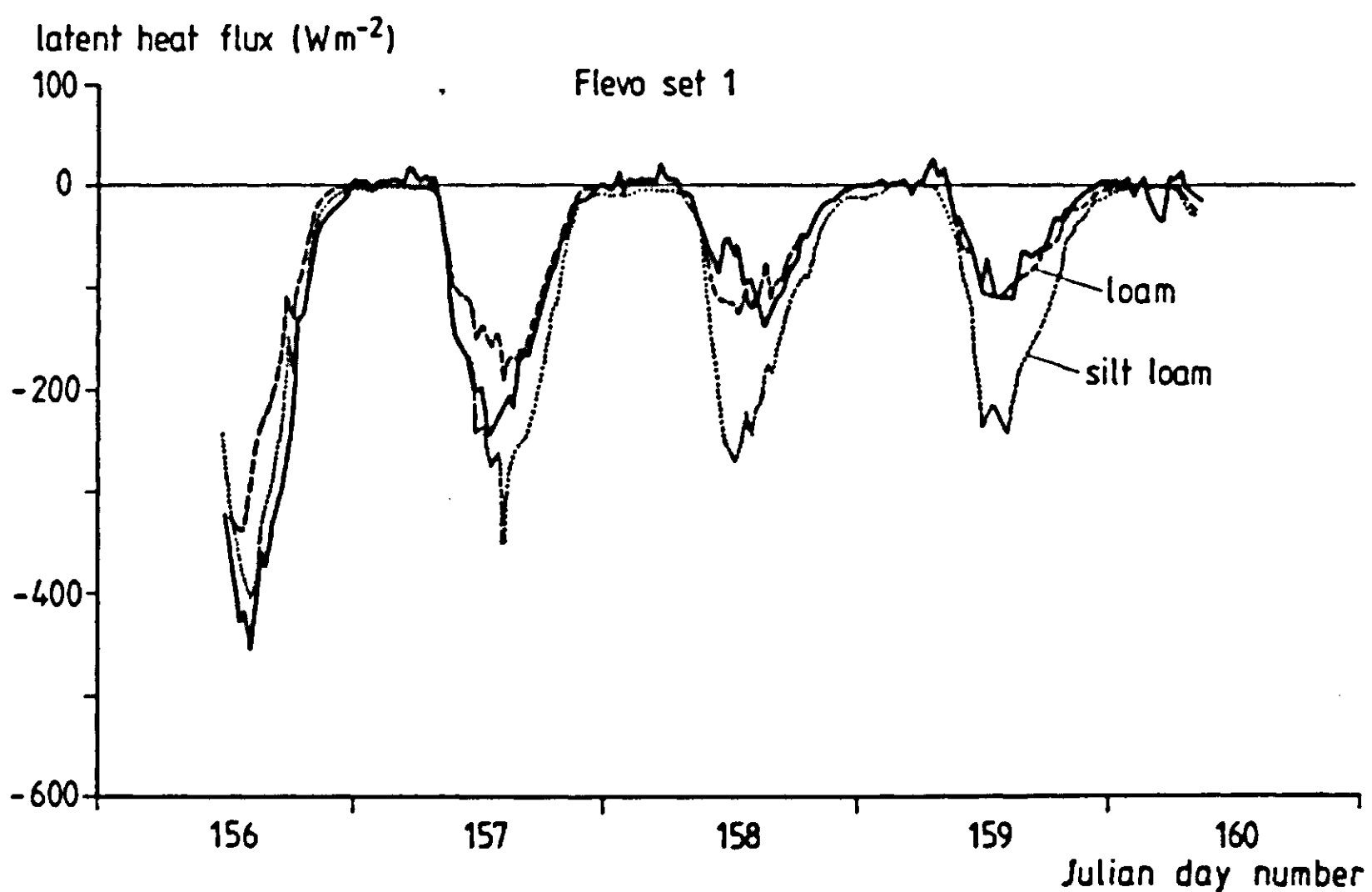


Figure 5.4 Measured (—) and simulated (---- and) latent heat flux.

Figure 5.5 shows the dramatic increase in Bowen ratio during the drying sequence. It appears that the soil type determines to a large extent the rate of increase of this ratio as time proceeds.

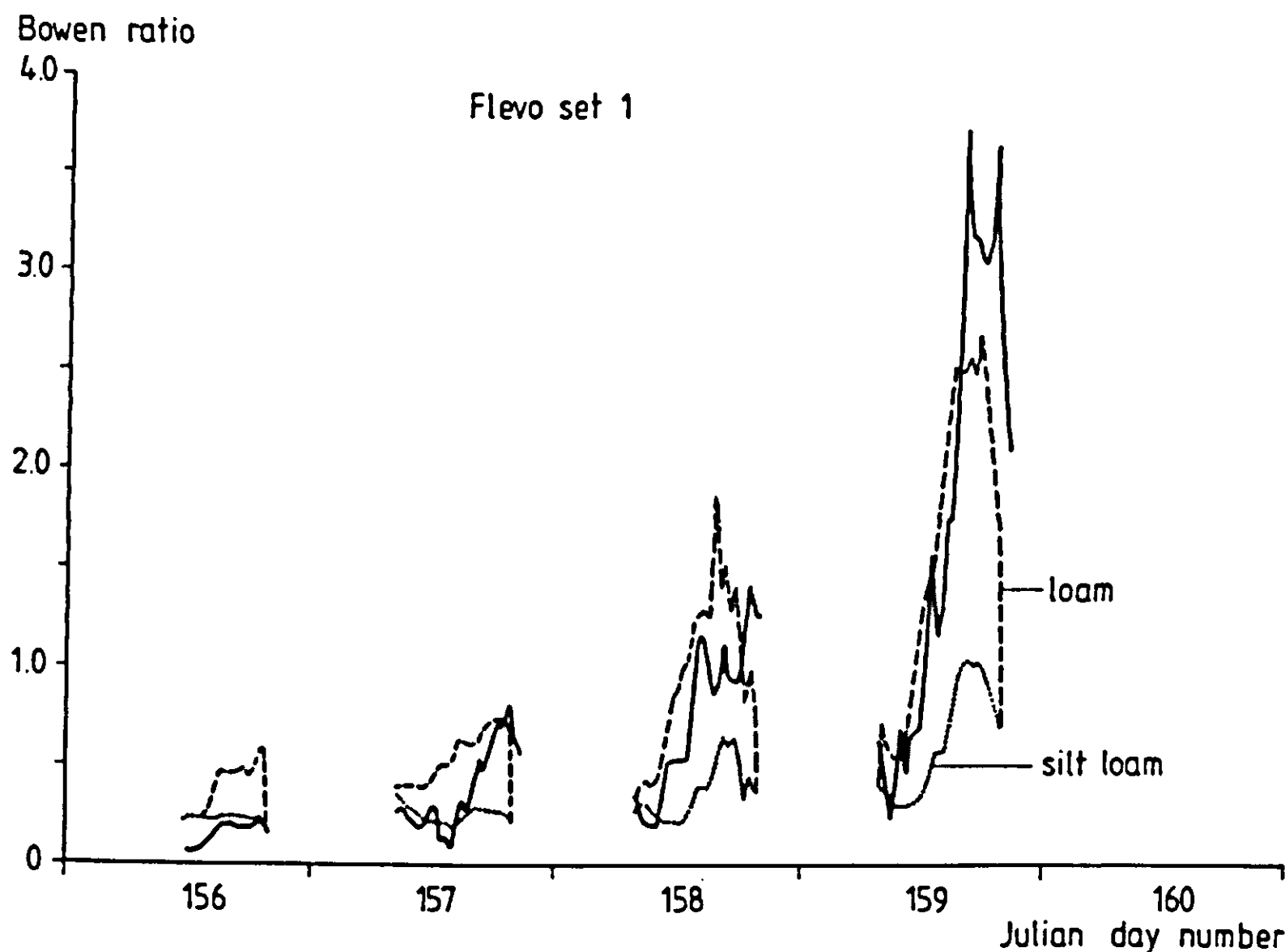


Figure 5.5 Measured (—) and simulated (---- and) development of the Bowen ratio, FLEVO set .

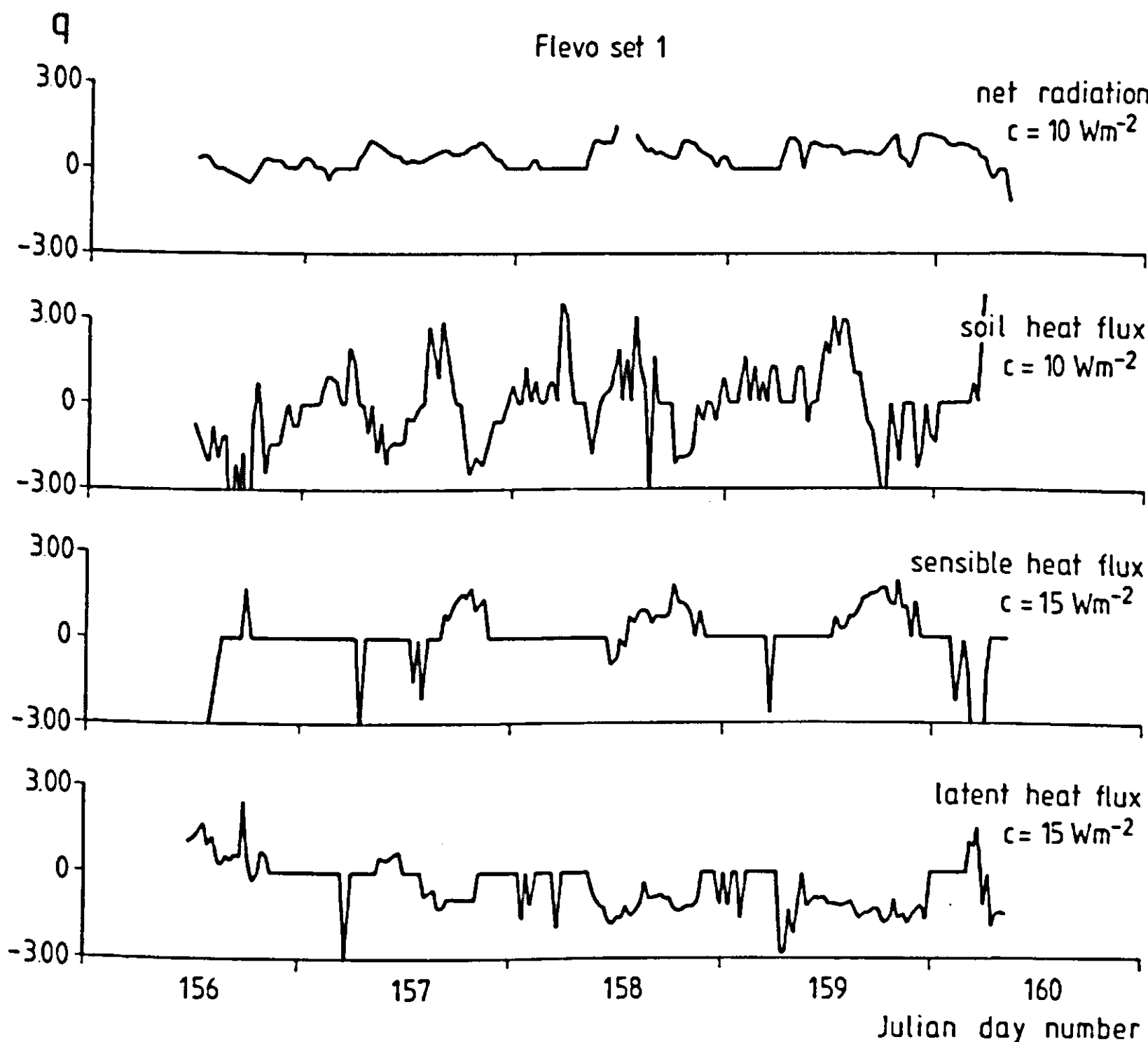


Figure 5.6 q-Values for the surface fluxes, FLEVO set 1. For explanation see text.

Evaluation of state variable predictions

For the silt loam, surface radiation temperature (Figure 5.7) is predicted rather well. The slight nocturnal overestimation may be associated with the excessive nighttime surface wetting, discussed above. However, also sky radiation temperature has a marked effect on surface radiation temperature during the night, and uncertainty in the former accounts for a maximum contribution of 45% to the prediction error variance. For the last night of the sequence, overestimation of net radiation is associated with the erroneous surface temperature prediction. Considering the expected errors (Table 5.2), the deviations as normalized in the parameter q should not be viewed as disturbing (Figure 5.15).

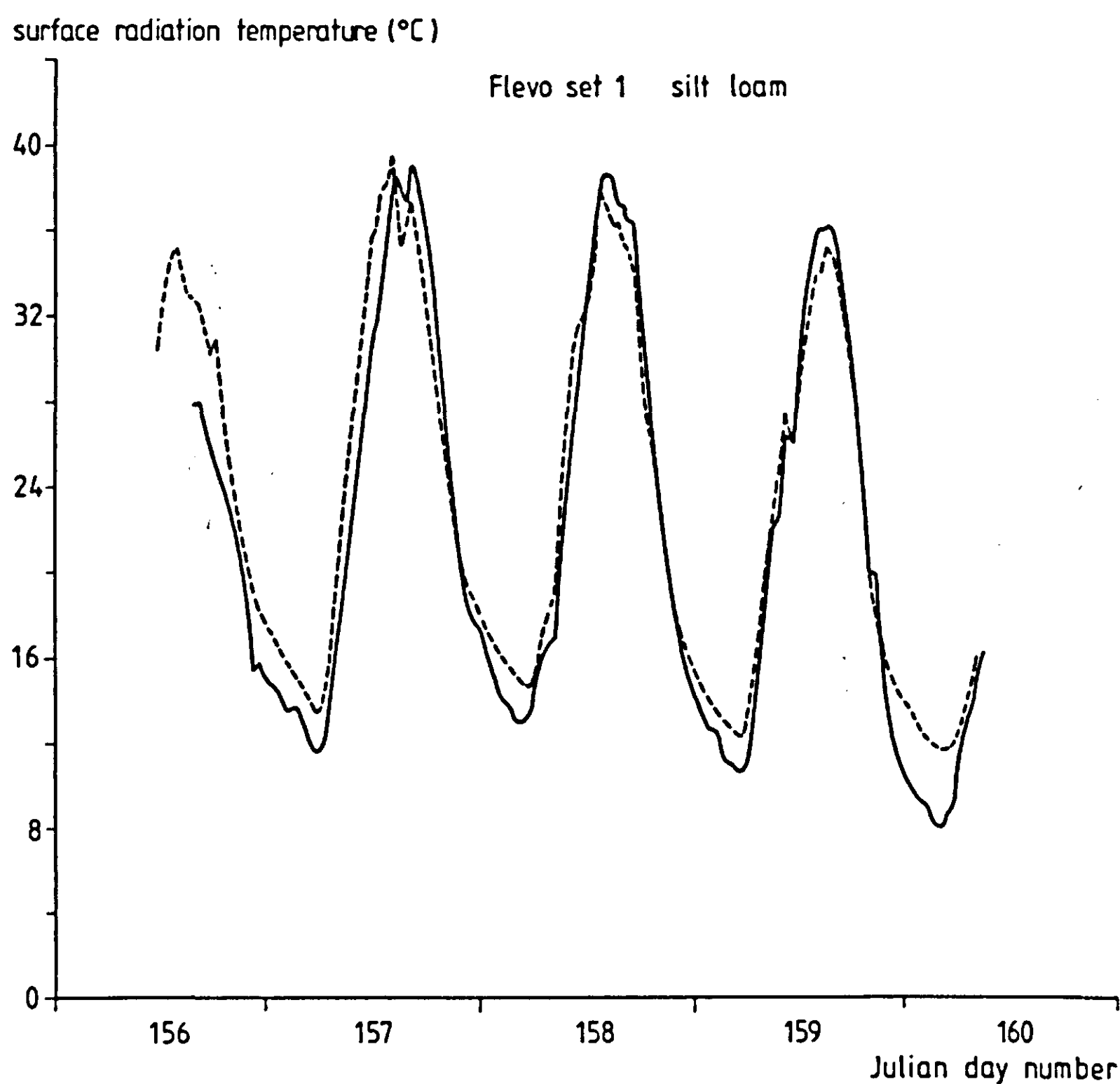


Figure 5.7 Surface radiation temperature for silt loam, measured (—) and simulated (----), FLEVO set 1.

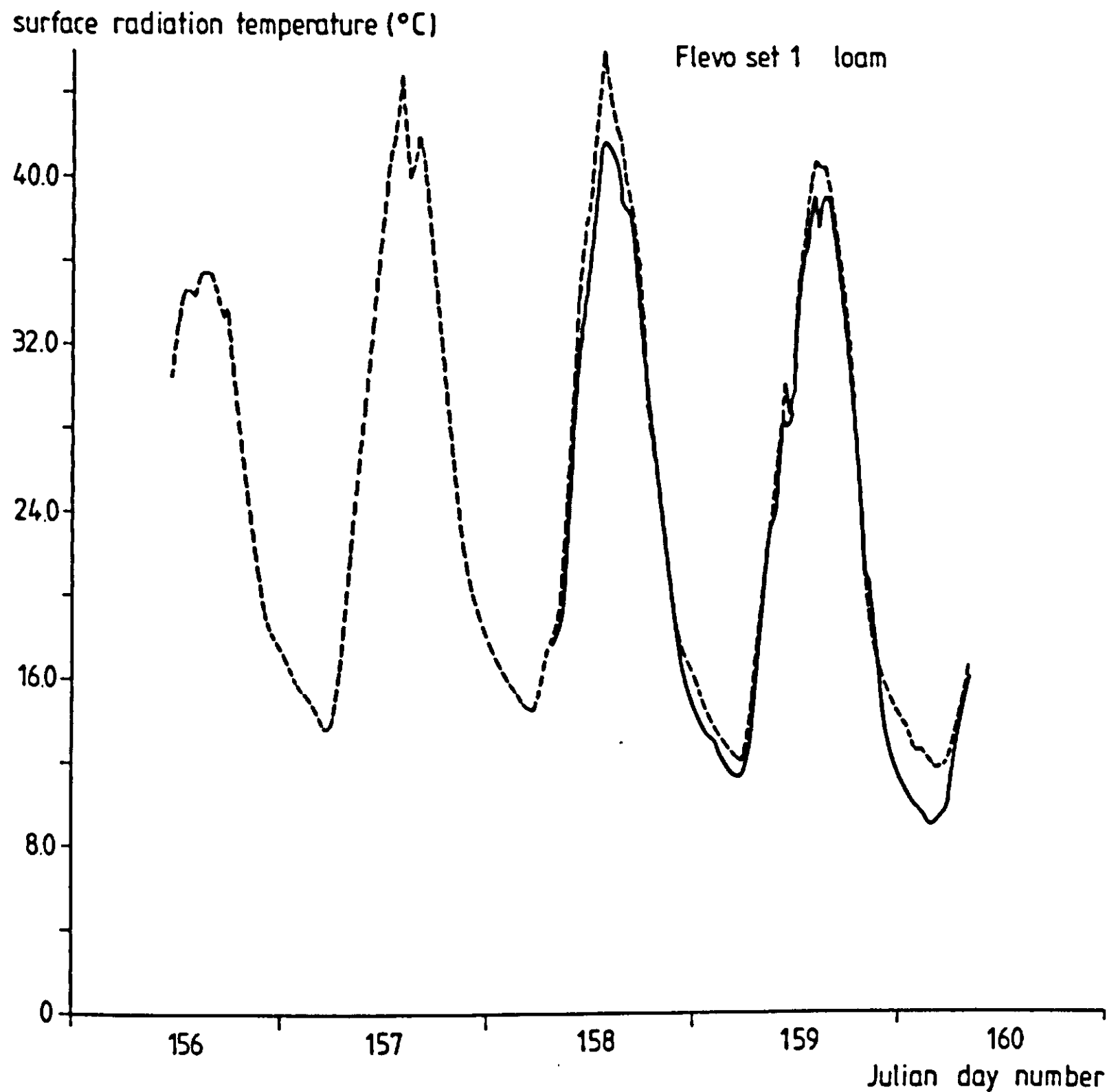


Figure 5.8 Surface radiation temperature for loam as measured (—) and simulated (----), FLEVO set 1.

A comparison between loam and silt loam radiation temperatures (Figures 5.7 and 5.8) shows the impact of the difference in 'surface hydrology', based on the different matric flux potential curves (previous chapter). The model, however, overestimates to some extent the radiation temperature for the loam plot, also during daytime. ~~overestimated~~

Topsoil moisture contents (Figures 5.9-5.12) changed only little at the depths 15-35 mm and 35-55 mm for both soils; the simulation results are in accordance with this observation. The gradual decrease in daytime moisture content over the four day period is predicted correctly for the various layers in both soils (note the faster drying for the loam surface layers); the amplitude for the 0-5 mm layers however, is grossly overestimated in the silt loam case. As stated before, the neglect of hysteresis or an erroneous value of the vapour transport coefficient might cause such a result. For the

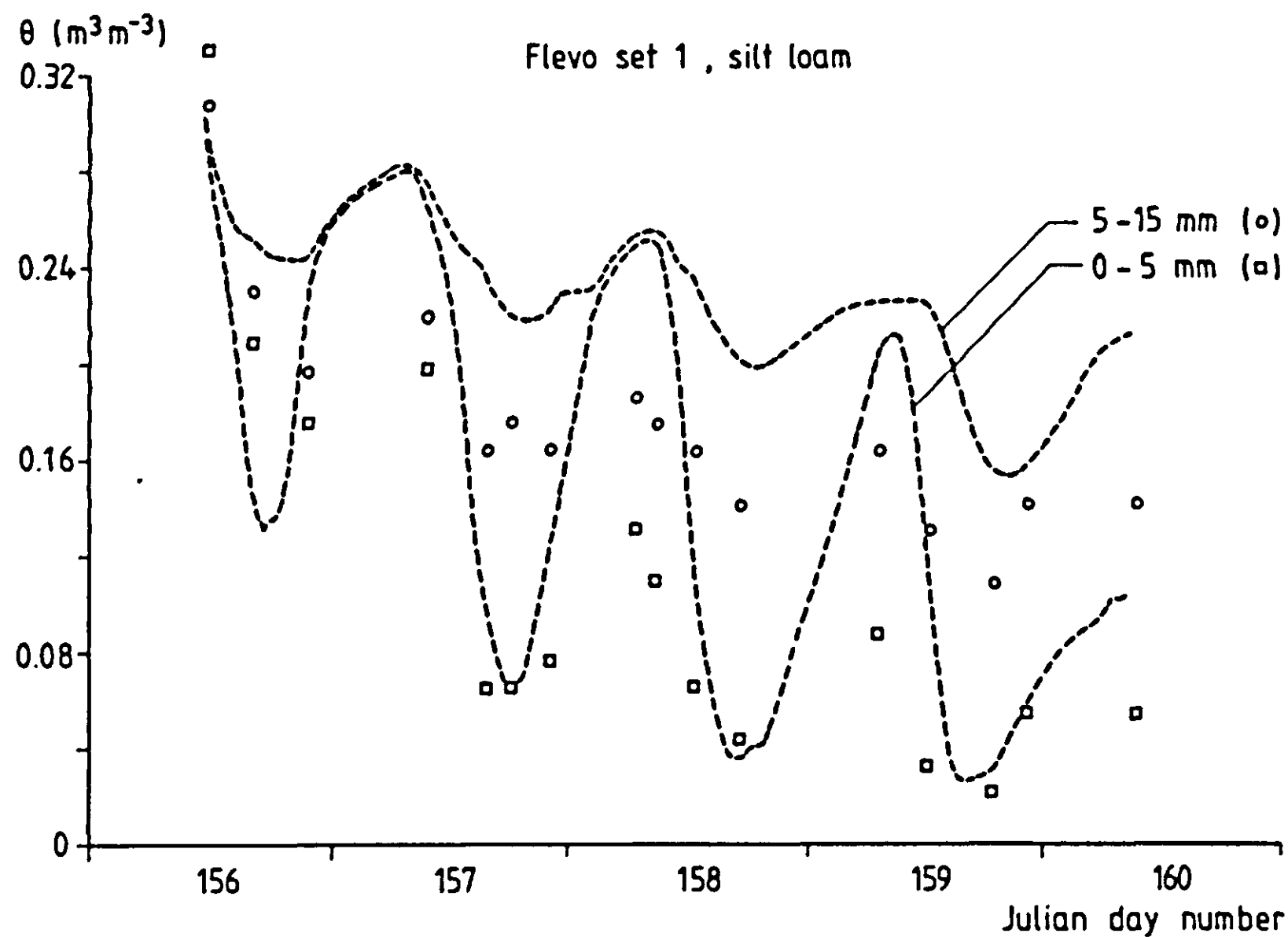


Figure 5.9 Soil moisture contents at various depth intervals, silt loam, FLEVO set 1; symbols represent observations, broken lines simulation results.



Figure 5.10 Soil moisture contents at various depth intervals, silt loam, FLEVO set 1.

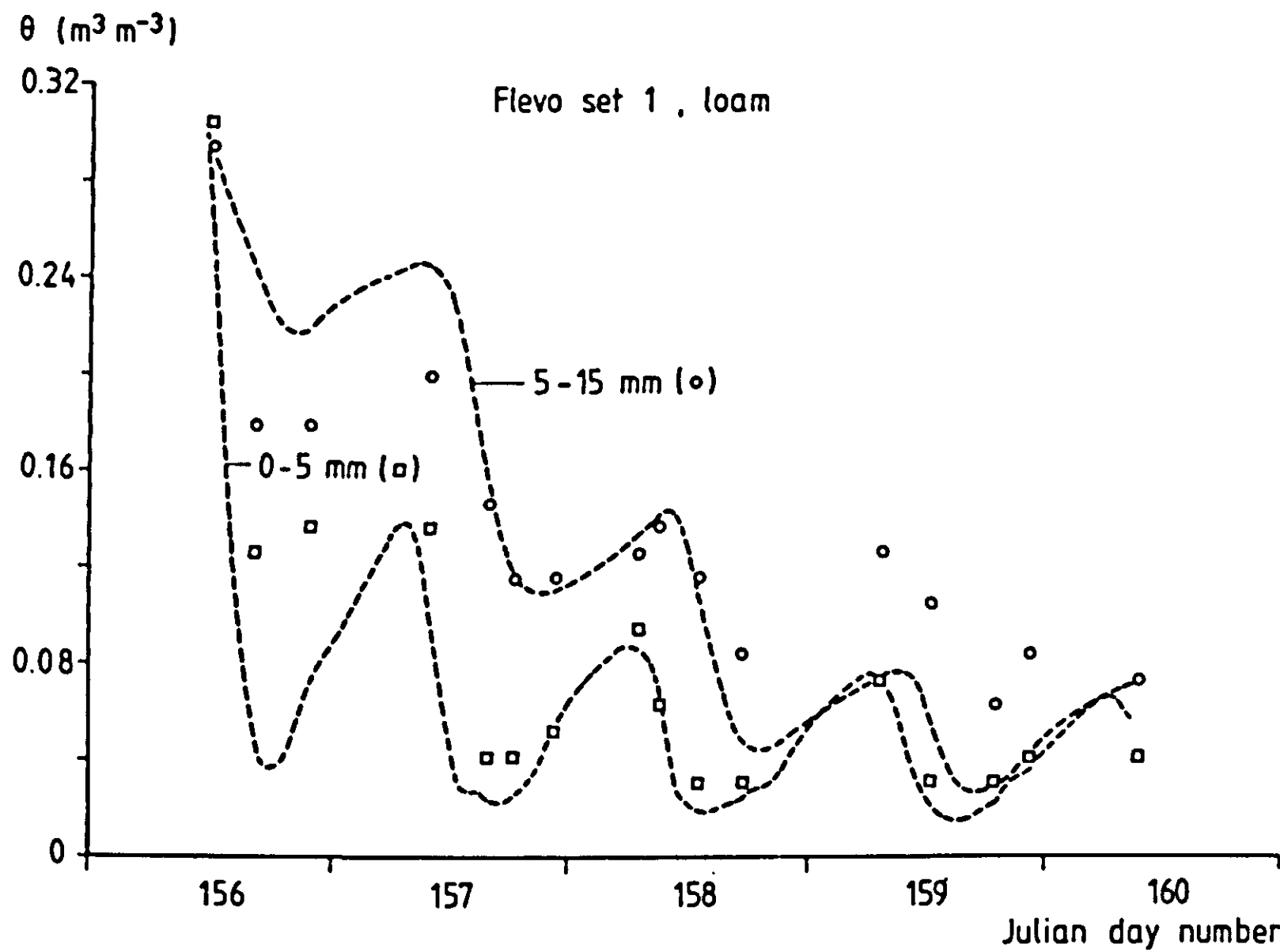


Figure 5.11 Soil moisture contents at various depth intervals, loam, FLEVO set 1; symbols represent observations, broken lines simulation results.

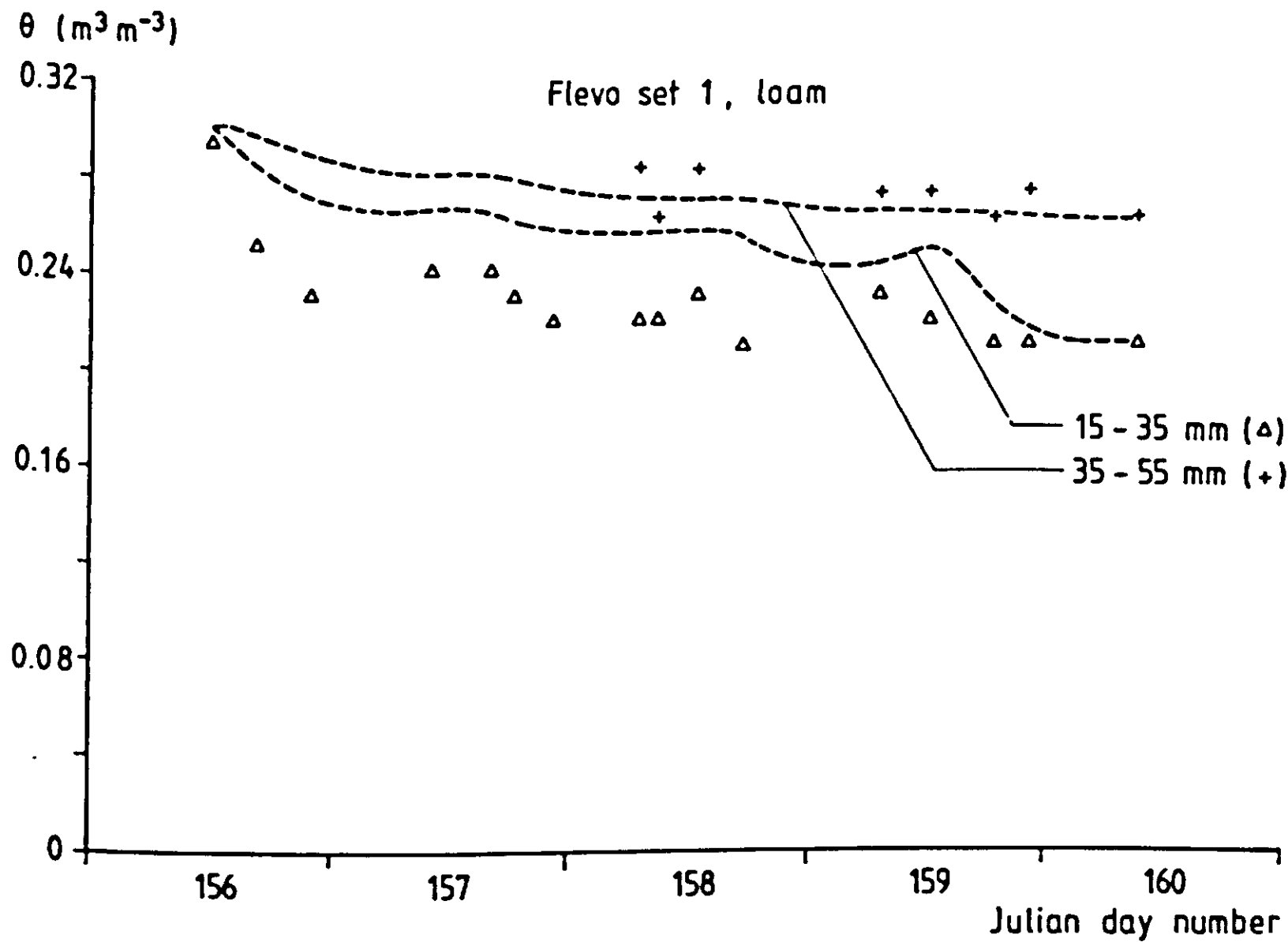


Figure 5.12 Soil moisture contents at various depth intervals, loam, FLEVO set 1.

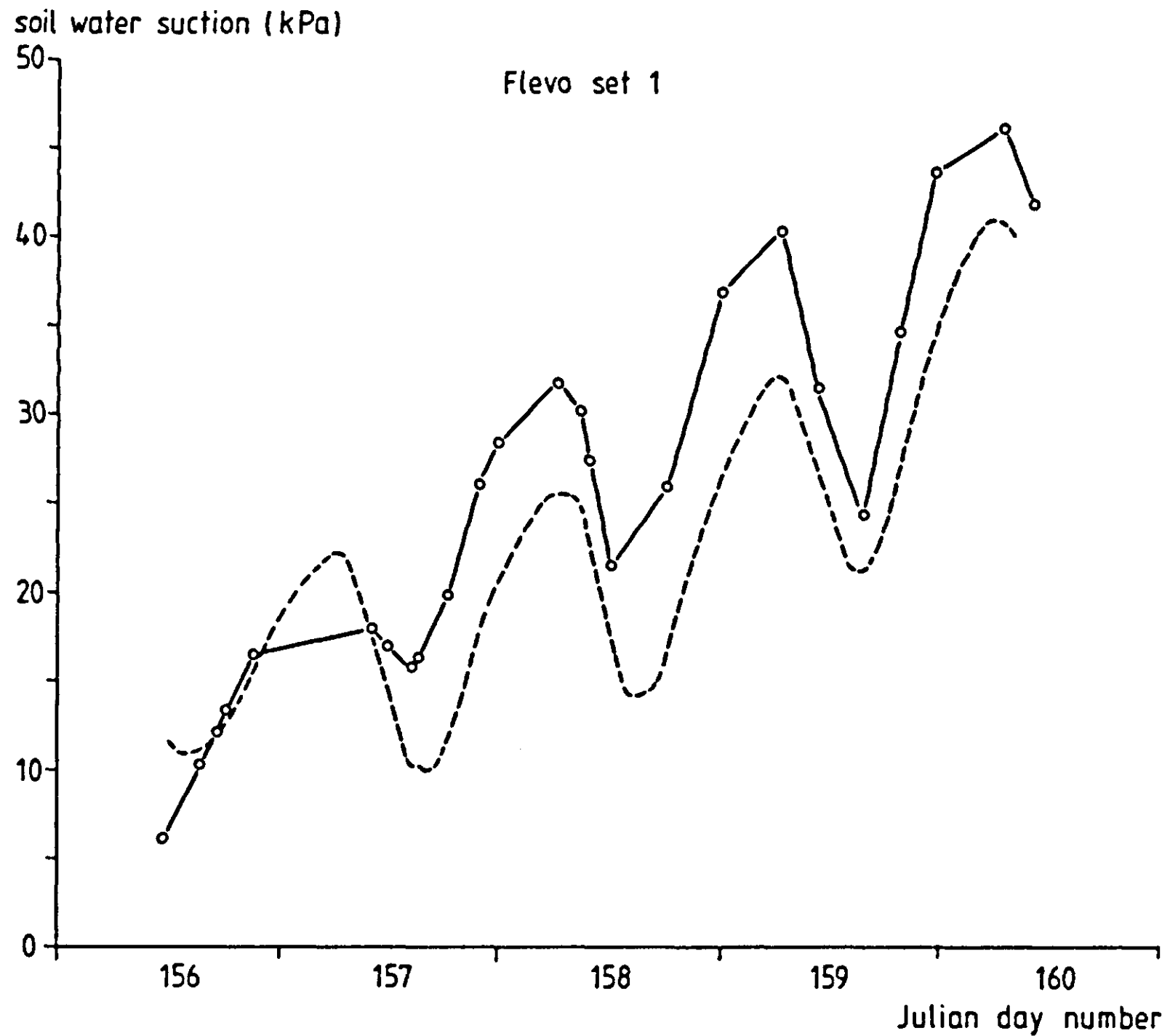


Figure 5.13 Soil water suction as measured (—) at 4 cm depth on silt loam, FLEVO set 1. The broken line shows the course, calculated on the basis of field measured $T(t)$ and $\theta(t)$, combined with laboratory measured $p_\theta(T)$ relationships. (Figure 4.37).

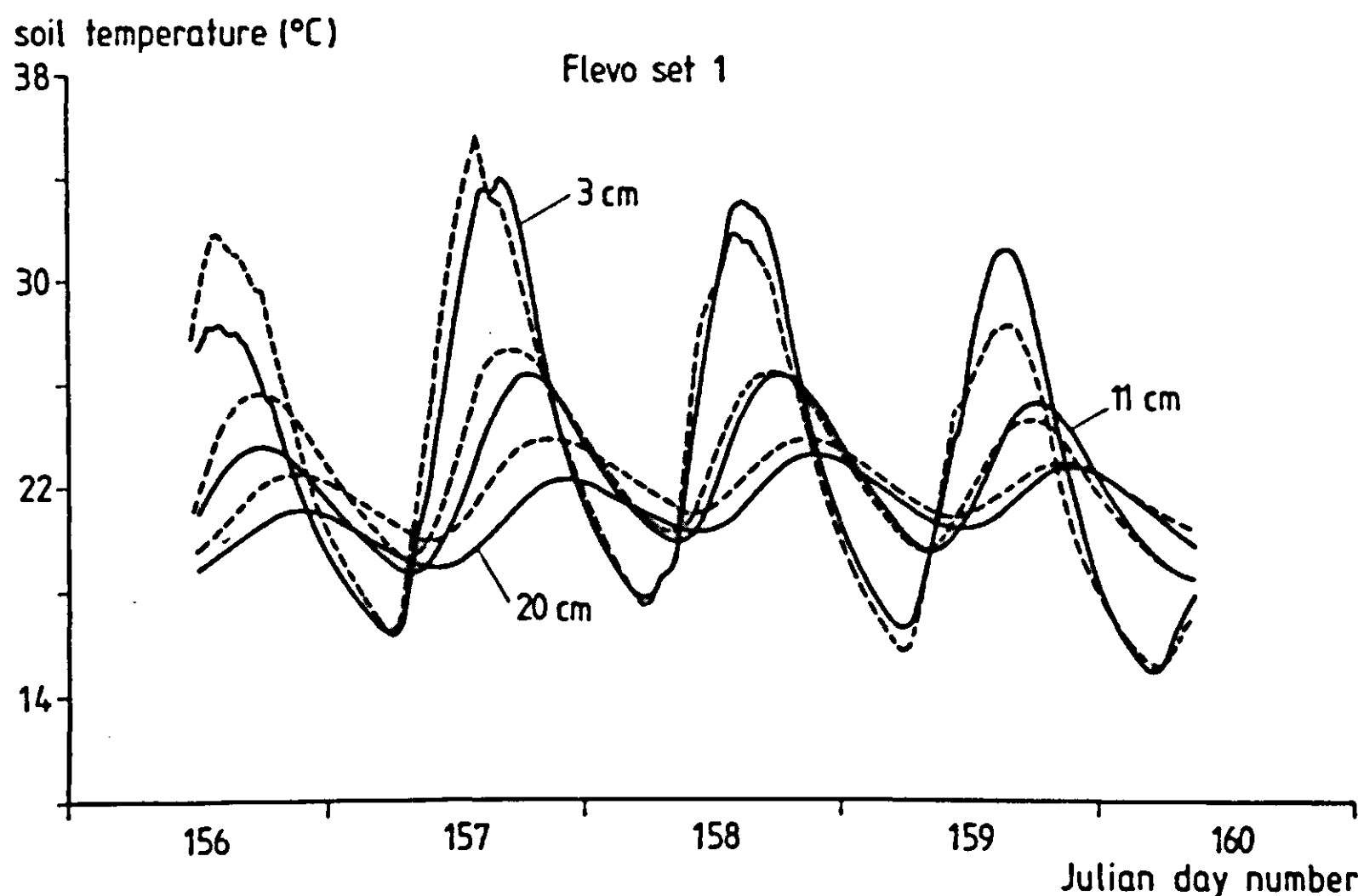


Figure 5.14 Measured (—) and simulated (----) soil temperatures at various depths, FLEVO set 1.

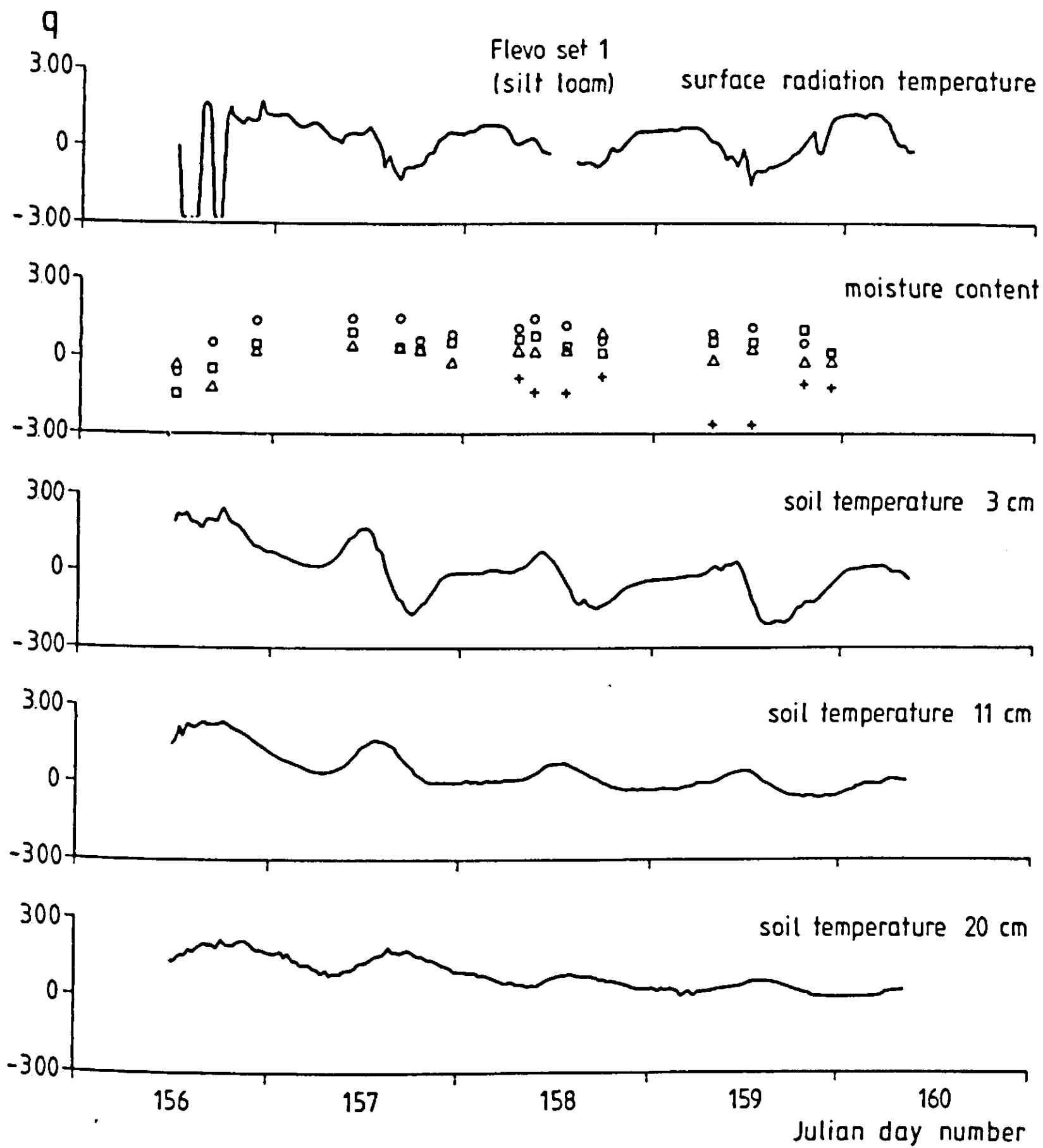


Figure 5.15 q-Values for the soil state variables, FLEVO set 1.
(□:0-5 mm; ○:5-15 mm; △:15-35 mm; +:35-55 mm).

loam case, where the same value for the vapour transfer coefficient was used in simulation, such a discrepancy is not observed. Moisture content in the 5-15 mm layer is consistently slightly overestimated for the silt loam. The diurnal amplitudes at this depth are predicted accurately for both soils. The values of q as depicted in Figure 5.15 mostly range from -1.5 to 1.5. Major sources of prediction error variance for moisture content in the top two layers are the uncertainties in sky emissivity parameters (accounting for up to 30% of the prediction error variance), in the hydraulic scale parameter α (up to 40%), and in the initial moisture content (up to 80%). For the layers 15-35 and 35-55 mm, the latter factor almost exclusively accounts for all the variance.

Soil temperatures appear to be predicted well at night, but not satis-

m; at 0.03 m depth, daytime temperatures are either over- or underestimated. On day 156, this is associated with an overestimation of the soil heat flux, at the expense of the latent heat loss. For this particular day, q-values for the soil temperature attain unacceptably high values (Figure 5.15). On the reason of this behaviour can only be speculated, at this stage.

5.1.3 FLEVO-2

Irregular weather conditions characterized circumstances during the FLEVO-2 experiment (Chapter 4). Over a five day period, cloudy and rainy days alternated with days exhibiting intermittent sunshine. As a result, surface energy fluxes and soil conditions show strongly fluctuating patterns; a specific feature for this dataset is the course of the surface soil heat flux, which shifted frequently during daytime from negative to positive and vice versa.

Tables 5.1 and 5.2 again list the input and output variables, along with the associated error intervals. The following options were used in running the model for the FLEVO-2 case:

IFBLD = 0 (no boundary layer simulation)
IFMFLP = 0 (hydrology formulated in terms of K-p)
IFKTB = 0 (hydraulic conductivity function specified in Van
Genuchten parameters)
IFGRAV = 1 (gravity term included in water flow equation)
IFCHTB = 1 (thermal conductivity specified in table)
IFNET = 0 (net radiation is not used as boundary condition)

The occurrence of rain during several days prescribes the gravity term to be taken into account. In the simulation run, the measured total of 33 mm precipitation was distributed uniformly over the 41 hour time span during which it was registered, resulting in an average flux of 0.81 mm h^{-1} . This averaging procedure was applied to prevent the time steps from decreasing to unacceptable small values, as would occur during peaks in rainfall intensity. Apart from the above, the treatment of this dataset was identical to the procedure described in the previous case. Because of the predominantly moist conditions, a difference in the behaviour of the loam and silt loam soil types could hardly be assessed; for this reason only the silt loam results are presented.

The figures 5.16-5.19 show the surface fluxes as measured and simulated, and Figure 5.29 depicts the corresponding q -values. The developments in the soil state variables can be seen from the Figures 5.21-5.24, whereas Figure 5.25 gives the $q-t$ series as calculated for the various output variables. One is reminded that all results shown and discussed are the output of one particular simulation run, and that to obtain these results, 'matching' was limited to the error intervals of the input variables (Table 5.1)

Evaluation of flux predictions

Net radiation for this dataset is predicted very well, with the exception of daynumbers 176-177 (Figure 5.16); this discordance is due to an increase in albedo which occurred in reality because of surface drying, but which is not effectuated in the simulation, since surface drying is not predicted correctly; the latter will be discussed below. Note that also the nighttime values are described rather accurately.

For the soil heat flux, the same as stated for the FLEVO-1 dataset applies; the spacing of temperature sensors is critical, especially where fluctuations are so pronounced as in the present case. For this reason, q reaches extreme values; some overestimation seems to occur during the first half of the day, whereas during the second half the heat flux is underestimated. Finally, a comparison with the FLEVO-1 data shows clearly the expected connection between nighttime soil heat flux and net radiation.

The latent and sensible heat fluxes (Figures 5.18 and 5.19) are predicted accurately, again with the exception of day 177. As mentioned, no distinction is made between the two different soil types, because the predominantly wet conditions prevented the difference in topsoil behaviour - which appears during drying only - to come about. The values of q are considered acceptable.

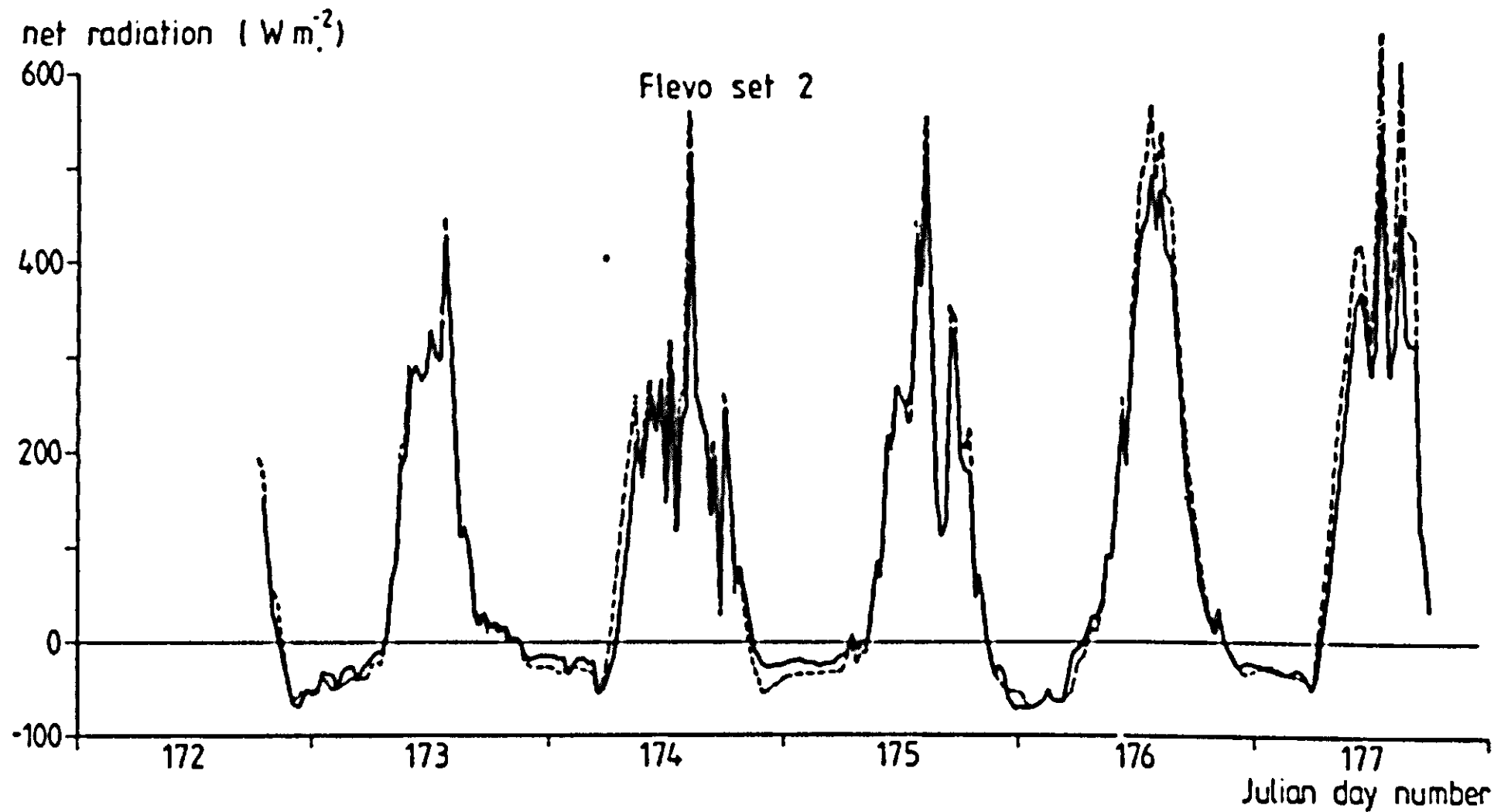


Figure 5.16 Measured (—) and simulated (----) net radiation, FLEVO set 2.

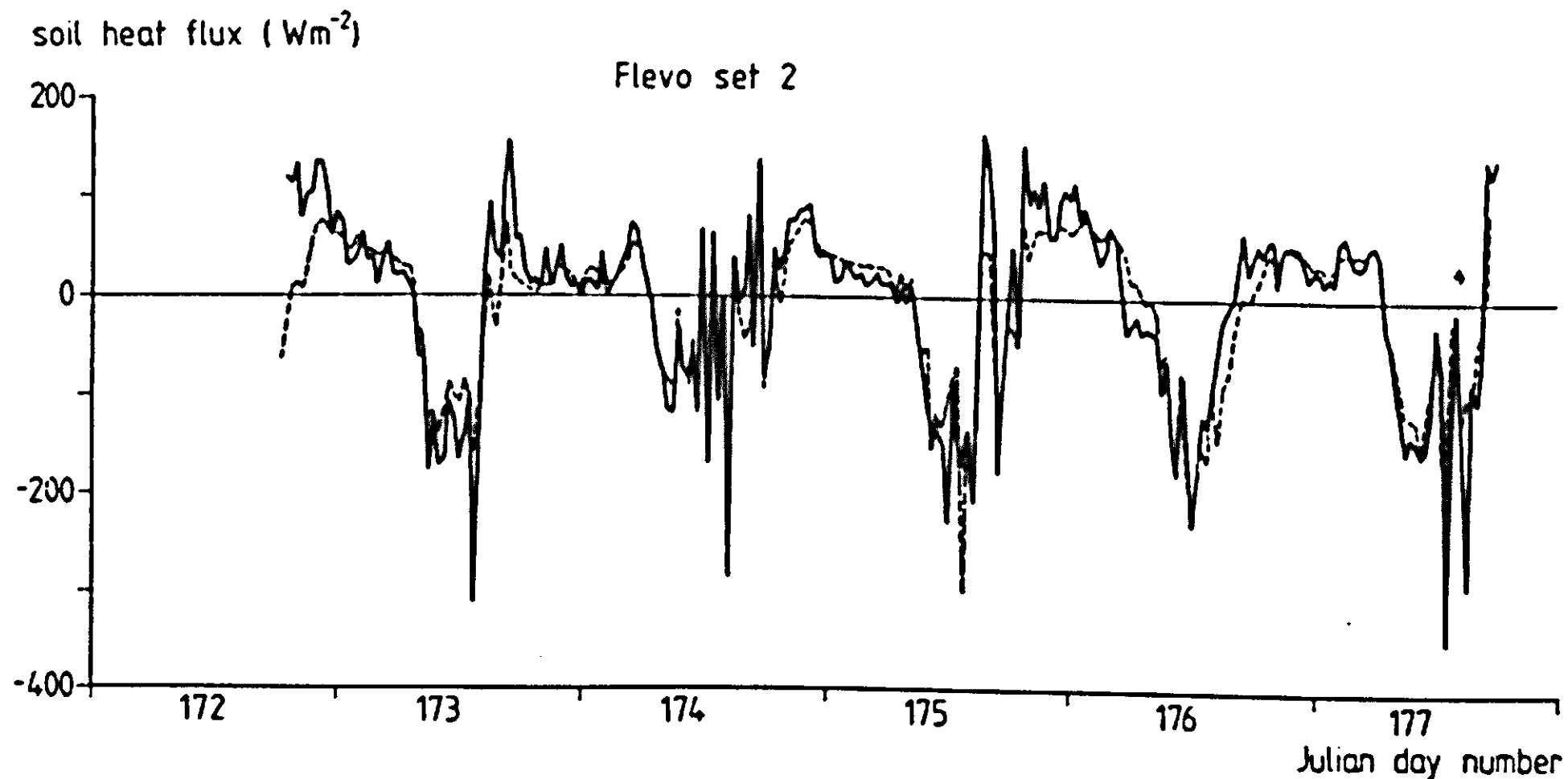


Figure 5.17 Measured (—) and simulated (----) soil heat flux, FLEVO set 2.

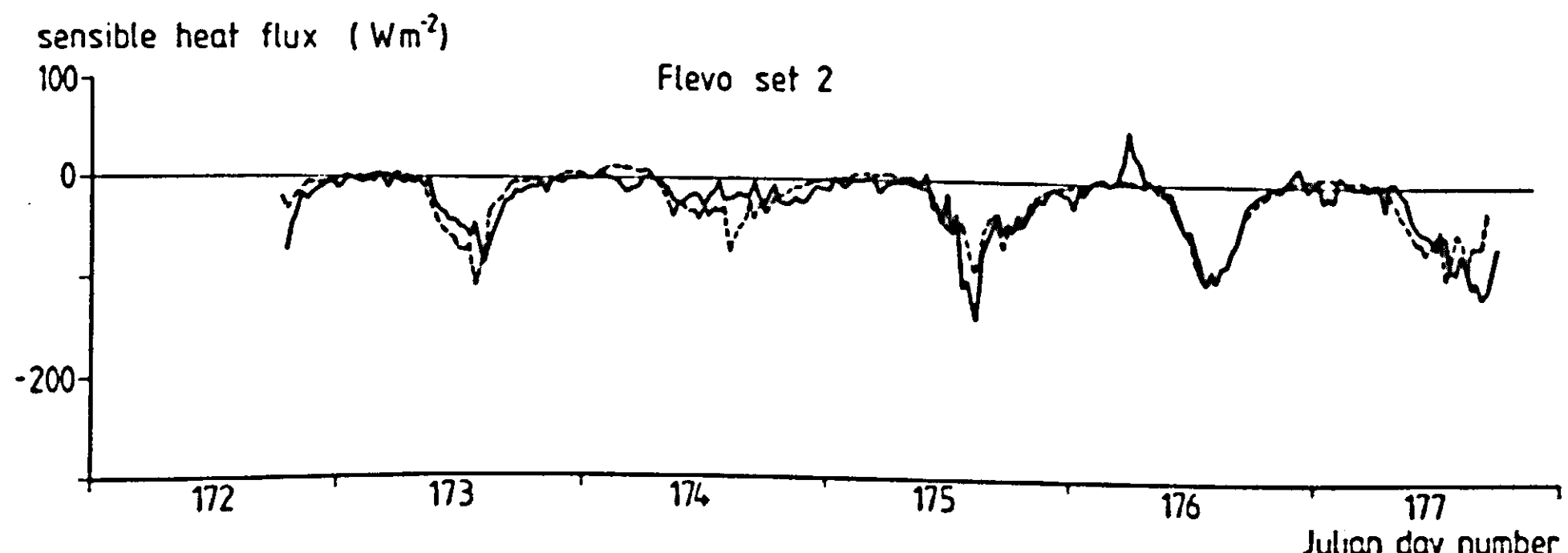


Figure 5.18 Measured (—) and simulated (----) sensible heat flux, FLEVO set

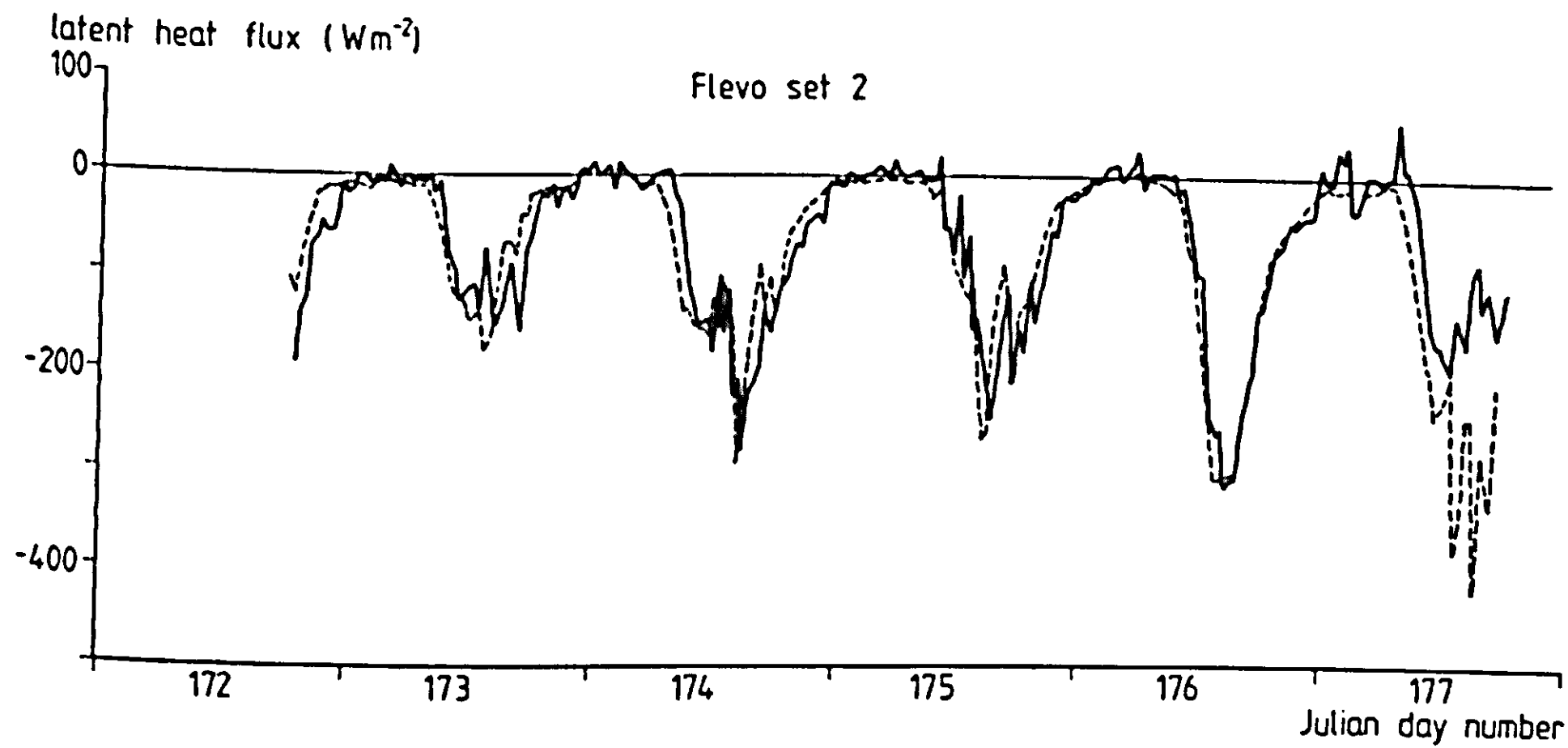


Figure 5.19 Measured (—) and simulated (----) latent heat flux, FLEVO set 2.

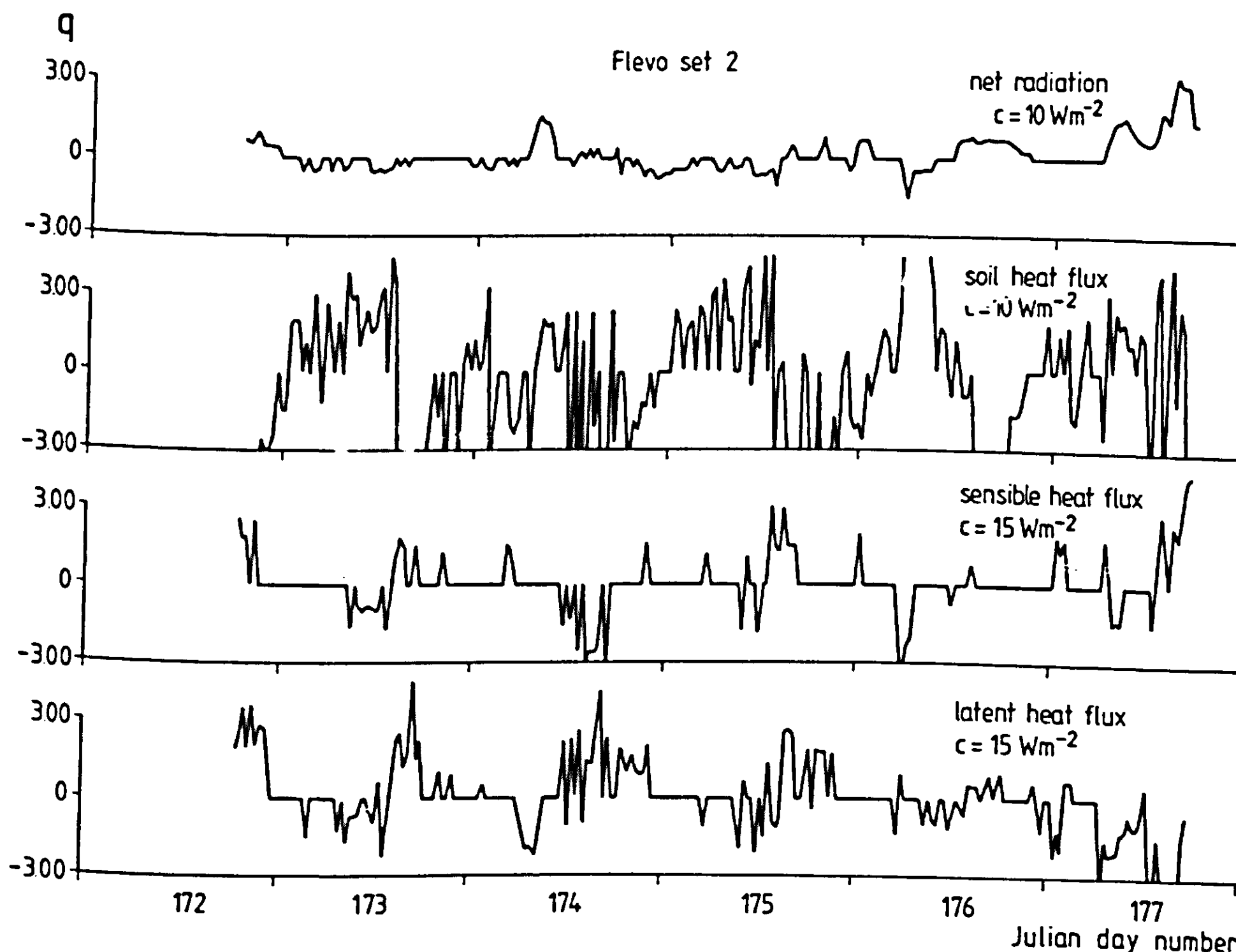


Figure 5.20 q-Values for the surface fluxes, FLEVO set 2.

Evaluation of state variable predictions

Predicted radiation temperature closely follows the measured curve (Figure 5.21), although the fluctuations at the half-hour scale are somewhat damped. The deviation observed for the night 175-176 might have the same causes as discussed for the dataset FLEVO-1. It is not clear why radiation temperature is overestimated on day 176; here one would expect an underestimation caused by too slow surface drying, as observed for day 177.

Moisture contents in the top 15 mm (Figure 5.22) are generally overestimated. Rain occurred on days 173-175, during which no measurements of moisture content were made. The hydraulic soil properties as measured and used for this simulation run were taken from the top 5 cm layer. Changes with depth in hydraulic soil properties may cause the predictions of moisture content at 15-55 mm to be a few percent beside the mark. Such deviations have a strong effect on surface drying process, which apparently is not simulated correctly after the rain has ceased; even when taking into account the uncertainties in all the measurements, it must be noted that the simulated results are quite different from the observations, as can be seen from Figure 5.25. It is concluded that for situations where rain and surface drying are intermittent, a good description of topsoil water movement requires extremely detailed soil information.

The soil temperatures are described fairly well, and q remains close to zero for all depths taken into consideration (Figures 5.24 and 5.25).

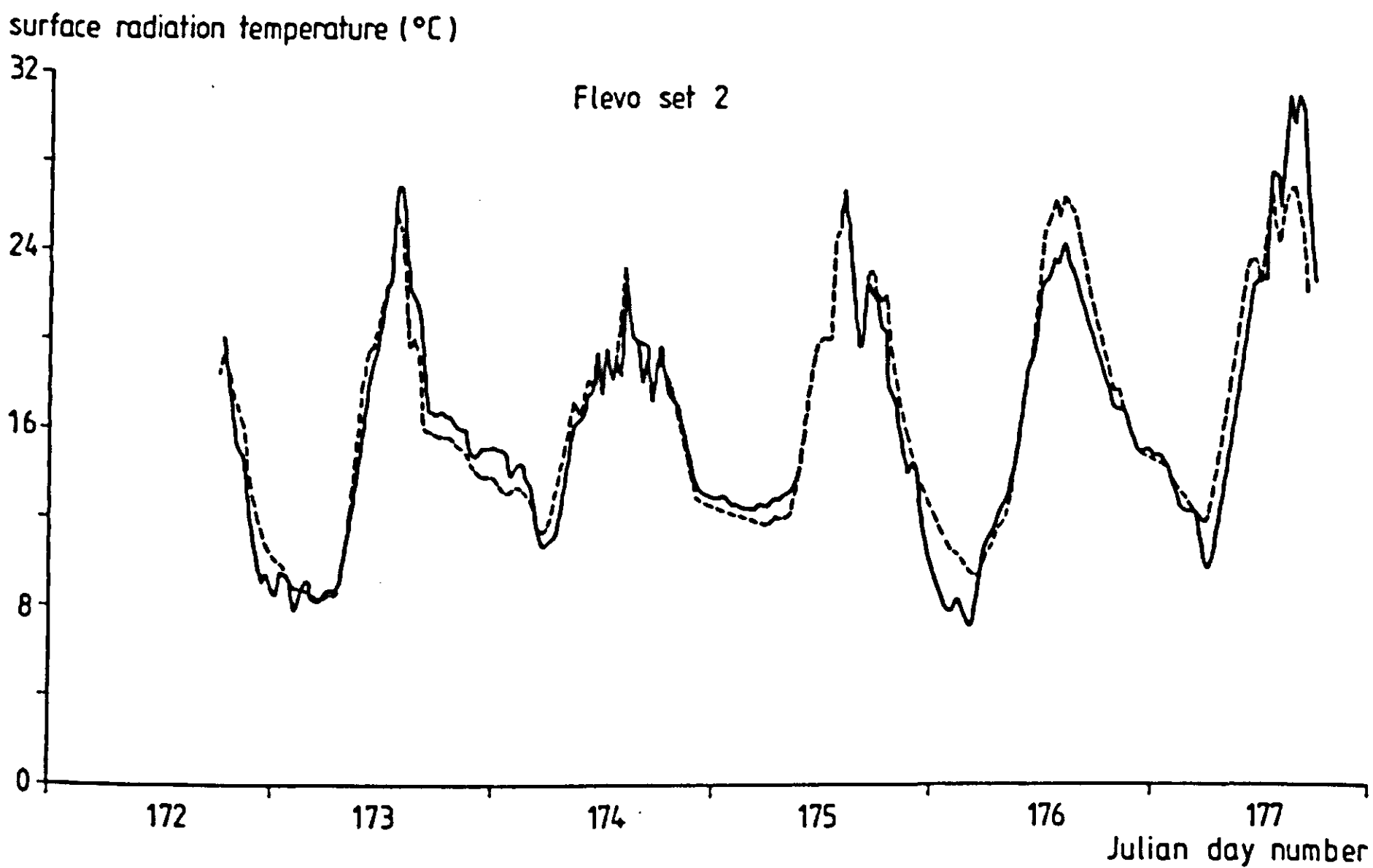


Figure 5.21 Surface radiation temperature for silt loam as measured (—) and simulated (----), FLEVO set 2. For the loam soil, almost identical courses were measured and simulated.

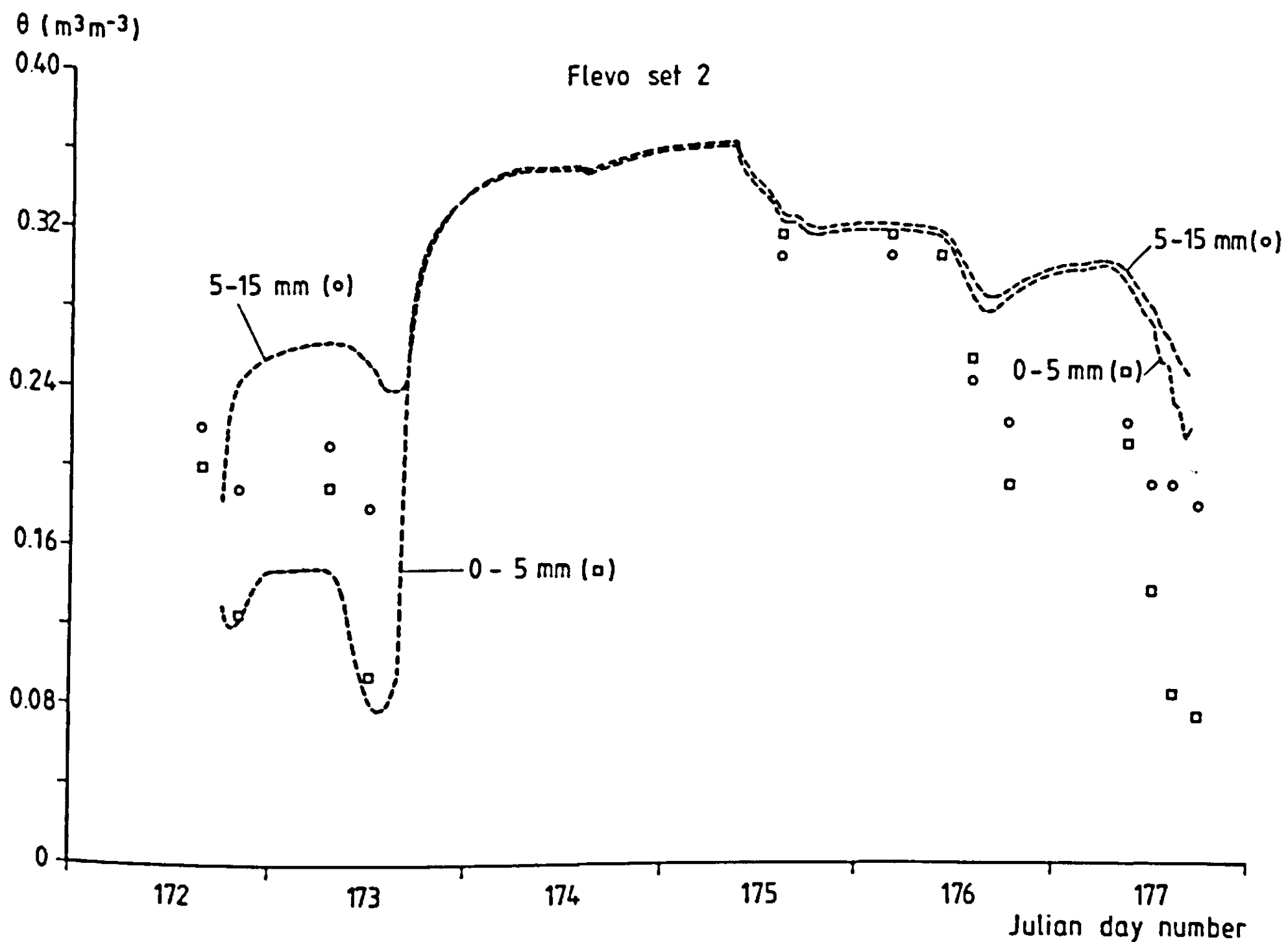


Figure 5.22

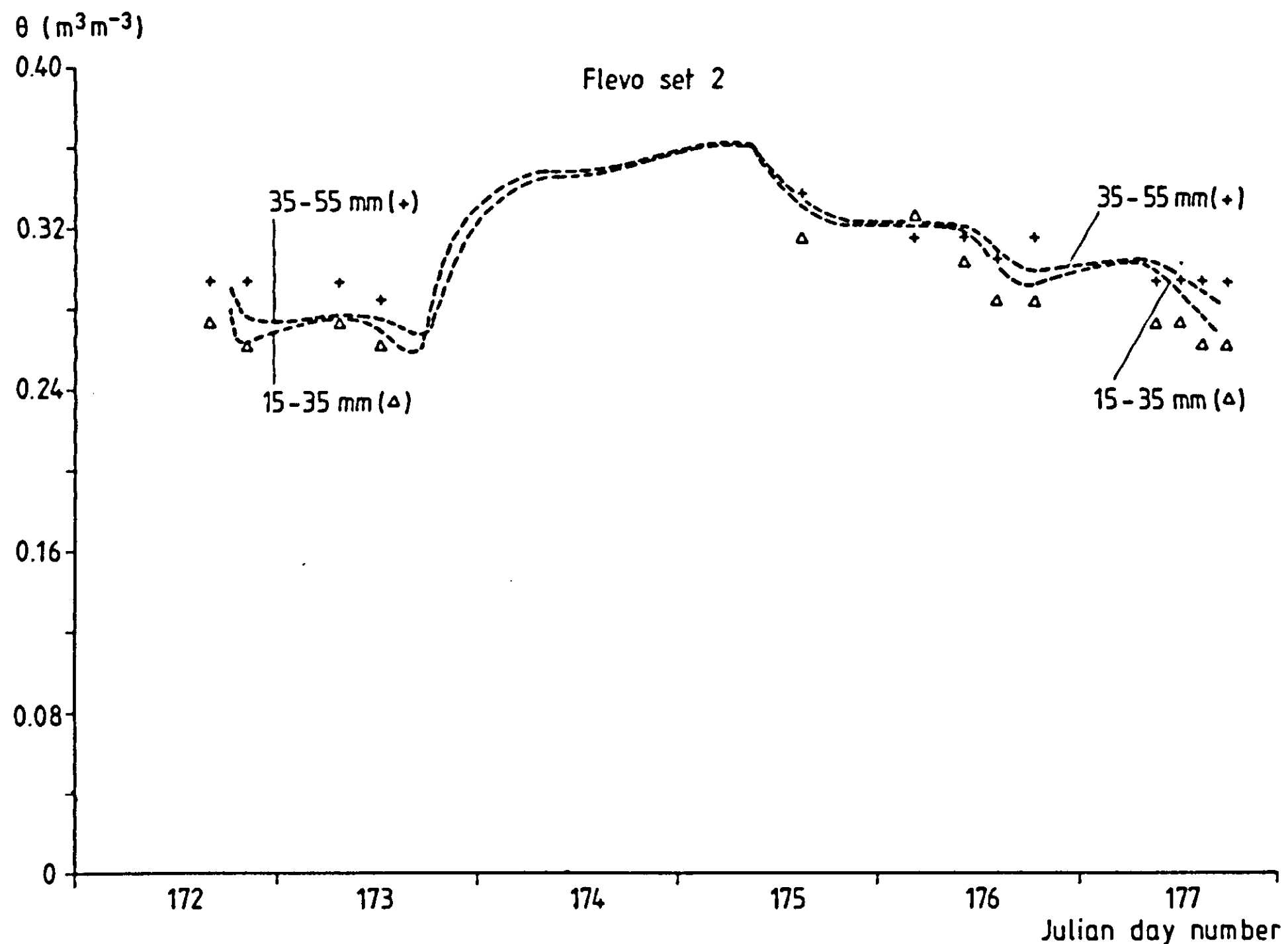


Figure 5.22, 5.23 Soil moisture content at various depth intervals, silt loam, FLEVO set 2; symbols represent observations, broken lines simulation results. The loam soil showed similar developments for this data-set.

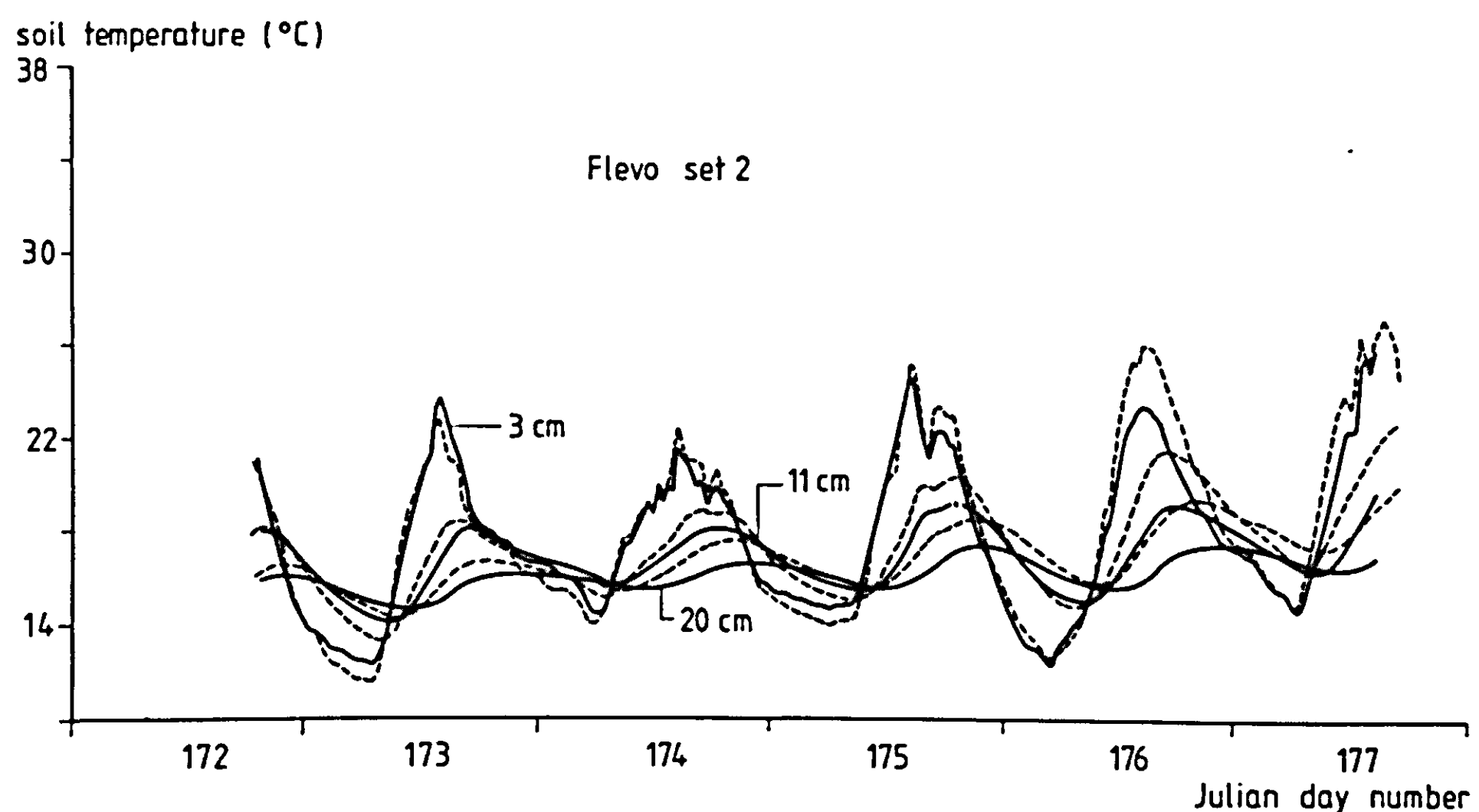


Figure 5.24 Measured (—) and simulated (----) soil temperatures at various depths, FLEVO set 2.

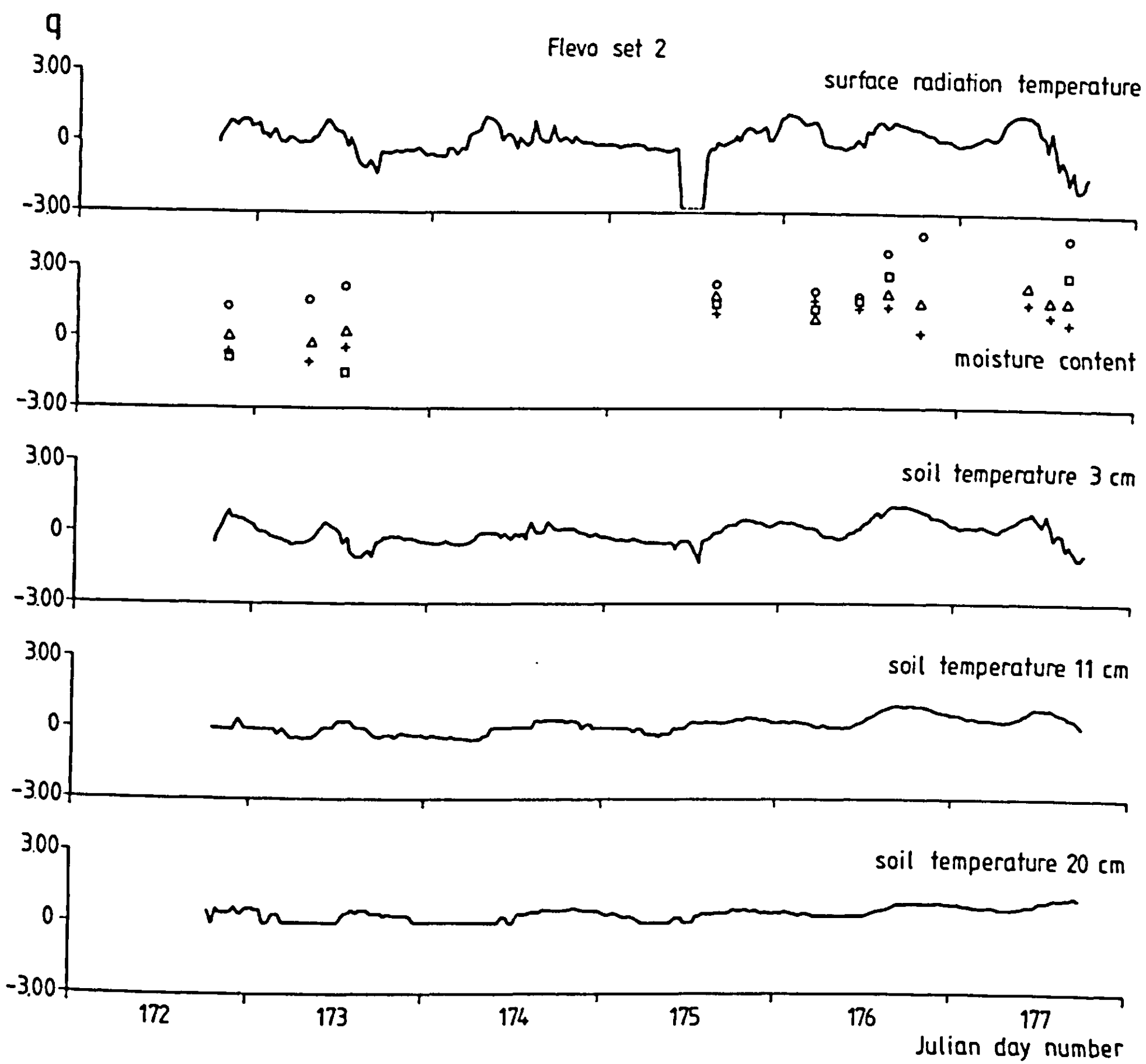


Figure 5.25 q-Values for the soil state variables, FLEVO set 2.
(□:0-5mm; ○:5-15mm; Δ:15-35 mm; +:35-55 mm).

5.1.4 TEXAS

Also the TEXAS experiment yielded a five day series of observations. In this case, the surface energy fluxes will not be considered in model validation, since most of these terms are known with too little accuracy to render them useful for a comparison with simulation results. The course of measured net radiation was used to formulate the energy flux boundary condition in the simulation exercise discussed below.

Specific for the TEXAS dataset is the sudden change in regime, caused by flooding of the dry soil after two days of measurement. Attention will be focussed upon the response of the soil state variables (temperature, radiation temperature, and moisture content) to this abrupt change and during subsequent drying.

The inputs again are listed in Table 5.1, and the errors in prediction and measurement, respectively, are presented in Table 5.2. The model options used for simulation of the TEXAS situation were:

IFMFLP = 1 (matric flux potential used in flow equation)
IFMTB = 0 (matric flux potential specified as rational expression)
IFGRAV = 1 (gravity term included in water flow equation)
IFKTB = 1 (hydraulic conductivity specified in a table)
IFCHTB = 0 (thermal conductivity calculated by De Vries model)
IFNET = 1 (net radiation used as boundary condition)

Measured and simulated time-series for surface radiation temperature, top-soil moisture content and soil temperature are plotted in the Figures 5.26, 5.27 and 5.28. For an interpretation of the differences between measured and simulated curves in the light of the occurring error variances, the corresponding q-values are shown in Figure 5.29.

Evaluation of state variable predictions

Surface radiation temperature is predicted reasonably well (Figure 5.26) although the maximum value measured during the first day is several K higher than the calculated value. The decrease in maximum daily surface temperature observed in the course of time is associated with an increase in soil moisture content, but is also partly due (days 175, 176) to a decrease in radiation (Fig. 4.8) as clouds became more frequent during the second half of the week. Nighttime surface temperatures are somewhat overestimated, possibly due to overestimation of thermal conductivity.

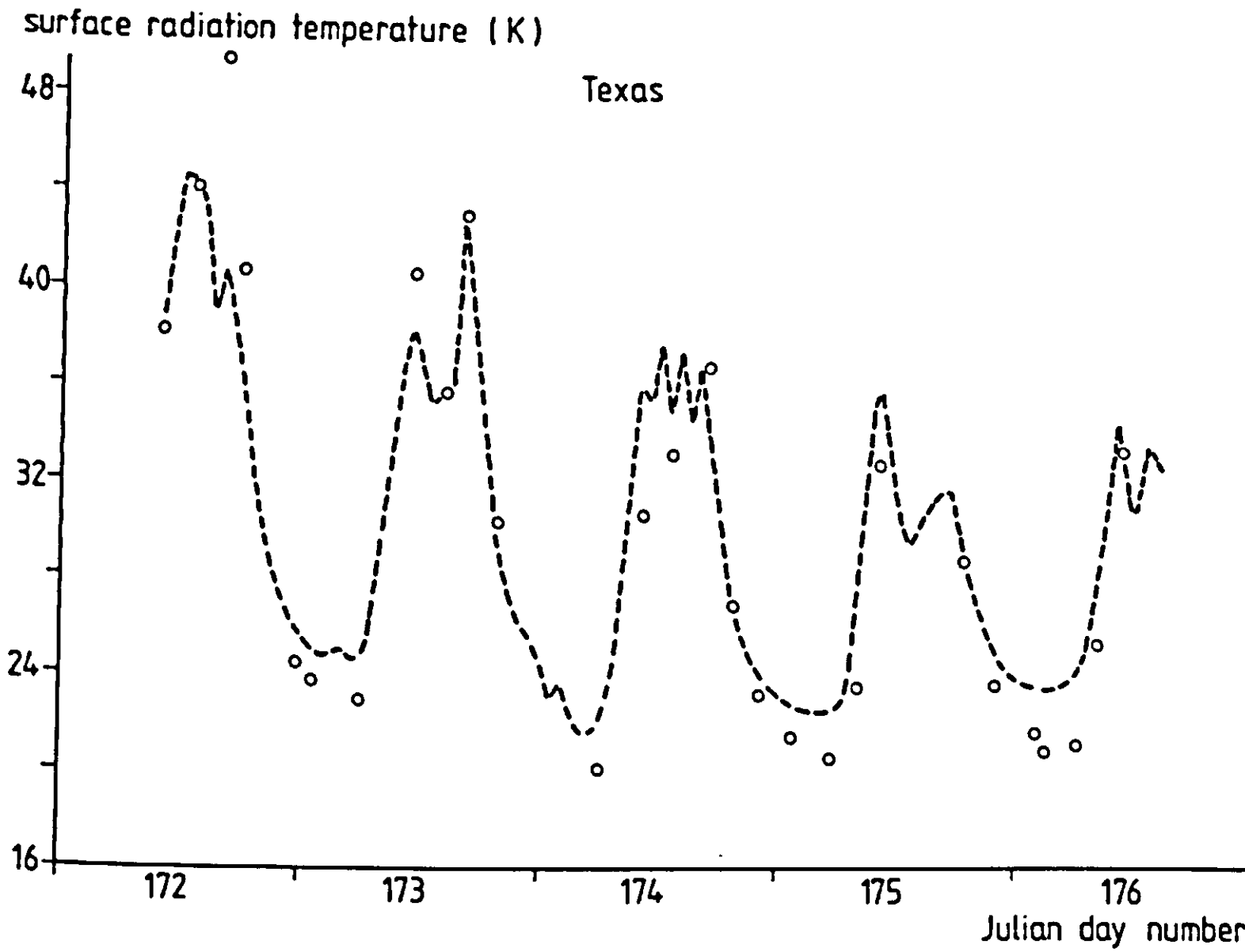


Figure 5.26 Measured () and simulated (----) surface radiation temperature for the TEXAS experiment.

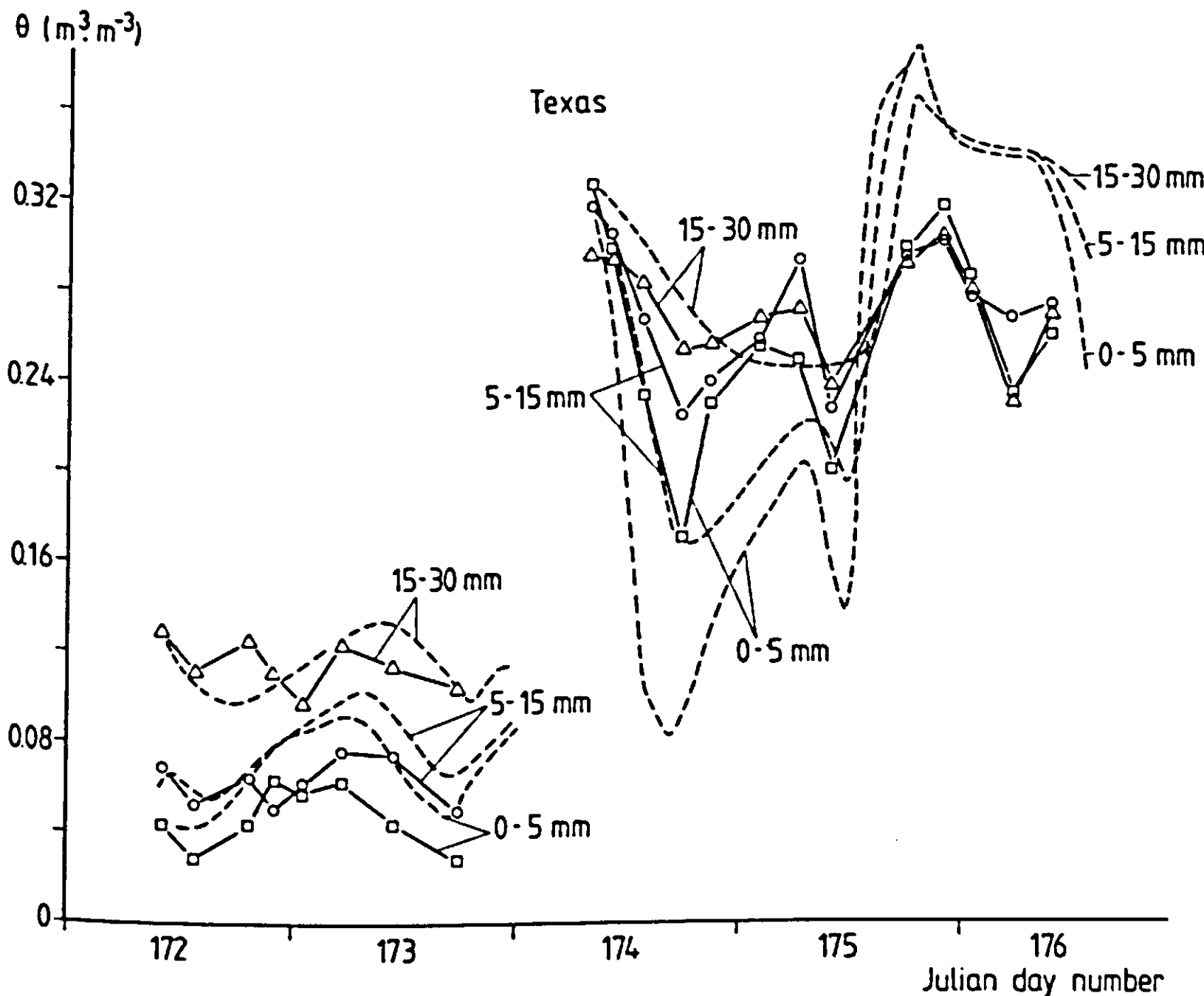


Figure 5.27 Measured (—) and simulated (----) courses of soil moisture content at various depths intervals, TEXAS.

Soil temperatures are also predicted within acceptable limits (for the q -values see Figure 5.29) for part of the sequence only; at some occasions predictions are too high, especially at 5 cm depth after wetting. Soil temperature at 25 cm and to a less extent at 10 cm depth is underestimated considerably before irrigation occurred in the night 173/174. These deviations may be due to erroneous $\lambda(\theta)$ prediction, invoked by the De Vries formulation (in this run the option IFCHTB=0 was used!). The results suggest that for dry soil the model underestimates $\lambda(\theta)$, whereas too high values seem to be calculated for the soil under wet conditions.

Soil moisture contents again appear difficult to predict. While variations in moisture content are within acceptable limits during the first two days of the experiment (Figure 5.28), fluctuations are much too pronounced for the second part of the week. During daytime, topsoil dries out to too low moisture contents and by subsequent redistribution during the night, the surface moisture content reaches too high values. Supposedly this is due to the neglect of hysteresis.

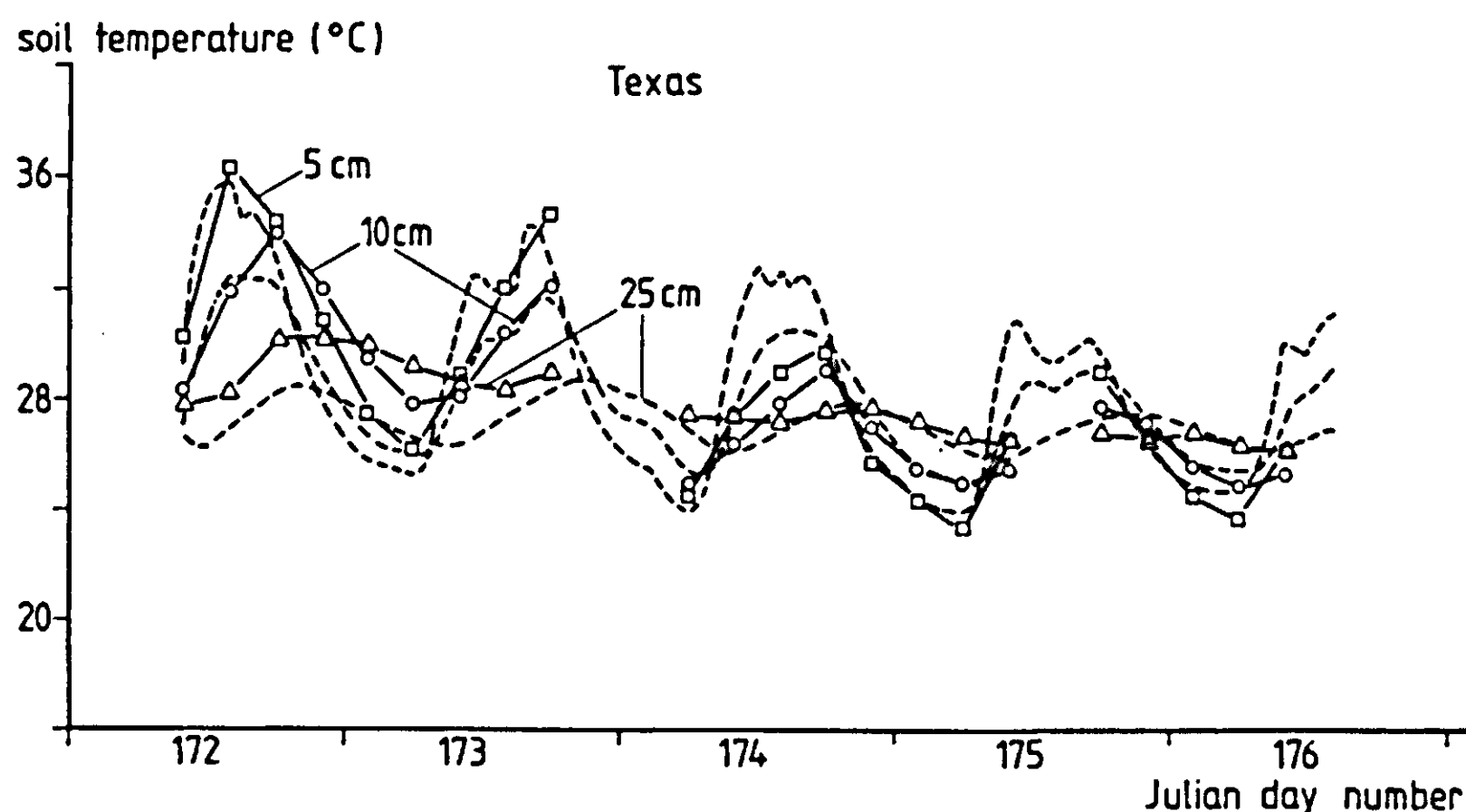


Figure 5.28 Measured (—) and simulated (----) soil temperature at 3 depths, TEXAS.

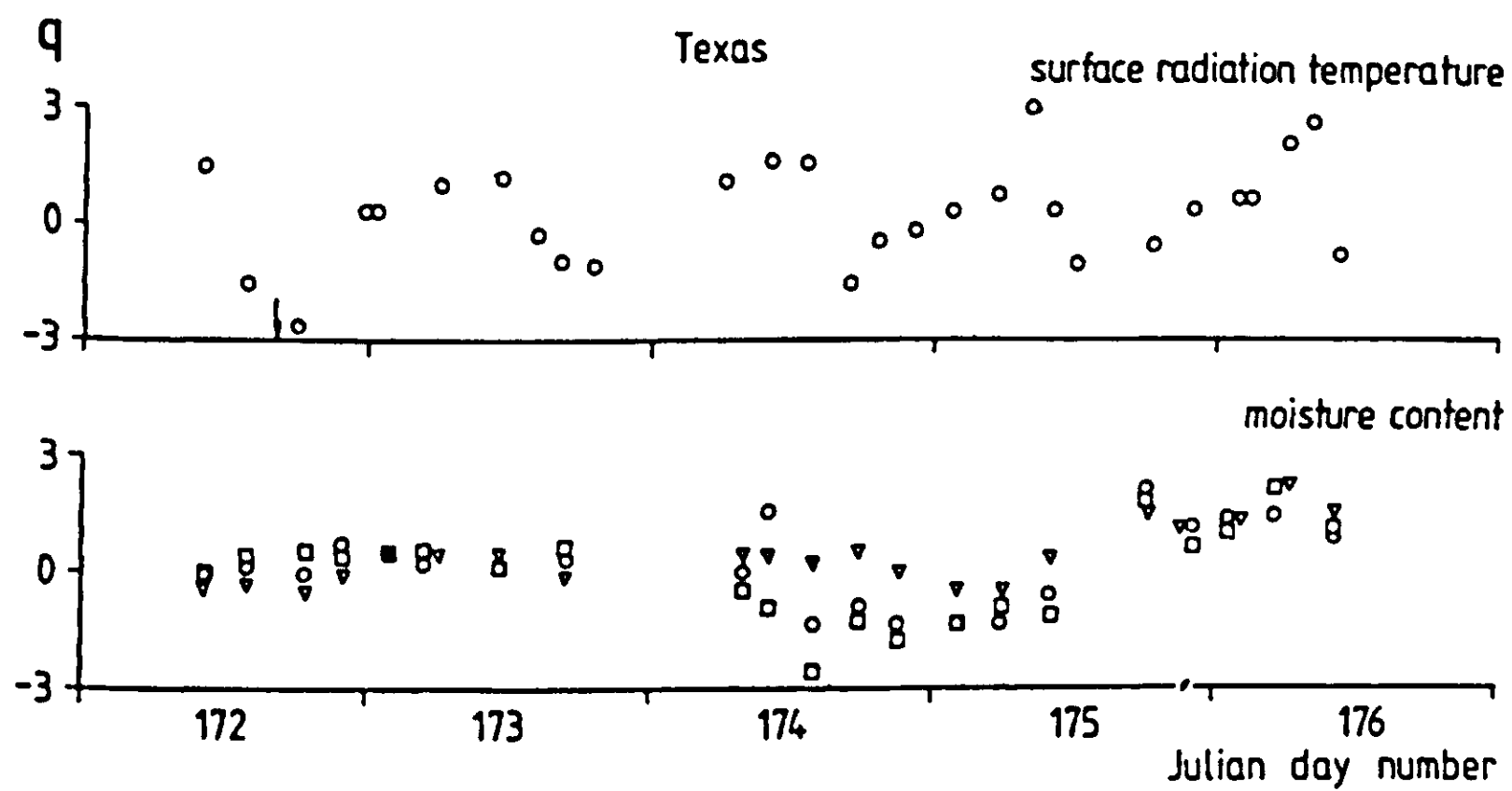


Figure 5.29 q-Values for the state variables, TEXAS. For explanation see subsection 5.1.1. (\square :0-5 mm; \circ :5-15 mm; ∇ :15-30 mm).

5.1.5 ARIZONA

Characteristic for the ARIZONA experiment, conducted by the USDA Water Conservation Laboratory at Phoenix, are the smooth cyclic patterns in the meteorological conditions, the arid climate (vapour pressure), and the high radiation levels. A feature of the resulting data series, of major interest in model validation, is the meticulously measured record of topsoil moisture behaviour during drying. The four days from which the observations are used here represent only a brief fraction of the total extent of the experiment.

The input data used for the validation runs are listed in Table 5.1, and the output error variances for the different terms again are given in Table 5.2. The following options of the SALSA model were chosen:

IFMFLP = 0 (K-p formulation of flow equation),

IFGRAV = 0 (no gravity term in water flow equation)

IFKTB = 1 (hydraulic conductivity specified in a table)

IFCHTB = 1 (thermal conductivity specified in table)

IFNET = 0 (measured net radiation not used as boundary condition).

The surface fluxes as measured and simulated are given in the Figures 5.30-5.33; to evaluate these results, Figure 5.34 shows the corresponding q-t series. For the soil state variables, the results are shown in Figures 5.35-5.39.

Evaluation of flux predictions

Net radiation (Figure 5.30) appears to be overestimated during daytime and underestimated at night, q-values ranging between -2 and +2 (Figure 5.34). With global radiation and longwave downward radiation as measured driving variables, and with correctly predicted surface temperatures, the main terms composing net radiation should be correct; the above deviations must therefore probably be ascribed to errors in soil albedo, emissivity, and/or longwave reflectivity.

The soil heat flux at the surface is not always predicted satisfactorily (Figures 5.31 and 5.34), yielding extreme values for the quotient q. Deviations, however, are not consistent to the extent that erroneous assumptions in the model should be expected.

This is not the case for the latent and sensible heat fluxes (Figures 5.32-5.34). For these variables, severe discrepancies between predictions and observations occur. (The measured values of latent heat flux are based on lysimeter data, and the sensible heat flux was determined as a rest

term). It should be recalled here that in the simulations for this dataset, the value of the aerodynamic roughness parameter z_0 was determined by 'matching' and was found to be extremely low (0.015 mm). (The soil heat flux was used as a criterion in the matching procedure). Aside from the fact that such a low value must be considered unrealistic, it can be noted that also the distribution of energy over the latent and sensible terms is not predicted correctly. During daytime, too much energy is spent on evaporation at

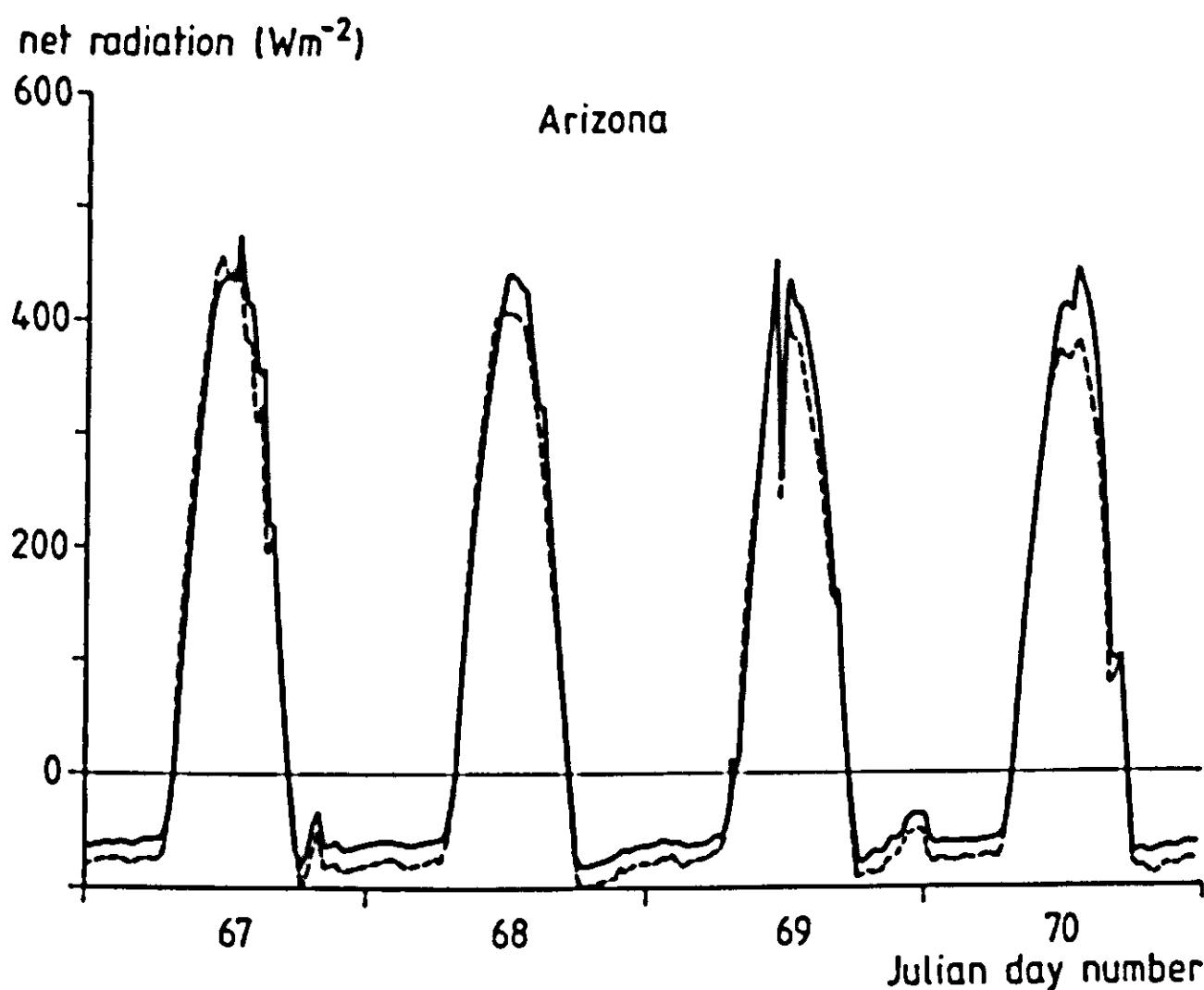


Figure 5.30 Measured (—) and simulated (---) net radiation for the ARIZONA experiment.

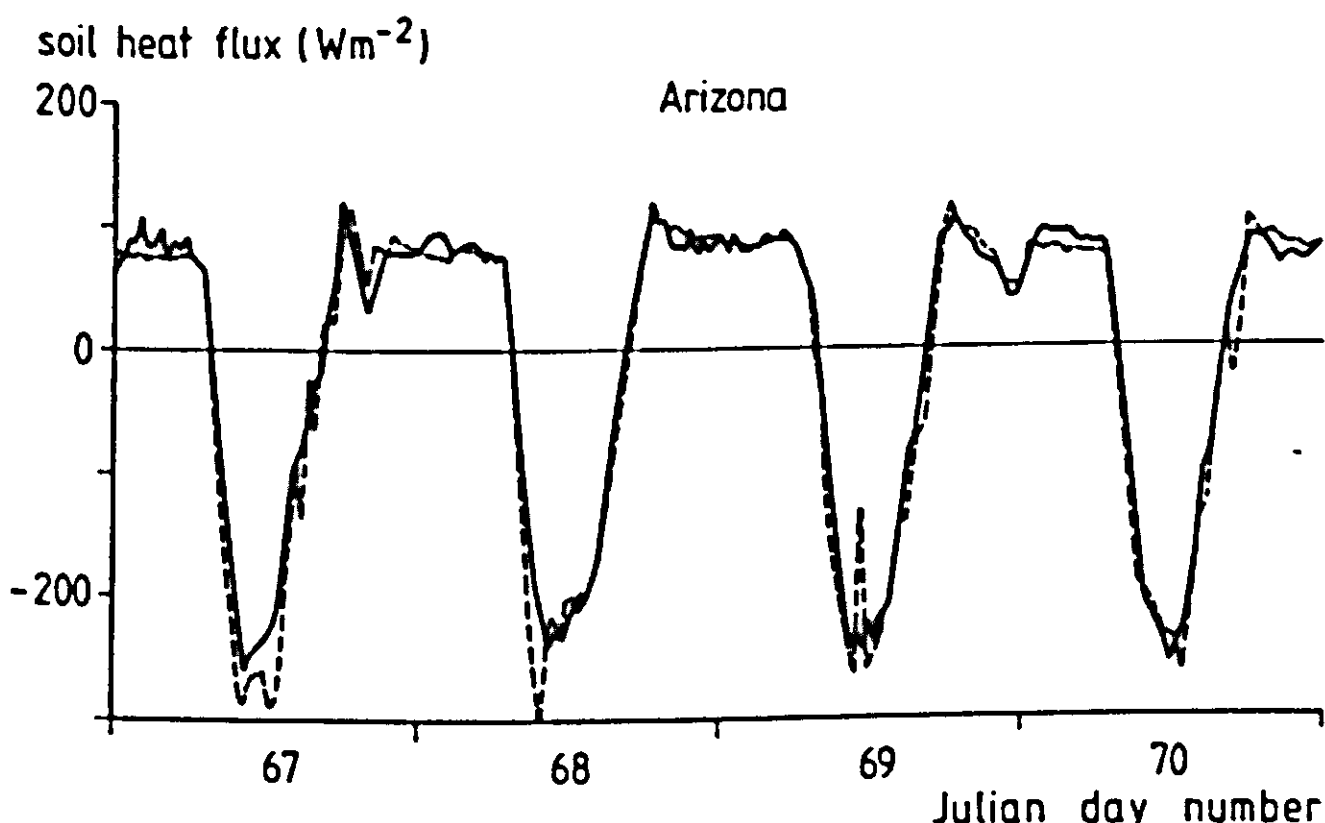


Figure 5.31 Measured (—) and simulated (---) soil heat flux for the ARIZONA experiment.

the expense of the sensible heat flux. To some extent this may be explained by the overestimation of nocturnal moisture redistribution, caused possibly by the neglect of hysteresis or by an erroneous value of the soil vapour transport coefficient. Another observation is that the relatively high evaporation rate as measured during the night is not predicted correctly by the

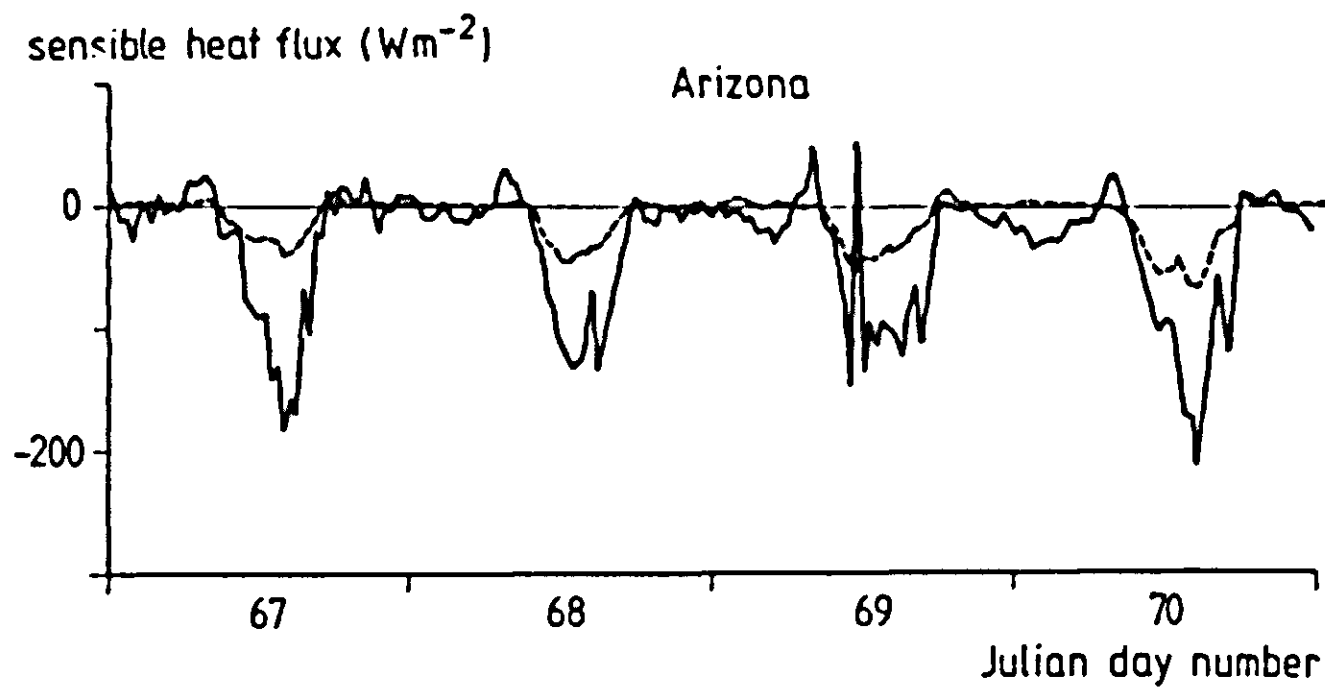


Figure 5.32 Measured (—) and simulated (---) sensible heat flux for the ARIZONA experiment.

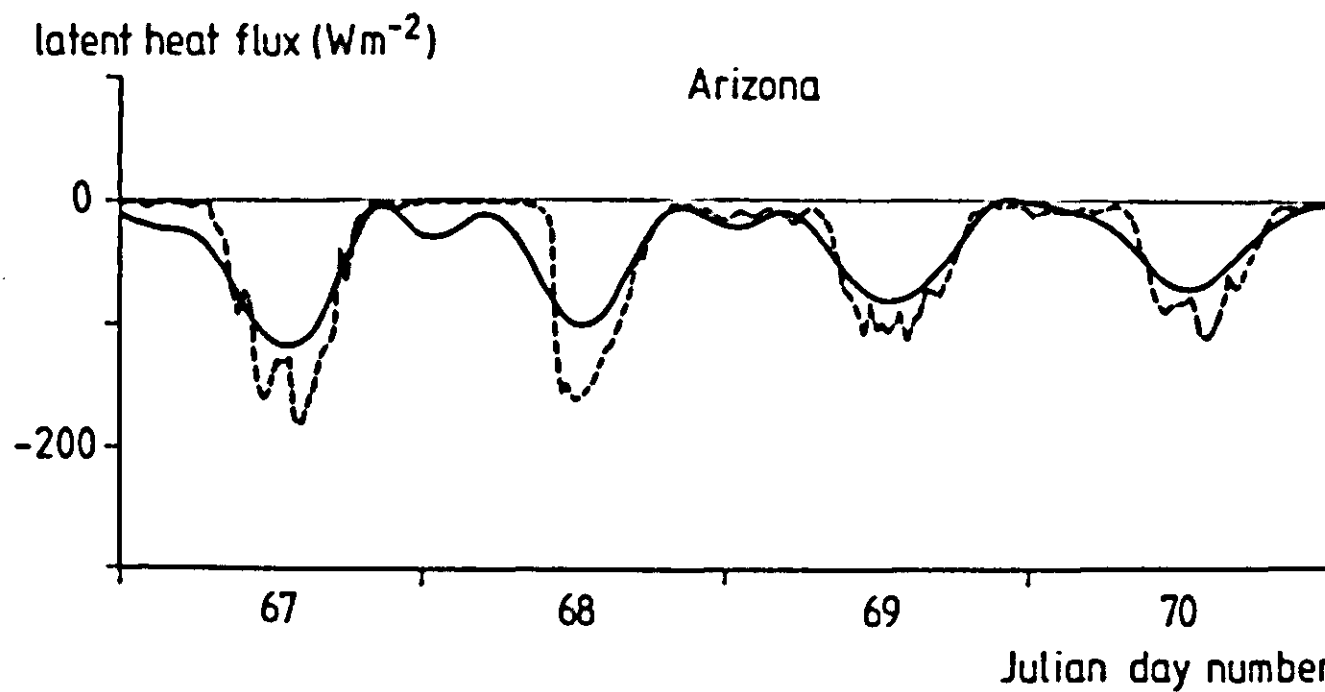


Figure 5.33 Measured (—) and simulated (---) latent heat flux for the ARIZONA experiment.

model. Irrespective of the above, the data suggest that the employed formulation of 'atmospheric resistance', using a single value of z_0 to describe the exchange coefficients for both heat and vapour in the atmosphere, must be considered inadequate for the present case. A fetch problem may have occurred, as could be concluded from the impossibility to derive a roughness parameter from the wind profile data of this experiment.

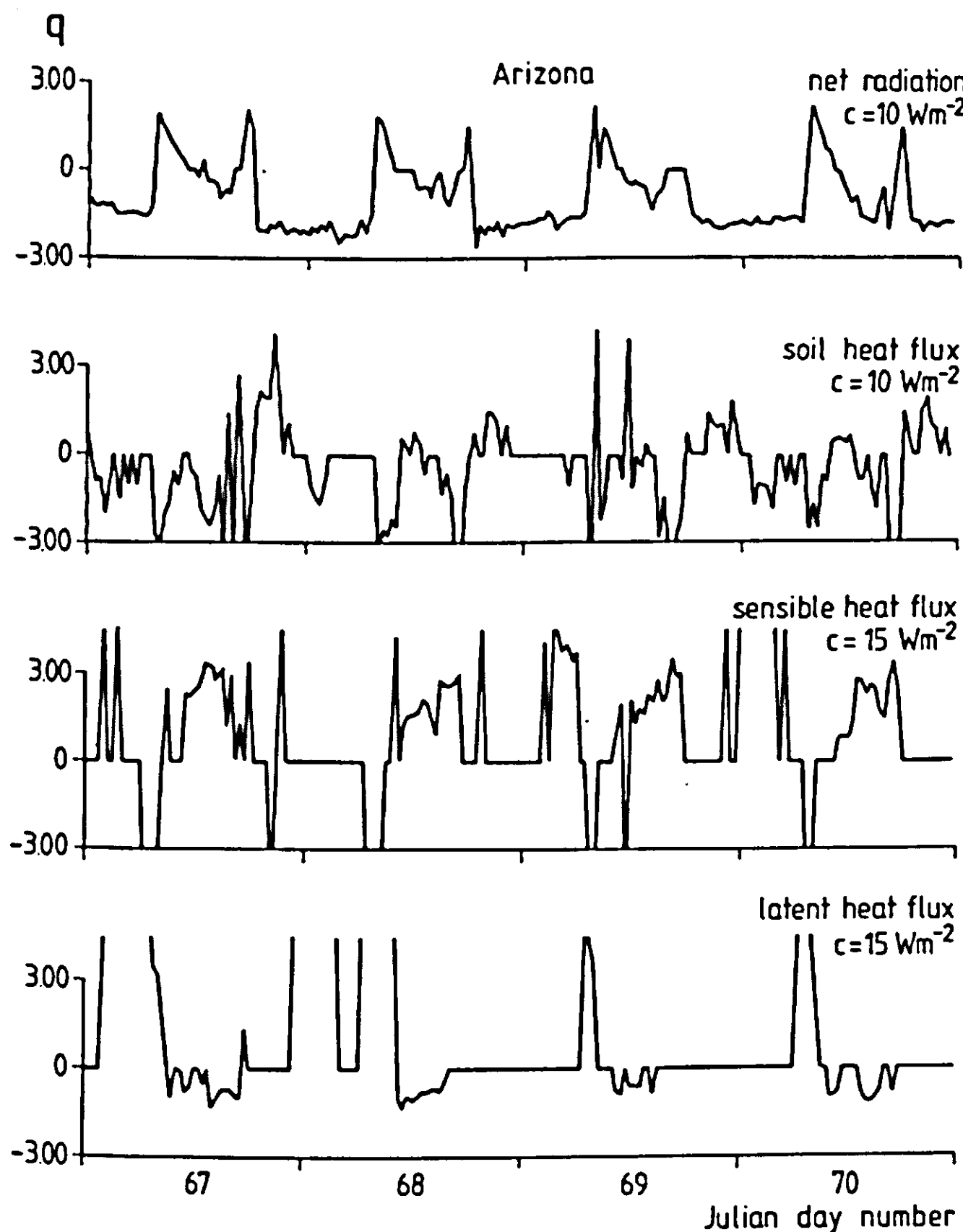


Figure 5.34 q-Values of the surface fluxes, ARIZONA. For explanation see subsection 5.1.1.

Evaluation of state variable predictions

Soil temperatures at all depths are predicted reasonably well, although some overestimation occurs (Figures 5.35 and 5.37). The curves shown in Figure 5.38 indicate that the disparity between prediction and observation is acceptable in view of the involved errors, q ranging mostly between -1.5 and +1.5.

For the volumetric moisture content, daytime values are described with acceptable accuracy, but too much redistribution occurs during the night. As observed before, this may contribute to the overestimation of evaporation during daytime. Figure 5.39 shows the corresponding q -values.

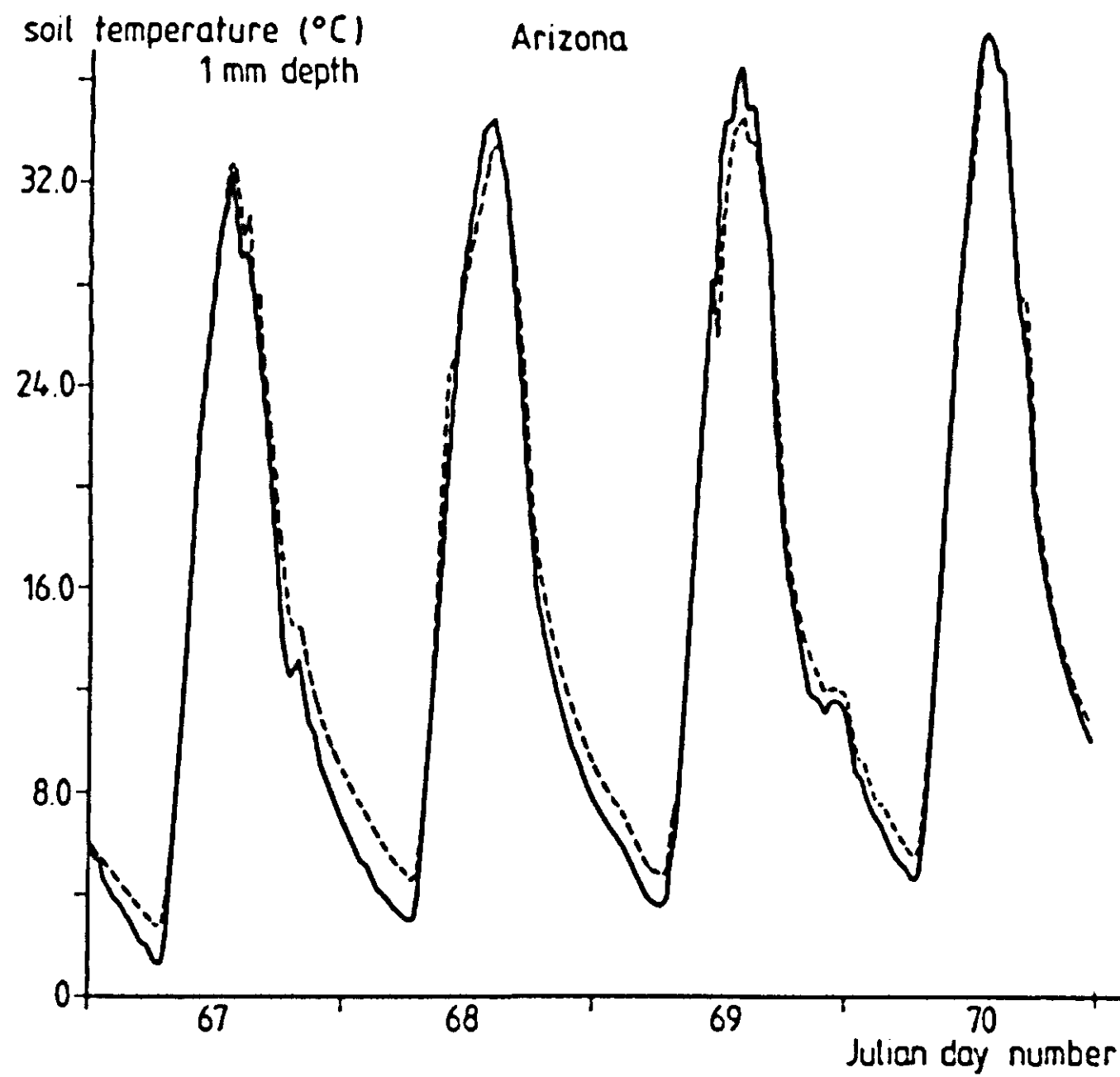


Figure 5.35 Measured (—) and simulated (----) 'surface' temperature, ARIZONA.

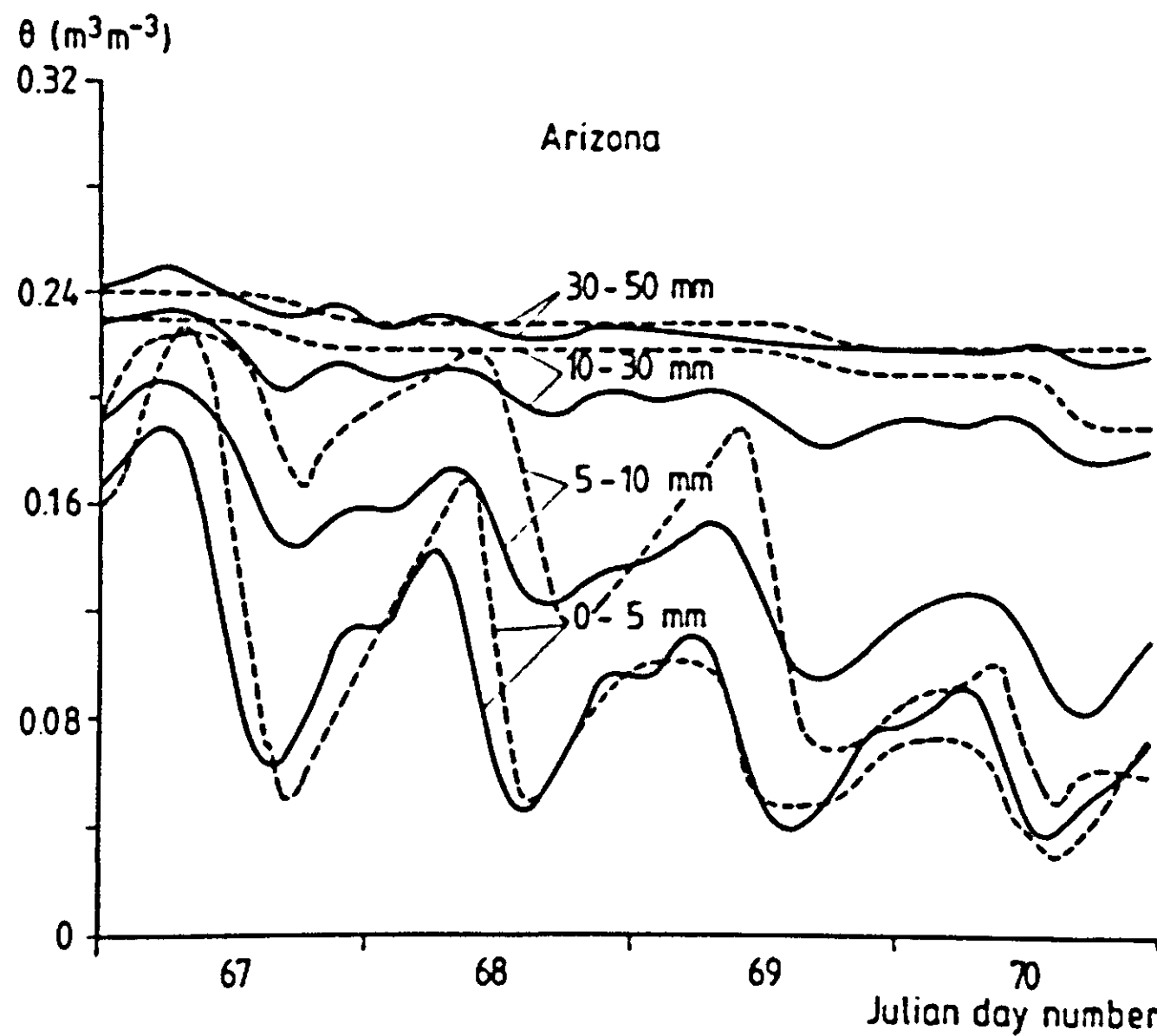


Figure 5.36 Measured (—) and simulated (----) soil moisture contents for various depths intervals, ARIZONA.

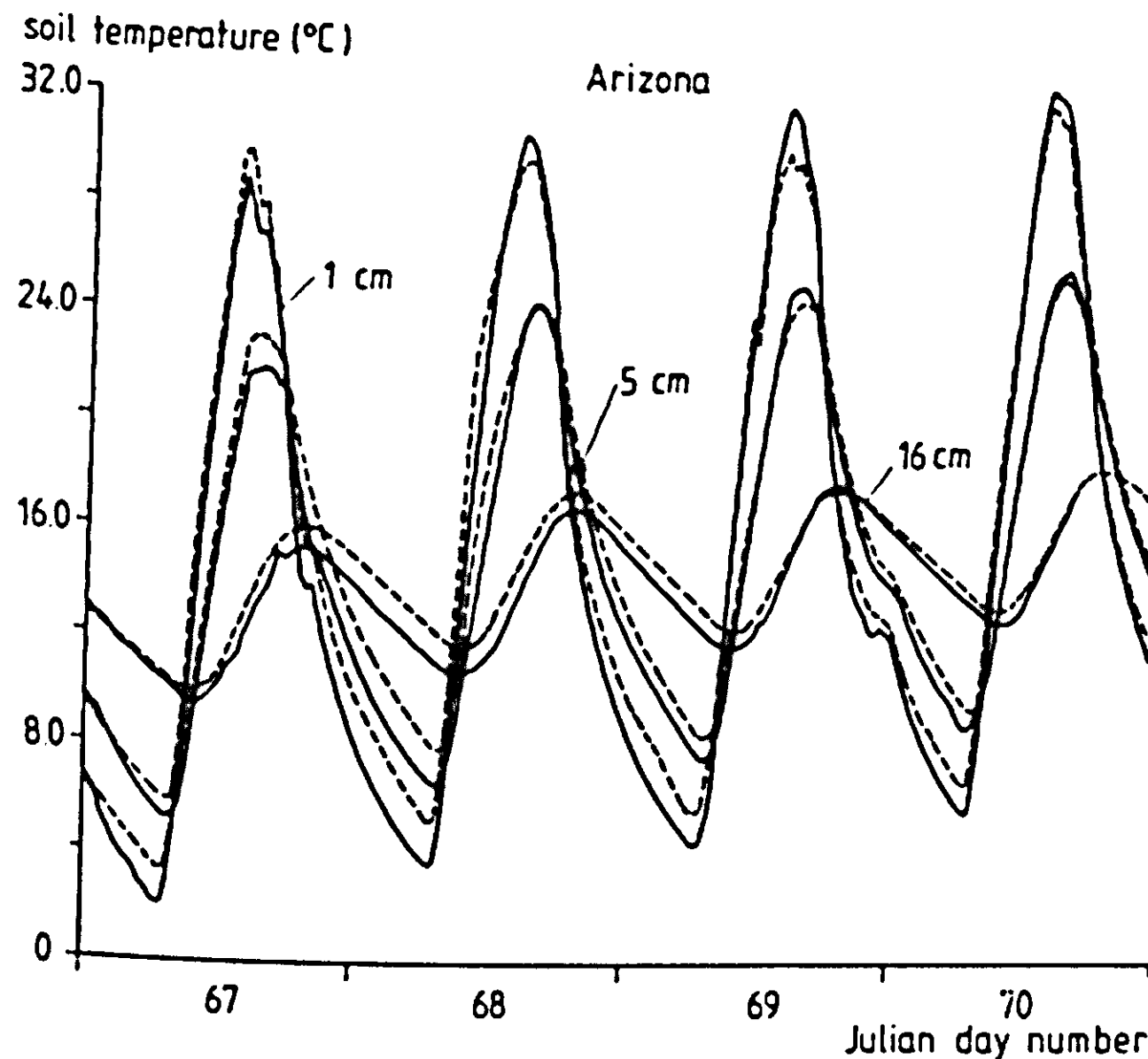
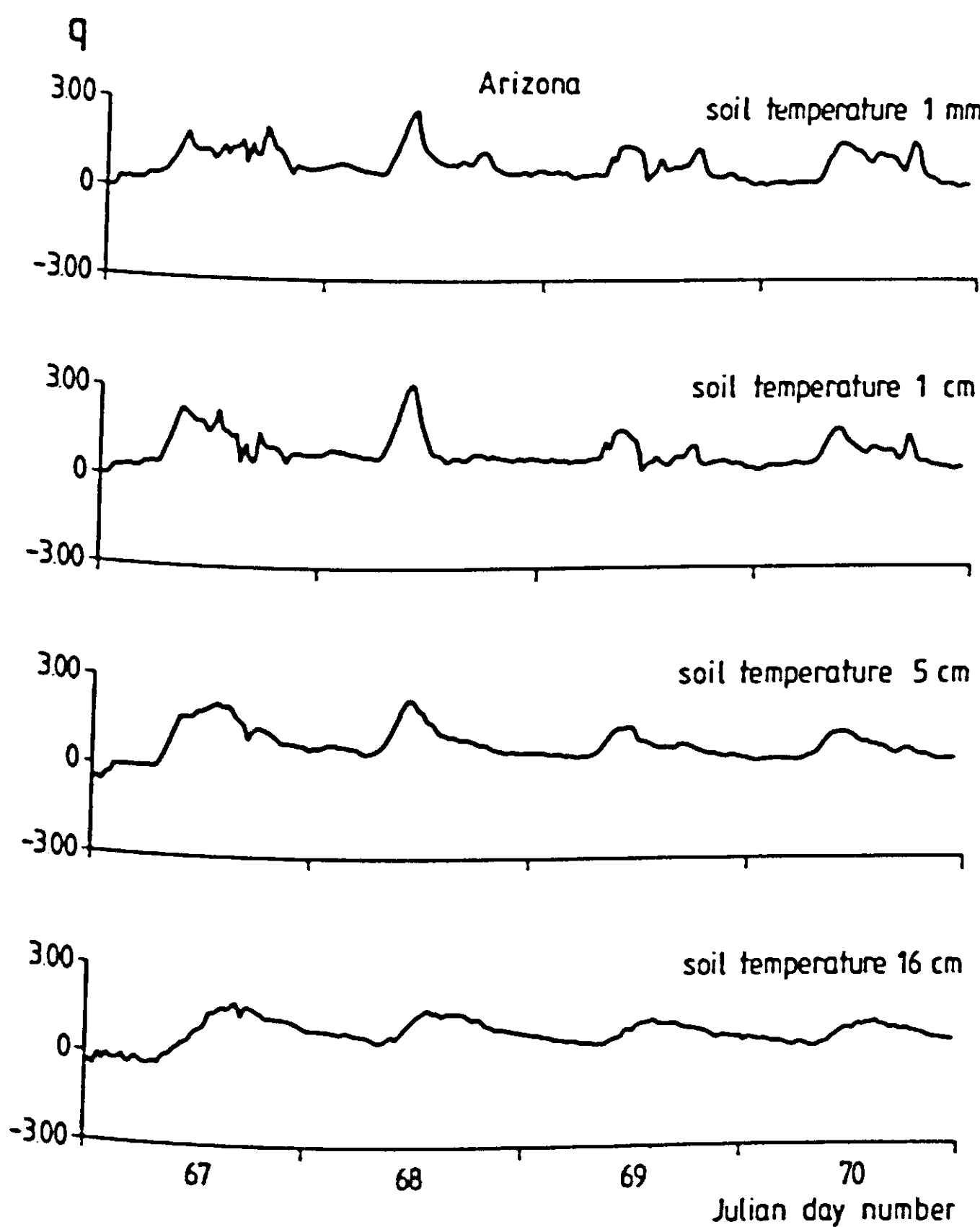


Figure 5.37 Measured (—) and simulated (---) soil temperatures at various depths, ARIZONA.

Figure 5.38 q -Values for the state variables, ARIZONA.



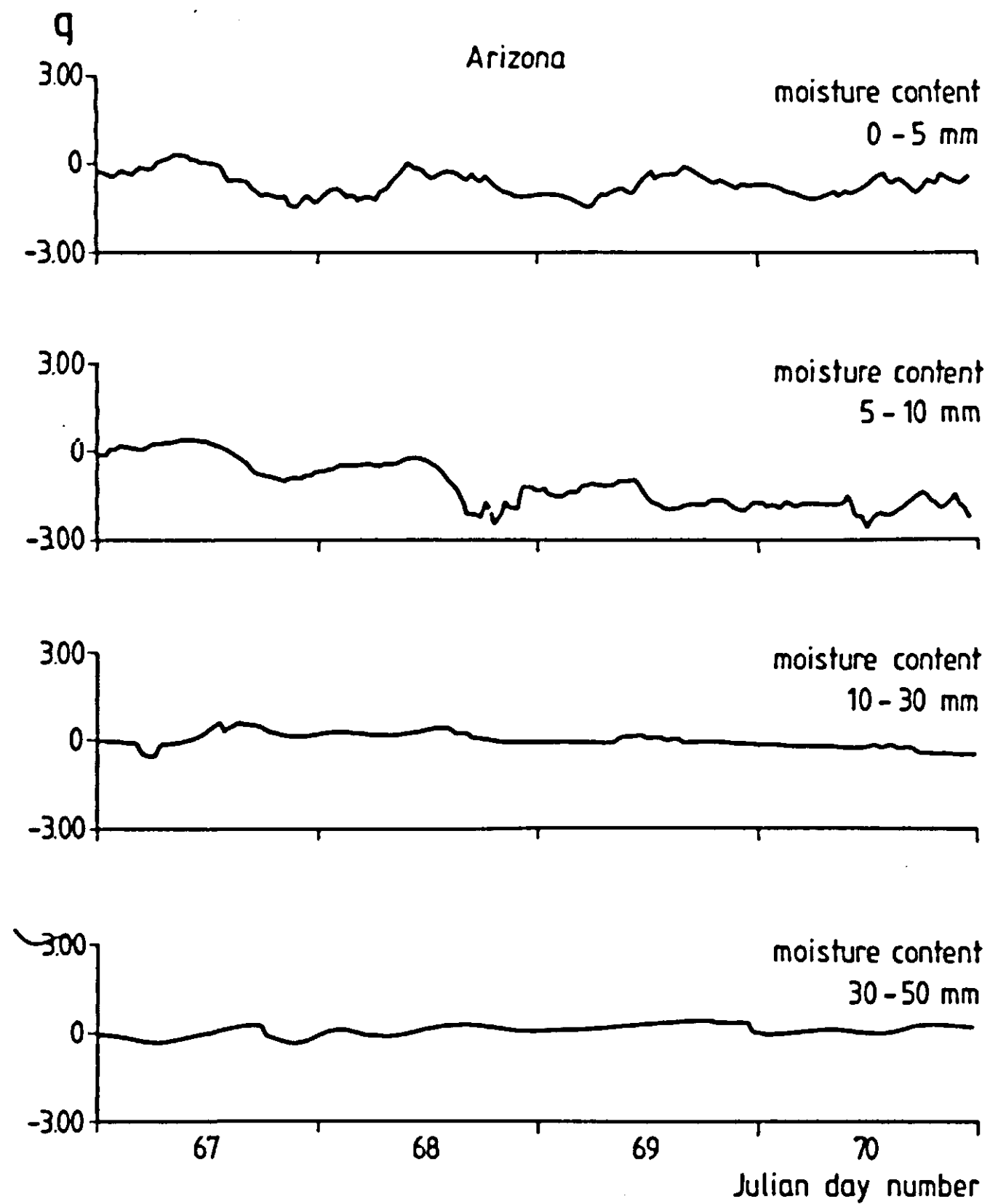


Figure 5.39 q-Values for soil moisture content at four depth intervals.

5.2 Comparison of the simulation model with an analytical solution under limiting conditions.

As an additional test of the model, some simulation results will be compared to an analytical solution of the surface energy balance and related soil water and heat flow equations. Unfortunately, to render such a comparison possible, the numerical algorithm must be simplified strongly, in order to match with the assumptions needed to achieve the analytical solution. The resulting simplified case can hardly be claimed to represent physical reality, and consequently one might question the usefulness of such a test. Nevertheless it is felt that a form of analytical validation is warranted here, as it may give an indication of the accuracy attained by the numerical procedures used in the current model; this is especially of interest since the experimental validation is liable to such wide error intervals as shown in the previous sections.

The analytical solution used for the present purpose is the Laplace-type model developed by Nicholaichuck (1974), mentioned already in Chapter 2. In this linearized model, all transport coefficients and capacities are treated as constants. Both the soil heat flow and soil water flow equations are included to describe the one-dimensional transport in the vertical direction for a semi-infinite soil column, subject to boundary conditions defined by the surface energy balance.

The heat flow equation is written as

$$(5.4) \quad C_s \frac{\partial T}{\partial t} = \lambda \frac{d^2 T}{dz^2} - C_w K \frac{dT}{dz}$$

where C_s and C_w are the volumetric heat capacities of bulk soil and water respectively, and the other symbols have their usual significance (cf Chapter 3). The second term on the RHS of the above equation is meant to cover the convective transport of heat by the soil water. Clearly, only that part of the flow which is induced by gravity is taken into account. The total flow of soil water is taken to be subject to the conservation equation:

$$(5.5) \quad \frac{\partial \theta}{\partial t} = D_\theta \frac{d^2 \theta}{dz^2} + D_T \frac{d^2 T}{dz^2} - \frac{dK}{dz}$$

where D_θ and D_T (both taken to be constant) are the classical 'isothermal' and 'thermal' soil water diffusivities as defined by Philip and De Vries (1957). As demonstrated in Chapter 3, this concept contains some pitfalls, and an additional inconsistency is introduced by the combined use of eqs. (5.4) and (5.5), since the coupling term is omitted in eq. (5.4), whereas it is retained in eq. (5.5).

The boundary conditions are derived from the energy balance equation:

$$(5.6) \quad R_n + \frac{\rho C}{r_a} (T_a - T_s) + \lambda \left(\frac{dT}{dz} \right)_s + LE = 0$$

where the second term represents the sensible heat flux in the air, the third term the soil heat flux and the last one the latent heat flux; E is the evaporative water flux at the surface. From eq. (5.6) the following boundary condition to the heat flow equation is derived:

$$(5.7) \quad \left(\frac{dT}{dz} \right)_s + K_2 T_s = K_1$$

with the constants K_1 and K_2 defined as

$$(5.8) \quad K_1 \equiv (-R_n - LE - \frac{\rho C_p}{r_a} T_a)/\lambda$$

$$(5.9) \quad K_2 \equiv \frac{\rho C_p}{r_a \lambda}$$

The gradient of water content at the surface, to be used as boundary condition to the water flow equation, is expressed as

$$(5.10) \quad \left(\frac{d\theta}{dz} \right)_s = K_3 + K_4 T_s$$

This relation follows from the flux equation and the condition of constant surface evaporation:

$$(5.11) \quad j_w = -D_\theta \frac{d\theta}{dz} - D_T \frac{dT}{dz} + K$$

$$(5.12) \quad j_{w,s} = -E$$

and it can be seen directly that therefore the parameters K_3 and K_4 are defined as

$$(5.13) \quad K_3 \equiv \frac{K + E_o}{D_\theta} - \frac{D_T}{D_\theta} K_1$$

$$(5.14) \quad K_4 \equiv \frac{D_T}{D_\theta} K_2$$

Nicholaichuck (1974) approximated all the terms $K_1 - k_4$ as constants. Gibbs and Baca (1981) extended this analysis by expressing the hydraulic conductivity as a linear function of moisture content and temperature. Since the diffusivities D_T and D_θ remain constant in their formulation, however, such that the dependence of K on θ and T appears only in the gravity term, the analysis by those authors is not considered to be physically more realistic than Nicholaichuck's description, which was adopted here.

Table 5.3 Values of soil parameters and initial conditions as used in the NICAN-LINTRA comparison.

variable	value	units
λ	1.0	$\text{W m}^{-1}\text{K}^{-1}$
C_s	$1.5 \cdot 10^6$	$\text{J m}^{-3}\text{K}^{-1}$
D_θ	$5.0 \cdot 10^{-7}$	m^2s^{-1}
D_T	$1.0 \cdot 10^{-9}$	$\text{m}^2\text{s}^{-1}\text{K}^{-1}$
K	$1.0 \cdot 10^{-15}$	m s^{-1}
T_i	20.0	$^\circ\text{C}$
θ_i	0.36	-
T (z=0.5 m)	20.0	$^\circ\text{C}$
$\theta(z=0.5 \text{ m})$	0.36	-
E	$1.1574 \cdot 10^{-7}$	m s^{-1}
T_a	20.0	$^\circ\text{C}$
R_n	700.	W m^{-2}
u (at 2 m)	2.0	m s^{-1}
z_o	10.0	mm

The analytical solution pertaining to the set of equations (5.4, 5.5) subject to conditions given by (5.7) and (5.10) makes use of Laplace transform methods. The solution is given in Appendix 9. A printout of the semi-analytical CSMP program (NICAN) that was written for this occasion to perform the calculations in the Nicholaichuck solution is given in Appendix 10; the procedure includes a convolution integral that is solved numerically. The actual derivation of the solution is considered too lengthy to be reproduced in this report, but a detailed description can be found in the cited thesis by Nicholaichuck and also in the work by Gibbs and Baca (1981).

To allow for a comparison with this Laplace model, the numerical model SALSA was trimmed down to a relatively short algorithm, listed in Appendix 10 under the name LINTRA (linearized transport). As stated, the main changes as compared to SALSA relate to the constancy of transport coefficients and capacities in the soil, a truncated heat convection term, and the elimination of the atmosphere compartment. Hydraulic conductivity is main-

Table 5.4 Predicted profiles of soil moisture content and temperature for t=3 hours.

depth mm	NICAN T(°C)	LINTRA T(°C)	NICAN $\theta(-)$	LINTRA $\theta(-)$
0.0	38.109	38.119	.	.
1.0	37.954	37.964	0.3234	0.3244
4.0	37.491	37.500	0.3259	0.3260
9.0	36.730	36.739	0.3288	0.3286
16.0	35.690	35.698	0.3323	0.3321
25.0	34.400	34.405	0.3364	0.3363
36.0	32.899	32.901	0.3411	0.3410
49.0	31.240	31.238	0.3459	0.3459
64.0	29.491	29.484	0.3506	0.3506
81.0	27.729	27.717	0.3548	0.3548
100.0	26.035	26.019	0.3582	0.3582
140.0	23.367	23.360	0.3618	0.3618
180.0	21.720	21.720	0.3624	0.3624
220.0	20.801	20.806	0.3618	0.3618
260.0	20.340	20.345	0.3610	0.3610
300.0	20.131	20.135	0.3605	0.3605
340.0	20.046	20.048	0.3602	0.3602
380.0	20.014	20.013	0.3601	0.3601

tained only to express the gravity term, and is replaced in the other terms by the two diffusivities D_θ and D_T in which both liquid and vapour contributions are lumped. Net radiation, air temperature, windspeed and evaporation rate are kept constant, and the initial soil moisture content and temperature are constant with depth.

Table 5.3 shows the values of the different parameters and conditions used in running both models LINTRA and NICAN for the example given here. The predicted moisture and temperature profiles, obtained by the two models, are given in Table 5.4 for the case where the soil is exposed to the fixed boundary conditions during three hours. The rate of heat accumulation in the soil is fairly high in this example, accounting for about 20% of the imposed net radiation. Viewing the analytical model as the reference case here, it

can be concluded from a comparison of the results that the numerical simulation model approaches the true solution to a very high degree of accuracy. For other cases, comparable results could be obtained.

5.3 Brief evaluation of simulated boundary layer development

Since datasets which are suitable for a validation of the complete SALSA model were not available to the present author, the performance of the 'atmosphere compartment' could only be tested to a limited extent. To this purpose, some features of predicted developments will be discussed. It may be recalled that the equations which express the transport processes and the production rates of kinetic energy, are identical to those, used by Nieuwstadt and Driedonks (1979) in their boundary layer model (with the exception of the surface exchange coefficients). The latter model was validated by experimental data for the case of nocturnal boundary layer development.

All the results presented in this subsection were generated by the same simulation run, unless mentioned otherwise. Conditions for this run were a geostrophic wind speed of 10 m s^{-1} , a very smooth surface ($z_0 = 0.1 \text{ mm}$) and an initial potential temperature of 20°C throughout the atmosphere. Initial conditions of wind speed and specific humidity were obtained by 'idling' for 48 h at constant surface temperature and surface humidity conditions. Initial conditions for the soil were taken from day 156, FLEVO set 1; soil properties were also taken from that dataset (silt loam). Simulation then started at the end of the afternoon (16.00 h) and proceeded to cover a period of 48 h. For global radiation, the measured data of day 159, FLEVO set 1, were used (Figure 4.6). The atmosphere was divided into eleven layers, doubling in thickness from the surface upward, with a thickness of 3 m for the first compartment.

Figure 5.40 depicts the terms of the surface energy balance, and Figure 5.41 shows the simulated conditions at screen height. The results can be considered not unrealistic if compared to observations, presented in section 4.5 for the various data sets. Calculated dewpoint temperature was added here as an extra check on the behaviour of simulated conditions at 1.5 m; predicted developments in this comparatively conservative quantity are interpreted as reasonable.

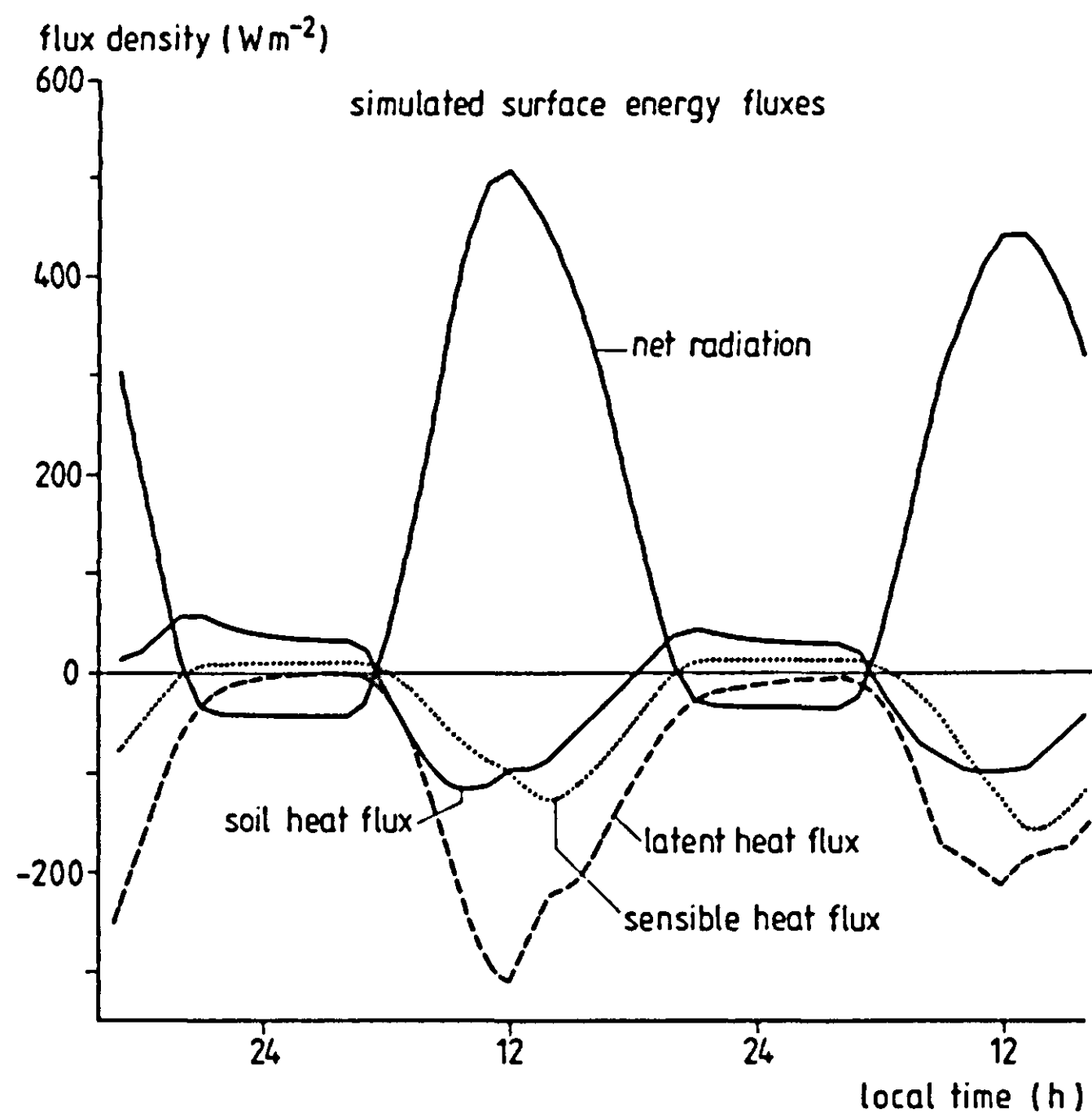


Figure 5.40 Surface fluxes as simulated by SALSA, including boundary layer development (IFBLD = 1). For the chosen set of system parameters and boundary conditions, see text.

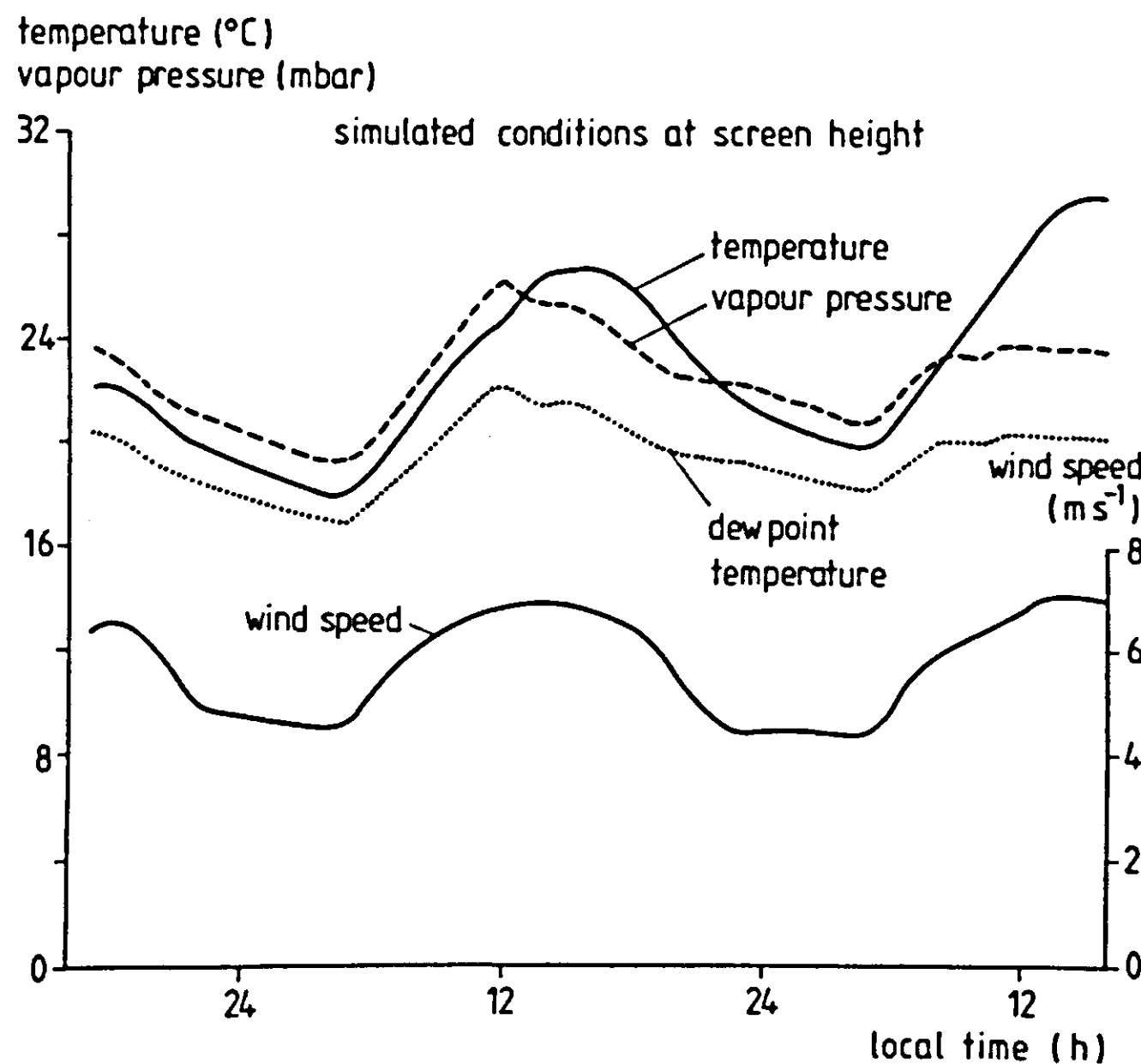


Figure 5.41 Atmospheric conditions at screen height as simulated by SALSA, including boundary layer development (IFBLD = 1).

Figure 5.42 shows the sensible heat flux in the lower atmosphere at various times of the day. In the mixed layer, fluxes should be approximately linear with height, which appears to be the case, except for the lower 15 m. Below that height, the heat flux divergence predicted at noon, as seen from the graph, accounts for a maximum rise in air temperature of about 1 K h^{-1} , which is viewed as acceptable at this hour.

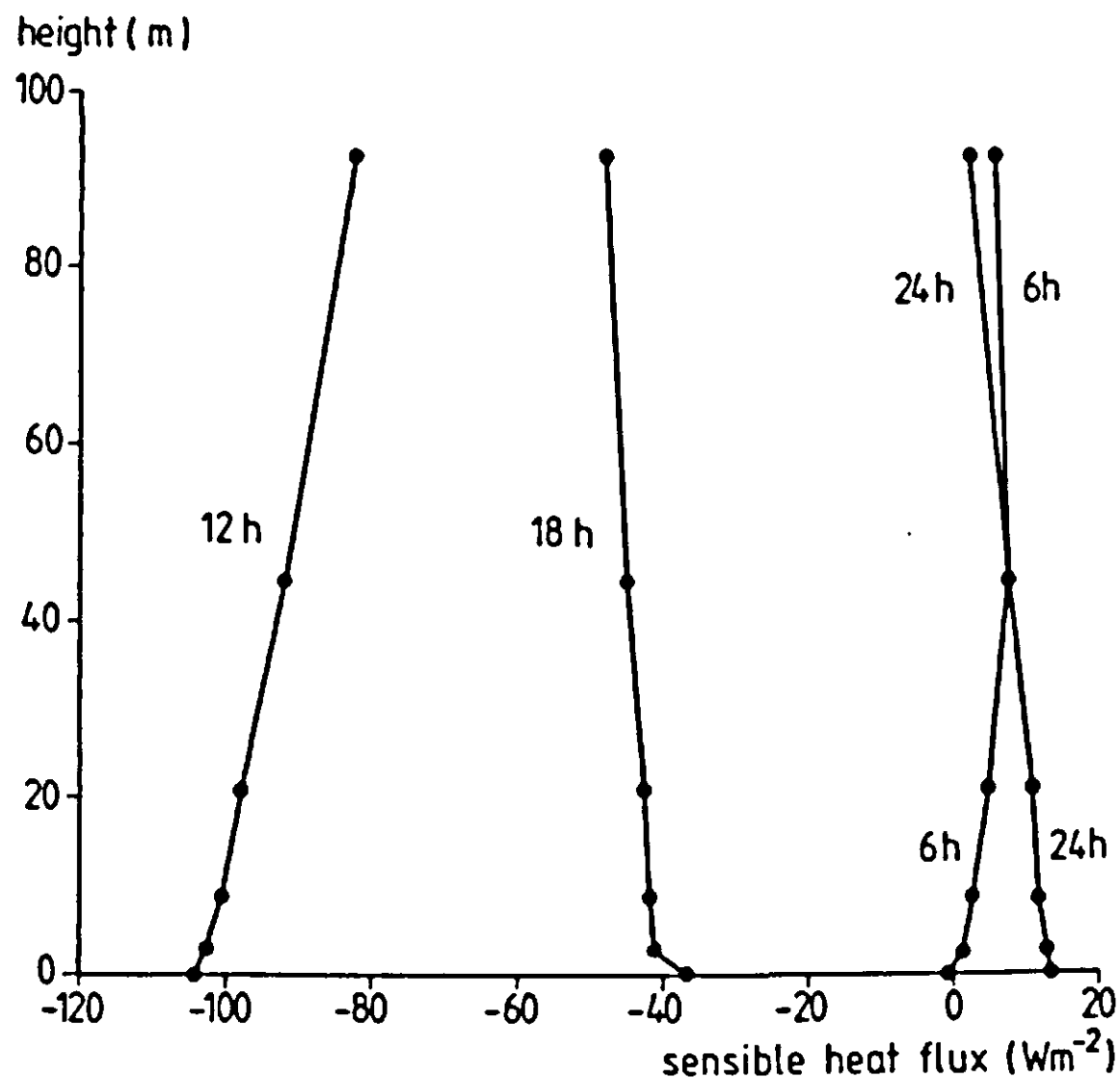


Figure 5.42 Profiles of the sensible heat flux in the lower atmosphere, as simulated by SALSA for different times of the day.

The normalized flux of momentum, τ_x/ρ , is presented in a similar way in Figure 5.43, and a more or less linear relation is found also for this case.

The development of the potential temperature profile is demonstrated in Figure 5.44. This picture illustrates the appearance of the nocturnal temperature inversion (with a base at 100–200 m height), which is dissolved subsequently in the morning hours. Also the difference in boundary layer height between day and night can be seen from this graph. The increase in maximum temperature at screen height – observed on the third day as compared to the second day – is due to drying of the soil surface. The corresponding developments in specific humidity are shown in Figure 5.45. The profiles of turbulent kinetic energy for the same simulation run are shown in Figure 5.46.

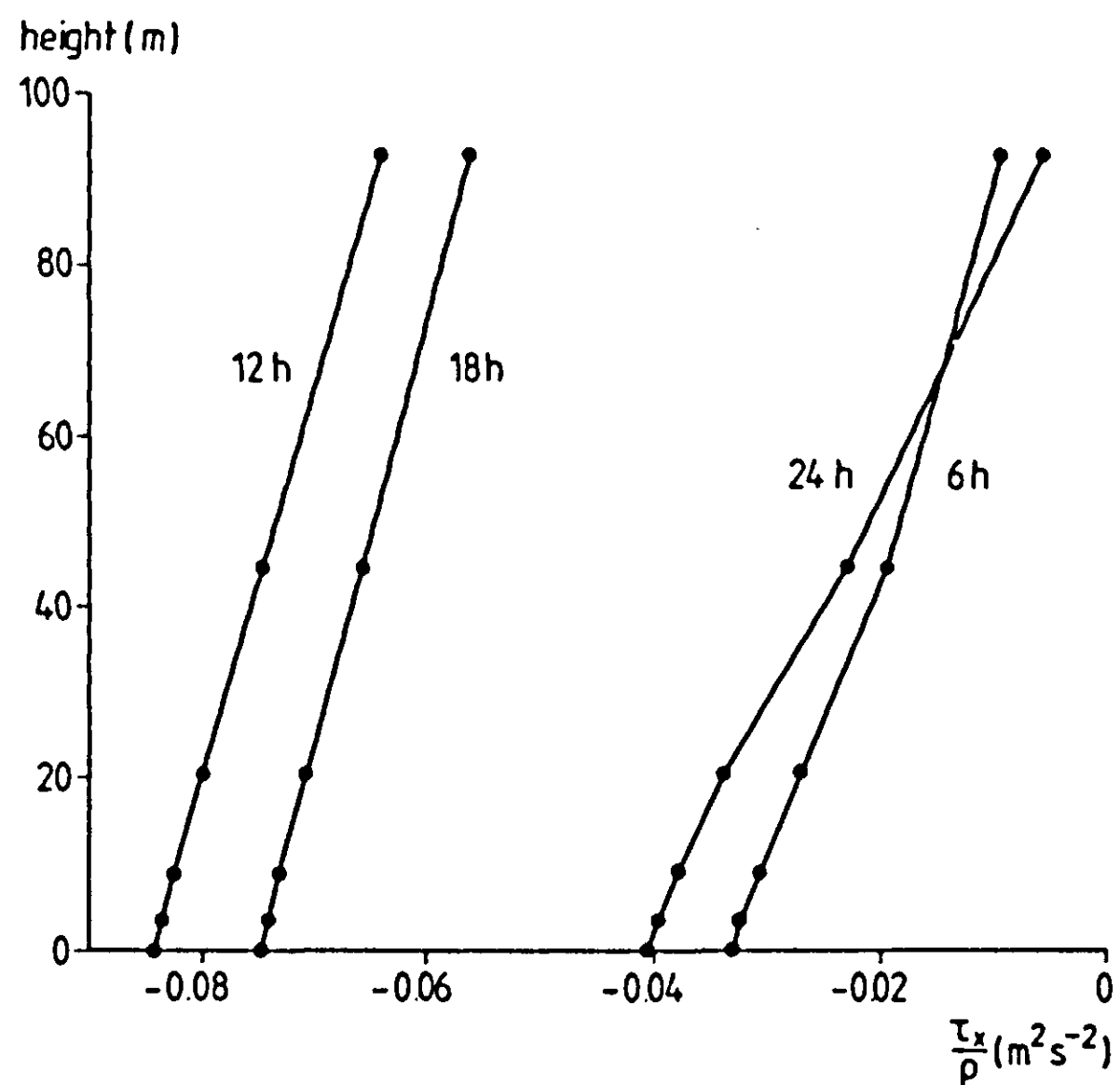


Figure 5.43 Profiles of the normalized flux of horizontal momentum, τ_x/ρ , as simulated by SALSA for different times of the day.

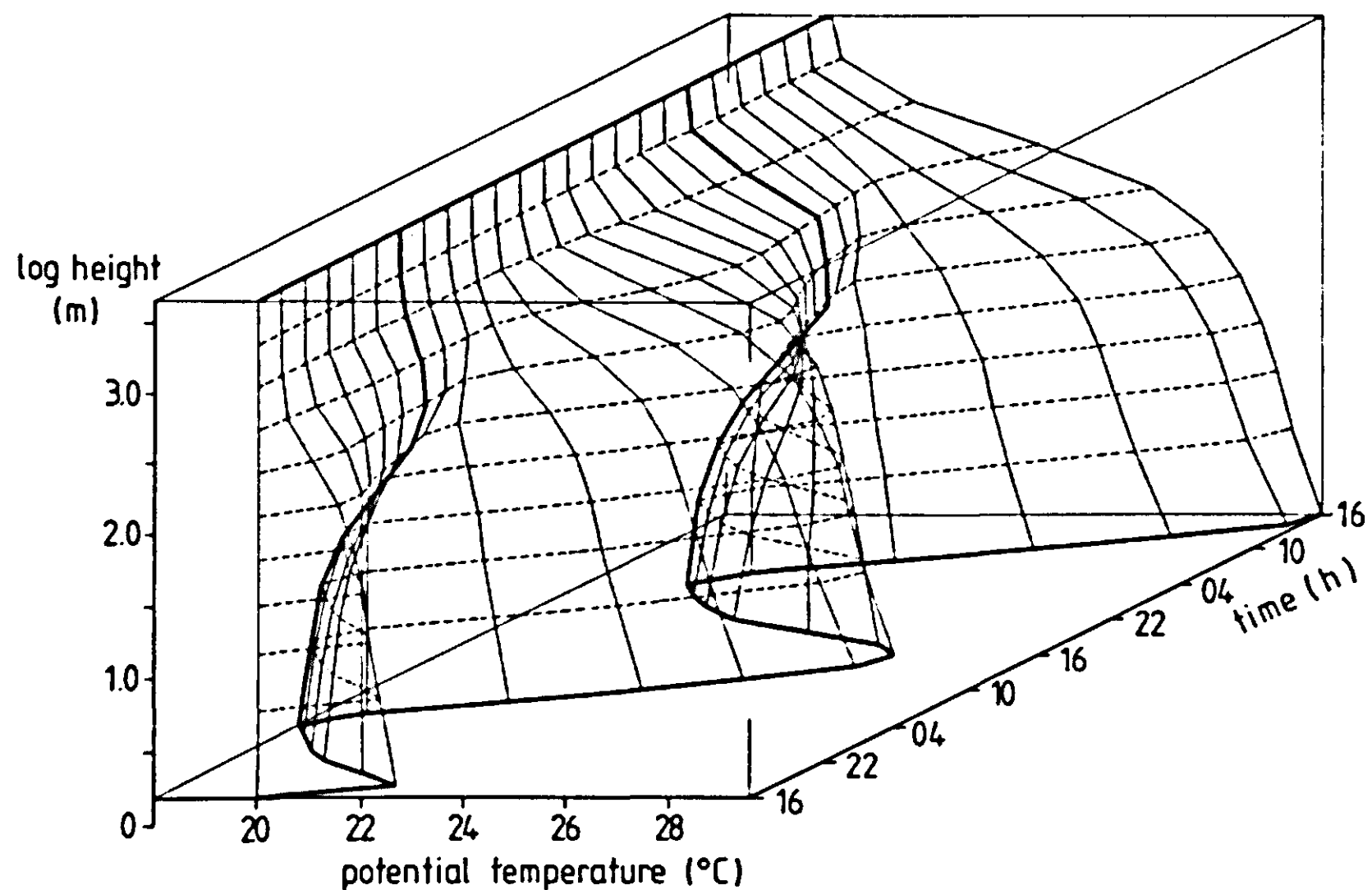


Figure 5.44 Simulated development of potential temperature in the lower atmosphere.

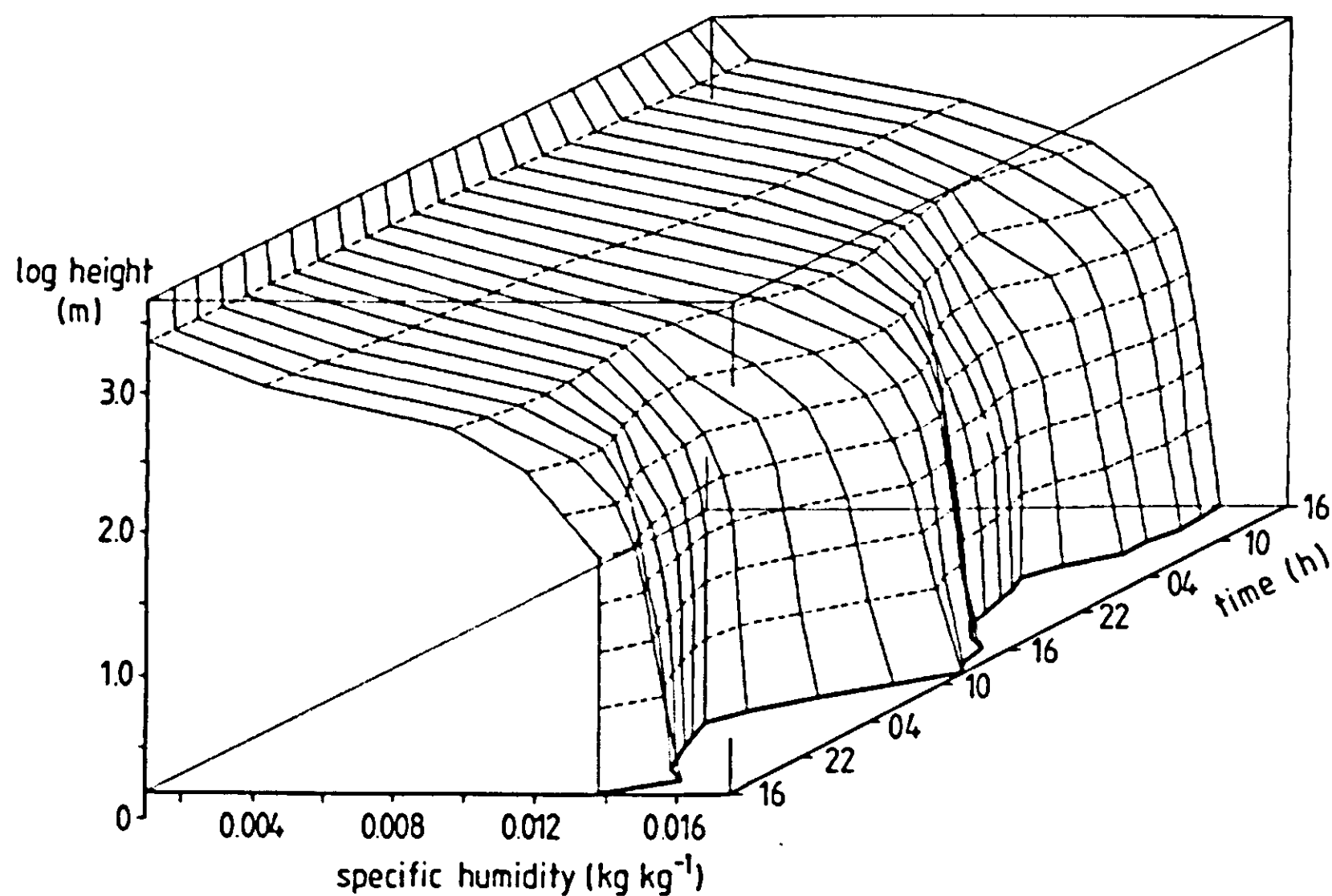
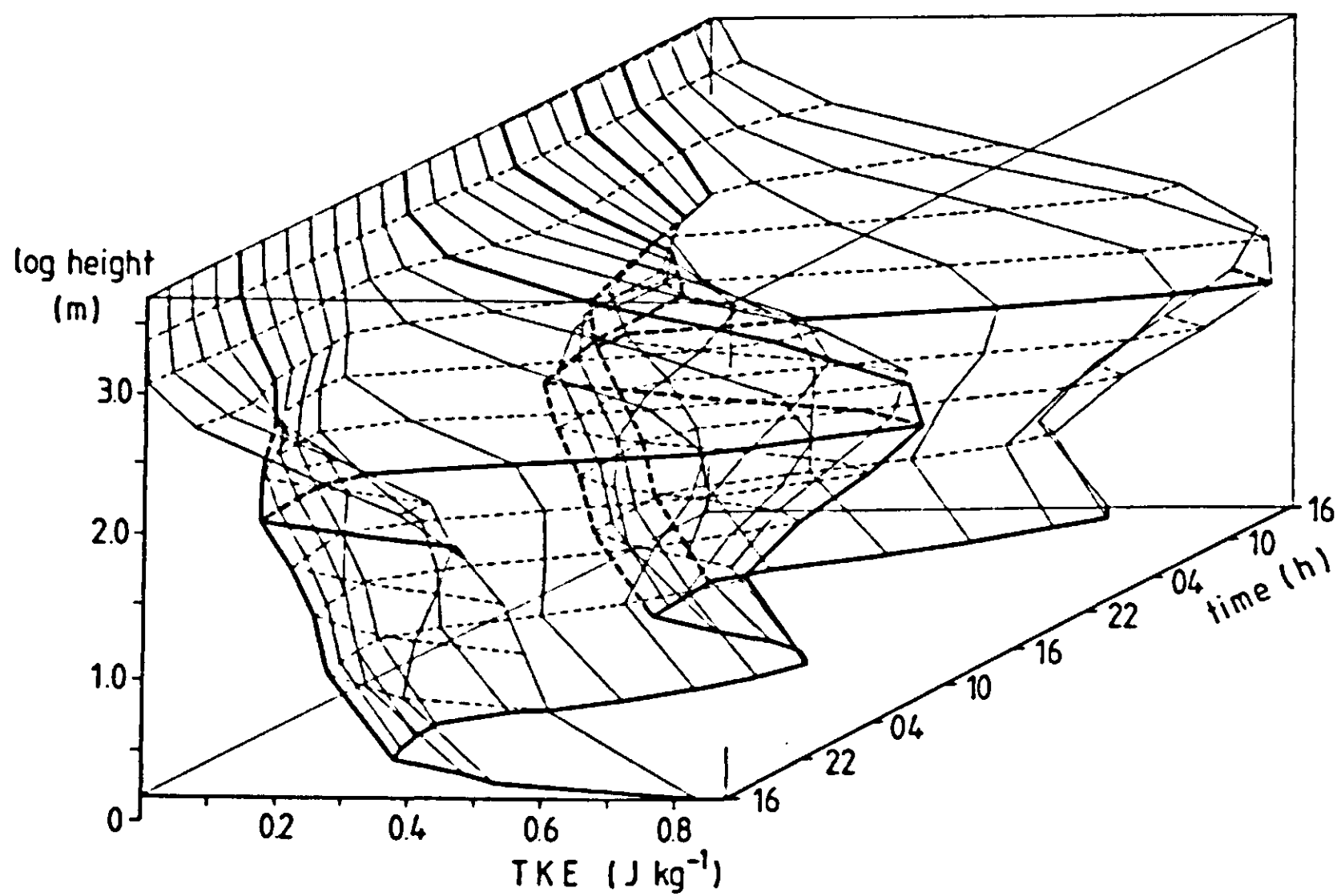
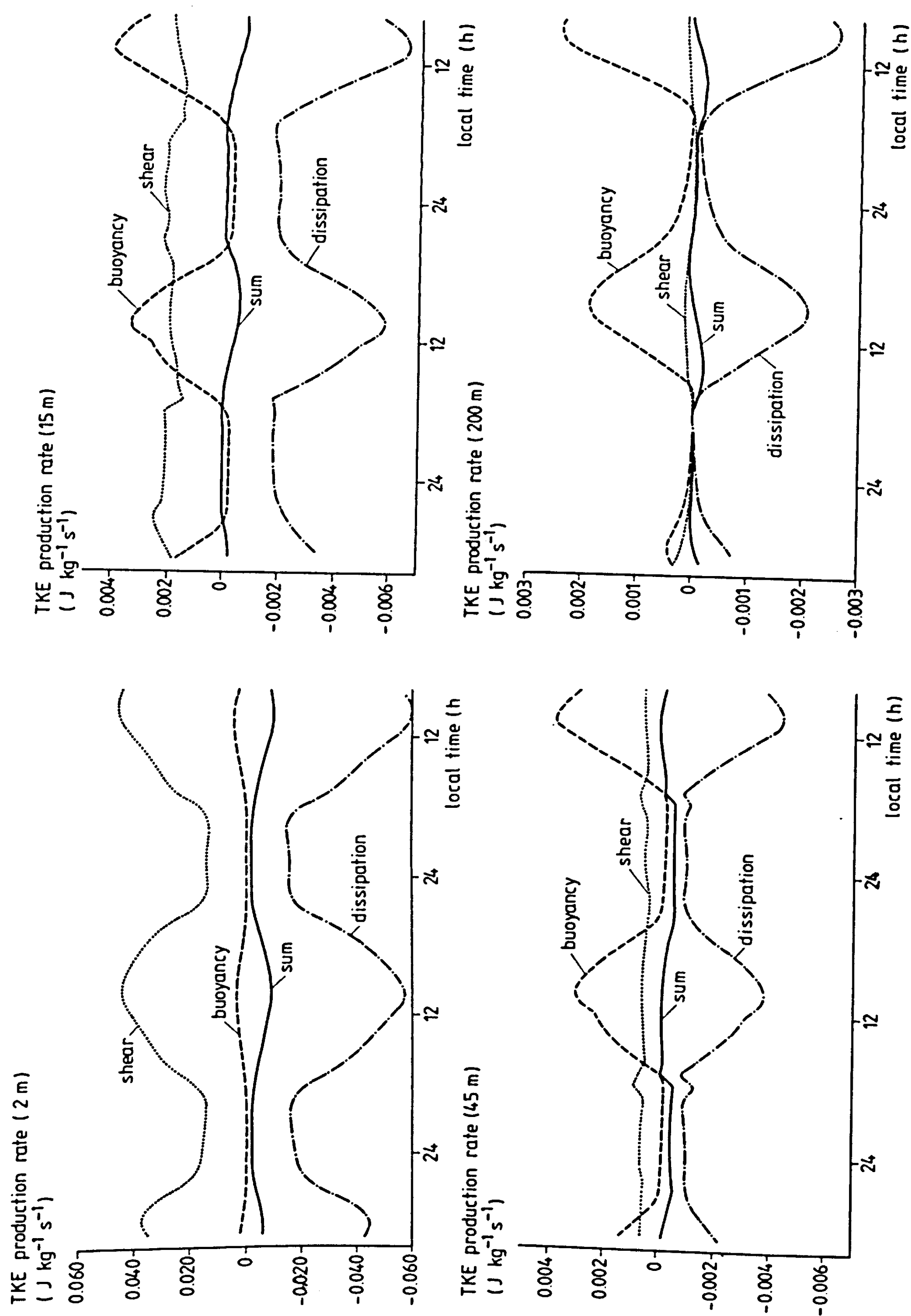


Figure 5.45 Simulated development of specific humidity in the lower atmosphere.

Figure 5.46 Simulated development of turbulent kinetic energy in the lower atmosphere.





Figures 5.47-5.50 Production rates of turbulent kinetic energy at different heights in the atmospheric boundary layer.

The courses of turbulent kinetic energy production terms at different fixed heights are depicted in the Figures 5.47 - 5.50. It can be observed that the sum of the various terms is relatively close to zero during most of the time at all four heights, which is in accordance with general experience.

In a more detailed study of model sensitivity, the effects of soil processes on conditions in the lower atmosphere, and vice versa, will be discussed in the next chapter.

CHAPTER 6. SENSITIVITY ANALYSIS

The term 'sensitivity analysis' has been used in the literature on modelling to indicate a wide range of activities related to the study of model behaviour. In the present context, 'sensitivity analysis' will be interpreted as a study of the effects of changes in system parameters, but also in model structure, on the values of output variables. Also, some relations between output variables will be inspected. The course of global radiation as a boundary condition will not be changed in the various simulation runs; also geostrophic wind and some empirical parameters, employed in the description of boundary layer development (cf. subsection 3.4.2), will be maintained at a fixed value. The present analysis, therefore, is by no means meant to be exhaustive; it focusses mainly on a number of soil properties. Due attention is given to the process of topsoil drying.

First, a brief discussion will be given on approaches to sensitivity analysis, as found in literature (section 6.1). Furthermore, the relevance of the 'atmosphere compartment' to the simulation of soil and surface processes is illustrated in section 6.2. Parameter sensitivity will be studied subsequently in section 6.3 for different stages of surface drying; also, the soil properties that determine the development of drying stages, and in particular the occurrence of 'drying fronts', are inspected in this chapter (section 6.4).

6.1 Approaches to sensitivity analysis

Several functions can be used to express sensitivity of systems. The most common expressions for the local sensitivity of some output variable $y(t)$ to changes in a system parameter p are the absolute sensitivity $\partial y(t)/\partial p$ and the relative sensitivity $\partial \ln y(t)/\partial \ln p = (\partial y/y)/(\partial p/p)$ (e.g. Horowitz, 1963; Himmelblau and Bischoff, 1968; France and Thornley, 1984; McCuen, 1973). DeCoursey (1976) advocated the use of the form $\partial \ln y(t)/\partial \ln(p-p_0)$ to reduce the effect of the choice of the reference level p_0 for the relevant parameter. To derive these functions for a given system, two basically different ways may be followed. In the study of biological systems, the 'parameter perturbation method' is widely applied to approximate the differential of interest as a finite difference quotient: changes in output variables are registered as a response to perturbations in

system parameters. A more elegant approach was developed in the field of systems control engineering. The involved method, yielding the time courses of the differentials $\frac{\partial y(t)}{\partial p}$, was described by Tomović and Vukobratović (1970) in their extensive treatise on 'general sensitivity theory'. Although the latter method appears to be impractical in the present case (as will be shown), its basic principles cannot be omitted in a brief review of sensitivity analysis because of their general validity and the contrast with the perturbation method.

General sensitivity theory.

Let a system be described by the time rate of change of a single state variable y as a function of a parameter p and time t :

$$(6.1) \quad \frac{\partial y}{\partial t} = f(y, p, t)$$

The sensitivity of this rate to perturbations in a parameter p can be written as the rate of change of the sensitivity u to that parameter:

$$(6.2) \quad \frac{\partial}{\partial p} \left(\frac{\partial y}{\partial t} \right) = \frac{\partial}{\partial t} \left(\frac{\partial y}{\partial p} \right) \equiv \frac{\partial u(p)}{\partial t}$$

where u is the so-called sensitivity function. Now by implicit differentiation one finds

$$(6.3) \quad \frac{\partial}{\partial p} (f(y(p), p, t)) = \frac{\partial f}{\partial y} \frac{\partial y}{\partial p} + \frac{\partial f}{\partial p}$$

which is, as follows from eqs. (6.1) and (6.2), equivalent with

$$(6.4) \quad \begin{aligned} \frac{\partial u}{\partial t} &= \frac{\partial f}{\partial y} \frac{\partial y}{\partial p} + \frac{\partial f}{\partial p} \\ &\equiv g(\phi, p, t)u(p, t) + h(\phi, p, t) \end{aligned}$$

with $u(p, t_0) = 0$ (p is supposed not to represent an initial condition). The function ϕ is the solution of eq. 6.1 for the unperturbed case (the current state variable of interest). If more than a single state variable is involved in the formulation of a particular differential $\frac{\partial y_j}{\partial t}$, eq. 6.4 is replaced by

$$(6.5) \quad \frac{\partial u_j(p)}{\partial t} = \sum_{i=1}^n \frac{\partial f_i}{\partial y_i} \frac{\partial y_i}{\partial p} + \frac{\partial f_j}{\partial p}$$

the solution of which is obtained by solving the matrix form of the rate equation:

$$(6.6) \quad \frac{\partial U}{\partial t} = G(\phi, p, t)U(p) + H(\phi, p, t)$$

under the condition $U(p, t_0) = 0$.

The matrices are then defined as

$$U \equiv \begin{vmatrix} \frac{\partial y_1}{\partial p_1} & \frac{\partial y_n}{\partial p_1} \\ \frac{\partial y_1}{\partial p_m} & \frac{\partial y_n}{\partial p_m} \end{vmatrix}, \quad G \equiv \begin{vmatrix} \frac{\partial f_1}{\partial y_1} & \frac{\partial f_n}{\partial y_1} \\ \frac{\partial f_1}{\partial y_n} & \frac{\partial f_n}{\partial y_n} \end{vmatrix} \quad \text{and}$$

$$H \equiv \begin{vmatrix} \frac{\partial f_1}{\partial p_1} & \frac{\partial f_n}{\partial p_1} \\ \frac{\partial f_1}{\partial p_m} & \frac{\partial f_n}{\partial p_m} \end{vmatrix}$$

So it appears that a total of n differential equations is required to solve the sensitivity function of a variable y_j to a single parameter, in the case where n state variables (including y_j itself) affect the differential $\frac{\partial y_j}{\partial t}$. Moreover, a total of n^2 and n derivatives must be formulated (programmed) to define the coefficient matrix G and the matrix H , respectively. The resulting differential equations can then be added to the simulation algorithm and be integrated (to yield the sensitivities u) by the usual procedure employed in the program to solve the original rate equations. Although this technique is attractive for relatively simple models, it becomes very impractical when applied to study the sensitivity of somewhat more complicated systems. In the following, therefore, the parameter perturbation method will be used.

The parameter perturbation method

Perturbation of parameters to which sensitivity is to be investigated provides a less elaborate type of sensitivity analysis. Usually, the finite difference form of the absolute sensitivity, $\Delta y(t)/\Delta p$, is calculated as an indicator. In section 6.3, some further remarks will be made with reference to the particular choice of the sensitivity indicator. The perturbation method may still call for extensive calculation efforts when applied to systems which involve a large number of parameters. Steinhorst et al. (1978) demonstrated, in a detailed example of sensitivity analysis, how an excessive number of simulation runs can be reduced by the use of so-called macro-parameters. A macro-parameter, in their terminology, represents a group of system parameters which are perturbed simultaneously. A high value for a given macro-parameter is then effectuated by taking high values for all contained system parameters. If the system appears to be insensitive to a certain macro-parameter, sensitivity to the individual parameters then needs no further study. The above authors varied the macro-parameters in different combinations according to a fractional, factorial design, and evaluated the main and interaction effects subsequently by analysis of variance of the output variables. For selected macro-parameters, the individual parameters were then studied in more detail. A condition for this approach to be valid is that negative interaction be absent among parameters, grouped into a macro-parameter.

In the SALSA model, most processes of interest - and hence the parameters involved - are interacting to some extent, and moreover the model is not very large, so that the use of macro-parameters is not warranted here. A perturbation scheme that allows for analysis of possible interaction phenomena, however, is valuable in general, and will be employed in studying the sensitivity of surface fluxes and conditions as discussed in section 6.3.

6.2 The relevance of boundary layer development to soil processes

As mentioned in Chapter 3, the mutual dependence of soil and atmosphere conditions called for a formulation of the development of atmosphere conditions which takes into account the computed surface fluxes. The (generally accepted) alternative situation - where boundary conditions measured at screen height are imposed on the soil system - is not suitable for the present type of sensitivity studies. It should, therefore, not be used where

one is interested in soil behaviour and surface fluxes over wide ranges of (soil) parameter values, since the courses of state variables close to the surface depend on the latter values themselves. The simulation results presented in this subsection serve to substantiate the above statement.

To this purpose it is attempted to demonstrate the contrast between results of the SALSA variant that includes boundary layer development (IFBLD=1) versus those of the shortened version that does not (IFBLD=0). In such an effort, one encounters the problem that for the latter case a series of boundary conditions must be generated which allows for a fair comparison. To overcome this difficulty, the complete version of SALSA (IFBLD=1) was run for two sets of soil parameters, which resulted in two series of simulated conditions at screen height. These conditions are air temperature, humidity, and windspeed, 'registered' at one-hour intervals for a period of four days. Subsequently, the courses of these variables, obtained as simulation output for the one soil type, were imposed as boundary conditions to the other soil - and vice versa - in a simulation run without boundary layer development. The soils used in this 'cross-combination' were taken to be different only in their hydraulic properties (moisture characteristic, hydraulic conductivity curve, and matric flux potential curve). The corresponding parameters are given in Table 6.1. All initial conditions, parameter values and model options were identical in all four runs, with the exception of the switch IFBLD, of course, and the initial soil moisture content, which should be related to the chosen hydraulic properties of the soil. Then, if the effect of soil conditions on surface fluxes via screen-height conditions (feedback via the atmosphere) would be negligible, the two runs for a given soil would result in identical courses of the surface fluxes (and other variables within the system).

Two contrasting soils were selected from the variety of soils listed in Table 3.8 : Mont Cenis silt loam (Vachaud, 1966), and Sable S2 (Stroosnijder, 1982). The initial soil water pressure for both cases was taken to be -5 kPa, as might be viewed as realistic under field conditions shortly after thorough wetting. The effect of gravity was taken into account (IFGRAV=1) and free drainage was allowed at the lower boundary of the system. For the boundary conditions geostrophic wind speed and global radiation, the same data as mentioned for the example given in section 5.4 were used .

Table 6.1 Hydraulic properties of Mont Cenis silt loam and Sable S2.

	Mont Cenis silt loam	Sable S2	
α	1.8070	10.020	Pa^{-1}
n	1.2814	1.3741	-
θ_r	0.0000	0.0000	-
θ_s	0.442	0.410	-
θ_i	0.38	0.23	
K_s	$1.41 \cdot 10^{-8}$	$409.58 \cdot 10^{-8}$	$\text{kg m}^{-1}\text{s}^{-1}\text{Pa}^{-1}$
A	$150.4 \cdot 10^{-6}$	$470.9 \cdot 10^{-6}$	$\text{kg m}^{-1}\text{s}^{-1}$
B	0.1670	0.0046	-

Drying of the topsoil appears to proceed quite differently for the two soils. Whereas the Mont Cenis silt loam is able to replenish the drying surface layers with subsoil water for several days, the Sable S2 soil rapidly develops a dry surface layer under the imposed conditions. (The process of topsoil drying in relation to hydraulic soil properties will be discussed in more detail in section 6.4). If attention is paid now to the surface fluxes and atmosphere conditons at screen height, it becomes clear how these are related to soil properties. Figure 6.1 shows the predicted behaviour of air temperature, humidity, and wind speed as developed over the two soils. The increase in daily maximum vapour pressure over the course of several days is less pronounced for Sable S2 than for Mont Cenis silt loam, since the latter maintains a higher evaporation rate. The reverse is true, as expected, for air temperature, which rises more rapidly in the case of Sable S2.

The surface fluxes of sensible and latent heat as simulated for the Mont Cenis soil by the complete model (IFBLD=1) are depicted in Figure 6.2. The same figure also shows the curves that result when at screen height the conditions, 'generated' over Sable S2 soil, are imposed on the Mont Cenis silt loam system. The low vapour pressure and high air temperature, acquired over the Sable S2 surface, induce an increased evaporation rate and a suppressed sensible heat flux when combined with the moist Mont Cenis soil surface. This happens to the extent that, during the last day of the

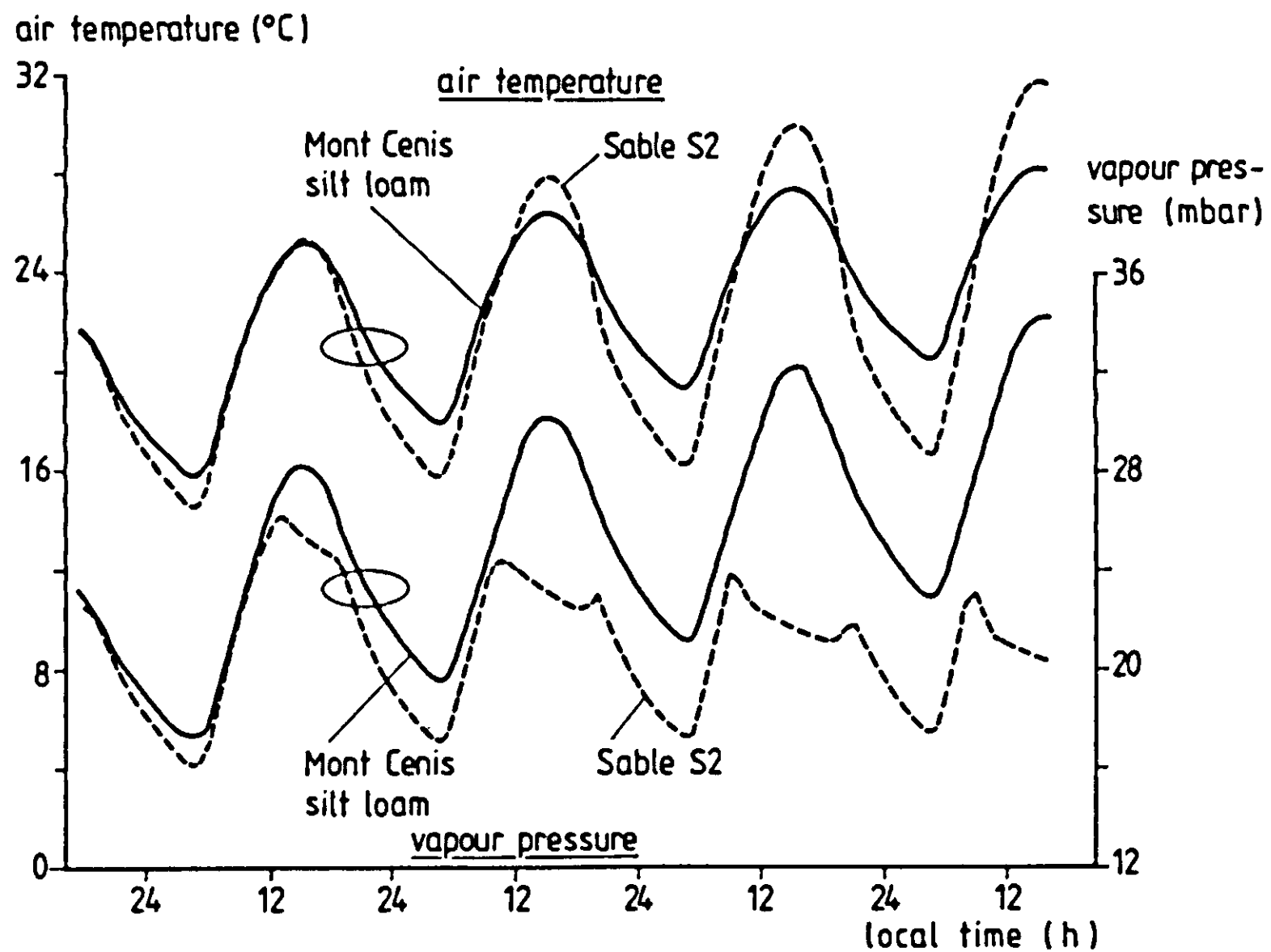


Figure 6.1 Simulated atmospheric conditions at 1.5 m above the surface for a silt loam and a sand soil; initial soil water pressure was -5 kPa in both cases.

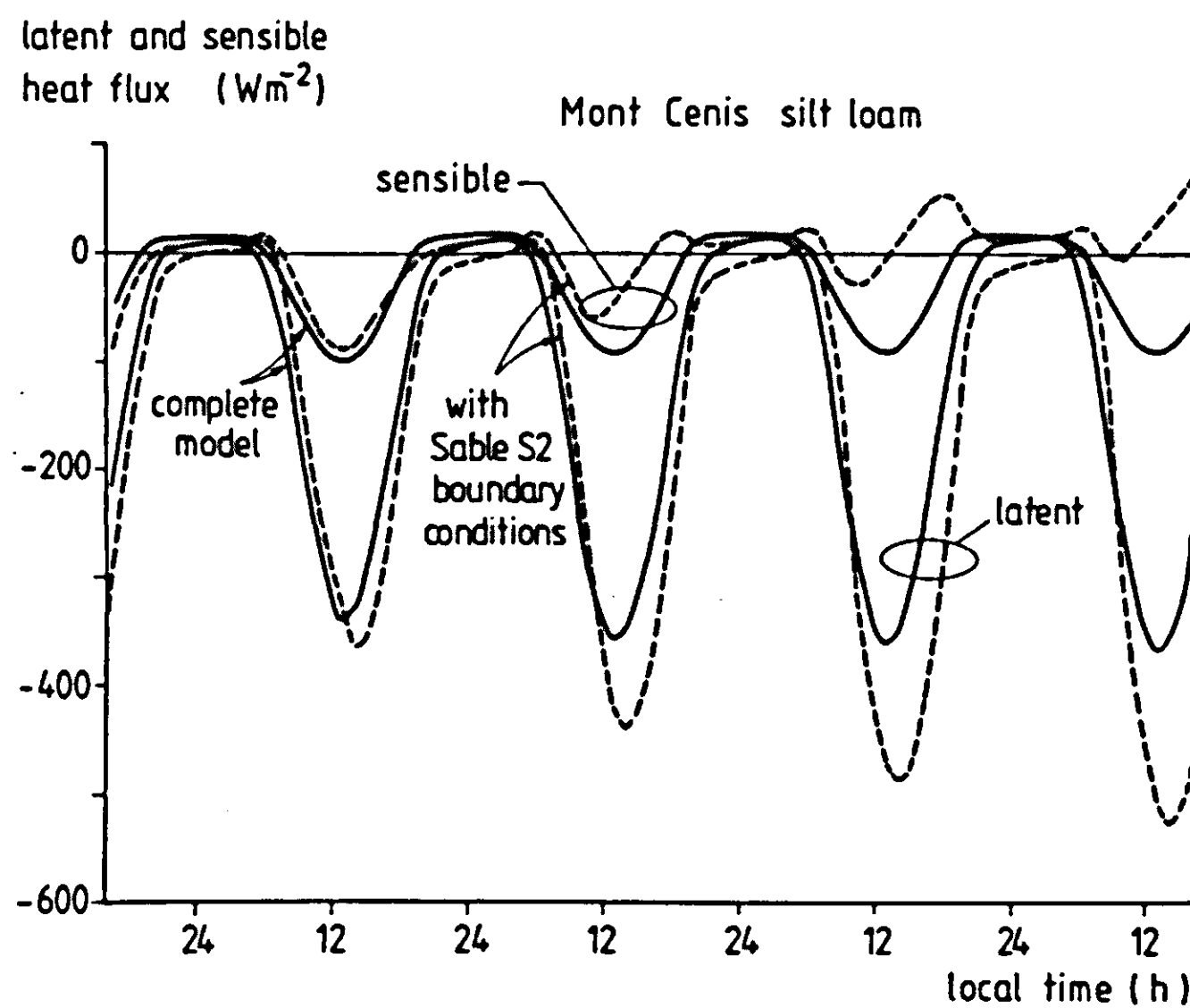


Figure 6.2 Surface fluxes of sensible and latent heat, simulated for a silt loam.

simulated period, the direction of the sensible heat flux is reversed to supply heat from the 'warm' atmosphere to the surface, cooled by excessive evaporation. A slight phase shift can be observed between the time series as obtained by the two model versions, respectively. This is due to the fact that conditions at screen height, obtained at given instants (e.g. 16.00 pm) from the 'complete' simulations, were maintained at their fixed values during one hour (16.00-17.00 pm) in the simulations with the shortened version of the model. Results analogous to those shown in Figure 6.2 were obtained for the Sable S2 soil, where the reverse effect could be observed; the contrast in that case was less pronounced, however, since soil conditions rather than atmospheric conditions were limiting evaporation.

The presented graphs expose clearly the relevance of soil behaviour to changes in air properties, and vice versa. This example serves to illustrate that for an accurate simulation of especially surface drying of bare soils, it is indispensable to use atmospheric boundary conditions that are in accordance with the development stage of the drying process. In reality, the picture sketched here will be found to be somewhat exaggerated, due to the underlying assumption of lateral homogeneity; the influence of soil conditions on the profiles of temperature and humidity in the developing boundary layer is therefore somewhat overestimated.

6.3 Sensitivity of some variables to major soil parameters; the drying stages I and III

It may be questioned which indicator of sensitivity is most suitable in the context of remote sensing imagery interpretation. Limiting the discussion to absolute sensitivity as defined in section 6.1, a choice could be made between (an approximation of) the differential sensitivity dy/dp , and the integral sensitivity $\Delta y/\Delta p$. Although both indicators have their advantages in specific cases, they share the disadvantage that division through dp and Δp , respectively, introduces a dependence on the scale chosen to express p , and thus renders impossible a direct comparison between the effects of different parameters. Moreover, the sensitivity itself becomes interesting mainly if combined with a certain interval Δp . It is assumed that one is primarily interested in the range of values that some output variable might attain, due to possible (field) variations in specified para-

meters. Attention is therefore focussed here on the quantity Δy , corresponding to a maximum range Δp , rather than on true sensitivity. The choice of Δp , inevitably introduces some subjectivity, but the gain is a direct picture of the relative importance of parameters.

The key parameters governing the surface energy balance under given meteorological conditions are albedo, emissivity, thermal conductivity and heat capacity, roughness length, and some hydraulic soil properties that determine surface drying. In this section the effects of these parameters - with the exception of the latter, as explained below - will be studied. The procedure involved uses a simplified version of the SALSA model.

The soil moisture content profile, as developing from a given initial state as a function of hydraulic properties and meteorological conditions, dominates the surface energy balance in a complicated manner; all transport coefficients, capacities and radiative properties are related to soil moisture content. The results of simulations with a model that describes the process of surface drying, therefore, can hardly be generalized in terms of sensitivity to basic soil parameters, other than those which directly affect moisture flow. Moreover, the development of moisture profiles is often a matter of several days, whereas the characteristic pattern in surface fluxes and state variables is based on 24-hour cycles. For these reasons, it was preferred here to consider first a system with steady state moisture movement. It can be argued that the study of such simplified systems yields less realistic results, but it is believed that the advantage of a higher degree of generalisation outweighs that disadvantage. Also, computation costs play a decisive role.

Defining the three stages of drying

To the above purpose, the schematized classical three stages of drying (Fischer, 1923) are employed. Stage I is defined by evaporation at the soil surface, where water supply is not limiting. Saturation deficit of the atmosphere, radiation, and some 'exchange resistance' determine to a large extent the evaporation rate, which could be referred to as 'potential evaporation' (although soil properties affect this flux also, as will be shown). The second stage, known as the 'falling rate' stage, represents a transient case, characterized by the development of the dry surface layer and a decreasing evaporation rate. By definition, stage II cannot be treated as a

steady state situation. Because of its more complicated nature, this subject will be discussed in detail separately in section 6.4. In stage III of the drying process, water evaporates from below a dry surface layer and is transported to the surface by diffusion in the vapour phase.

This schematic separation of stage was originally based on laboratory observations, and has not been subject to extensive study for field circumstances. Nevertheless, the concept has been supported by observations of Idso et al(1974) for a field situation; also the FLEVO data for Swifterbant loam (cf. Chapter 5) are in accordance with this separation of stages.

In the modelling trials to be discussed, the following working definition of the stages was applied. Stage I was treated as steady, evaporation taking place at the surface, the driving force being only the linearized gradient of vapour density between the evaporation site and screen height. In stage III, the evaporating surface was situated at a fixed depth, and the water transport was considered to be entirely in the vapour phase above this depth, the driving force again being the linearized density gradient. With respect to stage I, the 'resistance' to vapour transport was increased with a diffusion term for this case to account for transport in the soil. For both stages, all interactions between water vapour and soil material in the dry layer (including liquid water), were omitted. Aside from the above, the model employed was the complete SALSA model, i.e. including atmospheric developments. Again, the radiation data for day 156, FLEVO set 1, were used to define the energy flux boundary condition at the surface, and a geostrophic wind of 10 m s^{-1} was assumed in the following examples.

The two cases I and III were treated separately. To all system parameters considered, two values were assigned, based on the extremes to be expected under field conditions. A complete two-level factorial design was used to define the different combinations of high/low parameter values. For n parameters, this results in 2^n combinations. The simplified model was run for all combinations, and the output was treated by analysis of variance (ANOVA) for each instant (one-hour intervals). ANOVA yields the main effects of parameters, and the interactions of various orders between parameters. SPSS (Statistical Package for the Social Sciences, Nie and Hadlai Hull, 1981) software was used to perform the analyses.

Analysis of Stage I

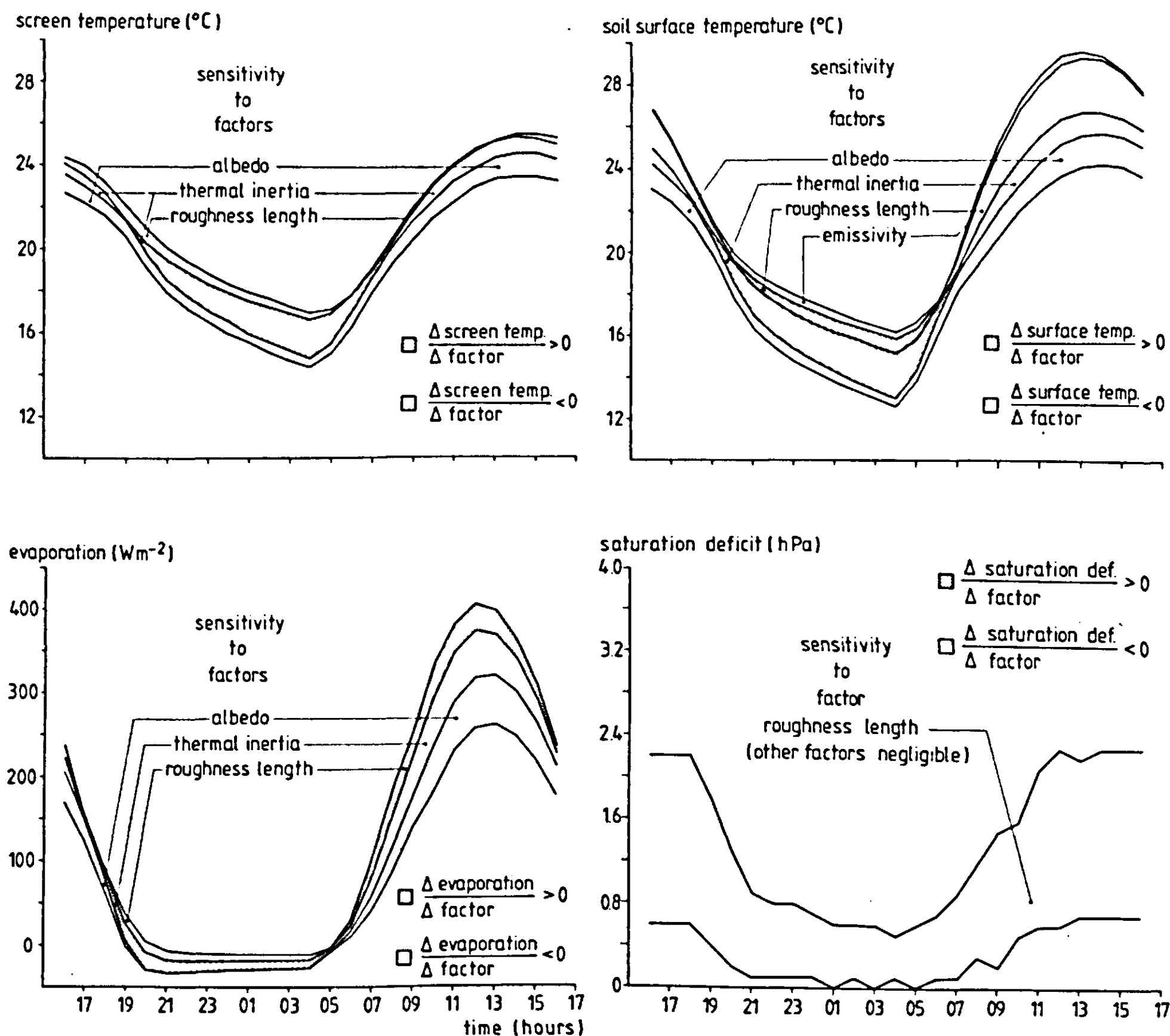
For the 'wet soil' situation, the parameters to be varied are albedo, emissivity, roughness length, thermal conductivity (λ), and heat capacity (C). As the latter (thermal) soil properties usually vary simultaneously, they were lumped into a single parameter, thermal inertia, defined as $p \equiv \sqrt{\lambda C}$. The frequent use of the thermal inertia concept in remote sensing literature was another reason to use this combined property. With the resulting four independent parameters, a total of 16 simulation runs was made, each for a period of 48 hours of which only the last 24 hours were analysed to reduce the effects of initial conditions. Table 6.2 lists the values, chosen for the parameters involved, based upon moist cq. wet soil conditions.

Table 6.2 Parameter values used in sensitivity analysis

	Stage I	Stage III		
albedo	.08	.14	.14	.38
emissivity	.94	.98	.92	.92
thermal cond. top	.60	2.30	.20	.40
thermal cond. sub	.60	2.30	.60	2.30
heat capacity top	$1.7 \cdot 10^6$	$3.0 \cdot 10^6$	$3.0 \cdot 10^5$	$6.0 \cdot 10^5$
heat capacity sub	$1.7 \cdot 10^6$	$3.0 \cdot 10^6$	$1.7 \cdot 10^6$	$3.0 \cdot 10^6$
thermal inertia top	1000	2630	250	500
thermal inertia sub	1000	2630	1000	2630
thickness toplayer	-	-	.009	.04
vapour diffusivity	-	-	$.22 \cdot 10^{-4}$	$1.1 \cdot 10^{-4}$
roughness length	.50	50	.50	50

The output variables for which sensitivity was investigated are surface temperature, latent heat flux, and temperature and saturation deficit of the air at 1.5 m height. Surface temperature was chosen since it is the variable of main interest in this study, and latent heat flux because of its relevance in an agronomical context. The other two variables are inspected in order to show the effect of soil conditions on the state of the lower atmosphere. For 25 hourly values and 4 output variables, a total of 100 ANOVA's was carried out.

Figures 6.3-6.6 show the main effects of parameter changes as they vary in time. These graphs call for some explanation. The information of interest is solely in the width and shading of the individual bands. The curves delineating these bands have no physical meaning themselves, because they result from addition of the effects of parameter variations. Also, the position of a particular band with respect to the vertical axis has no meaning: the total width of the entire band, obtained for each instant by summation of individual bands, was centered around the mean course of the relevant output variable. The following order of the individual bands was arbitrarily chosen. The mean curve itself is not depicted here, in order to focus attention on sensitivity rather than on absolute values. Individual band widths, measured in the units of the ordinate, directly show the (aver-



Figures 6.3-6.6 Results of a sensitivity analysis for stage I evaporation.
For explanation see text.

aged) absolute change in the output variable, due to a change in the indicated factor over the range mentioned in Table 6.2. The shading of each band determines whether the factor effect is positive or negative, as indicated in the figures. Bands narrower than 0.15 K, 0.15 K, 0.5 hPa, and 10 W m^{-2} were omitted from the figures for surface temperature, screen temperature, saturation deficit and latent heat flux, respectively.

If one is interested in the actual values of the output variables for a chosen combination of parameter values, these can be derived from the figures. In such factorial designs, the realisation of a dependent variable - in the absence of interaction among parameters - is expressed as the mean M plus half the sum of effects of all parameters 'present' (\equiv at high value), minus half the summed effects of parameters 'absent' (\equiv at low value). Thus, for a case with factors (parameters) a, b, and c 'present' and d, e, and f 'absent', the value of the dependent variable, noted as (abc) , would be calculated as

$$(6.7) \quad (abc) = M + \frac{1}{2}(A+B+C-D-E-F)$$

The capitals in this expression refer to the effects of parameters (factorial effect totals), to be read from the figures as band width and shading. In the case where interaction occurs, the relevant effects should be added on the RHS. In that situation, a plus sign must be assigned to combinations of letters appearing on the LHS (e.g. AC), and also to combinations of letters that are both absent on the LHS (e.g. DE); interaction effects between parameters which do not all pertain to either the 'absent' or 'present' class should be given a minus sign (e.g. AD, BEF, etc.). In this case of 'potential evaporation', the combinations AB, AC etc which could be added on the RHS to represent interaction effects, are all negligible. (i.e. the effects are smaller than the chosen critical minimum values mentioned before). The absence of interaction implies that the main effects of all factors are additive. In other cases (e.g. drying stage III) interaction may be considerable. A detailed treatment of the statistics of factorial experiments can be found in Snedecor and Cochran (1967).

From Figure 6.3 it can be seen that the variations in surface temperature, as expected to arise in the field from variations in albedo, thermal inertia and roughness length, all are of the same order of magnitude during daytime. Emissivity appears to play a minor role (note that surface temperature and not the radiation temperature is plotted!).

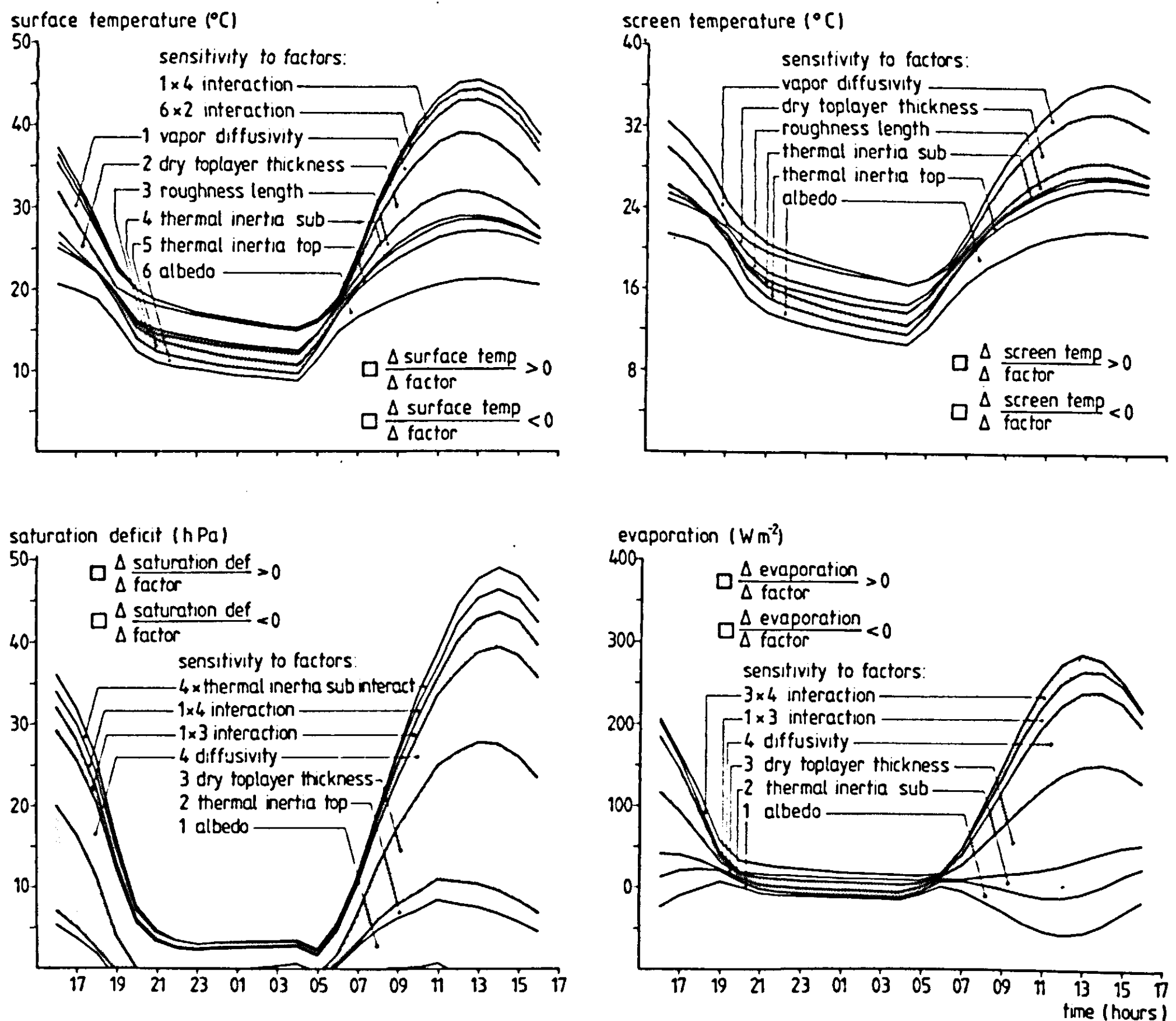
During the nighttime hours, thermal inertia dominates variability of surface temperature. Factors of relevant influence on air temperature at screen height are albedo and thermal inertia, but it can be observed that field variations in these parameters do not bring about changes of more than 1 or 2 K in air temperature in the case of stage-I evaporation. Saturation deficit, with very low overall values as expected at this stage, appears to be insensitive to all parameters; minor changes are due to variations in roughness length. For the latent heat flux, the parameters albedo, thermal inertia and roughness length again have effects of comparable magnitude, each giving rise to possible variations of about 50 Wm^{-2} .

Analysis of stage III.

In the simulation runs for stage III, again albedo, thermal inertia, and roughness length were varied. In this case, however, the thickness of the dry toplayer must be taken into account as a new parameter, while now two values of the thermal inertia must be chosen for the two layers considered. Moreover, vapour diffusivity is to be introduced as a system parameter. Variations in soil emissivity were omitted from the perturbation scheme, as these appear to have only a minor effect on the surface energy balance. So with the resulting total of six parameters to be varied, a full factorial two-level design asks for $2^6 = 64$ simulation runs in the case of stage III evaporation. The selected parameter values (Table 6.2) for the toplayer are based on reported ranges for dry soils, and for the subsoil on 'moist soil' values. This applies not, of course, to dry toplayer thickness (i.e. depth of the evaporation front), values for which are based on soil conditions to be expected during dry spells in NW Europe. These values may be considered as fairly arbitrary.

The output variables examined are again the surface temperature, latent heat flux, and air temperature and saturation deficit at screen height. The main effects are shown, along with some first order interaction effects, in the Figures 6.7-6.10. As in the previous case, these figures are the result of 100 analyses of variance (25 hourly values x 4 variables). For the inter-

interpretation of the graphs, one is referred to the explanation given for the stage I case. In the Figures 6.7-6.10, minimum values of 0.5 K, 0.3 K, 1 hPa and 10 W m^{-2} were used, respectively, for bands to be plotted.



Figures 6.7-6.10 Results of a sensitivity analysis for stage III evaporation. For explanation see text.

Whereas in the previous case interactions were negligible, they are relevant at stage III, at least for some parameters. It is recalled that an interaction effect AB between factors A and B is defined as the average response to A in the 'presence' (high value) of B, minus the average response to A in the 'absence' (low value) of B. The needed averages are taken over all possible combinations of the remaining factors.

Of the six parameters studied, albedo and dry layer thickness have the most pronounced effect on surface temperature (note the scale differences with the stage I figures). Also, during the daytime, roughness length and vapour diffusivity appear to be important parameters. Thermal inertia, especially of the subsoil (> 1 cm depth), plays only a minor role during the day. In this respect, some caution must be exercised when reading the figures, since the ranges chosen for topsoil inertia and subsoil inertia are different (Table 6.2). Thus a certain fraction of the toplayer thickness effect is due to the difference in topsoil and subsoil inertia. During the nighttime hours, thermal inertia dominates the picture. For screen temperature, similar effects can be observed from Figure 6.8. As expected, the soil parameters that are most important to the latent heat flux (Figure 6.10), also determine the saturation deficit of the air. The latter appears to be extremely sensitive to various soil properties, as seen in Figure 6.9. This does not surprise, since soil conditions that promote high surface - and air - temperatures are associated with low evaporation rates. Figures 6.9 serves as another illustration of the necessity to take into account the developments in the lower atmosphere when simulating surface processes.

6.4 Stage II: development of the dry surface layer; a case study

In the previous paragraph, the extreme cases of surface evaporation and evaporation from a fixed subsurface front were employed as a basis for sensitivity analysis. It was shown that the presence of a thin dry surface layer has a strong effect on the behaviour of surface temperature and other variables. The present section deals with the development of such dry surface layers as dependent on soil physical properties under given meteorological conditions. The results to be shown here may serve to indicate refinements in the sensitivity pictures sketched in the previous section, and to show how the hydraulic soil properties affect the evolution from evaporation stage I to stage III. To study the stage II development, the complete SALSA model was used, i.e. no a priori assumptions were made on soil liquid, vapour and heat movement; interactions between the different soil phases were included, and developments in the atmospheric boundary layer were simulated as well. In this case study, various aspects present themselves for discussion. These are the definition and behaviour of the drying front, and the role of the latent soil heat flux. Such aspects are not only of

relevance to the validity of the stage III-concept, they also have a wider significance as exemplified by dry-farming practices, where evaporation-inhibiting surface layers are aimed at. With reference to the previous paragraph, stage II can be viewed as the non-ideal stage III situation, where interactions between soil water and dry surface layer do occur. Therefore an analysis of stage II allows for a refinement of the conclusions arrived at in section 6.3.

The major physical soil characteristics that affect surface drying are the hydraulic conductivity curve and the moisture characteristic. As discussed in subsection 3.6.2, these two curves can be combined to yield the matric flux potential curve, which can conveniently be approximated for most soils in terms of an expression with three parameters, according to:

$$(6.8) \quad \Phi(\theta) = \frac{-A x}{x + B}$$

with $x \equiv 1 - \theta/\theta_s$. The parameters A and B (Table 3.8) play a key role in the development of drying fronts. To investigate their influence, the process of evaporation under free drainage conditions was studied. For orientation of the reader, some extreme examples of $\Phi(\theta)$ curves are plotted in Figure 6.11.

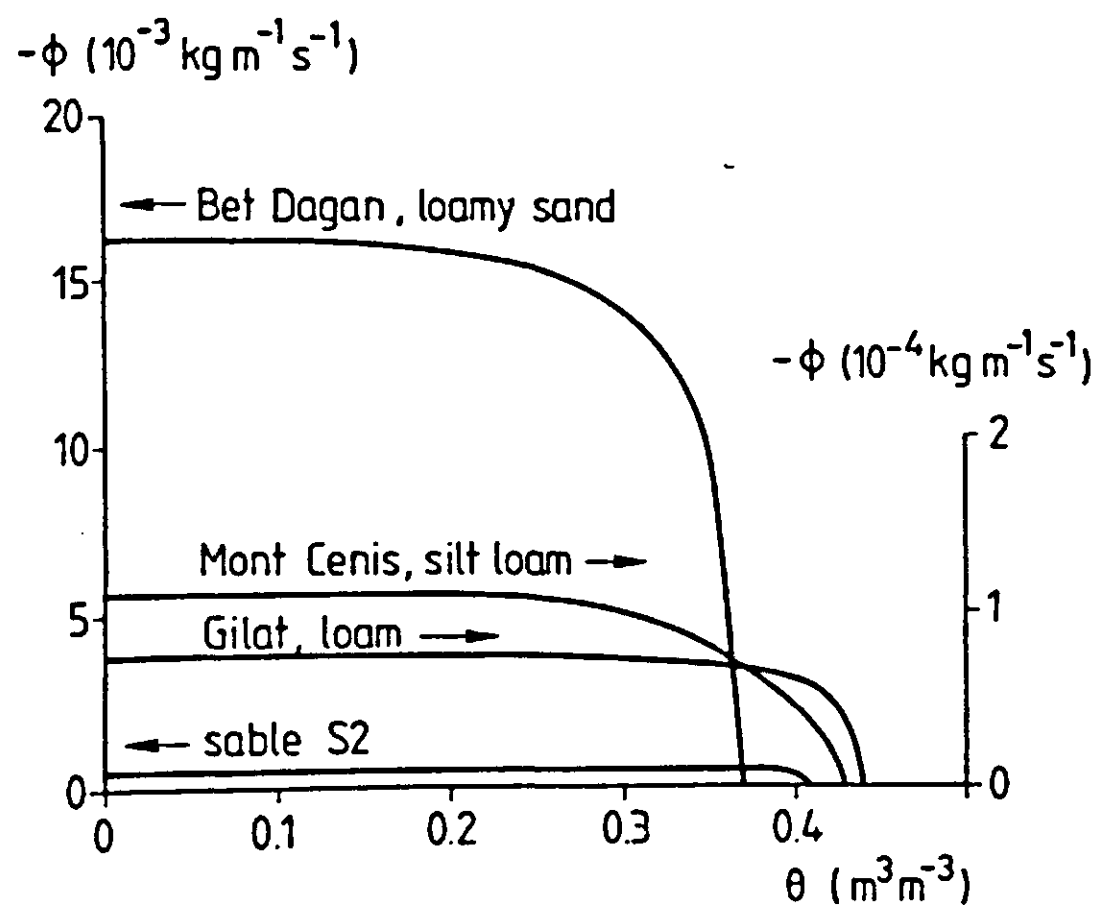


Figure 6.11 Matric flux potential as a function of moisture content for some example soils.

Drying of topsoil, under a given evaporative demand, depends to a large extent on the 'ability' of the soil to supply water to the evaporating surface, a property that can be expressed by the parameters A and B, mentioned above. A problem that presents itself in the free drainage case, however, is the choice of a reference level in the determination of these parameters. In Chapter 3 and in the previous section, A and B were taken to relate to saturation as a starting point of the $\Phi(\theta)$ curve. To render such variables useful in the description of the drying phenomenon in the absence of a water table, it seems more appropriate to use the 'field capacity' concept in a definition of a reference level. This becomes clear when it is realized, for example, that the extremely high A-values, found for some sandy soils (Table 3.8), may be due to high K-values pertaining only to the θ -range close to saturation. If these high water contents are maintained only during a brief period upon wetting, - that is when moisture content at field capacity lies below this range, - then that section of the $\Phi(\theta)$ curve that corresponds to this high degree of saturation plays no role in the surface drying process. In other words, in studying the effects of A and B by sensitivity analysis, it is inconvenient to take into account a gravity term that should be amended simultaneously with changes in A or B. So the problem comes down to defining a suitable moisture content θ_{ref} where gravity can be neglected. This moisture content then serves as a reference to the values A' and B', thus replacing θ_s in the definition of the independent variable x in equation 6.8. The quotes in A' and B' serve to indicate this change in reference level.

The reference moisture content could be designated as 'field capacity', following one of the accepted definitions. For example, the definition of field capacity may be based on a soil water pressure criterion. Alternatively, some threshold value of hydraulic conductivity might be employed. Unfortunately, for neither one of these criteria, the corresponding moisture content can be derived from the matric flux potential curve $\Phi(\theta)$ (nor from A and B, consequently). Whereas soil liquid transport is uniquely described by the gradient of Φ - i.e. any combination of $K(\theta)$ and $p(\theta)$ resulting in a certain $\Phi(\theta)$ gives identical θ -z-t developments when employed with certain boundary conditions - the $\Phi(\theta)$ characteristic cannot be used, reversely, to derive either of the basic characteristics $K(\theta)$ or $p(\theta)$, without a priori knowledge of one of these. In searching a suitable definition of θ_{ref} , therefore, it is useful to go back to the original $K(\theta)$ and $p(\theta)$ data as given in Table 3.8.

Three criteria for field capacity have been inspected for the soils listed in Table 3.8: (1) $p = -5 \text{ kPa}$, (2) $k = 0.1 \text{ mm/d}$, and (3) $k = 1 \text{ mm/d}$. Based on the first criterion, A' showed a fairly pronounced relation with θ_{ref} itself, which is inconvenient as it introduces a bias when studying the sensitivity of the system to A' . Criteria (2) and (3) provide a better physical basis for a definition of θ_{ref} . The higher k -value of the two (1 mm/d) was preferred here to the lower one, because it allows for a larger number of datapoints to be used in curve fitting (to determine A' and B' via an optimisation procedure). It may be argued that a critical value of 1 mm/d for k is high in the present context. For most of the soils listed, however, this value corresponds to soil water suctions ranging between 10 and 25 kPa (incidentally $5\text{-}10 \text{ kPa}$) which is not too different from the $1/10 - 1/3 \text{ bar}$, used frequently as a rule of thumb to estimate field capacity. Systematic relationships between θ_{ref} , based on criterion (3), and A' or B' were not found, in contrast to the suction case (1) mentioned above. In the following analysis, therefore, field capacity will be defined as the volumetric water content that corresponds to a hydraulic conductivity of 1 mm/d .

The values found for A' range between $0.5 \cdot 10^{-5}$ and $3.0 \cdot 10^{-5} \text{ kg m}^{-1} \text{ s}^{-1}$; as compared to the A -values listed in Table 3.8, this implies a strong decrease of the absolute value, obviously, and also of the variation in this parameter. The constant B' varies between 0.05 and 0.5 for the different soils, which is somewhat higher than the range for B indicated in the aforementioned table.

Using these extremes for A' and B' in different combinations, four simulation runs with the complete SALSA model were made for a one week period, starting from an initial moisture content of 0.30 over the whole profile in all cases. The remaining conditions and system parameters were chosen as mentioned in section 5.3. Small steps were used in discretizing the soil, to allow for relatively accurate profile description; from the top downward, compartments of $3*2, 3*3, 3*4, 3*5 \text{ mm}$ were used for the upper layers, respectively. The effects of A' and B' on the development of the dry surface layer are discussed below. The Figures 6.12 and 6.13 show the courses of latent heat flux and surface temperature, respectively, in order to characterize the specific situations elaborated upon in the following.

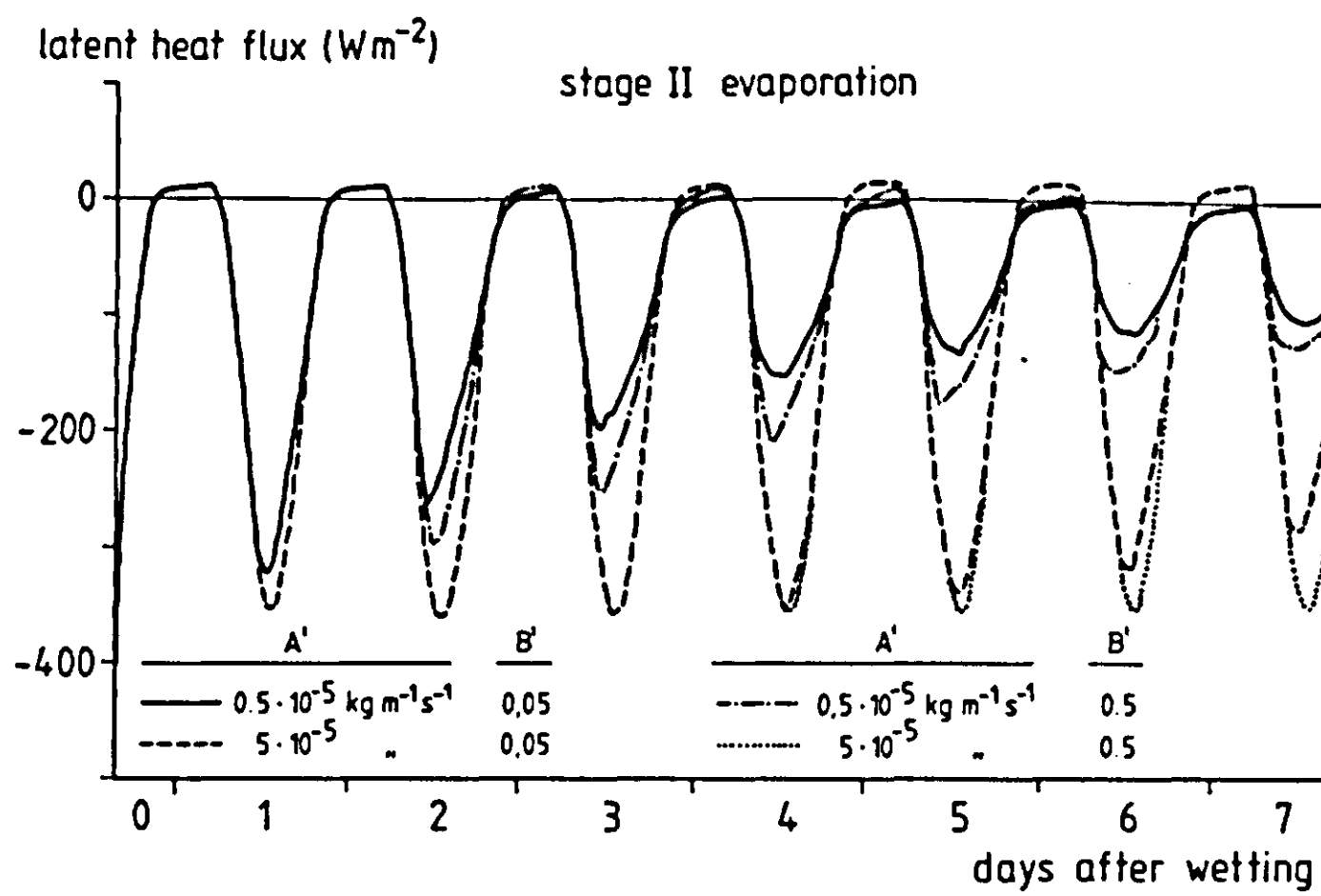


Figure 6.12 Latent heat flux, simulated for a one week drying sequence, for different combinations of soil hydraulic parameters A' and B'.

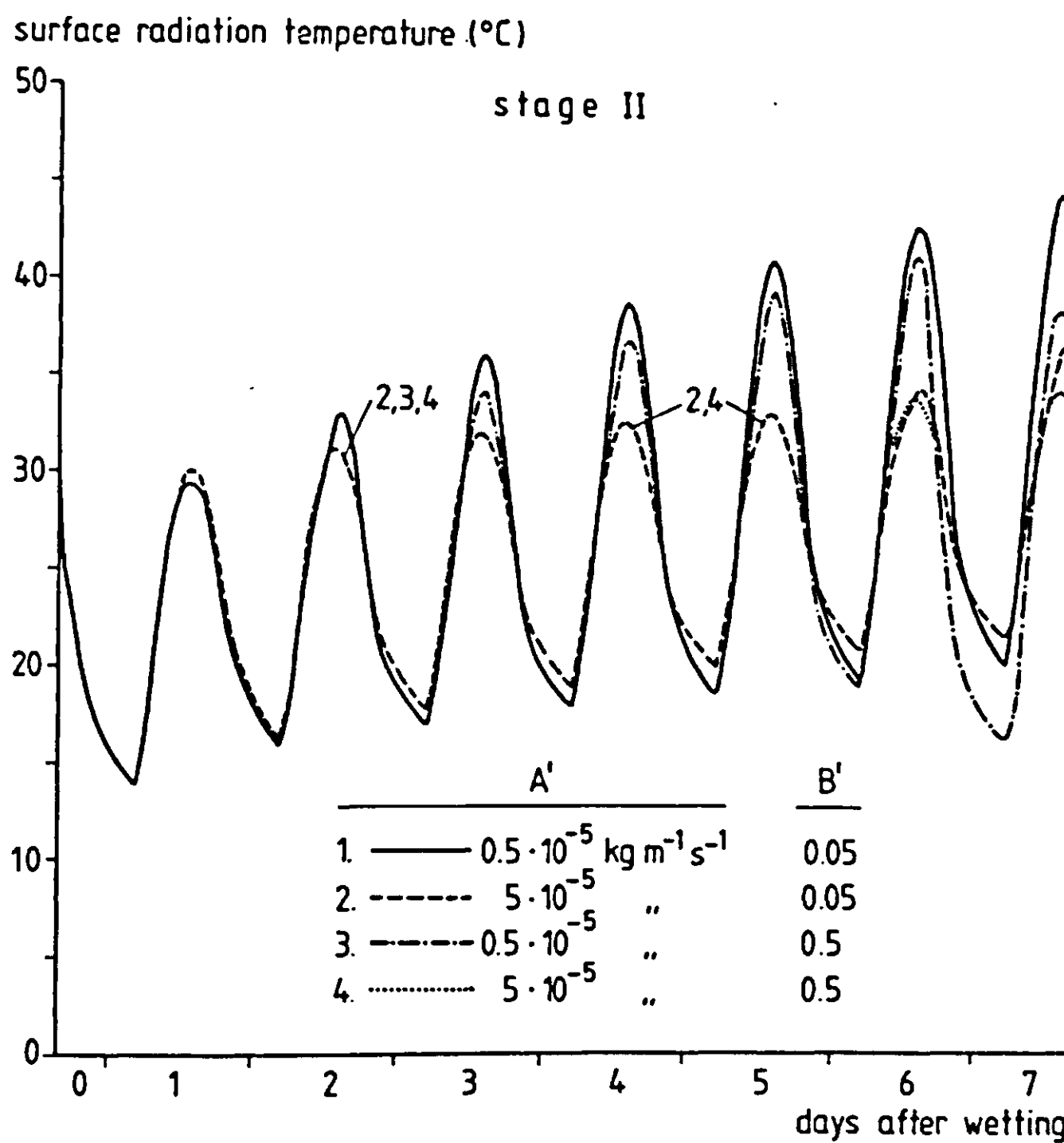


Figure 6.13 Surface temperature, simulated for a one week drying sequence, for different combinations of soil hydraulic parameters A' and B'.

The main questions to be discussed here are: (1) how pronounced is the developing drying front as a function of A' and B' , and (2) to what extent do these parameters affect the rate of arising and growth of the dry surface layer. The drying front phenomenon was studied earlier by e.g. Van Keulen and Hillel (1974). These authors based their analysis on the shape of the water diffusivity curve. Also Menenti (1984) discussed the drying front phenomenon and included a theoretical analysis of preferential evaporation sites within a pore system. The present analysis will focus only on the role of the two macroscopic parameters A' and B' . It may be recalled that vapour diffusivity within the soil is considered to be independent of moisture content; Adoption of supposed relations between vapour diffusivity and moisture content, as found in literature, would obscure the issue, while no general concensus has been achieved on this topic (Chapter 3).

Definition and shape of the front

Various thresholds can be used to define the drying front. In the context of the scheme followed in the previous section, which recognises three distinct stages of drying, a suitable definition seems to be the depth at which the vapour flux equals a certain fraction of the surface vapour flux. By locating the depths corresponding to different values of this fraction, a qualitative measure of the existence of such a drying front becomes available. An example is given in Figure 6.14, which refers to the soils with $A'=0.5 \cdot 10^{-5}$ (both) and $B'=0.05$ and 0.5 , respectively. It can be concluded that (1) during each day, the 'evaporation zone' moves downward over a considerable distance, (2) the 'evaporation zone' is rather diffuse, and (3) as B' increases, the 'front' becomes less pronounced. With reference to the sensitivity analysis of the simplified model (section 6.3) it can now be mentioned that these three effects tend to decrease the impact of dry layer thickness on the output variables. So in reality, sensitivity to dry layer thickness (to be defined for a fixed time of the day) will be less than in the idealized stage III case. The moisture content profiles, as developed after one week of drying, are shown in Figure 6.15. It can be observed from this picture that a lower B' value creates a more pronounced drying front, also in terms of the θ -z profile. An interesting feature is the relation with surface temperature. Comparison with Figure 6.13 makes clear that the soil, characterised by the lowest A' and B' values, reaches the highest surface temperatures during daytime. It is the most effective in preserving

soil moisture and hence shows the highest moisture content below the dry top layer. Generally it is assumed that the warmer spots on daytime thermal imagery indicate low soil moisture contents. The results shown here indicate that the reverse may be true, at least in cases where soils with different A' and B' values are present.

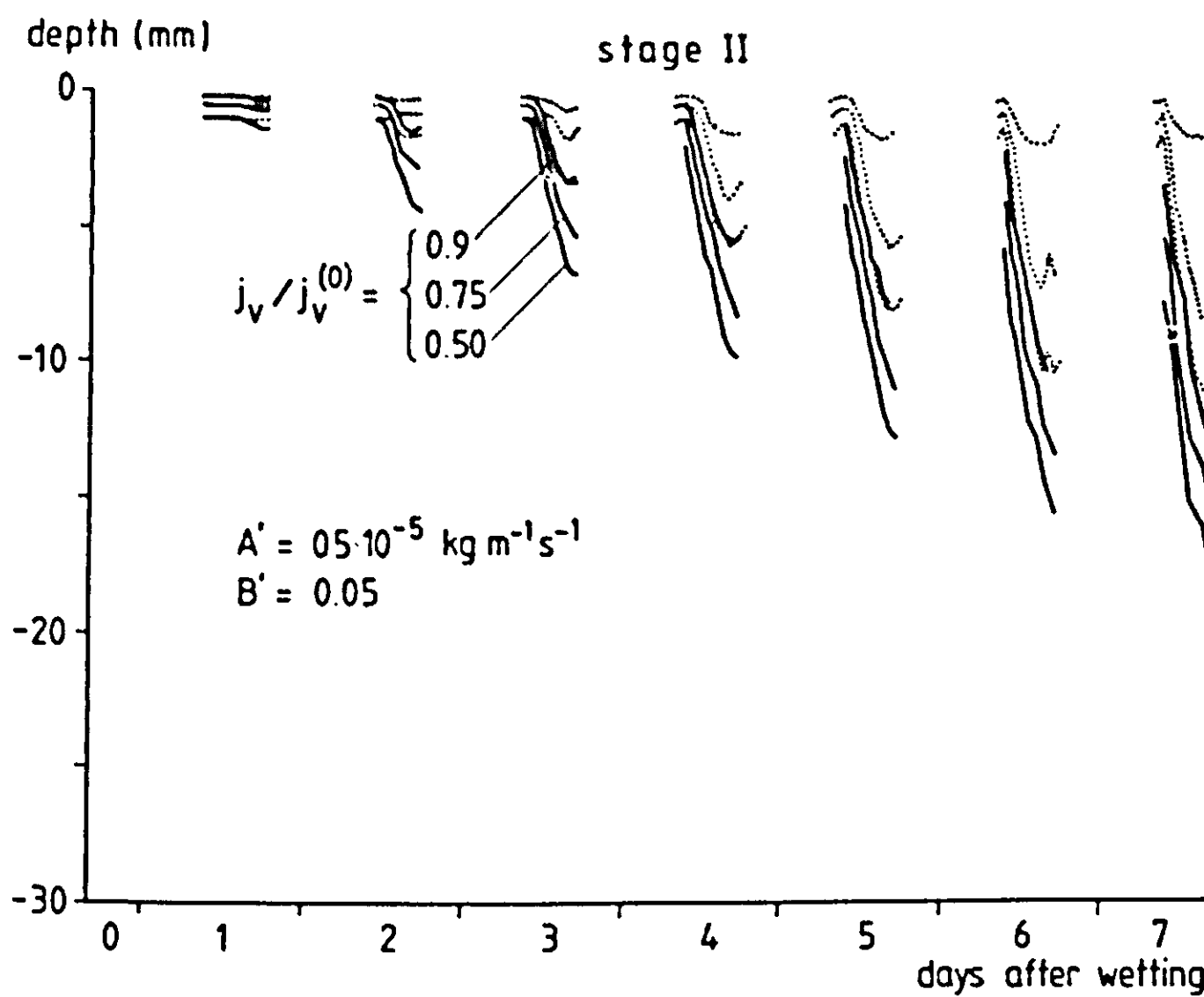


Figure 6.14 Depth at which the vapour flux equals chosen fractions of the surface vapour flux; depicted are the courses of only two of the soils mentioned in Figures 6.12 and 6.13. (The remaining two soils - with $A' = 5 \cdot 10^{-5} \text{ kg m}^{-1} \text{s}^{-1}$ - hardly developed a dry surface layer). Only daytime data, 09.00-17.00 h are plotted.

Other criteria that could be used to define a drying front are the site of maximum vapour flux divergence, or the site of maximum liquid flux convergence. Also, the zero flux plane for soil water vapour may serve as a valid criterion; below this plane, vapour moves downward during daytime, whereas it moves towards the surface from this depth upward (it is assumed that molecular diffusion is the governing transport process for soil water vapour). For the soil with $A'=0.5 \cdot 10^{-5}$ and $B'=0.05$, the development of the drying front as based on the three criteria mentioned, is plotted in Figure 6.16. (Only daytime data -09.00-17.00- were used since for evening, nighttime and early morning conditions, the concept of drying front loses significance). It appears that as soon as surface drying has commenced, the three thresholds do not yield very different courses of the drying front.

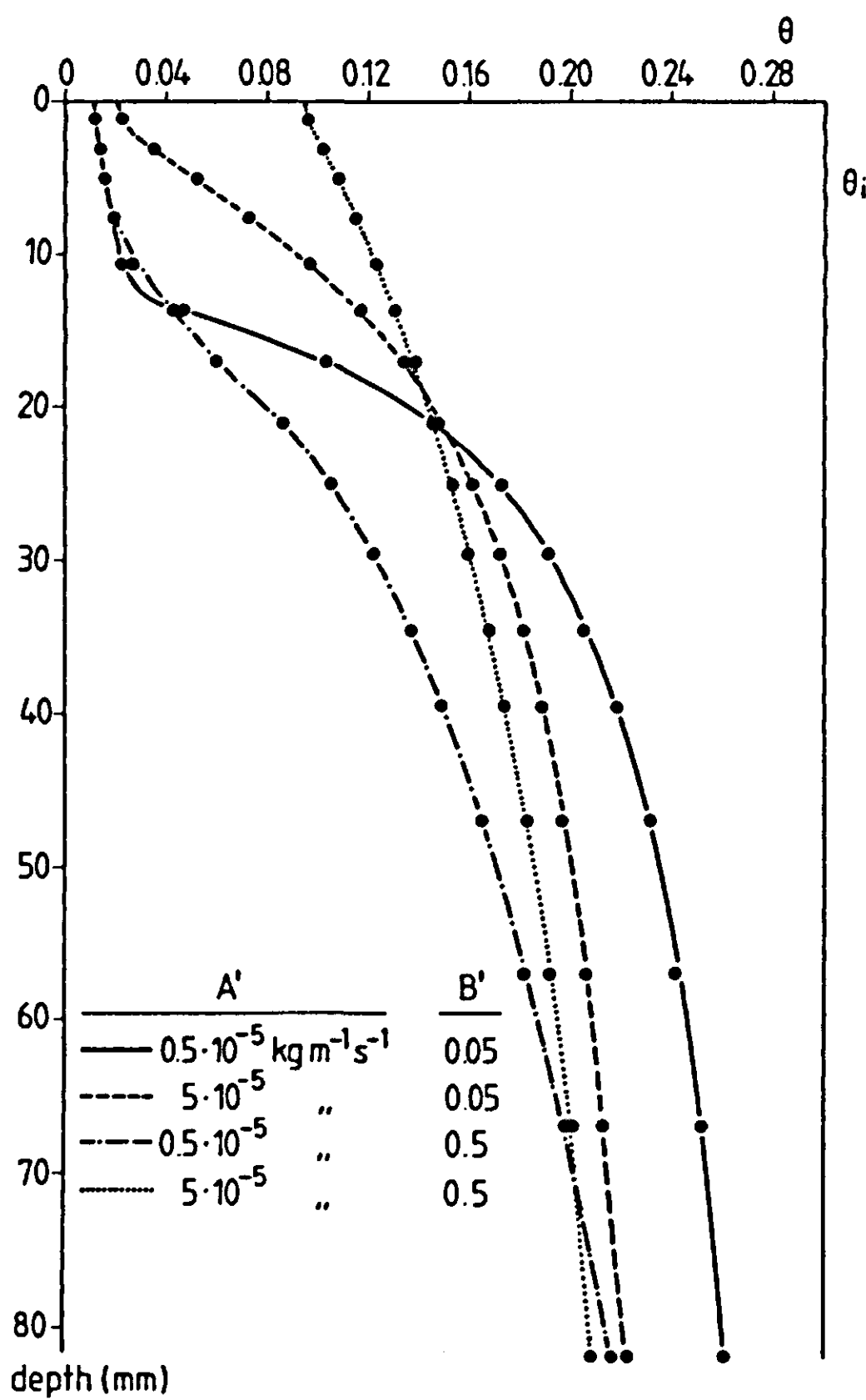


Figure 6.15 Moisture content profiles after one week of drying, for different combinations of soil hydraulic parameters A' and B'.

For higher B'-values, the differences in depth, resulting from the use of different definitions, are somewhat larger. The deviant behaviour of the zero flux plane in the beginning of the drying sequence, observed from Figure 6.16, is explained by the behaviour of temperature; surface temperature in that particular period is relatively low due to evaporative cooling, which implies that the maximum vapour density is found somewhat below the surface. Of the various criteria mentioned, the site of maximum liquid flux convergence will be employed as an indicator of front depth in the following, since this criterion is the most meaningful in relation to the sensitivity analysis described in section 6.3.

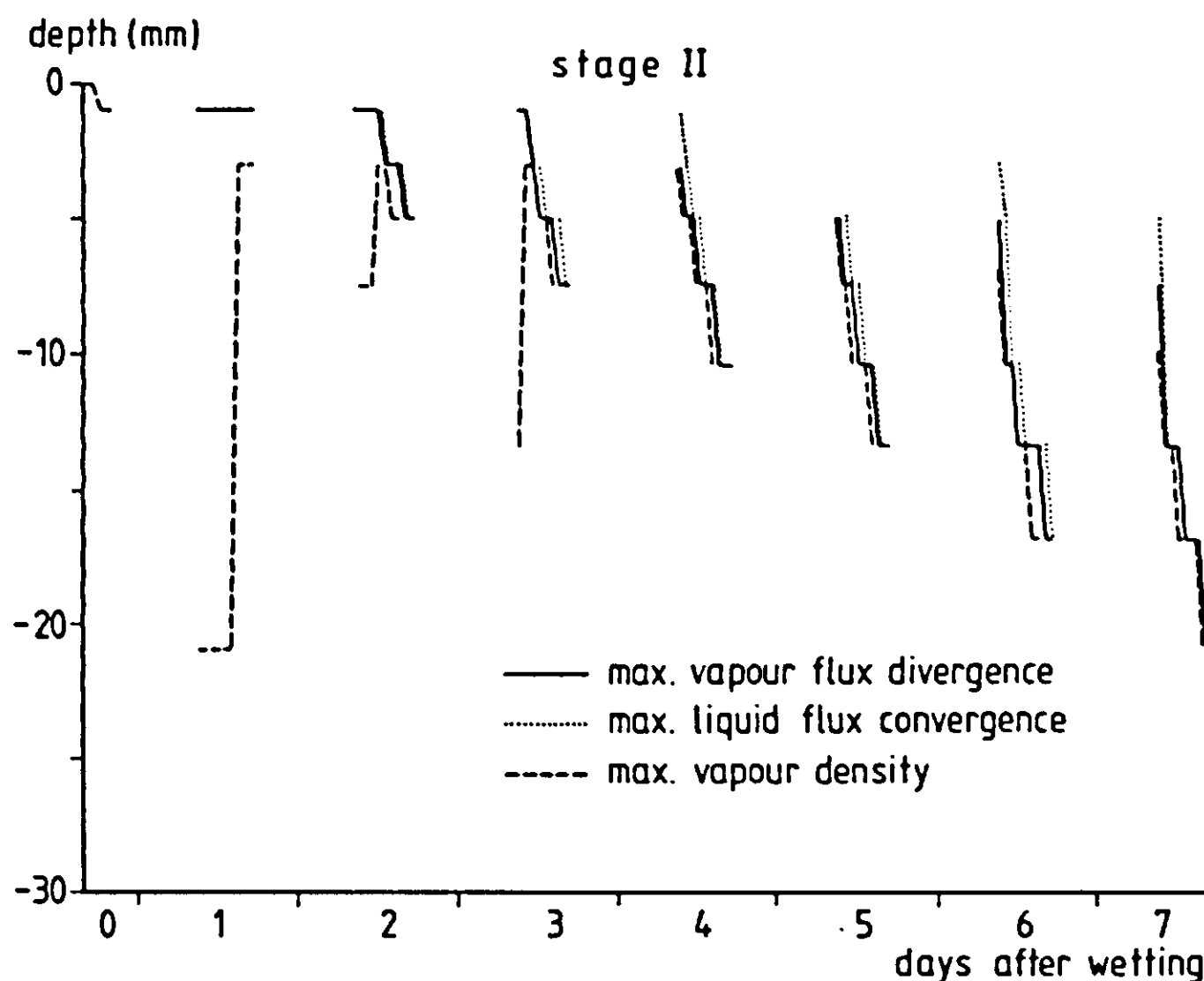


Figure 6.16 Development of the drying front as defined by various criteria. From the soils used in the previous figures, the fastest drying soil ($A' = 0.5 \cdot 10^{-5} \text{ kg m}^{-1} \text{ s}^{-1}$, $B' = 0.05$) was selected for this example.

Effect of A' and B' on dry layer growth and relative evaporation

Defining now the soil layer above the plane of maximum liquid flux convergence as the dry surface layer, the influence of the hydraulic parameters A' and B' on the growth of this layer can be examined. The role of the parameter A' is illustrated by Figure 6.17, showing an increase in drying rate as A' decreases. For this series of runs, B' was maintained at a constant value (0.05). The effect of variations in B' at constant A' ($0.3 \cdot 10^{-5} \text{ kg m}^{-1} \text{ s}^{-1}$) can be read from Figure 6.18. Clearly, A' is the more important parameter in the surface drying process as defined here. Alternatively, surface drying may be expressed in terms of relative evaporation E/E_0 . The 'potential evaporation' E_0 in this case is defined as the simulated evaporation for the particular soil, which supplies enough water to the surface to maintain a steady daily total evaporation in the course of time (Figure 6.12). This applies to the soil with the highest A' and B' values in the present example. The courses of relative evaporation as dependent on A' and B' are depicted in the Figures 6.19 and 6.20, respectively. Also from these results, it is concluded that A' is the parameter of primary importance. In view of the relative ease at which A' can be obtained by laboratory measurements, it is felt that this parameter deserves due attention. Its relevance

to dry farming practices may be clear from the above pictures. Further study seems required to arrive at more general formulations of topsoil drying as a function of A' , B' and θ_{ref} .

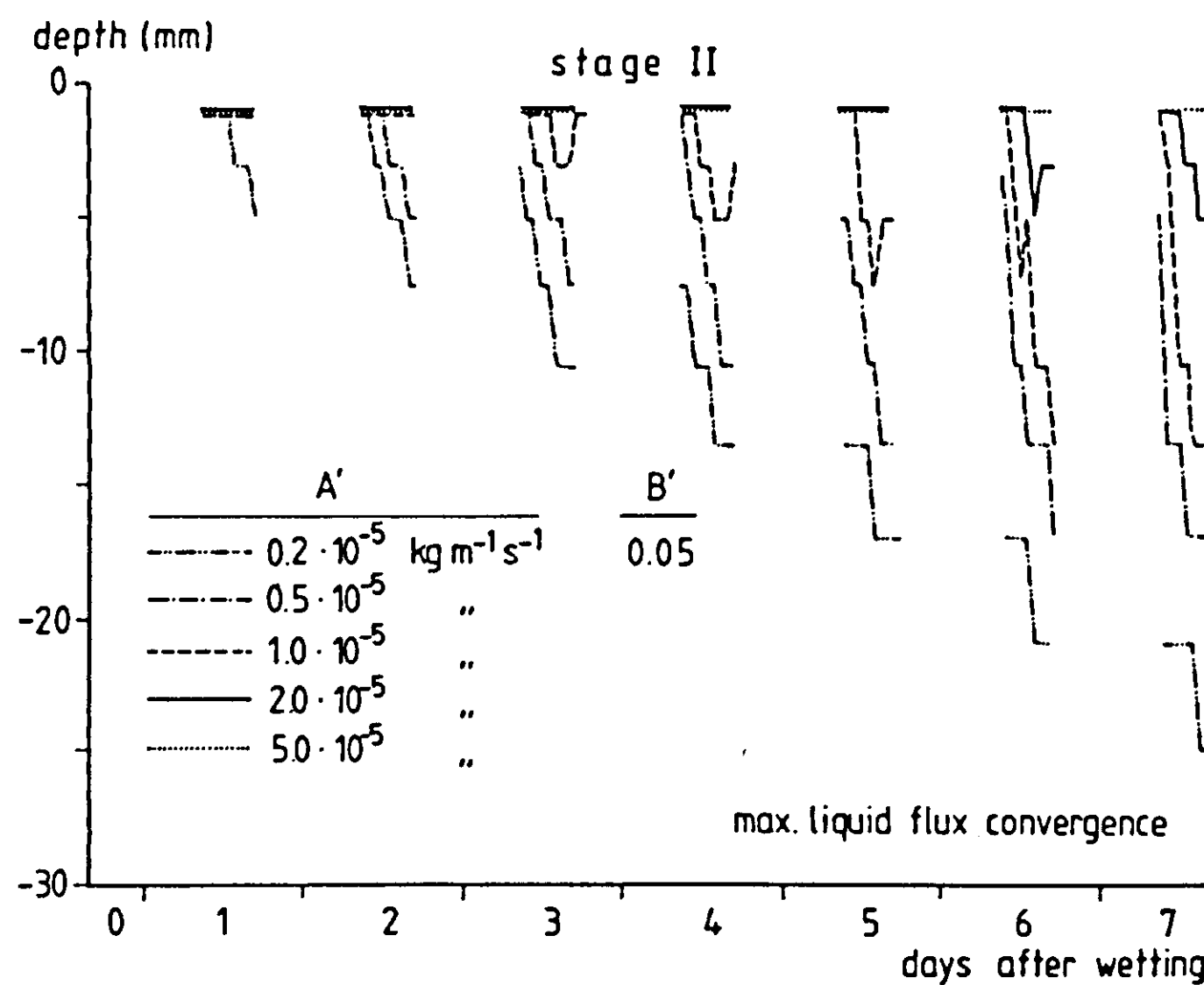


Figure 6.17 Development of the drying front for different A' -values at constant B' .

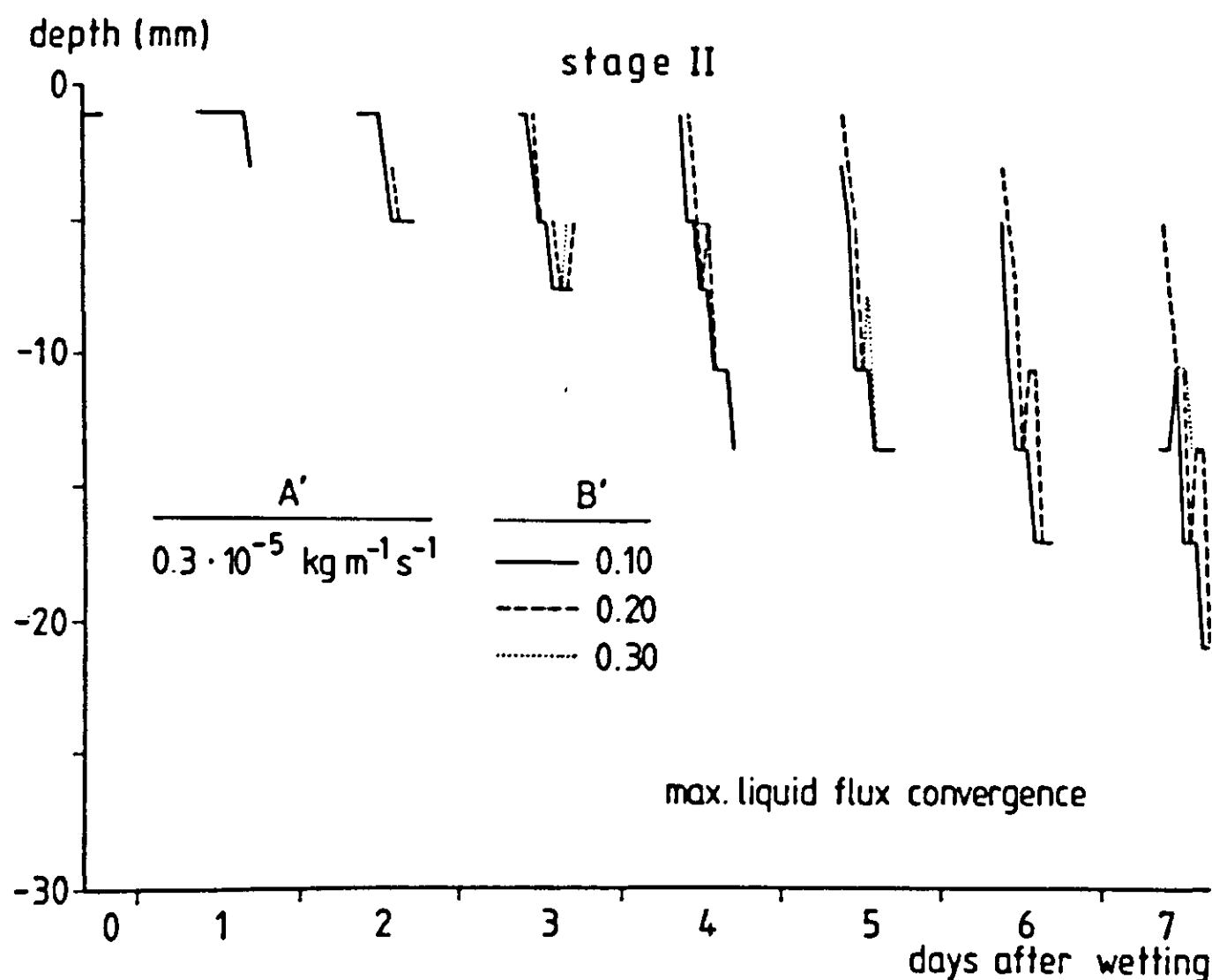


Figure 6.18 Development of the drying front for different B' -values at constant A' .

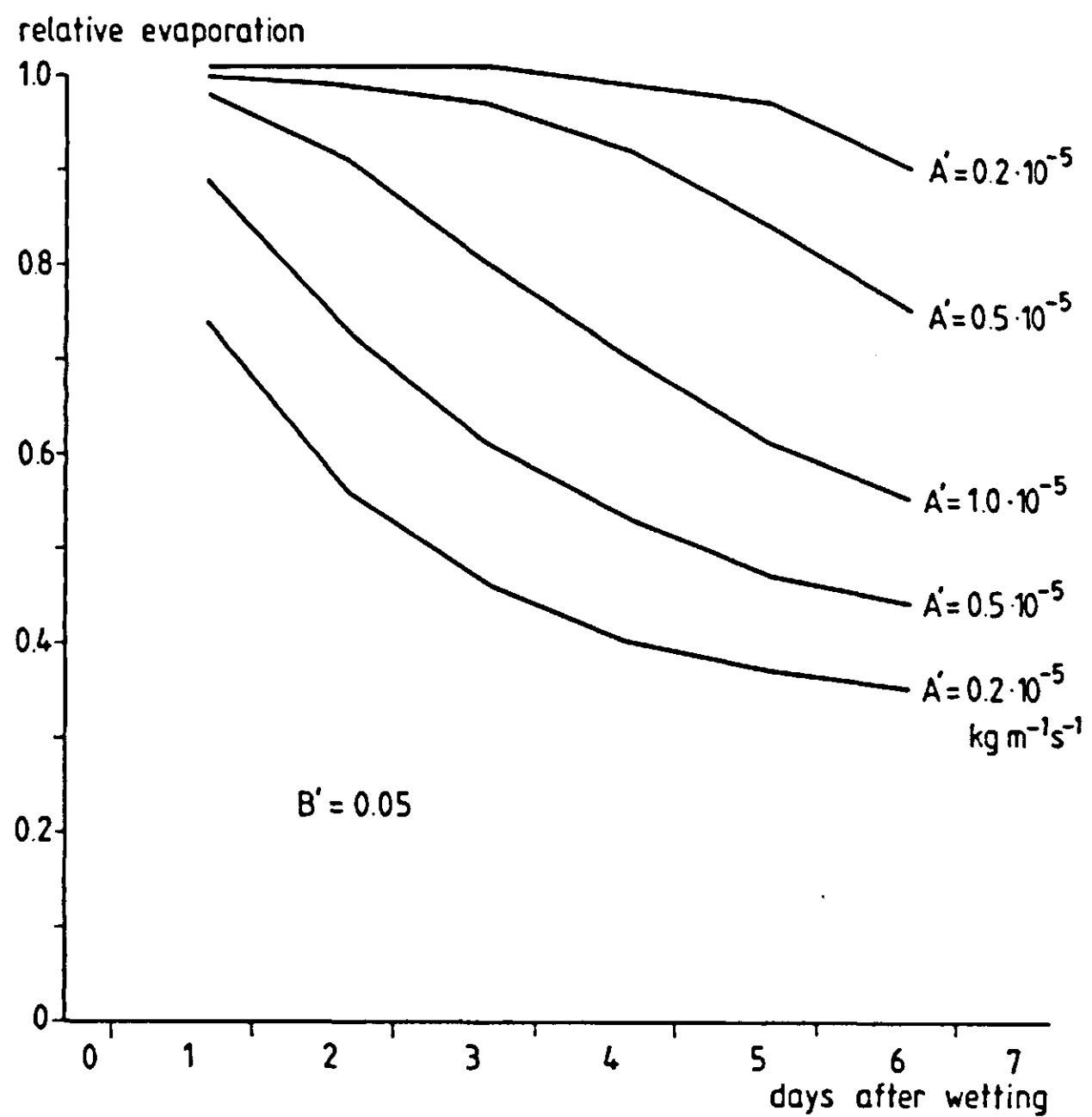
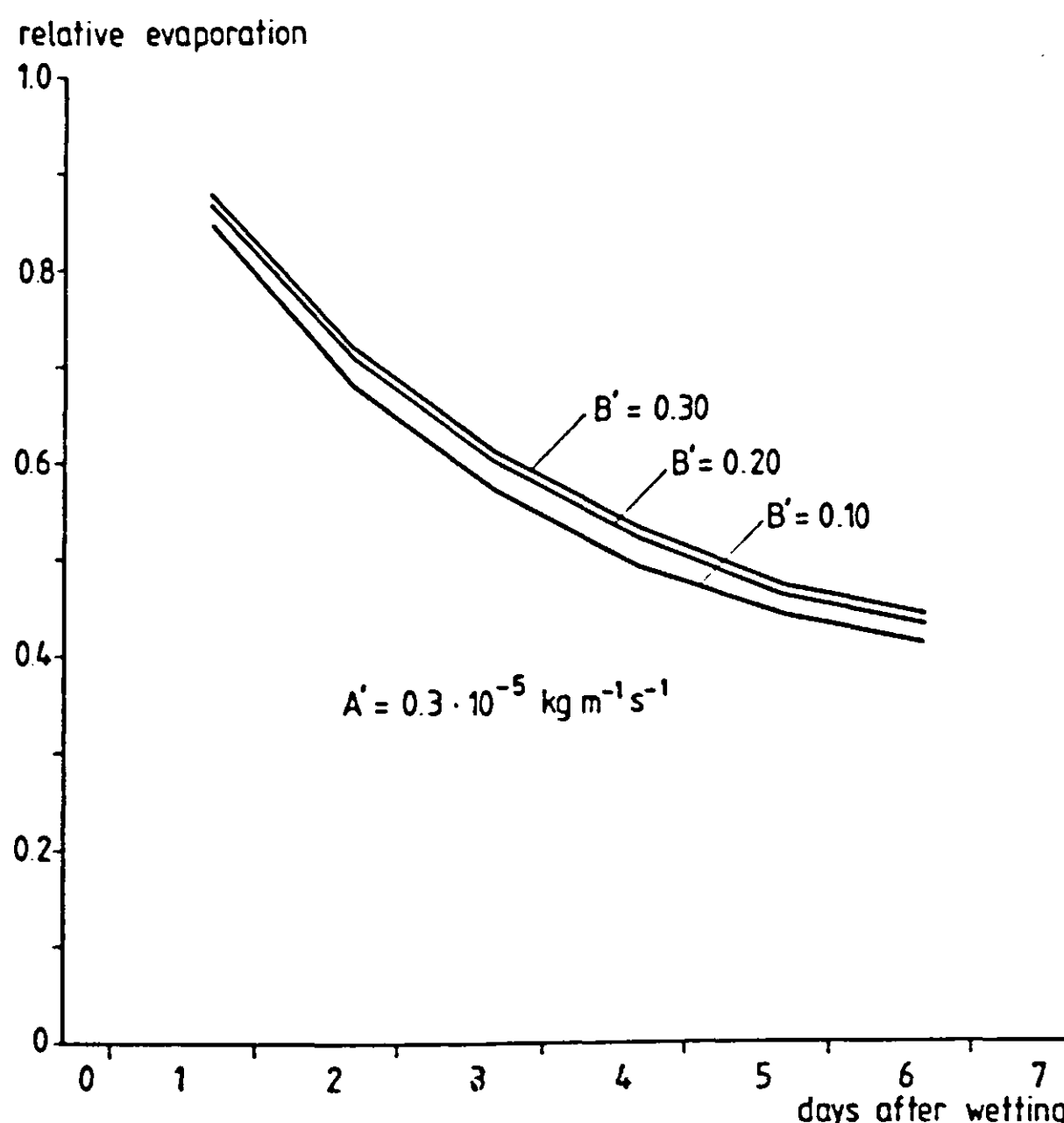


Figure 6.19 Daily evaporation relative to potential evaporation during a one week drying sequence, for various A' -values.

Figure 6.20 Daily evaporation relative to potential evaporation during a one week drying sequence, for various B' -values.



Nocturnal vapour condensation

In the sensitivity analysis for drying stage III, interaction between water vapour and dry soil was omitted. It was shown in the above section that, during stage II, rewetting of the dry toplayer occurs at night, and that this process tends to decrease sensitivity of output variables - e.g. surface temperature - to the thickness of the dry toplayer during daytime. Part of this redistribution of moisture is due to vapour movement. In view of the stage III analysis, it may be questioned how realistic the assumption of an inert toplayer is with respect to thermal behaviour at night.

The fast-drying soil, for which Figures 6.14 and 6.16 have shown some daytime developments, is used here as an example to illustrate the nighttime process of interest. Figure 6.21 gives an impression of the energy fluxes involved as drying proceeds. Net radiation (about -70 Wm^{-2}) appears to be countered for 60-70% by the conduction soil heat flux at $z=0$. (The remainder is covered by downward transport of sensible and/or latent heat from the atmosphere). This conduction term supplies heat from the uppermost soil compartment (2 mm) to the radiating surface. It is interesting to follow now the heat fluxes at some depth below the surface. To this purpose, a depth of 9 mm was chosen; this lies well within the range over which the drying front passes during development. The conduction flux and net latent heat flux, both at 9 mm, are depicted in Figure 6.21 as well. Net latent heat flux is defined here as the total amount of heat evolved from condensation in the 0-9 mm layer per unit of time and surface, i.e. the latent heat flux at $z = 9 \text{ mm}$ minus its value at the surface. It can be observed that cooling of the 0-9 mm layer, i.e. divergence of the total soil heat flux, plays no significant role during the major part of the night, the sum of the two terms at 9 mm almost equalling the surface conduction flux. The distribution over the two terms at 9 mm, however, changes drastically as the toplayer dries out. During the first four nights, conduction is the governing heat supply mechanism. In the nights following, conduction becomes less dominant (λ decreases) and the contribution of distillation increases. The course of early evening net latent heat flux shows an increase during the drying sequence: in the first half of the week, net evaporation from the 0-9 mm layer remains positive for a few hours after R_n has become negative; this is compensated for by positive (upward) conduction at the base of this layer. In the second half of the week, net condensation starts already one hour after R_n has turned negative. This sudden change can be explained on the basis of soil

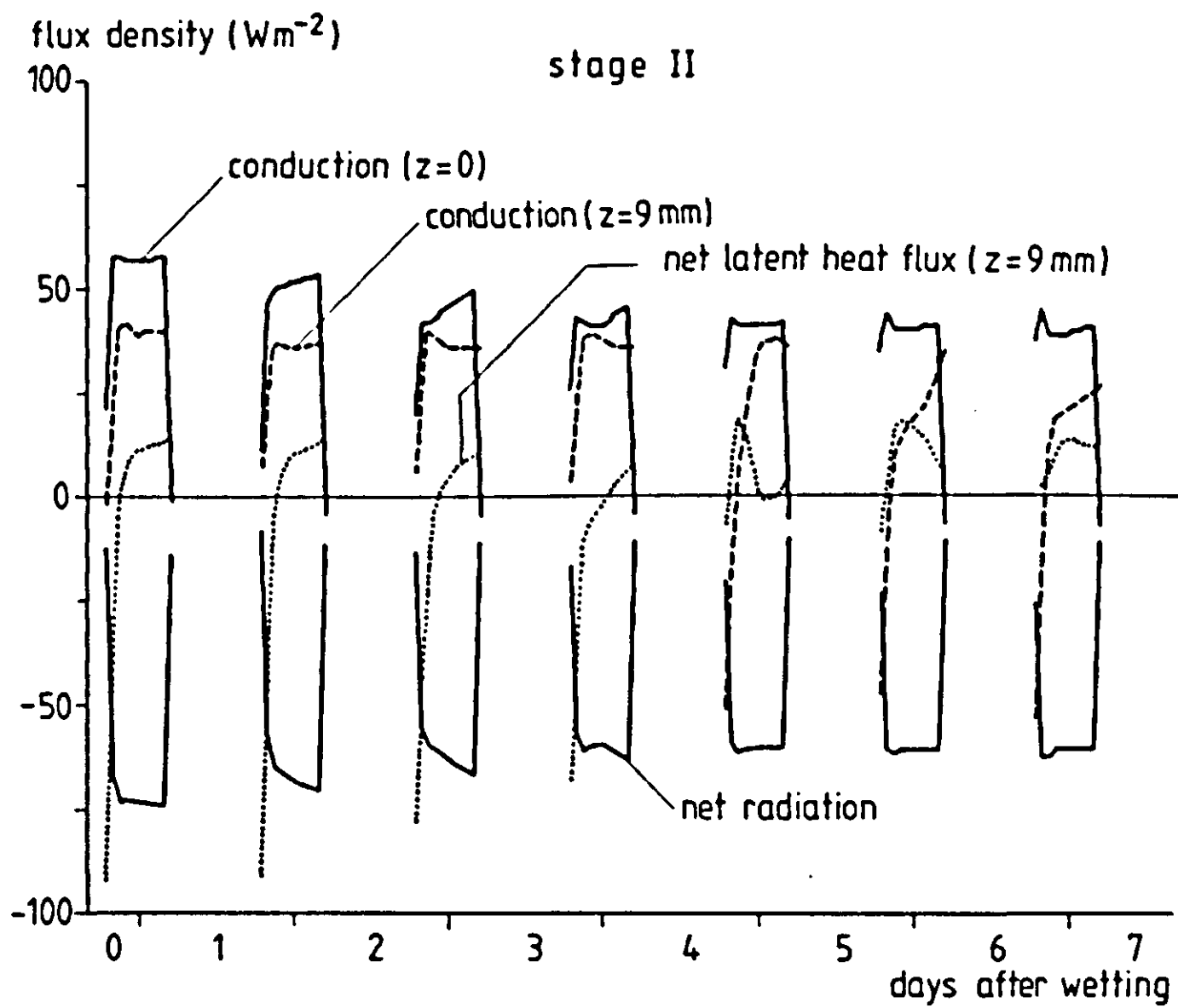


Figure 6.21 Energy fluxes in the top 9 mm of soil during drying; $A' = 0.5 \times 10^{-5} \text{ kg m}^{-1}\text{s}^{-1}$ and $B' = 0.05$. Only the time intervals where $R_n < 0$ are shown.

relative humidity, which drops below 100% during the afternoon. The role of relative humidity becomes apparent in the fifth and following nights, where distillation delivers enough heat for the conduction term at 9 mm to be negative during the evening hours; this could not be explained if vapour diffusion were governed by the temperature gradient only. The decrease of the net latent heat flux after some hours is associated with relative humidity approaching the value of 100%; this happens in short time (steep decrease in fifth night) as long as only a thin soil layer has dried out to low relative humidity values. For the example shown here, it can be concluded that condensation in the top layer makes up for up to 25% of net radiation, and for up to 40% of the conduction term at $z=0$, that is, of the total heat supply by the soil to the surface. Such a contribution is not negligible, and in view of the sensitivity study discussed in section 6.3 it can be stated that sensitivity of output variables to the thermal soil properties - at night - will be somewhat less, in reality, than was indicated in that section.

6.5. Comments on the relation T_s -LE

The effect of changes in system parameters on the course of various output variables has been demonstrated for the idealized drying stages I and III. As mentioned, a complete factorial design was used in combination with analysis of variance to identify the respective effects. The same data will now be submitted to an analysis of covariance in order to determine the relation between two output variables, and to identify the amount of 'noise' in this relation ascribed to the distinguished system parameters. The variables of interest to thermal remote sensing at present are the surface temperature T_s and the latent heat flux LE. Analysis of covariance is based on a linear regression between two variables, resulting in an expression of the dependent variable as a linear combination, e.g.:

$$(6.9) \quad (abc) = M + \beta(X-\bar{X}) + \frac{1}{2}(A+B+C-D-E-F)$$

for the example where factors a, b and c are present and d, e, and f absent; β is the regression coefficient, and the capitals are the main effects of the independent variables (system parameters) corrected for the covariate. In the case inspected here, T_s is the dependent and LE is used as the covariate. As the relation between these two variables is mainly of interest during daytime, only the data for the 08.00-20.00 h. period are given. Figure 6.22 shows the results for the stage III case. Clearly, albedo is the strongest source of noise in the T_s -LE relationship, the main effect ranging between -2 and -8 K. Roughness length and dry layer thickness show effects, comparable in absolute magnitude but of opposite sign, as expected. Vapour diffusivity and thermal inertia, the latter of both topsoil and subsoil, appear to have a minor influence on surface temperature, when LE is included as the covariate. The same analysis on the simulated stage I data yielded small effects for albedo, thermal inertia and emissivity (± 1.2 , -1.0 to +1.5, and -0.15 to +0.10 K, respectively). Roughness length, on the other hand, showed an effect of approximately the same magnitude as found for the stage III data, ranging from -4 to +1.5 K for an increase of this parameter over the range indicated in section 6.3. Interpretation of deviations in surface temperature - derived from thermal imagery - in terms of deviations in evaporation rate appears to be dangerous, as may be deduced from Figure 6.22. With the reported regression coefficients, and knowledge of the main

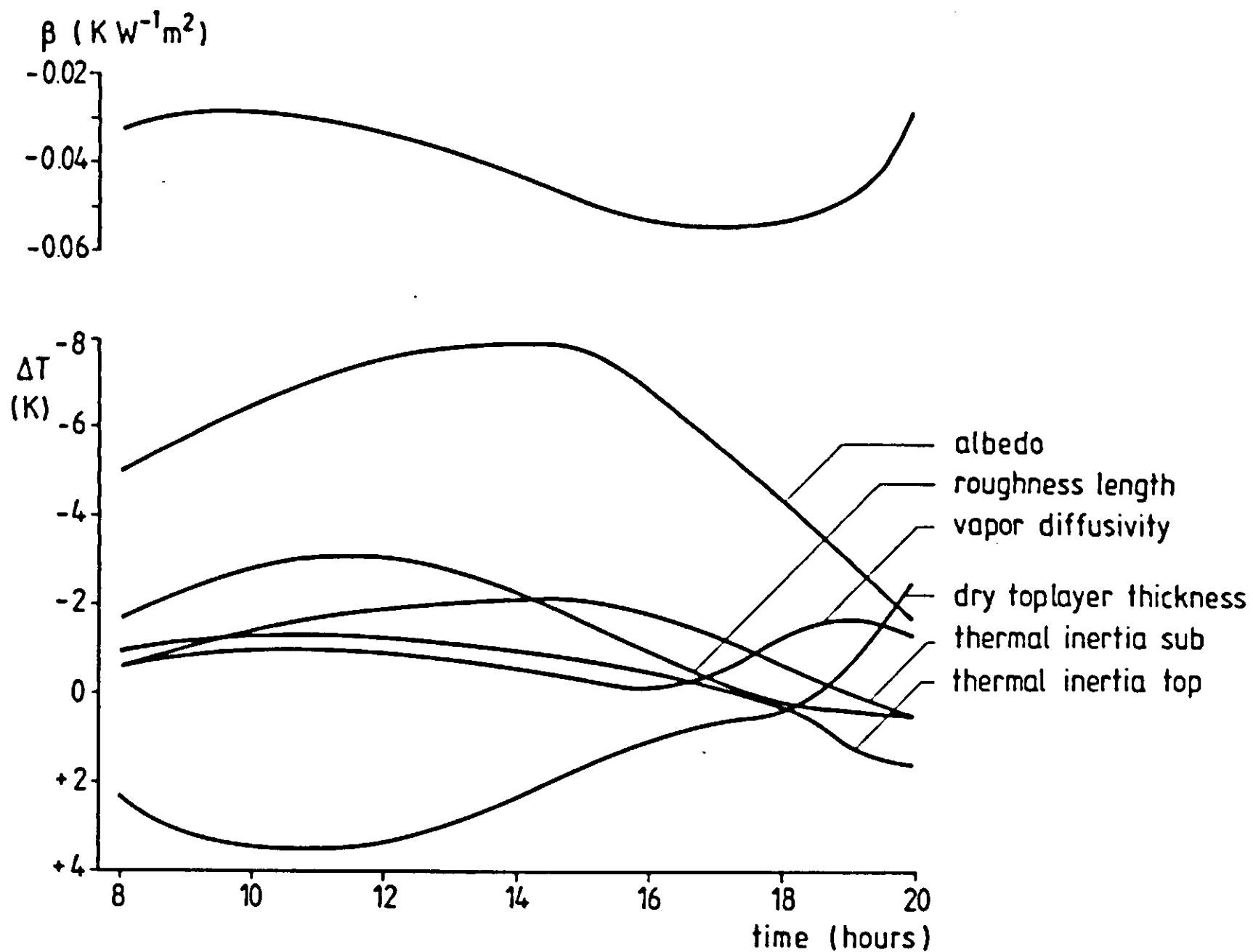


Figure 6.22 Main effects of various system parameters on surface temperature in stage III, corrected for covariate LE; indicated is also the course of the regression coefficient β between surface temperature and latent heat flux.

parameter effects, it can be shown that a 1 K deviation from the mean surface temperature, interpreted as being caused by a difference in evaporation rate, results in a value of $30-40 W m^{-2}$ for this estimated deviation in evaporation rate from its mean. (This corresponds to approximately $0.05 mm h^{-1}$). Whereas variations of several K can apparently be ascribed to variations in system parameters over the indicated ranges (6.3) without being associated with differences in evaporation rate, considerable errors can be expected in the estimates of LE derived from observed surface temperature.

CHAPTER 7. THERMAL REMOTE SENSING: STATE OF THE ART AND PERSPECTIVES FOR BARE SOILS.

Over the last decade, remotely sensed thermal data have been collected for investigations of different nature. In the process of imagery interpretation, various case-specific assumptions, which limit the applicability of the derived interpretation technique, have to be made. In the field of geological mapping, for example, thermal properties of dry rock materials have been assessed successfully from diurnal temperature amplitudes in order to delineate lithological boundaries (e.g. Abrams et al. 1984). The thermal inertia approach, followed in such applications, is based on the relation between soil heat flux and surface temperature amplitude, and has been shown to be conceptually sound under specific circumstances, where evaporation can be neglected (e.g. Tosi, 1983). In other cases the validity of this approach is questionable.

A completely different analysis is required when thermal imagery of (partially) vegetated surfaces is to be interpreted in terms of hydrological or crop physiological variables, i.e. evapotranspiration rate or drought stress, respectively (Nieuwenhuis, 1985; Jackson, 1977) Hatfield et al, 1983). Under the conditions of interest in that particular case, the soil heat flux plays only a minor role and is often considered negligible as compared to the latent heat flux, in contrast to the previous case.

Thermal infrared remote sensing has also been applied extensively to bare soil surfaces, where in general neither the soil heat flux nor the latent heat flux should be considered as dominant beforehand. This is precisely the situation of interest in the present case. The demand for regional hydrological information on bare soil surface may be illustrated by the recent work of Ward et al (1982), Moore et al (1983) and England et al (1983), on rainfall and soil moisture monitoring for the Sahel area, and by the investigations on water losses from aquifers in Northern Africa by Menenti (1984). These authors based their analyses on thermal imagery obtained by remote sensing, which is recognized to be indispensable to the estimation of surface variables on a regional scale. As shown in the previous chapter, a variety of processes affect the course of bare soil surface temperature, and drastic simplifications must be made in order to enable the quantitative interpretation of such a course. It is felt that within the context of remote sensing, the typical use of deterministic models, such as

the one presented in this report, should focus on the validation of these simplifying assumptions. In the present report, this has not yet been done exhaustively, and much work remains to be done in that respect. It is the author's opinion that if products derived from remotely sensed data are presented as quantitative information, they should always be accompanied by realistic estimates of expected errors, particularly when these are large. In practice, this is usually not the case. The ensuing scepticism from the side of workers in applied field physics cannot be expected to foster a positive attitude towards remote sensing from this group of potential users. Aside from this, of course, it is recognized that remotely data have great importance anyway in a qualitative sense, allowing the assessment of patterns and boundaries that could not be located by other means.

In the light of the results of the experiments, simulations and sensitivity analyses discussed in the previous chapters, some expectations may now be voiced with regard to the potential capabilities of thermal imagery of bare soil. To this purpose, the major approaches found in the literature on the interpretation of thermal images, will be inspected briefly as to the assumptions involved and the required additional information. Also, some aspects of interpretation techniques that were originally not designed to be applied to bare soil imagery, are taken into consideration. In this discussion it will be assumed that continuous records of the surface temperature can be obtained, thus disregarding the problems of timing and atmospheric distortion, which both are usually severe (Kahle et al, 1984).

In discussing the perspectives of thermal remote sensing, a distinction should be made between two types of information pertinent to the soil surface layer, viz. 1) that with respect to the value of certain state parameters (T, θ) and 2) that with respect to the surface fluxes, of which only LE will be treated.

7.1 Determination of soil state variables

Soil temperature

The variable obviously involved in thermal imagery is the temperature of the soil, albeit that the 'surface radiation temperature' is the one observed directly (provided the signal can be corrected for atmospheric distortion and sky radiation). This variable in itself is not of direct agronomical value. The radiation emitted at the surface is generated in the top 10-100 μm skin only. The relation of radiation temperature to true surface temperature T_s being given by eq.(4.14) it can be seen that uncertainties in the emissivity ϵ introduce an error in the derived value for T_s . If the soil emissivity in the relevant spectral window is known with an accuracy of ± 0.04 (cf. Table 3.3), the surface temperature can be estimated with an accuracy of approximately ± 3 K at best.

Although the surface temperature plays a central role in many of the surface processes, the course of soil temperature at various depths below the surface will be of a more general agronomical interest. Information on temperatures in the top few centimeters of soil may be relevant to the characterization of conditions for germination and root growth. Such information could also be valuable in the prediction of pest development. To obtain estimates of subsurface soil temperatures, a measured course of surface temperature should be combined with some model to describe heat transport in the soil. The general analytical model that describes the development of soil temperature with depth and time, expressed in terms of Fourier series, was extensively discussed by van Duin (1956) and by van Wijk (1963). Application of such models in the above manner yields a first estimate of expected errors in predicted soil temperatures, due to uncertainties in the thermal soil properties. Even for the detailed field experiments currently discussed, inaccuracies in $\lambda(\theta)$ and $C(\theta)$ were estimated to be as high as $\pm 15\%$ and 10%, respectively. This results in an error of $\pm 12-13\%$ in damping depths D of the diurnal temperature wave. Using these values in the Fourier model, one finds that the relative error in soil temperature amplitude $A_T(z)$ increases from zero at the surface to 20% at depths where $A_T(z) = 0.25 A_T(0)$. For a surface temperature amplitude of 20 K, this implies a maximum error of approximately ± 1 K in $A_T(z)$ at any depths. Neglecting trends due to seasonal changes or to meteorological events on a synoptic scale, the daily average soil temperature might be taken as constant with depth. So the

average surface temperature should be a fair indicator of average soil temperature. With a possible shift in average temperature of ± 3 K due to the input surface temperature, it may be roughly stated that the actual value of soil temperature can be predicted with no better accuracy than ± 3.5 K when also errors in temperature amplitude are taken into account (neglecting the effect of errors in D on the phase shift).

In the above, the governing moisture content was assumed to be known. As this variable changes with depth, and also variations in bulk density occur, the errors to be expected in modelled subsurface temperature are larger than the figures indicated here. Another aspect that has a bearing on uncertainty is the latent heat term, drawing off a certain fraction of the soil heat flux where subsurface evaporation occurs. Clearly, this effect tends to reduce the diurnal soil temperature amplitude at any depth. The error analysis presented in Chapter 5 takes into account all the error sources mentioned here, as well as the effects of spatial variability on the initial temperature chosen. The error standard deviations given in Table 5.2 for the predicted soil temperatures, however, should be corrected for application in the present problem, where the actual course of surface temperature is assumed to be known, whereas that course was not used as such in the validation trials. If, therefore, that fraction of the variance in T_{rs} (radiation temperature) which is due to sources that affect T_s (true surface temperature) as well is subtracted from the calculated variance in soil temperature, a rough estimate can be obtained of the uncertainties involved in predicted soil temperature fluctuations. Finally then, the shift of ± 3 K should be added in order to get an impression of the order of accuracy which can be obtained in the modelling of bare soil temperatures on the basis of remotely sensed surface temperature (and detailed information concerning thermal and hydraulic properties of the soil under study). According to the results of this work, expected standard deviations would range then between ± 3 and ± 5 K. It may be concluded that the combined use of remotely sensed surface temperature and detailed soil physical models does not improve the estimation of soil temperatures beyond the accuracy already attained by empirical models that use global radiation and air temperature as inputs.

Soil moisture content

Perhaps the item placed highest on the list of state variables to be derived from thermal surface information is the soil moisture content. This obviously concerns a 'secondary' quantity, related to temperature in some indirect manner. Numerous field studies have given evidence of relations between surface moisture content and the behaviour of surface temperature (Vleck and King, 1983; Cihlar, 1980; Idso et al, 1975, Heilman and Moore, 1980; Reginato et al, 1976; ten Berge et al, 1983). This behaviour has been expressed in terms of diurnal surface temperature amplitude, or difference between maximum surface and maximum air temperature, or simply momentary values were used. The resulting empirical relations, however, could not be generalized to yield dependable formulae for image interpretation. Nevertheless, starting from the idea that moisture content affects thermal properties, these relations gave rise to the hope that the thermal inertia concept, originally developed for geological applications, could also be applied to bare soils to yield information on the soil moisture content.

In situations where conduction is the predominant heat transfer mechanism in the (homogeneous) soil, combination of Fourier's law

$$(7.1) \quad G_s = -\lambda \frac{\partial T}{\partial z}$$

with a sinusoidal behaviour of the surface temperature T_s yields the relation between surface heat flux G_s and the frequency (ω) and amplitude (ΔT_s) of the surface temperature wave (Van Wijk, 1963):

$$(7.2) \quad \int_{t_1}^{t_2} G_s(t) dt = \Delta T_s \cdot \sqrt{\omega \lambda C} \cdot \int_{t_1}^{t_2} \sin(\omega t + \pi/4) dt$$

With reference to the diurnal cycle, the term $\sqrt{\omega \lambda C}$ is sometimes named the "diurnal heat capacity" (Price, 1980). Thermal inertia is defined as $P \equiv \sqrt{\lambda C}$ (although some authors have interpreted 'thermal inertia mapping' simply as the regional registration of the diurnal surface temperature amplitude). The 'thermal inertia approach' basically combines (remote) measurements of T_s with estimates of $G_s(t)$ to solve eq. 7.2 for $\sqrt{\lambda C}$. In the case of soil moisture mapping, this thermal property it subsequently translated into volumetric moisture content. Such a translation requires specific

soil information, primarily on bulk density, but also on mineralogical composition. Pratt and Ellyett (1979) extensively discussed these P-θ relations. It may be safely stated that for remote sensing applications, such specific soil information will not be available. (In the case of close-range thermal sensing, e.g. of trial fields to evaluate soil management effects, the situation may be better). Moreover, bulk density and moisture content near the soil surface can hardly even be considered homogeneous with respect to depth, a necessary assumption made in the inertia analysis.

Aside from the above, the major difficulty of the inertia methods resides in the estimation of the surface heat flux G_s . All procedures involve, explicitly or implicitly, the estimation - or neglect - of the remaining terms of the energy balance, i.e. net radiation R_n and the sensible and latent heat fluxes towards the atmosphere, H and LE. Frequently, the sum (H+LE) is large, and since G_s is found by subtraction of this term from R_n , relative errors in G_s can be expected to be large. Price (1977, 1980) formulated an analytical expression to relate daily mean evaporation rate and the diurnal heat capacity to the surface temperature amplitude. His procedure involves the use of an explicit function for global radiation, and the assumption that diurnal variations in H and LE depend linearly on T_s . As inherent to the problem of estimating G_s from the surface energy budget, also this method inevitably implies the necessity to enter surface exchange coefficients for heat and vapour, and the courses of atmospheric conditions at some height above the surface. Whereas the measurement or estimation of the latter on a regional scale present some difficulties that might be overcome, the estimation of the coefficients for heat and vapour exchange with the atmosphere is considered not feasible at present. Aside from wind speed - which could be known in the most favourable case - the parameter z_0 governs the exchange of sensible heat, and also of latent heat in drying stage I. For surfaces in drying stage III, the latent heat flux to the atmosphere is dominated by vapour diffusivity and path length (Chapter 6). Uncertainties in all these parameters are large in the sense that absolute errors in values of H and LE, calculated on the basis of chosen values for these parameters, must be expected to be large as compared to the absolute value of G_s . In other words, the estimated G_s is relatively sensitive to these parameters. Little is known about vapour diffusivity near the soil surface under field circumstances (cf. Chapter 3). The behaviour of effective z_0 values over non-homogeneous terrain is subject to recent studies

that reveal dramatic and unexpected shifts in this parameter (Kroon, 1985). Even for homogeneous trial fields, it appears difficult to determine z_0 with sufficient accuracy to render it useful for application in surface energy balance models (Chapter 5). The ranges chosen for parameter variation in the sensitivity analysis, presented in Chapter 6, were based on possible field variations. It is considered not realistic to presume that these intervals could be narrowed down for the purpose of regional terrain imagery interpretation.

Other authors proposed analytical approaches somewhat different from that of Price. Hechinger (1979) and England et al (1983) based their analyses on Fourier series methods. The latter group determined the atmospheric heat exchange coefficient, the total evaporation 'resistance' (including the soil diffusion term) and the soil thermal inertia by an optimisation procedure, minimizing the sum of squares between predicted and measured surface temperature. Since bare soil surface temperature, at least during daytime, is more sensitive to the transport parameters that govern H and LE than to soil thermal inertia (cf. Chapter 6), it can be expected that also this method does not give reliable estimates of the latter parameter.

Alternatively, look up tables or graphs have been used (Rosema, 1979; van der Griend et al, 1985; Schieldge, 1980). These are created by running (numerical) simulation algorithms for a variety of boundary conditions and soil parameters. The acquired simulated courses of surface variables are then combined to build a 'network' that can be used to infer thermal inertia upon entering a number of estimated or measured parameters, along with the observed surface temperature amplitude. It will be clear that this approach suffers basically from the same weaknesses as mentioned above.

The concept of thermal admittance, being the reciprocal of complex thermal conductance, has been proposed as an alternative to thermal inertia since it allows, theoretically, to take into account variations with depth of soil thermal properties from phase shifts of the temperature wave (Byrne and Davis, 1980; Menenti, 1984). Aside from the fact that phase shifts can only be established under very regular boundary conditions, it can be expected the same problems as described for inertia will present themselves, when the concept is applied to bare soils.

The figures shown in Chapter 6 demonstrate that surface temperature is most sensitive to thermal soil properties in the early morning hours. During daytime, other parameters dominate the picture. Therefore, information on

thermal properties is 'polluted' when minimum surface temperatures are combined with maximum surface temperatures to yield the temperature amplitude as an indicator of thermal inertia. It may be considered to use the nighttime half of the surface heat flux instead, in combination with the difference between minimum surface temperature and some reference temperature, for which the air temperature at dusk seems to be an appropriate variable. The nocturnal part of the G_s 'sine' wave then should be established on the basis of net radiation. At night the turbulent fluxes H and LE are usually negligible and G_s is closely tied to R_n (Chapter 5).

Recent developments show possibilities for the assessment of net radiation by remote means. The proposed procedure then would imply the reverse of the method described by Hares et al (1985) to determine daily positive heat flux by combining a measured ΔT_s with an estimated value of the thermal inertia, based on observed moisture content. (Naturally, the problems associated with translating inertia to soil moisture content would remain unaltered).

While thermal inertia appears to be not an attractive variable to monitor soil water status, the combined use of soil water transport models and remotely sensed flux boundary conditions could be thought of as an alternative. For water budgetting of crops, such an approach has been followed recently by Nieuwenhuis (1985). Stroosnijder et al. (1985) proposed an analogous procedure for bare soils, combined with microwave measurements. It might be attainable to keep track of total soil moisture storage, also for bare soils, in this manner, provided that the course of the latent heat flux can be assessed with sufficient accuracy. For a correct simulation of the distribution of water in the soil, and notably of the impact that the diurnal cycle has on this distribution, accurate information on soil hydraulic parameters would be required. To characterize a soil in this respect, the parameters A' , B' and θ_{ref} - as introduced in section 6.4 - are considered suitable.

It should be faced, however, that these properties themselves have a dynamic character in areas where tillage, soil slaking, crust formation etc. are natural. Consequently, they cannot be determined on a sufficiently large scale by ground measurements. Yet, the accurate knowledge of hydraulic parameters is crucial to a sensible simulation of soil water movement. The possibility of deriving such parameters from observed regional courses of evaporation over longer periods after initial wetting - under known boundary

conditions - would be an interesting topic for further research. It is admitted that the accuracy attained in the simulation of surface soil moisture dynamics is rather limited, even in those cases where extensive data on physical soil properties are available. Especially this is so where wetting and drying alternate. All experimental studies treated in this report serve to illustrate this (cf. Chapters 4 and 5).

7.2 Determination of the latent heat flux

Surface temperature measurements have been used in various ways to estimate evaporation rates, either from crop canopies or bare soil surfaces. Among the earliest detailed field studies was the one described by Idso et al (1975) and Reginato et al (1976). These authors reported an empirical relation between relative evaporation rate E/E_o and daily surface temperature amplitude, and between E/E_o and maximum surface minus air temperature. For evaporation terms, daily totals were used. These authors concluded that the obtained linear relations could be used successfully to estimate daily evaporation totals from thermal data for a specific site. They commented that the relations were valid throughout the year, which at first may seem surprising, with net radiation changing. It can be understood qualitatively, however, that an increase in net radiation reduces both the quotient E/E_o (by increasing E_o more than E) and enhances the temperature difference between surface and air temperature maxima. So fluctuations in radiation levels tend to move the observed pairs of $(E/E_o, (T_s-T_a)_{max})$ 'along the regression line' between the two variables. Changes in the governing windspeed, on the contrary, may be expected to bring about deviations, since an increase in windspeed decreases both E/E_o and $(T_s-T_a)_{max}$. For a wheat crop, the same group of authors (Jackson et al, 1977) employed the difference between crop canopy and air temperature (T_c-T_a) at 14.00 h as an indicator of evapotranspiration ET. In this case, their analysis involved explicitly the net radiation term; the ground heat flux was assumed to be negligible on a daily basis, and the evapotranspiration was expressed as

$$(7.3) \quad ET = R_n - B(T_c - T_a) \quad W m^{-2}$$

where B is an empirical constant. The value of B was found to be independent of windspeed for the specific experimental site.

There is no obvious reason why this approach would not be valid for the calculation of bare soil evaporation. More experimental work is required to validate the above type of relationship for a wider range of environmental conditions. Unfortunately, the results reported by Reiniger et al (1982) are not encouraging.

Nieuwenhuis et al (1985) modified the above formulation and replaced net radiation by the daily potential evapotranspiration, thus basing the 'reference value' of ET not only on available energy but also on the turbulent exchange coefficient. In addition, they proposed to use the difference ($T_c - T_c^*$) instead of ($T_c - T_a$), where the asterix is meant to indicate the condition of potential evapotranspiration; the daily potential evapotranspiration was then calculated by one of the accepted formulations. The calibration constant B, appearing in eq. (7.3), was found to change with the modifications introduced, as can be expected. The applicability of the Nieuwenhuis formulation to the problem of bare soil evaporation certainly asks for due attention. In view of the results given in section 6.5, however, it may be anticipated that variations in roughness length and albedo introduce a considerable scatter in the values of the calibration constant B.

The procedure proposed by Hatfield et al (1983) uses net radiation, surface and air temperature, and aerodynamic resistance as inputs, to estimate momentary values for ET. For various crops they obtained good results. For bare soils, however, their assumption of the soil heat flux being negligible will certainly be violated; also it seems that the estimation of roughness length for (smooth) bare soils, required in this method, is more difficult than for crops.

Other recent studies of regional evapotranspiration are those by England et al (1983) and Reiniger et al (1982). The latter authors used numerical algorithms combined with ground-measured surface temperatures as inputs, in order to calculate cumulative daily evapotranspiration. The obtained figures were not consistent with the ground-measured evapotranspiration and it was concluded that the use of thermal imagery did not improve ground-measured ET rates; the authors ascribed the discrepancy to temporal variations in surface temperature and to the difficulties encountered in the determination of the surface roughness parameter.

England et al (1983) attempted to estimate evaporation by an optimization procedure, matching observed and calculated surface temperatures by adjustment of three parameters: the atmospheric heat transfer coefficient,

an 'overall' evaporation resistance, and soil thermal inertia . Such an approach indeed seems more feasible for the determination of fluxes than for the determination of thermal inertia and the derived moisture content, as discussed in the previous section. An advantage as compared to the other approaches mentioned before is that no empirical constants have to be used. Two of the parameters obtained as output from their model indeed are closely related to the most relevant system parameters, as illustrated by the figures in section 6.3 of the present report. The third, thermal inertia, might as well be left out of the optimisation procedure, as also suggested by the authors.

Yet an other approach to the estimation of bare soil evaporation from thermal imagery was applied by Menenti (1984), who expressed the actual latent heat flux at the surface as a linear combination of the two partial differentials $\partial LE/\partial T_s$ and $\partial LE/\partial a$, where T_s is the surface temperature and a the albedo. Both T_s and a were obtained from remotely sensed data. The method involves the use of a reference point where LE, T_s and a are known.

Alternatively the author demonstrated the use of three reference points to form a plane, representing LE as a linearized function of T_s and a. Both these methods seem to be more promising than the other approaches mentioned, since no estimates of atmospheric boundary conditions or difficult-to-obtain parameters (z_0) are involved, except for the reference points. The use of ground based experimental sites-in this case to collect the required reference data - seems to be a prerequisite in general for a sensible estimation of the latent heat flux. It must be reminded, however, that even small errors in the measurement of T_s may result in large errors in calculated LE values. Large errors are also caused when variations in soil or environmental factors cause deviations in T_s , which are not correlated with variations in LE. For an example to illustrate this problem, shared with all the other methods discussed, one is referred to Chapter 6.

Literature

- Aase, J.K. and S.B. Idso, 1975. Solar radiation interactions with mixed prairie rangeland in natural and denuded conditions. *Archiv für Meteorologie, Geophysik und Bioklimatologie, Serie B*, 23: 255-264.
- Abrams, M.J., A.B. Kahle, F.D. Palluconi, and J.P. Schieldge, 1984. Geologic mapping using thermal images. *Remote Sensing of Environment* 16: 13-33.
- Aldridge, R. and F.J. Cook, 1983. Estimation of soil temperatures at 0.1 and 0.3 m depths. *New Zealand Soil Bureau Scientific Report No. 62*.
- Angstrom, A., 1925. The albedo of various surfaces of ground. *Geografiska Annaler* 7: 321-342.
- Arya, L.M., D.A. Farrel, and G.R. Blake, 1975. A field study of soil water depletion patterns in presence of growing soy bean roots: I. Determination of hydraulic properties of the soil. *Soil Science Society of America Proceedings* 39: 424-430.
- Arya, L.M. and J.F. Paris, 1981. A physico-empirical model to predict the soil moisture characteristic from particle size distribution and bulk density data. *Soil Science Society of America Journal* 45: 1023-1030.
- Asrar, G., and E.T. Kanemasu, 1983. Estimating thermal diffusivity near the soil surface using Laplace Transform: uniform initial conditions. *Soil Science Society of America Journal* 47: 397-401
- Baca, A.G. and R.G. Gibbs, 1981. Analytical models for simultaneous heat and moisture transport in soils. Rockwell International, Richland, Washington.
- Bavel, C.H.M. van, and R. Lascano, 1979. CONSERVB, a numerical method to compute soil water content and temperature profiles under a bare surface. Rept. 3058-1 Texas A&M University, College Station.
- Berge, H.F.M. ten, L. Stroosnijder, P.A. Burrough, A.K. Bregt, and M.J. de Heus, 1983. Spatial variability of physical soil properties influencing the temperature of the soil surface. *Agricultural Water Management* 6: 213-226.
- Boast, C.W. and T.M. Robertson, 1982. A micro-lysimeter method for determining evaporation from bare soil; description and laboratory evaluation. *Soil Science Society of America Journal* 46: 689-695.

- Bolt, G.H., and P.H. Groenevelt, 1972. Coupling between transport processes in porous media. Proceedings 2nd IAHR-ISSS symposium on the fundamentals of transport phenomena in porous media. Guelph, Ontario.
- Bouten, W. and A.R.P. Janse, 1979. Radar reflection in relation to slaking. Proceedings Workshop Bare Soils, EARSEL, Paris.
- Bowers, S.A. and R.J. Hanks, 1965. Reflection of radiant energy from soils. Soil Science 100: 130-138.
- Bresler, E., J. Heller, N. Diner, I. Ben-Asher, A. Brandt, and D. Goldberg, 1971. Infiltration from a trickle source: II. Experimental data and theoretical predictions. Soil Science Society of America Proceedings 35: 683-689.
- Brooks, R.H. and A.T. Corey, 1964. Hydraulic properties of porous media. Hydrology Paper Nr. 3, Civ. Eng. Dept. Colorado State University, Fort Collins.
- Budyko, M.I., 1958. Heat balance of the earth's surface. Translation by N.A. Stepanova, U.S. Department of Commerce, Washington D.C.
- Buchan, G.D., 1982. Predicting bare soil temperature I. Theory and models for the multi-day mean diurnal variation. Journal of Soil Science 33: 185-197.
- Buettner, K.J.K. and C.D. Kern, 1963. Infra red emissivity of the Sahara from Tyros data. Science, 142: 671.
- Buettner, K.J.K. and C.D. Kern, 1965. The determination of infra red emissivities of terrestrial surfaces. Journal of Geophysical Research 70: 1329-1337.
- Buettner, K.J.K. and R. Dana, 1968. Reply to comparison of two methods for determining infra red emittances of bare soils. Journal of Applied Meteorology 8: 169.
- Busch, N.E., 1973. On the mechanics of atmospheric turbulence. Workshop on micrometeorology. Ed. D.A. Haugen, American Meteorological Society 1-66.
- Businger, J.A., 1975. Aerodynamics of vegetated surfaces. In: Heat and mass transfer in the biosphere. Eds. D.A. de Vries and N.H. Afgan. Scripta Wash. D.C.: 139-167.
- Businger, J.A., 1981. Equations and concepts; in: Atmospheric turbulence and air pollution modelling. Ed. F.T.M. Nieuwstadt and H. van Dop, D. Reidel Publ.

- Buttner, K. and E. Sutter, 1935. Abkühlungs Grösse in den Dünen, Rückstrahlung Verschiedener Bodenbedeckungen. Strahlentherapie 54, 156-173.
- Byrne, G.F., and J.R. Davis, 1980. Thermal inertia, thermal admittance, and the effect of layers. Remote sensing of environment 9: 295-300.
- Camillo, P.J., R.J. Gurney, and T.J. Schmugge, 1983. A soil and atmospheric boundary layer model for evapotranspiration and soil moisture studies. Water Resources Research 19: 371-380.
- Campbell, G.S., 1974. A simple method for determining unsaturated conductivity from moisture retention data. Soil Science 117: 311-314.
- Carslaw, H.S. and J.C. Jaeger, 1962. Conduction of heat in solids. Oxford Press.
- Carlson, T.N. and F.E. Boland, 1978. Analysis of urban-rural canopy using a surface heat flux/temperature model. Journal of Applied Meteorology 17: 998-1013.
- Cary, J.W. and S.A. Taylor, 1962a. The interaction of the simultaneous diffusions of heat and water vapor. Soil Science Society of America Proceedings 26: 413-416.
- Cary, J.W. and S.A. Taylor, 1962b. Thermally driven liquid and vapor phase transfer of water and energy in soil. Soil Science Society of America Proceedings 26: 417-420.
- Cary, J.W., 1963. Onsager's relation and the non-isothermal diffusion of water vapor. Journal of Physical Chemistry 67: 126-129.
- Cary, J.W., 1964. An evaporation experiment and its irreversible thermodynamics. International Journal of Heat and Mass Transfer 7: 531-538.
- Cary, J.W., 1965. Water flux in moist soil: Thermal versus suction gradients. Soil Science 100: 168-175.
- Cary, J.W., 1975. Soil water hysteresis: temperature and pressure effects. Soil Science 120: 308-311.
- Cary, J.W., R.A. Kohl and S.A. Taylor, 1964. Water adsorption by dry soil and its thermodynamic functions. Soil Science Society of America Proceedings 28: 309-313.
- Cary, J.W., 1979. Soil heat transducers and water vapor flow. Soil Science Society of America Journal 43: 835-839.

- Cass, A., G.S. Campbell and T.L. Jones, 1984. Enhancement of thermal water vapor diffusion in soil. Soil Science Society of America Journal 48: 25-32.
- Chahal, R.S., 1963. Effect of temperature and trapped air on the energy status of water in porous media. Soil Science 98: 107-112.
- Chahal, R.S., 1965. Effect of temperature and trapped air on matric suction. Soil Science 100: 262-265.
- Chang, M. and D.G. Boyer, 1977. Fitting soil temperature by a periodic regression model. Texas Journal of Science 29: 169-174.
- Chia, L.S., 1967. Albedos of natural surfaces in Barbados. Quarterly Journal of the Royal Meteorological Society 93: 116-120.
- Choudhury, B.J., T.J. Schmugge and T. Mo, 1982. A parametrisation of effective soil temperature for microwave emission. Journal of Geophysical Research 87: 1301-1304.
- Cihlar, J., 1980. Soil water and plant canopy effects on remotely measured surface temperatures. International Journal of Remote Sensing 1: 167-173.
- Clapp, R.B. and G.M. Hornberger, 1978. Empirical equations for some soil hydraulic properties. Water Resources Research 14: 601-604.
- Cochran, P.H., L. Boersma and C.T. Youngberg, 1967. Thermal conductivity of a pumice soil. Soil Science Society of America Proceedings 31: 454-459.
- Coleman, G and D.G. Coursey, 1976. Sensitivity and model variance analysis applied to some evaporation and evapotranspiration models. Water Resources Research 12: 873-879.
- Conaway, J. and C.H.M. van Bavel, 1967. Evaporation from a wet soil surface calculated from radiometrically determined surface temperatures. Journal of Applied Meteorology 6: 650-655.
- Constantz, J., 1982. Temperature dependence of unsaturated hydraulic conductivity of two soils. Soil Science Society of America Journal 46: 466-470.
- Coulson, K.L. and D.W. Reynolds, 1971. The spectral reflectance of natural surfaces. Journal of Applied Meteorology 10: 1285-1294.
- Cruse, R.M., D.R. Linden, J.K. Radke, W.E. Larson, and K. Larntz, 1980. A model to predict tillage effects on soil temperature. Soil Science Society of America Journal 44: 378-383.

- McCuen, R.H., 1973. The role of sensitivity analysis in hydrologic modeling. *J. of Hydrology* 18: 37-53.
- Dane, J.H. and P.J. Wieringa, 1975. Effect of hysteresis on the prediction of infiltration, redistribution and drainage of water in a layered soil. *Journal of Hydrology* 25: 229-242.
- Dane, J.H., 1980. Comparison of field and laboratory determined hydraulic conductivity values. *Soil Science Society of America Journal* 44: 228-231.
- Davidson, J.M., D.R. Nielsen, and J.W. Biggar, 1963. The measurement and description of water flow through Columbia silt loam and Hesperia sand loam. *Hilgardia* 34: 15-??
- Delsol, F., K. Miyakoda and R.H. Clarke, 1971. Parameterized processes in the surface boundary layer of an atmospheric circulation model. *Quarterly Journal of the Royal Meteorology Society* 97: 181-208
- Dirksen, C., 1969. Thermo-osmosis through compacted saturated clay membranes. *Soil Science Society of America Proceedings* 33: 821-826.
- Dobson, M.C., F.T. Ulaby, M.T. Hallikainen and M.A. El-Rayes, 1985. Microwave dielectric behaviour of wet soil; Part II: dielectric mixing models. *Geoscience and Remote Sensing, GE-23*: 35-46.
- Driedonks, A.G.M., 1981. Dynamics of the well mixed atmospheric boundary layer. PhD thesis, Vrije Universiteit, Amsterdam.
- Duin, R.H.A. van, 1956. Over de invloed van grondbewerking op het transport van warmte, lucht en water in de grond. Verslagen van Landbouwkundige onderzoeken No 62.7, Wageningen Agricultural University.
- Dyer, A.J., 1974. A review of flux-profile relationships. *Boundary Layer Meteorology* 7: 363-372.
- East, W.H., 1950. Fundamental study of clay: X, waterfilms in monodisperse kaolinite fraction. *Journal of the American Ceramics Society* 33: 211-218.
- Ekern, P.C., 1965. The fraction of sunlight retained as net radiation in Hawaii. *Journal of Geophysical Research* 70: 785-793.
- Elrich, D.H., 1964. Note on an improved apparatus for soil moisture flow measurements. *Soil Science Society of America Proceedings* 28: 450-453.
- Elseftawy, Atef, and R.S. Mansell, 1975. Hydraulic conductivity calculations for unsaturated steady state and transient state flow in sand. *Soil Science Society of America Proceedings* 39: 599-603.

- Cass, A., G.S. Campbell and T.L. Jones, 1984. Enhancement of thermal water vapor diffusion in soil. Soil Science Society of America Journal 48: 25-32.
- Chahal, R.S., 1963. Effect of temperature and trapped air on the energy status of water in porous media. Soil Science 98: 107-112.
- Chahal, R.S., 1965. Effect of temperature and trapped air on matric suction. Soil Science 100: 262-265.
- Chang, M. and D.G. Boyer, 1977. Fitting soil temperature by a periodic regression model. Texas Journal of Science 29: 169-174.
- Chia, L.S., 1967. Albedos of natural surfaces in Barbados. Quarterly Journal of the Royal Meteorological Society 93: 116-120.
- Choudhury, B.J., T.J. Schmugge and T. Mo, 1982. A parametrisation of effective soil temperature for microwave emission. Journal of Geophysical Research 87: 1301-1304.
- Cihlar, J., 1980. Soil water and plant canopy effects on remotely measured surface temperatures. International Journal of Remote Sensing 1: 167-173.
- Clapp, R.B. and G.M. Hornberger, 1978. Empirical equations for some soil hydraulic properties. Water Resources Research 14: 601-604.
- Cochran, P.H., L. Boersma and C.T. Youngberg, 1967. Thermal conductivity of a pumice soil. Soil Science Society of America Proceedings 31: 454-459.
- Coleman, G and D.G. Coursey, 1976. Sensitivity and model variance analysis applied to some evaporation and evapotranspiration models. Water Resources Research 12: 873-879.
- Conaway, J. and C.H.M. van Bavel, 1967. Evaporation from a wet soil surface calculated from radiometrically determined surface temperatures. Journal of Applied Meteorology 6: 650-655.
- Constantz, J., 1982. Temperature dependence of unsaturated hydraulic conductivity of two soils. Soil Science Society of America Journal 46: 466-470.
- Coulson, K.L. and D.W. Reynolds, 1971. The spectral reflectance of natural surfaces. Journal of Applied Meteorology 10: 1285-1294.
- Cruse, R.M., D.R. Linden, J.K. Radke, W.E. Larson, and K. Larntz, 1980. A model to predict tillage effects on soil temperature. Soil Science Society of America Journal 44: 378-383.

- McCuen, R.H., 1973. The role of sensitivity analysis in hydrologic modeling. *J. of Hydrology* 18: 37-53.
- Dane, J.H. and P.J. Wieringa, 1975. Effect of hysteresis on the prediction of infiltration, redistribution and drainage of water in a layered soil. *Journal of Hydrology* 25: 229-242.
- Dane, J.H., 1980. Comparison of field and laboratory determined hydraulic conductivity values. *Soil Science Society of America Journal* 44: 228-231.
- Davidson, J.M., D.R. Nielsen, and J.W. Biggar, 1963. The measurement and description of water flow through Columbia silt loam and Hesperia sand loam. *Hilgardia* 34: 15-??
- Delsol, F., K. Miyakoda and R.H. Clarke, 1971. Parameterized processes in the surface boundary layer of an atmospheric circulation model. *Quarterly Journal of the Royal Meteorology Society* 97: 181-208
- Dirksen, C., 1969. Thermo-osmosis through compacted saturated clay membranes. *Soil Science Society of America Proceedings* 33: 821-826.
- Dobson, M.C., F.T. Ulaby, M.T. Hallikainen and M.A. El-Rayes, 1985. Microwave dielectric behaviour of wet soil; Part II: dielectric mixing models. *Geoscience and Remote Sensing*, GE-23: 35-46.
- Driedonks, A.G.M., 1981. Dynamics of the well mixed atmospheric boundary layer. PhD thesis, Vrije Universiteit, Amsterdam.
- Duin, R.H.A. van, 1956. Over de invloed van grondbewerking op het transport van warmte, lucht en water in de grond. Verslagen van Landbouwkundige onderzoeken No 62.7, Wageningen Agricultural University.
- Dyer, A.J., 1974. A review of flux-profile relationships. *Boundary Layer Meteorology* 7: 363-372.
- East, W.H., 1950. Fundamental study of clay: X, waterfilms in monodisperse kaolinite fraction. *Journal of the American Ceramics Society* 33: 211-218.
- Ekern, P.C., 1965. The fraction of sunlight retained as net radiation in Hawaii. *Journal of Geophysical Research* 70: 785-793.
- Elrich, D.H., 1964. Note on an improved apparatus for soil moisture flow measurements. *Soil Science Society of America Proceedings* 28: 450-453.
- Elseftawy, Atef, and R.S. Mansell, 1975. Hydraulic conductivity calculations for unsaturated steady state and transient state flow in sand. *Soil Science Society of America Proceedings* 39: 599-603.

- England, C.E., R. Gombeer, E. Hechinger, R.W. Herschy, A. Rosema (ed.) and L. Stroosnijder, 1983. The Group Agromet Monitoring Project (GAMP): Application of Meteosat data for rainfall, evaporation, soil moisture and plant growth monitoring in Africa. *ESA Journal* 7: 169-188.
- Farrell, D.A., E.L. Greacen and C.G. Gurr, 1966. Vapor transfer in soil due to air turbulence. *Soil Science* 102: 305-313.
- Feddes, R.A., 1971. Water, heat and crop growth. PhD thesis, Wageningen, Agricultural University.
- Fisher, E.A., 1923. Some factors affecting the evaporation of water from soil. *Journal of Agricultural Science* 13, 121-143.
- Forrester, J.W., 1961. *Industrial Dynamics*, Massachusetts Institute of Technology Press, Cambridge, Mass., USA.
- France, J. and J.H.M. Thornby, 1984. *Mathematical models in Agriculture*. Butterworths, London.
- Fuchs, M. and C.B. Tanner, 1966. Infrared thermometry of vegetation. *Agronomy Journal* 58: 596-601.
- Fuchs, M. and C.B. Tanner, 1968. Surface temperature measurements of bare soils. *Journal of Applied Meteorology* 7: 303-305.
- Fukuda, H., 1955. Air and vapor movement in soil due to wind gustiness. *Soil Science* 79: 249-258.
- Gardner, R., 1955. Relation of temperature to moisture tension of soil. *Soil Science* 79: 257-265.
- Geiger, R., 1961. *Das Klima der bodennahen Luftsicht*. 4th edition. Braunschweig, F. Vieweg & Sohn: 19-27.
- Genuchten, M.Th. van, 1980. A closed-form equation for predicting the hydraulic conductivity of unsaturated soils. *Soil Science Society of America Journal* 44: 892-898.
- Gerbermann, A.H., 1979. Reflectance of various mixtures of a clay soil and sand. *Photogrammetric Engineering and Remote Sensing* 45: 1145-1151.
- Ghuman, B.S. and R. Lal, 1982. Temperature regime of a tropical soil in relation to surface condition and its Fourier analysis. *Soil Science* 134: 133-140.
- Gibbs, A.G. and R.G. Baca, 1981. Analytical models for simultaneous heat and moisture transport in soils. Internal Report RH0-LD-49, Rockwell Int., Rickland, Washington.
- Goates, J.R. and S.J. Bennet, 1957. Thermodynamic properties of water absorbed on soil minerals: II. Kaolinite. *Soil Science* 83: 325-330.

- Gold, A. and J. Ben Asher, 1976. Soil reflectance measurement using a photographic method. *Soil Science Society of America Journal* 40: 337-341.
- Goudriaan, J., 1977. Crop micrometeorology, a simulation study. *Simulation Monographs Pudoc*, Wageningen, The Netherlands.
- Graham, W.G. and K.M. King, 1961. Shortwave reflection coefficient for a field of maize. *Quarterly Journal of the Royal Meteorological Society* 87: 425-428.
- Graser, E.A. and C.H.M. van Bavel, 1982. The effect of soil moisture upon soil albedo. *Agricultural Meteorology* 27: 17-26.
- Green, R.E., R.J. Hanks, and W.E. Larson, 1964. Estimates of field infiltration by numerical solution of the moisture flow equation. *Soil Science Society of America Proceedings* 28: 15-19.
- Greene-Kelly, R. 1962. Charge, densities and heats of immersion of some clay minerals. *Clay Minerals Bulletin* 5: 1-8.
- Griend, A.A. van de, P.J. Camillo, and R.J. Curney, 1985. Discrimination of soil physical parameters, thermal inertia, and soil moisture from diurnal surface temperature fluctuations. *Water Resources Research* 21: 997-1009.
- Grinsven, J.J.M. van, C. Dirksen, and W. Bouten, 1985/86. Evaluation of the Hot Air Method for measuring soil water diffusivity. *Soil Science Society of America Journal* 49/50: ...-..
- Groenevelt, P.H. and B.D. Kay, 1974. On the interaction of water and heat transport in frozen and unfrozen soils: II. The liquid phase. *Soil Science Society of America Proceedings* 38: 400-404.
- Groot, S.R. de, and P. Mazur, 1962. Non-equilibrium thermodynamics. North Holland Publishers, Amsterdam.
- Gupta, S.C. and W.E. Larson, 1979. Estimating soil water retention characteristics from particle size distribution, organic matter content, and bulk density data. *Water Resources Research* 15: 1633-1635.
- Gupta, S.C., J.K. Radke and W.E. Larson, 1981. Predicting temperatures of bare and residue covered soils with and without a corn crop. *Soil Science Society of America Journal* 45: 405-412.
- Gupta, S.K., 1983. A radiative transfermodel for surface radiation budget studies. *Journal Quantitative Spectroscopy and Radiation Transfer* 5: 419-427.

- Hadas, A., 1968. Simultaneous flow of water and heat under periodic heat fluctuations. Soil Science Society of America Proceedings 32: 297-301.
- Hadas, A., 1969. A comparison between predicted and measured values of thermal conductivity of a moist soil under a steady and fluctuating thermal regime. Israel Journal of Agricultural Research 19: 151-160.
- Hadas, A., 1977a. Evaluation of theoretically predicted thermal conductivities of soils under field and laboratory conditions. Soil Science Society America Journal 41: 460-466.
- Hadas, A., 1977b. Heat transfer in dry aggregated soil: I. Heat conduction. Soil Science Society America Journal 41: 1055-1059.
- Haise, H.R. and O.J. Kelley, 1950. Causes of diurnal fluctuations of tensiometers. Soil Science 70: 301-313.
- Hammel, J.E., R.I. Papendick, and G.S. Campbell, 1981. Fallow tillage effects on evaporation and seedzone water content in a dry summer climate. Soil Science Society America Journal 45: 1016-1022.
- Hanks, R.J., H.R. Gardner, and M.L. Fairbourne, 1967. Evaporation of water from soils as influenced by drying with wind or radiation. Soil Science Society America Proceedings 31: 593-598.
- Hares, M.A., J. Ben Asher, A.D. Matthias, and A.W. Warrick, 1985. A simple method to evaluate daily positive soil heat flux. Soil Science Society of America Journal 49: 45-47.
- Haridasan, M. and R.D. Jensen, 1972. Effect of temperature on pressure head-water content relationship and conductivity of two soils. Soil Science Society America 36: 703-708.
- Hasfurther, V.R. and R.D. Burman, 1974. Soil temperature modelling using air temperature as a driving mechanism. Transactions of the American Society of Agricultural Engineers, 17: 78-81.
- Hatfield, J.L., A. Perrier, and R.D. Jackson, 1983. Estimation of evapotranspiration at one time-of-day using remotely sensed surface temperatures. Agricultural Water Management 7: 341-350.
- Hechinger, E., 1979. Contribution a l'interpretation de données de télédétection: étude d'un modèle thermique de sols et de son emploi pour la réalisation d'images de télédétection dans le visible et l'infrarouge thermique. Thèse Université Louis Pasteur Strasbourg

- Heide, G. van der, and A.J. Koolen, 1980. Soil surface albedo and multi-spectral reflectance of shortwave radiation as a function of degree of soil slaking. *Netherlands Journal of Agricultural Science* 28: 252-258.
- Heilman, J.L. and D.G. Moore, 1980. Thermography for estimating near-surface soil moisture under developing crop canopies. *Journal of Applied Meteorology* 19: 324-328.
- Hillel, D., 1976. On the role of soil moisture hysteresis in the suppression of evaporation from bare soil under diurnally cyclic evaporativity. *Soil Science* 122: 309-314.
- Hillel, D., 1980. *Fundaments of soil physics*. Academic Press, New York.
- Himmelblau, D.M., and K.B. Bisschoff, 1968. *Process analysis and simulation: deterministic systems*. Wiley & Sons, NY.
- Horton, R. Jr., 1982. Determination and use of soil thermal properties near the soil surface. PhD-thesis, Las Cruces, New Mexico.
- IBM, 1975. *Continuous System Modeling Program III (CSMP III)*, Program Reference Manual SH19-7001-2, Program Number 5734-X59, IBM Corp., White Plains, N.Y.
- Idso, S.B. and R.D. Jackson, 1969. Comparison of two methods for determining infra red emittances of bare soils. *Journal of Applied Meteorology* 8: 168-169.
- Idso, S.B. and R.J. Reginato, 1974. Assessing soil water status via albedo measurements. Proceedings Arizona Section of the American Water Resources Association and Hydrology section of the Arizona Academy of Science.
- Idso, S.B., R.J. Reginato, R.D. Jackson, B.A. Kimball and F.S. Nakayama, 1974. The three stages of drying of a field soil. *Soil Science Society of America Proceedings* 38: 831-837.
- Idso, S.B., T.J. Schmugge, R.D. Jackson and R.J. Reginato, 1975. The utility of surface temperature measurements for the remote sensing of surface soil water status. *Journal of Geophysical Research* 80: 3044-3049.
- Idso, S.B., R.J. Reginato, R.D. Jackson, 1975. Assessing bare soil evaporation via surface temperature measurements. In: *Hydrology and Water Resources in Arizona and the South West; Proceedings of the American Water Resources Association*, Tempe, Arizona, 199-205.

- Idso, S.B., R.D. Jackson, R.J. Reginato, B.A. Kimball, and F.S. Nakayama, 1975. The dependence of bare soil albedo on soil water content. *Journal of Applied Meteorology* 14: 109-113.
- ISSS, 1975. Final Report Second Committee on terminology in soil physics. Bolt Chairman. *ISSS Bulletin Nr.* 48: 16-22.
- Jackson, R.D., 1972. On the calculation of hydraulic conductivity. *Soil Science Society of America Proceedings* 36: 380-382.
- Jackson, R.D., 1973. Diurnal changes in soil water content. In: *Field soil water regime*, Soil Science Society of America Special Publication 5.
- Jackson, R.D., R.J. Reginato, B.A. Kimball, F.S. Nakayama, 1974. Diurnal soil water evaporation: comparison of measured and calculated soil water fluxes. *Soil Science Society of America Proceedings* 38: 861-866.
- Jackson, R.D., R.J. Reginato, and S.B. Idso, 1977. Wheat canopy temperature: a practical tool for evaluating water requirements. *Water Resources Research* 13: 651-656.
- Jacobs, P., 1982. The thermal behaviour of a three dimensional object placed in the open field. PhD-thesis Agricultural University Wageningen, The Netherlands.
- Jensen, M.E., M. Asce, and R.J. Hanks, 1967. Non-steady state drainage from porous media. *Journal of the Irrigation and Drainage division. Proceeding of the American Society of Civil Engineers. Ir. 3.*
- Journel, A.G. and C.J. Huijbregts, 1978. *Mining Geostatistics*. Academic Press, London.
- Jurinak, J.J. 1963. Multilayer adsorption of water by kaolinite. *Soil Science Society of America Proceedings* 27: 269-272.
- Jurinak, J.J. and R.G. Burau, 1967. Heat of immersion studies on anion-treated ferric oxide. *Soil Science Society of America Proceedings* 31: 732-736.
- Jury, W.A., 1973. Simultaneous transport of heat and moisture through a medium sand. PhD-thesis, University of Wisconsin.
- Jury, W.A. and J. Letey, 1979. Water vapor movement in soil: reconciliation of theory and experiment. *Soil Science Society of America Journal* 43: 823-827.

- Jury, W.A. and J. Letey, 1979. Water vapor movement in soil: reconciliation of theory and experiment. *Soil Science Society of America Journal* 43: 823-827.
- Kahle, A.B., 1977. A simple thermal model of the earth's surface for geo-logic mapping by remote sensing. *Journal of Geophysical Research* 82: 1673-1680.
- Kahle, A.B., 1977. A simple thermal model of the earth's surface for geo-logic mapping by remote sensing. *Journal of Geophysical Research* 82: 1673-1680.
- Kahle, A.B., J.P. Schieldge, and R. Alley, 1984. Sensitivity of thermal intertia calculations to variations in environmental factors. *Remote Sensing of Environment* 16: 211-232.
- Kalma, J.D. and R. Badham, 1972. The radiation balance of a tropical pas-ture. I. The reflection of shortwave radiation. *Agricultural Meteorology* 10: 251-259.
- Kay, B.D. and P.H. Groenevelt, 1974. On the interaction of water and heat transport in frozen and unfrozen soils: I. Basic theory. The Vapor phase. *Soil Science Society of America Proceedings* 38: 395-400.
- Keulen, H. van, 1975. Simulation of water use and herbage growth in arid regions. *Simulation Monographs*, Pudoc, Wageningen.
- Keulen, H. van, and D. Hillel, 1974. A simulation study of the drying front phenomenon. *Soil Science* 118: 270-273.
- Kimball, B.A. and E.R. Lemon, 1971. Air turbulence effects upon soil gas exchange. *Soil Science Society of America Proceedings* 35: 16-21.
- Kimball, B.A., R.D. Jackson, R.J. Reginato, F.S. Nakayama, and S.B. Idso, 1976. Comparison of field measured and calculated soil heat fluxes. *Soil Science Society of America Journal* 40: 18-24.
- Kimball, B.A. and R.D. Jackson, 1975. Soil heat flux determination: a null aligment method. *Agricultural Meteorology* 15: 1-9.
- Kondrat'ev, K.Y., 1954. The radiant energy of the sun, Leningrad, Chapter 9, Albedo of the underlying surface and clouds. English summary by A. Kurlent and P. Larson, McGill University.
- Krischer, O. and H. Rohnalter, 1940. Wärmeleitung und Dampfdiffusion in feuchten Gatern. *Verein Deutsch. Ing. Forchsungsheft* 402: 1-18.
- Lamers, J.G., 1985. Soil slaking and the possibilities to record with infra-red line scanning. *International Journal of Remote Sensing* 6: 153-165.

- Lascano, R.J. and C.H.M. van Bavel, 1983. Experimental verification of a model to predict soil moisture and temperature profiles. *Soil Science Society of America Journal* 47: 441-448.
- Lettau, H.H., 1957. Computation of heat budget constituents of the earth-air interface. In: *Exploring the atmospheres first mile*, 1, 305. Eds. H.H. Lettau and D. Davidson, N.Y. Pergamon press.
- Lynn, D.W., 1984. Surface material mapping in the English Fenlands using airborne multispectral scanner data. *International Journal of Remote Sensing* 4: 699-713.
- Lynn, D.W., 1985. The timeliness of thermal infrared data acquisition for soil and surface material survey in humid temperate environments (to be published).
- Mahrer, Y., 1982. A theoretical study of the effect of soil surface shape upon the soil temperature profile. *Soil Science* 134: 381-387.
- Marel, H.W. van der, 1966. Cation exchange, specific surface, and absorbed H₂O molecules. *Zeitschrift für Pflanzenernährung, Düngung und Bodenkunde* 114: 161-175.
- Mehuys, G.R., L.H. Stolzy, J. Letey, and L.V. Weeks, 1975. Effect of stones on the hydraulic conductivity of relatively dry desert soils. *Soil Science Society of America Proceedings* 39: 37-42
- Meikle, R.W. and T.R. Treadway, 1979. A mathematical method for estimating soil temperatures. *Soil Science* 128: 226-242.
- Meikle, R.W. and A.J. Gilchrist, 1983. A methematical method for estimation of soil temperatures in England and Scotland. *Agricultural Meteorology* 30: 221-225.
- Menenti, M., 1984. Physical aspects and determination of evaporation in deserts, applying remote sensing techniques. PhD thesis and Report 10 of Institute for Land and Water Management Research, Wageningen, The Netherlands.
- Miller, E.E., 1980. Similitude and scaling of soil water phenomena. In: *Applications of Soil Physics*. Ed. D. Hillel, Academic Press, N.Y.
- Milly, P.C.D., 1982. Moisture and heat transport in hysteretic, inhomogenous porous media: a matric head based formulation and a numerical model. *Water Resources Research* 18: 489-498.
- Milly, P.C.D., 1984. A simulation analysis of thermal effects on evaporation from soil. *Water Resources Research* 20: 1087-1098.

- Milly, P.C.D., 1984. A linear analysis of thermal effects on evaporation from soil. *Water Resources Research* 20: 1075-1085.
- Monteith, J.L., 1959. The reflection of shortwave radiation by vegetation. *Quarterly Journal of the Royal Meteorological Society* 85: 386-392.
- Monteith, J.L., 1963. Gas exchange in plant communities. In: *Environmental control of plant growth*, Ed. E.T. Evans. Academic Press, New York: 95-112.
- Moore, R.E., 1939. Water conduction from shallow water tables. *Hilgardia* 12: 383-424.
- Moore, R.E., 1940. The relation of soil temperature to soil moisture:pressure potential, retention and infiltration rate. *Soil Science Society of America Proceedings* 5: 61-64.
- Moore, D.G., J.C. Harlan, J.L. Heilman, D.O. Ohlen and W.D. Rosenthal, 1983. Infra-red remote sensing for monitoring rainfall. *Agricultural Water Management* 7: 363-378.
- Moustafa, S., D. Jarrar, H. El-Mansy, H. Al-Shami, G. Brusewitz, 1981. Arid soil temperature model. *Solar Energy* 27: 83-88.
- Mualem, Y., 1973. Modified approach to capillary hysteresis, based on a similarity hypothesis. *Water Resources Research* 9: 1324-1331.
- Mualem, Y., 1976. A new model for predicting the hydraulic conductivity of unsaturated porous media. *Water Resources Research* 12: 513-522.
- Mualem, Y. and G. Dagan, 1976. Development of methods, tools and solutions for unsaturated flow with application to watershed hydrology and other fields. US-Israel Binational Science Foundation, Report Research Project 442.
- Mualem, Y. and H.J. Morel-Seytoux, 1978. Analysis of a capillary hysteresis model, based on a one-variable distribution function. *Water Resources Research* 14: 605-610.
- Nagpal, N.K. and L. Boersma, 1973. Air entrapment as a possible error in the use of a cylindrical heat probe. *Soil Science Society of America Proceedings* 37: 828-832.
- Nakayama, F.S., R.D. Jackson, B.A. Kimball, R.J. Reginato, 1973. Diurnal soil water evaporation: Chloride movement and accumulation near the soil surface. *Soil Science Society of America Proceedings* 37: 509-513.
- Nerpin, S.V. and A.F. Chudnovski, 1970. Physics of the soil. Israel Program of Scientific Translations, Kefer Press, Jerusalem.

- Nicholaichuck, W., 1974. A soil moisture and temperature prediction model under evaporative conditions. PhD-thesis, University of Guelph, Guelph, Ontario.
- Nielsen, D.R., J.W. Biggar, and K.T. Ehr, 1973. The spatial variability of field measured soil water properties. *Hilgardia* 42: 215-259.
- Nielsen, D.R., 1982. Soil physics research: a leap into the future without the academia of the past. Whither soil research. Proceedings International Soil Science Society congres India: 59-67.
- Nielsen, D.R., R.D. Jackson, J.W. Cary, D.D. Evans, 1972. Soil water. American Society Agronomy and Soil Science Society of America.
- Nielsen, D.R., P.M. Tillotson, and S.R. Vieira, 1983. Analyzing field measure soil water properties. *Agricultural Water Management* 6: 93-109.
- Nieuwenhuis, G.J.A., 1985. Integration of remote sensing with a soil water balance simulation model (SWATRE). Paper presented at International Workshop on Hydrologic Applications of Space Technology, August 1985, Florida.
- Nieuwenhuis, G.J.A., E.H. Smidt, and H.A.M. Thunnissen, 1985. Estimation of regional evapotranspiration of arable crops from thermal infrared images. *International Journal of Remote Sensing* 6: 1319-1334.
- Nieuwstadt, F.T.M. and A.G.M. Driedonks, 1979. The nocturnal boundary layer: a case study compared with model calculations. *Journal of Applied Meteorology* 18: 1397-1405.
- Nimah, M.N., and R.J. Hanks, 1973. Model for estimating soil water, plant and atmospheric interrelations. I. Description and sensitivity. *Soil Science Society of America Proceedings* 37: 522-527.
- Njoku, E.G., J.P. Schieldge, and A.B. Kahle, 1980. Joint microwave and infrared studies for soil moisture determination. Jet Propulsion Laboratory publication 80-57, Pasadena, California.
- Obukhov, A.M., 1946. Turbulence in an atmosphere with a non-uniform temperature. Trudy Instituta Teoretisiskoj Geofiziki Academii Nauk SSSR (translation Boundary Layer Meteorology 2: 7-29).
- Ouellet, C.E., 1973. Estimation of monthly soil temperatures from climatic data. Technical Bulletin, Agricultural Canada No 82.
- Orchiston, H.D., 1953. Adsorption of water vapor. I. Soils at 25°C. *Soil Science* 76: 453-465.

- Orchiston, H.D., 1954. Adsorption of water vapor. II. Clays at 25°C. *Soil Science* 78: 463-480.
- Palagin, E.G., 1976. On the prediction of soil temperatures from meteorological data during the winter period. *Boundary Layer Meteorology* 10: 331-336.
- Palluconi, F.D. 1983. Personal communication. Yet Propulsion Laboratory, California Institute of Technology, Pasadena.
- Parton, W.J. and J.A. Logan, 1981. A model for diurnal variation in soil and air temperature. *Agricultural Meteorology* 23: 205-216.
- Paulson, C.A., 1970. The mathematical representation of windspeed and temperature profiles in the unstable atmospheric surface layer. *Journal of Applied Meteorology* 9: 857-861.
- Peck, A.J., 1960. Change of moisture tension with temperature and air pressure: theoretical. *Soil Science* 89: 303-310.
- Peck, A.J., 1969. Entrapment, stability and persistance of air bubbles in soil water. *Australian Journal of Soil Research* 7: 79-90.
- Philip, J.R., 1955. Numerical analysis of equations of the diffusion type with diffusivity concentration-dependent. *Transaction of the Faraday Society* 51: 885-892.
- Philip, J.R. and D.A. de Vries, 1957. Moisture movement in porous materials under temperature gradients. *Transaction of the American Geophysical Union* 38: 222-231.
- Philip, J.R., 1967. Sorption and infiltration in heterogeneous media. *Australian Journal of Soil Research* 5: 1-10.
- Philip, J.R., 1980. Field heterogeneity: some basic issues. *Water Resources Research* 16: 443-448.
- Piggin, I. and P. Schwertfeger, 1973. Variations in the albedo of wheat and barley crops. *Archiv für Meteorologie, Geophysik und Bioklimatologie, Serie B*, 21: 365-391.
- Planet, W.G., 1970. Some comments on reflectance measurements of wet soils. *Remote Sensing of Environment* 1: 127-129.
- Portman, D.J., 1954. The measurement of radiation. *Publications on Climatology John Hopkins University* 7: 289-292.
- Poulovassilis, A., 1962. Hysteresis of pore water, an application of the concept of independent domain. *Soil Science* 93: 405-412.

- Poulovassilis, A. and E. Tzimas, 1975. The hysteresis in the relationship between hydraulic conductivity and soil water content. *Soil Science* 120: 327-331.
- Pratt, D.A. and C.D. Ellyett, 1979. The thermal inertia approach to mapping of soil moisture and geology. *Remote Sensing of Environment* 8: 151-168.
- Pratt, D.A., and C.D. Ellyett, 1979. The thermal inertia approach to mapping of soil moisture and geology. *Remote sensing of environment* 8: 151-168.
- Pratt, D.A., S.J. Foster and C.D. Ellyett, 1980. A calibration procedure for Fourier series thermal inertia models. *Photogrammetric Engineering and Remote Sensing* 46: 529-538.
- Prevot, L., R. Bernard, O. Taconet, D. Vidal-Madjar, J.L. Thony, 1984. Evaporation from a bare soil, evaluated using a soil water transfer model and remotely sensed surface soil moisture data. *Water Resources Research* 20: 311-316.
- Price, J.C., 1977. Thermal inertia mapping: A new view of the earth. *Journal of Geophysical Research* 82: 2582-2590.
- Price, J.C. 1980. The potential of remotely sensed thermal infrared data to infer surface soil moisture and evaporation. *Water Resources Research* 16: 787-795.
- Quirk, J.P., 1955. Significance of surface areas calculated from water vapor sorption isotherms by use of the B.E.T. equation. *Soil Science* 80: 423-430.
- Raats, P.A.C., 1975. Transformations of fluxes and forces describing the simultaneous transport of water and heat in unsaturated porous media. *Water Resources Research* 11: 938-942.
- Rahi, G.S. and R.D. Jensen, 1975. Effect of temperature on soil water diffusivity. *Geoderma* 14: 115-124.
- Rao, P.S.C., R.E. Jessup, A.C. Hornsby, D.K. Cassel, and W.A. Pollans, 1983. Scaling soil microhydrologic properties of Lakeland and Konawa soils using similar media concepts. *Agricultural Water Management* 6: 277-290.
- Rawitz, E., 1965. The influence of a number of environmental factors on the availability of soil moisture to plants. Ph.D. thesis Hebrew University, Rehovot, Israel.

- Reginato, R.J., S.B. Idso, J.F. Vedder, R.D. Jackson, M.B. Blanchard, R. Goettelman, 1976. Soil water content and evaporation determined by thermal parameters obtained from ground-based and remote measurements. *Journal of Geophysical Research* 81: 1617-1620.
- Reimer, A. and C.F. Shaykewich, 1980. Estimation of Manitoba soil temperatures from atmospheric meteorological measurements. *Canadian Journal of Soil Science* 60: 299-309.
- Reiniger, P., J. Huygen, and J. Mégier, and B. Seguin, 1982. Estimates of regional evapotranspiration in south-eastern France using thermal and albedo data from the heat capacity mapping mission satellite. *Proceedings International Symposium of Remote Sensing of Environment* 2: 1231-1238.
- Reisenauer, A.E., 1963. Methods for solving problem of multidimensional partially saturated steady flow in soils. *Journal of Geophysical Research* 68: 5725-5733.
- Richards, L.A., M.B. Russel and O.R. Neal, 1937. Further developments on apparatus for field moisture studies. *Soil Science Society of America Proceedings* 2: 55-64.
- Richter, J., 1972. Zur Abhängigkeit des Bodenwasserpotentials von der Temperatur. *Zeitschrift für Pflanzenernährung und Bodenkunde* 131: 254-261.
- Riha, S.J., K.J. McInnes, S.W. Childs, and G.S. Campbell, 1980. A finite element calculation for determining thermal conductivity. *Soil Science Society of America Journal* 44: 1323-1325.
- Ritsema, C.J., 1985. De invloed van de temperatuur op de bodemvochtspanning bij constant vochtgehalte. MSc thesis Wageningen Agricultural University, Dept. of Soil Science and Plant Nutrition.
- Rose, D.A., 1963. Water movement in porous materials. Part 1: Isothermal vapor transfer. *British Journal of Applied Physics* 14: 256-262.
- Rose, D.A., 1963. Water movement in porous materials. Part 2: The separation of the components of water movement. *British Journal of Applied Physics* 14: 491-496.
- Rose, D.A., 1971. Water movement in dry soils. II. An analysis of hysteresis. *Journal of Soil Science* 22: 490-507.
- Rosema, A., 1975. A mathematical model for simulation of the thermal behaviour of bare soils, based on heat and moisture transfer. NIWARS-publication No 11, Delft, The Netherlands.

- Rosema,A., 1979. Thermal sensing of soil moisture, evaporation and crop yield. Communication presented at the Ispra Course on the Application of Remote Sensing to Agricultural Production Forecasting, October 15-19, Ispra, Italy.
- Russo, D, and E. Bresler, 1980. Field determinations of soil hydraulic properties. Soil Science Society of America Journal 44: 697-702.
- Russo, D., 1983. Leaching characteristics of a stony desert soil. Soil Science Society of America Journal,. 47: 431-435.
- Rijks, D.A., 1967. Water use by irrigated cotton. I. Reflection of short wave radiation. Journal of Applied Ecology 4: 561-568.
- Rijtema, P.E. 1969. Soil moisture forecasting. Nota 513 ICW, Wageningen.
- Saha, R.S. and R.P. Tripathy, 1981. Effect of temperature on the soil water content-suction relationship. Journal of the Indian Society of Soil Science 29: 143-147.
- Saha, R.S. and R.P. Tripathy, 1979. Effect of temperature on hydraulic conductivity of soil. Journal of the Indian Society of Soil Science 27: 220-224.
- Sasamori, T., 1970. A numerical study of atmospheric and soil boundary layers. Journal of the Atmospheric Sciences 27: 1122-1137.
- Schieldge, J.P., A.B. Kahle, and R.E. Alley, 1982. A numerical simulation of soil temperature and moisture variations for a bare field. Soil Science 133: 197-207.
- Schieldge, J.P., A.B. Kahle, R.E. Alley and A.R. Gillespie, 1980. Use of thermal inertia properties for material identification. Society of Photo-Optical Instrumentation Engineers (SPIE) 238: 350-357.
- Schmidlin, T.W., F.F. Peterson, and R.O. Gifford, 1983. Soil temperature regimes in Nevada. Soil Science Society of America Journal 47: 977-982.
- Schroeder, C., D.W. DeMichele, U.W. Pooch and W.R. Teague, 1978. Modeling heat and moisture flow in soils. Simulation 31: 173-176.
- Schurer, K., 1975. A method for measuring infra red emissivities of near-black surfaces at ambient temperatures. Infra Red Physics 16: 157-163.
- Scotter, D.R., 1976. Liquid and vapor phase transport in soil. Australian Journal of Soil Research 14: 33-41.
- Scotter, D.R. and P.A.C. Raats, 1969. Dispersion of water vapor in soil due to air turbulence. Soil Science 108: 170-176.

- Sellers, W.D., 1965. Physical climatology. University of Chicago Press.
- Sepaskhah, A.R. and L. Boersma, 1979. Thermal conductivity of soils as a function of temperature and water content. Soil Science Society of America Journal 43: 439-444.
- Simmons, C.S., D.R. Nielsen and J.W. Biggar, 1979. Scaling of field-measured soil water properties. Hilgardia 47: 74-154.
- Sisson, J.B., A.H. Ferguson, and M.Th. van Genuchten, 1980. A simple method for predicting drainage from field plots. Soil Science Society of America Journal 44: 1147-1152.
- Smith, M.W., 1977. Computer simulation of microclimatic and ground thermal regimes: test results and program description. Minister of Supply and Services Canada, catalog no R71-18/76-72.
- Snedecor, G.W. and W.G. Cochran, 1967. Statistical methods 6th edition. Iowa State University Press.
- Soer, G.J.R., 1977. The TERGRA model - a mathematical model for the simulation of the daily behaviour of crop surface temperature and actual evaporation. Nota ICW 1014 Wageningen, The Netherlands.
- Staple, W.J., 1965. Moisture tension, diffusivity and drying. Canadian Journal of Soil Science 45: 78-85.
- Staple, W.J., 1969. Moisture redistribution following infiltration. Soil Science Society of America Proceedings 33: 840-847.
- Steinhorst, R.K., H.W. Hunt, G.S. Innis and K.P. Haydock, 1978. Sensitivity analysis of the ELM model. In: Grasland simulation model, Ecol. Studies 26. Ed. G.S. Innis, Springer New York.
- Stroosnijder, L. and H.D.J. van Heemst, 1982. La meteorologie du Sahel et du terrain de l'etude. In: La productivité des paturages Sahéliens, Ed. F.W.T. Penning de M.A. Vries and Djitéye, Pudoc, Wageningen, The Netherlands.
- Stroosnijder, L., 1982. Le milieu Sahélien et les terrains expérimentaux. In: La productivité des paturages Sahélien, Eds. F.W.T. Penning de Vries et M.A. Djitéye, Pudoc, Wageningen, The Netherlands.
- Stroosnijder, L., R.J. Lascano, R.W. Newton and C.H.M. van Bavel, 1985/86. Estimating net rainfall, evaporation and water storage of a bare soil from sequential L-band emissivities. To be published in Journal of Remote Sensing.

- Taylor, S.A. and J.W. Cary, 1964. Linear equations for the simultaneous flow of matter and energy in a continuous soil system. *Soil Science Society of America Proceedings* 28: 167-172.
- Taylor, S.A. and G.L. Stewart, 1960. Some thermodynamic properties of soil water. *Soil Science Society of America Proceedings* 24: 243-247.
- Taylor, S.E. 1979. Measured emissivity of soils in the south-east United States. *Remote Sensing of Environment* 8: 359-364.
- Tennekes, H., and J.L. Lumley, 1972. A first course in turbulence MIT Press, Cambridge, Massachusetts, and London, England.
- Thom, A.S., 1975. Momentum, mass and heat exchange of plant communities. In: *Vegetation and the atmosphere*, Ed. J.L. Monteith, Academic Press, London.
- Thomas, M.D., 1928. Aqueous vapor pressure of soils: 4. Influence of irre-placeable bases. *Soil Science* 25: 485-493.
- Tomović, R. and M. Vukobratović, 1972. General sensitivity theory. American Elsevier Publishing Company, New York.
- Tosi, N., 1983. A simulation model supporting HCMM investigation on geological objectives. *International Journal of Remote Sensing* 4: 353-369.
- Toy, T.J., A.J. Kuhaida Jr. and B.E. Munson, 1978. The prediction of mean monthly soil temperature from mean monthly air temperature. *Soil Science* 126: 181-189.
- Tsang, L., E. Njoku and J.A. Kong, 1975. Microwave thermal emission from a stratified medium with non-uniform temperature distribution. *Journal of Applied Physics* 46: 5127-5133.
- Unsworth, M.H. and J.L. Monteith, 1975. Longwave radiation at the ground. *Quarterly Journal of the Royal Meteorological Society* 101: 13-24.
- Vachaud, G., 1966. Verification de la loi de Darcy generalisee et determination de la conductivit  capillaire a partir d'un infiltration horizontale IHS Symp. Wageningen, 277-292.
- Vachaud, G. and J.L Thony, 1971. Hysteresis during infiltration and redistribution in a soil column at different initial water contents. *Water Resources Research* 7: 111-127.
- Vann, J.R. and M.G. Cline, 1975. Estimating the mean annual soil temperature of areas correlated as the same soil series where both elevation and latitude vary. *Journal of Soil and Water Conservation* 30: 85-87.

- Vauclin, M., R. Haverkamp and G. Vachaud, 1979. Resolution numerique d'une equation de diffusion non-lineaire. Presses Universitaire de Grenoble, France.
- Vauclin, M., G. Hamon and G. Vachaud, 1983. Simulation of coupled flow of heat and water in a partially saturated soil. Determination of the surface temperature and evaporation rate from a bare soil. Zeszyty Problemowe Postepow Nauk Rolniczych 220: 285-299.
- Vershinin, P.V., M.K. Melnikova and B.N. Michurin, 1966. Fundamentals of agrophysics; Translation US Dept. of Commerce.
- Viswanadham, Y. 1982. Examination of the empirical flux-profile models in the atmospheric surface boundary layer. Boundary Layer Meteorology 22: 61-77.
- Vleck, J. and D. King, 1983. Detection of subsurface soil moisture by thermal sensing: results of laboratory, close range, and aerial studies. Photogrammetric Engineering and Remote Sensing 49: 1593-1597.
- Vries, D.A. de, 1952. Het warmtegeleidingsvermogen van grond. Mededelingen Landbouwhogeschool, Wageningen, The Netherlands.
- Vries, D.A. de, 1963. Thermal properties of soils. In: Physics of plant environment, Ed. W.R. van Wijk. North Holland Publishers, Amsterdam.
- Wadsworth, H.A. 1944. An interpretation of the moisture content-surface force curve for soils. Soil Science 58: 225-242.
- Ward, N.R., G.G. Wilkinson, G. Dugdale, and J.R. Milford, 1982. Soil moisture mapping in the Sahel by satellite. Proceedings of the Annual Technical Conference of the Remote Sensing Society, Liverpool.
- Warrick, A.W., G.J. Mullen and D.R. Nielsen, 1977. Scaling field measured soil hydraulic properties using a similar media concept. Water Resources Research 13: 355-362.
- Warrick, A.W. and A. Amoozegar-Fard, 1979. Infiltration and drainage using spatially scaled soil hydraulic properties. Water Resources Research 15: 1116-1120.
- Warrick, A.W. and D.R. Nielsen, 1980. Spatial variability of soil physical properties in the field. In: Applications of soil physics, Ed. D. Hillel, Academic Press, New York.

- Wartena, L. 1973. Checking of some formulae for the calculation of longwave radiation from clear skies. *Archief für Meteorologie, Geophysik und Bioklimatologie, Serie B*, 21: 335-348.
- Watson, K., 1973. Periodic heating of a layer over a semi-infinite solid. *Journal of Geophysical Research* 78: 5904-5910.
- Weeks, L.V., S.J. Richards, and J. Letey, 1968. Water and salt transfer in soil resulting from thermal gradients. *Soil Science Society of America Proceedings* 32: 193-197.
- Westcot, D. and P.J. Wierenga, 1974. Transfer of heat by conduction and vapor movement in a closed soil system. *Soil Science Society of America Proceedings* 38: 9-14.
- Wierenga, P.J., D.R. Nielsen, and R.M. Hagan, 1969. Thermal properties of a soil, based upon field and laboratory measurements. *Soil Science Society of America Journal* 44: 354-360.
- Wilkinson, G.E., and A. Klute, 1962. The temperature effect on the equilibrium energy status of water held by porous media. *Soil Science Society of America Proceedings* 26: 326-329.
- Woodside, W., and J.H. Messmer, 1961. Thermal conductivity of porous media, (1) unconsolidated sands. *Journal of Applied Physics* 32: 1683-1699.
- Wijk, W.R. van, 1963. *Physics of plant environment*. North Holland Publishers, Amsterdam.
- Zdunkowski, W.G. and D.C. Trask, 1971. Application of a radiative-conductive model to the simulation of nocturnal temperature changes over different soil types. *Journal of Applied Meteorology* 10: 937-948.

APPENDIX 1 Listing of the SALSA model

***** SALSA *****

* Soil-Atmosphere Linking Simulation Algorithm *

* Author: H.F.M. ten Berge
* Wageningen Agricultural University
* Dept. of Soil Science and Plant Nutrition
* De Dreijen 3, 6703 BC, Wageningen, The Netherlands
*

/ DIMENSION CHSL02(26), HRH(26) , KSAT(26) , W15(26) ,
/ 1 CHSL05(26), KFCSA(26) , POR(25) , W30(26) ,
/ 2 FC(26) , KFCSW(26) , VGA(26) , WREL15(26) ,
/ 3 FO(26) , KFSAC(26) , VGN(26) , WSAT(26) ,
/ 4 FQ(26) , KFSW(26) , VGM(26) , WRES(26) ,
/ 5 BDRAT(26) , DZ(26) , DZZ(26) , ZZ(26)
/ DIMENSION CHAV(26) , INVLH(12) , MFLP(26) ,
/ 1 CHSOIL(26) , INVLM(12) , OBU(12) , TKEAV(12) ,
/ 2 DAV(26) , K(26) , P(26) , TPAV(12) ,
/ 3 DUDZZ(12) , KAV(26) , PHIH(12) ,
/ 4 DVDZZ(12) , KH(12) , PHIM(12) , VPD(26) ,
/ 5 FA(26) , KM(12) , RH(26) , VPDS(26) ,
/ 6 HCSOIL(26) , KV(12) , STAPAR(12) , WREL(26) ,
/ 7 DATM(26)

STORAGE BD(26), TCM(26), TCMM(26)
STORAGE ACCPRX(12), DIVHFL(26), HFLX(26) , TPFLX(12)
STORAGE ACCPRY(12), DIVWFL(26), HFLCON(26), UVOLFLX(12)
STORAGE EPRBU0(12), DIVQ(12) , HFLVAP(26), VVOLFLX(12)
STORAGE EPRDIS(12), DIVTKE(12), QFLX(12) , WFLX(26)
STORAGE EPRSRX(12), DIVUV0(12), RMOLFLX(12), WFLLIQ(26)
STORAGE EPRSRY(12), DIVVV0(12), TKEFLX(12), WFLVAP(26)
STORAGE DIVTP(12)

FIXED I,J,N,NN

FIXED IFBLD, IFNET, IFMFLP, IFCHTB, IFKTB, IFGRAV, IFMTB

*-----

*-----

*-----

INITIAL

NOSORT

*-----

*-----

* ____ Run control parameters

*-----

PARAM IFBLD=1, IFMFLP=1, IFCHTB=1, IFKTB=0, IFGRAV=1, IFMTB=0

PARAM IFTCOR=0, IFNET=0

PARAM READEL=1800.

PARAM STDAY=0., STHOUR=0.

TIMER TIME=57600., FINTIM=403200., PRDEL=3600.

*TIMER TIME=57600., FINTIM=59400., PRDEL=600.

METHOD MILNE

*_____Parameters
*-----
*_____geometry parameters
PARAM N=25, NN=11
*_____soil composition parameters
PARAM F01 =0.01
PARAM FC1 =0.037
PARAM FQ1 =0.347
PARAM POR1 =0.566
PARAM BDSTAN=1300.
TABLE BD(1-25)=25*1300.
*_____soil radiation parameters
PARAM EWET=0.94, EDRY=0.91, AWET=0.13, ADRY=0.31, WCRITA=0.26
PARAM LONREF=0.10, EMIASS=1.0
*_____Soil hydraulic parameters
PARAM SCALE=1.
PARAM MFA = 150.4E-6
PARAM MFB = 0.167
PARAM WSAT1 =0.44
PARAM WRES1 =0.00
PARAM VGA1 =1.307E-4
PARAM VGN1 =1.2814
PARAM KSAT1 =1.41E-8
PARAM A =0.10
PARAM BCARY =1.0
*_____Soil thermal parameters
PARAM GC =0.0 , GO =0.5
PARAM GQ =0.14 , GW =0.14
PARAM GA =0.2
*_____Atmospheric parameters
PARAM YUC=0.2
PARAM CORIOL=1.37E-4, ALPHA=4.E-4, ATPRES=1.E5
PARAM ZNOT=0.0005 , UG=10.0, VG=0.0
*_____sky parameters
PARAM SKYA=0.65, SKYB=0.04, CLON=0.10, SKYTEM=0.0

*_____Functions

*-----
FUNCTION GLORTB= 57600.,430., 61200.,340., 64800.,210., ...
68400.,080., 72000.,010., 75600.,000., ...
100800.,000., 104400.,070., 108000.,170., ...
111600.,310., 115200.,450., 118800.,570., ...
122400.,670., 126000.,740., 129600.,770., ...
133200.,750., 136300.,690., 140400.,600., ...
144000.,480.

FUNCTION CHTB= 00.,0.25, 0.48,1.60

FUNCTION VPDSTB= 00.,4.84E-3 , 02.,5.55E-3 ,...
04.,6.35E-3 , 06.,7.25E-3 ,...
08.,8.26E-3 , 10.,9.38E-3 ,...
12.,1.06E-2 , 14.,1.21E-2 ,...
15.,1.36E-2 , 18.,1.53E-2 ,...
20.,1.73E-2 , 22.,1.94E-2 ,...

24., 2.17E-2	,	26., 2.43E-2	, ...
28., 2.72E-2	,	30., 3.03E-2	, ...
32., 3.37E-2	,	34., 3.75E-2	, ...
36., 4.16E-2	,	38., 4.61E-2	, ...
40., 5.10E-2	,	42., 5.64E-2	, ...
44., 6.22E-2	,	46., 6.85E-2	, ...
48., 7.55E-2	,	50., 8.24E-2	, ...
52., 9.06E-2	,	54., 9.93E-2	, ...
56., 1.09E-1	,	58., 1.18E-1	, ...
60., 1.29E-1	,	62., 1.41E-1	, ...
64., 1.54E-1	,	66., 1.67E-1	

FUNCTION PSIHTB= -3., 2.77,
-1.5, 2.2,
-0.5, 1.39,
-0.1, 0.53,
1.0,-4.7

-2., 2.43, ...
-1., 1.83, ...
-.25, 0.96, ...
.00, 0.00, ...

FUNCTION PSIMT3= -3.0, 1.74,
-1.5, 1.34,
-0.5, 0.79,
-0.1, 0.28,
1.0,-4.70

-2.0, 1.5, ...
-1.0, 1.12, ...
-.25, 0.54, ...
0.00, 0.00, ...

*-----Physical constants

CONSTANT	BOLZ	=5.67E-3	,	CHA	=25.E-3	,	CHC	=2.9
CONSTANT	CHO	=0.25	,	CHQ	=8.8	,	CHW	=0.57
CONSTANT	DNOT	=2.29E-5	,	G	=9.8	,	HCC	=2.4E6
CONSTANT	HCO	=2.5E6	,	HCQ	=2.1E6	,	HCW	=4.2E6
CONSTANT	KAR	=0.41	,	LVAP	=2.454E6	,	MH20	=18.E-3
CONSTANT	PSCH	=66.0	,	RGAS	=8.31	,	RHOCP	=1.2E3
CONSTANT	RHOAIR	=1.2	,	CP	=1.0E3	,	TZERO	=273.2
CONSTANT	RHOL	=1.0E3	,	PI	=3.14	,	HCA	=1.2E3
CONSTANT	MAIR	=28.8E-3	,	RHOCLY	=2650.			

*-----100-----Initial conditions and static boundary conditions; atmosphere

TABLE QI(1-11)	=	5*.013,.012,.011,.009,.004,2*.001
TABLE VI(1-11)=	1.11,1.57,1.89,2.15,2.33,2.30,1.59,-.39,-.99,-.06,-.06	
TABLE UI(1-11)=	2.76,3.99,4.93,5.86,6.94,8.3,9.9,10.5,3*10.0	

TABLE TPI(1-11) = 11*20.

TABLE TKEI(1-11)=.33,.51,.57,.54,.48,.38,.22,.075,.006,.001,.0005

U1	=	UI(1)
Q1	=	QI(1)
T1	=	TPI(1)

TABLE UVOLX(1-11)	=	11*0.01
TABLE VVOLX(1-11)	=	11*0.01
TABLE TPFLX(1-11)	=	11*0.01
TABLE QFLX(1-11)	=	11*0.00
TABLE UVOLX(12)	=	0.0
TABLE VVOLX(12)	=	0.0
TABLE TPFLX(12)	=	0.0

TABLE QFLX(12) = 0.0
TABLE TKEFLX(12) = 0.0
TABLE EPRSRX(12) = 0.0
TABLE EPRSRY(12) = 0.0
TABLE EPRBU0(12) = 0.0
TABLE TKEFLX(1) = 0.0
INCON RAM = 100.
INCON H = 10.
INCON V1 = 0.

*____ 200 Initial conditions and static boundary conditions; soil

*-----
TS = 30.
TABLE WI(1-25) = 25*0.38
TABLE TI(1-10) = 31., 31., 30., 30., 29., 28.3, 27.7, 27.2, 26.3, 25.3
TABLE TI(11-20) = 23.4, 22.2, 21.4, 20.8, 20., 19.3, 19.3, 19.1, 19., 18.8
TABLE TI(21-25) = 18.1, 17.3, 17.3, 17.3, 17.3
TABLE WFLX(26) = 0.0
TABLE HFLX(26) = 0.0

*____ 300 Auxiliary state variables; atmosphere

*-----
INVCOR = CORIOL/(ALPHA*ABS(UG))

*____ 400 Auxiliary state variables; soil

*-----
* dry soil composition
DO 400 I=1,N

BDRAT(I) = BD(I)/BDSTAN

400 CONTINUE

DO 410 I=1,N

FC(I) = FC1*BDRAT(I)

FO(I) = FO1*BDRAT(I)

FQ(I) = FQ1*BDRAT(I)

POR(I) = 1.-FC(I)-FO(I)-FQ(I)

410 CONTINUE

*____ soil hydraulic properties

DO 420 I=1,N

WSAT(I) = WSAT1

WRES(I) = WRES1

VGA(I) = VGA1

VGN(I) = VGN1

VGM(I) = 1.-1./VGN(I)

KSAT(I) = KSAT1

HRH(I) = RHOL/(A*FC(I)*RHOCLY)

W30(I) = 1./HRH(I)

WREL15(I) = (((VGA(I)*15.0E05)**VGN(I))+1.)*...
(-VGM(I))

W15(I) = (WSAT(I)-WRES(I))*WREL15(I)+WRES(I)

420 CONTINUE

```

*---- soil thermal properties De Vries model
  IF(IFCHTB.EQ.1) GOTO 500

430   KAW      = 0.66/(1.+((CHA/CHW)-1.)*GA)+0.33/ ...
          (1.+((CHA/CHW)-1.)*(1.-2.*GA))
  KQW      = 0.66/(1.+((CHQ/CHW)-1.)*GQ)+0.33/ ...
          (1.+((CHQ/CHW)-1.)*(1.-2.*GQ))
  KOW      = 0.66/(1.+((CHO/CHW)-1.)*GO)+0.33/ ...
          (1.+((CHO/CHW)-1.)*(1.-2.*GO))
  KCW      = 0.66/(1.+((CHC/CHW)-1.)*GC)+0.33/ ...
          (1.+((CHC/CHW)-1.)*(1.-2.*GC))
  KWA      = 0.66/(1.+((CHW/CHA)-1.)*GW)+0.33/ ...
          (1.+((CHW/CHA)-1.)*(1.-2.*GW))
  KQA      = 0.56/(1.+((CHQ/CHA)-1.)*GQ)+0.33/ ...
          (1.+((CHQ/CHA)-1.)*(1.-2.*GQ))
  KOA      = 0.66/(1.+((CHO/CHA)-1.)*GO)+0.33/ ...
          (1.+((CHO/CHA)-1.)*(1.-2.*GO))
  KCA      = 0.66/(1.+((CHC/CHA)-1.)*GC)+0.33/ ...
          (1.+((CHC/CHA)-1.)*(1.-2.*GC))

  DO 440 I=1,N
  CHSL02(I) = 1.25*(KWA*.02*CHW+KOA*FO(I)*CHO+KQA...
          *FQ(I)*CHQ+KCA*FC(I)*CHC+(POR(I)- ...
          .02)*CHA)/(KWA*.02+KOA*FO(I)+KQA*...
          FQ(I)+KCA*FC(I)+(POR(I)-0.02))
  CHSL05(I) = (.05*CHW+KOW*FO(I)*CHO+KQW*FQ(I)*CHQ...
          +KCW*FC(I)*CHC+KAW*(POR(I)-.05)*CHA)/...
          (.05+KOW*FO(I)+KQW*FQ(I)+KCW*FC(I)+ ...
          KAW*(POR(I)-.05))
  KFCSA(I) = KOA*FO(I)*CHO+KQA*FQ(I)*CHQ+KCA*FC(I)*CHC
  KFSAC(I) = KOA*FO(I)+KQA*FQ(I)+KCA*FC(I)
  KFCSW(I) = KOW*FO(I)*CHO+KQW*FQ(I)*CHQ+KCW*FC(I)*CHC
  KFSW(I)  = KOW*FO(I)+KQW*FQ(I)+KCW*FC(I)

440   CONTINUE

```

*---- 500 __discretisation; atmosphere

```

*-----500 CONTINUE
  TABLE TCMM(1-5)      = 3.,6.,12.,24.,48.
  TABLE TCMM(6-11)     = 96.,192.,384.,768.,1536.,3072.
  ZZ(1)                = 0.5*TCMM(1)
  SUM                  = 0.0
  DO 510 I=2,NN
  ZZ(I)                = SUM+TCMM(I-1)
  SUM                  = ZZ(I)

510   CONTINUE
  DZZ(1)               = 0.5*TCMM(1)
  DO 520 I=2,NN
  DZZ(I)               = 0.5*(TCMM(I-1)+TCMM(I))

520   CONTINUE

```

*---- 600 __discretisation; soil

```

*-----600 CONTINUE
  TABLE TCM(1-10)      = 3*2.E-3,3*3.E-3,3*4.E-3,5.E-3
  TABLE TCM(11-20)     = 2*5.E-3,3*10.E-3,3*20.E-3,30.E-3,40.E-3
  TABLE TCM(21-25)     = 5*60.E-3

```

```
DZ(1) = 0.5*TCM(I)
DO 610 I=2,N
DZ(I) = 0.5*(TCM(I)+TCM(I-1))
610 CONTINUE

*____700____opening of access files
*-----CALL OPENS

*-----DYNAMIC NOSORT
*-----800____dynamic boundary conditions
*-----IF(KEEP.EQ.0.AND.IFBLD.EQ.1) GOTO 900
IF(IMPULS(0.,READEL).EQ.0.AND.IFBLD.EQ.1) GOTO 900
IF(KEEP.EQ.0.AND.IFBLD.EQ.0) GOTO 950
IF(IMPULS(0.,READEL).EQ.0.AND.IFBLD.EQ.0) GOTO 950
IF(IFBLD.EQ.0) GOTO 350
RADTIM=57600.+AMOD((TIME-57600.),86400.)
GLORAD=AFGEN(GLORTB,RADTIM)
* CLOC = AFGEN(CLOCTB,TIME)
CLOC=0.
VPA = (8./5.)*Q(1)*ATPRES
EMISKY = (SKYA+SKYB*(SQRT(0.01*VPA)))*(1.+CLON*...
          CLOC*CLOC)
LONGIN = EMISKY*BOLZ*((TP(1)+TZERO)**4)
GOTO 900

850 READ(50,860) GLORAD,T1,VPA,U1,RAIN,CLOC
860 FORMAT(21X,6F)
Q1=(VPA/ATPRES)*(5./8.)
EMISKY=(SKYA+SKYB*SQRT(0.01*VPA))*(1.+CLON*CLOC*CLOC)
LONGIN=EMISKY*BOLZ*((T1+TZERO)**4)

*____rain
WFLIN=0.
GOTO 950

*____900____transport coefficients, auxiliary state variables; atmosphere
*-----option: boundary layer development
*-----stability at interfaces
900 TPAV(1) = 0.5*(TS+TP(1))
DO 905 I=2,NN
TPAV(I) = (TP(I)*TCMM(I)+TP(I-1)*TCMM(I-1))/ ...
           (TCMM(I)+TCMM(I-1))
905 CONTINUE
```

```
DO 930 I=1,NN
RMOFLX(I)      = SQRT(UVOFLX(I)**2+VVOFLX(I)**2)
OBU(I)          = (TPAV(I)+TZERO)*((ABS(RMOFLX(I)))** ...
                 1.5)/(KAR*G*TPFLX(I))
STAPAR(I)       = ZZ(I)/OBU(I)
IF(I.EQ.1) STAPAR(I)=0.5*STAPAR(I)
IF(STAPAR(I).LT.-3.) STAPAR(I)=-3.
IF(STAPAR(I).GT.1.0) STAPAR(I)=1.0
IF(STAPAR(I).GE.0.0) GOTO 910
PHIM(I)         = (1.-16.*STAPAR(I))**(-0.25)
PHIH(I)         = PHIM(I)*PHIM(I)
GOTO 920
910  PHIM(I)       = 1.+4.7*STAPAR(I)
PHIH(I)         = PHIM(I)
920  INVLM(I)     = PHIM(I)/(KAR*ZZ(I))+INVCOR
INVLH(I)        = PHIH(I)/(KAR*ZZ(I))+INVCOR
930  CONTINUE
```

*----- Local turbulent transport coefficients at interfaces

```
DO 940 I=2,NN
TKEAV(I)        = (TCMM(I)*TKE(I)+TCMM(I-1)*TKE(I-1))/ ...
                  (TCMM(I)+TCMM(I-1))
KM(I)           = (1./INVLM(I))*((YUC*TKEAV(I))**0.5)
IF(TKEAV(I).LE.0.) KM(I)=0.0
KH(I)           = KM(I)*INVLM(I)/INVLH(I)
KV(I)           = KH(I)
940  CONTINUE
GOTO 960
```

*----- option: no boundary layer development

```
950  TPAV(1)        = 0.5*(TS+T1)
      TPFLX(1)      = H/(RHOAIR*CP)
      RMOFLX(1)     = U1/RAM
      OBU(1)         = (TPAV(1)+TZERO)*(ABS(RMOFLX(1))**1.5)/ ...
                        (KAR*G*TPFLX(1))
      STAPAR(1)      = 0.5*ZZ(1)/OBU(1)
      IF(STAPAR(1).LT.-3.) STAPAR(1)=-3.
      IF(STAPAR(1).GT.1.0) STAPAR(1)=1.0
```

*----- surface exchange coefficients (integrated profiles Paulson)

```
960  PSIM            = AFGEN(PSIMTB,STAPAR(1))
      PSIH            = AFGEN(PSIHTB,STAPAR(1))
      SURWIN          = SQRT(U1*U1+V1*V1)
      RAM             = ((ALOG(ZZ(1)/ZNOT)-PSIM)**2)/(SURWIN* ...
                        KAR**2)
      RAH             = (ALOG(ZZ(1)/ZNOT)-PSIH)*(ALOG(ZZ(1)/ ...
                        ZNOT)-PSIM)/(SURWIN*KAR**2)
      RAV             = RAH
```

```
*_____1000 Transport coefficients, auxiliary state variables; soil water
*-----
*_____Soil vapour state profile
1000 DO 1020 I=1,N
      VPDS(I) = AFGEN(VPDSTB,T(I))
      IF (W(I).LT.W15(I)) GOTO 1005
      RH(I) = 1.0
      GOTO 1015
1005 IF (W(I).LT.W30(I)) GOTO 1010
      RH(I) = 0.3+0.2*(W(I)-W30(I))/(W15(I)-W30(I))
      GOTO 1015
1010 RH(I) = HRH(I)*W(I)*0.8
1015 VPD(I) = RH(I)*VPDS(I)
1020 CONTINUE
      RHS = RH(1)

*_____effective vapour diffusivity
      DO 1025 I=1,N
      DATM(I) = DNOT*((T(I)+TZERO)/TZERO)**1.75
1025 CONTINUE
      DO 1030 I=2,N
      DAV(I) = BCARY*(DATM(I)+DATM(I-1))/2.
1030 CONTINUE

*_____Soil water pressure
      IF (IFMFLP.EQ.1.AND.IFGRAV.EQ.0) GOTO 1080
      DO 1035 I=1,N
      WREL(I) = (W(I)-WRES(I))/(WSAT(I)-WRES(I))
1035 CONTINUE
      IF (IFMFLP.EQ.1) GOTO 1050
      DO 1045 I=1,N
      IF (W(I).LT.W15(I)) GOTO 1040
      P(I) = -(1./VGAC(I))*(WREL(I)**(-1./VGM(I))-1.)...
              **(1./VGN(I))
      GOTO 1045
1040 P(I) = RHOL*RGAS*(T(I)+TZERO)*(ALOG(RH(I)))/MH20
1045 CONTINUE
      DO 1047 I=1,N
      P(I) = P(I)/SCALE
1047 CONTINUE

*_____Hydraulic conductivity Van Genuchten-Mualem
1050 IF (IFKTB.EQ.1) GOTO 1060
      DO 1055 I=1,N
      IF (W(I).LE.WRES(I)) K(I)=0.0
      IF (W(I).GT.WRES(I)) K(I)=KSAT(I)*SQR(WREL(I))*...
              (1.-(1.-WREL(I)**(1./VGM(I)))**VGM(I))...
              **2.
1055 CONTINUE
      GOTO 1070
*_____Hydraulic conductivity from table
1060 DO 1065 I=1,N
      K(I) = AFGEN(KTB,W(I))
1065 CONTINUE
```

```
1070 KAV(1) = 0.0
      DO 1075 I=2,N
      KAV(I) = (SCALE**2)*SQRT(K(I-1)*K(I))
1075 CONTINUE
      KAV(N+1)=(SCALE**2)*K(N)
      IF (IFMFLP.EQ.0) GOTO 1100
*---- MFLP profile, rational expression
1080 IF (IFMTB.EQ.1) GOTO 1090
      DO 1085 I=1,N
      MFLP(I) = -SCALE*MFA*(1.-WREL(I))/(MFB+1.-WREL(I))
1085 CONTINUE
      GOTO 1100
*---- MFLP from table
1090 DO 1095 I=1,N
      MFLP(I) = SCALE*AFGEN(MTB,W(I))
1095 CONTINUE

*---- 1100 Transport coefficients, auxiliary state variables- soil heat
*-----
*---- soil heat capacity
1100 DO 1105 I=1,N
      HCSOIL(I) = FC(I)*HCC+FQ(I)*HCQ+FO(I)*HCO+W(I)*HCW
1105 CONTINUE

*---- soil thermal conductivity, De Vries
1110 IF (IFCHTB.EQ.1) GOTO 1150
      DO 1140 I=1,N
      FA(I) = POR(I)-W(I)
      IF (W(I).GT.0.02) GOTO 1120
      CHSOIL(I) = 1.25*(CHW*W(I)*KWA+FA(I)*CHA+KFCSA(I))/...
                   (KFSAC(I)+KWA*W(I)+FA(I))
      GOTO 1140
1120 IF (W(I).GT.0.05) GOTO 1130
      CHSOIL(I) = CHSL02(I)+(W(I)-0.02)*(CHSL05(I)-
                   CHSL02(I))/0.03
      GOTO 1140
1130 CHSOIL(I) = W(I)*CHW+FA(I)*KAW*CHA+KFCSW(I)/...
                   (W(I)+KAW*FA(I)+KFSW(I))
1140 CONTINUE
      GOTO 1170
*---- soil thermal conductivity from table
1150 DO 1160 I=1,N
      CHSOIL(I) = BDRAT(I)*AFGEN(CHTB,W(I))
1160 CONTINUE
*---- local average soil thermal conductivity
1170 CHAV(1) = CHSOIL(1)
      DO 1180 I=2,N
      CHAV(I) = (CHSOIL(I-1)*TCM(I-1)+CHSOIL(I)*TCM(I))...
                   /(TCM(I-1)+TCM(I))
1180 CONTINUE
```

*---- 1200 Implicit calculation surface energy balance

```
ALB = AWET+(ADRY-AWET)*(WCRITA-W(1))/WCRITA
IF(W(1).GT.WCRITA) ALB=AWET
EMISOI = EDRY+(EWET-EDRY)*W(1)/WSAT(1)
TSO = T(1)
TS = IMPL(TSO,0.1,FOTS)
H = RHOAIR*CP*(T1-TS)/RAH
RADEMI = -EMISOI*BOLZ*(TS+TZERO)**4
NETRAD = (1.-ALB)*GLORAD+(1.-LONREF)*LONGIN+RADEMI
IF (IFNET.EQ.1) NETRAD=NETREA
FOTS = (NETRAD+H)/(CHSOIL(1)/DZ(1))+T(1)
QS = RHS*AFGEN(VPDSTB,T(1))/RHOAIR
E = RHOAIR*(Q1-QS)/RAV
LE = LVAP*E
TSAPP = ((-RADEMI+(1.-EMISOI)*BOLZ*(SKYTEM
+TZERO)**4)/(EMIASS*BOLZ))**0.25-TZERO ...
```

*---- 1300 Fluxes and rates of change; atmosphere

```
IF(IFBLD.EQ.0) GOTO 1400
UVOLX(1) = U(1)/RAM
VVOLX(1) = V(1)/RAM
TPFLX(1) = H/(RHOAIR*CP)
QFLX(1) = E/RHOAIR
TKEFLX(1) = 0.0
DO 1310 I=2,NN
UVOLX(I) = KM(I)*(U(I)-U(I-1))/DZZ(I)
VVOLX(I) = KM(I)*(V(I)-V(I-1))/DZZ(I)
TPFLX(I) = KH(I)*(TP(I)-TP(I-1))/DZZ(I)
QFLX(I) = KH(I)*(G(I)-Q(I-1))/DZZ(I)
TKEFLX(I) = KM(I)*(TKE(I)-TKE(I-1))/DZZ(I)
```

1310 CONTINUE

*---- flux divergencies atmosphere

```
DO 1320 I=1,NN
DIVUVOC(I) = (UVOLX(I+1)-UVOLX(I))/TCMM(I)
DIVVVC(I) = (VVOLX(I+1)-VVOLX(I))/TCMM(I)
DIVTPC(I) = (TPFLX(I+1)-TPFLX(I))/TCMM(I)
DIVTKEC(I) = (TKEFLX(I+1)-TKEFLX(I))/TCMM(I)
DIVQC(I) = (QFLX(I+1)-QFLX(I))/TCMM(I)
```

1320 CONTINUE

*---- acceleration by pressure gradient

```
DO 1330 I=1,NN
ACCPRY(I) = -CORIOL*(U(I)-UG)
ACCPRX(I) = +CORIOL*(V(I)-VG)
```

1330 CONTINUE

*---- turbulent kinetic energy production (J/(kg.s))

*---- EFRSRX, EPRSRY, EPRBVO at interfaces, EPRDIS at centres

```
DUDZZ(1) = U(1)/DZZ(1)
DVDZZ(1) = V(1)/DZZ(1)
DO 1340 I=2,NN
DUDZZ(I) = (U(I)-U(I-1))/DZZ(I)
DVDZZ(I) = (V(I)-V(I-1))/DZZ(I)
```

1340 CONTINUE

```
DO 1350 I=1,NN
EPRS RX(I) = (UV OFLX(I)*DUDZZ(I)*DZZ(I)+UV OFLX(I+1)*...
              DUDZZ(I+1)*DZZ(I+1))/(DZZ(I)+DZZ(I+1))
EPRS RY(I) = (VV OFLX(I)*DVDZZ(I)*DZZ(I)+VV OFLX(I+1)*...
              DVDZZ(I+1)*DZZ(I+1))/(DZZ(I)+DZZ(I+1))
EPRBUO(I) = -(TPFLX(I)*DZZ(I)+TPFLX(I+1)*DZZ(I+1))*...
              G/((TP(I)+TZERO)*(DZZ(I)+DZZ(I+1)))
EPRDIS(I) = -((YUC*TKE(I))**1.5)*(INVLM(I)+...
              INVLM(I+1))/2.
1350 CONTINUE
EPRDIS(I) = -((YUC*TKE(1))**1.5)*INVLM(1)

*-----rates of change main state variables; atmosphere
DO 1360 I=1,NN
TKERCH(I) = EPRS RX(I)+EPRS RY(I)+EPRBUO(I)+...
              EPRDIS(I)+DIVTKE(I)
URCH(I) = ACCPRX(I)+DIVUV0(I)
VRCH(I) = ACCPRY(I)+DIVVVO(I)
TPRCH(I) = DIVTP(I)
QRCH(I) = DIVQ(I)
1360 CONTINUE

*-----1400 Fluxes and rates of change; soil water
*-----soil vapour flux
1400 WFLVAP(1) = -E
DO 1405 I=2,N
WFLVAP(I) = DAV(I)*(VPD(I)-VPD(I-1))/DZ(I)
1405 CONTINUE

*-----liquid flux
WFLLIQ(1) = -WFLIN
*-----liquid flux k-p option
IF (IFMFLP.EQ.1) GOTO 1420
DO 1410 I=2,N
WFLLIQ(I) = -KAV(I)*((P(I-1)-P(I))/DZ(I)+RHOL*G)
1410 CONTINUE
WFLLIQ(N+1) = -KAV(N+1)*RHOL*G
GOTO 1460
*-----liquid flux, MFLP option, gravity included
1420 IF (IFGRAV.EQ.0) GOTO 1440
DO 1430 I=2,N
WFLLIQ(I) = (MFLP(I)-MFLP(I-1))/DZ(I)-KAV(I)*RHOL*G
1430 CONTINUE
WFLLIQ(N+1) = -KAV(N+1)*RHOL*G
GOTO 1460
*-----liquid flux, MFLP option, no gravity
1440 DO 1450 I=2,N
WFLLIQ(I) = (MFLP(I)-MFLP(I-1))/DZ(I)
1450 CONTINUE

*-----total water flux
1460 DO 1470 I=1,N+1
WFLX(I) = WFLLIQ(I)+WFLVAP(I)
1470 CONTINUE
```

*_____ flux divergence and rate of change of soil water content

DO 1480 I=1,N
DIVWFL(I) = (WFLX(I+1)-WFLX(I))/TCM(I)
WRCH(I) = DIVWFL(I)/RHOL

1480 CONTINUE

*____ 1500 ____ Fluxes and rate of change ; soil heat

*-----

*____ conduction

HFLCON(1) = -(TS-T(1))*CHSOIL(1)/DZ(1)
DO 1500 I=2,N
HFLCON(I) = CHAV(I)*(T(I)-T(I-1))/DZ(I)

1500 CONTINUE

*____ latent heat

*____ HFLVAP(1) was NOT covered as part of the surface energy balance

DO 1510 I=1,N
HFLVAP(I) = LVAP*WFLVAP(I)

1510 CONTINUE

*____ total soil heat flux

DO 1520 I=1,N
HFLX(I) = HFLCON(I)+HFLVAP(I)

1520 CONTINUE

*____ flux divergence and rate of change soil temperature

DO 1530 I=1,N
DIVHFL(I) = (HFLX(I+1)-HFLX(I))/TCM(I)
TRCH(I) = DIVHFL(I)/HCSOIL(I)

1530 CONTINUE

GFLX = HFLCON(1)+HFLVAP(1)

*____ 1600 ____ Output and disposal

*-----

IF (KEEP.EQ.0) GOTO 1700

TSINT = TSINT+TSAPP*DELT
RNINT = RNINT+NETRAD*DELT
GINT = GINT+GFLX*DELT
HINT = HINT+H*DELT
LEINT = LEINT+LE*DELT
SUMTIM = SUMTIM+DELT
IF (IMPULS(0.,PRDEL).EQ.0) GOTO 1700

HOURS=STHOUR+TIME/3600.

HOUR=AMOD(HOURS,24.)

DAY=STDAY+HOURS/24.

TYPE 1603, DAY,HOUR,DELT

1603 FORMAT(X,F6.2,X,F6.2,X,F6.2)

* calculation integrated output variables

TSPRI = TSINT/SUMTIM
RNPRI = RNINT/SUMTIM
GPRI = GINT/SUMTIM
HPRI = HINT/SUMTIM
LEPRI = LEINT/SUMTIM
BOW = 0.
IF(HOUR.GT.8.AND.HOUR.LT.20.) BOW=HPRI/LEPRI

```
1640 WRITE(51,1640) DAY,HOUR,TSAPP,NETRAD,GFLX,H,LE,T1,SURWIN,Q1,BOW
      FORMAT(F7.3,X,F4.1,X,F5.2,X,4(F7.2,X),F4.1,X,F5.2,X,F6.4,X,F5.2)
      WRITE(51,1641) (W(I),I=1,25)
1641 FORMAT(25(F4.3,X))
1642 WRITE(51,1642) (WFLLIQ(I),I=1,12)
1642 FORMAT(12(E9.2,X))
      WRITE(51,1642) (VPD(I),I=1,12)
      WRITE(51,1642) (HFLVAP(I),I=1,12)
      WRITE(51,1642) (HFLVAP(I),I=1,12)
      WRITE(51,1643) (T(I),I=1,25)
      WRITE(51,1642) (HFLCON(I),I=1,12)
1643 FORMAT(25(F4.1,X))

*   reset integrals of print variables
TSINT          = 0.
RNINT          = 0.
GINT           = 0.
HINT           = 0.
LEINT          = 0.
SUMTIM         = 0.
```

*-----1700---Integration of rates of change

```
*-----1700 CONTINUE
      U          = INTGRL(UI,URCH,11)
      V          = INTGRL(VI,VRCH,11)
      TP         = INTGRL(TPI,TPRCH,11)
      Q          = INTGRL(QI,QRCH,11)
      TKE        = INTGRL(TKEI,TKERCH,11)
      W          = INTGRL(WI,WRCH,25)
      T          = INTGRL(TI,TRCH,25)
      IF(IFBLD.EQ.0) GOTO 1710
      U1         = U(1)
      V1         = V(1)
      Q1         = Q(1)
      T1         = TP(1)
```

1710 CONTINUE

```
*-----TERMINAL
CALL CLOSES
CALL OPENS
* END RERUN .....
END
STOP
```

```
SUBROUTINE OPENS
OPEN (UNIT=50,ACCESS='SEQIN',FILE='METEO.IN')
OPEN (UNIT=51,ACCESS='APPEND',MODE='ASCII',FILE='MONT.OUT')
RETURN
END
```

```
SUBROUTINE CLOSES
CLOSE(UNIT=50,FILE='METEO.IN')
CLOSE(UNIT=51,FILE='MONT.OUT')
RETURN
END
```

ENDJOB

APPENDIX 2 Algorithm for the calculation of soil thermal conductivity according to the De Vries (1963) model.

NOSORT
FIXED NCOM, I, NCOM1, NCOM2

STORAGE FC(26), FO(26), FQ(26), POR(26)
STORAGE W(26), CHSOIL(26), CHSL02(26), KFCSA(26), CHSL05(26),...
KFSA(26), KFCSW(26), KFSW(26), FA(26)

TIMER FINTIM=1., DELT=2.

METHOD RECT

PARAM NCOM=25

TABLE W(1-5)=0., 0.02, 0.04, 0.06, 0.08

TABLE W(6-10)=0.10, 0.12, 0.14, 0.16, 0.18

TABLE W(11-15)=0.20, 0.22, 0.24, 0.26, 0.28

TABLE W(16-20)=0.30, 0.32, 0.34, 0.36, 0.38

TABLE W(21-25)=0.40, 0.42, 0.44, 0.46, 0.48

* AD 6 ****Dry soil composition

PARAM FO1 =0.004 , FO2 =0.004

PARAM FC1 =0.1 , FC2 =0.1

PARAM FQ1 =0.31 , FQ2 =0.31

PARAM POR1 =(.59,.58,.55,.54,.53,.51,.50)

* AD 8 ****Soil thermal properties

PARAM GC =0.0 , GO =0.5

PARAM GQ =0.14 , GW =0.14

PARAM GA =0.05

*** 4 *** Physical constants

CONSTANT BOLZ =5.67E-8 , CHA =100.E-3 , CHC =2.9

CONSTANT CHO =0.25 , CHQ =8.8 , CHW =0.57

CONSTANT DNOT =2.29E-5 , G =9.8 , HCC =2.4E6

CONSTANT HCO =2.5E6 , HCQ =2.1E6 , HCW =4.2E6

CONSTANT KAR =0.41 , L =2.454E6 , M =18.E-3

CONSTANT PSCH =66.0 , RGAS =8.31 , RHOCP =1.2E3

CONSTANT RHOL =1.0E3 , VIP =1.002 , HCA =1.2E3

CONSTANT MAIR =28.8E-3 , RHOCLY=2650.

DO 600 I=1,NCOM

FC(I)=FC1

FO(I)=FO1

FQ(I)=FQ1

POR(I)=POR1

600 CONTINUE

** 8 *** Non-dynamic soil thermal properties
* Data and calculation of principal properties, De Vries 1975.

800 KAW =0.66/(1.+((CHA/CHW)-1.)*GA)+0.33/ ...
KQW =0.66/(1.+((CHQ/CHW)-1.)*(1.-2.*GA)) ...
KOW =0.66/(1.+((CHO/CHW)-1.)*(1.-2.*GQ)) ...
KCW =0.66/(1.+((CHC/CHW)-1.)*(1.-2.*GC)) ...
KWA =0.66/(1.+((CHW/CHA)-1.)*GW)+0.33/ ...
KQA =0.66/(1.+((CHQ/CHA)-1.)*GQ)+0.33/ ...
KOA =0.66/(1.+((CHO/CHA)-1.)*GO)+0.33/ ...
KCA =0.66/(1.+((CHC/CHA)-1.)*GC)+0.33/ ...
DO B10 I=1,NCOM
CHSL02(I) =1.25*(KWA*.02*CHW+KOA*FO(I)*CHO+KQA*FQ(I)*...
CHQ+KCA*FC(I)*CHC+(POR(I)-.02)*CHA)/(KWA* ...
.02+KOA*FO(I)+KQA*FQ(I)+KCA*FC(I)+(POR(I) ...
-.02))
CHSL05(I) =(.05*CHW+KOW*FO(I)*CHO+KQW*FQ(I)*CHQ+KCW* ...
FC(I)*CHC+KAW*(POR(I)-.05)*CHA)/(.05+KOW* ...
FO(I)+KQW*FQ(I)+KCW*FC(I)+KAW*(POR(I)-.05))
KFCSA(I) =KOA*FO(I)*CHO+KQA*FQ(I)*CHQ+KCA*FC(I)*CHC

** 14 *** Calculation of the thermal conductivity profile

1401 DO 1420 I=1,26
FA(I) =POR(I)-W(I)
IF (W(I).GT.0.02) GO TO 1400
CHSOIL(I) =1.25*(CHW*W(I)*KWA+FA(I)*CHA+KFCSA(I))/ ...
(KFSW(I)+KWA*W(I)+FA(I))
GO TO 1420
1400 IF (W(I).GT.0.05) GO TO 1410
CHSOIL(I) =CHSL02(I)+(W(I)-.02)*(CHSL05(I)-CHSL02(I))...
/0.03
GO TO 1420
1410 CHSOIL(I) =W(I)*CHW+FA(I)*KAW*CHA+KFCSW(I)/ ...
(W(I)+KAW*FA(I)+KFSW(I))
1420 CONTINUE

TERMINAL
NOSORT
TYPE 1111, (W(I),CHSOIL(I),I=1,25)
1111 FORMAT(F4.2,2X,F5.2)
END
STOP
ENDJOB

$$(dP)_S = \left(\frac{\partial P}{\partial T}\right)_S dT = \frac{\Delta \overline{H}_a}{V} dT$$

APPENDIX 3 On the derivation of equation 3.59

For the interfacial region, the second law of thermodynamics states:

$$(A3.1) \quad dU = TdS - PdV + \gamma dA$$

where U is the internal energy, S is the entropy, V the volume and A the interfacial area. The interfacial tension γ is defined as the interfacial free Helmholtz energy per unit of surface area:

$$(A3.2) \quad \gamma = \left(\frac{\partial F}{\partial A}\right)_{V,T}$$

where F is defined as:

$$(A3.3) \quad F = U - TS$$

At constant moisture content and neglecting changes in density ($dV = 0$), a change in free energy may be written as:

$$(A3.4) \quad dF = \left(\frac{\partial F}{\partial T}\right)_{A,V} dT + \left(\frac{\partial F}{\partial A}\right)_{T,V} dA = -SdT + \gamma dA$$

Using Cauchy's rule for cross differentiation, it follows that

$$(A3.5) \quad -\left(\frac{\partial S}{\partial A}\right)_T = \left(\frac{\partial \gamma}{\partial T}\right)_A$$

Combination of (A3.2), (A3.3) and (A3.5) finally results in

$$(A3.6) \quad \gamma = \left(\frac{\partial U}{\partial A}\right)_{V,T} + T\left(\frac{\partial \gamma}{\partial T}\right)_{V,A}$$

where the first term on the RHS is the interfacial energy, and the second term is the latent heat of interface formation, L_i :

$$(A3.7) \quad L_i \equiv T\left(\frac{d\gamma}{dT}\right)_{V,A} = -T\left(\frac{dS}{dA}\right)_{V,T} \quad J \text{ m}^{-2}$$

For incomplete wetting and in the absence of wetting angle hysteresis, Young's law relates the wetting angle ϕ for a three-component system to the respective interfacial tensions:

$$(A3.8) \quad \cos \phi = \frac{\gamma_{sl} - \gamma_{sg}}{\gamma_{lg}}$$

Now if the above is applied to the soil-water-air system, combination of eq. (A3.8) with eq. (3.55) and differentiation to T gives:

$$(A3.9) \quad \left(\frac{\partial p}{\partial T}\right)_\theta = \frac{-2}{R} \cos \phi \frac{d\gamma_{lg}}{dT} = \frac{2}{R} \frac{d}{dT} (\gamma_{sl} - \gamma_{sg}) \quad \text{Pa K}^{-1}$$

(It must be realized that p in eq. 3.55 is the pressure equivalent of the potential of water in the duct, i.e. the pressure of free or extrametric water in thermodynamic equilibrium with the water under consideration). According to eq. (A3.7), the latent heat of interface formation can here be written as

$$(A3.10) \quad L_i = T \frac{d}{dT} (\gamma_{sl} - \gamma_{sg}) \quad \text{J m}^{-2}$$

Now combination of (A3.9) and (A3.10) yields

$$(A3.11) \quad \left(\frac{\partial p}{\partial T}\right)_\theta = \frac{2}{R} \frac{L_i}{T} \quad \text{Pa K}^{-1}$$

In this equation, the factor 2/R represents the amount of surface area per unit of volume for a cylinder section. So the heat of interface formation per unit of interface area (L_i in J m^{-2}) is distributed over the total volume of liquid in the duct, to yield the pressure-temperature relationship. Expressed per unit of mass in the duct, the associated change in enthalpy can be written as

$$(A3.12) \quad \frac{2}{\rho R} \frac{L_i}{T} \equiv \frac{\Delta \bar{H}_a}{T} \quad \text{J kg}^{-1} \text{K}^{-1}$$

thereby defining the heat of adsorption or heat of wetting $\Delta \bar{H}_a$. Using this definition, the p-T relation is written as

$$(A3.13) \quad \left(\frac{\partial p}{\partial T}\right)_\theta = \frac{\Delta \bar{H}_a}{VT} \quad \text{Pa K}^{-1}$$

where V is the specific volume of the liquid.

So eq. (3.59) appears as a result of Young's Law, combined with basic interface thermodynamics. It is assumed that the relevant properties can be averaged over all available water in the duct, where a single water phase with pressure p' and entropy S' is present. In that case, as shown in subsection 3.6.1 by making use of the Clapeyron equation, the driving force $\nabla p'$ vanishes.

Now it can also be shown that in a situation where two liquid phases are distinguished in the duct (free or 'extrametric' and adsorbed or 'matric' water), the net result is the same for the hypothetical case that the transport coefficients K of the two phases are identical. The latent heat of interface formation is distributed in that case over only a fraction α of the liquid, and the change in enthalpy per unit volume of liquid is larger by a factor $1/\alpha$. The Clapeyron equation then reads:

$$(A3.14) \quad \frac{dp}{dT} - \frac{dp'}{dT} = \frac{1}{\alpha} \frac{\Delta \bar{H}_a}{VT}$$

where $\Delta \bar{H}_a$ is still defined according to eq. (A3.12), i.e. taking into account all liquid in the considered capillary. Combining (A3.13) with (A3.14) yields

$$(A3.15) \quad \frac{dp'}{dT} = \left(1 - \frac{1}{\alpha}\right) \frac{\Delta \bar{H}_a}{VT} < 0$$

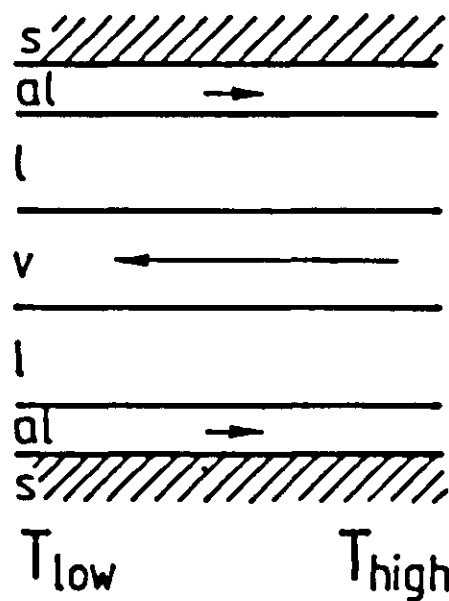
If it is noted that a force $(\partial p / \partial T)VT$ acts upon a fraction $1-\alpha$ of the liquid, and a force $(\partial p' / \partial T)VT$ upon a fraction α , it becomes evident that if the mobility of the liquid is independent of its phase, two equal mass fluxes with contrary directions arise due to the presence of a T-gradient at constant θ :

$$K\alpha\left(1 - \frac{1}{\alpha}\right) \frac{\Delta H_a}{VT} = -K(1-\alpha)\frac{\Delta H_a}{VT}$$

Figure A3.1 visualises the above theory.

thermo-osmosis

$$\nabla p \equiv 0; \nabla \theta \neq 0$$



$$\nabla \theta \equiv 0; \nabla p \neq 0$$

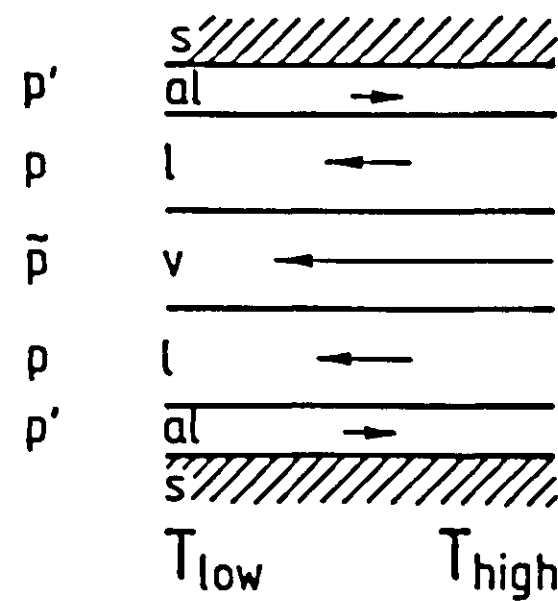


Figure A3.1 Qualitative visualisation of soil water pressure gradients in three distinguished phases, induced by a temperature gradient; arrows indicate the direction of the flow. For the meaning of symbols see text, subsections 3.6.1 and 3.6.3.

APPENDIX 4 Some additional considerations based on TIP

To analyse the relations between liquid fluxes and heat fluxes in a moist soil, use will be made of the framework of Thermodynamics of Irreversible Processes (TIP).

The central equation in TIP is the equation of entropy production (De Groot and Mazur, 1962):

$$(A4.1) \quad T\sigma = - j_s \nabla T - j_w \nabla \mu_w - \frac{1}{T} \frac{dS}{dt} = - j_r \nabla T - j_w \nabla \mu_r$$

where σ is the rate of entropy production per unit volume, j_s is the entropy flux, j_w the water flux and μ_w the chemical potential of the water. Considering again only liquid water and neglecting gravity, equation (A4.1) can be written either as:

$$(A4.2a) \quad T\sigma = - j'_q \frac{\nabla T}{T} - j_1 \bar{V} \nabla p$$

with

$$(A4.3a) \quad j'_q \equiv Tj_s - Tj_1 S$$

or

$$(A4.2b) \quad T\sigma = - j''_q \frac{\nabla T}{T} - j_1 \bar{V}' \nabla p'$$

with

$$(A4.3b) \quad j''_q \equiv Tj_s - Tj_1 S'$$

S , V and p are the partial specific entropy, the specific volume and the pressure of soil water in the free or 'extramatic' state; the corresponding quantities for the adsorbed or 'matric' state are denoted as S' , V' and p' , respectively.

The fluxes j'_q and j''_q are called the reduced heat fluxes. Either one of the two above formulations (2-3a, 2-3b) can be chosen, depending on which water phase one wishes to view as the reference liquid. This choice defines the corresponding reduced heat fluxes. Equations (A4.2) dictate the combina-

tions of fluxes and conjugated forces that should be used to define basic sets of macroscopic fluxes that preserve the entropy production equation and the Onsager reciprocal relations (De Groot and Mazur, 1962; Raats, 1975).

As an example, the simplified case is considered of liquid transfer in a duct where two homogeneous phases exist: a fraction α of the liquid present in the adsorbed ('matric') state with corresponding properties S' and p' , the remainder of the liquid being free with properties S and p . The transfer coefficients are denoted by K' and K respectively. Using eqs. (3.58), (A4.2) and (A4.3), one may then calculate, for both phases separately, the fluxes of mass and entropy, which after summing up finally result in the matrix of 'overall' coefficients for both chosen formulations a and b respectively:

$$\begin{array}{|c|cc|} \hline & -\nabla p \bar{V} & -\nabla T/T \\ \hline j_1 & (1-\alpha)K + \alpha K' & -\alpha K' \frac{\Delta H_a}{\bar{V}} \\ & & \\ j'_q & -\alpha K' \frac{\Delta \bar{H}_a}{\bar{V}} & \lambda T + \left(\frac{\Delta \bar{H}_a}{\bar{V}}\right)^2 \alpha K' \\ \hline \end{array}$$

$$\begin{array}{|c|cc|} \hline & -\nabla p' \bar{V} & -\nabla T/T \\ \hline j_1 & (1-\alpha)K + \alpha K' & (1-\alpha)K \frac{\Delta H_a}{\bar{V}} \\ & & \\ j''_q & (1-\alpha)K \frac{\Delta \bar{H}_a}{\bar{V}} & \lambda T + K(1-\alpha)\left(\frac{\Delta \bar{H}_a}{\bar{V}}\right)^2 \\ \hline \end{array}$$

In this notation, the fluxes (left column) are written as the sum of the conjugated forces (top line), multiplied by the corresponding transport coefficients (the matrix elements).

The cross coefficients should be equal within each of these matrices, in accordance with Onsagers theorem. It must be mentioned that here, contrary to the previous appendix, the difference in enthalpy $\Delta \bar{H}_a$ relates to the 'matric' water only, that is, the total latent heat of interface formation is expressed per unit of mass of 'matric' water. So for any choice of α (ranging from 1 to values approaching 0) the product $\alpha \Delta \bar{H}_a$ should be constant, assuming that enough water is present to have liberated all the latent heat involved.

These matrices can be transformed to determine the transport coefficients in the case where $\nabla \theta$ and $\nabla T/T$ are to be used as the primary driving forces. Using eqs. (3.58), (3.59) and the relation $\nabla p_i = (\partial p_i / \partial \theta)_T \nabla \theta + (\partial p_i / \partial T)_\theta \nabla T$, and assuming for simplicity that

$K = K'$, the following matrices result:

	$-\nabla\theta$	$-\nabla T/T$		$-\nabla\theta$	$-\nabla T/T$
j_1	D	0		D	0
j'_q	$-\alpha K \frac{\Delta \bar{H}}{V} \left(\frac{\partial p}{\partial \theta} \right)_T$	$\lambda T + (1-\alpha) \left(\frac{\Delta \bar{H}}{V} \right)^2 \alpha K$		$(1-\alpha) K \frac{\Delta \bar{H}}{V} \left(\frac{\partial p}{\partial \theta} \right)_T$	$\lambda T + \alpha(1-\alpha)K \left(\frac{\Delta \bar{H}}{V} \right)^2$

The coefficient D is the well known diffusivity defined as $K(\partial p / \partial \theta)$. The vanishing of the upper off diagonal coefficient was the subject of discussion in section 3.6.1. It can be seen that Onsagers reciprocal relations are not valid here, which does not surprise, as the fluxes were not transformed consistently along with the transformation of the forces. Raats (1975) discussed these Meixner transformations in detail. Note that if $0 < \alpha < 1$ and $K' \neq 0$, the reduced heat flux can never be identified with a true conduction flux in either of the cases $\nabla p = 0$, $\nabla p' = 0$, or $\nabla \theta = 0$.

It can be observed that $j'_q = j''_q$ for $\nabla \theta = 0$; this becomes evident when one realizes that for this condition the mass fluxes in both phases are equal, but of opposite direction (The latter was shown in Appendix 3). Consequently, the choice of the reference entropy in the last term on the RHS of eqs (A4.3) does not have influence on the magnitude of the reduced heat flux in this particular situation. If on the other hand $\nabla \theta \neq 0$, it appears that the reduced heat fluxes are not identical. This serves to illustrate that the reduced heat fluxes are not necessarily to be identified with a true sensible heat flux. The latter is only the case if all transported mass finally is brought to the reference state defined by S resp. S' in eqs (A4.3). In physical terms, this will occur when the liquid leaves the system to enter a reservoir with designated entropy.

APPENDIX 5 Heat transfer by convection in the soil under a gradient in virtual temperature

For the sake of completeness it is shown first that evaporation from a subsurface front cannot be maintained by convective heat supply from above as the only energy source.

Virtual temperature can be written as:

$$(A5.1) \quad T_{vi} = \frac{1 + r/\epsilon}{1 + r} \cdot T$$

where r is the mixing ratio (kg water/kg dry air) and $\epsilon (=5/8)$ is the ratio of the molecular weights $M_{\text{water}}/M_{\text{dry air}}$; temperatures are in Kelvin. In other words, T_{vi} is the temperature that dry air would have at the actual density of the air under consideration, maintaining constant total pressure.

The following will be assumed: (1) the surface air is completely dry and at temperature T_0 ; (2) at evaporation front the air temperature is T_E , relative humidity is h_E , mixing ration is r_E ; (3) $T_{E,vi} > T_0$ (required for instability); (4) all heat, transported by convection, is used for evaporation (no loss to soil heating); combination of the above results in:

$$(A5.2) \quad C_p(T_0 - T_E) V_{in} = L h_E r_{sat}(T_E) V_{out}$$

where V is the total flux of air on a dry mass basis. An additional condition that is imposed naturally is that V_{in} and V_{out} are equal (with opposite directions).

The instability condition can then be written as

$$(A5.3) \quad T_0 < \frac{1 + r_E/\epsilon}{1 + r_E} T_E \approx \frac{1 + h_E r_{sat}(T_E)/\epsilon}{1 + h_E r_{sat}(T_E)} T_E$$

It follows now from combination with the above that

$$(A5.4) \quad \frac{1 + h_E r_{sat}(T_E)/\epsilon}{1 + h_E r_{sat}(T_E)} T_E > \frac{L h_E r_{sat}(T_E)}{C_p} + T_E$$

which will be written as

$$(A5.5) \quad \frac{1 + Ah}{1 + Bh} - C > Dh + C$$

with $A \equiv r_{\text{sat}}(T_E)/\epsilon$, $B \equiv r_{\text{sat}}(T_E)$, $C \equiv T_E C_p$, $D \equiv L r_{\text{sat}}(T_E)$. Upon equating LHS and RHS of A5.5, the roots

$$h = 0$$

and
$$h = \frac{AC - BC - D}{BD}$$

are found. In the second root, the denominator BD is positive. The numerator is negative since the term D is one order of magnitude larger than the other terms. As the solution of A5.5 is the interval $(AC - BC - D)/BD < h < 0$, it appears that no h-values with physical significance exist under the imposed conditions; hence heat supply through 'hot dry air flow' from the surface downward cannot solely maintain subsurface evaporation.

Of course heat is also supplied from the surrounding soil mass by conduction and local cooling. How significant is the convective term in this combined mechanism? The following example gives an indication.

For surface temperatures (dry air) of 30, 40, 50 and 60 °C, minimum T_E values of 26, 34, 41 and 47 °C are allowed in order to keep the stratification unstable (saturated air at evaporation front). This implies maximum temperature differences $\Delta T (=T_o - T_E)$ of 4, 6, 9 and 13 K. Using eq. A5.2. with $C_p = 1000 \text{ J kg}^{-1}$, L ranging from $2.39 \cdot 10^6$ to $2.44 \cdot 10^6 \text{ J kg}^{-1}$ and $r_{\text{sat}}(T_E)$ between $2.02 \cdot 10^{-2}$ and $6.25 \cdot 10^{-2}$, it appears that only a fraction 0.078 - 0.085 of the required heat is supplied by thermal convection. The remainder is supported by local changes in heat content and by conduction.

APPENDIX 6 Determination of the matric flux potential curve for core samples; a new method

The $\Phi-\theta$ curve can be determined from a series of simple flux and weight measurements under steady state conditions. The procedure described below was used to determine the $\Phi-\theta$ curves of the two Swifterbant soils, shown in Figure 4.38.

Assumptions underlying the method are:

1. the gravity term in the water flow equation can be neglected
2. the soil sample is homogeneous on a macroscopic scale
3. the flow is unidimensional.

It is recalled that under these conditions, the flux of soil liquid at any location can be written as (cf. section 3.6.2).

$$(A\ 6.1) \quad j_{liq} = - \frac{d\Phi}{dz}$$

A soil core sample (e.g. 100 cc) is brought to equilibrium with a chosen reference soil water pressure p_0 (state 0). A porous membrane at the lower end of the soil core connects the soil water to the water in a burette, equipped with a marriotte arrangement to fixate the pressure level. The matrix flux potential Φ_0 corresponding to this equilibrium situation is defined to be zero.

The following step is to expose the surface of the sample to an evaporative demand until a steady upward moisture flow is established (to be observed from flux and/or weight measurements). The flux j_i and the sample weight w_i characterize this state i. The procedure is repeated for increasing evaporative demands, resulting in a series of values for j_i and w_i , respectively, pertaining to steady states i. During all measurements, the base of the sample is maintained at constant pressure.

Let the curve in Figure A6.1 represent the matric flux potential curve to be determined. This curve now can be constructed from the above measurements in the following manner. For each state i, the value Φ_i , prevailing at the surface of the evaporating sample, is given as the product of sample height Δz and the governing flux, according to eq. A6.1 and the definition of Φ_0 :

$$(A6.2) \quad \Phi_i = - j_i \Delta z$$

The corresponding surface moisture contents θ are now sought, to yield the pairs (θ_1, Φ_1) which represent the curve to be determined. The surface moisture contents are calculated step by step through linear interpolation. The procedure is depicted in Figure A6.2.

Point A represents the initial condition (θ_0, Φ_0) . θ_0 is calculated from W_0 and the sample dry weight (to be measured as the last step of the procedure). To locate point B, the surface moisture content in state 1, θ_1 , can be calculated upon assumption of linearity in the θ -z profile. The flux j_1 should be taken small enough in order not to introduce a significant error by this simplifying assumption. θ_1 then is found from the equation

$$(A6.3) \quad W_0 - W_1 = a \Delta z (\theta_0 - \theta_1)$$

where a is the sample surface area. The flux j_1 was measured, so now both coordinates of B (θ_1, Φ_1) are known. To determine θ_2 , - pertaining to point C on the curve - the value of Φ_1 must be used as indicated in Figure A6.2. With the linear Φ -z profile (eq. A6.1, steady state), the depth z_{21} where $\Phi = \Phi_1$ can be calculated. At z_{21} , θ equals θ_1 . Now the θ -z profile is assumed to be linear over two segments: from $z = 0$ to $z = z_{21}$, and from $z = z_{21}$ to $z = \Delta z$. Thus the surface moisture content θ_2 can be calculated and be combined with Φ_2 to yield point C on the curve. Similarly, for state 3 the depths z_{31} and z_{32} are located at the sites where $\Phi = \Phi_1$ and $\Phi = \Phi_2$, respectively. The moisture contents at these depths are θ_1 and θ_2 , and these values are used to calculate θ_3 at the surface from W_3 , the θ -z profile now being divided into three linear segments. All the other points on the curve are determined similarly. Clearly, the whole procedure is easily cast into a numerical algorithm, which requires only the measured pairs (W_i, j_i) and the constants a , Δz and W_d (oven dry weight) as input variables.

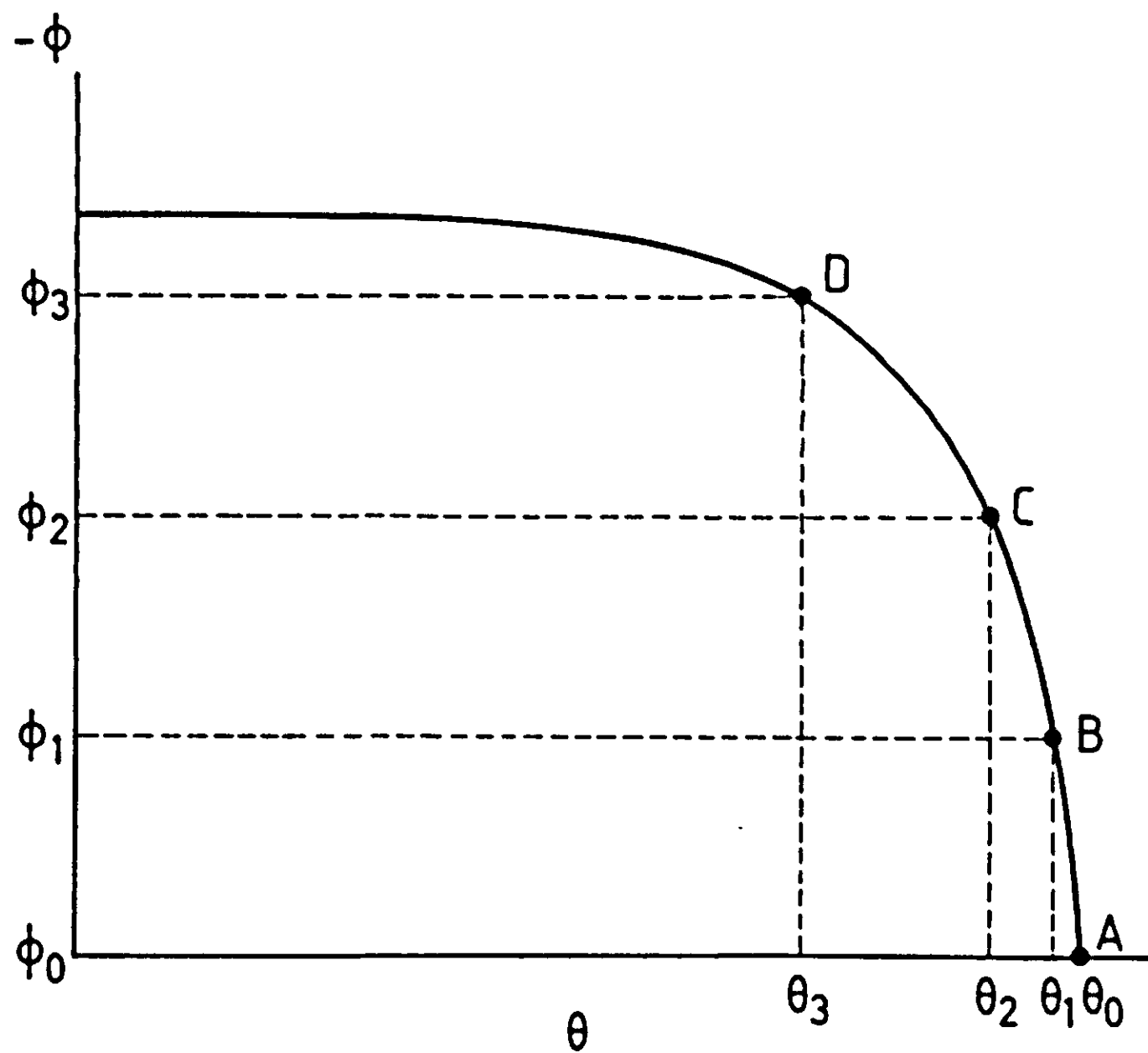


Figure A6.1 Example of a $\phi(\theta)$ curve, to be determined by the described procedure.

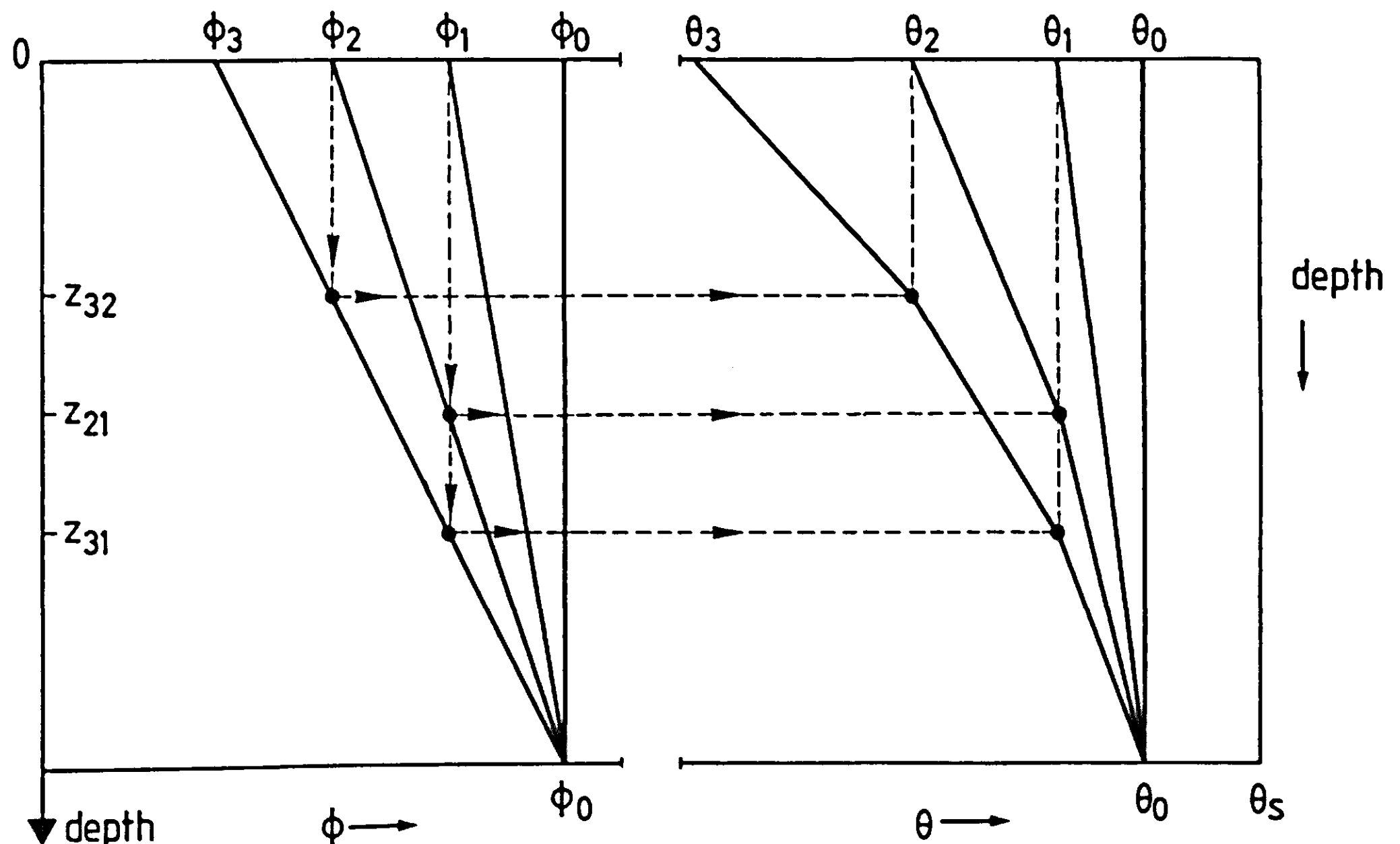


Figure A6.2 Profiles of $\phi(1)$ and $r(2)$ as calculated from flux- and weight measurements in different steady states.

APPENDIX A7 Description of the surface step method to determine soil thermal conductivity on core samples (Stroosnijder, 1984).

The described method makes use of the establishment of a constant interface temperature when two semi-infinite bodies, each at its own initial temperature, make contact. Applying a step increase of the surface temperature, the reduced temperature $T(z,t)$ at time t and distance z from the interface can be written as

$$(A7.1) \quad \bar{T}(z,t) \equiv \frac{T(z,t) - T_i}{T_o - T_i} = \operatorname{erfc} \left(\frac{z}{2\sqrt{Dt}} \right) \equiv \operatorname{erfc} (u)$$

where T_i is the initial temperature, T_o the imposed surface temperature, and D the thermal diffusivity (Carslaw and Jaeger, 1962).

When $T(z,t)$ is measured and T_i and T_o are known, eq. (A7.1) can be solved for D . The thermal conductivity λ is then subsequently calculated by making use of an estimated value of the heat capacity.

The constant surface temperature T_o is imposed at the surface of a soil core sample by fusing the sample with a PVC core of known thermal properties and at known initial temperature. The contact temperature that arises is a function of the initial temperatures and the contact coefficients of the soil and PVC materials, respectively:

$$\frac{T_o - T_{i,\text{soil}}}{T_{i,\text{PVC}} - T_o} = \frac{\sqrt{(\lambda C)}_{\text{PVC}}}{\sqrt{(\lambda C)}_{\text{soil}}}$$

The contact temperature can be measured directly and in that case the procedure needs no further comment. Alternatively, T_o may be calculated from measured $T(z,t)$ -values by an interpolation procedure. Writing the diffusivity as

$$D = \frac{z^2}{4} \frac{1}{u^2 t}$$

one may use two measured values of T_z in the above equations to yield the same value for D , and hence for $u^2 t$. So the relation

$$(u^2 t)_{t1} = (u^2 t)_{t2}$$

is used. In order to obtain u-values, the measured T_z values must be used to calculate the reduced T-values. To this purpose the unknown T_o must be invoked. This variable can be assessed by a graphical procedure: For a number of different T_o values, the corresponding u-values are calculated. Plotting of the ratio $(u^2 t)_{t1}/(u^2 t)_{t2}$ vs the assumed values of T_o yields the true T_o as the point where this ratio equals unity.

APPENDIX A8 Details on FLEVO, TEXAS, ARIZONA experiments

Table A8.1 Properties measured for Swifterbant soils

property/function	remarks	depth (cm)	silt	loam
			loam	
moisture characteristic suctions	0.25, 1, 2, 4, 7, 10, 20, 50, 100, 1500, kPa 16 cores; lab.	7.5 - 12.5 17.5 - 22.5 27.5 - 32.5 37.5 - 42.5	+	+
moisture characteristic suction	0.25, 1, 100 1500 kPa 200 cores; lab.	0 - 5 5 - 10	+	+
moisture characteristic	div. θ , T = 2,10,15,20, 25,30,35,45 °C lab.	0 - 10	+	-
bulk density	16 cores 200 cores 20 plates	7.5 - 12.5 17.5 - 22.5 27.5 - 32.5 37.5 - 42.5 0 - 5 5 - 10 0.0 - 0.5 0.5 - 1.5	+	+
hydraulic conductivity	1 kPa; 10 cores	0 - 5	+	+
matrix flux potential	complete curve; 16 cores	0 - 5	+	+
emissivity	$\theta \approx 0.10, 0.20, 0.30, 0.40$ 12 cores; lab.	0 - 5	+	-
albedo	in situ	0.0 - 0.5	+	-
thermal conductivity	surface step method; lab.	0 - 5	+	-
thermal conductivity	in situ; 9 heat probes	2,3,4,5,8	+	-
thermal conductivity	null alignment in situ	0 - 30	+	-
texture	fractions, 0-2, 2-16, 16-50, 50-75, 75-100, 100-150 μm microtrac laser	0 - 5	+	+

Table A8.2 Properties measured for Buffalo silty clay

property/function	remarks	depth (cm)
moisture characteristic	suctions 0,25, 1, 2, 4 7, 10, 20, 50, 100, 1500 kPa 15 cores; lab.	0 - 5
hydraulic conductivity	complete curve; hot air method; 15 cores	0 - 10
bulk density	at 1 cm increments at 2 cm increments at 5 cm increments	0 - 15 15 - 25 25 - 50
albedo	in situ as $f(\theta)$	0.0 - 0.5
texture	fractions 0-2, 2-50, >50 μm	0 - 5

Tabel A8.3 Dynamic variables measured in FLEVO experiment

Variable	height/depth	freq.	instrument / technique	recording / readout	integration field plots
global radiation	1.5 m	2/hr	Kipp solari-albedo-meter	TFDL data-logger	+
reflected global radiation	1.5 m	2/hr	TFDL data-logger	+	5
T _{dry} (air)	1.5 m	1/hr	thermistor	-	*
T _{dry} (air)	0.5 m	2/hr	thermistor	TFDL data-logger	-
T _{dry} -T _{wet} (air)	0.5 m	2/hr	Cu-Co th.cpl.	TFDL data-logger	+
T _{wet} -T _{wet} (air)	0.5-0.2 m	2/hr	Cu-Co th.cpl.	TFDL data-logger (100 x ampl)	+
T _{dry} -T _{dry} (air)	0.5-0.2 m	2/hr	Cu-Co th.cpl.	TFDL data-logger (100 x ampl)	+
windspeed	0.2,0.5,0.8 m	2/hr	cup-anemometers	TFDL data-logger	+
radiation temp. (soil)	1.5 m (soil)	2/hr (8-14 um)	Heimann KT15	TFDL data-logger	+
soil temperature	1,3,3.5,5.5,11.5 21,54 cm	2/hr	thermistor	TFDL data-logger	-
soil temperature	5,10,20,25,30,35 40,45,50	2/hr	thermistor	TFDL data-logger	-
soil temperature	1,4,9,14,20,35,50 35-55 mm	2-5/day	Cu-Co th.cpl. gravimetric (5x)	TFDL data-logger	-
soil water content	0-5,5-15,15-35, 35-55 mm	2-5/day	gravimetric (5x)	TFDL data-logger	-
soil water suction	4,9,14,20,35,50 cm	2-5/day	Hg.manom.tension.	-	1,2,3,4
cumulative evaporation	0-12 cm	1/day	microlysimeter	-	moving
rainfall	-	1/hr	autom.rain gauge	+	*
cloud cover	-	1/hr	-	-	**

* Kloostertuin nearby (1 km) weather station; ** KNMI Lelystad

Table A8.4 Dynamic variables measured in TEXAS experiment.

Variable	height/depth freq.	Instrument/ technique	recording/ readout	Integration plots	field plots
global radiation	1.5 m		1/hr	Kipp	Omnidata Polycorder
refl. glob. rad.	1.5 m		1/hr	Kipp	Omnidata Polycorder
net radiation	2.0 m		1/hr	Fritschen S.A.	Omnidata Polycorder
T _{dry} (air)	1.5 m		1/hr	thermistor	Omnidata Polycorder
T _{wet} (air)	1.5 m		1/hr	thermistor	Omnidata Polycorder
windspeed	2.0 m		1/hr	cup-anemometer	Omnidata Polycorder
radiation temp.	1.0 m		6-12/d	Barnes	
soil					1-10
sky rad. temp.	.		6-12/d	Barnes	.
soil temperature	5,10,25,100 cm		6/d	Cu-Co th.cpl.	-
soil water cont.	0-5,5-15,15-35 mm		6/d	gravimetric (10x)	A-F
soil water cont.	5,10,20,30,40,50		1/d	Troxler	1-10
	60,70,80,90,100 cm			neutron probe	A-F
soil water cont.	0-15 (1 cm incr.)		6/d	Troxler	
	15-25 (2 cm incr.)			gamma probe	-
	25-50 (5 cm incr.)				A-F
cum. evaporation	0-12 cm		6/d	microlysimeter	1-10
rainfall				rainingauge	+
irrigation				rainingauge	+
				fluxmeter	random (10 spots)

Table A8.5 Dynamic variables measured in ARIZONA experiment (by USDA Water Conservation Laboratory)

variable	height/depth	frequency	instrument/technique
global radiation	.	2/hr	Eppley Pyranometer
reflected radiation	.	2/hr	Eppley Pyranometer; Kipp Solarimeter
all wave radiation	.	2/hr	Funk Radiometer; Saturn Radiometer
net radiation	0.2, 0.5 m		
Tair dry	0.2, 0.5, 3.90 m	2/hr	Cu-Co thermocouples
Tair wet	0.2, 0.5 m	2/hr	Cu-Co thermocouples
windspeed	0.2, 0.5, 0.9, 1.75 m	2/hr	
soil temperature	1, 5, 7.5, 10, 20, 30, 40, 50, 80, mm	2/hr	Cu-Co thermocouples
	0.16, 0.32, 0.64, 1.28 m		
soil water content	0-5, 0-10, 10-30, 30-50, 50-90, 50-100 mm	2/hr	gravimetric (6x)
	0.10-0.15, 0.15-0.20, 0.20-0.30, 0.30-		
	0.40, 0.40-0.50; 0.50-0.60, 0.60-0.70,		
	0.70-0.80, 0.80-0.90, 0.90-1.00 m		
soil heat flux	5 mm	2/hr	disks, null alignment
soil evaporation	0-1.6 m	2/hr	weighing lysimeter
tank evaporation	.	2/hr	open pan

APPENDIX 9 The Nicholaichuck model

The non-dimensional solution of the heat flow equation is written as:

$$(A9.1) \quad \frac{T(z,t) - T_{in}}{T_{in}} = \left(\frac{\kappa_1}{\alpha T_{in}} - \frac{\kappa_2}{\alpha} \right) g_o(z_o, t_o, R_1)$$

with

T_{in} : initial soil temperature

$$(A9.2) \quad z_o \equiv \alpha z$$

$$(A9.3) \quad t_o \equiv t/\tau$$

$$(A9.4) \quad \alpha \equiv F_4/2F_1$$

$$(A9.5) \quad R_1 \equiv -\kappa_2/\alpha$$

$$(A9.6) \quad \tau \equiv 1/\alpha^2 F_1$$

(note that the scaled depth z_o has no relation to the roughness length z_o as used in Chapters 3-7)

The function g_o is defined as

$$(A9.7) \quad g_o(z_o, t_o, R_1) = \frac{1}{2(2-R_1)} \exp(2z_o) \operatorname{Erfc}\left(\frac{z_o}{2\sqrt{t_o}} + \sqrt{t_o}\right) - \frac{1}{2R_1} \operatorname{Erfc}\left(\frac{z_o}{2\sqrt{t_o}} - \sqrt{t_o}\right) - \frac{(1-R_1)}{R_1(R_1-2)} \exp[R_1(R_1-2)t_o + R_1z_o] \cdot \operatorname{Erfc}\left[\frac{z_o}{2\sqrt{t_o}} + (R_1-1)\sqrt{t_o}\right]$$

The distribution of soil moisture at time t is given by the expression

$$(A9.8) \quad \theta(z,t) = \theta_{in} + v_p(z,t) + v_h(z,t)$$

where θ_{in} is the initial volumetric moisture content. The function $v_p(z,t)$ in this equation is defined as

$$(A9.10) \quad v_p(z,t) = C_1 \sum_{i=1}^2 B_i g_o(z_o, t_o, R_1)$$

where

$$(A9.11) \quad C_1 \equiv \frac{(K_1/\alpha T_{in} - K_2/\alpha)}{\tau D_\theta \alpha^2 - 1}$$

and g_o is the function mentioned above, where R_1 can be replaced by R_2 , defined as

$$(A9.12) \quad R_2 \equiv \frac{-2}{\tau D_\theta \alpha^2 - 1}$$

Furthermore, B_1 and B_2 are given by

$$(A9.13) \quad B_1 \equiv \frac{-D_T T_{in} \tau \alpha^2 R_1}{R_1 - R_2}$$

$$(A9.14) \quad B_2 \equiv \frac{D_T T_{in} \tau \alpha^2 R_2}{R_1 - R_2}$$

V_h in eq (A9. 8) is a linear combination of two more complicated functions:

$$(A9.15) \quad V_h \equiv C_2 f_1(z, t) + f_2(z, t) +$$

with

$$(A9.16) \quad C_2 \equiv \frac{1}{\alpha} (K_3 + K_4 T_{in}) - C_1 (B_1 + B_2)$$

$$f_1(z, t) \equiv \left(\frac{z}{2} + \frac{1}{4\beta} + \frac{\beta\tau}{\eta} t_o \right) \cdot \exp(2\beta z_o) \cdot \operatorname{Erfc}\left(\frac{1}{2}\sqrt{\frac{\eta}{\tau}} \frac{z}{\sqrt{t_o}} + \beta \sqrt{\frac{\tau}{\eta}} \sqrt{t_o}\right)$$

$$(A9.17) \quad - \frac{1}{4\beta} \operatorname{Erfc}\left(\frac{1}{2}\sqrt{\frac{\eta}{\tau}} \frac{z}{\sqrt{t_o}} - \beta \sqrt{\frac{\tau}{\eta}} \sqrt{t_o}\right) \\ - \sqrt{\frac{\tau t_o}{\pi \eta}} \cdot \exp\left(\beta z_o - \left(\frac{\eta}{4\tau} \frac{z_o^2}{t_o} + \frac{\beta^2 \tau}{\eta} t_o\right)\right)$$

$$(A9.18) \quad f_2(z, t) \equiv \int_0^t H_{10}(t'_o) \cdot H_{20}(z_o, t_o - t'_o) dt'_o$$

$$(A9.19) \quad \text{with} \quad H_{10}(t'_o) \equiv -\frac{\tau}{\eta} \sum_{i=1}^2 d_i g_o(o, t'_o, R_i)$$

where the coefficients d_1 are defined as

$$(A9.20) \quad d_1 \equiv \frac{K_4}{\alpha^2} (K_1 - K_2 T_{1n}) - C_1 B_1 (R_1 - 2\beta)$$

$$(A9.21) \quad d_2 \equiv - C_1 B_2 (R_2 - 2\beta)$$

and the function H_{20} represents the expression

$$H_{20}(z_o, t_o) \equiv \sqrt{\frac{\eta}{\pi\tau}} \frac{1}{\sqrt{t_o}} \cdot \exp\left(-\left(\frac{1}{2}\sqrt{\frac{\eta}{\tau}} \frac{z_o}{\sqrt{t_o}} - \beta \sqrt{\frac{\tau}{\eta}} \sqrt{t_o}\right)^2\right)$$

$$(A9.22) \quad - \beta \cdot \exp(2\beta z_o) \cdot \operatorname{Erfc}\left(\frac{1}{2}\sqrt{\frac{\eta}{\tau}} \frac{z_o}{\sqrt{t_o}} + \beta \sqrt{\frac{\tau}{\eta}} \sqrt{t_o}\right)^2$$

The convolution integral expressed by eq. (A9. 18) is solved numerically by the CSMP-program listed in Appendix 10. The scaled time t_o is the current variable, and by the nature of the occurring integral, the output produced by the program NICAN will only be correct for that point of (scaled) time that corresponds to the FINTIM value, used in the definition of the function H_{20} . So if the program is used to calculate profiles after three hours real time, as in the example given in Chapter 5 (Table 5.9), only the $\theta(z)$ and $T(z)$ values for $t=3$ hours are correct, and not those for the preceding points in time. Hence a complete run must be made for each specific point in time for which one wishes to obtain a prediction.

APPENDIX 10 Listings of the models NICAN and LINTRA

***** GIBAC *****
*
* A semi-analitical model for the calculation of temperature and
* moisture profiles in homogeneous soils, based on Nicholaichucks,W.,
* 1974, and Gibbs,A.G. and R.G.Baca,1981.
*
* Author:H.F.M.ten Berge
* Wageningen Agricultural University,
* Dept.of Soil Science and Plant Nutrition
* De Dreijen 3, 6703 BC, Wageningen, The Netherlands
*

STORAGE	ERFC1A(26),	ERFC2A(26),	ERFC4A(26),	ERFC1B(26)
STORAGE	ERFC2B(26),	ERFC4B(26),	ERFC11(26),	ERFC12(26)
STORAGE	F1ARG1(26),	F1ARG2(26),	F1ARG3(26)	
STORAGE	F1LOC(26),	FTERM1(26),	FTERM2(26),	FTERM3(26)
STORAGE	GDA(26),	GDB(26),	GARG1A(26),	GARG2A(26)
STORAGE	GARG3A(26),	GARG4A(26),	GARG1B(26),	GARG2B(26)
STORAGE	GARG3B(26),	GARG4B(26),	GTER1A(26),	GTER2A(26)
STORAGE	GTER3A(26),	GTER4A(26),	GTER1B(26),	GTER2B(26)
STORAGE	GTER3B(26),	GTER4B(26),	H2O(26)	
STORAGE	H2ARG1(26),	H2ARG2(26),	HTERM1(26),	HTERM2(26)
STORAGE	T(26),	VH(26),	VP(26),	W(26)
STORAGE	X(26),	XO(26)		

FIXED I

INITIAL

NOSORT

*** 1 *** Parameters and constants

CONSTANT PI	=3.14159		
PARAM CH	=1.0,	CL	=4180.
PARAM CS	=1.0E3,	DT	=1.E-9
PARAM DTH	=5.E-7		
PARAM ES	=1.1574E-7		
PARAM K0	=1.E-15		
PARAM L	=2.454E6, M		=0.0
PARAM N	=0.0,	RHOL	=1.0E3
PARAM RHOS	=1.5E3,	RN	=700.
PARAM TA	=20.,	TI	=20.
PARAM WI	=0.36,	RHOA	=1.2
PARAM CPA	=1.0E3,	Z	=2.0
PARAM ZNOT	=0.01,	KAR	=0.41
PARAM WS	=2.0,	TIMOUT	=10800.

*** 2 *** Geometry of the system

```
*****  
TABLE X(1-5)      =0.0,1.E-3,4.E-3,9.E-3,16.E-3  
TABLE X(6-10)     =25.E-3,36.E-3,49.E-3,64.E-3,81.E-3  
TABLE X(11-15)    =10.E-2,12.E-2,14.E-2,16.E-2,18.E-2  
TABLE X(16-20)    =20.E-2,22.E-2,24.E-2,26.E-2,28.E-2  
TABLE X(21-25)    =30.E-2,32.E-2,34.E-2,36.E-2,38.E-2  
TABLE X(26)       =39.5E-2
```

*** 3 *** Output and run control

```
*****  
RENAME TIME=T0  
TIMER FINTIM=35.E-21,PRDEL=35.E-22,DELT=30.E-24  
METHOD TRAPZ  
FINISH TIJD=10830.  
PRINT TIJD,DUT0,...  
T(1-25),W(1-26)
```

*** 4 *** Calculation of the system constants

```
*****  
HEC          =((ALOG(Z/ZNOT))**2.)/(WS*(KAR**2.))  
H            =RHOA*CPA/HEC  
K1           =(RHOL*L*ES-H*TA-RN)/CH  
K2           =-H/CH  
K3           =(K0-M*WI-N*TI+ES-DT*K1)/DTH  
K4           =(DT*K2+N)/DTH  
F1           =CH/(RHOS*CS)  
F4           =(RHOL*CL*K0)/(RHOS*CS)  
  
ALPHA        =F4/(2.*F1)  
BETA         =M/(2.*ALPHA*DTH)  
TOU          =1./(F1*(ALPHA**2.))  
ETA          =1./(DTH*(ALPHA**2.))  
  
P1           =N*ALPHA*TI*TOU  
P2           =DT*TI*TOU*(ALPHA**2.)  
R1           =-K2/ALPHA  
R2           =(M*ALPHA*TOU-2.)/(TOU*DTH*(ALPHA**2.)-1.)  
B1           =(P1-P2*R1)/(R1-R2)  
B2           =-(B1+P2)  
C1           =(K1/(ALPHA*TI)-K2/ALPHA)/(TOU*DTH*...  
              *(ALPHA**2.)-1.)  
C2           =(K3+K4*TI+M*WI/DTH)/ALPHA-C1*(B1+B2)  
D1           =K4*(K1-K2*TI)/(ALPHA**2.)-C1*B1*(R1-2.*BETA)  
D2           =-C1*B2*(R2-2.*BETA)  
COEFT        =K1/(ALPHA*TI)-K2/ALPHA  
DO 100  
X0(I)        =ALPHA*X(I)  
100 CONTINUE  
FIN=TIMEOUT/TOU
```


***** DYNAMIC

***** NOSORT

*** 5 *** Semi-analytical solution

TIJD =T0*T0U
DUTO =FIN-T0
DO 200 I=1,26
GARG1A(I) =X0(I)/(2.*SQRT(T0))+SQRT(T0)
GARG2A(I) =X0(I)/(2.*SQRT(T0))-SQRT(T0)
GARG3A(I) =R1*(R1-2.)*T0+R1*X0(I)
GARG4A(I) =X0(I)/(2.*SQRT(T0))+(R1-1.)*SQRT(T0)
GARG1B(I) =GARG1A(I)
GARG2B(I) =GARG2A(I)
GARG3B(I) =R2*(R2-2.)*T0+R2*X0(I)
GARG4B(I) =X0(I)/(2.*SQRT(T0))+(R2-1.)*SQRT(T0)
ERFC1A(I) =ERFC(GARG1A(I))
ERFC2A(I) =ERFC(GARG2A(I))
ERFC4A(I) =ERFC(GARG4A(I))
ERFC1B(I) =ERFC1A(I)
ERFC2B(I) =ERFC2A(I)
ERFC4B(I) =ERFC(GARG4B(I))

GTER1A(I) =1./(2.*(2.-R1))*EXP(2.*X0(I))*ERFC1A(I)
GTER2A(I) =+1./(2.*R1)*ERFC2A(I)
GTER3A(I) =+(1.-R1)/(R1*(R1-2.))*EXP(GARG3A(I))
GTER4A(I) =ERFC4A(I)
GTER1B(I) =1./(2.*(2.-R2))*EXP(2.*X0(I))*ERFC1B(I)
GTER2B(I) =1./(2.*R2)*ERFC2B(I)
GTER3B(I) =+(1.-R2)/(R2*(R2-2.))*EXP(GARG3B(I))
GTER4B(I) =ERFC4B(I)
GOA(I) =GTER1A(I)-GTER2A(I)-GTER3A(I)*GTER4A(I)
GOB(I) =GTER1B(I)-GTER2B(I)-GTER3B(I)*GTER4B(I)

T(I) =COEFT*GOA(I)*TI+TI

IF (M.EQ.0.0) GOTO 150
F1ARG1(I) =0.5*SQRT(ETA/T0U)*X0(I)/SQRT(T0)+BETA* ...
 SQRT(T0U/ETA)*SQRT(T0)
F1ARG2(I) =0.5*SQRT(ETA/T0U)*X0(I)/SQRT(T0)-BETA* ...
 SQRT(T0U/ETA)*SQRT(T0)
F1ARG3(I) =BETA*X0(I)-(ETA/(4.*T0U))*X0(I)*X0(I)/ ...
 T0-BETA*BETA*T0U*T0/ETA
 =ERFC(F1ARG1(I))
 =ERFC(F1ARG2(I))
FTERM1(I) =(X0(I)/2.+1./((4.*BETA)+BETA*T0U*T0/ETA)* ...
 EXP(2.*BETA*X0(I))*ERFC11(I)
FTERM2(I) =1./((4.*BETA)*ERFC12(I)

FTERM3(I) =SQRT(TOU*T0/(PI*ETA))*
F1LOC(I) EXP(F1ARG3(I))
GO TO 170 =FTERM1(I)-FTERM2(I)-FTERM3(I)

150 F1ARG1(I) =0.5*SQRT(ETA/TOU)*X0(I)/SQRT(T0)
F1ARG2(I) =-0.25*ETA/TOU*X0(I)*X0(I)/T0
ERFC11(I) =ERFC(F1ARG1(I))
F1LOC(I) =X0(I)*ERFC11(I)-2.*SQRT(TOU/(PI*ETA)) ...
*SQRT(T0)*EXP(F1ARG2(I))
170 H10 =-(TOU/ETA)*(D1*G0A(1)+D2*G0B(1))
H2ARG1(I) =-(0.5*SQRT(ETA/TOU)*X0(I)/SQRT(DUTO)-
BETA*SQRT(TOU/ETA)*SQRT(DUTO))***2. ...
H2ARG2(I) =(0.5*SQRT(ETA/TOU)*X0(I)/SQRT(DUTO)+BETA ...
*SQRT(TOU/ETA)*SQRT(DUTO))***2.
HTERM1(I) =(SQRT(ETA/(PI*TOU))/SQRT(DUTC))*EXP(H2ARG1(I))
HTERM2(I) =+BETA*EXP(2.*BETA*X0(I))*ERFC(H2ARG2(I))
H2O(I) =HTERM1(I)-HTERM2(I)
F2ARG(I) =H10*H2O(I)
F2LOC =INTGRL(0.,F2ARG,26)
VH(I) =C2*F1LOC(I)+F2LOC(I)
VP(I) =C1*B1*G0A(I)+C1*B2*G0B(I)

W(I) =VP(I)+VH(I)+WI

200 CONTINUE

IF(KEEP.LT.0.5) GO TO 1
IF(TIJD.EQ.10800.) WRITE(7,300) (TIJD,T(I),W(I),I=1,26)
300 FORMAT(2X,F8.1,3X,F8.3,3X,F8.4)
IF(TIJD.GT.10750.) CALL PRINT
1 CONTINUE
END
STOP
ENDJOB

***** LINTRA *****
*
* A model for simulating transport processes near the surface
* of a bare soil .
* This is a strongly simplified version of the the soil com-
* partment of SALSA. Thermal conductivity and soil water
* diffusivities (thermal and isothermal) are assumed to be con-
* stant.
*
* Author:H.F.M.ten Berge
* Wageningen Agricultural University,
* Dept.of Soil Science and Plant Nutrition,
* De Dreijen 3, 6703 BC, Wageningen, The netherlands
*

STORAGE DEPTH(26) , HFL(26) , HFLC(26) , HFLM(26)
STORAGE RDF(26) , T(26) , TCM(26) , W(26)
STORAGE WFLI(26) , WFLLIQ(26), WFLT(26)
FIXED I,J,NCOM

INITIAL
NOSORT

*** 1 *** Parameters
*** Geometry of the system
NCOM =25
TABLE TCM(1-5)=2.E-3,4.E-3,6.E-3,8.E-3,10.E-3
TABLE TCM(6-10)=12.E-3,14.E-3,16.E-3,18.E-3,20.E-3
TABLE TCM(11-15)=5*20.E-3
TABLE TCM(16-20)=5*20.E-3
TABLE TCM(21-25)=5*20.E-3
RDF(1) =1./(0.5*TCM(1))
DO 500 I=2,NCOM
RDF(I) =1./(0.5*(TCM(I-1)+TCM(I)))
500 CONTINUE
RDF(NCOM+1) =1./(0.5*TCM(NCOM))
*** Physical constants ***
CONSTANT KAR =0.41 , L =2.454E6
CONSTANT RHOL=1.0E3, RHOCP =1.2E3
*** Soil thermal properties ***
PARAM CH =1.0 , HCS =1.0E3
PARAM HCW =4180.0, RHOS =1.5E3
*** Soil hydraulic properties ***
PARAM HYCON =1.E-15
PARAM DT =1.E-9
PARAM DTH =5.E-7

*** Initial soil profile conditions ***

PARAM WI =0.36, TI =20.0

*** Boundary conditions and atmospheric conditions ***

PARAM ES =1.1574E-7

PARAM RN =700.

PARAM TA =20.0

PARAM WS =2.0

PARAM Z =2.0

PARAM ZNOT =0.01

PARAM TBNDL0 =20.

PARAM WBNDL0 =0.36

*** 2 *** Run control and options

TIMER FINTIM=10800., PRDEL=900., DELT=5.0

FINISH T1 =100. , T1 =0. , W1 =1. , W1 =0. , TS =100.

METHOD RKSFX

PRINT TS,T(1-10),T(12),T(14),T(16),T(18),T(20),...
T(22),T(24),T(25),W(1-10),W(12),W(14),W(16),W(18),...
W(20),W(22),W(24),W(25)

*** 3 *** Initial values of dynamic boundary layer parameters

USTAR =(KAR*WS)/ALOG(Z/ZNOT)

HEC =(ALOG(Z/ZNOT))**2./(WS*KAR**2.)

*** 4 *** Initial soil profile conditions

DO 1200 I=1,NCOM

W(I) =WI

WCONTI(I) =W(I)*TCM(I)

T(I) =TI

HCONTI(I) =T(I)*HCS*RHOS*TCM(I)

1200 CONTINUE

TS =TI

DYNAMIC

NOSORT

*** 5 *** Calculation of soil surface temperature by energy
balance; no boundary layer stability correction.

TS0 =T(1)

TS =IMPL(TS0,0.1,FOTS)

EHL ==ES*RHOL*L

SHL ==-(RHOCP/HEC)*(TS-TA)

FOTS =(RN+EHL+SHL)/(RDF(1)*CH)+T(1)

*** 6 *** Calculation of the energy balance components

```
*****  
2400 EHL  
      SHL  
      HFLC(1)  
      ENBAL  
      ==ES*RHOL*L  
      ==-(RHOCP/HEC)*(TS-TA)  
      ==-(TS-T(1))*CH*RDF(1)  
      =RN+EHL+SHL+HFLC(1)
```

*** 7 *** Calculation of total moisture fluxes (vapor and liquid)

```
*****  
      WFLI(1)          =ES  
      WFLT(1)          =0.0  
      DO 2700 I=2,NCOM  
      WFLT(I)          =(T(I)-T(I-1))*DT*RDF(I)  
      WFLI(I)          =(W(I)-W(I-1))*DTH*RDF(I)-HYCON  
2700  CONTINUE  
      WFLT(NCOM+1)     =(TBNDLO-T(NCOM))*DT*RDF(NCOM+1)  
      WFLI(NCOM+1)     =(WBNDLO-W(NCOM))*DTH*RDF(NCOM+1)-HYCON  
      DO 2705  
      WFLLIQ(I)        =I=1,NCOM+1  
      CONTINUE  
      DO 2710 I=1,NCOM  
      WFLNET(I)        =WFLLIQ(I+1)-WFLLIQ(I)  
2710  CONTINUE
```

*** 9 *** Calculation of soil heat flux by conduction

```
*****  
      HFLC(1)          ==-(TS-T(1))*CH*RDF(1)  
      DO 2800  
      HFLC(I)          =I=2,NCOM  
      =CH*(T(I)-T(I-1))*RDF(I)  
2800  CONTINUE  
      HFLC(NCOM+1)     =CH*(TBNDLO-T(NCOM))*RDF(NCOM+1)
```

*** 10 *** Calculation of heat flux by liquid mass flow

```
*****  
      HFLM(1)          =0.0  
      DO 2910  
      HFLM(I)          =I=2,NCOM+1  
      =-HYCON*RHOL*HCW*T(I-1)  
2910  CONTINUE
```

*** 11 *** Calculation of total heat fluxes

```
*****  
      DO 3100  
      HFL(I)           =I=1,NCOM+1  
      =HFLC(I)+HFLM(I)  
3100  CONTINUE  
      DO 3110  
      HFLNET(I)        =I=1,NCOM  
      =HFL(I+1)-HFL(I)  
3110  CONTINUE
```

*** 12 *** Integration of moisture fluxes and calculation of new
* water contents

```
*****  
WCONT          =INTGRL(WCONTI,WFLNET,25)  
DO 3200        I=1,NCOM  
    W(I)          =WCONT(I)/TCM(I)  
3200  CONTINUE  
    #1            =W(1)
```

*** 13 *** Integration of heat fluxes and calculation of new
* temperatures

```
*****  
HCONT          =INTGRL(HCONTI,HFLNET,25)  
DO 3300        I=1,NCOM  
    T(I)          =HCONT(I)/(RHOS*TCM(I)*HCS)  
3300  CONTINUE  
    T1            =T(1)
```

```
*****  
*****  
*****  
END  
STOP  
ENDJOB
```

SAMENVATTING

Aan het bodemoppervlak worden warmte en vocht uitgewisseld tussen bodem en atmosfeer. Voor onbegroeide grond hebben, - in tegenstelling tot het geval waar een plantendek aanwezig is -, een aantal fysische bodemeigenschappen een sterke invloed op het hydrologisch en, hiermee nauw verbonden, thermisch gedrag van de bovengrond. Stralingseigenschappen, thermische eigenschappen en hydraulische kenmerken van de bodem bepalen in zekere mate de verdeling van beschikbare energie over de diverse componenten van de energiebalans aan het oppervlak. Van deze samenhang tracht men in de 'remote sensing' gebruik te maken bij de interpretatie van warmtebeelden voor landbouwkundige doeleinden.

In de hier gerapporteerde studie werd een numeriek simulatiemodel ontwikkeld, met het doel de relaties tussen de fluxen aan het oppervlak en de toestandsvariabelen in bodem en atmosfeer te beschrijven. Het model SALSA (Soil-Atmosphere Linking Simulation Algorithm) simuleert ontwikkelingen in bodem en atmosfeer, waarbij globale straling en geostrophische wind als randvoorwaarden opgelegd worden. Een dergelijk model kan gebruikt worden om de invloed van bodemeigenschappen op de oppervlakte-temperatuur, welke met behulp van warmtebeelden geschat kan worden, na te gaan. Diverse modellen werden reeds eerder ontwikkeld om de energiebalans van het oppervlak te beschrijven. Een overzicht hiervan wordt gegeven in Hoofdstuk 2. De meeste modellen echter nemen slechts in geringe mate de fysische bodemeigenschappen in beschouwing, en vrijwel steeds wordt de toestand van de atmosfeer onafhankelijk van die van de bodem beschouwd. In hoofdstuk 6 wordt aangetoond dat dit tot grote fouten kan leiden.

Hoofdstuk 3 beschrijft de theorie en de aannamen welke aan het model ten grondslag liggen. Uitvoerig wordt hierbij ingegaan op o.a. straling aan het bodemoppervlak, het transport in de atmosferische grenslaag, en de koppeling tussen vocht- en warmtetransport in de bodem. Met betrekking tot deze kopplingsverschijnselen worden verschillende theoretische benaderingen met elkaar vergeleken. Voor het transport in de vloeibare fase leidt dit tot een vereenvoudiging van de bestaande mechanistische beschrijving. In Appendices 3 en 4 wordt dit geval verder uitgewerkt in het kader van Thermodynamica van Irreversibele Processen (TIP).

Voor de karakterisering van de hydraulische bodemeigenschappen worden enkele nieuwe parameters geïntroduceerd. Deze parameters (A' en B') definiëren een eerste orde rationele functie, welke goed blijkt te voldoen als uitdrukking voor de 'matrix flux potentiaal' als functie van vochtgehalte. Bij de simulatie van vochttransport waarbij de zwaartekrachtsterm verwaarloosd kan worden, of waarbij sterke gradiënten optreden, verdient het gebruik van de 'matrix flux potentiaal' de voorkeur boven dat van de hydraulische doorlatendheid en vochtkarakteristiek.

Naast de modelbeschrijving zijn in Hoofdstuk 3 ook vele bodemfysische gegevens uit de literatuur samengebracht in tabelvorm. De in het veld te verwachten maximale variatie in de diverse parameters kan uit deze data geschat worden, en wordt in Hoofdstuk 6 gebruikt in een gevoeligheidsanalyse.

Om het model te toetsen zijn veldexperimenten uitgevoerd in Oostelijk Flevoland en in Texas. Verder is gebruik gemaakt van experimentele gegevens verzameld door het USDA Water Conservation Laboratory te Phoenix, Arizona. Met de beschikbare experimentele gegevens kon slechts een verkorte versie van het SALSA model getoetst worden, omdat gegevens over grenslaagontwikkeling ontbraken en bovendien de proefgebieden steeds veel te klein waren om de gebruikte eendimensionale beschrijving te rechtvaardigen. Daarom werden steeds de op enige hoogte boven het proefveld gemeten condities als randvoorwaarden gebruikt. Alle systeemparameters werden onafhankelijk gemeten, berekend of geschat, d.w.z. niet door 'calibratie' bepaald. Hierdoor kunnen voorspelde toestandsvariabelen en fluxen ter validatie vergeleken worden met meetwaarden. (Een uitzondering hierop werd gemaakt voor de parameter ruwheidslengte in de TEXAS en ARIZONA gevallen. Deze kon niet uit de gemeten windsnelheden worden afgeleid en moest door 'calibratie' bepaald worden).

De vergelijking tussen meetwaarden en voorspellingen wordt behandeld in Hoofdstuk 5. Daar wordt aandacht geschonken aan de te verwachten fout in meetwaarde en voorspelling, waarbij gebruik wordt gemaakt van een dimensieloze variabele q , die de mate van overeenkomst tussen voorspelling en meting uitdrukt. In verband hiermee wordt de ruimtelijke variabiliteit van bodemeigenschappen in rekening gebracht door gebruikmaking van semivariantie-analyse en van het 'schalen' van hydraulische eigenschappen. Eerstgenoemde analyse werd tevens gebruikt bij het bepalen van meetlocaties voor detailstudie. Overeenkomst tussen metingen en voorspellingen blijkt het best te zijn voor de twee FLEVO datasets, welke betrekking hebben op respectievelijk

een droge, zonnige week en een regenachtige week met wisselende bewolking. Dat de modeltoetsing minder goede resultaten oplevert - in sommige opzichten - voor de ARIZONA en TEXAS data, wordt geweten aan de geringe afmetingen van beide proefvelden en het grote contrast met de (begroeide) omgeving.

Zowel in meting als voorspelling blijkt het bodemvochtgehalte nabij het oppervlak een duidelijke dagelijkse gang te vertonen, al wordt deze door het model wat overschat. Deze overschatting wordt toegeschreven aan het verwaarlozen van hysteresis in de vochtkarakteristiek.

Lokale variatie in hydraulische eigenschappen binnen het FLEVO proefveld, als gevolg van geringe textuurverschillen, blijkt variatie in het hydraulisch en thermisch gedrag van de bovengrond (1 à 2 cm) te veroorzaken. Dit effect wordt eveneens gesimuleerd. Ook het verloop van de uitdroging over een aantal dagen wordt door het model goed beschreven in de meeste gevallen. Problemen treden op wanneer bevochtiging (door regen) en uitdroging elkaar afwisselen. Deels wordt dit toegeschreven aan het hysteresis-probleem, maar bovendien blijkt zeer nauwkeurige informatie m.b.t. hydraulische eigenschappen vereist te zijn, d.w.z. ook geringe veranderingen die optreden als functie van de diepte dienen gekend te zijn. Het zal duidelijk zijn dat dit laatste voor een praktijksituatie niet het geval kan zijn; het gebruik van dergelijke deterministische modellen voor het doen van actuele voorspellingen voor de praktijk wordt dan ook als zeer beperkt gezien (i.e. buiten 'bodemfysische proefvelden'). Bodemtemperaturen op enige diepte blijken ook niet steeds nauwkeurig te voorspellen. Wanneer echter de geïntroduceerde fouten in rekening genomen worden blijkt de discrepantie tussen metingen en voorspellingen acceptabel (Hoofdstuk 5).

Samenvattend kan worden gesteld dat, ondanks de genoemde problemen, de experimentele modelvalidatie geen aanleiding geeft, significante fouten te veronderstellen in het gebruikte model.

Voor de bestudering van de gevoeligheid van variabelen voor systeemparameters werden de laatstgenoemde gevarieerd over het gehele traject waarover variaties verwacht kunnen worden in het veld. Wanneer extreme waarden voor parameters gekozen worden, dient men ervoor te zorgen dat de gebruikte randvoorwaarden aan het systeem realistisch blijven, d.w.z. dat zij zouden bestaan bij de gekozen combinatie van parameterwaarden en initiële condities. Wanneer meteorologische condities nabij het bodemoppervlak (bijv. op hut-hoogte) opgelegd worden als randvoorwaarde, is hieraan moeilijk te voldoen. Daarom wordt in Hoofdstuk 6 het 'complete' model gebruikt voor gevoe-

ligheidsanalyse, d.w.z. de model-versie welke de ontwikkeling van de atmosferische grenslaag eveneens simuleert. In een voorbeeld wordt aangetoond hoezeer de condities op hut-hoogte afhankelijkheid zijn van de bodemgesteldheid. De gevoeligheden van oppervlaktetemperatuur, luchttemperatuur, verzwadigingsdeficiënt (beide op huthoogte) en latente warmteflux voor een aantal bodemeigenschappen worden berekend voor twee vereenvoudigde gevallen; deze betreffen uitdrogingsstadium I ('potentiële verdamping') en stadium III (verdamping vanaf een vooraf bepaalde diepte beneden het oppervlak). Een dergelijke vereenvoudiging is gewenst omdat het zich in de loop der tijd wijzigend bodemvochtprofiel alle betrokken parameters beïnvloedt, en hiermee de gevoeligheid voor die parameters (bijv. albedo, warmtecapaciteit etc.) versluiert. In een aparte paragraaf wordt daarna het proces van de uitdroging zelf (stadium II) beschouwd in afhankelijkheid van de reeds genoemde hydraulische parameters A' en B'.

In de gevoelighedsanalyse voor stadia I en III wordt aan een aantal parameters een hoge of lage waarde toegekend, zodanig dat alle mogelijke combinaties van hoge en lage waarden gebruikt worden. Na het probleem voor alle combinaties door te rekenen, kunnen de gemiddelde parameter-effecten en hun interacties berekend worden d.m.v. variantie-analyse. In stadium I blijkt de oppervlaktetemperatuur overdag het gevoeligst voor ruwheidslengte, albedo en 'thermische inertia'. 's Nachts heeft de laatstgenoemde parameter het grootste effect. Voor stadium III hebben overdag albedo en de dikte van de droge toplaag het grootste effect, en in mindere mate de diffusiecoëfficiënt van waterdamp en de ruwheidslengte. De thermische bodemeigenschappen blijken in dit stadium alleen 's nachts van enig belang.

De ontwikkeling van de droge toplaag in stadium II blijkt sterk afhankelijk van de parameter A' en in meerdere mate van B' (samen bepalen deze parameters de matrix flux potentiaal curve). Hetzelfde kan geconcludeerd worden voor de verdampingsreductie. Genoemde resultaten kunnen gebruikt worden om de snelheid waarmee gevoeligheden veranderen bij de overgang van stadium I naar stadium III, te preciseren.

Genoemde hydraulische parameters hebben tevens een uitgesproken effect op de vorm van het vochtfront. De gesimuleerde verlopen van de diepte van het verdampingsfront in de tijd, volgens een aantal definities, worden eveneens met elkaar vergeleken, en blijken nauw met elkaar overeen te komen.

Aan het einde van Hoofdstuk 6 wordt nagegaan in welke mate de mogelijke variaties in bodemeigenschappen 'ruis' veroorzaken in het verband tussen oppervlakte-temperatuur en verdampingssnelheid. Variaties in albedo, ruwheidslengte en dikte van de droge toplaag blijken overdag fouten in de orde van 100 W m^{-2} te kunnen veroorzaken, wanneer gebruik gemaakt wordt van een linear verband tussen $(T_s - \bar{T}_s)$ en $(LE - \bar{LE})$.

In het laatste hoofdstuk wordt een overzicht gegeven van bestaande methoden ter interpretatie van warmtebeelden. Hierbij zijn ook methoden opgenomen welke tot op heden alleen werden toegepast op 'begroeide' situaties. Op grond van experimentele gegevens en gevoelighedsanalyse wordt geconcludeerd dat het gebruik van 'thermische inertia' in strikte zin ter bepaling van het bodemvochtgehalte nabij het oppervlak te zeer met onzekerheden behept is om bruikbare resultaten op te leveren. In plaats daarvan zal verder onderzoek zich moeten richten op de verdampingssnelheid, al zijn de hierboven genoemde resultaten niet veelbelovend, zoals uit eerdere hoofdstukken blijkt. Er wordt de nadruk op gelegd dat deze conclusies zich beperken tot het geval van onbegroeide bodem. In aanwezigheid van begroeiing spelen bodemfysische factoren een veel geringere rol in de energiebalans, die dan meer betrekking heeft op het vegetatie-dek.

CURRICULUM VITAE

Hein ten Berge werd geboren te Tilburg op 26 april 1956. Hij volgde de Gymnasium B opleiding aan het St. Thomas-college te Venlo en behaalde in 1974 het eindexamen.

In datzelfde jaar werd aangevangen met de studie Bodemkunde en Bemestingsleer (N33) aan de Landbouwhogeschool te Wageningen, waar hij in januari 1978 het kandidaatsexamen deed. De praktijktijd werd daarna in 1978 doorgebracht in Venezuela (Ministerio del Ambiente) in de bodemkartering, en vervolgens in 1979 bij het USDA Sedimentation Laboratory te Oxford Mississippi. De doctoraalfase werd afgesloten in 1981 met examens in de vakken bodemnatuurkunde, informatica, landbouwplantenteelt, en meteorologie.

In oktober 1981 werd de schrijver aangesteld als onderzoeksassistent bij de vakgroep Bodemkunde en Plantevoeding. Hij werd door de Landbouwhogeschool, de Begeleidingscommissie Remote Sensing (Rijkswaterstaat) en de European Geophysical Union in de gelegenheid gesteld enkele buitenlandse congressen te bezoeken, en een reis te maken langs een aantal onderzoeksinstellingen in de USA. Sinds 1 januari 1985 is hij als wetenschappelijk medewerker tijdelijk aangesteld aan de Landbouwhogeschool, en neemt als zodanig deel aan de onderzoeks- en onderwijsactiviteiten van genoemde vakgroep.